Proceedings Volume 2, 2011

Earthquake Geology and Archaeology: Science, Society and Critical Facilities

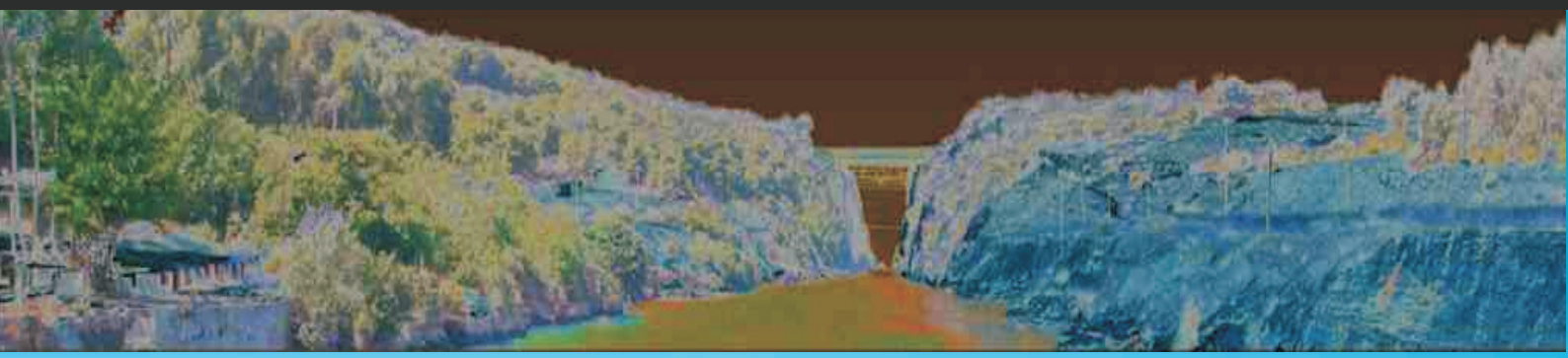

Editors

C. Grützner, R. Pérez-López, T. Fernández Steeger, I. Papanikolaou
K. Reicherter, P.G. Silva, and A. Vött

PROCEEDINGS

2nd INQUA-IGCP 567 International Workshop on Active Tectonics, Earthquake Geology, Archaeology and Engineering

19-24 September 2011
Corinth (Greece)

ISBN: 978-960-466-093-3

Proceedings

Earthquake Geology and Archaeology: Science, Society and Critical facilities

2nd INQUA-IGCP 567 International Workshop on Active Tectonics, Earthquake Geology, Archaeology and Engineering

Editors

C. Grützner, R. Pérez-López, T. Fernández-Steeger, I. Papanikolaou
K. Reicherter, P.G. Silva and A. Vött

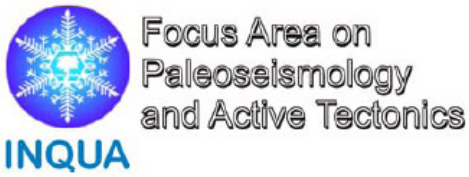

This **Volume of Proceedings** has been produced for the **2nd INQUA-IGCP 567 International Workshop on Active Tectonics, Earthquake Geology, Archaeology and Engineering** held in Corinth (Greece), 19-24 September 2011. The event has been organized jointly by the INQUA-TERPRO Focus Area on Paleoseismology and Active Tectonics and the IGCP-567: Earthquake Archaeology.

This scientific meeting has been supported by the INQUA-TERPRO #0418 Project (2008-2011), the IGCP 567 Project, the Earthquake Planning and Protection Organization of Greece (EPPO – ΟΑΣΠ) and the Periphery of the Peloponnese

UCL

Aon Benfield UCL Hazard Centre

Birkbeck UNIVERSITY OF LONDON

RWTH AACHEN UNIVERSITY

Ο.Α.Σ.Π.

JGU JOHANNES GUTENBERG UNIVERSITÄT MAINZ

ΕΘΝΙΚΟ & ΚΑΠΟΔΙΣΤΡΙΑΚΟ ΠΑΝΕΠΙΣΤΗΜΙΟ ΑΘΗΝΩΝ
NATIONAL & KAPODISTRIAN UNIVERSITY OF ATHENS

VNiVERSiDAD D SALAMANCA

AEQUA

Instituto Geológico y Minero de España

GSSI

paleoseismicity.org

Printed by
The Natural Hazards Laboratory,
National and Kapodistrian University of Athens

Edited by
INQUA-TERPRO Focus Area on
Paleoseismology and Active Tectonics
& IGCP-567 Earthquake Archaeology

INQUA-IGCP 567 Proceedings, Vol.2

I.S.B.N. 978-960-466-093-3
PRINTED IN GREECE

paleoseismicity.org

Vol. 2: Earthquake Geology and Archaeology: Science, Society and Critical facilities (C. Grützner, R. Pérez-López, T. Fernández-Steeger,, I. Papanikolaou, K. Reicherter, P.G. Silva & A. Vött, Eds.). ISBN 978-960-466-093-3. Printed in Greece, 2011. 2nd INQUA-IGCP 567 International Workshop, Corinth (Greece).

Vol. 1: Archaeoseismology and Palaeoseismology in the Alpine-Himalayan collisional Zone (R. Pérez-López, C. Grützner, J. Lario, K. Reicherter & P.G. Silva, Eds.). ISBN 978-84-7484-217-3. Printed in Spain, 2009. 1st INQUA-IGCP 567 International Workshop. *Baelo Claudia*, Cádiz (Spain).

Preface

After the very successful 1st Workshop on Earthquake Archaeology and Paleoseismology held in the ancient roman site of Baelo Claudia (Spain, 2009), the INQUA Focus Group on Paleoseismology and Active Tectonics decided to elaborate a bi-annual calendar to support this joint initiative with the IGCP-567 "Earthquake Archaeology". This second joint meeting moved to the eastern Mediterranean, a tectonically active setting within the Africa-Eurasia collision zone and located in the origins of the pioneer's works on archaeoseismology. However, for the coming year 2012, at least a part of us will move also to the New World, where the 3rd INQUA-IGCP 567 international workshop will take place in Morelia, Mexico in November 2012. It is planned to proceed with the meeting, so we are thinking of Aachen, Germany, to be the host in 2013, possibly together with Louvain, Belgium.

The aim of this joint meeting is to stimulate the already emerging comparative discussion among Earthquake Environmental Effects (EEE) and Earthquake Archaeoseismological Effects (EAE) in order to elaborate comprehensive classifications for future cataloguing and parametrization of ancient earthquakes and palaeoearthquakes. One of the final goals our collaborative workshops is the integration of archaeoseismological data in Macroseismic Scales such as the Environmental Seismic Intensity Scale ESI-2007 developed within the frame of the International Union for Quaternary Research (INQUA). In this second workshop we offer again a multidisciplinary and cross-disciplinary approach and program, since there is an urgent necessity to share the knowledge and objectives among geologists, seismologists, geodesists, archaeologists and civil engineers in order to improve seismic hazard assessments and analyses in a near future. Also, we intend to sharpen geoscientists and their research more in the direction of critical facilities, which are of world-wide public and political interest after the dramatic catastroph in Fukushima, Japan.

The last two years provided significant dreadful earthquake scenarios, which were in most of the cases oversized in relation to the data provided by the historical and instrumental seismicity. The Haiti Mw 7.0 (Haiti, Jan 2010), Malua Mw 8.8 (Chile, May 2010), Christchurch Mw 6.3 (New Zealand, Feb 2011), Tohoku Mw 9.0 (Japan, Mar 2011) and Lorca Mw 5.1 (Spain, May 2011) events illustrates that both extreme subduction earthquakes or moderate events can generate severe damage in relation to relevant secondary coseismic effects or Earthquake Environmental Effects (EEE). Most of these recent events have clearly demonstrated that the vibratory ground shaking is not the unique, or even most significant, source of direct damage, and it is by no means the only parameter that should be considered in seismic hazard assessments. The lessons offered by the aforementioned events corroborate once again the relevance of liquefaction, tsunamis, rockfalls, landslides, ground subsidence, uplift or failure as a major source of hazard. But this also underpins the need of re-evaluating the significance of macroseismic intensity as an empirical measurement of earthquake size. In fact, as highlighted in the last volume produced by the INQUA Focus Area (Serva et al., 2011), intensity is a parameter able to describe a complete earthquake scenario, based on direct field observation and suitable to be preserved in the geological, geomorphological and archaeological records.

With this aim the INQUA TERPRO #0418 Project (2008-2011) has implemented a world-wide online EEE Catalogue based on Google Earth in order to promote the use of the ESI-2007 Scale for seismic hazard purposes www.eeecatalog.sinanet.apat.it/terremoti/index.php. On the other hand the IGCP-567 is promoting an interesting shared approach of EEE data and EAE data for the same purpose. Examples of this variety of original research coming from this collaborative approach are the Geological Society of London Special Volume 316 (2009) ***Paleoseismology: Historical and Prehistorical records of Earthquake Ground Effects for Seismic Hazard Assessment*** (K. Reicherter, A.M. Michetti & P.G. Silva, Eds.), the Geological Society of America Special Papers 471, ***Ancient Earthquakes*** (2010) (M. Sintubin, I.S. Stewart, T. Niemi & E. Altunel, Eds.) and the Special Volume of Quaternary International (2011) ***Earthquake Archaeology and Paleoseismology*** (P.G. Silva, M. Sintubin & K. Reicherter, Eds.). In the same way, this abstract volume contains more than 80 contributions from researchers of more than 27 different countries and illustrates the upgrading shared knowledge on palaeo-, ancient, historical and instrumental earthquakes and images an impressive growth of our community. Our workshop was co-ordinated through the newly established website www.paleoseismicity.org, where earthquake info and blogs are openly shared.

Finally, we wish all participants a fruitful conference and workshop in the vicinity of the ancient sites of the Classical Greece around the Corinth Gulf, where earthquake science, wonderful landscapes, ancient cultures, amazing sunny days, fantastic "Greek cooking", nice beaches, daily cool beers, wine tasting events and late night gin tonics mixed with hot discussions are waiting for all of us. A special **"efharisto poli"** goes to Christoph Grützner and Raul Pérez-López for their invaluable work with the organisation and the abstract handling.

The Organizers of the 2nd INQUA-IGCP 567 Workshop

Dr. Ioannis Papanikolaou
Agricultural University of Athens (GRE)
Aon-Benfield Hazard Research Centre,
University College London, (UCL) (UK)

Prof. Klaus Reicherter
RWTH Aachen University (GER)

Prof. Andreas Vött
University of Mainz (GER)

Prof. Pablo G. Silva
University of Salamanca (ESP)

FIRST PALEOSEISMIC EVIDENCES IN ECUADOR: THE PALLATANGA FAULT RECORD

Baize, Stéphane (1), Laurence Audin (2), Thierry Winter (3), Alexandra Alvarado (4), Luis Pilatasig (5), Mercedes Taipe (4), Paul Kauffmann (1), Pedro Reyes (4)

(1) Institut de Radioprotection et de Sûreté Nucléaire, BP 17, 92262 Fontenay-aux-Roses, France. stephane.baize@irsn.fr
(2) Institut de Recherche pour le Développement, ISTERRE, Grenoble, France.
(3) Bureau de Recherche Géologiques et Minières, Service Risques Naturels, Orléans, France.
(4) Escuela Politécnica Nacional, Instituto de Geofísica, Quito, Ecuador.
(5) Ministerio de Recursos Naturales No Renovables, Quito, Ecuador.

Abstract (First paleoseismic evidences in Ecuador: the Pallatanga fault record): *The Pallatanga fault (PF) is a prominent strike-slip fault of Central Ecuador. This structure is suspected to have hosted large earthquakes, including the 1797 Riobamba event (M~7.5). The scope of the study is to evaluate the paleoseismic history of the fault, together with enhancing the seismotectonic model of this part of the Andes and improving the seismic hazard assessment. From 3 trenches, we could infer that the PF experienced several strong events (M7.2 to 7.7) in the last 8500 years. According to a new mapping campaign, we also could evidence that the fault propagates north to the Riobamba outskirts, suggesting that faulting occurred nearby this big city.*

Key words*: Paleoearthquakes, Holocene, Pallatanga fault, Ecuador*

INTRODUCTION

The Pallatanga fault (PF) is a NNE-SSW segment of the Dolorès-Guayaquil Megashear. This mega-structure is the large deformation zone accommodating the dextral displacement between the Northern Andean Block and the South America Plate with a rate of 6 to 8 mm/a. The PF is a 50 km-long fault, for which a previous morphotectonic study validated its Holocene right-lateral motion (Winter *et al*., 1993). This fault is probably the source of one of the largest crustal earthquake in South-America, occurred in Riobamba in 1797 (M~7.5: Beauval *et al*., 2010) (figure 1). The "Riobamba Antigua" city was destroyed (25,000 casualties) and then replaced at its current place. It may also have generated a Mw6.1 event in 1911.

The scope of the study is to (1) assess the occurrence of potential large paleoearthquakes and quantify their number, magnitudes and recurrence times, (2) improve the seismotectonic model of the area, and (3) enhance the seismic hazard assessment of this inhabited region (Riobamba city, 200,000 inhabitants).

PREVIOUS MORPHOTECTONIC STUDY OF PF

A detailed topographic survey in the Pangor Rio valley (Winter *et al*., 1993) evidenced the fault plane characteristics (N40°E, 75°W) and allowed estimating the "near-field" displacement to be ~40m for the dextral component and ~8m for the reverse one. Winter *et al.* (1993) deduced a cumulated striae dipping slightly to the south (10°). They also proposed an average slip rate of 2.9 to 4.6 mm/yr, according to regional geomorphic correlation.

RESULTS OF THE TRENCH SURVEY

We focused on paleoseismological analyses at Rumipamba and on a detailed mapping of the active fault trace continuation towards Riobamba city.

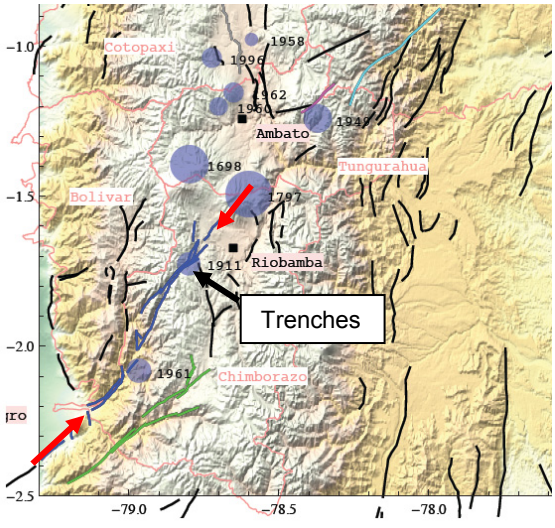

Figure 1: Location of the study area, with the main faults and historical seismicity. Figure extract from Beauval et al. (2010). Blue disks: historical events, with magnitude proportional to radius (ex. 1797: M=7.6; 1911: M=6.2; 1958: M=5). Specific faults: Pallatanga fault in blue and bounded by red arrows, Guamote-Huigra fault in green, Llanganates fault in cyan, Pucara fault in magenta. Pink lines: provinces boundaries. Names of provinces in pink; names of towns in black.

At Rumipamba, the fault trace runs parallel to the mountain front and cuts perpendicularly the erosional features going downhill (figure 2). The mountain slope sedimentation is exclusively dominated by ash falls, with rare colluvium and alluvium. Unfortunately,

we could not find any channel deposits in test trenches and it was thus impossible to find linear features that could account for lateral offsetting. In further developments, we thus used the "morphological slip vector" of Winter et al. (1993).

In the three excavated trenches, ash falls are strongly pedogenetized in black organic soils (andisols), over thicknesses of 2 to 3.5 meters.

Figure 2: South-eastward view of the mountain front, cut by the Rumipamba segment of the PF. Trenches were excavated in the the same area.

Available ^{14}C datings of these soils (23 samples) range from 6650 cal BC to 1650 cal AD, scattered into 7 classes of ages (-6650, -5500, -3500, -2800, -1800, 800, 1650). They lie above the volcanic basement (Mesozoic-Tertiary).

The trenches' survey pointed out several interbeds with variable oxidized material contents -including basement fragments and root remnants- in the vicinity of the fault strands. Our basic assumption is that these "clastic layers" are stratigraphic markers of earthquakes (colluvial wedges) because they are associated with the erosion of a basement scarp appeared during surface faulting.

Among the 3 trenches, the trench #2 is especially interesting in order to reconstruct the paleoseismic history of the fault. There, the stratigraphic series is more complete and stratigraphic units can be correlated on each side of the fault (figure 3). In trenches #1 and #3, the fault strands are obvious but correlations are difficult. In trench #2, the fault splits in 3 strands propagating from the basement fault gouge up to the Holocene deposits and the modern soil. The fault zone downthrows the eastern wall by about 3 m.

By performing a retrodeformation of the trench, we could infer 5 strong events with individual vertical throws from 0.25 m up to 0.90 m (table 1). Assuming a slip vector dipping of 10° (Winter *et al.,* 1993), the total throws are between 1.45 to 5.20 m, which provides magnitudes from 7.2 to 7.7 according to Wells & Coppersmith (1994) relations. To generate such earthquakes, the same empirical relations suggest that the fault rupture can be as long as 60 to 140 km (which is larger than the mapped PF).

Some uncertainties remain after trench survey. For example, the retrodeformation of trench #2 can lead to only 4 paleoearthquakes because arguments for separating events #4 and #5 (Table 1) are weak. The last event in 1797 should then have a higher magnitude than mentioned in table 1. Moreover, the event #2, which is also recorded in trench #1 and well constrained by ^{14}C datings, is associated with 2 successive and discordant colluvial wedges. If we assume this is not partly due to non-tectonic processes (climate degradation for ex.), then arises the issue of possible under-representation of earthquake number in trench #2 (and correlative overestimation of magnitude).

EQ	Date approx. (cal y.)	Vertical throw (cm)	Total throw (cm)	Mw	SRL (km)
5	1797	25	145	**7.2**	60
4	~1,000	60	345	**7.5**	100
3	~0	90	520	**7.7**	140
2	~ -1,000	90	520	**7.7**	140
1	~ -4,500	70	400	**7.6**	120

Table 1: synthetic table of the earthquake history along the Rumipamba segment of the Pallatanga fault. Vertical throw is the observed data; total throw is calculated from vertical throw and morphological slip vector; Mw is calculated from total throw with W&C (1994) relation (average displacement); SRL is estimated from total throw

CONTRIBUTION OF MAPPING

From its southern tip (Western Cordillera front) to the trench site (figure 1), the PF is mapped and reaches a length of about 60 km. Given the previous conclusion of large fault ruptures (SRL>60 km), it has been decided to investigate the "unknown" northern continuation of the Rumipamba segment where morphological features suggested its existence and where the rupture may have propagated during large past events. The interest is that section is also that it can help in improving the seismotectonic model of the region and in clarifying the seismic hazard assessment of this inhabited area.

Before field mapping, fault traces were tracked down with analysis of remote-sensing images (SPOT5). Field control and mapping allow validating most of this preliminary work thanks to morphologic and geologic observations. The Rumipamba segment splits into 2 fault zones when entering the Inter-Andean valley (figure 4). The western branch (Rumipamba-Huacona and La Merced segments) seems to rotate into a N-S direction, with pure lateral kinematics, whereas the eastern ones changes to a NE-SW strike, with a more important vertical component (Cajabamba, Gatazo and Lican-Riobamba segments). This last segment cuts the Riobamba basin and seems to offset the surface deposits of the Upper Pleistocene (40 ka, Bernard *et al*., 2008) and later morphological features. The scarp is almost 100 m high and, locally, we could find a dextral offset of 50 m of a valley slope. To the north-east, some morphological features (mountain front spurs, stream profiles) and outcrops (normal faulting and tilting of recent sediments) suggest that active deformation propagates from the Riobamba basin north-eastwards along the Cordillera Reale front (Penipe area), along the Chambo segment.

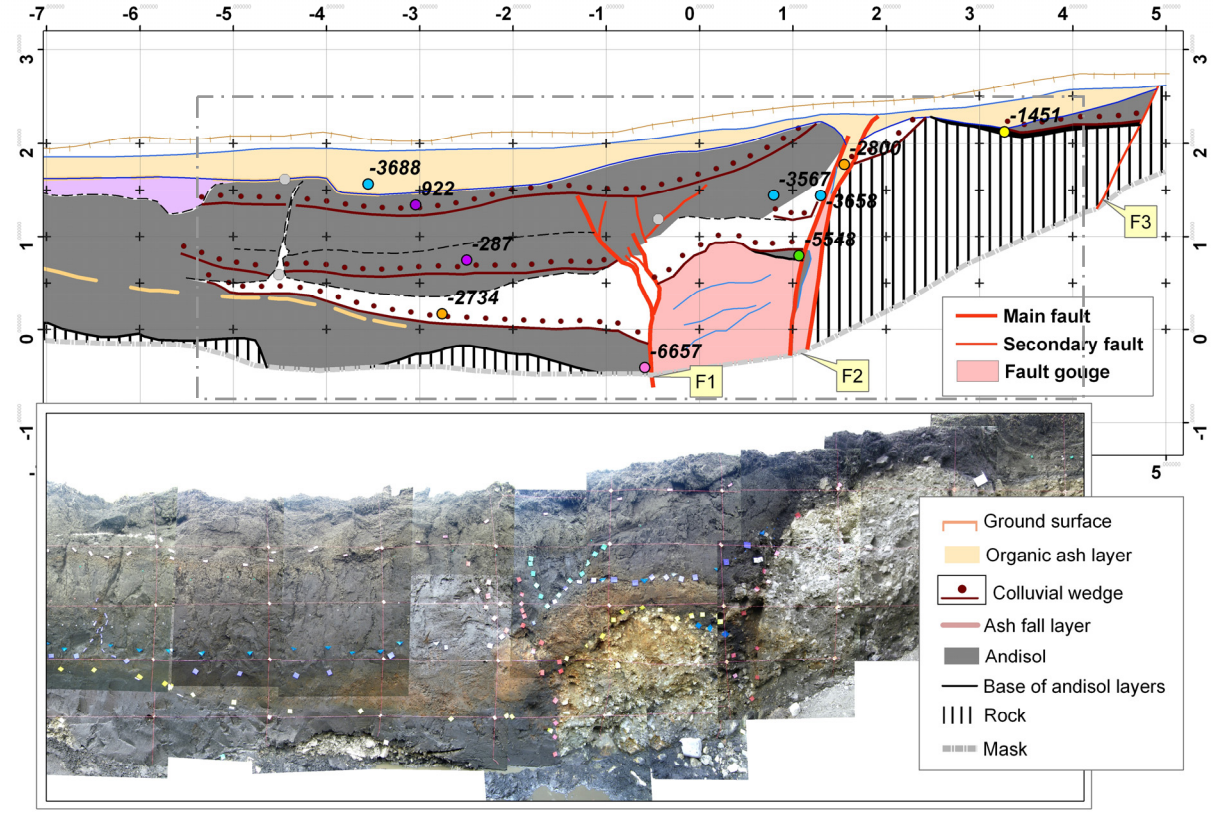

Figure 3: Mosaic picture and sketch interpretation of trench #2. Ages are given in cal BC/AD.

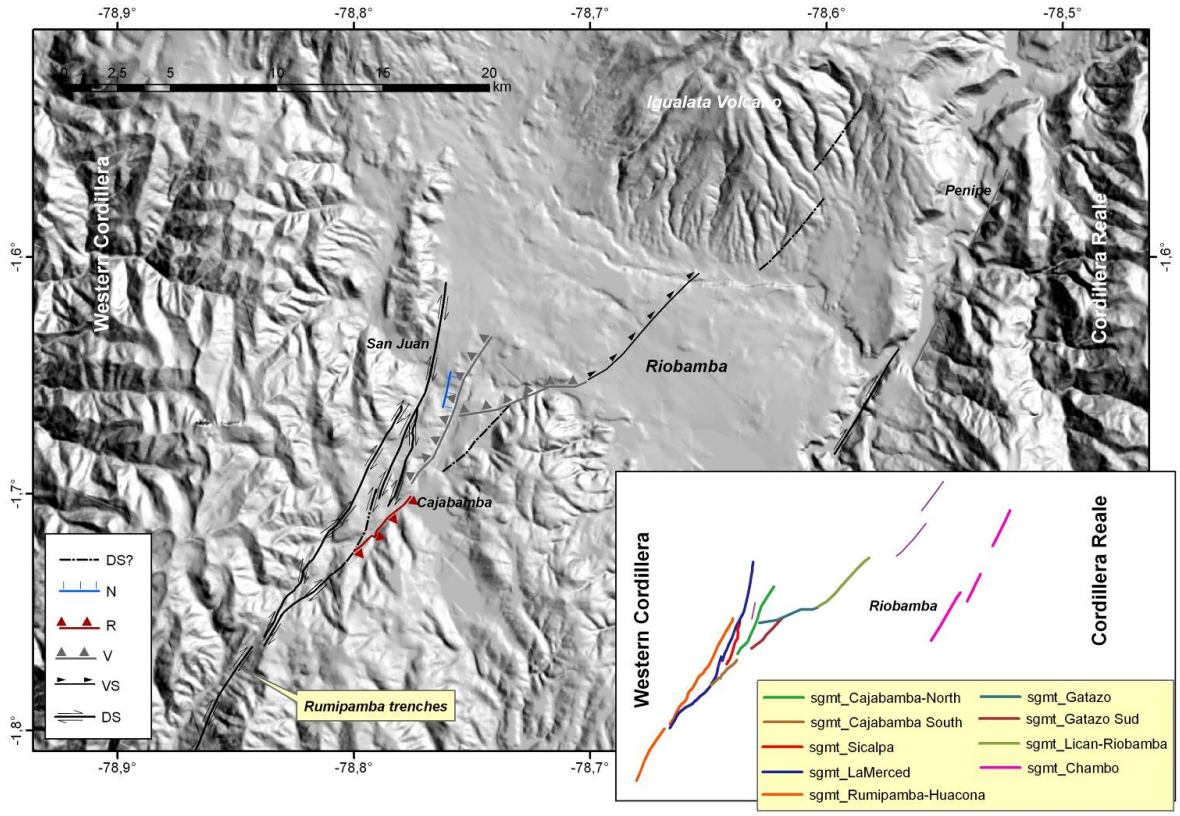

Figure 4: Sketch map of the northern extension of the PF within the Riobamba basin, and example of the morphological imprint of the fault. DS: segment with prevailing dextral component; N: with normal component (symbols on the downthrown block side); R: with reverse component; V: segment with undifferenciated vertical offset; VS: segment with vertical and dextral strike-slip component (symbols on the upthrown block side, for the 3 last).

These preliminary conclusions need to be completed by further mapping, especially in the Chambo valley and along the western rim of the Inter-Andean valley (north of San Juan).

All along the prospected area, several places have been quoted to be potential sites for further paleoseismic investigations.

DISCUSSION

For the first time in Ecuador, paleoseismic investigations prove the occurrence of 4 or 5 strong events which shook the Riobamba region in the past. We probably found the trace in sediments of the Riobamba event (1797) and then confirm that it has been generated by the Pallatanga fault. Magnitudes, inferred from geological signal and applying empirical relations, range between 7.2 and 7.7, which is in agreement with the independent estimation of the Riobamba earthquake by Beauval *et al.* (2010). Reccurrence times of these events seem variable (Table 1: 800 to 3,500 years) with a mean value around 1,000-1,500 years.

Nonetheless, the trench survey and its interpretation are soiled by uncertainties and arises the issue of under or over-representation of the event number, which is a crucial point in seismic hazard assessment (Mc Calpin, 2009). In addition, the 3 trenches revealed variable tectono-sedimentary signals. These nuances weaken the above conclusions dealing with magnitudes of paleoearthquakes and hazard assessment for the PF, and we clearly need additional investigations to strengthen the results. In this first-step work, we assumed for instance during magnitude assessment that the observed coseismic offsets are “average” values of the event slip and this has clearly to be validated. The mapping clearly shows that the trenches were not performed at the northern tip of the fault and new trenching sites must be found out to increase the slip vs rupture length dataset.

Dealing with the fault slip rate of the fault, our results based on radiometric datings outstandingly validate the rate published by Winter *et al.* (1993). Roughly, trenches show vertical displacement of about 3 meters of recent soils -i.e. 20 meters following the hypothesis of a 10° slip vector- which have been produced during the last 5,000 years. This leads to a mean slip rate of ~4 mm/a. With respect to the total displacement rate (~6-8 mm/a) of the North-Andean Block, it suggests that other segments accommodate a significant part of the relative motion of North Andean Block wrt South America. Up to now, no other faults are potential candidates.

What we know from our mapping campaign is that deformation probably propagates both to the north (along the western edge of the Inter-Andean valley) and to the north-east (towards the eastern rim of the Cordillera Reale). This last segment could be the structural link between the Pallatanga fault (to the south) and the Pucara/Llanganates faults (to the north), one of these being probably the source of the Pelileo destructive earthquake (1949) (Beauval *et al.*, 2010). This propagation of deformation to the north also drastically increases the seismic hazard for Riobamba city, because rupture segments probably run all along the outskirts of this vulnerable big city.

Acknowledgements: The authors give special thanks to the Indian communities of Rumipamba and neighboring villages, for their warm welcome and “technical” contribution to logistics and trench cleaning. Thanks also to the various authorities of Ecuador who make this research possible (prefecture and the civil safety services). We also benefit of the help and fruitful discussions with people from the Escuela Politecnica Nacional de Quito.

References

Beauval, C., H. Yepes H., W. H. Bakun, J. Egred, A. Alvarado & J.-C. Singaucho, (2010). Locations and magnitudes of historical earthquakes in the Sierra of Ecuador (1587–1996). Geophys. J. Int., doi: 10.1111/j.1365-246X.2010.04569.x.

Bernard, B., B. van Wyk de Vries, D. Barba, H. Leyrit, C. Robin, S. Alcaraz & P. Samaniego, (2008). The Chimborazo sector collapse and debris avalanche: Deposit characteristics as evidence of emplacement mechanisms. Journal of Volcanology and Geothermal Research 176, 36–43.

Mc Calpin, J. P., (2009). Paleoseismology. INTERNATIONAL GEOPHYSICS SERIES, volume 95, Academic Press, 802 pages.

Wells, D. L. & K. J. Coppersmith, (1994). New empirical relationships among magnitude, rupture length, rupture width, rupture area and surface displacement. Bull. Seism. Soc. America 84, 974-1002.

Winter, T., J.P. Avouac & A. Lavenu, (1993). Late Quaternary kinematics of the Pallatanga strike-slip fault (Central Ecuador) from topographic measurements of displaced morphological features. Geophys. J. Int. 115, 905-920.

EARTHQUAKE ARCHAEOLOGY

INQUA PALEOSEISMOLOGY AND ACTIVE TECTONICS

SOME NOTES ON EARTHQUAKE AND FAULT RELATIONSHIPS FOR DIP-SLIP EVENTS

Salvatore Barba (1) and Debora Finocchio (1, 2)

(1) Istituto Nazionale di Geofisica e Vulcanologia, Via di Vigna Murata 605, Roma, Italy. salvatore.barba@ingv.it
(4) Università di Urbino, Italy

Abstract (Some notes on earthquake and fault relationships for dip-slip events): *We developed a conceptual model for dip-slip earthquakes to predict the coseismic surface throw and the dislocation as a function of depth along-dip (1-D averaged). By performing a Monte Carlo experiment in Matlab to test the conceptual model against earthquake data for years 1990-2006, we found that, for reverse faulting, the surface throw is better reproduced with the slip distributions which show a maximum slip closer to the surface. Our model predicts a surface throw for reverse faulting earthquakes that is larger than that contained in the Wells and Coppersmith (1994) relationships. The use of downward or upward directivity in the rupture changes dramatically the assessment and the perception of the earthquake hazard, as shown by the catastrophic 2011 Japan earthquake.*

Key words*: Normal fault, thrust fault, coseismic rupture, Monte Carlo model.*

INTRODUCTION

It is commonly accepted in the literature that deviatoric stress increases with depth (see, e.g., Das and Scholz, 1983; Henry and Das, 2001). The coseismic dislocation is predicted to initiate at the base of the seismogenic layer and to propagate upward. However, two classes of observations, coseismic throw and depth directivity, are hardly explained with such hypotheses in the case of dip-slip earthquakes. Reverse-faulting earthquakes occurred in the past 20 years exhibited a much larger throw at the surface, with respect to normal-faulting earthquakes of similar magnitudes. Also, in certain cases of reverse-faulting earthquakes, seismological observations show a downward directivity of the rupture (Carminati et al., 2004).

METHOD AND DATA

In this work we developed a conceptual model for dip-slip earthquakes to predict the coseismic surface throw and the dislocation as a function of depth along-dip (1-D averaged). To this purpose, we determined relationships among the surface throw and the earthquake parameters (slip, dip, depth, and moment magnitude Mw) for two emblematic normal and reverse faults. Finally, assuming that the (1-D averaged) slip-distribution at depth may be related to the deviatoric stress, we discussed the difference between our model and Das e Scholz (1983) model. This work is thus developed in two parts: the generation of synthetic relationships between coseismic throw and magnitude, and the comparison of model predictions with a 20-years long earthquake dataset (*Table 1*). We made a Monte Carlo experiment in Matlab to test the conceptual model against data.

The synthetic relationships are based on standard seismic catalogues. We determined the frequency distributions for dip, Mw and seismic moment from the USGS catalogue, and the depth distributions from regional earthquake catalogue. Based on these distributions, we generated a very large synthetic earthquake catalogue. For each of these synthetic earthquakes we set the average slip, the length and the width of the rupture based on a-priori relationships. Then, we predicted the surface throw based on two classes of slip distributions at depth: one class based on four a-priori distributions (our

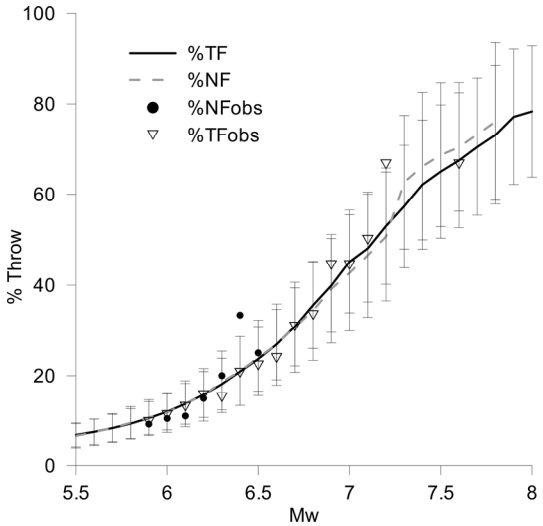

Fig. 1: Cumulative percentage of earthquakes that ruptured the surface for reverse (TF) and normal faulting (NF). Lines represent the model prediction, the symbols represent the data.

choice), and one class based on literature data, which have been grouped in three slip distributions at depth. These four (or three) distributions differ as it follows: (1) the maximum slip is in the center of the rupture, (2) it is closer to the bottom or (3) to the top edge of the rupture; (4) the slip is uniform. For each magnitude bin we computed the average and the

standard deviation of the predicted surface throw. Last, we compared the predicted maximum and average surface throw with the observed throw for earthquakes occurred in years 1990-2008. As a cross check, we computed the percentage of synthetic earthquakes that produce surface throw, as a function of magnitude (*Fig. 1*).

RESULTS

We found differences between reverse and normal faulting earthquakes. For reverse faulting, the surface throw is better reproduced with the slip distributions which show a maximum slip closer to the surface, or with the uniform slip (*Fig. 2*). For normal faulting, the best fit occurs when the maximum slip is closer to the bottom edge of the rupture.

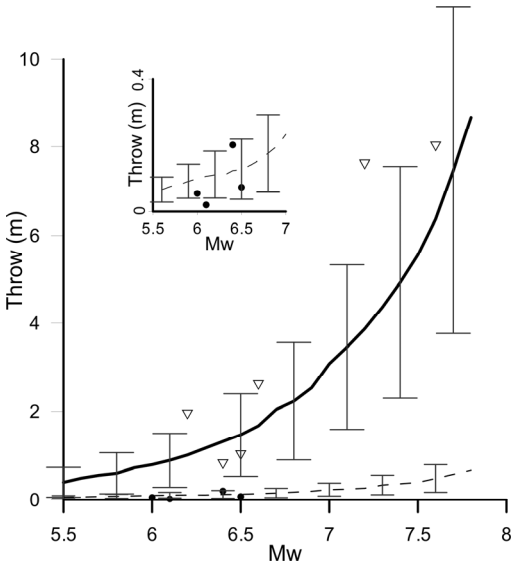

Fig. 2: Surface throw as a function of moment magnitude. Lines represent the model prediction, the symbols represent the data. For convenience, an enlargement is shown in the inset.

DISCUSSION AND CONCLUSIONS

We observed some differences with the outcomes of Wells e Coppersmith (1994) and Das e Scholz (1983). Our model predicts a surface throw for reverse faulting earthquakes that is larger than that contained in the Wells and Coppersmith (1994) relationships. The opposite occurs for normal faulting earthquakes. In the dataset of Wells and Coppersmith (1994), the fault dimensions are derived sometimes from seismological data, sometimes from geodetic data. As we used only earthquakes occurred in recent times, our dataset is based on seismological data and is therefore more homogeneous. Although we have fewer data, our result appears robust. In the hypothesis that the slip distribution can be used as a proxy for deviatoric stress, the maximum of the deviatoric stress is expected to be close to the upper edge of the fault rupture at least for earthquakes with low dip angle (<45 degrees). Das e Scholz (1983) model was developed based on a dataset of Californian earthquakes, where thrusts exhibit larger dip angles. We believe this dataset is not representative of global earthquakes.

The use of downward or upward directivity in the rupture changes dramatically the assessment and the perception of the earthquake hazard, as shown by the catastrophic 2011 Japan earthquake. Also, the importance of a bias in the predicted surface throw can be more important in very large earthquakes. We propose to discuss our findings in the light of the very recent and large earthquakes.

Acknowledgements: We thank Paolo Fasoli for part of the literature review and Martin Mai for the discussion about the slip models.

References

Carminati, E., C. Doglioni, and S. Barba (2004), Reverse migration of seismicity on thrusts and normal faults, *Earth-Science Reviews*, 65(3-4), 195-222.

Das, S., and C. H. Scholz (1983), Why large earthquakes do not nucleate at shallow depths, *Nature*, 305, 621 – 623.

Henry, C., and S. Das (2001), Aftershock zones of large shallow earthquakes: fault dimensions, aftershock area expansion and scaling relations, *Geophysical Journal International*, 147(2), 272-293.

Wells, D. L., and K. J. Coppersmith (1994), New empirical relationships among magnitude, rupture length, rupture width, rupture area, and surface displacement, *Bulletin of the Seismological Society of America*, 84(4), 974-1002.

Table 1: Earthquakes with coseismic surface throw, years 1990-2006 (Mw>=5.9).

N	Code	Date	Location	Mw	Depth (Km)	Type	Avg Throw (m)
1	EV-022	1990/11/06	Iran	6.6	11.1	TF	2.6
2	EV-073	1992/08/19	Turkey	7.2	17	TF	3
3	EV-101	1993/05/17	California	6.1	7	NF	0.02
4	EV-117	1993/09/29	India	6.2	14.1	TF	1.93
5	EV-187	1995/05/13	Greece	6.5	14	NF	0.05
6	EV-192	1995/06/15	Greece	6.5	14	NF	0.02
7	EV-206	1995/10/01	Turkey	6.4	9	NF	0.2
8	EV-282	1997/09/26	Italy	6	6	NF	0.03
9	EV-330	1999/09/07	Greece	6	10	NF	0.08

N	Code	Date	Location	Mw	Depth (Km)	Type	Avg Throw (m)
10	EV-331	1999/09/20	Taiwan	7.6	9	TF	5
11	EV-405	2002/02/03	Turkey	6.5	5	NF	0.15
12	EV-414	2002/06/22	Iran	6.5	11	TF	1
13	EV-431	2002/11/03	Alaska	7.2	4.2	TF	4
14	EV-518	2005/02/22	Iran	6.4	7	TF	0.8
15	EV-532	2005/10/08	Pakistan	7.6	19.1	TF	3.7

EARTHQUAKE ARCHAEOLOGY

INQUA PALEOSEISMOLOGY AND ACTIVE TECTONICS

HOLOCENE COASTAL NOTCHES IN THE MEDITERRANEAN: PALAEOSEISMIC OR PALAEOCLIMATIC INDICATORS?

Boulton, S. J. (1) and Stewart, I. S. (1)

(1) School of Geography, Earth and Environmental Sciences, University of Plymouth, Plymouth, Devon, PL4 8AA, U.K.
Sarah.boulton@plymouth.ac.uk

Abstract (Holocene Coastal Notches in the Mediterranean: Palaeoseismic or Palaeoclimatic indicators?): *Bioerosion and bioconstruction along rocky coastlines can lead to the development of coastal notches that are preserved when uplifted or submerged above or below the swash zone and thus can be used to quantify relative vertical coastal motions in tectonically active areas. There are two main models for the genesis of notch profiles. The first is tectonically driven, with notches forming during relative still-stands of sea-level; notches are subsequently raised (or lowered) relative to sea-level due to local seismic events. The second model favours a climatic origin for notch formation, where stable periods of Holocene climate allow enhanced erosion. Here, we explore these two models using a database of Eastern Mediterranean notches. We conclude that the spatial and temporal distribution of the notches favours a dominantly tectonic control on formation.*

Key words*: notches, tectonics, climate, Holocene.*

INTRODUCTION

Along rocky coastlines bioerosion and bioconstruction can lead to the development of coastal notches that can be preserved when uplifted or submerged above the swash zone (Stewart and Morhange, 2009). As these geomorphic features form at sea level, palaeoshorelines could be used to quantify relative coastal uplift and subsidence in tectonically active areas when the sea level history is known (e.g., Pirazzoli & Thommeret, 1977; Pirazzoli et al., 1981, 1982, 1989, 1991, 1994a, 1994b; Stiros et al., 1992; Stewart et al., 1997; Stiros et al., 2000; Antonioli et al., 2006; Shaw et al., 2008).

Despite this large body of work there is some disagreement on the process of notch formation. The most commonly assumed theory is that notches form when the rate of sea level change matches the uplift (or subsidence) rate along a coastline resulting in a relative sea level still stand. Notches are then raised higher than sea level when a seismic event results in rapid coastal uplift preserving the feature from further erosion. However, in many other areas it is not clear whether notches reflect short-term seismic events or the long-term uplift rate averaged over many seismic cycles (Stewart & Vita Finzi, 1996). Rarely, can individual notches be matched to documented earthquakes (Pirazzoli, 1994a).

Recently, Cooper et al. (2007) have linked notch formation to Holocene periods of climatic stability. Specifically, when the rate of sea level rise is lower than the tectonic uplift rate but when climatic conditions favour high productivity, increased levels of bioerosion develop a notch. This enhanced erosion ceases during periods of rapid climate change (RCC), allowing notches to become emergent due to continuing coastal uplift. Cooper et al. (2007) discount any correlation between notches and individual seismic events, stating that individual earthquakes are too small to raise a notch clear above sea level and too numerous to explain the formation of the four notch intervals that they observed on the Perachora Peninsula (Greece). This is a dramatic reinterpretation of coastal notches which, if correct, means these phenomena cannot be used for palaeoseismic indicators and associated seismic hazard assessments. So what drives notch development: tectonic instability (earthquakes) or climatic stability (enhanced bioerosion)?

If tectonic uplift is the dominant control in the Mediterranean, then notches will develop only in coasts where slow regional emergence is augmented by abrupt uplift events (earthquakes) and the age of notches will relate broadly to local palaeoseismic episodes. If climate is the dominant control on notch formation, then notches can also form on subsiding coasts and will date only to periods of climatic stability (no RCC) that are consistent across the region. Mayewski et al., (2004) propose five periods of stable climate dating to 8000-6000, 5400-4200, 3800-3300, 2500-1200 and 1000-600 years BP. That implies that no more than five notches ought to be formed in any one place, each corresponding to an intervening periods of no RCC during the last 10,000 yrs (Mayewski et al., 2004). Yet in some parts of the Mediterranean coast more than five notch levels are recorded; along the coast of Crete, nine to ten well preserved superimposed shorelines can be observed (Pirazzoli et al., 1982) and eight are present on Rhodes (Pirazzoli et al., 1989).

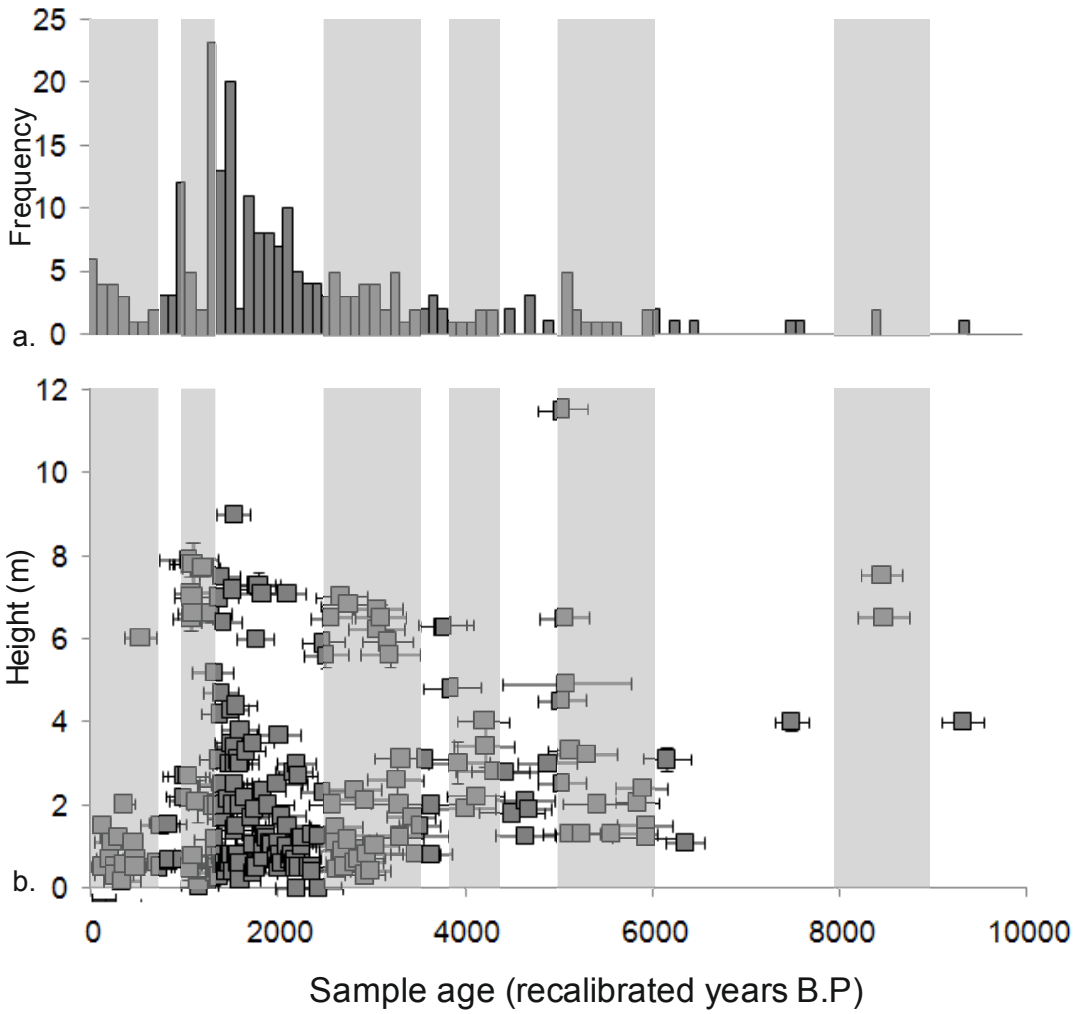

Figure 1a) Histogram showing frequency of samples against age from notches around the Eastern Mediterranean in 100 year groups; b) Graph of radiocarbon age against height of all notch data for the Eastern Mediterranean region. Grey bars on both graphs indicate the periods of proposed Holocene rapid climate change.

Such field observations seem inconsistent with the climate model. However, to appraise any relationship with climate in a more robust manner requires a systematic analysis of the Holocene palaeo-shoreline data for the Mediterranean region as a whole. To do that, we have compiled a dataset of palaeo-shoreline data that span several decades of published research in the region. The database itself comprises 428 dated samples derived from 40 separate studies that were undertaken at locations from across the whole of the Eastern Mediterranean. These data are used to examine age and height relationships and test correlations with periods of RCC.

The results of the database are summarised in figure 1. Generally, with the exception of a few outliers, the initial phase of notch development in the Mediterranean occurs in the period 5000 – 6500 years BP (Fig. 1). This period correlates with the mid-Holocene slowdown of global sea-level rise. The eustatic slowdown at this time ensures that along many tectonically uplifting coasts, rates of emergence and sea level rise are in unison and so notch development takes place. It is noteworthy that under the climate model this period is one of rapid climate change and so a time window in which notch formation ought to be muted.

Indeed, overall, figure 1 shows that there appears to be no correlation between stable climatic periods and notch occurrence, with numerous notches dating to periods of RCC (grey bars). This strongly suggests that climate is not the controlling factor for notch formation. Instead, it appears that the complex age and height pattern of notches around the region more likely reflects local tectonic histories of slow interseismic crustal deformation overprinted by abrupt seismic movements of the coastline. Discriminating ambiguous palaeoseismic information from this complex shoreline record, however, remains a difficult task.

Acknowledgements: We would like to thank Richard Martin for his help in constructing the notch database.

References

Antonioli, F., Ferranti, L., Lambeck, K., Kershaw, S., Verrubbi, V., Dai Pra, G., (2006). Late Pleistocene to Holocene record of changing uplift rates in southern Calabria and northeastern Sicily (southern Italy, Central Mediterranean Sea). *Tectonophysics*, 422, 23-40.

Cooper, F.J., Roberts, G.P., Underwood, C.J., (2007). A comparison of 10^3-10^5 climate stability and the formation of coastal notches. *Geophysics research letters*, 34, L14310, doi:10.1029/2007GL030673

Mayewski, P.A., Rohling, E., Stager, C., Karlén, K., Maasch, K., Meeker, L.D., Meyerson, E., Gasse, F., van Kreveld, S., Holmgren, K., Lee-Thorp, J., Rosqvist, G., Rack, F., Staubwasser, M., and Schneider, R., (2004), Holocene climate variability, *Quaternary Research* 62, 243-255.

Pirazzoli, P.A., Thommeret, J., (1977). Datation radiométrique d'une ligne de rivage à +2.5 m près de Aghia Roumeli, Crète, Grèce. *Le Comte Rendu d'Academie Science*, Paris, Series D, 97, 1255-1257.

Pirazzoli, P.A., Thommeret, J., Thommeret, Y., Laborel, J., Montaggioni, L.F. (1981). Les rivages emerges d'Antikythira (Cerigotto): correlations avec le Crete occidentale et implications cinematiques et geodynamics. Niveax Marins et Tectonique Quaternaires dans l'Aire Mediterraneene, Paris, UNRS and Universitie Paris I, pp. 49-65.

Pirazzoli, P.A., Thommeret, J., Thommeret, Y., Laborel, J., Montaggioni, L.F. (1982). Crustal block movements from Holocene shorelines: Crete and Antikythira (Greece). *Tectonophysics*, 86, 27-43.

Pirazzoli, P.A. 1986, Marine notches In: van de Plassche, O. (Ed), Sea-level Research: A Manual for the Collection and Evaluation of Data, Geo Books, Norwich pp. 361–400.

Pirazzoli, P.A., Montaggioni, L.F., Saliege, J.F., Segonzac, G., Thommeret, Y., Vergnaud-Grazzini, C., (1989). Crustal block movements from Holocene shorelines: Rhodes Island (Greece). *Tectonophysics*, 170, 89-114.

Pirazzoli, P.A., Laborel, J., Saliege, J.F., Erol, O., Kayan, I., Person, A. (1991). Holocene raised shorelines on the Hatay coasts (Turkey): Palaeoecological and tectonic implications. *Marine Geology*, 96, 295-311.

Pirazzoli, P.A., Stiros, S.C., Laborel, J., Laborel-Deguen, F., Arnold, M., Papageorgiou, S., Morhange, C. (1994a). Late-Holocene shoreline changes related to palaeoseismic events in the Ionian Islands, Greece. *The Holocene*, 4, 397-405.

Pirazzoli, P.A., Stiros, S.C., Arnold, M., Laborel, J., Laborel-Deguen, F., Papageorgiou, S., (1994b). Episodic uplift deduced from Holocene shorelines in the Perachora Peninsula, Corinth area, Greece. *Tectonophysics*, 229, 201-209.

Shaw, B., Ambraseys, N.N., England, P.C., Floyd, M.A., Gorman, G.J., Higman, T.F.G., Jackson, J.A., Nocquet, J,-M., Pain, C.C., Piggott, M.D., (2008). Eastern Mediterranean tectonics and tsunami hazard inferred from the AD 365 earthquake. *Nature Geoscience*, 1, 268-276.

Stewart, I.S., Vita-Finzi, C., (1996). Coastal uplift on active normal faults: The Eliki Fault, Greece. *Geophysical Research Letters*, 23, 1853-1856.

Stewart, I.S., Morhange, C. (2009). Coastal geomorphology and sea-level change. In J.C. Woodward (Ed.). *The physical geography of the Mediterranean* (pp. 383–413). Oxford: Oxford University Press.

Stewart, I.S., Cundy, A., Kershaw, S., Firth, C., (1997). Holocene coastal uplift in the Taormina area, northeastern Sicily: Implications for the southern prolongation of the Calabrian seismogenic belt. *Journal of Geodynamics*, 24, 37-50.

Stiros, S.C., Arnold, M., Pirazzoli, P.A., Laborel, J., Laborel,, Papageorgiou, S., (1992). Historical coseismic uplift on Euboea Island, Greece. *Earth and Planetary Science Letters*, 108, 109-117.

Stiros, S.C., Laborel, J., Laborel-Deguen, F., Papageorgiou, S., Evin, J., Pirazzoli, P.A., (2000). Seismic coastal uplift in a region of subsidence: Holocene raised shorelines of Samos Island, Aegean Sea, Greece. *Marine Geology*, 170, 41-58.

EARTHQUAKE ARCHAEOLOGY

INQUA PALEOSEISMOLOGY AND ACTIVE TECTONICS

ANALYSING THE LANDSLIDE SUSCEPTIBILITY WITH STATISTICAL METHODS IN MAILY-SAY, KYRGYZSTAN

Braun, Anika (1), Tomas M. Fernandez-Steeger (1), Hans-Balder Havenith (2), Almaz Torgoev(2), Romy Schlögel (3)

(1) Department of Engineering Geology and Hydrogeology, RWTH Aachen University, Lochnerstraße 4-20, 52064 Aachen, GERMANY. Email: braun@lih.rwth-aachen.de
(2) Georisks and Environment, Department of Geology, University of Liège, B20 Sart Tilmann, 4000 Liège, BELGIUM.
(3) School and Observatory of Earth Sciences, Institut de Physique du Globe de Strasbourg, 5 rue Descartes, F-67084 Strasbourg Cedex

Abstract (Analysing the landslide susceptibility with statistical methods in Maily-Say, Kyrgyzstan): *A landslide susceptibility analysis was carried out for Maily-Say, a former uranium mining town in Kyrgyzstan. Numerous landslides threaten inhabitants, infrastructure and uranium tailings. Besides typical factors responsible in this region, like seismicity, geology, geomorphology and climatic conditions, land use plays an important role in Maily-Say. In order to predict landslide susceptibility and to clarify the interplay of different factors two statistical methods were implemented, a bivariate statistical method and a data mining approach based on a multi-temporal digital landslide inventory. Generally, with both methods areas could be mapped that show a high potential for future landslides. Furthermore, the correlation of landslides with the landform and loess deposits provide some information on the seismic effects on slope stability.*

Key words*: landslide susceptibility, bivariate statistical analysis, data mining*

INTRODUCTION

In this study a landslide susceptibility analysis in Maily-Say, Kyrgyzstan, was undertaken. In the vicinity of the former uranium mining and milling town more than 200 landslides were present in 2007. Besides frequent damage to houses and infrastructure, landslides already caused several fatalities. Landslides damming the main river during spring runoff lead to flooding (Havenith et al., 2006b). Numerous radioactive, partially instable uranium tailings and waste dumps are threatened by landslides. Since the main river leads to the Ferghana Valley, a densely populated and agricultural region covered mainly by Uzbekistan, the destabilisation of nuclear waste tailings in Maily-Say bears the potential of a major environmental catastrophe (Blacksmith Institute, 2006).

The term landslide susceptibility implies the spatial probability of occurrence of slope failures (Aleotti & Chowdury, 1999). By analysing geological and geomorphological situations that have lead to slope failures in the past, it is possible to predict the landslide susceptibility to a certain degree (Varnes, 1984). In this study two different statistical methods were used for predicting the landslide susceptibility in Maily-Say, a bivariate statistical approach and data mining. Besides pointing out endangered areas, the study aimed at analysing the main factors causing slope failures in Maily-Say and their temporal development with the help of a multi-temporal landslide inventory.

The idea behind this approach is to extract a maximum of information from a simple dataset (geology, digital elevation model, landslide inventory) to provide a first localisation of endangered areas without having been to the field.

SETTING

Maily-Say is located in the western foothills of the seismically active Tien Shan high mountain belt, on the northern rim of the Ferghana Basin. The Tien Shan is an old orogenic belt from Variscan times which was reactivated during the collision of India and Eurasia 55 Ma ago and started to rise 10 Ma ago (Molnar & Tapponier, 1975; Bullen et al., 2001), see figure 1. The peaks exceed heights of 7000 m. The geology in Maily-Say is related to the transitional position between high mountains and a basin dominated by partially soft Jurassic, Cretaceous and Paleogene sedimentary rocks, see figure 4. A relatively weathering resistant formation is the Cretaceous limestone that was also mined for

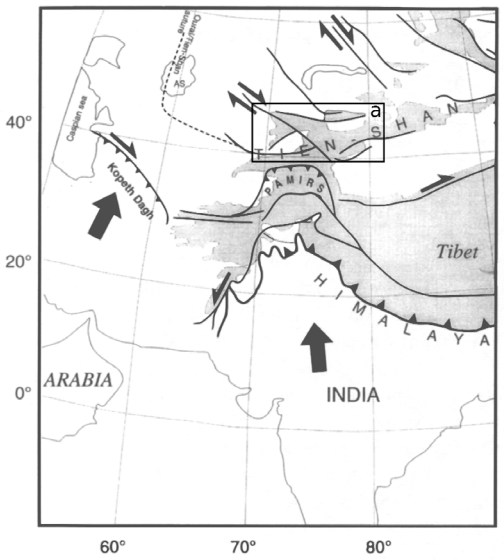

Fig. 1: Schematic tectonic map of Southern Central Asia, from Bossu et al. (1996) with the outline of figure 2 (a).

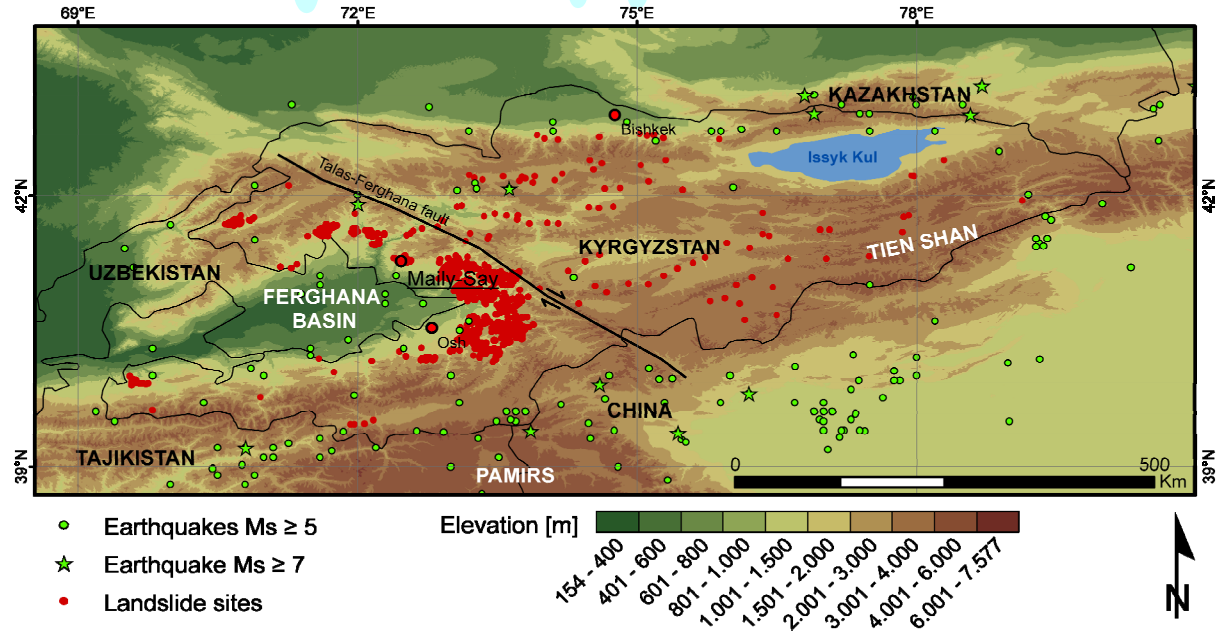

Fig. 2: Digital elevation model of Kyrgyzstan (SRTM data from Reuter et al. (2007)) with mapped landslide sites and Ms ≥ 5 earthquakes, based on data of the Kyrgyz and world seismic catalogue.

uranium. The landscape is characterised by a quiet rough relief with heights reaching from 700 m to 4000 m. The climate is predominantly dry-continental with snowfall in winter and high run off in spring.

Due to the tectonic, geological, geomorphological and hydrometerological conditions this region in general is highly prone to landslides (Roessner et al., 2005), see also figure 2). In Maily-Say also the uranium mining activities from 1946 to 1968 are supposed to have an important impact on the destabilisation of slopes. Actually, before 1946 there were only few landslides present (Havenith et al., 2006b). Then, landslide activity increased due to mining activities (Torgoev et al., 2002). Until 1962 the number of landslides reached 157. The direct link between mining activities and landslides may be explained by rock weakening because of the extraction works, collapse of underground mining galleries and rising groundwater levels in the abandoned galleries (Havenith et al., 2006b). But also indirect processes like changed land use due to population growth and increasing traffic may play a role. After the mining activities stopped in 1968, the increase of landslide activity was going on and even accelerating in the 90s. Large landslides, like the Koytash, the Tektonik and the Isolith landslides, involving up to 5 Million m^3 of rocks and soils formed during this period (Minetti, 2004). It is not clear, whether this are still long-term effects of the mining activities or if other factors, like seismic events or climatic trends contribute to this development. For instance a massive collapse of the Tektonik landslide occurred 7 weeks after a Ms 6,2 earthquake in 1992, at 20 km in the south of Maily-Say (Havenith et al., 2006b). Unfortunately documentation e.g. on earthquake damages are scarce, so it is not possible to draw clear connections between earthquake events and single landslides.

METHODS, RESULTS AND DISCUSSION

A multi-temporal landslide and scarp inventory of the years 1962, 1984, 1996, 2002 and 2007 as well as geological and geomorphological data for the Maily-Say Valley were available and prepared in ArcGIS (ESRI). The landslide and scarp inventories were developed on the basis of existing digital inventories, aerial photographs from the 50s and 60s, satellite images from 2002 and 2007 and field observations.

Bivariate statistical analysis

For the bivariate statistical analysis landslide and scarp maps were compared to different factor maps on a pixel base using a GIS. According to the method of van Westen (1997), a weight index (W_i) was calculated expressing the probability of landslide occurrence for each raster cell according to the distinct parameter. Parameters investigated were e.g. slope angle, altitude, curvature, distance to rivers as erosion base, geology, distance to faults and loess deposits. Loess deposits in the Maily-Say valley mainly remained on plateaus which are due to the

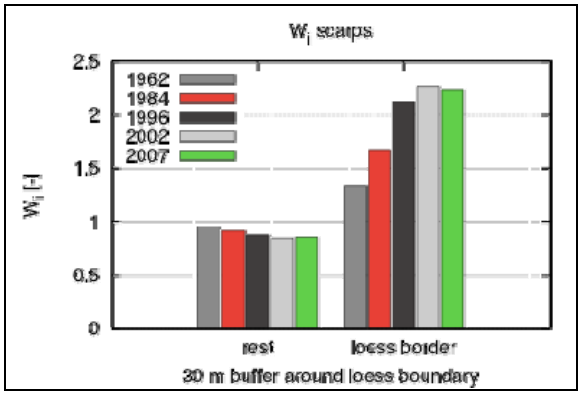

Fig. 3: Histogram showing the W_i for scarps vs. loess boundary.

lacking slope angle not very vulnerable to landslides. Often there are steeper slopes at the verge of these plateaus and the loess deposits. This is where loess landslides are likely to occur. Therefore, a 30 m buffer around the boundaries of loess was also analysed. The weight indices were compared for scarps and landslide bodies separately and between the different years. A landslide susceptibility map was created following the InfoVal method (Saha et al., 2005) based on the 1962 landslide inventory.

In the following paragraph some interesting results are summarized. A seismic triggering is suggested by the correlation of the landslide scarps with convex landforms and with the boundaries of loess deposits.

Basically, concave landforms are supposed to be more susceptible to landslides because of runoff convergence and lower depth to water table. On the other hand, in convex landforms the seismic waves are amplified when reflected at the surface. Havenith et al. (2006a) observed this phenomenon in the Suusamyr region, also within the Tien Shan. Hence, the correlation of landslide scarps with concave landforms indicates a seismic triggering. The correlation of landslide scarps with the boundaries of loess (see figure 3 and 4) is increasing over time and stagnating after 1996. Earthquakes can directly trigger loess landslides, e.g. by loess liquefaction as observed in China and Tajikistan (Wang et al., 2004) or indirectly by forming fractures that allow rapid infiltration and resulting collapse during the next rainfall event (Havenith & Bourdeau, 2010). The fact that this observed trend is rising abruptly between 1984 and 1996 and then stagnating may indicate a connection to the 1992 Ms 6,2 earthquake event near Maily-Say. Not only a direct triggering but also a weakening effect of the aforementioned processes and a temporal delayed failure of slopes is possible.

In addition to that, evidence for a climatic change was figured out. A shift of landslide correlation with slope aspect from S in 1962 and 1984 to NW in 1996 indicates the contribution of a wetter climate to increasing slope failure.

The method caused problems e.g. in implementing the geology (figure 4). Here landslides correlate strongly with the Sarybia formation, a Jurassic sandstone formation. This is because only a very small extend of this formation is included into the analysis extend. This small extend includes a very large landslide, which leads to an overestimation.

The landslide susceptibility map created with this method based on the 1962 landslide inventory was compared to landslide inventories of the years after 1962. The comparison showed agreement between regions mapped as highly susceptible and landslides that formed after 1962.

Data Mining

With data mining methods it is possible to detect landslides in a dataset using classification algorithms. This method aims at simulating the reasoning process, e.g., the one of a geologist as in this case (Fernandez-Steeger, 2002). An artificial neural network (ANN) and a Bayesian network were developed for analysing the multi-temporal landslide inventory. Since this method can handle large input

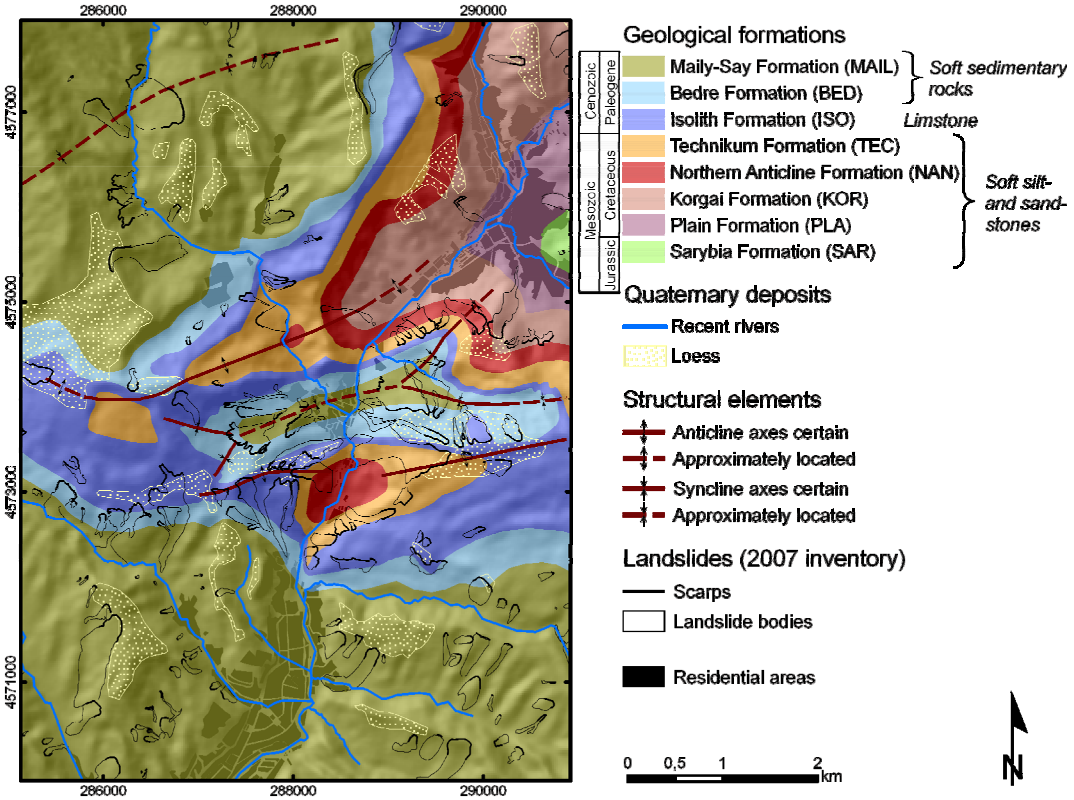

Fig. 4: Geological map of the working area showing distribution of loess deposits and outlines of landslides in 2007. Geology after de Marneffe (2010).

datasets, an abundance of geological, morphological and hydrological factors were used as input data. The dataset was prepared in a ArcGIS on a pixel base, while the main modelling was executed with the PASW Modeler 14 (SPSS Inc.), a user interface for common data mining algorithms as well as data pre- and post-processing The results of the classification were transferred back to the GIS for evaluation. While the ANN was adjusted quite optimal to the landslides and provided good classifications, the Bayesian networks developed the ability to identify also zones for possible future landslides. At this point of the work the contribution of each factor to the result is still not very transparent. Further development is needed here. Whereas ANNs have already successfully been implemented for landslide susceptibility analysis (Fernandez-Steeger, 2002; Lee et al., 2003) there are no studies based on Bayesian networks. A comparison between the results of the InfoVal method and a Bayesian network is shown in figure 5

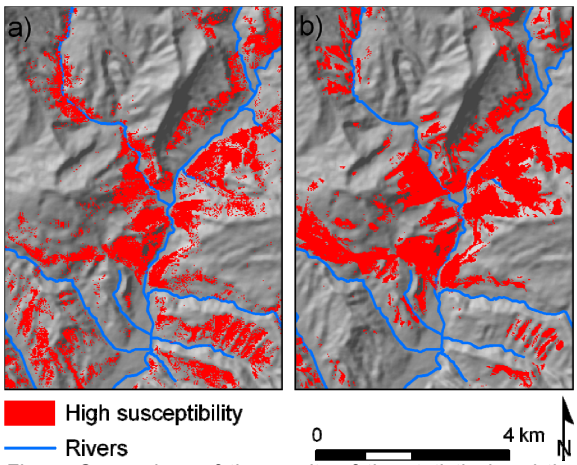

Fig. 5: Comparison of the results of the statistical and the data mining approach, a) InfoVal method, b) Bayesian networks. Both based on landslide data from 1962.

CONCLUSIONS

Two statistical methods were applied to analyse landslide susceptibility in Maily-Say, Kyrgyzstan. Both methods provide the possibility of a remote landslide analysis based on relatively simple datasets. This is an advantage for remote places like Kyrgyzstan, where landslide sites are not easily accessible or experts are simply lacking. Especially the bivariate statistical method is a simple method that provides a useful first idea of landslide susceptibility. The data mining approach is also promising for the task of predicting landslide susceptibility, but the whole process of data preparation, modelling and validation requires more time and mathematical skills.

References

Aleotti, P., Chowdhury, R. (1999). Landslide hazard assessment: summary review and new perspectives. *Bulletin of Engineering Geology and the Environment*, 58, 21–44.

Blacksmith Institute (2006). The world's worst polluted places-The Top Ten.

Bossu, R., Grasso, J. R., Plotnikova, L. M., Nurtaev, B., Fréchet, J., Moisy, M. (1996). Complexity of Intracontinental Seismic Faultings: The Gazli, Uzbekistan, Sequence. *Bulletin of the Seismological Society of America*, 86, 959–971.

Bullen, M.E., Burbank, D.W., Garver, J.I., Abdrakhmatov, K.Y. (2001). Late Cenozoic tectonic evolution of the northwestern Tien Shan: New age estimates for the initiation of mountain building. *Geological Society of America Bulletin*, 113, 1544–1559.

De Marneffe, C. (2010): Cartographie et modelisation 3D de la geologie de la vallee de Mailuu-Suu, Tien Shan, Master's Thesis, University of Liège, unpublished, 93p.

Fernandez-Steeger, T. M. (2002). Erkennung von Hangrutschungssystemen mit Neuronalen Netzen als Grundlage für Georisikoanalysen. Ph.D. Thesis, Karlsruhe University.

Havenith, H. B., Bourdeau, C. (2010). Earthquake-induced Landslide Hazards in Mountain Regions: A Review of Case Histories from Central Asia. *Geologica Belgica*, 13, 135–150.

Havenith, H. B., Strom, A., Caceres, F., Pirard, E. (2006a). Analysis of landslide susceptibility in the Suusamyr region, Tien Shan: statistical and geotechnical approach. *Landslides*, 3, 39–50.

Havenith, H. B., Torgoev, I., Meleshko, A., Alioshin, Y., Torgoev, A., Danneels, G. (2006b). Landslides in the Mailuu-Suu Valley, Kyrgyzstan-Hazards and Impacts. *Landslides*, 3, 137–147.

Lee, S., Ryu, J.-H., Lee, M.-J., Won, J.-S. (2003). Use of an artificial neural network for analysis of the susceptibility to landslides at Boun, Korea. *Environmental Geology*, 44, 820–833.

Minetti, L. (2004). Kyrgyz Republic proposed naturall disaster mitigation project, *1st IDA Preparation Mission*. Ministry of Environment and Emergency (MEE), Bishkek, 40p, inedit.

Molnar, P., Tapponier, P. (1975). Cenozoic Tectonics of Asia: Effects of a continental collision. *Science*, 189, 419–426.

Reuter, H. I., Nelson, A., Jarvis, A. (2007). An evaluation of void filling interpolation methods for SRTM data. *International Journal of Geographic Information Science*. 21:9, 983-1008.

Roessner, S., Wetzel, H. U., Kaufmann, H., Sarnagoev, A. (2005). Potential of Satellite Remote Sensing and GIS for Landslide Hazard Assessment in Southern Kyrgyzstan (Central Asia). *Natural Hazards*, 35, 395–416.

Saha, A. K., Gupta, R. P., Sarkar, I., Arora, M. K., Csaplovics, E. (2005). An approach for GIS-based statistical landslide susceptibility zonation-with a case study in the Himalayas. *Landslides*, 2, 61–69.

Torgoev, I. A., Alioshin, Y. G., Havenith, H. B. (2002). Impact of uranium mining and processing on the environment of mountainous areas of Kyrgyzstan. In: Merkel, Planer- Friedrich and Wolkersdorfer (eds), *Uranium in the aquatic environment*, pp. 93–98, Springer, Berlin Heidelberg New York.

Wang, L., Wang, Y., Wang, J., Li, L., Yuan, Z. (2004). The Liquefaction Potential of Loess in China and its Prevention. *13th World Conference On Earthquake Engineering*, Vancouver, B.C., Canada, 13p.

Vandenhove, H. Q. H., Clerc, J.-J., Lejeune, J.-M., Sweeck, L., Sillen, X., Mallants, D., Zeevaert, T. (2003). Final report in frame of EC-TACIS Project N◦ SCRE1/N◦ 38 remediation of uranium mining and milling tailing in Mailuu-Suu district Kyrgyzstan, Mol (Belgium).

Van Westen, C. J. (1997). Statistical landslide hazard analysis. In: *Application guide, ILWIS 2.1 for Windows*. ITC, Enschede, The Netherlands, 73–84.

Varnes, D. J. (1984). Landslide hazard zonation: a review of principles and practise. *UNESCO*, Paris, 63 p.

EARTHQUAKE ARCHAEOLOGY

INQUA PALEOSEISMOLOGY AND ACTIVE TECTONICS

TECTONIC INTERPRETATION OF THE 2008 WENCHUAN EARTHQUAKE: WHY IT ONLY PROPAGATED IN ONE DIRECTION - THE FUTURE?

Burchfiel, B. C. (1), Royden, L. H. (1)

(1) Department of Earth, Atmospheric and Planetary Sciences, 54-1010, Massachusetts Institute of Technology, Cambridge, MA 02139, USA. EMAIL: bcbruch@mit.edu

Abstract (Tectonic interpretation of the 2008 Wenchuan earthquake): *The 2008 Wenchuan earthquake, (M = 7.9) occurred on a listric thrust fault that at the hypocenter (15-20 km) dipped ~30-40° NW and steepened upward to near vertical at the surface (Zhang et al., 2008) Maximum slip was 9 m vertical and 6 m right-slip. The fault propagated from the epicenter to the northeast for ~ 200 km with increasing right-slip eastward and broke across at least two fault segment boundaries. Although the earthquake occurs along the steep topographic slope of the Longmen Shan at eastern margin of the Tibet plateau, it was unexpected because data suggests that the recurrence interval on the fault zone was 2500 to 4000 years.*

Key words: *Earthquake, Wenchuan, China, 2008*

INTRODUCTION

The earthquake fault, Pengguan-Beichuan fault, broke in two segments, the main segment was along the east side of a major uplift of Precambrian basement rocks, the Pengguan massif, in the Longmen Shan at the eastern margin of the Tibet plateau, southwestern Sichaun, China, and propagated northeast into Paleozoic rocks. The Pengguan uplift is a northeast plunging anticline with its sedimentary cover still exposed at the north end. The east side of the anticline is the Pengguan-Beichuan fault. Because of the plunge to the north the east vergent thrust sheets are exposed also to the north and are cut by the Pengguan-Beichuan fault (figure 1). These geological relations were discussed by Burchfiel et al., (1995).

The question of why the fault only propagated to the northeast and its long recurrence interval can be explained by the geological framework in the area that was known in 1995. The west side of Pengguan uplift and the Pengguan-Beichuan fault are cut off at the south end by the Wenchuan-Maowen fault, a steep fault that has active right-slip, but was not reactivated during the earthquake, that also cuts off the sedimentary cover and Mesozoic thrust sheets so that the southern Penguan Precambrian has no sedimentary cover and it is not clear how much it has been uplifted. How these two faults interact is critical, but is at present unknown. The Wenchuan-Beichuan fault has a low-grade mylonitic fabric that shows the west side down (a normal fault), that is consistent with the geology where the rocks west of the Penguan massif are metamorphosed Paleozoic that belong to the Mesozoic thrust sheets.

DISCUSSION

Why the earthquake did not propagate also to the southwest and what are the prospects of a large earthquake to the southwest can be explained by the geological framework of the area. To the south, the Precambrian is uplifted again in the Baoxing massif that also has the characteristics of an east vergent fold with a steep thrust along its eastern side (Fig. 1). The Wenchuan-Maowen fault appears to continue south and cuts off the west side of the Baoxing uplift and Paleozoic and even Triassic strata lie west of the fault against Precambrian rocks to the east.

Regionally east of the Chengdu plain (the Quaternary area east of Pengguan uplift) is an single curving fold, the Longchaun anticline) that intersects the Longmen Shan obliquely in the north but trends away from the Longmen Shan to the south and curves south east of Chengdu and continue farther south east of Emei shan (Figure 1). Within the southern Chengdu plane several north-plunging anticlines appear and grow in amplitude southward so that the elevation to the south rises and rapidly becomes the eastern part of the Tibetan Plateau. These folds involve Precambrian rocks in the south. Thus what appears to be a horizontal decollement with the sedimentary section beneath the Chengdu plane in the north that connects the Longchaun anticline with the Pengguan-Beichuan fault, in the south the decollement must drop into the Precambrian rocks where the topography becomes part of the Tibetan Plateau.

The geometry of active deformation suggests stresses focused mainly at the Pengguan uplift in the north, become distributed southward from the 2008 epicenter across a broad of the area suggesting that the stress is being relieved in the southern area where is more distributed and being relieved by a broader and more active area of seismic activity.

However, along the topographic eastern margin of plateau, mountains increase in elevation so that at the Siguniang Shan (4 girls) they reach more than 6200 m and at Gonga Shan farther south they reach 7550 m. The mountain front east of the 4 girls is very

steep, suggesting again rapid uplift like along the Pengguan massif. This is similar to the conditions at the area of the Wenchuan earthquake, and needs to be tectonically and geomorphologically researched for recurrence interval in this area that may also be longer that recorded history. looked at in terms of the even though the stress appears to be more distributed to the east in this region. Like all geology relations there are ambiquities: the steepness of the topographic margin of the plateau in this area is a clue as to how structurally active the plateau margin is but the broader distribution of active structures and earthquakes suggests stresses are being distributed. Farther east there is second steep mountain front on the east side of Emei Shan with an active fault at its base. Another alarming relationship.

The change in structure from north to south east of the Longmen Shan can be interpreted to be related to the geometery of the Xianshuihe fault, an arcuate NW-tending fault major active right-slip that separates two major crustal provinces in SW China: a province to the south that is part of a crustal fragment that rotates clockwise at 10-12 mm/yr around the Eastern Himalayan syntaxis, from the Longmen Shan province that moves NE ~parallel to the eastern margin the Tibetan Plateau with only a very slow convergence rate (1-2 mm/yr) with respect to South China to the east as shown by GPS data. In fact, the convergence rate is so slow that the eastern part of the Tibetan Plateau moves east nearly at the same rate as South China as first shown by King et al. (1997). The slow convergence rate across the topographic margin of Tibet Plateau explains the large recurrence interval of the Wenchuan earthquake, but does not easily explain the steep topographic margin and the rise in elevation of the front to the south.

West of Kanding Xianshuihe fault curves more sharply that either to the NW or SE forming a restraining bend indicates there is a component of compression across the fault that forms the high topographic area east of the fault and where basement rocks are involved in the structure. At the bend the mountains reach 7550m where the large Cenozoic pluton that underlies the Gonga Shan. If so the it is also where to the east of the fault the Tibetan plateau was elevated and the folds that come from the southern part of the Sichuan basin involve Precambrian rocks. There are cross structures here; WNW trending thrust faults that involve Precambrian cut across the N-S trending folds from the southern Sichuan basin that also involve Precambrian. The decollement here is in the basement beneath the folds and probably beneath the huge NW-trending Danba antiform of Precambrian east of Kanding. This raises the question of how deep is the decollement and how does it interact with the Xianshuihe fault; the decollement is deep and the Xianshuihe fault may be a crustal feature.

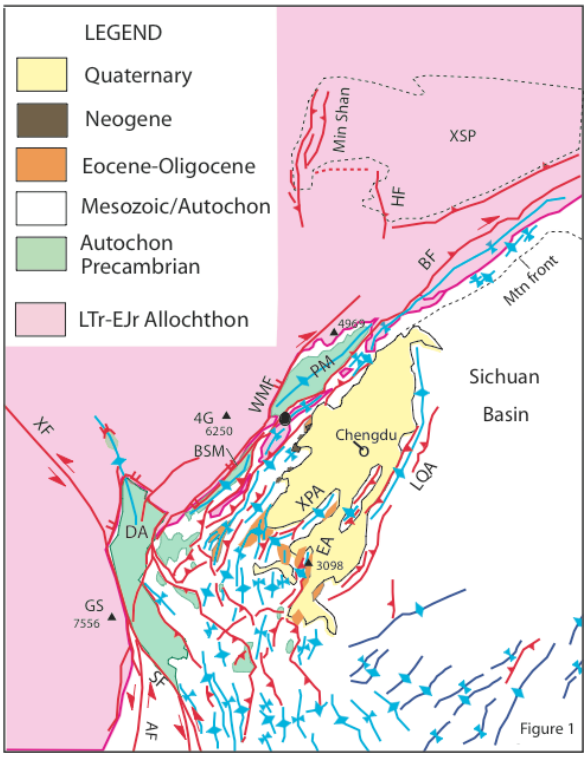

Fig. 1: Generalized map of the Longmen Shan and Southern Sichuan basin area showing structures of late Cenozoic to active age. Faults are in red decorated with barbs for thrust faults, arrows for strike-slip faults and double ticks for normal faults. Blue are the folds of late Cenozoic age, except in the southeast where they are of Middle Cretaceous age (dark blue). These structures overprint the early Mesozoic Longmen Shan thrust faults that moved the Songpan Ganze Unit (pale red) eastward above the Yangtze Unit (white).The area of the southwestern Sichuan basin shown in yellow, the Chengdu plain, has a thin cover of Pleistocene sediments derived from the Longmen Shan and ponded behind the active Longquan anticline (LQA). Large black dot at south end of Pengguan massif (PM) is location of the 2008 Wenchuan earthquake epicenter. 4G=Four Girls peaks, AF=Anninghe fault, BF=Beichuan fault, BSM=Baoxing massif, DA=Danba antiform, EA=Emei Shan anticline, GS=Gonga Shan, HF=Huya fault, PM=Pengguan massif, SF=Shimian fault, WMF=Wenchuan-Maowen fault, XF=Xianshuihe fault, XSP=Xushan platform, XPA=Xiong Po anticline.

Acknowledgements: This work was supported by NSF Grant 000357.

References

Burchfiel, B. C., Z. Chen., Y. Liu, & L. H. Royden, (1995). Tectonics of the Longmen Shan and adjacent regions. International Geological Review, 37(8), 661-736.

King, R. W., F. Shen, B. C. Burchfiel, Z. Chen, Y. Liu, L. H. Royden, E. Wang, X. Zhang, & J. Zhao, (1997). Geodetic measurement of crustal motion in southwest China. Geology, 25 (2), 179-182.

Zhang, P-Z., X-Z. Wen, Z-K. Shen, & J-H. Chen, (2008). Oblique, High-Angle, Listric-Reverse Faulting and Associated Development of Strain: The Wenchuan Earthquake of May 12, 2008, Sichuan. Annual reviews of Earth and Planetary Sciences, 38, 353-382.

EARTHQUAKE ARCHAEOLOGY

INQUA PALEOSEISMOLOGY AND ACTIVE TECTONICS

CHARACTERIZATION OF LATE PLEISTOCENE-HOLOCENE EARTHQUAKE-INDUCED "HOMOGENITES" IN THE SEA OF MARMARA THROUGH MAGNETIC FABRIC. IMPLICATION FOR CO-SEISMIC OFFSETS DETECTION AND MEASUREMENTS

Campos Corina (1)(2), Beck Christian (1), Crouzet Christian (1), Carrillo Eduardo (3)

(1) Institut des Sciences de la Terre ISTerre, UMR CNRS 5275, Grenoble University, 73376 Le Bourget du Lac Cedex, France. Email : Corina.Guzman@etu.univ-savoie.fr
(2) Departamento de Ciencias de la Tierra, Universidad Simón Bolívar, Sartenejas, Baruta, Venezuela. Email: campossc@usb.ve.
(3) Instituto de Ciencias de la Tierra, Universidad Central de Venezuela, Av. Los Ilustres, Caracas, Venezuela. Email: eduardo.carrillo@ciens.ucv.ve.

Abstract: The Marmara Sea is located in the eastern part of the Mediterranean region, in an area with strong seismic instability associated with the activity of North Anatolian Fault. In order to analyze the impact of seismicity on the sedimentation in the Marmara Sea we have studied three giant piston cores (27 to 37.7m long). They represent the last 20 kyr of sedimentation. The upper section (marine stage) is predominantly composed by fine grained terrigenous material (clay-silty) and in less percentage by the silty-sandy laminated intervals. The lower section (non marine) is composed by abundant fine grained terrigenous material, numerous turbidites sequences and levels with deformation structures (possible seismites). Some turbidites show an abrupt contact separating the coarse grain basal part (bed load) of the fine grain upper part (suspended load), this later are defined as "homogenites"

Key words*:* Sea of Marmara, Earthquakes, Turbidites, Homogeneites.

Introduction

The Marmara Sea (Northwestern Turkey) is a pull-apart basin developed along the North Anatolian Fault (Hancock and Barka, 1981). East-West elongated (200 km) it is composed of several aligned sub-basins (Tekirdağ, Orta, Kumburgaz and Çinarcic basin) (Fig.1). The North Anatolian Fault (N.A.F) is a 1200-km-long dextral strike-slip fault (Şengör et al., 2004) and is considered as a major active boundary between Anatolia and Eurasia plates. (Armijo el al., 1999; McClusky et al., 2000; Flerit et al., 2003).

The northern branch of the N.A.F. crosses the different deep sub-basins, where giant pistons cores (from 27 to 37,7 m) have been retrieved, with location based on high resolution seismic reflection imaging. This survey aimed to detect and characterize co-seismic sedimentary episodes - especially "homogenites" – for a 20 000 yr-long period. Different previous studies have demonstrated the interest of sedimentary record (isolated marine basins and lakes) as archives of seismic activity (Hempton and Dewey, 1983; Calvo et al., 1998; Chapron et al., 1999; among many others). Movements of water masses (seiche effect, reflected turbidites) and mass wasting (triggered by major earthquakes) are inferred to combine themselves for specific depositions which locally compensate vertical offset of seafloor, as in the Sea of Marmara central basin (Beck et al, 2007; Stegmann et al., 2007; Strasser et al., 2006). Thus, the present work is dedicated to the Central (Orta) and eastern (Çinarcic) basins to detect, characterize, and correlate, these sedimentary "events", as a contribution to pecise paleoseismic data (associated fault offset, chronology).

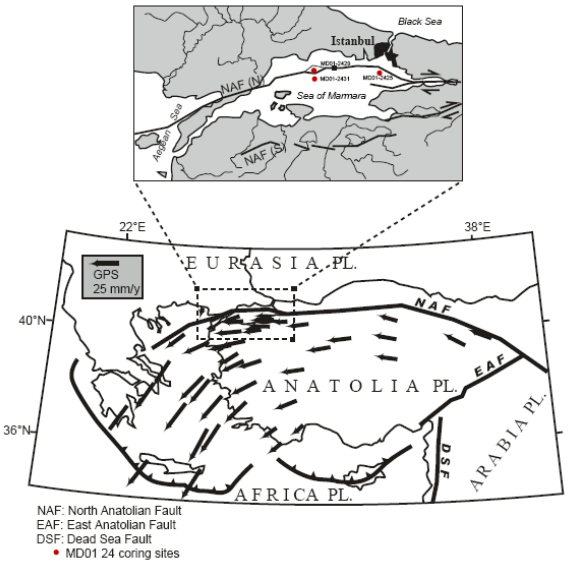

Fig.1 Simplified geodynamic setting of the Sea of Marmara for the present day with coring locations (after Armijo et al., 1999; Beck et al., 2007). GPS velocity vector with fixed Eurasia Plate, from McClusky et al., 2000. The Anatolia Plate is bounded by major strike-slip faults systems (North and East) and subduction (South).

The objective of this work is identify and characterize the impact of seismicity over the sedimentation and distinguish them from "normal" sedimentary processes as hemipelagic-type fallout and flooding,

subsequently we hope to determine the earthquake recurrence and contribute to improve hazard estimates. We have studied 3 giant piston cores collected during the MARMACORE Cruise in August-Septembre 2001. The cores were taken in the Çinarcic basin (MD01-2425), and in the Orta basin (MD01-2429, MD01-2431), at depths between 1230 and 1170m. The sedimentary record in theses cores represent the sedimentation of the last 20 kyr.

METHODS

One of the challenges is the distinction between fine-grained, slow and continuous, hemipelagic sedimentation, from quite instantaneous re-suspension and re-deposition. For this we combined different tools in order to characterize the textures: grain size (laser diffraction grain size analyzer, Malvern TM), anisotropy of magnetic susceptibility (Kappabridges MFK1-FA AGICO) and X-ray imagery (D.G.O.'s SCOPIX). Compositions were controlled through magnetic susceptibility (BARTINGTON TM MS2 contact sensor), and microscopic analysis. The chronology was established from ^{14}C (AMS measurements) derived from wood, plants and sapropelic muds. We calibrated the ages with Oxcal Program v4.1. The ages found represent the Holocene and part of the late Pleistocene.

RESULTS

The analyzed sections are composed of fine grained terrigenous material (clay-silty) intercalated with silty-sandy laminated intervals, turbidites sequences and liquefaction features as ball and pillow. The upper marine part is predominantly compose by the clay-silty slightly calcareous and in less percentage by the silty-sandy laminated intervals, theses intervals consist of milimetric's lenticular and parallel planar beddings.

In the lower non marine part the fine grained terrigenous material is abundant but we find numerous turbidites sequences with thicknesses ranging from centimeters to decimeters. This turbidites can show erosive bases, normal gradation and ripples, others can show an abrupt contact separating the coarse grain basal part (bed load) of the fine grain upper part (suspended load)(Fig.2), this later are defined as "homogenites". In this non marine section we can also find in less proportion the slumps and the levels with deformation structures (possible seismites).

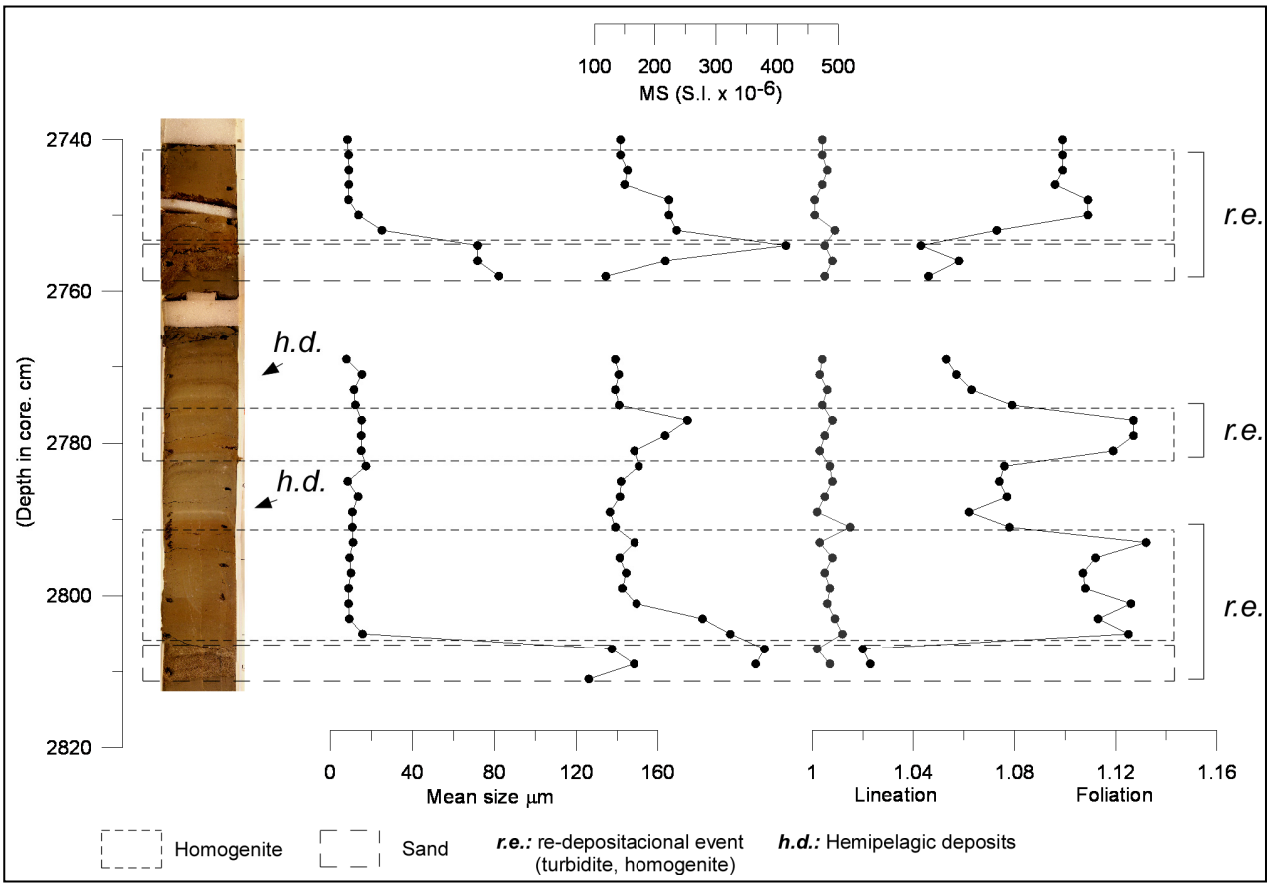

Fig.2 Textural and compositional characterization of three homogenites present in the non marine section (core MD01-2425). The mean size, magnetic susceptibility and lineation magnetic don't show differences between the hemipelagic normal sedimentation and the homogeneous coseismic sedimentation. The foliation magnetic (AMS) is higher in the homogenites than the hemipelagic deposits, this high foliation contrast has to be explained by different arrays of phyllosilicates, associate a specific settling conditions related to water mass oscillation.

The Magnetic Susceptibility signature in the marine part is in general lower than the non marine part (average in the marine part is$10x10^{-5}$ SI and $30x10^{-5}$ SI in the non marine part). In general this signature is strong in the silty-sandy laminated intervals and in the turbidites sequences. In the turbidites sequences this signature has a behavior similar to the one observed in the profiles of grain-size, being higher in the sand layers than the fine grain, and showing constants values in the homogenites. On the other hand, the foliation determined from the Anisotropy of Magnetic Susceptibility is much higher in the levels the fine grain size belonging to the homogenites (average of 1.12) than any other level of thin grain size (average 1.06) (Fig.2). As both types of levels (homogenites and hemipelagic deposits) have similar grain-sizes and not very different composition, this high foliation contrast has to be explained by different arrays of phyllosilicates, which, at their turn, cannot be explained by different compactions. Thus, we infer specific settling conditions related to water mass oscillation.

In the study area others analyses are in processes such as the carbonates contents, clay minerals, analysis of terrigenous fraction (mineralogy), organic matter, etc.

References

Armijo, R., Meyer, B., Hubert, A., Barka, A. (1999). Westward propagation of the North Anatolian Fault into the northern Aegean: timing and kinematics. *Geology* 27 (3), 267–270.

Beck C., Mercier de Lepinay B., Schneider J.L., Cremer M., Cagatay N., Wendenbaum E., Boutareaud S., Menot G., Schmidt S., Weber O., Eris K., Armijo R., Meyer B., Pondard N., Gutscher M.A., Turon J.L., Labeyrie L., Cortijo E., Gallet Y., Bouquerel H., Gorur N., Gervais A., Castera M.H., Londeix L., de Resseguier A., Jaouen A. (2007) Late Quaternary co-seismic sedimentation in the Sea of Marmara's deep basins, *Sedimentary Geology*, 199, 65-89.

Calvo, J.P., Rodriguez-Pascua, M., Martin-Velazquez, S., Jimenez, S., De Vicente, G. (1998). Microdeformation of lacustrine laminate sequences from Late Miocene formations of SE Spain: an interpretation of loop bedding. *Sedimentology* 45, 279–292.

Chapron, E., Beck, C., Pourchet, M., Deconinck, J.-F. (1999). 1822 AD earthquake-triggered homogenite in Lake Le Bourget (NW Alps). *Terra Nova* 11, 86–92.

Flerit, F., Armijo, R., King, G.C.P., Meyer, B., Barka, E. (2003). Slip partitioning in the Sea of Marmara pull-apart determined from GPS velocity vectors. *Geophysical Journal International* 154, 1–7.

Hancock, P.L., Barka, A.A. (1981). Opposed shear senses inferred from neotectonic mesofractures systems in the North Anatolian fault zone. *J. Struct. Geol*. 3, 383–392.

Hempton, M.R., Dewey, J.F. (1983). Earthquake-induced deformational structures in young lacustrine sediments, East Anatolian Fault, southwest Turkey. Tectonophysics 98, 7–14.

McClusky, S., Bassalanian, S., Barka, A., Demir, C., Ergintav, S., Georgiev, I., Gurkan, O., Hamburger, M., Hurst, K., Hans-Gert, H.-G., Karstens, K., Kekelidze, G., King, R., Kotzev, V., Lenk, O., Mahmoud, S., Mishin, A., Nadariya, M., Ouzounis, A., Paradissis, D., Peter, Y., Prilepin, M., Relinger, R., Sanli, I., Seeger, H., Tealeb, A., Toksöz, M.N., Veis, G.(2000). Global positioning system constraints on plate kinematics and dynamics in the eastern Mediterranean and Caucasus. *Journal of Geophysical Research* 105, 5695–5719.

Sengör, A.M.C., Tuysuz, O., Imren, C., Sakinc, M., Eyidogan, H., Gorur, N., Le Pichon, X., Claude Rangin, C. (2004). *The* North Anatolian Fault. A new look. Ann. Rev. Earth Planet. Sci. 33, 1-75.

Stegmann, S., Strasser, M., Anselmetti, F.S., Kopf, A. (2007). Geotechnical in situ characterisation of subaquatic slopes: The role of pore pressure transients versus frictional strength in landslide initiation. *Geophysical Research Letters*, 34, L07607

Strasser, M, Anselmetti, F.S., Fäh, D., Giardini, D., Schnellmann, M. (2006). Magnitudes and source areas of large prehistoric northern Alpine earthquakes revealed by slope failures in lakes. *Geology*, 34 (12)

PALEOSEISMOLOGICAL EVIDENCE FOR HISTORICAL SURFACE RUPTURE EVENTS IN S. MIGUEL ISLAND (AZORES)

Carmo, Rita (1), José Madeira (2), Ana Hipólito (1), Teresa Ferreira (1)

(1) Centro de Vulcanologia e Avaliação de Riscos Geológicos, Universidade dos Açores, Complexo Científico, 3º Piso – Ala Sul, Rua Mãe de Deus, 9500-321 Ponta Delgada, Açores, Portugal. Email: Rita.L.Carmo@azores.gov.pt
(2) Dpto. Geologia, LATTEX/IDL, Faculdade de Ciências da Universidade de Lisboa, Edifício C6, Campo Grande, 1749-016 Lisboa, Portugal. Email: jmadeira@fc.ul.pt

Abstract (Paleoseismological evidence for historical surface rupture events in S. Miguel Island (Azores)): *The Azores archipelago is located in the triple junction between the Eurasian, Nubian and North American lithospheric plates. The Achada das Furnas plateau, located in the central part of S. Miguel Island, between Fogo and Furnas volcanoes, is dominated by several basaltic cinder cones that define several WNW-ESE and E-W alignments. Two E-W trending scarps were identified by aerial photo analysis. Trenches were open across the scarps to confirm their tectonic nature exposing two active normal faults (the Altiprado Faults). At least four paleoearthquakes were deduced, three of which in historical times. Radiocarbon ages are in agreement with this interpretation.*

Key words*: Azores, active faults, paleoseismology*

GEOLOGICAL SETTING

The Azores archipelago is located at the Eurasia (Eu), Nubia (Nu) and North America (NA) triple junction (*Fig. 1*). The Mid Atlantic Ridge separates the NA from Eu and Nu plates, while the Azores-Gibraltar Fault Zone (Terceira Rift and Gloria Fault) is the boundary between Eu and Nu plates. The archipelago comprises nine islands distributed by three groups: the western islands lie on NA plate while the central and eastern groups are located along the western segment of the Azores-Gibraltar Fault Zone (*Fig. 1*). As a result of its complex tectonic setting, the Azores archipelago is subject to frequent seismic and volcanic activity.

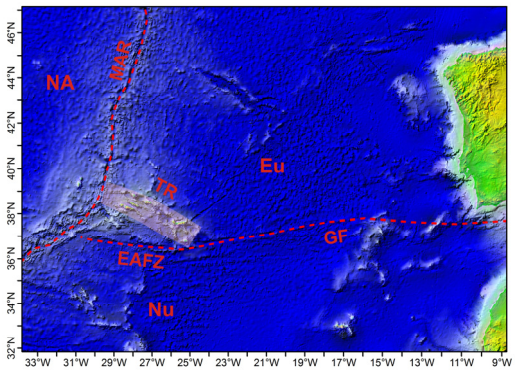

Fig. 1: Azores tectonic setting. NA – North American plate; Eu – Eurasian plate; Nu – Nubian plate; MAR – Mid Atlantic Ridge; TR – Terceira Rift (s.l.); EAFZ – East Azores Fracture Zone; GF – Gloria Fault. World topography and bathymetry from ESRI (2008).

S. Miguel Island was settled in 1439-1443. It has three active explosive central volcanoes with summit calderas linked by zones of fissural volcanism. The main tectonic structures trend NW-SE to WNW-ESE, NNW-SSE and NE-SW.

The Achada das Furnas plateau, located in the central area of the island, between Fogo and Furnas volcanoes, is dominated by several basaltic cinder cones defining WNW-ESE and E-W alignments (*Fig. 2*). Aerial photo analysis identified the presence of two E-W trending scarps produced by the Altiprado Faults (AF1 and AF2, *Fig. 2*).

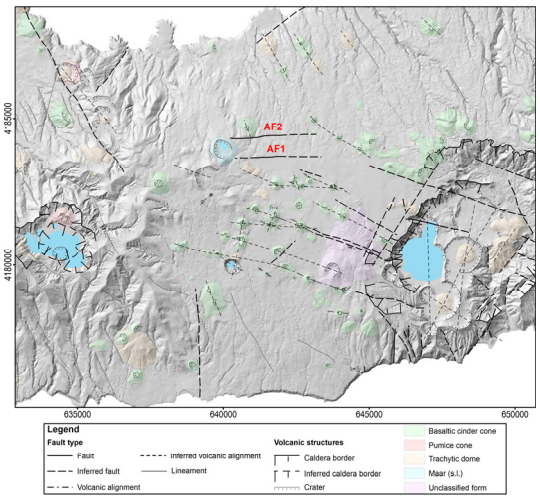

Fig. 2: Main tectonic and volcanic structures of Achada das Furnas plateau.

THE ALTIPRADO FAULTS

Altiprado Fault 1

The Altiprado Fault 1 (AF1) trace is marked by an 835 m-long, 3 m-high, south-facing scarp, trending N87ºE (*Fig. 3*). To the east and to the west its trace becomes uncertain.

A ~18 m-long trench exposed the fault, trending N87ºE and dipping 65ºS, displacing a stratigraphic succession that comprises 6 pumice fall deposits (units) separated by paleosols produced by eruptions of Fogo and Furnas volcanoes (*Fig. 4*): 1 - olive-brown paleosol containing basalt lapilli fragments, corresponding to Fogo A deposit (4520±90 years BP; Wallenstein, 1999); 2 – pumice fall deposit composed of alternating yellowish lapilli and light olive brown ash beds, probably related to Fogo C deposit; 3 - strong brown pumice ash fall deposit with some lapilli at the base (3a), and a yellowish pumice fall deposit in the central part (3b); probably Fogo D deposit; 4 - grey pumice ash deposit, corresponding to Furnas C deposit (1900 years BP; Guest et al., 1994), topped by a very dark grey soil (1440-1500 cal AD); 5 - stratified pumice fall deposit of alternating beds of fine to medium greyish white lapilli and ash containing sanidine crystals (from 1563 AD historical eruption in Fogo volcano), topped by a very dark grey paleosol rich in coal fragments (1660-1700 cal AD); 6 - remobilised deposit from the underlying unit.

The AF1 affects all stratigraphic units and the existing scarp is an uneroded free-face almost devoid of soil that corresponds to the projection of the fault to the surface (*Fig. 4*). Several WNW-ESE to E-W trending fractures and open cracks, sometimes filled with material from overlying units, and a colluvium composed of material of units 3 and 4 were also exposed in the trench (*Fig. 4*).

Units 2 to 4 (soil 1440-1500 cal AD) are displaced by 1.0m and units 5 (soil 1660-1700 cal AD) and 6 by 0.38m, indicating two surface rupturing paleoearthquakes of Mw 6.7 and 6.4 (using the Wells & Coppersmith's, 1994, M/MD correlation), respectively, accounting for an accumulated dip-slip of 1.38m.

Two earthquakes in 571-511 years indicate a recurrence interval that ranges from 286 to 256 years, yielding a slip rate of 2-3 mm/year.

Altiprado Fault 2

The Altiprado Fault 2 trace is marked by an almost imperceptible 1690 m-long and ~40 cm-high south facing scarp, trending N87ºE (*Fig. 3*). To the east its location becomes uncertain.

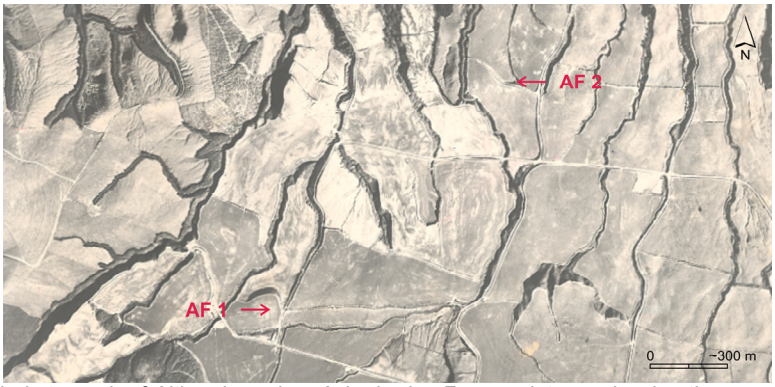

Fig. 3: Vertical aerial photograph of Altiprado region, Achada das Furnas plateau, showing the geomorphic expression of Altiprado Faults (Aerial photo from Direcção Geral de Planeamento Urbanístico, 1974).

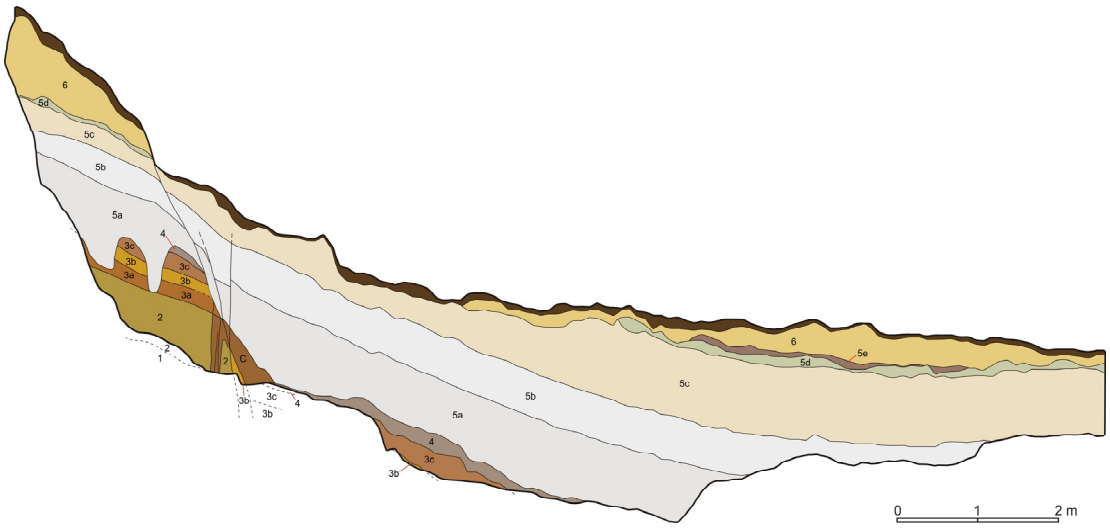

Fig. 4: Map of the east wall of the Altiprado Fault 1 trench.

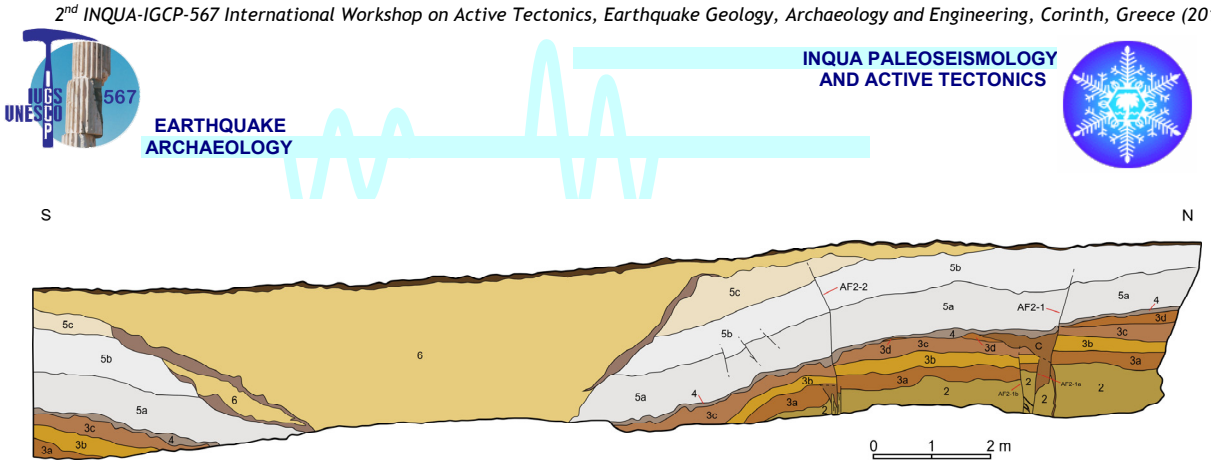

Fig. 5: Map of the west wall of the Altiprado Fault 2 trench.

A 29 m-long trench exposed two subvertical faults (AF2-1 and AF2-2) that display frequent changes in dip sense (N75-89ºE, generally dipping 62-88ºS) and an E-W trending paleo-channel (filled with unit 6) (*Fig. 5*). The exposed stratigraphic sequence is the same observed in AF1 trench, with exception of unit 1 that is absent (*Fig. 5*). There are also open fractures trending ENE-WSW to E-W, sometimes filled with material from overlying units, and a colluvium, containing material of unit 3, deposited against the AF2-1 fault (*Fig. 5*).

The faults produced differential vertical separations on units 2 and 3 (younger than ~4500 years BP), and on units 4 (~1900 years BP; soil 1440-1500 cal AD) and 5 (1563 AD): AF2-1 - accumulated dip-slip of 33cm (26+7cm); AF2-2 - accumulated dip-slip of 15cm (11+4cm). Assuming that the ruptures in AF2-1 and AF2-2 were produced by the same earthquakes, displacement values of 0.37m (0.26+0.11cm) and 0.11m (0.07+0.04cm), correspond to earthquakes of Mw of 6.4 and 6.0, respectively (using the Wells & Coppersmith's, 1994, M/MD correlation). The accumulated displacement is 0.48m (0.37m+0.11m).

The existence of an E-W trending paleo-channel suggest that it may have been developed at the base of a previous fault scarp, once the regional drainage system in this area is oriented N-S.

Altiprado Faults evolution

The Altiprado Faults evolution was deduced from geometric analysis of the trenches. As they are geographically close and affect the same stratigraphic succession, this allows correlating their evolution (*Fig. 6*):

a) Deposition of units 1 (4520±90 years BP) to 3;
b) Surface rupture at AF2-1 and AF2-2 with normal separations of 26cm and 11cm, respectively (Mw 6.4 earthquake);
c) Erosion truncating unit 3, with the formation of gullies in AF1 fault zone, and fault scarp retreat at AF2-1 with the formation of a colluvial wedge (C) with material from unit 3;
d) Deposition of unit 4 (~1900 years BP) and soil development (1440-1500 cal AD);
e) Surface rupture (Mw 6.7) at AF1 with normal separation of 1.0m;
f) Erosion with minor fault scarp retreat with formation of a colluvial wedge (C) in AF1;
g) Deposition of unit 5 (1563 AD – Fogo Volcano historical eruption) with sin-eruptive ruptures (Mw 6.0?) in AF2-1 and AF2-2, without geomorphic expression, of 7cm and 4cm, respectively;
h) Erosion truncating the top of unit 5 and formation of a new paleo-channel in AF2 fault zone; development of a soil (1660-1700 cal AD);
i) Erosion truncating unit 5 and deposition of unit 6;
j) Surface rupture (Mw 6.4) at AF1 with normal separation of 0.38m;
k) Erosion truncating units 5 and 6; development of present top soil.

DISCUSSION

Analysing the geological history, the first surface rupture earthquake is associated to AF2, originating an accumulated dip-slip of 37cm in AF2-1 and AF2-2. It occurred in pre-historical times, after the deposition of unit 3 (Fogo D deposit, <4500 years BP) and before 1900 years BP (unit 4 - Furnas C deposit).

The second surface rupture event occurred in AF1, after the development of unit 4 paleosol (1440-1500 cal AD) and before the deposition of unit 5 (1563 AD - historical eruption), with normal separation of 1.0m. Since the settlement of S. Miguel Island began in 1439-1440 AD and taking into account the historical

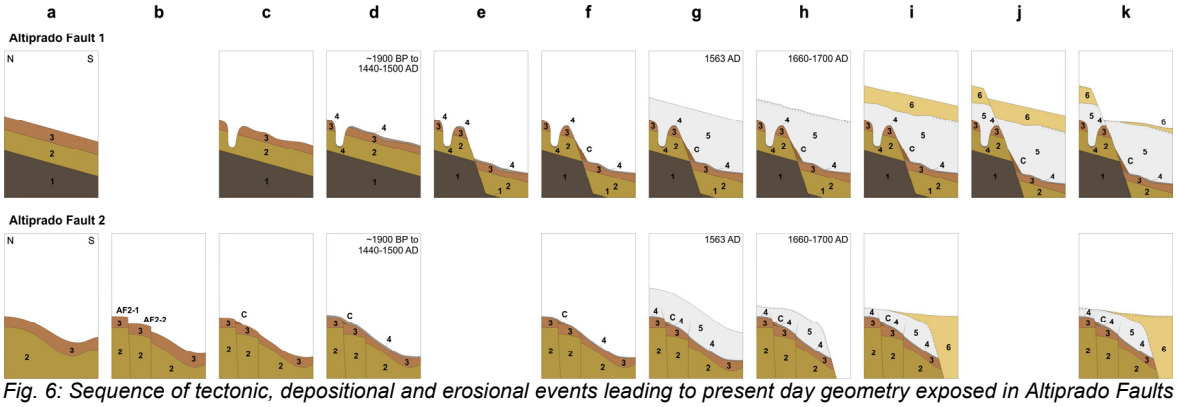

Fig. 6: Sequence of tectonic, depositional and erosional events leading to present day geometry exposed in Altiprado Faults 1 and 2 trenches.

earthquakes in the island and the youthful aspect of the scarp, this event is probably related to October 22nd, 1522 historical earthquake. This was one of the most destructive events that occurred in Azores, causing 5000 deaths. The epicentre was located inland, a few km southwards from AF1 (*Fig. 7*) and triggered several landslides and severe damage, mainly in the central eastern part of the island.

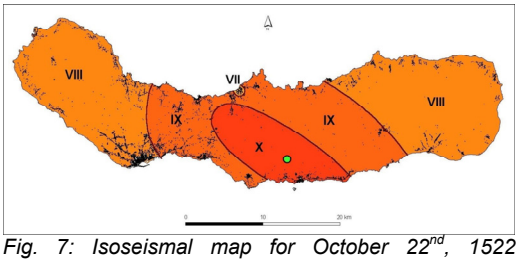

Fig. 7: Isoseismal map for October 22nd, 1522 earthquake (Silveira et al., 2003).

The third rupture is associated with AF2. As it is not clear if the last displacement (11cm in AF2-1 and AF2-2) is affecting only the lower part of unit 5 (1563 AD) or affects the entire unit, this could be associated with the intense seismic activity that accompanied the 1563 historical eruption of Fogo volcano. The earthquakes were felt in a wide region and caused severe damage in Ribeira Grande and Ribeira Seca villages. Otherwise it could have occurred after this volcanic event.

The fourth earthquake is related with AF1 and occurred after the deposition of unit 6 (>1660-1700 cal AD) with normal separation of 0.38m.

If the last three earthquakes occurred in historical period, the recurrence interval for Altiprado Faults zone is 163 years.

There is no evidence of a high magnitude earthquake (Mw 6.4) with inland epicentre in historical records, as well in the instrumental seismicity data that could justify the most recent displacement. However, there is a long time record of seismic swarms in this area, with earthquakes of low to moderate magnitude (*e.g.* 1967, 1989 and 2005).

The most recent seismic swarm started on May 10th, 2005 and continued till the end of that year, registering more than 46000 earthquakes (*Fig. 8*). The strongest events occurred on September 20th and 21th and had ML 4.1 and 4.3, respectively, causing several landslides and ground cracking.

GPS monitoring data allowed Trota (2008) to verify that there was also ground deformation associated

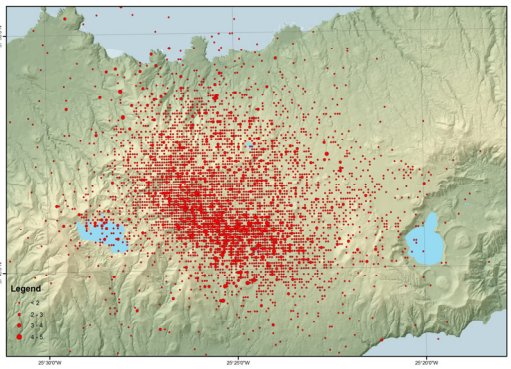

Fig. 8: Epicentre distribution of 2005 seismic swarm (May 10th to December; data from CVARG/CIVISA, 2005).

with the seismic activity. Considering the seismicity pattern, the low seismic energy released and the GPS data, this activity has been related to a magmatic intrusion. The previous seismic swarms were not geodetic monitored and the seismic network was limited, so there are no evidences of previous episodes of crustal deformation and the seismic parameters may have significant errors associated. Nevertheless, one possibility is that the 0.38m displacement observed in AF1 trench could be an accumulated value as a consequence of several moderate earthquakes during the periods of seismic activity increments in this area that might have been associated with crustal deformation.

Acknowledgements: Rita Carmo is supported by a PhD Grant from Fundo Regional da Ciência e Tecnologia. Fieldwork was financed by Centro de Informação e Vigilância Sismo-Vulcânica dos Açores (CIVISA).

References

Guest, J.E., Duncan, A.M., Cole, P.D., Gaspar, J.L., Queiroz, G., Wallenstein, N., Ferreira, T. (1994) – Preliminary report on the volcanic geology of Furnas volcano, São Miguel, Azores. ESF Furnas Laboratory Volcano, Eruptive History and Volcanic Open File Report 1, 24 p.

Silveira, D., Gaspar, J.L., Ferreira, T., Queiroz, G (2003) - Reassessment of the historical seismic activity with major impact on S. Miguel island (Azores). *Natural Hazards and Earth System Sciences* 3, 615-623.

Trota, A. (2008) - *Crustal deformation studies in S. Miguel and Terceira islands (Azores). Volcanic unrest evaluation in Fogo/Congro area (S. Miguel)*. PhD thesis, Azores Univ., 281p.

Wallenstein, N. (1999) – *Estudo da história recente e do comportamento eruptivo do Vulcão do Fogo (S. Miguel, Açores). Avaliação preliminar do "hazard"*. PhD thesis, Azores Univ., 266p.

EARTHQUAKE ARCHAEOLOGY

INQUA PALEOSEISMOLOGY AND ACTIVE TECTONICS

FAULT TECTONICS REGARDING THE NEOTECTONIC PERIOD AND INFLUENCE OF TECTONIC STRUCTURES ON GLACIAL PROCESS IN AREAS OF THICK QUATERNARY COVER

Jolanta Čyžienė

Lithuanian Geological Survey. Konarskio, 35. 03123-Vilnius. LITHUANIA. Email: jolanta.cyziene@lgt.lt

Abstract (Fault tectonics regarding the neotectonic period and influence of tectonic structures on glacial process in areas of thick Quaternary cover): *Through the Quaternary period Lithuania has been covered by continental ice sheets originated in Fennoscandia which corresponds to all glaciations known so far in the Eastern Europe, this causing very complicated structure of the Quaternary cover. This paper discusses the coincidence of outlines of main morphological features with regional tectonic structures and also whether tectonic processes influence on Quaternary development. To understand the tectonic processes influence on Quaternary sediments, neotectonic structures and movements were estimated on the basis of studies of the sub-Quaternary relief, Quaternary succession, modern relief and drainage system. A comparison of sub-Quaternary relief and present surface with tectonic structure and neotectonic activity of studied territories has revealed a frequent coincidence of linear and areal geological and geomorphological objects.*

Key words*: Quaternary, (neo)tectonics, Baltic, palaeoinsicions*

INTRODUCTION

The territory of Lithuania and adjacent areas in the Baltic Sea Region, located in the south-western margin of the East European Craton, could be considered as a region of low seismic activity due to the Early Precambrian crust and distant location to the active tectonic regions. Nevertheless, more than 40 seismic events (historical and instrumental) with a M≤4.5 and intensities up to VI-VII (MSK-64 scale) were reported in the Baltic countries and adjacent territories since year 1616 (Pačėsa, 2007), and two strong earthquakes that took place in the Kaliningrad region on 21 September 2004, the magnitudes being 4.4 and 5.0. Recent seismic activity of Baltic Sea Region often related to glacio-isostatic rebound of the Fennoscandian Shield, but also could be triggered by plate-scale North Atlantic ridge-push forces (Pascal et al., 2010). The territory of Lithuania is one of classical regions with Quaternary cover formed during continental glaciations. The average thickness of Quaternary cover in Lithuania is approximately 130 m and varies from 10-30 m in the northern part of country – the area of prevailing glacial erosion – up to 200-300 m in marginal highlands and the buried valleys or palaeoincisions. The processes of accumulation, erosion during the glaciations and ice-free periods, developed under the influence of neotectonic movements, have created the wide variety of Quaternary sediments and landforms. These processes made great impact creating the present shape of the sub-Quaternary surface and modified tectonic structures. Structural units of the landscape generated by a combination of tectonic activity and climate (morphostructures) often coincide with deep pre-Quaternary structures (Šliaupa, 1998) The coincidence of the faults defined by geophysical and well data to morphotectonic lineaments was considered as strong evidence, determining its "activity" during the glacial and post-glacial times (Šliaupa, 2003). To understand the tectonic processes influence on Quaternary sediments, neotectonic structures and movements were estimated on the basis of studies of the sub-Quaternary relief, Quaternary succession, modern relief and drainage system. This paper presents discussions on the possibilities to detect (neo)tectonic characteristics in the regions with Quaternary cover formed during continental glaciations and assumptions for the morphotectonic evidence.

GEOLOGICAL SETTING

Lithuania is situated within the Baltic sedimentary basin. The sedimentary succession of Lithuania is subdivided into four major structural-sedimentary complexes: Baikalian, Caledonian, Hercynian and Alpine and consists of Upper Vendian to Quaternary sedimentary rocks resting on an Early Proterozoic crystalline basement. The thickness of the sedimentary cover ranges from 0.2 km in the East to 2.3 km in west Lithuania. All of the complexes are separated by unconformities within the sedimentary succession that represents periods of non-deposition and erosion. A set of faults are recognized in the sedimentary cover that are most distinct in the Caledonian complex. The displacements of some reverse faults exceed 200 m in western Lithuania (e.g. Telšiai fault). The oldest traces of the tectonic activity are recorded in the sub-Jotnian rocks that were preserved in a small area in west Lithuania. A limited extensional faulting took place in Vendian and Cambrian times, as it was identified in seismic

profiles in western and central Lithuania. This extensional event(s) is related to the initial stages of establishment of the passive margin due to breaking apart of the Rodinian supercontinent. In western Lithuania these basement blocks were draped by Cambrian rocks, and they are overlain by Vendian deposits in the eastern Lithuania. It was rather quiet during Ordovician and Silurian times, no structuring was documented except some gentle flexuring. The tectonic forces drastically increased in latest Silurian – earliest Devonian times relating to far-field stress transmission generated by Scandian orogeny in Scandinavian Caledonides. The dense family of compressional and transpersional faults was established in western Lithuania, while faulting was only scarce in the eastern half of Lithuania that is accounted to stronger lithosphere and longer distance the stress source. The W-E and WSW-ENE oriented faults show transpressional geometries, whereas the NE-SW striking faults are compressional features (Šliaupa et al., 2002). The morphology of faults is rather variable, ranging from single-plain fault to complex flower structure and terraced fault sets. The faulting associated to formation of local uplifts along the hanging walls of the faults. The Telšiai reverse fault, formed in transpressional regime, is the largest tectonic feature in the sedimentary cover of Lithuania. This fault trends W-E for a few hundred kilometres, it shows variable geometry along the strike that associate with changing abundance and scale of local uplifts. Faults are rather rare in the younger structural complexes where flexures are most common features of tectonic displacement. Structural-sedimentary complexes differ by their geological composition and independently by the structural pattern. Especially high variety of genesis and lithological composition of the Quaternary deposits is reflected in drastic changes both in vertical and lateral distribution of Quaternary sediments. Surface formations and geomorphological features in a large part of Lithuanian territory were formed during the Late Nemunas (Late Weichselian) Glaciation.

ASSUMPTION FOR THE MORPHOTECTONIC EVIDENCE

The studies focusing on mutual relationships between glacial landforms and tectonic structures in areas glaciated in the Pleistocene usually take into account two aspects. The first one concerns the influence exerted by pre-glacial tectonic structures on the behaviour of the ice-sheet, controlling thereby same glacial landforms. One of the issues under consideration is the influence of fault zones reactivated by ice-sheet load upon location and course of subglacial tunnels. The second aspect is related to post-glacial neotectonic movements, the most prominent manifestations of which are tectonically-controlled erosional scarps, either undermining or displacing glacial landforms. Essential question concerns coincidence of outlines of main morphological features with regional tectonic structures and also whether tectonic processes influence on Quaternary development, and in which way.

Neotectonic movements of the Earth's crust are reflected by deformation processes often accompanied by tectonic activity. Number of publications reported that the last deglaciation of northern Fennoscandia was accompanied by a high seismic activity. The earthquakes triggered landslides in glacial till, seismically-induced soft sediment deformation structures, "seismites", are common in trench exposures in the vicinity of the faults in northern Sweden. Deformation of sandy-silty sediments, potentially caused by earthquakes, have also been encountered in central and southern Sweden (e.g., Mörner, 2004), but are less common than in the north. The deglaciation history in Lithuania is longer, but there is so far not recorded and no published evidence of paleoseismic events. It must be pointed out that the late- to postglacial fault scarps identified in northern Sweden are all developed in the Precambrian crystalline basement, and mainly in rocks of Proterozoic age. Morphologically prominent faults occur also in the Caledonian bedrock in the mountain range, but so far no recent fault movements along any of these features have been indicated (Lagerback & Sundh, 2008). The geological setting of Lithuania is very different compared to Sweden. The study area is covered entirely by Quaternary sediments of glacial origin (average thickness of sediments is 130 m). Two major types of faults prevail in Lithuania, i.e. the oldest, defined only in the Precambrian crystalline basement and do not dissecting the sedimentary cover and younger that penetrate into the sediments overlying the crystalline basement. In comparison to Sweden, no faults so far have been detected in Quaternary succession. Fault tectonics regarding the neotectonic period in Lithuania, as well as in all Baltic region, is rather subtle problem. It is difficult to determine the influence of tectonic structures on glacial process in the Pleistocene and testing its influence on the process of the mass movements in glaciotectonic and neotectonic young-alpine structures. Tectonic deformations of the sub-Quaternary relief during Neogene-Quaternary or Quaternary period, i.e. a part of a tectonic and denudation factors imprinting the sub-Quaternary surface, are the key problem. Numerous evidences reported from the Baltic Region indicate that steps, elevations and depressions of the sub-Quaternary surface are partly of tectonic nature (Šliaupa & Popov, 1998).

Large-scale landforms and neotectonic movements were investigated in close connection to structural features of the pre-Quaternary and Quaternary deposits. Those movements were predetermined at large by ancient pre-Quaternary tectonic structures showing inherited trends of movements. In Lithuania the commonly used term "neotectonic fault zone" concerns, in fact, mostly a system of linear elements defined by remote sensing, morphometric, and geomorphological-structural investigations. The influence of linear tectonic zones is shown in a sharp change of the composition and structure of the Quaternary cover. Based on available data of geological mapping at scale 1:50 000 (coverage c.a.

48 % of the country), especially from the areas with dense network of boreholes, several factors having morphotectonic implications must be pointed out:

- block structures of Quaternary cover;
- palaeoincisions of pre-Quaternary surface and inside of Quaternary cover;
- linear structures of present topography;
- river valleys (tunnel valleys);
- ravines;
- palaeolacustrine basins and zones of distortions;
- glaciodislocations, rafts of pre-Quaternary rocks;
- intrusions of mineralised water and springs (Čyžienė & Satkūnas, 2008).

DISCUSSION

A particular role belongs to deep palaeoincisions of sub-Quaternary surface and tunnel valleys of present topography. The palaeoincisions are distinct feature of pre-Quaternary surface and particularly are proper for the Baltic Highland reaching even 280 m in depth. Network of especially deep palaeoincisions is determined in the Molėtai Lakeland (north of Vilnius). Genetically palaeoincisions of pre-Quaternary surface are analogous to the tunnel valleys, which were formed during subglacial erosion by meltwater under the glaciodynamic pressure. In the cases of clear correspondence of palaeoincisions with tunnel valleys, their morphotectonic implication could be concluded (Čyžienė & Satkūnas, 2008). However, reliable determination of spatial form and presence of network of palaeoincisions requires very dense network of boreholes and is dependent on ways of interpretation and interpolation of topography of pre-Quaternary surface (e.g. Šliaupa et al., 1999). Therefore, different patterns of forms and networks of palaeoincisions are presented by different researchers.

The problem of the genesis of palaeoincisions of sub-Quaternary surface in Lithuania is of great practical importance. The genesis of these particular forms is discussed taking into account all factors that could influence the formation of palaeoincisions in the environment of continental glaciations. Analysis of palaeohydrography during the interglacial periods shows that basis of erosion could not be the reason for incision of river valley 100-120 m below the present sea level. The basis of fluvial erosion at the end of the Neogene-beginning of the Quaternary most probably was not lower than 50-60 m above the present sea level and this could not affect incision or river valleys deeper than +50 m (Satkūnas, 2000). Bottom of deepest palaeoincisions of Vilnius environs occur at an altitude of 10-56 m below the present sea level. According to the age of tills, occurring in vicinities of the studied palaeoincisions, these forms have been formed during the Dainava (Elsterian) and Žemaitija (Saalian) glaciations. The lithology and rhythmic structure of the material filling the palaeoincisions show that they have been formed as a consequence of subglacial erosion under glacial pressure. Morphological similarity of palaeoincisions and ravines of present topography indicated the same origin of both these forms. The ravine Tapeliai (10 km north-east of Vilnius) was studied, using special borehole data. Sand and gravel (total thickness 44 m) filling the ravine has a rhythmic structure characteristic of the palaeoincisions of sub-Quaternary surface. This property also shows the general similarity of ravines of present topography and palaeoincisions (Satkūnas, 2008).

Tunnel valleys of present topography are revealed on the geomorphological map (Guobytė, 2000) and their good correspondence with photo-lineaments are concluded (Guobytė, 1995). Besides that, the tunnel valleys in most cases are interpreted as neotectonically active linear zones (Šliaupa, 2005). The coincidence of palaeoincisions and the tunnel valleys in many cases still has to be confirmed by boreholes, which are generally absent in the tunnel valleys. Therefore, due to lack to the direct data the palaeoincisions in places seems hardly correlating with tunnel valleys (Čyžienė & Satkūnas, 2008). On the other hand, it still remains underestimated presence of paleoincisions that do not reach the surface of pre-Quaternary rocks.

A comparison of sub-Quaternary relief and present surface with tectonic structure and neotectonic activity of territories has revealed a frequent coincidence of linear and areal geological and geomorphological objects.

Acknowledgements: Thanks to the Marie Curie Programme „Transfer of Knowledge“ in the Sixth Framework Programme for the support of the project "Morphotectonic Map of European Lowland Area”.

References

Čyžienė, J., Satkūnas, J. (2008). Morphotectonic of Quaternary landforms, examples from Baltic region. *Volume of abstracts of the third conference of MELA project Cartographical approach of the morphotectonic of European lowland area*, 20-23.

Guobytė, R. (1995). Geological mapping of the Molėtai area, 1:50 000. *Geological Report No. 5478, Lithuanian Geological Survey* (*LGT).*

Guobytė, R. (2000). Geomorphological map of Lithuania, 1:200 000. *Geological Report No. 4378, Lithuanian Geological Survey (LGT).*

Lagerbäck, R., Sundh, M. (2008). Early Holocene faulting and paleoseismicity in northern Sweden. *Research Paper C 836, Geological Survey of Sweden*, 80 p.

Mörner, N.-A. (2004). Active faults and paleoseismicity in Fennoscandia, especially Sweden. Primary structures and secondary effects. *Tectonophysics, 380*, 139-157.

Pačėsa, A. (2007). Seismological observation in Lithuania. *Volume of abstracts of the international workshop Seismicity and seismological observations of the Baltic sea region and adjacent territories, September 10-12, 2007, Vilnius, Lithuania, LGT,* 66-69.

Pascal, C., Roberts, D., Gabrielsen, R.H. (2010). Tectonic significance of present-day stress relief phenomena in formerly glaciated regions. *Journal of the Geological Society*, 167, 363-371.

Satkūnas, J. (2000). Formation of palaeoincisions in the environment of continental glaciations: an example of Eastern Lithuania. *Geologija*, 31, 52-65.

Satkūnas, J. (2008). Morphotectonic implication of tunnel valleys in areas with thick Quaternary cover. *Volume of abstracts of the third conference of MELA project*

Cartographical approach of the morphotectonic of European lowland area, 42-45.

Šliaupa, A. (1998). Neotectonic structures of Lithuania and Adjacent Territories. *Litosfera,* 2, 37-46.

Šliaupa, A. (2005). Neotectonic map of Lithuania and adjacent areas, 1:1 000 000. *Evolution of geological environment in Lithuania, Vilnius, Lithuanian Geological Survey, Report, CD*.

Šliaupa, S., Popov, M. (1998). Linkage between Basement and Neotectonic Linear Structures in Lithuania. *Litosfera,* 2, 23-36.

Šliaupa, S. (2002). Kinematic features of the Telšiai fault in Western Lithuania: structural and permeability prognosis.. *Geologija, 38,* 24-30.

Šliaupa, S. (2003). Geodynamic evolution of Baltic sedimentary basin. *Doctoral thesis, Geological Institute, Vilnius*, 207 p.

PLIO – PLEISTOCENE TECTONIC ACTIVITY IN THE SOUTHWEST OF PORTUGAL

Figueiredo, Paula M. (1, 2), Cabral, João (1,2), Rockwell, Thomas K. (3)

(1) IDL, Instituto Dom Luiz, pmfigueiredo@fc.ul.pt
(2) Geology Department, Science Faculty, Lisbon University
(3) Geological Department, San Diego State University

Abstract: *Southwest Portugal, located close to the Eurasia-Núbia plate boundary, is characterized by moderate seismicity, although strong events may occur, as in 1755 (Mw≥8), 1969, (Mw 7.9), and more recently in 2007 (Mw 6.3) and 2009 (Mw 6.1), all located in the offshore. No historical earthquakes with onshore rupture are known for this region. Inland, recent neotectonic and paleoseismological studies corroborate seismogenic activity during the Pleistocene, at the S.Teotónio–Aljezur–Sinceira Fault System, suggesting that these structures are active and are potential sources for moderate seismicity. At the coastline, several features such as old beach sediments, paleo abrasion platforms and paleo cliffs were recognized. A sequence of poorly preserved surfaces with thin deposits may correspond to Pleistocene marine terraces, suggesting a higher uplift rate than expected for this region.*

Key words*: Pleistocene, Uplift, active tectonics, Portugal*

INTRODUCTION

Southwestern Portugal is located close to the Eurasia-Nubia plate boundary, near the Azores-Gibraltar fracture zone. East of the Gloria transform fault, this boundary becomes complex and diffuse, where deformation is distributed across a few hundred kilometres wide zone, related to the NW-SE convergence of Iberia and Nubia at a rate of ca. 4-5 mm/yr. In this area is located the inferred seismogenic source zone of the 1755 earthquake and tsunami (estimated ≥ Mw 8), and also of the Mw 7.9 1969 event. (Zittelini *et al*., 2009).

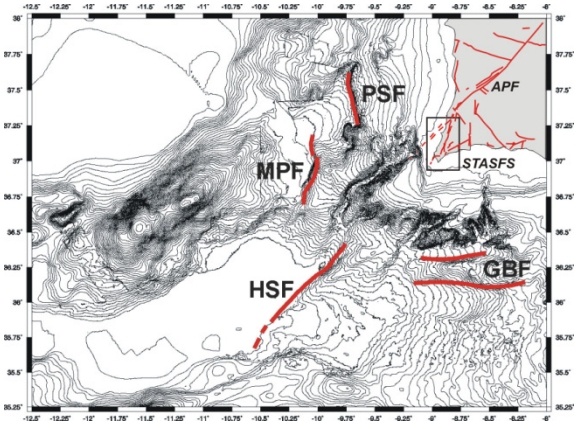

Fig. 1: Main Neotectonic structures located in southwern Portugal. Onshore structures: APF, Alentejo-Placencia Fault; STASFS, São Teotónio-Aljezur-Sinceira Fault System. Offshore Structures: PSF, Pereira de Sousa Fault; MPF, Marquês de Pombal Fault; HSF, Horseshoe Fault; GBF, Guadalquivir Bank Faults.

This seismogenic source zone is characterized by several structures trending NNE-SSW to NE-SW, as the Marquês de Pombal and the Horseshoe faults, and other faults trending close to E-W, such as the Guadalquivir Bank and SWIM faults (Figure 1). To understand and study the recent tectonic activity in this sector of Iberia, it is necessary to study the individual inland structures but also inland deformation evidences that may be related to some of the referred offshore active structures. This abstract depicts both perspectives.

DISCUSSION

The São Teotónio –Aljezur- Sinceira Fault System

The São Teotónio–Aljezur–Sinceira fault system (STASFS) corresponds to the nearest inland brittle structure that may correlate to the ongoing plate boundary deformation in the offshore. It extends NNE-SSW for 50 km, parallel and close to the southwest Portuguese coast (Figure 1), and comprises left-lateral strike-slip faults, deforming a large regional abrasion platform ca. 10 km wide, considered of probable late Miocene age, and which was reoccupied during the Pliocene and the Pleistocene. Four small Cenozoic tectonic basins, filled with Miocene to Pleistocene sediments, occur along the STASFS.

Post-Pliocene vertical displacements of up to 100 m may have occurred related to tectonic activity in the STASFS, but generally these only reach a few tens of meters. Dias (2001) estimated a slip-rate of ca. 0.03-0.06 mm/yr, based on the vertical offset of morphological features. However, as the main slip on these structures is strike-slip, those values are a minimum estimative. Dias (2001), taking into account

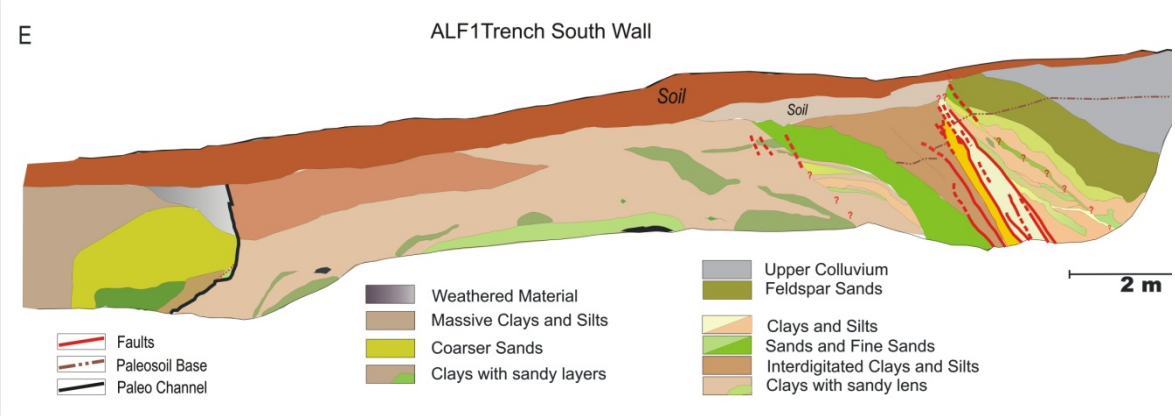

Fig. 2: South wall of trench ALF1, located at the Alfambras basin. Description of geology included in the figure.

the length of the known fault also estimated a maximum magnitude of Mw 7, an average co-seismic displacement of 1 m and a recurrence period of 19210 - 32017 yr, based upon Wells & Coppersmith empirical relationships.

Recently, through detailed geomorphologic and field work studies, several paleoseismic sites were selected. At the Alfambras basin, two trenches were excavated: in the ALF-1 trench (Figure 2), one of the active (?) fault branches was identified, although no paleo-earthquakes were individualized. This fault deforms post-Miocene sediments that may be Pleistocene. OSL samples were collected to better constrain the ages. A paleosoil, probably 700 ka old, is also faulted showing a vertical displacement of ca. 1 m. We saw no deformation within the upper soil units; therefore we could not state an obvious correlation between the fault trace and the topography which would imply a more recent activity. Since no piercing points were identified, no lateral displacement was quantified at this site.

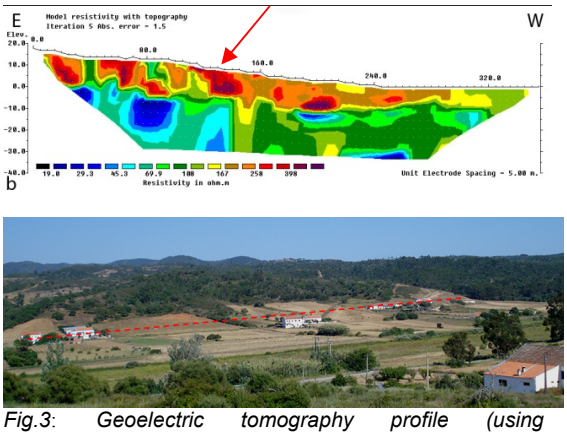

Fig.3: Geoelectric tomography profile (using Schlumberger method) *at Monte Ferreiros site, strong contrast coincides with geomorphologic trace interpreted in the lower image.*

More paleoseismic sites were selected farther north in the Aljezur and Alfambras basins, where geoelectric tomography profiles (Figures 3 & 4) up to 50 m depth were obtained corroborating the existence of several fault traces near the topographic surface.

The Framangola site (at Alfambras basin) is located close to a feature recognized as a shutter ridge and two trenches were opened at the alluvial plain to investigate the Holocene sequence. Unfortunately, the very coarse sediments and the high water table did not allow us to safely investigate this trench site at a deeper level: a thick gravel sequence was recognized as likely to be related to several landslides triggered during the 1755 earthquake based upon archaeological artefacts.

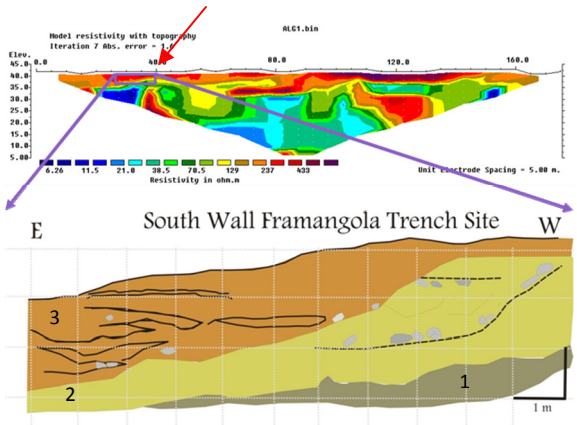

Fig.4. Geoelectric tomography profile (using Schlumberger method) *at Framangola site at the alluvial plain, strongest contrast coincides with previously identified fault trace; the trench units identified also correlate with the tomography (1) Clays and fine silts; (2) Very coarse Gravel (3) Silty sandy & fine conglomerate*

At its northern end, near São Teotónio, the STASFS joins the Alentejo-Placencia fault (APF), the iberian fault with higher length. In this area the tectonic deformation becomes distributed, suggesting than APF may have several splays along this intersection and it is difficult to scrutinize the relationship between both structures. No Holocene or late Pleistocene deposits were recognized in association with the identified fault segments, which increase the uncertainty concerning the recent activity. Presently it is still not clear whether the STASFS extend to the north of the APF.

Towards the south, at the southern sector of the STASFS, south of the Sinceira basin, the local morphology does not evidence any significant Plio-Pleistocene vertical deformation related with this fault system, and it seems that this fault system may splay into several faults. In fact, several parallel faults occur in the Mesozoic bedrock sediments where limestones dominate. Several karst pits are filled with Plio-Pleistocene sands (Faro-Quarteira sands) mainly at the coastal section Martinhal – Zavial where the STASFS should intersect the coastline. The elongated shape those karst sometimes present, suggested a structural control by a previous structural fabric on the karst development (Dias and Cabral, 2002).

The Coastal region

The southwestern Portuguese littoral is characterized by coastlines with two distinct morphologies: one trending N-S, presenting high cliffs in Paleozoic schists and greywackes that reach up to 100 m height, with several overhanging fluvial valleys and a narrow abrasion platform, and another trending E-W, formed mainly in Mesozoic limestones, forming an irregular and lower coastline, with karst wells filled with Plio-Pleistocene sands (generally of the Faro-Quarteira Sands regional stratigraphic unit) as referred above.

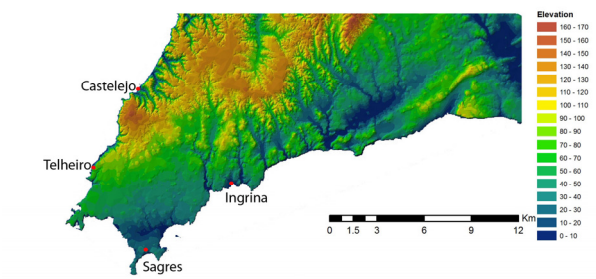

Fig.5 Digital Terrain Model of the Sagres region, southwest STASFS showing the location of sites referred in the text.

Fig. 6 Pleistocene beach sediments resting over a poorly preserved abrasion surface cut on Triassic sediments at 65-76 m height at Telheiro (adapted from Dias, 2001). Beach sands overlie a basal pebbly deposit. At the top of the sequence occur several eolionites apparently with distinct paleosoils, suggesting several eolic sedimentation events.

Detailed field surveys were conducted in both coastlines in order to recognize paleo shore-line features and beach deposits in a wide raised abrasion platform considered late Miocene in age and reoccupied during Pliocene and Pleistocene times (figure 5).

The highest beach sediments we were able to identify are at Fonte Santa, circa 350 m elevation, and underlying aeolionites considered to be Pliocene.

In the western coast, north of Sagres, where the cliffs are very abrupt and the drainage is strongly incised, we recognized a raised beach consisting of a coarse, pebbly layer underlying beach sands at 76 m height (Figures 5 & 6). Two samples of sand were collected for OSL dating. The basal unconformity surface apparently dips gently southwards (~2º).

Further to the north, at the Castelejo beach (Figure 5 & 7), we identify an aeolionite with several paleosoils and colluviums that overlies a marine abrasion platform on Palaeozoic schists circa 2 m elevation, almost coincident with the modern one. We collected OSL samples at the base of this sequence with a resulting age of ca.64 ka. Underlying the aeolionite and overlying the abrasion platform two conglomerate beach deposits with a thin beach sand layer between them were identified and OSL samples were collected. We interpreted this to represent aeolian deposition during MIS 4, when sea level was lowered to expose the offshore sandy marine sediments, and the underlying platform to be the late stage 5 (MIS 5a) marine terrace. Correlative sediments were also identified further to the north, at Amoreira beach.

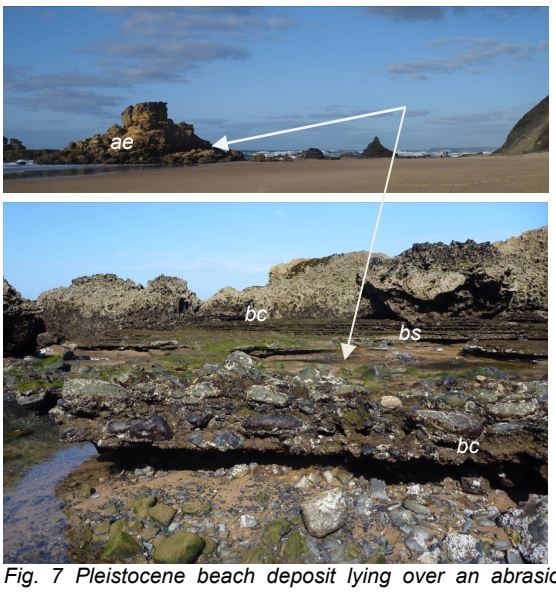

Fig. 7 Pleistocene beach deposit lying over an abrasion platform cut on Carboniferous schists, at 2 m height (bc - beach conglomerate; bs – beach sand). Above this deposit outcrops a sequence of strongly carbonate cemented eolianites, likely to be MIS 4 (ae).

At the E-W trending southern coast, detailed geomorphologic studies combined with field survey and paleosoils characterization, suggest that the culminant abrasion platform, which is well preserved near Sagres, dipping gently to the Southeast, may

actually correspond to a sequence of closely spaced, poorly preserved, middle Pleistocene marine terraces.

A raised abrasion platform cut on Mesozoic limestones, at ~12 m elevation, and the corresponding paleo-cliff were recognized at the Ingrina beach, though no beach sediments were encountered (Figure 8). This raised abrasion platform at Ingrina, probably corresponds to the MIS 5e abrasion surface.

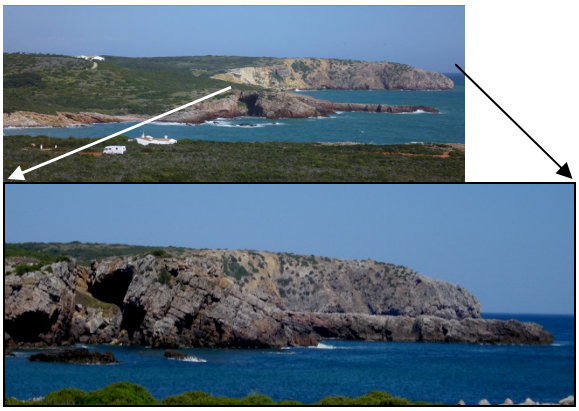

Fig. 8. Pleistocene raised abrasion platform at Ingrina beach, at 12m elevation.

West of Ingrina beach, there is a surface slightly under 50 m height, that probably corresponds to an abrasion surface, with several residual reliefs up to 5 m high. This surface is overlain by a thin clayey sand deposit, which is generally covered by abundant rounded quartz pebbles, thus suggesting that the surface may correspond to a marine terrace at 45-50 m. Samples were collected for OSL dating. A poorly preserved surface around 60-65 m may correspond to the surface identified at Telheiro, but no beach sediments were recognized.

All these surfaces are covered by several eolianite bodies, likely to have been reactivated trough time.

CONCLUSIONS

Trenches excavated across the São Teotónio–Aljezur–Sinceira fault system (STASFS), which extends NNE-SSW for 50 km parallel to the southwest Portuguese coast, exposed faulted alluvium that is inset below the regional marine abrasion surface. Sparse age control based on paleosol development, along with the geomorphic position of these alluvial terrace deposits relative to the marine deposits, suggests that this faulting occurred in the middle to late Pleistocene timeframe, although we have yet to find evidence of Holocene activity.

We mapped a raised abrasion platform at an elevation of ~75 m near Sagres, which dips gently to the SE and may represent part of a sequence of poorly expressed, early to middle Pleistocene terraces. OSL samples and marine shells were collected for dating at Telheiro, where beach deposits are present at 76 m elevation. In the same region at Castelejo, we dated an aeolionite that directly overlies a marine abrasion platform at 2 m elevation, with a resulting age of ca. 64 ka. We interpreted this to represent aeolian deposition during MIS 4, when sea level was lowered to expose the offshore sandy marine sediments, and the underlying platform to be the late stage 5 (MIS 5a) marine terrace.

The 12 m terrace at Ingrina, cut across carbonate rocks, probably corresponds to the MIS 5e abrasion surface. If this uplift rate is applicable for the entire Quaternary, this implies a late Miocene to Pliocene age of the aeolionites and marine deposits at Fonte Santa, which lie at an elevation of nearly 350 m. These observations imply a long-term uplift rate of about 0.06 mm/yr.

These are still preliminary results, to confirm with further studies.

We attribute the observed deformations to the continued NW-SE 4 to 5 mm/yr convergence of Iberia and Nubia, with the STASFS accommodating some of the ongoing plate boundary activity.

Acknowledgements : This work was funded by Fundação da Ciência e Tecnologia, through a PhD scholarship (SFRH/BD/36892/2007) and Research Project "Paleoseismological study of active faults in Mainland Portugal" (PTDC/CTE-GIN/66283/2006), co-financed by FEDER.

References

Cabral, J. (1995). Neotectónica em Portugal Continental, Mem. Nº31, *Inst.Geol.Min.*, 265 p.

Carrilho, F. (2005). *Estudo da Sismicidade do Sudoeste de Portugal Continental*, Diss. Mestrado, Dep.Fisica, Univ. Lisboa, 172 p.

Dias, R. (2001). *Neotectónica da Região do Algarve*, Dissertação de Doutoramento, Univ. Lisboa, 369 p.

Dias, R. P., Cabral, J. (2002): Interpretation of recent structures in an area of cryptokarst evolution - neotectonic versus subsidence genesis. *Geodinamica Acta*, 15 (4), 233-248.

Manuppella, G. (Coord.) (1992) - Carta Geológica da Região do Algarve, escala 1/100 000., Serviços Geológicos de Portugal.

Wells, D., Coppersmith, K. (1994). New empirical relationships among magnitude, rupture length, rupture width, rupture area and surface displacement. Bulletin of the Seismological Society of America, Vol.84 (4), 974-1002.

Zitellini N., Gracia E., Matias L., Terrinha P., Abreu M.A., DeAlteriis G., Henriet J.P., Danobeitia J.J., Masson D.G., Mulder T., Ramella R., Somoza L., Diez S. (2009) - The quest for the Africa–Eurasia plate boundary west of the Strait of Gibraltar, *Earth and Planetary Science Letters Vol.280, 1-4*, 15 April 2009, 13-50.

EARTHQUAKE ARCHAEOLOGY

INQUA PALEOSEISMOLOGY AND ACTIVE TECTONICS

GEODETIC EVIDENCE OF THE CONTROL OF A MAJOR INACTIVE TECTONIC BOUNDARY ON THE CONTEMPORARY DEFORMATION FIELD OF ATHENS (GREECE)

Michael Foumelis (1), Ioannis Fountoulis (2), Ioannis D. Papanikolaou (3, 4), Dimitrios Papanikolaou (2)

(1) Department of Geography, Harokopio University of Athens, 70 El. Venizelou Str., Kallithea, 176 71, Athens, Greece, Email: mfoumelis@hua.gr
(2) Department of Dynamics Tectonics & Applied Geology, Faculty of Geology and Geoenvironment, National and Kapodistrian University of Athens, Panepistimioupolis, Ilissia, 157 84, Athens, Greece
(3) Laboratory of Mineralogy & Geology, Department of Geological Sciences and Atmospheric Environment, Agricultural University of Athens, 75 Iera Odos Str., 118 55, Athens, Greece
(4) AON Benfield UCL Hazard Research Centre, Department of Earth Sciences, University College London, WC 1E 6BT, London, UK

Abstract (Geodetic evidence for control of a major inactive tectonic boundary on contemporary deformation field of Athens (Greece)): *A GPS-derived velocity field from a dense geodetic network established in the broader area of Athens is presented, whereas local variations of strain rates across a major inactive tectonic boundary separating metamorphic and non-metamorphic geotectonic units are also highlighted. An apparent differentiation of the eastern part of Athens plain with negligible deformation rates, from the western part where relatively higher strain rates are observed, indicate its control of the above mentioned boundary on the contemporary deformation field of the region. These findings are in agreement with previous geological observations, however, due to the dense local GPS network it was fatherly possible to localize and quantify the effect of such a major inherited tectonic feature on the deformation pattern of the area.*

Key words*: GPS velocities, strain rates, tectonics, Athens Basin*

INTRODUCTION

Detailed instrumental observations of the tectonic movements in Athens Basin by geodetic or other methods are absent. The contribution of previous geodetic GPS studies to examine the kinematic field of Attica are limited to observations from regional networks, designed to monitor large-scale rather than local tectonic movements (Clarke et al., 1998; Veis et al., 2003). With a limited number of stations within the region, a general picture of the motion is gained, while changes within are hardly addressed.

In the present study a comprehensive GPS-derived velocity field for the broader area of Athens is presented. Variations of strain rates across a major tectonic boundary occurring in the region are highlighted and implication on the contemporary kinematics and dynamics of the region are discussed.

GEOLOGICAL SETTING

The Athens basement belongs to alpine formations outcropping in the mountains and the hills of the area. Recent post-alpine sediments (syn-rift deposits) often cover the slopes of the mountains as well as areas of low altitude.

The area presents a complex alpine structure comprising mainly by Mesozoic metamorphic rocks of Attica geotectonic unit, occurring at Pendeli and Hymmetus mountains and Mesozoic non-metamorphic rocks of the Eastern Greece geotectonic unit, occurring at Parnitha, Poikilo and Aegaleo mountains. The boundary between the metamorphic and non-metamorphic geotectonic units, although generally accepted to be of tectonic origin, its exact geometric and kinematic characteristics are yet to be determined, since no direct geological mapping could be undertaken. The entire tectonic structure within the area is covered by an allochtonous system, called “Athens schists”, tectonically overlaid on the two previously mentioned units, as well as Neogene and Quaternary deposits. It is traced northwards from the Aegean coast of Southern Evia, through Aliveri to Kalamos in northeast Attica and continues to the southwest into the plain of Athens. Within the area of interest its locations coincide approximately with the riverbed of Kifissos R. (Papanikolaou et al., 1999; Mariolakos & Fountoulis, 2000; Xypolias et al., 2003) (Fig. 1), also confirmed by geophysical investigations at the northern part of the basin (Papadopoulos et al., 2007). Results of seismic tomography indicate the presence of abnormally high seismic velocities in the central part of the basin, most likely related to this major boundary, extending towards the southeast at Saronikos Gulf (Drakatos et al. 2005).

According to Papanikolaou & Royden (2007) this boundary represents a broad extensional detachment with significant portion of dextral shear, whereas opinions of a right-lateral strike slip fault zone have also been reported (Mariolakos & Fountoulis, 2000; Krohe et al. 2009). Considering a depth of about 30 km for the metamorphics (Lozios, 1993), it is clear that this tectonic boundary has accommodated more

than 25 km of displacement. It was active throughout Late Miocene times and gradually became inactive during Early Pliocene (Papanikolaou & Royden, 2007). However, it forms a major boundary that separates the E-W trending higher slip-rate active faults in the western part of Attica from the NW-SE trending lower slip-rate faults in the eastern part (Mariolakos & Papanikolaou, 1987; Papanikolaou et al. 2004).

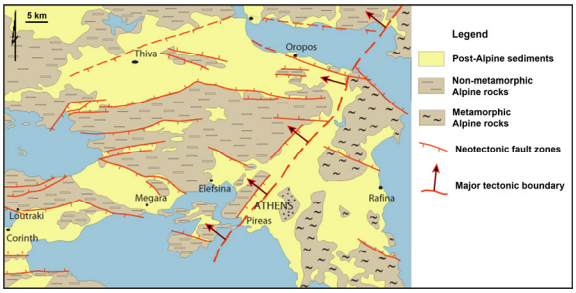

Fig. 1: Simplified neotectonic map of Attica showing the approximate location of the major tectonic boundary separating metamorphic and non-metamorphic alpine rocks (modified from Papanikolaou et al. 1999).

GPS NETWORK ESTABLISHMENT

Given the lack of previous instrumental observations, the design of the geodetic network was primarily focused on the investigation of the local tectonic regime. The minimum number of survey points required is imposed by the tectonic complexity of the region and the degree of fragmentation of the crust.

The established Athens Geodetic Network (AGNET) consisted of a total number of 41 campaign GPS sites (Fig. 2) including already available benchmarks of the Hellenic Military Geographical Service (HMGS), as well as sites previously installed by the Hellenic Mapping and Cadastral Organization (HEMCO) and the National Technical University of Athens (NTUA). Continuous (real-time) GPS station operate in the region by Metrica company (MET0), National Observatory of Athens (NOA1) and National & Kapodistrian University of Athens (UOA1), and despite their relatively limited observations at the time, they where considered in the analysis as well. The network covers essentially both the basins of Athens and Thriassio as well as their bordering mountain ranges, showing a relatively uniform spatial distribution. With an average distance between stations of approximately 5 km, a sufficient sampling of local deformation field is accomplished.

GPS MEASUREMENTS AND ANALYSIS

GPS campaigns were carried out from 2005 to 2008 (3.2 yr) following an annual re-occupation strategy. The benchmarks of the HMGS were first measured during network establishment and together with selected GPS sites once more on 2008. Measurements were conducted using LEICA geodetic GPS receivers equipped with SR299/399, AT202/302 and Ach1202Pro antennas. Carrier phase observations were recorded every 10 seconds from each station for a period of at least four hours. In an effort to achieve optimal results, selected stations were occupied for several days per epoch (independent sessions). To avoid large tropospheric errors an initial elevation cut-off angle of 10° was used.

Collected data were processed using Leica Geo Office v.1.1 and Bernese ver. 4.2 (Beutler et al., 2001). The realization of the reference frame was performed using the coordinates and velocity of Dionysos (DION) continuous GPS station, located on the metamorphic alpine basement. DION was tied to the ITRF2000 at epoch 2005.0 by almost a decade of observations from numerous sites of the EUREF permanent network (Prof. D. Paradissis, personal communication). It can be argued that connecting the local network to the ITRF through DION reference station would be sufficient, taking into account the network extend. Details on data collection and processing could be found in Foumelis (2009).

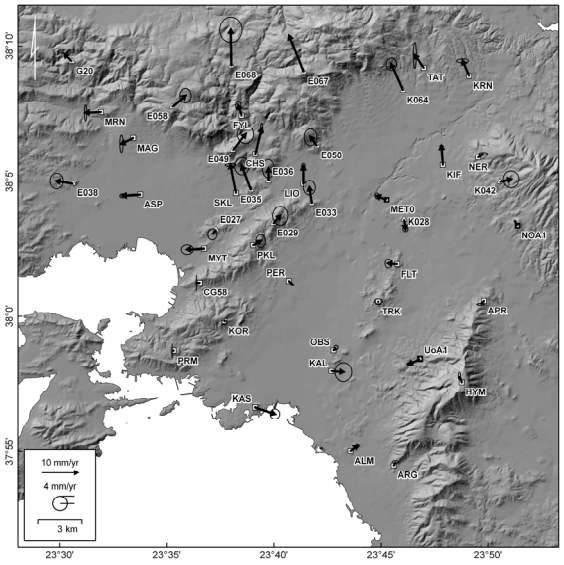

Fig. 2: Annual GPS velocities of broader Athens area, relative to DION, for the period 2005-2008. The error ellipses represent the 1-sigma confidence region. Velocities of E067 and G20 benchmarks from Veis et al. (2003), and NOA1 from the EUREF website, after transformation to the specific ITRF.

Repeated campaign observations allow the determination of the displacement vector as a function of time. The estimation of velocities and the corresponding errors was carried out on a statistical basis, by analysis of time series of each individual component of motion, by least square adjustment. Uncertainties were determined using the average scatter of residuals of the linear regression, providing more realistic error estimates. The estimated GPS velocity field is presented in a local DION-fixed reference frame in order to allow the recognition of local scale displacement patterns (Fig. 2). Site velocities from previous geodetic studies (E067 & G20) as well as EUREF solutions (NOA1) were also considered for the sake of completeness.

STRAIN RATES

In order to provide results independent from the choice of the reference frame, strain analysis was performed by the *grid_strain* Matlab™ software package (Teza et al., 2008). It allows the definition of the deformation pattern by providing the intensity and direction of principal components of strain tensor together with corresponding errors, by means of a modified linear least-squares (LS) inversion, under the hypothesis of uniform strain field condition. Inputs for calculating strain were horizontal GPS annual velocities and their corresponding errors. In this sense results express the linear strain rates in the region.

For the purpose of the analysis, GPS sites located on the mountains bordering the Athens Basin, specifically on the metamorphic basement of Pendeli and Hymettus mountains to the East (APR, ARG, HYM, NER and TAT) and on the non-metamorphic formations of eastern Parnitha Mt. and Aegaleo Mt. (E067, CHS, KOR, PKL and PRM) were selected. The analysis involved initially the calculation of a single strain tensor based on all selected stations and then, by gradual segmentation of the area for a more detailed investigation of spatial variations of the deformation regime. All calculations are referred to the center of mass of each set of sites considered.

From single strain tensor calculations, an extension of 0.27 ±0.06 μstrain/yr along a NNW–SSE direction (N 347°) is shown, with a negative eigenvalue (compression) for the minimum principal axes (Fig. 3). It is nevertheless evident that a single strain tensor is insufficient to express adequately the apparent heterogeneity of the local displacement field. Further examination of the strain field (Fig. 4) indicate negligible compressional rates at the southern part of the basin compared to the dominant extensional regime of relatively higher strain rates (0.91 ±0.09 μstrain/yr) at the northern part between Pendeli and Parnitha ranges.

A more detailed consideration of the strain field between the two geotectonic units was performed by triangulation of the selected GPS sites (Fig. 5). Herein, it is interesting to note the major differentiation between the western and the eastern parts of Athens Basin with significantly lower strain rates in the latter. Moreover, the gradual increase of the extension rates at the western part of Athens plain moving to the North is clearly depicted, while a counterclockwise rotation of the maximum principle axis of the strain tensor is also observed. The compressional regime at the southeastern part of the basin should be underlined.

DISCUSSIONS

The stress field in the region is characterized by extension in a NNE–SSW direction, also confirmed by regional geodetic measurements (Veis et al., 2003). However, the 5-km spacing of the geodetic network allowed investigating local variations of the strain rates.

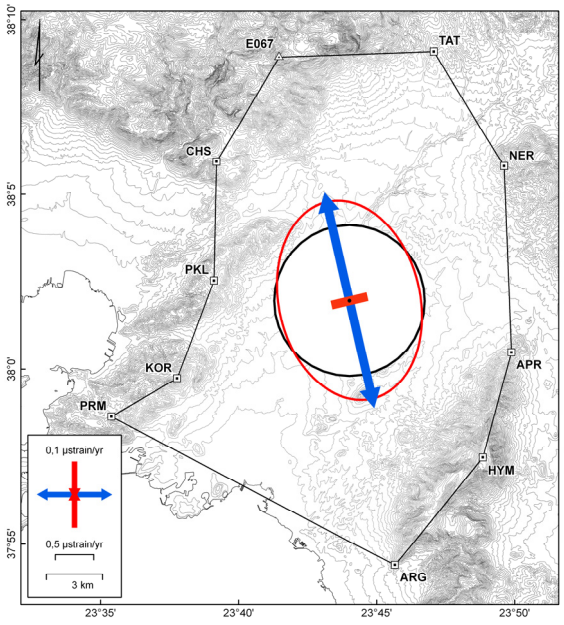

Fig. 3: Principle axes of the strain rate tensor for the area of interest, calculated from velocities of selected GPS sites, in background contour lines of 20m interval.

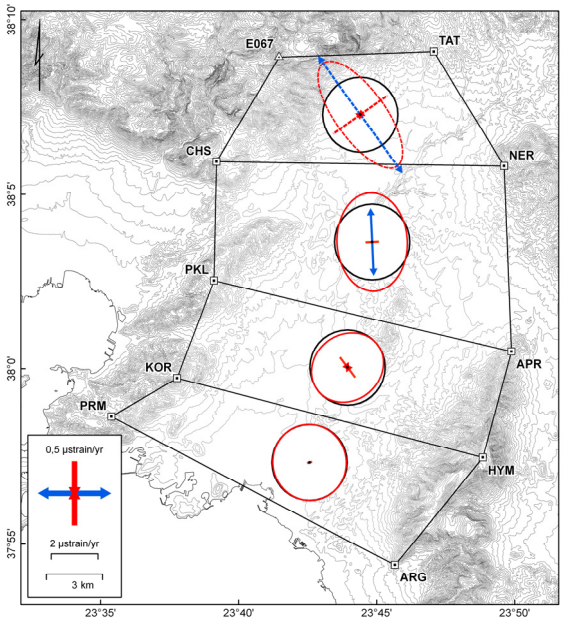

Fig. 4: Principle axes of the strain rate tensors within Athens Basin. Dashed lines indicate local estimates around which GPS data are poorly distributed from a geometrical point of view.

A differentiation of strain rates across the inactive tectonic boundary is evident with significantly higher rates at the western part of Athens Basin. Given its inactive characteristics, a passive control should be considered. Such behavior has also been mentioned during the Athens 1999 earthquake from SAR interferometric observations of the spatial expansion of the co- and post-seismic displacement field (Foumelis et al., 2009).

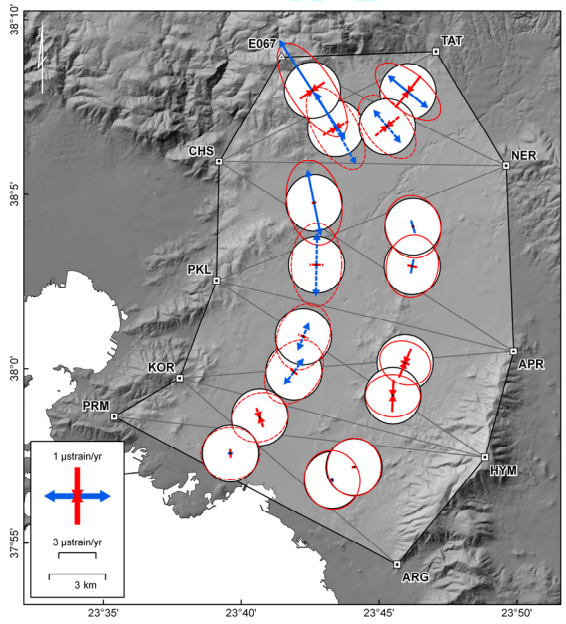

Fig. 5: Detailed strain analysis by different triangulations of selected GPS sites. Principle axes of the strain rate tensors are calculated at the center of mass of each triangle.

The broader area is essentially a transitional zone between the Corinth Gulf and Beotia to the west, characterized by E-W trending active faults with significant seismic activity and those of southern Attica and Cyclades islands to the east, showing low deformation rates (Mariolakos & Papanikolaou, 1987; Papanicolaou & Lozios, 1990). Thus, the observed high strain rates at the northern part of the basin should be attributed to the high crustal velocities observed within Parnitha Mt. an area controlled mainly by E-W trending active fault zones (Ganas et al. 2005; Papanikolaou & Papanikolaou, 2007) although the role of NE-SW trending faults should be important as well (Mariolakos & Fountoulis, 2000).

Acknowledgements: The authors would like to acknowledge Prof. E. Lagios for his support and supervision during GPS measurements, Prof. D. Paradissis for his suggestions, Dr. V. Sakkas for processing of UOA1 data and METRICA company for MET0 station data provision.

References

Beutler, G., H. Bock, E. Brockmann, R. Dach, P. Fridez, W. Gurtner, U. Hugenntobler, D. Ineichen, J. Johnson, M. Meindl, L. Mervart, M. Rothacher, S. Schaer, T. Springer & R. Weber, (2001). Bernese GPS Software Version 4.2. U. Hugentobler, S. Schaer & P. Fridez (eds.), Astronomical Institute, University of Berne, Switzerland, 515p.

Clark, P.J., R.R. Davies, P.C. England, B. Parsons, H. Billiris, D. Paradissis, G. Veis, P.A. Cross, P.H. Denys, V. Ashkenazi, R. Bingley, H.-G. Kahle, M.V. Müller, & P. Briole, (1998). Crustal strain in central Greece from repeated GPS measurements in the interval 1989-1997. *Geophysical Journal International* 135 (1), 195-214.

Drakatos, G., V. Karastathis, J. Makris, J. Papoulia & G. Stavrakakis, (2005). 3D crustal structure in the neotectonic basin of the Gulf of Saronikos (Greece). *Tectonophysics* 400, 55-65.

Foumelis, M., (2009). Study of crustal deformation in the broader area of Athens by means of Differential GPS and SAR Interferometry. Dissertation thesis, Department of Geology and Geoenvironment, University of Athens, 358p (in Greek).

Foumelis, M., I. Parcharidis, E. Lagios & N. Voulgaris, (2009). Evolution of post-seismic ground deformation of Athens 1999 earthquake observed by SAR interferometry. *Journal of Applied Geophysics* 69, 16-23.

Ganas, A., S. Pavlides & V. Karastathis, (2005). DEM-based morphometry of range-front escarpments in Attica, central Greece and its relation to fault slip rates. Geomorphology 65, 301-319.

Krohe, A., E. Mposkos, A. Diamantopoulos & G. Kaouras, (2009). Formation of basins and mountain ranges in Attica (Greece): The role of Miocene to recent low-angle normal detachment faults. *Earth-Science Reviews* 98 (1-2), 81-104.

Lozios, S., (1993). Tectonic analyisis of the metamorphic rocks in NE Attica (in Greek). Dissertation thesis, Department of Geology, University of Athens, 299p (in Greek).

Mariolakos, I. & I. Fountoulis, (2000). The Athens earthquake September 7, 1999 neotectonic regime and geodynamic phenomena. *Ann. Geol. Pays Hellen.* 38 (B), 165-174.

Mariolakos, I. & D. Papanikolaou, (1987). Deformation pattern and relation between deformation and seismicity in the Hellenic Arc. *Bull. Geol. Soc. Greece* 19, 59-76 (in Greek).

Papadopoulos T.D., N. Goulty, N.S. Voulgaris, J.D. Alexopoulos, I. Fountoulis, P. Kambouris, V. Karastathis, C. Peirce, S. Chailas, J. Kassaras, M. Pirli, G. Goumas & E. Lagios, (2007). Tectonic structure of Central-Western Attica (Greece) based on geophysical investigations - Preliminary Results. *Bull. Geol. Soc. Greece* 40 (3), 1207-1218.

Papanikolaou, D., E. Bassi, H. Kranis & G. Danamos, (2004). Paleogeographic evolution of the Athens basin from upper Miocene to Present. *Bull. Geol. Soc. Greece* 36 (2), 816-825 (in Greek).

Papanikolaou, D., E. Lekkas, Ch. Sideris, I. Fountoulis, G. Danamos, Ch. Kranis, S. Lozios, I. Antoniou, E. Vassilakis, S. Vasilopoulou, P. Nomikou, I. Papanikolaou, E. Skourtsos & K. Soukis, (1999). Geology and tectonics of Western Attica in relation to the 7-9-99 earthquake. Newsletter of E.C.P.F.E., issue no. 3, 30-34.

Papanikolaou, D. & S. Lozios, (1990). Comparative neotectonic structure of high (Korinthia-Beotia) and low rate (Attica-Cyclades) activity. *Bull. Geol. Soc. Greece* 16, 47-65 (in Greek).

Papanikolaou, D. & I. Papanikolaou, (2007). Geological, geomorphological and tectonic structure of NE Attica and seismic hazard implications for the northern edge of Athens plain. *Bull. Geol. Soc. Greece* 40 (1), 425-438.

Papanikolaou, D. & L. Royden, (2007). Disruption of the Hellenic Arc: Late Miocene extensional detachment faults and steep Pliocene-Quaternary normal faults – or – What happened to Corinth ? *Tectonics* 26, TC5003, doi:10.1029/2006TC002007.

Teza, G., A. Pesci & A. Galgaro, (2008). Grid_strain and grid_strain3: Software packages for strain field computation in 2D and 3D environments. *Computers & Geosciences* 34, 1142-1153.

Xypolias, P., S. Kokkalas & K. Skourlis, (2003). Upward extrusion and subsequent transpression as a possible mechanism for the exhumation of HP/LT rocks in Evia island (Aegean Sea , Greece). *Journal of Geodynamics* 35, 303-332.

Veis et al. (2003). Tectonic displacements along the Aegean and the Alkyonides- Perachora-Parnitha triangle. Applied Research Project, Earthquake Planning and Protection Organization. Athens, 74p (in Greek).

EARTHQUAKE ARCHAEOLOGY

INQUA PALEOSEISMOLOGY AND ACTIVE TECTONICS

NEOTECTONICS AND COMPARISON OF THE ENVIRONMENTAL SEISMIC INTENSITY SCALE (ESI 2007) AND THE TRADITIONAL SCALES FOR EARTHQUAKE INTENSITIES FOR THE KALAMATA (SW GREECE) EARTHQUAKE (MS=6.2R, 13-09-1986)

Fountoulis, Ioannis (1), Mavroulis, Spyridon (1)

(1) National and Kapodistrian University of Athens, Faculty of Geology and Geoenvironment, Department of Dynamic Tectonic and Applied Geology, Panepistimiopoli, Zografou 15784 Athens, GREECE. Email: fountoulis@geol.uoa.gr , smavroulis@yahoo.gr

Abstract: *The Kalamata (13-09-1986, Ms=6.0R, SW Peloponnese) earthquake can be classified as a medium to small scale event based on the tectonic structures that triggered the earthquake and the effects caused on human, structural and natural environment. The aim of this paper is to present the geotectonic and seismotectonic regime of the earthquake affected region based on field data along the seismic fault zone and an attempt is made towards the: (i) estimation of the intensity values according to the European Macroseismic Scale (EMS 1998) and the Environmental Seismic Intensity Scale (ESI 2007) and the determination of their geographical distribution in a macroscale, (ii) interpretation of the intensity values data and their distribution according to the seismotectonic, geodynamic and geotechnical regime, and (iii) conduction of a comparative evaluation review on the application of both EMS 1998 and ESI 2007. The application of both EMS 1998 and ESI 2007 and the comparative evaluation of the results indicate that the estimated values of EMS 1998 and ESI 2007 were almost in agreement, despite the fact that the geographical locations of assessment data were different suggesting that the application and use of both scales appears to represent a useful and reliable tool for seismic hazard estimation.*

Key words*: Kalamata, earthquake, neotectonics, environmental effects*

INTRODUCTION

Kalamata is located very close (< 70km) to the Hellenic (Ionian) Trench region in which the subduction zone of the African plate beneath the European (Aegean) one exists and thus is one of the most seismically active areas of Europe (Figure 1).
On 13 September 1986, a shallow depth (< 10km) earthquake struck the wider Kalamata area resulting in 20 casualties, extensive damages and many environmental effects. The epicenter of the main earthquake was located about 10km NNE of the city of Kalamata, and its magnitude was Ms=6.2 (Papazachos, et al., 1988). Two days later, a second shock of Ms=5.4R (Papazachos, et al., 1988) occurred closer to the Kalamata city at the same depth. The focal mechanism of the main shock shows an E-W extension (Lyon-Caen et al., 1987; Papazachos, et al., 1988).

Seismological studies of Papazachos et al. (1988), and Lyon-Caen et al. (1988) indicated that aftershocks defined two clusters and an about 450 west-dipping fault plane. The foci depths of the seismic sequence were ranging between 11 and 0.9km. Based on the variety of orientations and dips calculated for the sub-faults activated during the aftershock sequence, since the analysis of the northern cluster indicates the existence of two types of orientation, which are dipping in four different angles and the southern cluster is characterized by an almost uniform behaviour activated later in the sequence, Tselentis et al. (1989) concluded that the area is tectonically very complex which is in agreement with the neotectonic structure described by Mariolakos et al. (1989; 1992, 1993) and Mariolakos & Fountoulis (1998).

Stiros and Kontogianni (2008) applied two first-order leveling traverses crossing the wider Kalamata area and measured subsidence of about 7cm NE of the Kalamata city in epicentral area of the southern cluster. The Kalamata earthquake produced a maximum intensity VIII+ on the IMM or EMS 1992 scale (Elnashai et al., 1987; Gazetas et al., 1990), while Panou et al. (2004) based on building damages estimated the intensity up to IX - X for the city of Kalamata.

The aim of this paper is to present the geotectonic and seismotectonic regime of the earthquake affected region based on field data along the seismic fault zone and an attempt is made towards the: (i) estimation of the intensity values in terms of the European Macroseimic Scale (EMS 1998; Grünthal, 1998) and Environmental Seismic Intensity Scale (ESI 2007; Michetti et al., 2007) and the determination of their geographical distribution in a macroscale, (ii) interpretation of the intensity values data and their distribution according to the seismotectonic, geodynamic and geotechnical regime, and (iii) conduction of a comparative evaluation review on the application of both EMS 1998 and ESI 2007.

GEOLOGY - TECTONICS - NEOTECTONICS - FAULT ZONES - FAULTS

In the broader Kalamata area the following four alpine geotectonic units from the lower to the upper occur (Psonis, 1986; Mariolakos et al., 1993): (a) the

Mani unit consisting mainly of marbles, (b) the Arna unit consisting of quartzites and phyllites, (c) the Tripolis unit which consists of neritic carbonates and flysch formation and (d) the Pindos unit consisting of thin-bedded pelagic carbonates and clastic formations. From the structural point of view, the four above-mentioned geotectonic units form a succession of three nappes. The Mani unit (slightly metamorphosed) is considered to be the relatively autochthonous one. The Arna unit overthrusts the Mani unit, the Tripolis unit (second nappe) overthrusts the Arna unit and the Pindos unit (third nappe) overthrusts the Tripolis unit (Figure 2). The Late Pliocene-Early Pleistocene marine deposits consist of marls, sandstone and conglomerates (Marcopoulou-Diacantoni et al. 1989; Mariolakos et al., 1993). The Middle-Late Pleistocene deposits consist mainly of red colored siliceous sands-sandstones and conglomerates. Alluvial deposits, clastic material and talus represent the Holocene.

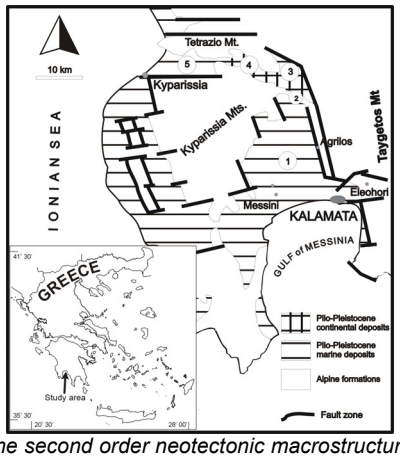

Fig. 1: The second order neotectonic macrostructures within the first order neotectonic macrostructure of the Kalamata-Kyparissia graben. The numbers correspond to the following second order neotectonic macrostructures: 1: Kato Messinia graben, 2: Meligalas horst, 3: Ano Messinia graben, 4: Dorion basin, 5: Kyparissia-Kalo Nero graben

The meizoseismal area is located at the eastern margin of the Kalamata - Kyparissia graben and constitutes the northward prolongation of the Gulf of Messinia (Figure 1). Large and composite fault zones define its margins and second order macrostructures are observed within as well as at the margins representing smaller grabens and horsts (Figure 1) (Mariolakos & Fountoulis, 1998). The E-W striking Dimiova - Perivolakia graben is bounded by the Kato Karveli - Venitsa fault zone to the north, by the Arahova to the east, by the Xerilas fault zone (XFZ) to the south and by the Nedon fault zone (NFZ) to the west (Figure 2). This macrostructure constitutes one of the most interesting minor order neotectonic macrostructures because of the occurrence of the Pindos unit. Mariolakos et al. (1989) interpreted the kinematic regime of this macrostructure suggesting that this graben rotates around an N-S axis located at the area of Arahova westwards. At the western part of the fault zone the total throw is more than 2.000m (Mariolakos et al., 1986; Mariolakos et al., 1989). The most of the environmental effects and damages caused during the seismic activity of September 1986 were observed within this graben. The marginal fault zones consist of many faults, which are not continuous and differ on strike even when they belong to the same fault zone, as they form conjugate fault systems.

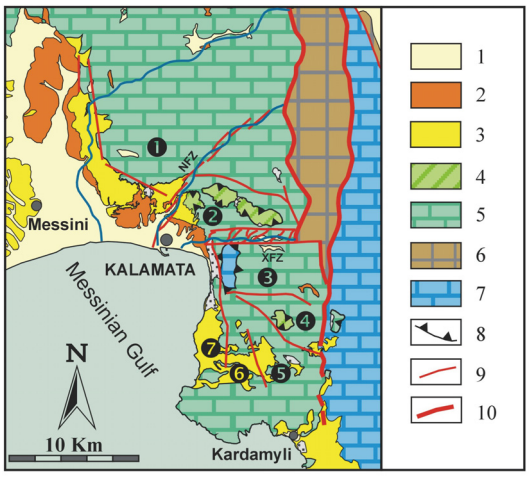

Fig. 2: Simplified geological map showing the four alpine geotectonic units overthrust one on top of the other, as well as the post-alpine sediments of the region of the Kalamata area. 1: Holocene deposits; 2: Continental deposits; 3: Early Pleistocene marine deposits; 4: Pindos unit; 5: Gavrovo-Tripolis unit; 6: Arna unit; 7: Mani unit; 8: Overthrust; 9: Fault; 10: Detachment fault. The numbers in the black circles correspond to the smaller order neotectonic macrostructures of the Kato Messinia sub-graben 1: Asprochoma-Koutalas horst, 2: Dimiova-Perivolakia graben, 3: Kalathion Mt. horst, 4: Altomyra semi-graben, 5: Kambos graben, 6: Vardia-Koka horst, 7: Kitries-Mantinia sub-graben, XFZ:Xerilas Fault zone, NFZ:Nedon Fault Zone.

SPATIAL DISTRIBUTION OF ENVIRONMENTAL EFFECTS

During the above-mentioned seismic activity, fault reactivation (seismic faults), new faulting and seismic fracturing were observed (the latter distinguished by no displacement) (Figure 3). The reactivated faults strike in different directions (N-S, E-W, NNE-SSW) and the throw of the faults due to the reactivation is generally small (max=20cm) and of normal character. The maximum throw has been observed at a seismic fault caused by the main aftershock Ms=5.6 R.

Numerous seismic ruptures trending N-S, NNE-SSW, NE-SW, E-W and NW-SE were mapped in the affected area, in most cases in en echelon arrangement (Mariolakos et al., 1989). These seismic fractures presented a vertical displacement of several mm up to 25-30cm and they often presented a horizontal component showing sinistral or dextral displacement.

The majority of rock falls were observed in several sections along the slopes of the Tzirorema, Karveli and Xerilas streams and the Nedon river valleys as well as in the wider area of Eleochori, Karveli and Ladas villages (Figure 3). They were observed in areas characterized by steep slopes (> 50 per cent) and they were related almost everywhere to small or

large faults with some of them reactivated during the earthquake and others not.

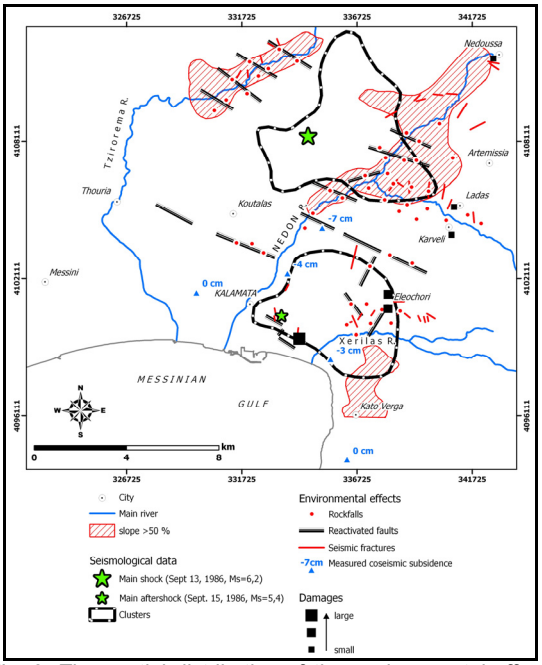

Fig. 3: The spatial distribution of the environmental effects observed during the Kalamata earthquake sequence (based on data from Mariolakos et al., 1992; Gazetas et al., 1990; Fountoulis, 2004; Stiros & Kontogianni, 2008).

SPATIAL DISTRIBUTION OF DAMAGES

The damages were limited to an area of triangular shape, which is defined to the south by the fault zone of the Xerilas River, to the east by the fault zone of Nedousa - Arahova and to the west by the fault zone of the Nedon River (Figure 3). No damages were recorded to the west of the Nedon fault zone and south of the Xerilas fault zone and especially in areas where the geological basement has the same seismo-geological behavior as those in the city of Kalamata and Eleohori village, which caused serious damage. Based on field observations, the damage is not determined only by the age, type, height and other characteristics of buildings. There were cases with two nearly identical constructions in the same area; one remained intact while the other was destroyed. In other cases the building destruction is linked to zones of seismic fracturing that were observed in the construction basement. Of course, this is not the rule. In many other cases the building destruction is linked to zones of seismic fracturing that were observed in the construction basement. Of course, this is not the rule.

CONCLUSIONS

Taking into account the aforementioned we can draw the following conclusions:
The damages were limited to the area that can be regarded as a transitional area between the tectonic basin Kalamata - Kyparissia and the tectonic horsts of Asprohoma - Koutala to the north and the Kalathio Mt. to the south. On the contrary, in Messini and in Verga, damages of that size were not observed because those areas belong to different neotectonic macrosturctures that were not reactivated during the earthquakes of 1986 (central region of the tectonic basin of Kato Messinia and tectonic horst of Kalathio Mt respectively).

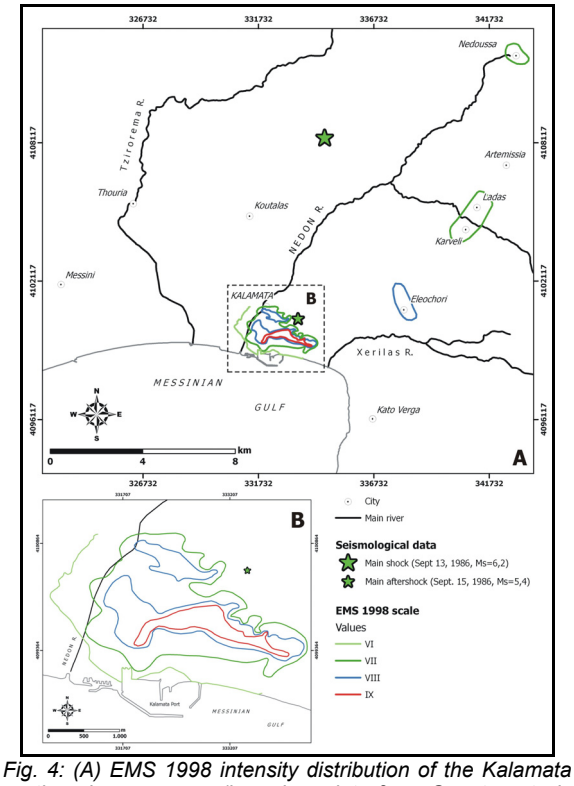

Fig. 4: (A) EMS 1998 intensity distribution of the Kalamata earthquake sequence (based on data from Gazetas et al., 1990; Panou et al., 2004). (B) EMS 1998 intensity distribution of the Kalamata earthquake sequence for Kalamata city (based on data from Panou et al., 2004).

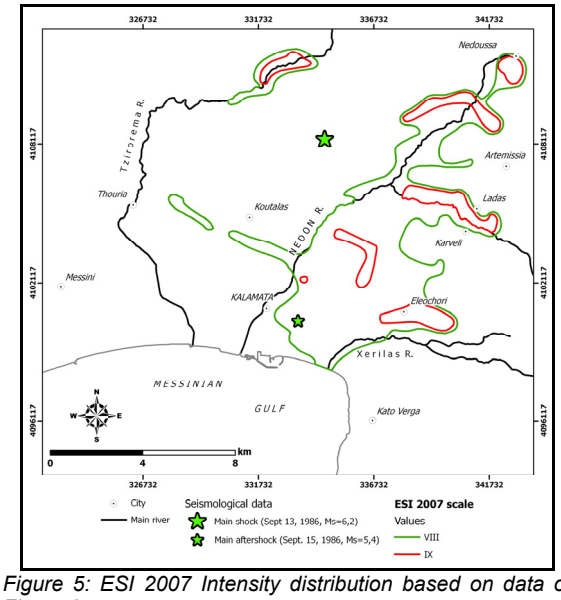

Figure 5: ESI 2007 Intensity distribution based on data of Figure 3.

Rock falls were observed mainly in the tectonic graben that was activated and also north of it, at Tzirorema. On the other hand, on the steep slopes of the Kalathio Mt. that belong to the homonymous

neotectonic macrostructure, which was not reactivated, no rock falls were observed.

An important factor in the distribution of the damages and rock falls in the greater area was the reactivation of old faults or the creation of new soil ruptures. In this way, the fact that the destruction of buildings was observed in Giannitsanika (higher intensity in Figure 4) and not near the coast can be explained, although the foundation ground - red siliceous clastic formation - in the first case theoretically presents better geotechnical characteristics in comparison to the loose coastal deposits.

The ESI 2007 scale appears to fit better than the EMS scale in the neotectonic regime of the area as its boundaries coincide better with the boundaries of the activated graben and the observations we have done concerning the distribution of the environmental effects. The application of both EMS 1998 and ESI 2007 and the comparative evaluation of the results indicate that the estimated values of EMS 1998 and ESI 2007 were almost in agreement, despite the fact that the geographical locations of assessment data were different suggesting that the application and use of both scales appears to represent a useful and reliable tool for seismic hazard estimation.

References

Elnashai, A., Pilakoutas, K., Ambraseys, N. & Lefas, I. (1987). Lessons learnt from the Kalamata (Greece) earthquake of 13 September 1986. *European Earthquake Engineering*, 1, 11-19.

Fountoulis, I. 2004. The neotectonic macrostructures and the geological basement, the main factors controlling the spatial distribution of the damage and geodynamic phenomena resulting from the Kalamata (13 September 1986) and Athens (7 September 1999) earthquakes. *WIT Press: In Earthquake Geodynamics: Seismic Case Studies. Edited by: E. L. Lekkas, Series: Advances in Earthquake Engineering*, vol. 12, p. 45-63.

Gazetas, G., Dakoulas, P. & Papageorgiou, A. (1990). Local soil and source-mechanism effects in the 1986 kalamata (Greece) earthquake. *Earthquake Engineering and Structural Dynamics,* vol. 19, 431-456.

Grünthal, G. 1998. (ed.): European Macroseismic Scale 1998 (EMS-98). Cahiers du Centre Européen de Géodynamique et de Séismologie 15, Centre Européen de Géodynamique et de Séismologie, Luxembourg, 99 pp.

Lyon-Caen, H., Armijo, R., Drakopoulos, J., Baskoutas, J., Delibassis, N., Gaulon, R., Kouskouna, V., Latoussakis, J., Makropoulos, K., Papadimitriou, P., Papanastassiou, D. & Pedotti, G. (1988). The 1986 Kalamata (South Peloponnesus) earthquake: Detailed study of a normal fault, evidences for east-west extension in the Hellenic arc, *J. Geophys. Res.* 93, 14.967–15.000.

Marcopoulou-Diacantoni, A., Mirkou, M.R., Mariolakos, I., Logos, E., Lozios, S. & Fountoulis, I. (1989). Stratigraphic observations in the post alpine deposits in Thouria-Ano Amfia area (Messinia Province, Greece) and their neotectonic interpretation. *Bull. Geol Soc. Greece,* XXIII/3, pp. 275-295, (in Greek).

Mariolakos, I., Sabot, V., Alexopoulos, A., Danamos, G., Lekkas, E., Logos, E., Lozios, S., Mertzanis, A. & Fountoulis, I. (1986). Microzonic study of Kalamata (Geology, Tectonics, Neotectonics, Geomorphology). *Report of EPPO (Earth Planning Protection Organization),* (in Greek).

Mariolakos, I., Fountoulis, I., Logos, E. & Lozios, S. (1989). Surface faulting caused by the Kalamata (Greece) earthquakes (13.9.1986). *Tectonophysics*, 163, pp. 197-203.

Mariolakos, I., Fountoulis, I. & Nassopoulou, S. (1992). The influence of the neotectonic macrostructures, fractures and the geological basement in the distribution of the damages in the Kalamata earthquake (13-9-1986). *Proc. 1st Greek Congress on Antiseismic Engineering and Technical Seismology Technical Chamber of Greece*, 1, pp. 55-68, (in Greek).

Mariolakos, I., Schneider, H., Fountoulis, I. & Vouloumanos, N. (1993). Paleogeography, sedimentation and neotectonic implications at the Kambos depression and Kitries Bay area (Messinia, Peloponnese, Greece). *Bull Geol. Soc. Greece*, XXVIII/1, pp. 397-413, 1993.

Mariolakos, I. & Fountoulis, I. (1998). Is it safe to built on fault surfaces in a seismically active area? *Proc. 8th International IAEG Congress*, pp. 665-670, Balkema.

Michetti A.M., Esposito, E., Guerrieri, L., Porfido, S., Serva, L., Tatevossian, R., Vittori, E., Audemard, F., Azuma, T., Clague, J., Comerci, V., Gürpinar, A., Mccalpin, J., Mohammadioun, B., Mörner, N.A., Ota, Y. & Roghozin, E. (2007). Environmental Seismic Intensity Scale 2007 - ESI 2007. In: Guerrieri L. and Vittori E. (Eds.), Memorie Descrittive della Carta Geologica d'Italia, 74, 7-54, Servizio Geologico d'Italia – Dipartimento Difesa del Suolo, APAT, Roma, Italy.

Panou, A., Theodoulidis, N. & Savvaidis, A. (2004). Correlation between (H/V) ratio and seismic damage: The case of the city of Kalamata. In SESAME project, *Report of the WP04, H/V Technique: Empirical Evaluation, Project* No. EVG1-CT-2000-00026.

Papazachos, V., Kiratzi, A., Karacostas, B., Panagiotopoulos, D., Scordilis, E. & Mountrakis, D. (1988). Surface fault traces, fault plane solution and spatial distribution of the aftershocks of the September 13, 1986 earthquake of Kalamata (Southern Greece). *PAGEOPH,* vol. 126, No. 1, 55-68.

Psonis, K. 1986. Geological map of Greece, Kalamata sheet, scale 1/50,000, Geological Survey of Greece: Athens.

Stiros, S. & Kontogianni, V. (2008). Modelling of the Kalamata (SW Greece) earthquake faulting using geodetic data. *Journal of Applied Geodesy,* 2, 179-185; DOI 10.1515/JAG.2008.020

QUANTIFICATION OF RIVER VALLEY MAJOR DIVERSION IMPACT AT KYLLINI COASTAL AREA (W. PELOPONNESUS, GREECE) WITH REMOTE SENSING TECHNIQUES

Fountoulis Ioannis D. (1), Vassilakis Emmanuel (1), Mavroulis Spyridon (1), Alexopoulos John (2), Erkeki Athanasia (3)

(1) School of Geology and Geoenvironment, Department of Dynamics, Tectonics and Applied Geology, National and Kapodistrian University of Athens, 15784, Greece. Email: evasilak@geol.uoa.gr
(2) School of Geology and Geoenvironment, Department of Geophysics and Geothermy, National and Kapodistrian University of Athens, 15784, Greece.
(3) School of Geology and Geoenvironment, Laboratory of Natural Hazards, National and Kapodistrian University of Athens, 15784, Greece.

Abstract: *The effects of the geological, tectonic and neotectonic structure and the impact of the human presence and activity on the drainage network of Pineios river are presented here in order to determine the causes of its diversion and the implications to the shoreline. We used, analyzed and evaluated (a) geomorphological, geological, tectonic and neotectonic data of the study area, (b) historical information and archaeological findings from buried and eroded archaeological sites of the wider study area, (c) published data related to drill cores and radiocarbon dates, and (d) remote sensing datasets, as satellite and aerial photos of different capturing periods, as well as real-time kinematic differential GPS measurements for the definition of the current shoreline. It is concluded that the detected shoreline displacements and drainage diversions are the result of the combination of active tectonics and human activity during the last 100 kyrs.*

Key words*: Kyllini peninsula, Pineios river, RTK DGPS, river evolution, coastal erosion*

INTRODUCTION

The Pineios River development and history takes place in one of the most tectonically and seismically active areas in Greece. The intense and continuous tectonic activity in the area is highly related to its location on the external part of the Hellenic arc and adjacent to the convergent boundary where African plate is subducted beneath the Aegean as well as the diapirism of near surface evaporitic domes. The highest seismicity levels recorded in the area (Hatzfeld *et al*., 1990) as well as the generation of many historic strong earthquakes confirm the neotectonic observations, which show that the area is undergoing a complicated tectonic deformation.

The most important fault zones in the study area are the Panopoulo fault zone (Panopoulo FZ), Pineios fault zone (Pineios FZ) and the strike - slip fault zone that gave rise to the Andravida earthquake (08-06-2008, ML=6,5). These major faults form several neotectonic blocks in the study area including the Gastouni graben (hangingwall of Pineios fault zone), the uplifted area of Varda (footwall of Pineios fault zone) and the Kyllini horst (Fig. 1).

GEOCHRONOLOGICAL INTERPERETATION

In order to determine the effect of the ongoing active tectonics on the Pineios River diversion during the late 18th or the early 19th century, we calculated relative uplift rates for several sites of the study area based on $^{230}Th/^{238}U$ dating of corals made by Stamatopoulos *et al*. (1988) and dating of marine deposits in Kyllini peninsula estimated by Mariolakos *et al*. (1988):

a. 0,39 mm/yr for Psari area (103 kyrs)
b. 0,50 mm/yr for Neapoli area (118 kyrs)
c. 0,67 mm/yr for Aletreika area (209 kyrs)
d. 0,16 to 0,48 mm/yr for the eastern (inland) part of Kyllini peninsula (125 kyrs)

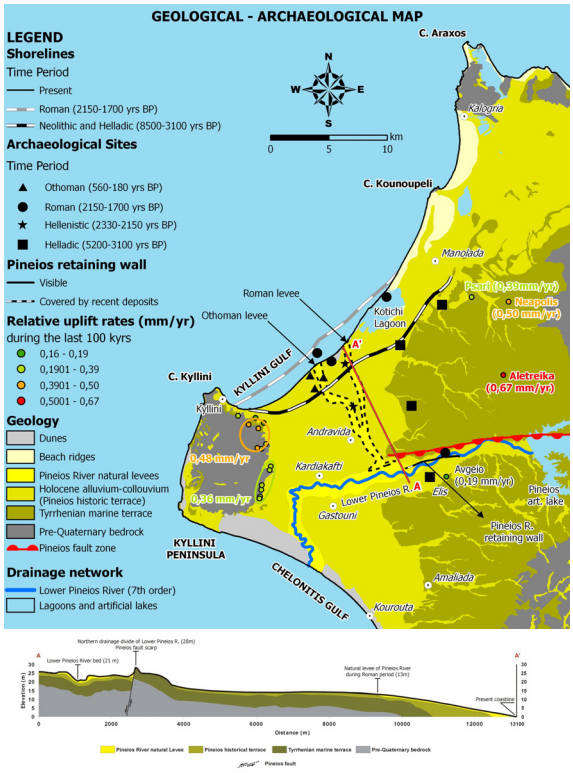

Fig. 1: Sketch map of the contemporary Pineios river deltaic area (at the hanging wall of the Pineios fault) and the former deltaic area at the footwall of the same fault. The estimated shorelines for the Roman and Neolithic periods are shown. The archaeological sites and the sampling sites of the geochronological analysis are also noted, along with the calculated uplift rates for the last 100kyrs.

The general conclusions after the interpretation of the geochronological data are:

a. The maximum relative uplift rate (0,67 mm/yr) characterizes an area (Aletreika) located on the footwall side and very close to the Pineios FZ.
b. The relative uplift rate of the Gastouni graben (hangingwall of Pineios FZ, 0,19 mm/yr) is less even than the lowest value of the Pineios FZ footwall relative uplift rate (0,39 mm/yr).
c. The northeastern part of Kyllini peninsula has higher relative uplift rate (0,48 mm/yr) than the southeastern part (0,30 mm/yr)
d. The maximum relative uplift rate of the footwall of Pineios FZ is significantly higher than the maximum relative rates of the eastern part of Kyllini peninsula and the Gastouni graben.

HISTORICAL COASTLINE DATA

It is more than obvious that the major percentage of the coastline displacements in the study area, during the last 8kyrs, are related to active structures and the tectonic instability as this affects the alongshore redistribution of sediments from the Pineios delta. After the organization of all the available geological and historical data we were able to estimate and reconstruct the paleo-coastline in several periods for the last 100kyrs (Fig. 2). It is quite easy to accept that during Tyrrhenian most of the area of Kyllini was under the water since the marine sediments were deposited.

The palaeo-delta of Pineios River was developed N of Kyllini peninsula before and during Neolithic period. The Neolithic and Helladic shoreline was located 3,5 km onshore from the present shoreline. During the Roman period, Pineios River flowed directly S of the Kotychi lagoon forming a levee, which is now abandoned, eroded and stands as a low sea cliff. An acceleration of coastal deposition and consequently delta propagation took place. The Roman shoreline was 1,5 km seaward from the present shoreline. During the Othoman period, Pineios occupied the channel 5 km S of Kotychi lagoon forming another levee standing well above the floodplain at the shoreline and indicating coastal retreat. This channel is in the process of filling. The minimum age of this levee is about 200 yrs BP.

The Pineios diversion to the south of Kyllini peninsula took place during the late 18th century. Following this diversion, the pre-18th-century-A.D. Pineios River delta shoreline in now undergoing marine transgression and intense coastal erosion, as is to be expected in a former delta now essentially starved of new sediment. The pre-18th-century-A.D. northern channels of Pineios River and few smaller streams can still be seen in their courses to the northwest, now dry. The dominant geomorphic processes in the modern delta of Pineios River are progradation and aggradation with large volumes of river sediment.

Based on the palaeogeographic reconstructions developed by Kraft *et al.* (2005) and the late Holocene environmental changes from Kotychi Lagoon recorded by Kontopoulos and Koutsios (2010) we note that:

a. the shoreline in the Pineios delta advanced by 3,5 km into the sea in the 6.350 yrs period from Neolithic (8.500 yrs BP) to Roman (2.150 yrs BP) period, which shows a coastal progradation rate of the order of 0,55 m/yr, and
b. the shoreline in the Pineios delta retreated by 1,75 km in the 2.150 yrs period from Roman period (2.150 yrs BP) to present which shows a retrogradation rate as 0,81 m/yr from Roman period to present.

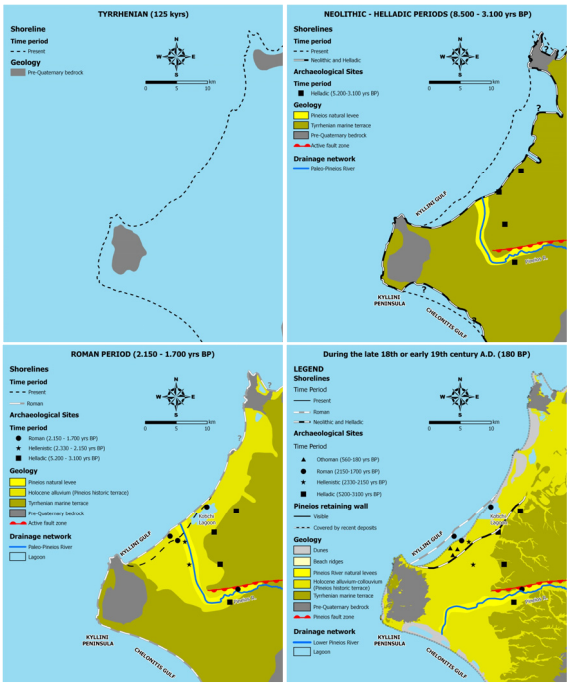

Fig. 2: Shoreline displacements in the study area during the last 8 kyrs.

REMOTE SENSING CONTRIBUTION

In order to determine whether or not progradation or retrogradation took place in Pineios former and current deltas in recent years, we initially mapped the shorelines at different times in the 27-year-period from 1972 to 1999 using (a) topographic maps at 1:5.000 scale (1972), (b) two datasets of aerial photos (1987, 1996), (c) satellite images (1999). Then, these data were compared with the present shoreline (2011), which was traced with the use of real-time kinematic differential GPS.

The initial phase was to collect the available remote sensing data and create a time series of images along the contemporary coastline. The oldest data available were the topographic maps acquired from the Geographic Agency of the Hellenic Army that was also based on photogrammetry techniques on previously acquired aerial photographs.

Using 42 air photographs acquired during 1987 we generated an ortho-mosaic for the same year. During this photogrammetric procedure a high resolution (2-meters) DEM was produced, and used for the ortho-

rectification of a 15-meter resolution Landsat-7 ETM+, panchromatic image. All the data were registered with an ortho-mosaic produced by 1996 aerial photographs (Fig. 3).

Next, by using image interpretation techniques we traced the coastline in the different periods. The difficulty was to identify the exact points of contact between the seawater and the land. This was made by equalizing the image histogram and in some cases applying a threshold value. The use of the panchromatic part of the spectrum for all the collected remote sensing data provides the homogeneity of the methodology.

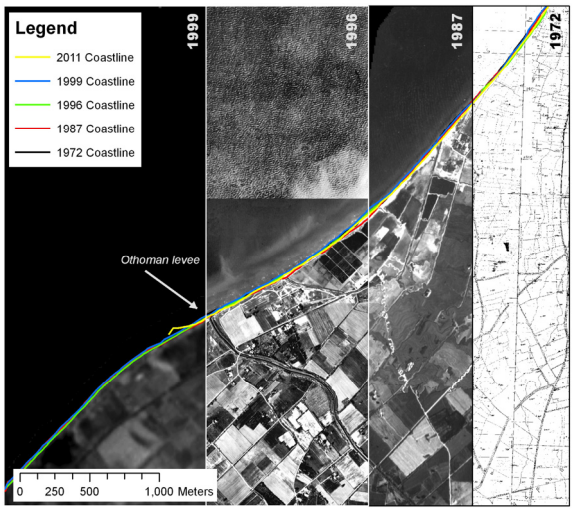

Fig. 3: Parts of the digital data used for the interpretation of recent coastline displacement.

Establishing 4 GPS bases along the shore and use the technology of real time kinematic GPS point acquisition completed the methodology. The accuracy of the present coastline was very good as the specifications of the equipment give less than 10cm (Fig. 4).

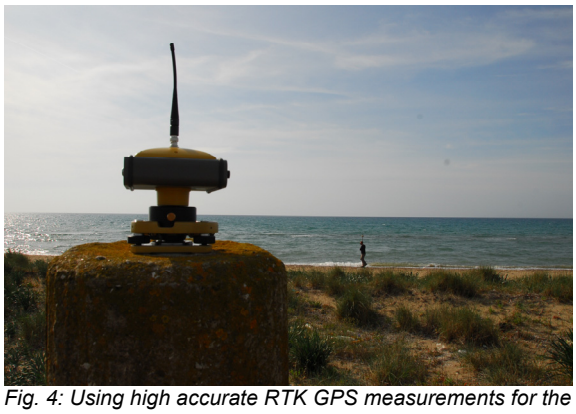

Fig. 4: Using high accurate RTK GPS measurements for the tracing of the present coastline.

The combination of all the traced coastlines on the remote sensing data with the RTK GPS recorded coastline have shown that both the former and the current delta fronts of Pineios River are divided into various sub-areas characterized by different type, phase and rate of shoreline displacement. Moreover, there is no systematic progradation or retrogradation in these delta fronts according to the data covering the last 40-year-period from 1972 to 2011 (Fig. 5). Nevertheless, there are parts of the coastline, especially where the Roman and Othoman levees used to function, that most of 50 meters of the beach have been eroded.

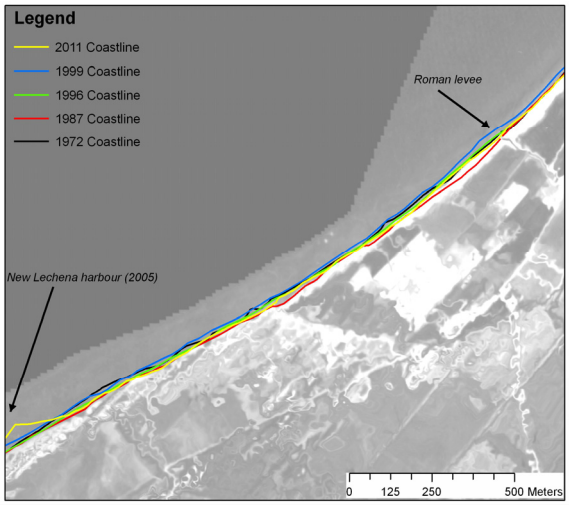

Fig. 5: Synthetic image with all the traced coastlines at a part of the study area where Pineios river used to flow into the sea before 1800's.

CONCLUSIONS

It is obvious that the western part of Pineios drainage basin is developed in an area (Gastouni graben), which is uplifted with lower relative uplift rate in comparison with the other surrounding areas. Hence, the Lower Pineios River was and is forced to flow in this graben, close and parallel to Pineios FZ.

Furthermore, the age of Pineios FZ initiation progressively decreases from E to W. A similar decrease from E to W is also observed in the throw of Pineios FZ. The throw of the western part was gradually increased until a critical point in time (probably during 18th century A.D.) when the relative uplift rate of the Pineios FZ footwall was larger than the relative uplift rate of the hanging wall. Since then, Pineios River was blocked, not able to flow N-wards and over the morphology escarpment formed by the fault and consequently enforced to shift S-wards. Moreover, the combined uplift movement of the footwall of Pineios FZ in the E and the northeastern (inland) part of the Kyllini peninsula in the W resulted in the slightly uplifted margin of the northwestern part of Gastouni graben, the block of the northwards flow of Pineios River and the initiation of the southwards flow of the river.

This natural trend of Pineios southward diversion during 18th century was supported and enforced by the human activity in the study area and especially by the construction of the ancient retaining wall of Pineios River (Papaconstantinou, 1991) during the Hellenistic period (2.330-2.150 B.C.) in order to protect the northern banks from the destructive river action.

The study area is undergoing intense and differential tectonic deformation, which has continued since Pliocene.

The areas of maximum thickness are constantly subsiding during the sedimentation phase and strictly related to the Pineios delta and river sediment loads and transport. Moreover, the southern area presents higher subsidence rates than the northern one.

The study area is also divided to three subareas that uplift with different rates (Fig. 6): (i) the footwall of Pineios fault zone (0,39-0,67 mm/yr), (ii) the Gastouni graben (0,19 mm/yr), (iii) the eastern (inland) part of Kyllini peninsula (0,36-0,48 mm/yr). The western part of Pineios basin is corresponding to the subarea with the lowest relative uplift rate (0,19 mm/yr, Gastouni graben).

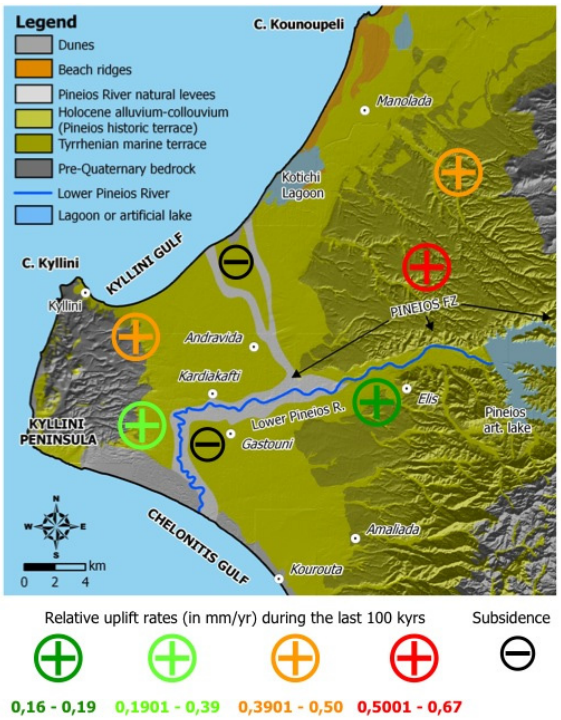

Fig. 6: Areas of uplift and subsidence around the Pineios river former and contemporary deltas.

The diversion of Pineios River to the south of Kyllini peninsula during the 18th century is a case of fluvial antecedence upon the slightly uplifted margin of the Gastouni graben and is the result of the gradually increase of the throw along the western part of the Pineios fault zone during historic times marked by strong and destructive earthquakes during the late 18th or early 19th century A.D. This natural process and trend is supported and enforced by the human activity in the study area during historic times as it is revealed by significant human constructions in the area.

References

Fountoulis, I., 1994. Neotectonic evolution of the Central-Western Peloponnese. Ph.D Thesis, Faculty of Geology, National and Kapodistrian University of Athens, GAIA 7, 386pp. (in Greek, abridged English version)

Hatzfeld, D., Pedotti, G., Hatzidimitriou, P., Makropoulos, K., 1990. The strain pattern in the western Hellenic arc deduced from a microearthquake survey: Geophys. J. Int., v. 101, p. 181-202.

Kamberis, E., 1987. Geology and oil-geologic study of the post alpine sediments of NW Peloponnese. PhD Thesis. National Technical University of Athens, Greece (in Greek).

Kontopoulos, N., Koutsios, A. 2010. A late Holocene record of environmental changes from Kotihi lagoon, Elis, Northwest Peloponnesus, Greece, Quaternary International, v. 225, 2, p. 191-198.

Kraft, J.C., Rapp, (Rip), G., Gifford, J.A., Aschenbrenner, S.E., 2005. Coastal change and Archaeological Setting in Elis. Hesperia 74, 1-39.

Lekkas, E., Papanikolaou, D., Fountoulis, I., 1992. Neotectonic Map of Greece, Pyrgos - Tropaia sheets, scale 1:100.000, Research project of the University of Athens, Department of Geology, Division of Dynamic, Tectonic, Applied Geology, Athens

Lekkas, E., Papanikolaou, D., Fountoulis, I. 1995. The Pyrgos earthquake - The geological and geotechnical conditions of the Pyrgos area (W. Peloponnese, Greece). XV Congress of the Carpatho-Balcan Geological Association, Seminar on active faults, Geol. Soc. Greece, 42-46, Athens.

Mariolakos, I., Lekkas, E., Danamos, G., Logos, E., Fountoulis, I., Adamopoulou, E., 1988. Geological - Tectonic Study of the Earthquake affected areas in Elis Prefecture (Kyllini Peninsula). Research project of the University of Athens, Department of Geology, Division of Dynamic, Tectonic, Applied Geology, 108 p., Athens 1989 (in Greek).

Mariolakos, I., Papanikolaou, D., Lagios, E. 1985. A Neotectonic Geodynamic Model of Peloponnesus Based on Morphotectonics, Repeated Gravity Measurements and Seismicity. Geol. Jb., v. B 50, p. 3-17.

Mavroulis, S. 2009. Fault activity assessment in NW Peloponnesus – The Andravida Earthquake (08/06/2008). Msc Thesis, Inter-University Post-Graduate Studies Programme on "Prevention and Management of Natural Disasters", Department of Geology and Geo-Environment of the National and Kapodistrian University of Athens, and Department of Geoinformatics and Topography of the Technological Educational Institute of Serres. 622 p.

Mavroulis, S., Fountoulis, I., Lekkas, E., 2010. Environmental effects caused by the Andravida (08-06-2008, ML = 6.5, NW Peloponnese, Greece) earthquake. In: A. Williams, G. Pinches, C. Chin, T. McMorran and C. Massey, Editors, Geologically Active: 11th IAEG Congress, Taylor & Francis Group, Auckland, New Zealand (2010), pp. 451-459.

Papaconstantinou, E., 1991. Architectonic elements of the ancient Agora of Elis in the retaining wall of the Pineios River. First International Symposium on Achaia and Elis in Antiquity, Athens, p. 329-334 (in Greek).

Papanikolaou, D., Fountoulis, I., Metaxas, C., 2007. Active faults, deformation rates and Quaternary paleogeography at Kyparissiakos Gulf (SW Greece) deduced from onshore and offshore data, Quatern. Int. 171-172, pp. 14-30.

Stamatopoulos L., Voltaggio, M., Kontopulos, N., Cinque, A., La Rocca, S., 1988. $^{230}Th/^{238}U$ dating of corals from Tyrrhenian marine deposits of Varda area (North-western Peloponnesus), Greece. Geogr. Fis. Dinam. Quat., v. 11, p. 99-103.

COULD LARGE PALAEOEARTHQUAKES BREAK GIANT STALACTITES IN CACAHUAMILPA CAVE? (TAXCO, CENTRAL MÉXICO)

Garduño-Monroy VH. (1), R. Pérez-López (2), MA Rodríguez-Pascua (2), J. García Mayordomo (2)*
I. Israde-Alcántara(1) and J. Bischoff (3)

(1) Universidad Michoacana San Nicolás de Hidalgo. Morelia. México. Email: vgmonroy@umich.mx
(2) IGME – Instituto Geológico y Minero de España, Área de Investigación en Riesgos Geológicos. Madrid, España. Email: r.perez@igme.es , m.rodríguez@igme.es
(3) United States Geological Survey. 345 Middlefield Road, MS 211, Menlo Park, CA 94025. EE.UU. jbischoff@usgs.gov
* Corresponding author

Abstract (Could large palaeoearthquakes break giant stalactites in Cacahuamilpa cave? (Taxco, central Mexico)): *the Cacahuamilpa cave, an outstanding karstic system located in the nearby of Taxco, Central Mexico, shows several damaged dripstones: stalagmites and stalactites. This cave is determined by large E-W horizontal phreatic galleries, with large dripstones, mainly stalagmites, stalactites and travertine columns. The size of these speleothems reaches a maximum value of 30 m for stalagmites (The Champagne Bottle) and 10 m for stalactites. Oriented and fallen stalagmites and broken stalactites were dated by U-Th technique, and we have obtained a probable age of 1540 BP. We also have modelled the earthquake magnitude for breaking these stalactites and a minimum magnitude M7 was estimated. The cave is located 250 km away from the Middle American Trench, responsible of large earthquakes as the Michoacán, M8.1 in 1985. Besides these large subduction zone earthquakes, there are also large active intraplate normal and strike slip faults, but with low reoccurrence intervals that can generate large earthquakes in the region.*

Key words*: speleoseismology, stalagmites, earthquake, Mexico*

THE CACAHUAMILPA CAVE SYSTEM

Cacahuamilpa cave (CC) is located within the Guerrero State of Mexico, near of Taxco city, well-known for its silver mining industry. This karst system is located within the Ixtapan Valley, a NW-SE elongated valley, 60 km long and 40 km wide. The Nevado de Toluca volcano (4558 m asl) is the highest peak and the karst is determined by two main fluvial channels: the San Jeronimo (running N-S) and the Chontalcoatlán (E-W). Both rivers meet under the La Corona hill and both appear outside of the carbonitic massif and from their hypogeum tunnelling at Dos Bocas. The lowest topographic point corresponds with the cave entrance of Cacahuamilpa, 1000 m asl. The Amacuzac River rises from the cave pit (Fig. 1). The CC belongs to the La Estrella Karstic System (LAKS). LAKS is configured by several caves in the surrounding of Cacahuamilpa: Cuevas Pacheco, Cueva Agua Brava, Gruta de Acuitlapán and Cuevas de La Estrella, among other minor caves.

The geology of the cave is described as the Morelos Unit, a stratified limestone and dolostone deposit of Lower Cretaceous (Fries, 1960), with a maximum thickness of 900 m. Furthermore appears Albian limestone (Xochicalco and Cuautla Units) and the Mezcala Unit, formed by sandstone with interlayered black limestone (Fries, 1960). Quaternary deposits are volcanic andesitic rocks and basalts and the youngest ones are Holocene travertines. Hydrothermal activity related with active volcanoes (i.e. Nevado de Toluca) is described in Ixtapan and Tonatico (35º-40ºC)(Fries, 1960).

The cave topography is mainly determined by a large horizontal phreatic tube (Fig. 2)(Bonet, 1971), with semi circular cross section. Large dripstones appear along the cave: (1). *El Chivo*, travertine; (2) and (3): *La Tortuga* and *El Guerrero*, cracked and toppled flowstone and columns. (4) *El Guerrero* dripstones. (5) The *Botella de Champán*, the greatest stalagmite 36 m high, (6) The *Calendario Azteca* (Sun Stone) and the Volcán (7), a cone-shaped large flowstone.

This work aims to demonstrate the possibility that large earthquakes (with magnitude M>7) could break giant speleothemes, and giving the fingerprint to obtain large palaeoearthquakes in the geological record that affected the area.

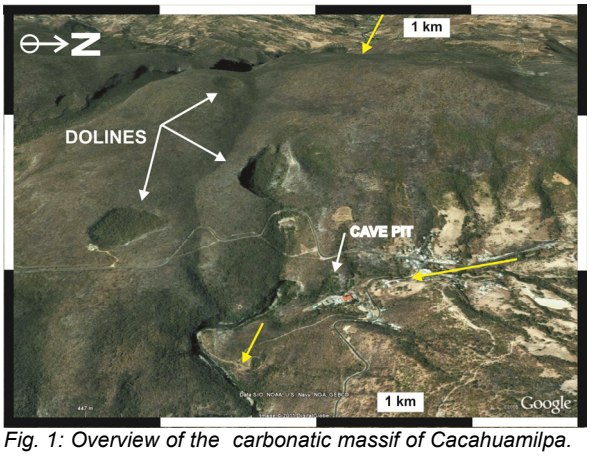

Fig. 1: Overview of the carbonatic massif of Cacahuamilpa. Main fluvial channels run from NW- to SE. The topography of the cave is related with the hydraulic gradient. Yellow arrows indicate the hydraulic gradient.

DAMAGED SPELEOTHEMS

Spelaeoseismology is a new branch of palaeoseismology, which studies ancient earthquakes from the karstic record in caves (Lacave and Koller, 2004; Kagan et al., 2005; Pérez-López et

al., 2009). Earthquakes are well recorded in caves by multiple damage affecting dripstones, travertine, also by ceiling collapse and faulting. Furthermore, the age of damage could be well constrained by using techniques such as U-Th disequilibrium of speleothems (e.g. Kagan et al., 2005).

Fig. 2. Cave topography in plant of Cacahuamilpa. Numbers indicate sites where broken speleothems are described. Red stars show those sites where sampled were collected. 1. El Chivo, 2 y 3. La Tortuga. 4. El Guerrero. 5. Botella de Champán. 6. Calendario Azteca o piedra del Sol. 7. El volcán. After cave topography from Bonet, 1971.

Different damaged speleothems (seismothems) appear along the cave: broken stalagmites, stalactites, cracked columns and travertines. The Calendario Azteca stalactite, or Sun Stone, represents one of the most spectacular dripstone ever described in caves around the world. The total length estimated is 13 m approximately, and it shows an outstanding size for a hanging structure, 3.5 m of diameter and estimated longitude of 12 m. This E-W trending stalactite appears broken in six slices of concentric carbonate mega stones from the soda straw line (cm). Despite that this stalactite represents a national natural monument several samples were collected with the aim to obtain the age and the carbonate precipitation rate for dripstones in this time interval. At this moment data are still processing at the laboratory.

	ABUNDANCE g/gsample		Activity (dpm/s)	
234U	6.90E-11	±1.4845E-13	0.95341	±0.0020526
238U	9.52E-07	±1.7109E-09	0.7105	±0.0012766
230Th	2.95E-13	±8.7190E-15	0.013429	±0.00039744
232Th	1.66E-09	±4.9300E-11	0.00040293	±0.000012
	Activity Ratio			
234U/238U	1.34E+00	±0.0037630	**AGE yr BP**	**1548±47**
230Th/234U	1.41E-02	±0.00041796		
230Th/232Th	3.30E+01	±1.4		
232Th/238U	5.67E-04	±1.6921E-05		
230Th/238U	1.89E-02	±5.6E-04		

Table 1. Radiometric dating by U-Th disequilibrium of the growth stalagmite post breaking (see Fig. 3 down). The sample wt is 0.52 g. Sample CAVO11-09.

Other spectacular seismothems and fallen stalagmites are similarly oriented and could be related with the same phenomenon (Fig.2, 7th site, El Volcán)(Fig.3). In this site, 4 stalagmites ranging between 4.2 and 1.7 m, with a diameter between 0.57 and 0.4 m, appear broken and oriented E-W. We have dated the breaking by U-Th on the subsequent growing post the oriented toppling (Table 1).

The natural period of vibration of stalagmites for H/D ranging between 3 and 4 and acceleration measures suggest earthquakes larger than M 7 close to the cave (50 km away). We have used the technique described in Maestro et al. (2011). In both cases the fallen structures have the same lithological composition (carbonates) and similar geometric relationships (H/D factor). However, in this case no strong water-flows are related to the toppled stalagmites. Nevertheless, the natural vibration of such large dripstone could be the responsible of the broken pieces (Cadorin et al. 2001). Assuming gravitational instability, the stalagmites would be oriented to the slip side instead of perpendicular (Fig.3).

SEISMIC SOURCES

The convergence between the Cocos plate and the North American plate at 53 mm/yr (GPS velocity, De Mets et al. 1990; Pardo & Suarez, 1995), configures and active area dominated by subduction earthquakes along the Middle American Trench (MAT) (Fig. 4). During the last century, thirteen instrumental earthquakes with magnitude greater than 7 have been recorded (1967-2011) in the trench zone of the MAT, and in a direction perpendicular to the cave (ca 250 km away). Moreover, the great Oaxaca earthquake of 1931 (M 8.1), the historic earthquake of Michoacán (1858) of 7.5 (Singh et al,. 1985) and the Acambay earthquake of M7 (1912), suggest a complex relationship between subduction earthquakes and intraplate earthquakes due to normal lithospheric faulting.

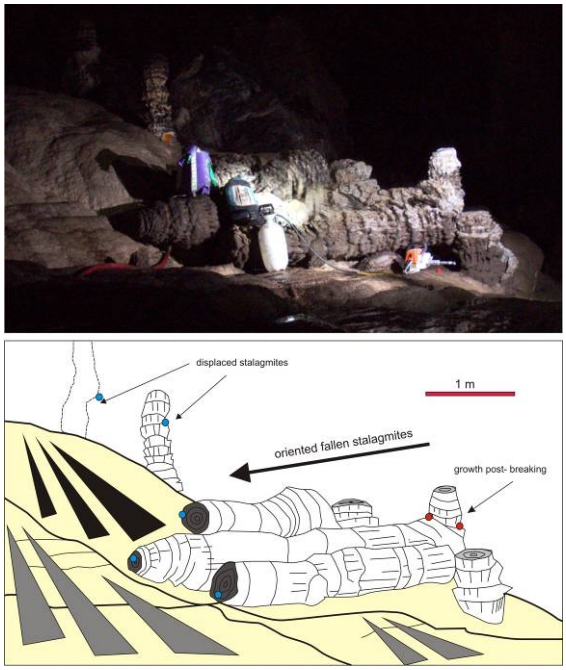

Fig. 3. Up: Broken and oriented stalagmites located at El Volcán (see Fig. 2). Down: Photo interpretation of the fallen speleothems. The axis orientation is E-W, approximately. Red dots indicate sample collected points and blue ones points to be sampled in the future field work. Black and grey triangles indicate the maximum slope direction.

The Michoacán earthquake of the 19th of September, 1985 was the more devastated with a magnitude of 8.1. This earthquake caused 9.500 fatalities, about 30.000 people were injured and more than 100.000 people were homeless, whereas severe damage was caused in buildings of Mexico DF and in different states of central Mexico also (http://earthquake.usgs.gov/earthquakes/world/events/1985_09_19.php).

Therefore, both the MAT subduction earthquakes as the large intraplate normal and strike-slips faults (e.g. the Morelia-Acambay Fault System, The Oaxaca Fault zone)(Garduño-Monroy et al., 2009), could generate large earthquakes to affect large speleothems within the Cacahuamilpa cave. It is interesting to describe large palaeoearthquakes triggered by intraplate faults in this zone due to, at present there is no instrumental record for such sized earthquakes. Therefore, infrequent large intraplate earthquake could be hibernating and palaeoseismic studies in the surroundings will be worthy to fill up the gap in the historical records.

RESULTS

Preliminary results suggest a potential palaeoearthquake dated c.a.1548 ±48BP, obtained from U-Th disequilibrium dating technique (Table 1.). The magnitude of the potential earthquake has been speculated from the geometry and mechanical properties of the stalagmites. Results suggest M>7. The geometry factor is defined by the relationship between the high and width (H/D), and the mechanical properties assuming a crystalline carbonate. Hence, we can conclude that:

(1) The broken and oriented stalagmites within the Cacahuamilpa cave could be related with palaeoearthquakes.
(2) The large size of damaged speleothems could be related with large earthquakes (M>7), in agreement with the tectonic framework of the Pacific side of Mexico: the convergence between Cocos and North American plates.
(3) Palaeoearthquakes in this zone could be related to either subduction earthquakes or large intraplate earthquakes but with long reoccurrence intervals.

The next step is to assign the potential seismic source. More accurate data are required to reconstruct the complete history of the broken speleothems in Cacahuamilpa. However, the earthquake hypothesis appeared as the strongest cause for this large damage. The interest of this work is for finding large shallow earthquakes (>M7) in a zone which is located 250 km far from the Middle American Trench.

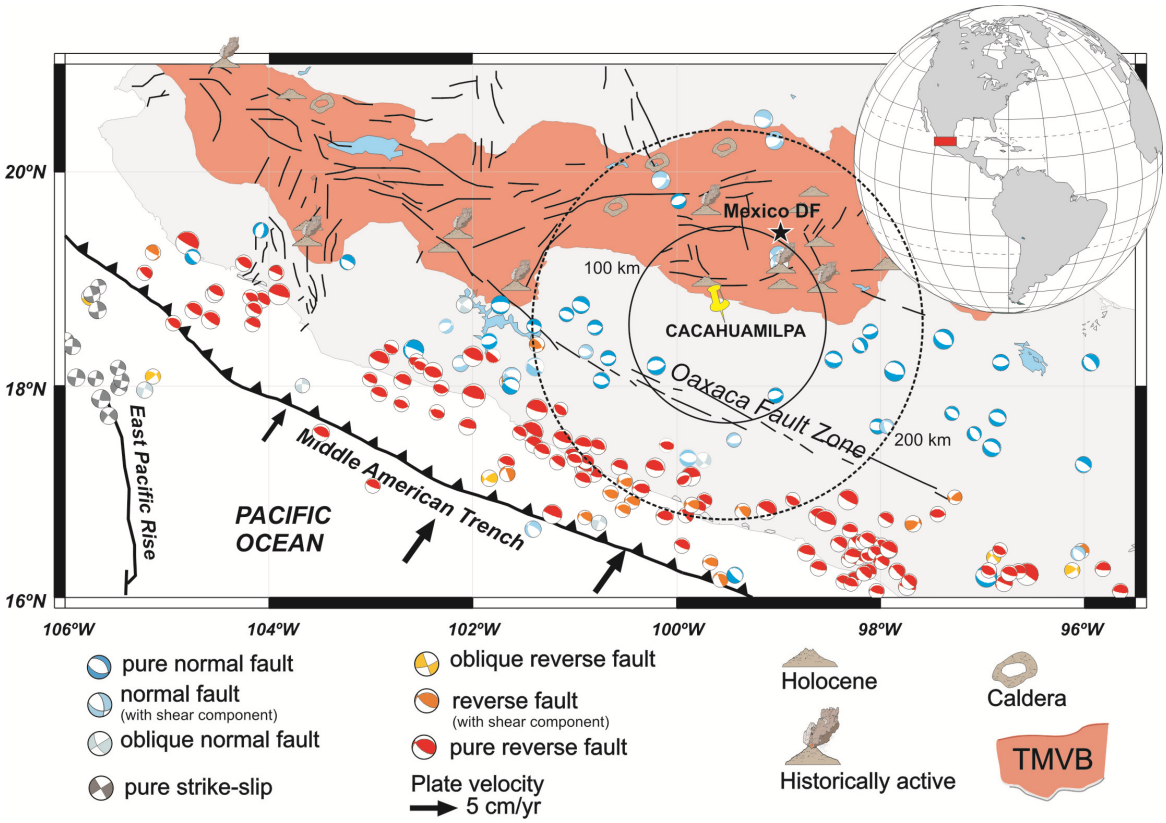

Fig. 4. Tectonic frame of Mexico. Most of earthquakes are related to the subduction between the Cocos plate and North American plate. Earthquakes represented here were obtained from Harvard online catalog (http://www.globalcmt.org/). After Pérez-López et al. (2011). TMVB: Trans Mexican Volcanic Belt

Acknowledgements: We are very grateful to *Parque Nacional Grutas de Cacahuamilpa* to give us all permissions to access to all parts of the cave, for extract samples and provide people to support us during the underground field work. Thanks are given to the CONACYT ministerial Mexican project entitled: *Estudio tectónico, de paleosismología y de efectos sísmicos arqueológicos en lagos del Holoceno y actuales del Cinturón Volcánico Transmexicano y del bloque Jalisco*.

References

Bonet, F. (1971). Espeleología de l aRegión de Cacahuamilpa. Universidad Autónoma Nacional Mexicana Instituto Geológico. Boletín nº 90. 98 p.

Cadorin, J.-F., Jongmans, D., Plumier, A., Camelbeeck, T., Delaby, S. and Quinif, Y. (2001). "Modelling of speleothems failure in the Hotton cave (Belgium). Is the failure earthquake induced?" Netherlands Journal of Geosciences 80(3–4): 315–321.

DeMets, C., R.G. Gordon, D.F. Argus, and S. Stein, (1990).Current plate motions. Geophysics Research Journal International 101: 425-478.

Garduño-Monroy V. H., R. Pérez-López, I. Israde-Alcantara, M. A. Rodríguez-Pascua, E. Szynkaruk, V. M. Hernández-Madrigal, M. L.García-Zepeda, P. Corona-Chávez, M. Ostroumov, V. H. Medina-Vega, G. García-Estrada, O. Carranza, E. Lopez-Granados and J. C. Mora Chaparro. (2009).Geometry and Paleoseismology of the Southwestern Part of the Morelia-Acambay Fault System, Central Mexico. Geofisica Internacional 48(3): 319- 335.

Kagan, E. J., Agnon, A., Bar-Matthews, M. & Ayalon, A. (2005). Dating large, infrequent earthquakes by damaged cave deposits. Geology 33(4), 261–264.

Fries, C. (1960). Geología del Estado de Morelos y de partes adyacentes de México y Guerrero, región central meridional de México. Instituto Geológico de México, Boletín nº 60(9), 236p.

Lacave C. & M. G. Koller . (2004). What Can Be Concluded About Seismic History From Broken And Unbroken Speleothems? Journal of Earthquake Engineering, Vol. 8, No. 3 (2004) 431–455.

Maestro A, G. Jané, J. García-Mayordomo, B. Fernández-Revuelta, M.A. Rodríguez-Pascua, J.J. Martínez-Díaz & R. Pérez-López. (2011). Cause Of The Rupture And Distribution Of Broken Submarine Carbonate Chimneys In The Gulf Of Cádiz (Southwestern Spain). Quaternary Int. In Press.

Pardo, M. & Suárez, G. (1995). Shape of the subducted Rivera and Cocos plates in southern Mexico: seismic and tectonic implications. Journal of Geophysical Research 100: 12,357-12,373.

Pérez-López R., Rodríguez-Pascua, M.A., Giner-Robles, J.L., Martínez-Díaz, J.J., Marcos-Nuez, A., Silva, P., Bejar, M. and Calvo, J.P. (2009). Spelaeoseismology and palaeoseismicity of the "Benis Cave" (Murcia, SE of Spain): coseismic effects of the 1999 Mula earthquake (mb 4.8). Geological Society of London, Special Publications, 316: 207-216.

Pérez-López R., D. Legrand, V.H. Garduño-Monroy, M.A. Rodríguez-Pascua , J.L. Giner-Robles. (2011). Scaling laws of the size-distribution of monogenetic volcanoes within the Michoacán-Guanajuato Volcanic Field (Mexico). Journal of Volcanology and Geothermal Research 201: 65–72.

Singh, S. K., Gerardo Suárez & T. Domínguez. (1985). The Oaxaca, Mexico, earthquake of 1931: lithospheric normal faulting in the subducted Cocos plate. Nature 317:56-58.

THREE-DIMENSIONAL INVESTIGATION OF THE AD 1621 PEDRO MIGUEL FAULT RUPTURE FOR DESIGN OF THE PANAMA CANAL'S BORINQUEN DAM

Gath, Eldon M. (1) and Tania Gonzalez (1)

(1) Earth Consultants International, 1642 E. 4th Street, Santa Ana, California, 92701, USA. Email: gath@earthconsultants.com

Abstract (Three-dimensional investigation of the AD 1621 Pedro Miguel fault rupture fro desing of the Panama canal`s Bronquen dam): *Using a series of trenches, we excavated the Pedro Miguel fault in 3-D to measure the displacement magnitude and kinematics of the AD 1621 rupture. The purpose of the study was to use the Most Recent Event event as a proxy for a future rupture of the fault through the foundation of Borinquen Dam, a major new component of the Panama Canal Expansion. The study used a small, fault-affected, cobble-filled channel as the target for displacement measurements. Hundreds of ground survey points were obtained for contacts, faults, the channel thalweg and margins. The channel is offset 3.0±0.2 m right-laterally, and 0.5±0.5 m reverse-vertically, with the vertical component occurring only within a few meters of the main fault tip. The fault rupture is expressed as a low-angle, one-sided, transpressive flower structure, exploiting weak bedding planes to propagate an en-echelon stepping rupture across the landscape. Mitigation of this rupture will be an important requirement for the dam designers.*

Key words*: Panama, paleoseismology, dam design, fault rupture*

Introduction

As part of the Panama Canal's Expansion Project, a four-segment earthen dam is being designed to form an ~7 km-long waterway to bypass the existing Miraflores and Pedro Miguel Locks (Fig. 1). Borinquen Dam will retain the Gatun Lake water elevation ~11 m above the Miraflores Lake elevation, and as such, must be designed to resist seismic loads. Extensive prior paleoseismic investigations (Rockwell et al., 2010) of the Pedro Miguel fault have shown the dam must also be designed to resist fault rupture.

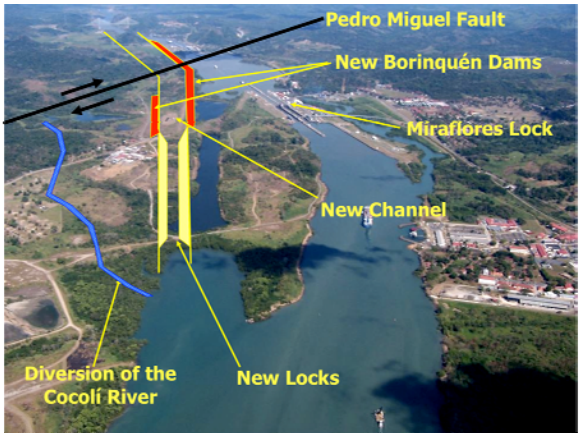

Fig. 1: Aerial view, looking NW, of the Pacific approach to the Panama Canal, showing the proposed location of the new locks, channel, and Borinquen Dam. The northerly-trending Pedro Miguel fault cuts through the proposed dam foundation about midway between the existing Miraflores and Pedro Miguel locks.

The Pedro Miguel fault is a right-lateral strike-slip fault that passes through the planned Borinquen Dam's foundation (Fig. 1). In earlier work, we (ECI, 2007, 2008, 2010) determined that the fault has had multiple Holocene ruptures, a late Quaternary slip rate of ~5 mm/yr, a Holocene recurrence interval of 500±100 years, and its Most Recent Event (MRE) on May 2, 1621. Attempts to constrain the displacements from the MRE resulted in only minimum values of ~2 m near the dam site, but a well constrained 2.8 m at the fault's northern end where it severed the Camino de Cruces (Gath and Rockwell, 2009). The purpose of this latest investigation (ECI, 2010) was to attempt to reconcile these two displacement results at the dam's location.

Fig. 2: The investigation's target was a small channel that appeared to be offset 3-4 meters. The fault (red line) was inferred to extend through the area, right-laterally offsetting a channel that approaches from the photo's upper right corner and exits along the bottom left (shown by the geologists and the blue lines).

From earlier studies and recent construction exposures, we knew the fault location to within a few meters (Fig. 2). The purpose of this paper is to present the technical details of the study's findings, and to also present and discuss the methodology of the investigation, including the planning, execution, findings, and modifications that were made along the way, because there were many.

Investigation

The investigation began with a simple plan (Fig. 3) to expose the fault on both sides of the small geomorphically defined area, and then characterize the channel geometry on both sides of the fault. Once the site was delineated, the channel margins could be slowly excavated towards the fault trace using a series of thin slices. Unfortunately, the initial fault-perpendicular trench (T-48 in Fig. 4) did not expose the fault where expected, and we failed to recognize the significance of a fault that was exposed elsewhere in the trench. The second fault-locator trench (C in Fig. 4) immediately filled with water from a sudden storm and was abandoned for four days until it could be pumped out. The two fault-parallel trenches (A and left part of B in Fig. 4) intended to define the channel geometry into and out of the fault did not expose any channel deposits or channel morphology. After four initial trenches, our investigation was definitely in trouble, with no fault and no channels to show for the work done to that point.

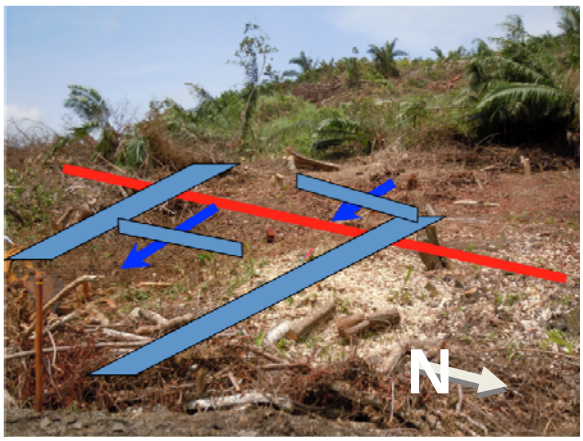

Fig. 3: The original plan was to locate the fault (red line) on opposite sides of the displaced channel (blue arrows) by trenching perpendicular to the fault (large gray rectangles), then locate the channel margins by trenching parallel to the fault and perpendicular to the channel form (small gray rectangles). Using hand excavations and continuous survey control, we would then excavate the channel margins progressively closer to the fault, until they were in fault-contact on both sides of the fault.

Fig. 4 diagrammatically shows the trenches that were finally excavated as we tried to sort out the details of the site and salvage some data for use by the dam designers. Once T-48 and 48-C failed to expose the faults where expected (Fig. 4), and trenches 48-A and B failed to expose the channels where expected, we lengthened 48-B until we found both the fault and the channel (Fig. 6). Fortunately, the channel was still fully contained on the hanging wall of the fault, and was not yet in fault contact, so we had not removed that important interaction point with our excavation.

Fig. 5 shows a modification of Fig. 3 to reflect the pattern of the faults and channels at the site, as defined by the final trenches. The challenge was to continue the excavations but be careful that the excavations did not remove the geologic data and relationships that were vital to the measurement of the channel displacements. This was accomplished by excavating from the outer edges of the site inward, and by always keeping a mental map of the site and the goal, a preserved and measurable channel offset.

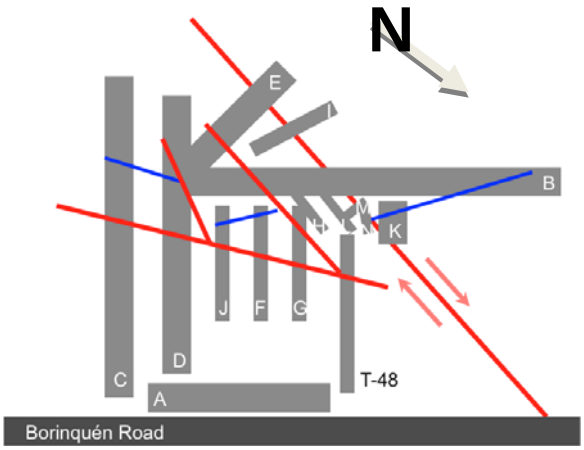

Fig. 4: Schematic layout of our final trenching study. Trenches are shown as rectangles, the faults are in red, and the channel structure is shown by the blue lines, trending across the middle of the study area. The complex nature of the fault rupture pattern meant that the initially simple geomorphic offset inferred from the pre-trenching landscape was incorrect. The channel was effectively trapped within the fault zone, and each transpressive "petal" of the fault offset the channel progressively. The channel that we trenched first appears to have been man-made, to facilitate surface drainage to a culvert under Borinquen Road.

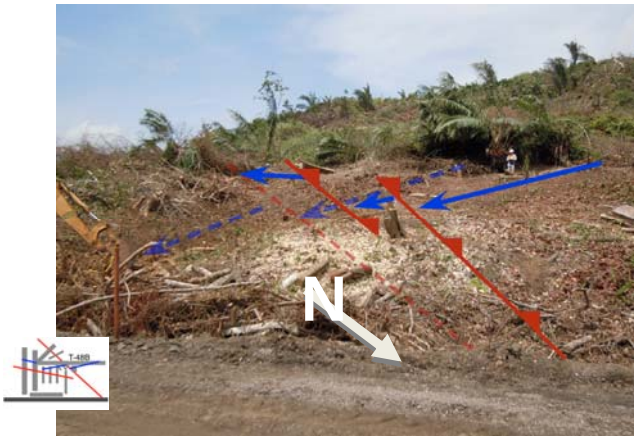

Fig. 5: Pedro Miguel fault trenching site immediately south of the old Borinquén Road (base of photo), following brush removal, but before trenching started. The fault and channel locations, as interpreted from the geomorphology, are shown with the lighter, dashed lines, whereas the actual fault and channel locations found after trenching are shown diagrammatically with the bold and solid lines.

Fig. 7 shows the channel on the hanging wall above the fault, whereas Fig. 8 shows the structural complexity of the fault zone that forced us to evolve the initial investigation plan to accommodate the unexpected. The extreme low angle of the fault acted as a bulldozer of the surface soils pushing them out and over the channel alluvium, but this also

served to bury, and thereby preserve, the channel deposits under the fault petal.

Fig. 6: Trench 48-B - the discovery trench, showing the fault (right) and the channel deposits (left), looking out over the Panama Canal in the background.

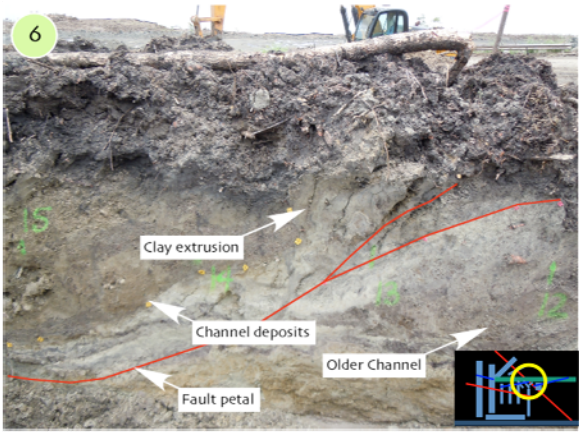

Fig. 7: Interpreted image of part of Trench 48-B showing the low-angle fault and the channel deposits on the hanging wall. The area shown as a "clay extrusion" is interpreted to be a weathered mole track from the MRE as it is intruded into, and deformed, the modern surface soils..

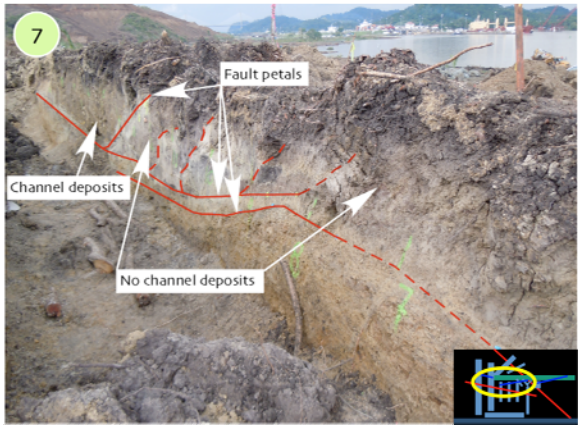

Fig. 8: Interpreted image of Trench 48-B, looking back towards Fig. 7, showing the low-angle fault petals where they have broken upwards to the surface, and the lack of alluvial deposits on the eastern (right) wall.

The purpose of digging 48-K (Fig. 9) was to continue the exposure of 48-B up-dip of the fault to get as close as possible to the spot where the fault first cut the base of the channel. With the fault dipping to the west and the channel flowing to the east, this could occur suddenly. In Fig. 9 it appears that the deepest part of the channel is touching the fault, but there are still 3-5 cm of separation. In 48-M (Fig. 10) however, the base of the channel is the fault, and the SE channel margin is completely removed by the fault. Thus, our channel margin's northern piercing point lies between 48-K and 48-M (±2 m), and the thalweg's piercing point lies within 48-M (±0.5 m).

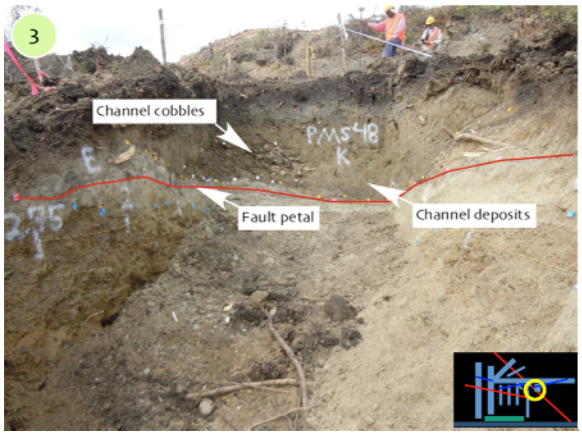

Fig. 9: Interpreted image of the end of Trench 48-K, with 48-B (Fig. 7) ~ 1 meter on the other side (to the south) of the trench. This image shows the channel deposits still above the fault trace.

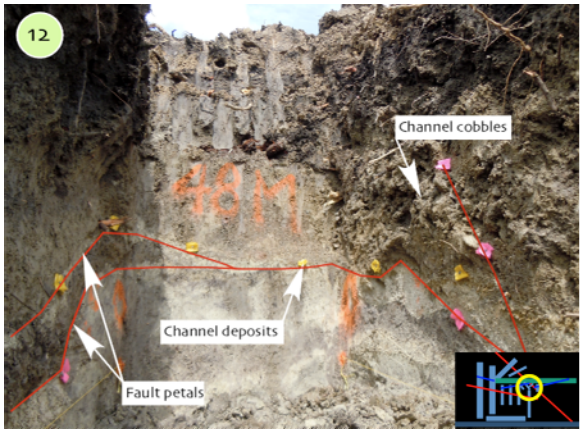

Fig. 10: Looking easterly at the interpreted image of the end of Trench 48-M, excavated ~1 m to the left (east) of 48-K (Fig. 7). This photo shows the base of the channel deposits now in fault contact in the head of the trench, and truncated by the fault on the right side.

In addition to the fault complexity shown in Fig. 8, it is important to note that there were no alluvial deposits visible on the fault's footwall in the northern wall of the trench. However, trenches 48-F, G, H, J, & M all exposed channel deposits and cobbles (Figs 4, 10 and 11). This is because the channel margin on the footwall lies 0.5-1.0 m north of the north face of Trench 48-B. Thus Trench 48-B missed taking out

the southern margin of our target channel by less than 1 m. With the southern margin so tightly constrained, the most accurate offset measurements came from that side.

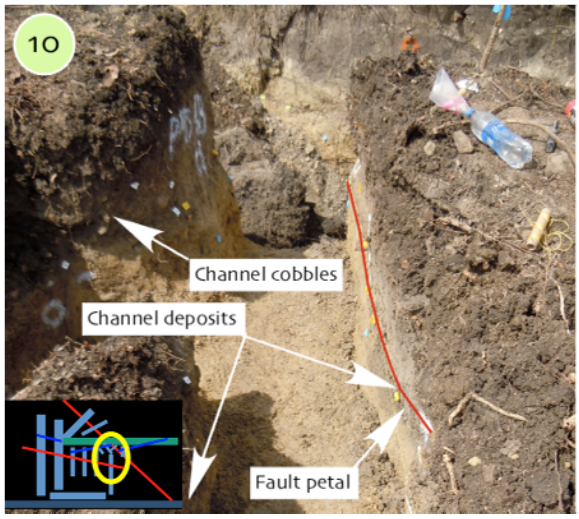

Fig. 11: Interpreted image of Trench 48-H, with 48-B (Fig. 8) exposed through the window at the end of the trench. This image shows the limits of the channel deposits on the footwall side of the fault, and shows a secondary fault petal on the right wall vertically truncating the cobble deposits within the excavated width of the trench.

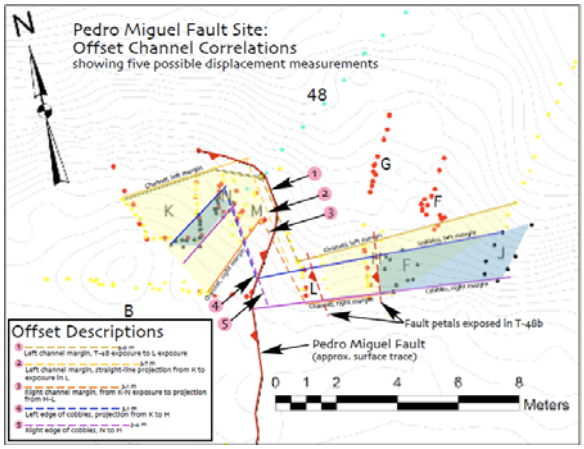

Fig. 12: Geologically interpreted map of the channel offsets based on hundreds of survey points collected. The yellow area reflects the full margins of the sandy channel deposits whereas the blue area defines the cobble-filled channel thalweg. The northern margin of the channel is more poorly constrained (±2 m), while the southern margin and thalweg margins are constrained to less than ±1 m. The right-lateral offset across the fault is measured at 3.0±0.2 m. A 0.5 m vertical offset occurred at the tip of the main fault petal, resulting in the upward bowing and erosional removal of the channel thalweg, but this uplift is localized to only a few meters from the fault tip and is not present away from the fault. Farther east, the fault tip over-rides and protects the alluvial channel deposits.

Conclusions

Although the study was much more complicated than initially planned, we were successful in locating the fault, in exposing a young channel that was offset across the fault, and in measuring the offset of that channel by the most recent earthquake. Using 15 trenches and hundreds of surveyed data points, we were able to constrain the MRE rupture to 3.0±0.2 m of right-lateral displacement, and 0.5±0.5 m of localized reverse-slip uplift at the surface tip of the fault. Because the fault is expressed through the dam as an en-echelon stepping, transpressional flower structure that exploits the weak bedding planes of the near-surface strata, it will be a difficult fault to mitigate in the design of Borinquen Dam (Fig. 13).

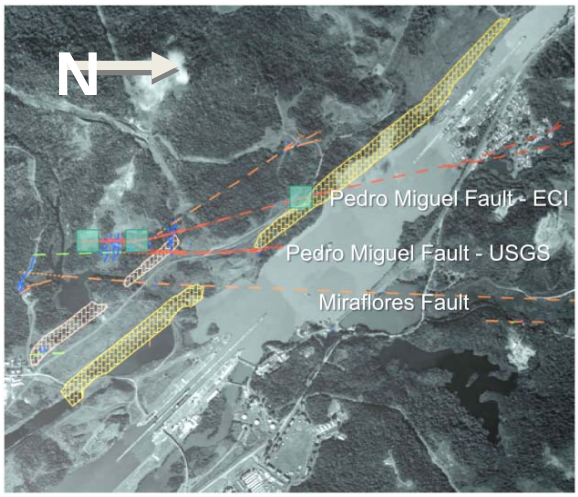

Fig. 13: Map of the Pedro Miguel and Miraflores faults through the Borinquen Dam area (hachured). Areas where we have conducted paleoseismic trenching are shown with the green squares; the green square directly over the dam location is the location of this study.

Acknowledgements

Thanks to Kay St. Peters and Barrett Salisbury for excellent field assistance and data mapping. Appreciation is due to the Autoridad del Canal de Panama for permission to conduct this study and to Ms. Pastora Franceschi for arranging all the details.

References

Earth Consultants International (ECI), 2007, Paleoseismic Trenching of the Pedro Miguel Fault in Cocolí, Located Immediately Southwest of the Panamá Canal, Panamá; consulting report for the Autoridad del Canal de Panamá (ACP), Project No. 2614.02.

ECI, 2008, Quantitative Characterization of the Pedro Miguel Fault, Determination of Recency of Activity on the Miraflores Fault, and Detailed Mapping of the Active Faults Through the Proposed Borinquén Dam Location; consulting report for the ACP, Project No. 2708.05.

ECI, 2010, Additional Trenching of the Pedro Miguel and Miraflores faults in Cocoli, immediately southwest of the Panamá Canal; consulting report for the ACP, Project No. 3012.

Gath, E.M. and Rockwell, T.K., 2009, Coseismic offset of the Camino de Cruces confirms the Pedro Miguel fault as the cause of the AD 1621 Panamá Viejo earthquake; in Pérez-Lopez, R. and others (eds), *Archeoseismology and Palaeoseismology*:: 1st INQUA-IGCP-567 Int. Workshop on Earthquake Archaeology and Palaeoseismology, Baelo Claudia, Spain, p. 32-34.

Rockwell, T. and others, 2010, Neotectonics and paleoseismology of the Limón and Pedro Miguel faults in Panamá: Earthquake Hazard to the Panamá Canal: B. of the Seis. Soc. America, v. 100, p. 3097-3129.

EARTHQUAKE ARCHAEOLOGY

INQUA PALEOSEISMOLOGY AND ACTIVE TECTONICS

VELOCITY FIELD IN BULGARIA AND NORTHERN GREECE FROM GPS CAMPAIGNS SPANNING 1993-2008

Georgiev, Ivan (1), Dimitar Dimitrov (1), Pierre Briole (2), Emil Botev (3)

(1) Department of Geodesy, National Institute of Geophysics, Geodesy and Geography, Bulgarian Academy of Sciences, Sofia 1113, Acad. Bonchev Str., Bl. 3, BULGARIA, E-mail: ivan@bas.bg
(2) Ecole Normale Superieure, Paris 75230, 45 rue d'Ulm, FRANCE
(3). Department of Seismology, National Institute of Geophysics, Geodesy and Geography, Bulgarian Academy of Sciences, Sofia 1113, Acad. Bonchev Str., Bl. 3, BULGARIA

Abstract (Velocity Field in Bulgaria and Northern Greece from GPS Campaigns Spanning 1993-2008): *We use GPS observations during the period from 1993 to 2008 to obtain the velocities of about 100 points in Bulgaria measured in more than 30 campaigns. Along with data from 21 points in Northern Greece, measured between 1999 and 2008, the results constrain the present-day motion in the region. Points in FYROM and Albania are also included in the processing to outline the picture of recent motions from Black to Adriatic Sea. The velocity field shows overall motion to the south relative to stable Eurasia and increasing motion from north to south confirming the extensional regime in Southwest Bulgaria and Northern Greece. The results can be used to constrain the north boundary of South Balkan extensional region.*

Key words*: GPS, velocity field, Bulgaria and Nortern Greece, South Balkan Extensional Region*

MOTIVATION

The region of South Bulgaria, especially Southwest Bulgaria and the Rhodopes Mountains, is the most active tectonic and seismotectonic area of the country with proved recent active tectonic structures and crustal movements. The strongest earthquake in continental Europe in the last two centuries occurred in the Krupnik-Kresna region. The territory belongs to the southern part of the Central-Balkan neotectonic region – a zone with recent extension of the crust and with complex interaction between the horizontal and vertical movements of the tectonic structures (Zagorchev, 2001). The geological and geophysical data confirm the recent activity of the fault structures formed during the Late Neogene and the Quaternary. The area is located in the northern part of the North Aegean region and is strongly affected by its tectonics and high seismicity. This is the main reason for establishing in the early 2000 a relatively dense geodynamic GPS network in Southwest Bulgaria for long-term monitoring of recent crustal movements. The network is repeatedly measured in the period 2001 - 2008. Along with GPS data from the new National GPS network of Bulgaria and a few EUREF campaigns spanning the period 1993 - 2008 we obtained velocities of about 100 points in Bulgaria. We use also GPS data from several campaigns in Northern Greece, few points in FYROM and Albania to obtain the velocity field and to constrain tectonics in the region. The obtained results can be used to constrain the northern boundary of the South-Balkan extensional province.

GPS DATA

GPS data used in the solution include campaigns on the territory of Bulgaria, Northern Greece, FYROM and Albania and comprise 158 points. In Bulgaria GPS data span the period 1993 – 2008. The data from the nineties are mainly from the EUREF campaigns in Bulgaria. Most of the data are from extensively measured geodynamic network in Southwest Bulgaria and points from the new National GPS network. The typical duration for each point measurement in the successive campaigns is 48 hours. The points with long observation history are 98. In Northern Greece we analyzed data from 21 points collected in 1999, 2000 and 2008. The data from 2008 are from joint Bulgarian-Greek GPS campaign with 48 to 72 hours measurements. Data from 5 points in FYROM are included in the solution from campaigns in 1996, 2000 and 2008. The data from 1996 and 2000 are measured in two EUREF campaigns, courtesy given by the Agency of Cadastre and the 2008 campaign is performed jointly by Department of Geodesy, Sofia, and Faculty of Civil Engineering, University "Ss. Cyril and Metodius", Skopje. Albanian data comprise 34 stations in four campaigns from 2003 till 2009 and are committed by the Laboratory of Alpine Belts Geodynamics, University of Grenoble, France.

All the data are processed and analyzed by the Bernese 5.0 software. The reference frame is ITRF2005 and the processing follows the EUREF standards (see for example Boucher and Altamimi, 2007). The reference and kinematic frame are defined by points of the European Permanent Network (EPN) included in the solution. The details of

the processing strategy can be found in Georgiev (Georgiev et al., 2007).

RESULTS AND DISCUSSION

Fig. 1 shows the obtained velocities of all 158 points in Bulgaria, Northern Greece, FYROM and Albania relative to (stable) Eurasia. The results filled in the gap in velocity field in the Eastern Mediterranean to the north of the extensively studied Marmara and Aegean regions. Results from other authors are also presented on the figure (Reilinger et al., 2006, Hollenstein et al., 2008, Floyd et al., 2010) to show the position of Bulgarian and Northern Greece territory in the East Mediterranean geodynamic settings. The velocities of the Albanian stations and points in Bulgaria (red vectors, points mainly from the National GPS network) show the velocity field in east-west direction from Black to Adriatic Sea.

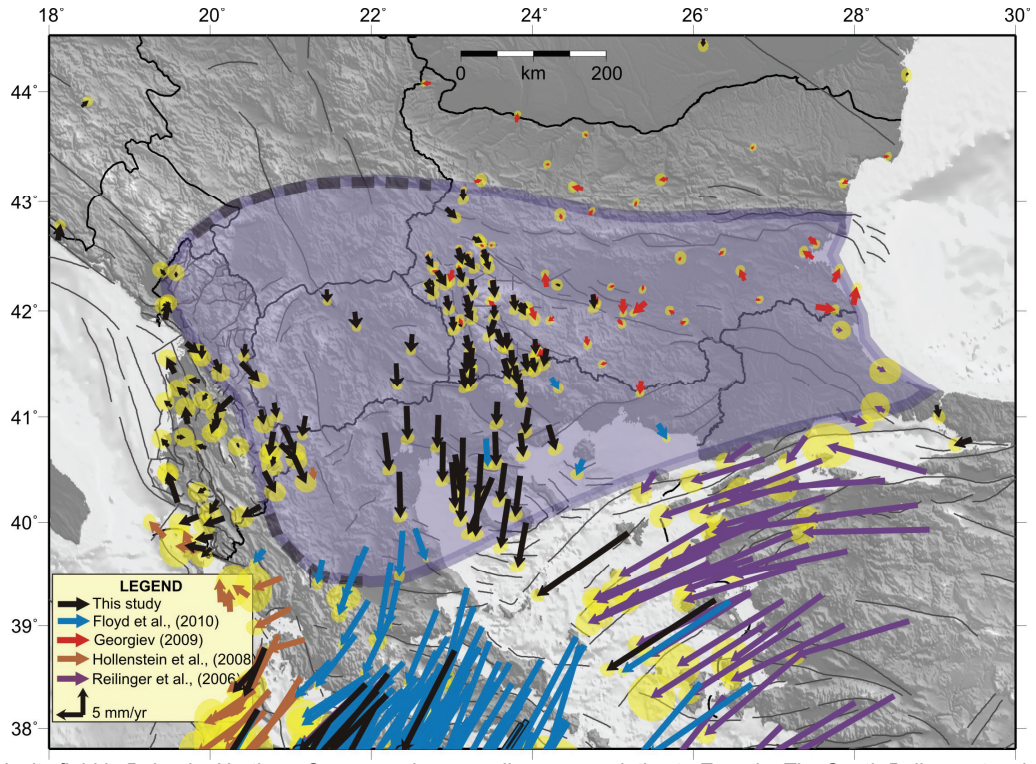

Fig. 1: Velocity field in Bulgaria, Northern Greece and surrounding areas relative to Eurasia. The South Balkan extensional region is outlined according to Burchfiel et al. (Burchfiel at al., 2006)

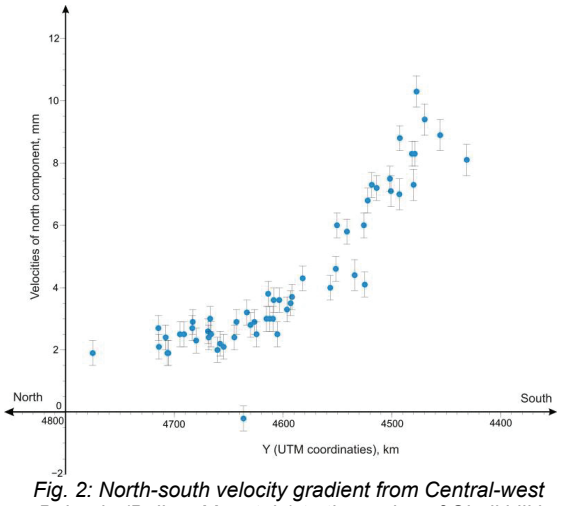

Fig. 2: North-south velocity gradient from Central-west Bulgaria (Balkan Mountain) to the region of Chalkidiki

The obtained velocities in Southwest Bulgaria and Northern Greece indicate an overall motion to the south. The results show an increasing rate from 2 mm/y in Central-west Bulgaria (Balkan Mountain) to 10 mm/y for the region of Chalkidiki. On the north-south profile from the Balkan Mountain till the Chalkidiki peninsula the north component of the estimated velocities are drawn (Fig. 2). The increasing velocities from north to south are clearly seen on this 400 km long profile confirming the north-south extensional regime in the region (see also McClusky et al., 2000, Hollenstein et al. 2008).

One point deviates from the overall south motion in Southwest Bulgaria and it is clearly seen on the velocity gradient profile (Fig. 2). This is a point from the local geodynamic network of the Department of Geodesy around the Krupnik fault, located on its northern edge. The result is in good agreement with the dipping of the fault obtained by geologic and seismotectonic data.

The points in northern and eastern part of the Bulgarian territory (red vectors) are not dense enough to draw unquestionable conclusions. But from the obtained results it is clear that North Bulgarian territory, north from the Balkan Mountain, is

part of Eurasia with velocities practically near to zero. On the Fig. 1 are shown the slightly changed borders of the South Balkan extensional region proposed by Burchfiel et al. (Burchfiel at al., 2006). According to this model the northern border of the extensional region follow approximately the Balkan Mountain. Our data as a whole, although not sufficiently dense in Southeast Bulgaria, seems to confirm this hypothesis. The question which remains is the behavior of few points located on the southeastern Black sea coast showing north-northeast motion. We need a denser network in this region to clear these two questions – to confirm the northern border of the South Balkan extensional region and to resolve the motion along the Black Sea coast.

Acknowledgements: We gratefully acknowledge the support of all agencies in the countries for the measurements: Military Geographyc Service and Agency of Geodesy, Cartography and Cadastre, Sofia, Bulgaria; Faculty of Civil Engineering, University "Ss. Cyril and Metodius", Skopje, FYROM; Aristotle University of Thessaloniki, Greece and Laboratory of Alpine Belts Geodynamics, University of Grenoble, France.

References

Boucher, C., Altamimi, Z. (2007). Memo: Specifications for reference frame fixing in the analysis of a EUREF GPS campaign, Version 27-03-2007.

Burchfiel, B.C., King, R.W., Todosov, A., Kotzev, V., Durmurdzanov, N., Serafimovski, T., Nurce, B. (2006), GPS results for Macedonia and its importance for the tectonics of the Southern Balkan extensional regime. Tectonophys 413 (3-4), 239-248.

Floyd, M. A., et al. (2010), A new velocity field for Greece: Implications for the kinematics and dynamics of the Aegean. J. Geophys. Res., 115 (10), B10403, doi:10.1029/2009JB007040.

Georgiev I., Gabenski, P., Gladkov, G., Tashkov, T., Danchev, P., Dimitrov D. (2006). NATIONAL GPS NETWORK: Processing the observations from the Main order. Geodesy N 18, Special edition, Military Geographic Service of the Bulgarian Army, 209p.

Georgiev I., (2009). National and Permanent GPS networks of Bulgaria – processing of the observation, analysis and application in geodynamic Thesis to obtain the degree Doctor of Science", Department of Geodesy, National Institute of Geophysics, Geodesy and Geography, Sofia, Bulgaria, 258p.

Hollenstein et al. (2008). Crustal motion and deformation in Greece from a decade of GPS measurements, 1993–2003. Tectonophysics 449, 17–40.

Matev, K. (2011). GPS constrains on current tectonics of Southwest Bulgaria, Northern Greece and Albania. Thesis to obtain the degree "Doctor" of University of Grenobe, Laboratory of Alpine Belts Geodynamics, University of Grenoble, France, Department of Geodesy, National Institute of Geophysics, Geodesy and Geography, Sofia, Bulgaria, 203p.

McClusky, S., Balassanian, S., Barka, A. Demir, C. Ergintav, S., Georgiev, I., Gurcan, O., Hamburger, O., Hurst, K, Kahle, H., Kastens, K., Kekelidze, G., King, R,, Kotzev, V., Lenk, O., Mahmoud, S., Mishin, A., Nadariya, M., Ouzounis, A.. Paradissis, D., Peter. Y., Prilepin, M., Reilnger, R., Sanli, I., Seeger, H., Tealeb, A., Toksoz, M., Veis, G. (2000). Global Positioning System Constraints on Plate Kinematics and Dynamics in the Eastern Mediterranean and Caucasus. Journal of Geophysical Research - Solid Earth, Vol. 105, No.B35, 5695-5719.

Reilinger, R., et al. (2006), GPS constraints on continental deformation in the Africa-Arabia-Eurasia continental collision zone and implications for the dynamics of plate interactions, J. Geophys. Res., 111, B05411, doi:10.1029/2005JB004051.

Zagorchev, I. (2001). South Western Bulgaria, Geological Guidebook. Sofia, Bulg. Acad. Sci., 98p.

ACROCORINTH - GEOLOGICAL HISTORY AND THE INFLUENCE OF PALEOSEISMIC EVENTS TO RECENT ARCHAEOLOGICAL RESEARCH

Gielisch, Hartwig (1)

(1) EurGeol. Dr. Hartwig Gielisch, DMT GmbH & Co. KG, Am Technologiepark 1, 45307 Essen Germany
Phone, +49 201 172 1888, email: hartwig.gielisch@dmt.de

Abstract (Acrocorinth - Geological history and the influence of paleoseismic events to recent archaeological research): *The Acrocorinth is the result of two major tectonical events. From Upper Cretaceous to Eocene the Acrocorinth limestone, origins from the Mesozoic carbonate platforms, were mixed with cherts of the Böotian Ocean in an accretionary wedge of the Central Hellenic Melange Belt. The melange units were covered by Neogene Acrocorinth conglomerates. Pliocene Corinthian marls cover all older units. In the Pleistocene the hill was pushed up very rapidly through the Tertiary units. Pleistocene marine terraces occur in 220 m a. s. l. at Acrocorinth of Pre-Paleotyrrhean age, thus verifying an uplift of more than 200 m in the last 400,000 years. All sediments are covered by the several sheets? of debris, the results of several major paleoseismic events. These breccias contain as components Mesozoic and Cainozoic rocks occurring at the Acrocorinth and cover probably? the remaining nine temples described by Pausanias. In order to find the missing temples it is essential to know, which part of the sediments is in-situ or are part of landslides triggered by paleoseismic events.*

Key words*: conglomerates, rapid uplift, debris breccias, covered temples*

INTRODUCTION

Acrocorinth is located in the northern Argolis south of the Corinthian golf and directly south of the ruins of ancient Corinth. The geological history of the hill is subdivided in two major tectonical events: the genesis of a melange during a continent-continent collision in the lower Tertiary and a rapid uplift in the younger Pleistocene. Several paleoseismic events form the actual shape of the hill.

GEOLOGICAL HISTORY OF THE ACROCORINTH

The geological history of Acrocorinth starts in the middle Mesozoic. Neritic lime- and dolostones formed on the Parnassus-carbonate platform as part of the Centralhellenic Systems, while in the center of the Böotian Ocean, a sub basin of the Pindos Ocean, pelagic cherts and ophiolitic sequences were built.

During the closing of the Böotian Ocean carbonates, cherts and ophiolites were tectonically mixed as part of an accretion in the subduction trench thus forming a mélange belt between the Parnassus- and Pelagonian-plates (GIELISCH, 1993, 1994). The youngest components of these mega-breccias are of Eocene age. The alpine orogenesis of Greece is completed in the Lower to Middle Miocene.

During the Upper Miocene the alpine Hellenides were fragmented by a phase of intense brittle faulting. The major systems of the Greek intra-mountainous graben-systems developed during the Upper Miocene and the Lower Pliocene.

During and directly after these phases of brittle faulting the Acrocorinth conglomerates have been deposited over the Mesozoic units. Components of the conglomerates comprise mainly local and regional geological units (carbonates, cherts, serpentinites of the ophiolites, quartzites) (RICHTER et al., 1992). Exotic clasts like olivine-gabbros,

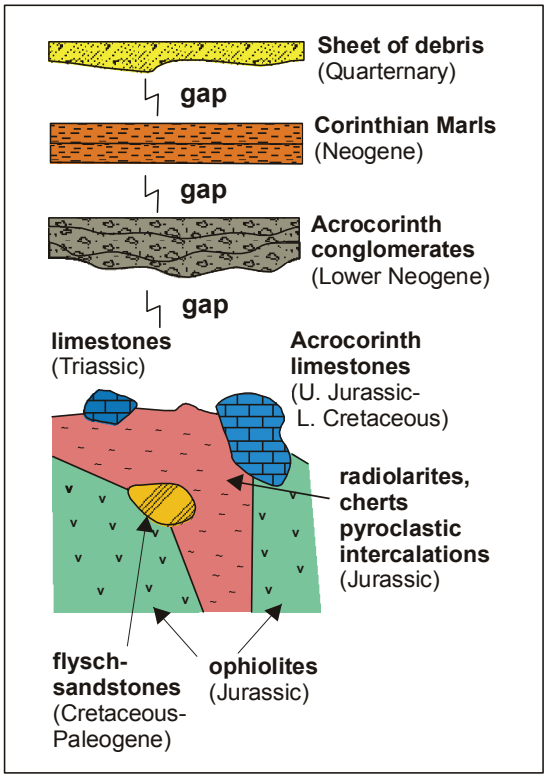

Fig. 1: Schematic profile of sequences in the Corinthian area showing the stratigraphical position of the main geological units

marbles and other metamorphic rocks show a connection to source rocks, which are nowadays located further away. Following after the Acrocorinth conglomerates, the Corinthian Marls formed in the Neogene and cover all other geological units (s. fig. 1).

In the beginning of the Pliocene the Graben of Corinth started to sink. As compensation for the deepening of the graben the Parnassus-Ghiona Mountains rose in the north, while in the south the Trapazona Mountains and isolated areas north, including Acrocorinth have been up-lifted pushing through the Neogene and Quaternary sediments. At Acrocorinth marine terraces are developed at 220 m a.s.l.. The age of the terraces is Pre-Paleotyrrhean (460,000 to 400,000 a) thus verifying an uplift of the hill of some 200 m in the last 400,000 years (SEDAT, 1986).

Today the components of the Mesozoic mélange form the top of the Acrocorinth hill as well as a smaller hill west of Acrocorinth, (Penteskufion). Acrocorinth conglomerates occur east and west of the hill, pushed up during the up-lift of Acrocorinth, with circular dip directions outwards on the flanks. West of the Penteskufion the conglomerate also occurs, dipping also into a westerly direction. In the eastern and western areas the conglomerates are covered by Corinthian Marls. In the south of Acrocorinth, conglomerates do not outcrop. Here the Corinthian Marls are directly in contact with Mesozoic units. On the northern flank conglomerates do also not outcrop. The outcropping units on the northern flank of the hill are interpreted to be breccias with angular components and not conglomerates.

PALAEO-EARTHQUAKES

In ancient times, beginning from the Mycenaean period until the Turkish invasion, the Acrocorinth was the acropolis and fortress of the ancient city of Corinth. Nearly every civilization left archaeological remains on the top and the flanks of the hill. Following PAUSANIAS (II. 4.6) in Roman times (A.D. 160) ten smaller temples and sanctuaries (BOOKIDIS & STROUD (1987) were located on the northern flank of the hill:

":::[2.4.6] As you go up this Acrocorinthus you see two precincts of Isis, one if Isis surnamed Pelagian (Marine) and the other of Egyptian Isis, and two of Serapis, one of them being of Serapis called "in Canopus." After these are altars to Helius, and a sanctuary of Necessity and Force, into which it is not customary to enter….." PAUSANIAS (II. 4.6)

The Demeter and Persephone temple, one of these sanctuaries, has been excavated in the 1970ies and 80ies by the American School of Classical Studies. Locations of the remaining 9 temples or sanctuaries are unknown. But where are the ruins of the sanctuaries?

The Graben of Corinth is a seismic high risk area. Several major earthquakes affected this area in the last 2000 years. Following PHILLIPSON (1892) and v. FREYBERG (1952) three bigger earth quick destroyed the area in historical times: 420 B.C., 77 A.C. and 551 A.C.

One of the biggest was the earthquake of 551 A.D. This earthquake affected mainly Acrocorinth and thereafter the acropolis on the Acrocorinth remained inhabited until the 8th century. The northern flanks of the hill collapsed and a mixture of natural rocks and cultural debris formed talus deposits, which cover the main parts of the northern flanks (s. Fig. 2). These slide breccias have been cemented in the following centuries and can therefore, be misinterpreted as conglomerates. However, the angular to sub-angular character of the clasts point to an origin as breccias in contrast to the well-rounded clasts of the Acrocorinth conglomerates. In summary, it was possible it identify four different generations of slide breccias:

I. Very coarse sheet of debris: components sharp-edged, up to 50 cm diameter, lightly cemented with powdery, carbonate matrix. This breccia shows a fining upwards, the components become smaller to the top of the unit. The unit is older than unit II. No other dating was possible.

Fig.2: Sheets of debris at the Northern flank of the Acrocorinth: a: base of unit IV; b: base of unit I

II. Fine-coarsed sheet of debris: components angular rounded with diameters of 5 to 10 cm. The components are firmly cemented by carbonate matrix and building pedocretes. The unit is older than 700 B.C.. The small theatre in the temple of Demeter was cut into this unit and this temple was built around 700 B.C..

III. Medium-coarsed sheet of debris: components angular of up to 20 cm diameter. The components are firmly cemented by a carbonate matrix. Also here pedocrete genesis is possible to observe. This breccia is young the unit II, because it overlies unit II. The breccia contains in addition to the natural components bricks and human processed stones. This unit could be the sheet of debris of the earth quick from 420 B.C., because it overlies the theatre of the temple of Demeter.

IV. Fine-to medium coarsed sheet of debris: components sharp-edged, up to 10 cm diameter, lightly cemented with terra fusca and terra rossa. The base of the breccia shows bricks, destroyed pottery and traces of cinders (s. Fig. 3). The breccia contains a lot of terrestrial *Stylommatophora* shells. In the year 146 B.C. the Romans destroyed Corinth fighting against the Archaean League. The city was completely razed and Corinth was nearly 100 year's uninhabitated. Julius Ceasar refounded the city as Colonia Laus Iulia Corinthiensis in 44 B.C. shortly before his assassination. This horizon could be the level of the Roman ravage in the year 146. B.C.. In this case the unit IV is younger than 146 B.C..

Pausanias visited the area around 160 A.D., 83 years after the major earth quake from 77 A.D. The unit IV conforms to a typical rock fall landslide and based on this study it is the final bigger unit becoming exist as result of such an event. Hence unit IV could be the sheet of debris of the 551 A.D. seismic event.

Fig. 3: Unit IV a: shells of Stylommatophora; b: level of the Roman ravage; c: conglomerates of the Corinthian Marls

Corinth and parts of the fortifications on Acrocorinth were rebuilt during the rule of Justinian I, Caesar of Byzantium. In this time the Byzantine Empire was nearly 200 years converted to Christianity and there was no reason to rebuild ancient heathen temples. In order to locate the remaining ruins of the 9 missing temples it is necessary to identify the level between unit III and unit IV and start excavations at this level.

Following another earthquake on the 21st February 1858 the city was given up and rebuilt 6 km northwest of the ancient settlement.

CONCLUSIONS

BOOKIDIS & STROUD (1987) describe the northern flank sediments as conglomerates. These conglomerates at Acrocorinth are of a Neogene age and excavations in these sediments will probably not lead to any successes looking for remains from the Roman period.
Recent studies indicate that the the northern flanks of Acrocorinth are covered by breccias resulting from palaeoseismic events. Sedimentary characteristics do indicate an origin as cemented talus deposits, some of which triggered by paleo-earthquakes. These breccias are most probably younger than the Roman period because of cultural debris. A Neogene age can be excluded.
Archaeological excavations in and below these recent sediments may locate the remaining of sanctuaries described by PAUSANIAS 160 A.D.

References

Bookidis, N. & Stroud, R. (1987). Demeter and Persephone in ancient Corinth. 33 p., American School of Classical Studies, ISBN 0876616716, Princton, New Jersey.
Freyberg, B. v. (1952). Der Bau des Isthmus von Korinth.- Ann. geol. Pays Hell., 4, p. 157-188, Athens.
Gielisch, H. Dragastan, O. & Richter, D.K. (1993). Lagoonal to tidal carbonate sequences of Upper Jurassic/Lower Cretaceous age in the Corinthian area: Melange blocks of the Parnassos Zone.- Bull. Geol. Soc. Greece, Vol. XXVI-II/3, 663676, Athen.
Gielisch, H. (1994). Mikrofazies und stratigraphische Stellung des Jura-Kreide-Übergangsbereichs der Parnass-Kiona-Zone zwischen Mittelgriechenland und Argolis.- Dissertation, 223 p., Bochumer geol. u. geotechn. Arb., Bd. 43, Bochum.
Pausanias (II, 4.6) from http://www.theoi.com/Text/Pausanias1A.html
Philippson, A. (1892). Der Peloponnes – versuch einer KLandeskunde auf geologischer Grundlage. 642 p., Berlin.
Sedat,R (1986). Das Stufenland von Korinth (Griechenland).- 183 p., Diss., Bochum.
Richter, D.K., Dragastan, O. & Gielisch, H. (1992): Microfacies, diagensis and biostratigraphy of the Jurrassic/Cretaceous lagoonal Acrocorinth-Limestone (Parnassos Zone NE-Peloponnesos, Greece).- Bochumer geol. u. geotechn. Arb., 39, 1-70, Bochum.

INTERPRETING OFFSHORE SUBMERGED TSUNAMI DEPOSITS: AN INCOMPLETELY COMPLETE RECORD

Beverly N. Goodman-Tchernov (1)

(1) Moses Strauss Department of Marine Geosciences, Leon Charney School of Marine Sciences, University of Haifa, Mt. Carmel, Israel 31905. bgoodman@univ.haifa.ac.il

Abstract (Interpreting Offshore Submerged Tsunami Deposits: An Incompletely Complete Record): *The complications and challenges of understanding and interpreting offshore submerged tsunami deposits is presented here and discussed in relation to recently and previously published tsunami studies. Regular annual storm activity impacts the shallow uppershelf and littoral zone, and rarer larger storms can impact deeper water depths. These events combined, with subwater surface currents, can regularly or periodically alter the seabottom, manipulating and reworking previously laid tsunamigenic horizons. Because of this, offshore deposits must be carefully considered within their meteorological and coastal morphological contexts. The differentiation between storm and tsunami deposits has long been a primary concern for understanding the sedimentological signature of paleotsunami deposits. Here, examples of paleotsunami deposits offshore on the Mediterranean coast of Israel will be presented with a discussion of how to address the issue of 'completeness' of the offshore record in order to properly place these evidence in the overall context of tsunami records.*

Key words*: tsunami, sedimentology, uppershelf, Mediterranean*

INTRODUCTION

Recent research offshore from Caesarea, Israel (Reinhardt et al. 2006, Goodman-Tchernov et al. 2009, Fig. 1) argues for the presence of preserved tsunamites from multiple paleotsunami events. The specific horizons were identified based on the presence of tsunamigenic characteristics anchored in granulometry, shell taphonomy, sedimentological structures, erosional features, and terrestrial and marine mixing. While these horizons are well documented and laterally extensive, there are variations in the thickness and some events mentioned in historical documentation that are not present. The question arises whether the physical record is incomplete, or the historical records fabricated. The offshore record is highly problematic due to regularly occurring high-energy storm events which can disturb and rework remains from tsunami events (Dawson 2007, Shanmugam 2011). In addition, this reworking varies by a multitude of factors including depth, seafloor sedimentology and morphology, ultimately leaving a heterogeneous footprint. A deposit of one composition might survive intact due to width, material hardness, or mechanical strength, while another is easily erased. This absence and presence is seen when comparing across cores. In Caesarea, current research is aimed at tackling the complicated story in the near offshore environment through detailed analysis of sediment cores and the comparative study of modern storm impact and deposits.

STORM IMPACTS

In mid-December 2010, a large storm hit the Israeli coastline with measured wave heights of 13.7 meters, just after a comparative storm/non-storm study was launched. A storm of this magnitude is only known to have a reoccurrence cycle of 2-3 times a century. The impact of the storm on the coastline was significant, dismantling and transporting large sections of concrete from a modern wave breaker, scouring the base of the ancient aqueduct, stripping the upper layer of sand from the seabottom in many parts of the harbor, and scraping 1-2 meters off of the face of coastal cliffs (see Fig. 2). A small underwater excavation survey and sediment study was completed in the summer and fall of 2010, preceding the storm. Following the storm, the same areas were

Fig. 1: Caesarea, Israel. Aerial photograph of the coastline with the submerged ancient harbor. Tsunamis in antiquity struck the harbour, likely contributing to the harbour's ultimate demise.

revisited. This rare large storm had a great effect on the areas studied, and the deposits give a glimpse into the degree of impact that large storms may have had in antiquity, providing a reference point for differentiating between normal sea conditions, large storms, and tsunamis.

Fig. 2: December 15, 2010, Caesarea, Israel. Two days after height of major decadal storm. Rubble eroded from buildings and concrete slabs moved from the outer breakwater cover a structure on the harbour pier.

Normal, storm, and tsunami conditions were defined in sediment cores with the use of particle size distribution contour mapping (Goodman-Tchernov et al. 2009, see Fig. 3). Now, the recent large storm has provided a modern analog for comparison.

DISCUSSION

Offshore sedimentological research presents a unique preservation scenario, one in which there is no one-for-one record as one might find in certain varved lake sediments. The finds offshore of Caesarea are surprising, in the regard that *any* record remains in 20 meters water depth and shallower. Observations from the recent large storm clearly demonstrate that storms are capable of altering the record substantially, and it is therefore significant that finds demonstrate the presence of some preservation. What does remain, could be argued, is telling about the types of materials that are capable of withstanding later storm impacts. It could also be argued that the presence of events in the historical record that lack physical correlation in the offshore sediments should not be dismissed. Such absences might relate to the size or characteristic of the tsunami deposit—that it was not substantial enough to survive later storms. Future work might investigate cores from deeper waters, beyond any storm influence (~30m water depth) to see whether indications of those 'missing' events are present.

Offshore tsunami deposits, particularly in the zone of storm-influence, do not represent a complete depositional sequence, rather, they are a representation of specific sets of circumstances dictated by deposit composition, thickness, and surrounding geomorphological conditions that nonetheless provide an important and independent window into paleotsunami impacts.

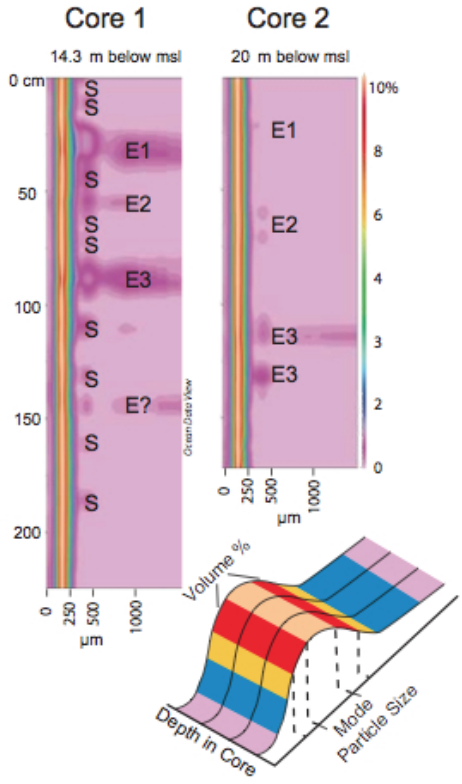

Fig. 3: Particle size distribution contour mapping used to differentiating between storm and tsunami events (from Goodman-Tchernov et al. 2009). 'S' indicates storms, 'E' indicates tsunami events. The lack of storm events in core 2 is interpreted as the product of water depth and distance from the shore.

Acknowledgements: Appreciation expressed to Israel Antiquities Authority (K. Sharvit), Hatter Laboratory for Coastal Archaeology (M. Artzy), Israel Science Foundation, Israel Ministry of Infrastructure, and H. Dey.

References

Dawson, A. G., and I. Stewart (2007), Tsunami deposits in the geological record, *Sediment.Geol., 200*(3-4), 166-183.

Goodman-Tchernov, B. N., H. W. Dey, E. G. Reinhardt, F. McCoy, and Y. Mart (2009), Tsunami waves generated by the Santorini eruption reached Eastern Mediterranean shores, *Geology, 37*(10), 943-946.

Reinhardt, E. G., B. N. Goodman, J. I. Boyce, G. Lopez, P. van Hengstum, W. J. Rink, Y. Mart, and A. Raban (December, 2006), The tsunami of 13 December A.D. 115 and the destruction of Herod the Great's harbor at Caesarea Maritima, Israel, *Geology, 34*(12), 1061-1064.

Shanmugam, G. (2011), Process-sedimentological challenges in distinguishing paleo-tsunami deposits, *Natural Disasters.*

EARTHQUAKE ENVIRONMENTAL EFFECTS, INTENSITY AND SEISMIC HAZARD ASSESSMENT: THE EEE CATALOGUE (INQUA PROJECT #0418)

Guerrieri, Luca (1), Anna Maria Blumetti (1), Elisa Brustia (1), Eliana Esposito (2), Mauro Lucarini (1), Alessandro M. Michetti (3), Sabina Porfido (2), Leonello Serva (1) & Eutizio Vittori (1), & the INQUA TERPRO Project #0811 Working Group

(1) Dipartimento Difesa del Suolo, Servizio Geologico d'Italia, ISPRA, Via V. Brancati 48, 00144 Roma, ITALY. Email: luca.guerrieri@isprambiente.it
(2) Istituto per l'Ambiente Marino e Costiero, CNR, Calata Porta di Massa - 80133 Napoli, ITALY
(3) Dipartimento di Scienze Chimiche e Ambientali, Università dell'Insubria, Via Valleggio, 11, 22100 Como, ITALY

Abstract (Earthquake Environmental Effects, intensity and seismic hazard assessment: the EEE Catalogue (INQUA Project #0418): *Earthquake Environmental Effects (EEE) are the effects produced by an earthquake on the natural environment, either directly linked to the earthquake source or triggered by the ground shaking. These include surface faulting, regional uplift and subsidence, tsunamis, liquefaction, ground resonance, landslides, and ground failure phenomena.*
The EEE catalogue is a data collection of Earthquake Environmental Effects from modern, historical and paleoseismic earthquakes compiled at global level by the INQUA TERPRO Project #0811 WG.
The damages caused by recent catastrophic seismic events have been mostly linked to the vulnerability of physical environment enhancing the crucial role of EEEs, including tsunamis, for seismic hazard purposes. Therefore, these events have confirmed that the EEE Catalogue is an essential tool to complete traditional SHA based on PGA maps, since it allows to identify the natural areas most vulnerable to earthquake occurrence and to objectively compare in time and in space the earthquake intensity through the ESI scale.

Key words*: Earthquake Environmental Effects, ESI intensity scale, seismic hazard.*

INTRODUCTION

Earthquake Environmental Effects (EEE) are the effects caused by an earthquake on natural environment, including surface faulting, regional uplift and subsidence, tsunamis, liquefactions, ground resonance, landslides and ground failure, either directly linked to the earthquake source or provoked by the ground shaking (Michetti et al., 2007).
Most of the damage resulting from moderate to large earthquakes is typically related with the vulnerability of the physical environment. This point has been sadly and dramatically confirmed by the two relevant seismic events occurred in the last months in countries with strong economy and modern building codes, i.e., the February 22, 2011, Mw 6.3 Christchurch and the March 11, 2011, Mw 9.0 East Japan earthquakes.

The March 11, 2011, earthquake occurred in the Pacific Ocean near the coast of NE Japan. Most of the damage in terms of dead toll (more than 20,000 people) and destruction was caused by the huge tsunami (run up values larger than 38 m; more than 5 km inland penetration in the Sendai coastal plain). Comparatively, the amount of damage induced by the vibratory ground motion itself was modest. The size of the 2011 tsunami was fairly larger than those recorded in the affected area in the last century, but comparable with the tsunamis affecting the same areas in 869 A.D. recently well documented by means of geological and paleoseismic studies (Sawai et al., 2007; HERP, 2009).
Nevertheless, the relevance of EEE has been also shown by the moderate-size event occurred on February 22, 2011, very close to the town of Christchurch, New Zealand.

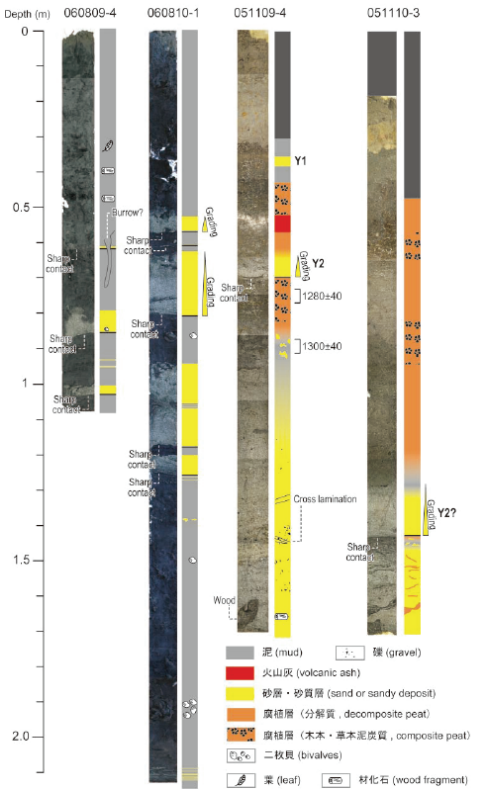

Fig. 1: – Geological record of past tsunamis at Watari and Yamamoto, Myagi prefecture (Sawai et al., 2007). The characteristics and spatial distribution of these deposits allowed to identify ancient tsunamis comparable with the March 11, 2011 event.

This was basically an aftershock of the 2010 September 4, Mw 7.0 event. However, while the main shock did not cause victims or large damage, the 2011 event caused the death of at least 75 people and the destruction of several districts in the Christchurch area. This scenario of bad damage was mainly linked to local effects of site amplification, which depends largely on the stratigraphic characteristics (geological history) of the recent deposits over which the town is built; as well, the same sediments are particularly susceptible to liquefaction. As a consequence, also houses designed in agreement with the local seismic codes have collapsed, due to liquefaction within the foundation soils.

Both events, although not comparable in size and geodynamic setting, have confirmed once again i) the relevance of earthquake environmental effects as a major source of seismic hazards, in addition to vibratory ground motion; ii) the need of re-evaluating the significance of macroseismic intensity as unequivocal measurement of the final earthquake impact on the local natural and built environment, and iii) the relationships between epicentral intensity, earthquake size, and source geometry. As a matter of fact, intensity is a parameter able to describe a complete earthquake scenario, based on direct field observation. Thus, the knowledge of the characteristics and spatial distribution of EEE induced by past earthquakes will strongly improve standard seismic hazard assessments, that typically consider only the vibratory ground motion hazard.

THE EEE CATALOGUE

Nowadays, a significant amount of data about Earthquake Environmental Effects is available for a very large number of recent, historical and paleo-earthquakes. However available information is located in several different sources (scientific papers, historical documents, professional reports), and often difficult to access.

The EEE Catalogue has been promoted with the aim to properly retrieve the available information about EEE at global level and archive it into a unique database, in order to facilitate their use for seismic hazard purposes. Its implementation has been endorsed at global level by the INQUA TERPRO Project #0811, through a Working Group coordinated by ISPRA - Geological Survey of Italy.

The EEE catalogue collects the characteristics, size and spatial distribution of coseismic effects on nature in a standard way from modern, historical and paleoearthquakes. For each event, we have assessed epicentral and local intensities based on EEE data through the ESI 2007 scale (Michetti et al., 2007), that integrates and completes the traditional macroseismic intensity scales, allowing to assess the intensity parameter also where buildings are absent or damage-based diagnostics saturates. This procedure has allowed an objective comparison in terms of earthquake intensity, for events occurred in different areas and/or in different periods.

The information is collected at three levels of increasing detail (Earthquake, Locality, Site). Also available imagery documentation (photographs, video, sketch maps, stratigraphic logs) can be uploaded into the database.The quality of the database in terms of completeness, reliability, and resolution of locations is strongly influenced by the age of the earthquake so that it is expected to be very variable.

Nevertheless, even where the information is less accurate (historical earthquakes), the documented effects are typically the most relevant i.e. most diagnostic for intensity assessment. Similarly, the information from paleoseismic investigations, although poorly representative of the entire scenario, still includes significant data (i.e. local coseismic fault displacements) very helpful of a minimum size of the earthquake.

A first official release of the EEE Catalogue has been done in the frame of the XVIII INQUA Congress, held in Bern in July 2011. However, the implementation of the EEE catalogue is always in progress at http://www.eeecatalog.sinanet.apat.it/login. Data can be explored on a public interface (Fig. 2) based on Google Earth at http://www.eeecatalog.sinanet.apat.it/terremoti/index.php. Earthquake records validated by the Scientific Committee of the Project can be also downloaded from the site.

THE ADDED VALUE

The major added value of the EEE Catalogue in terms of seismic risk is the possibility to explore the scenarios of environmental effects induced by past earthquakes and therefore identify the areas where the anthropic settlements and infrastructures are more exposed to this source of potential hazard. To this end, a good accuracy of EEEs location becomes crucial. Typically, EEEs from recent earthquakes are mapped with good accuracy immediately after the event. Nevertheless, even for some historical earthquakes it is possible to retrieve with very good detail this information. It is the case of the December 28, 1908 Messina Straits earthquake and consequent tsunami (Fig. 3), where the EEE Catalogue allows to locate the earthquake/tsunami effects over the present urban texture with a spatial resolution of a few meters, pointing out the areas characterized by the highest risk. Furthermore, the EEE Catalogue allows to reveal possible trends in the spatial distribution of primary and secondary effects. For example, Fig. 4 shows the spatial distribution of EEEs induced by the October 8 2005, Muzaffarabad, Pakistan, earthquake (Ali et al., 2009): it is quite evident that the location and amount of surface faulting is consistent with the spatial distribution of coseismic slope movements, in terms of both areal density and size.

A similar result is shown by the spatial distribution of EEEs induced by the 1811-1812 New Madrid, Missouri, earthquakes, mapped in Fig. 5. Indeed, the most relevant primary and secondary effects are located along the Mississippi valley near New

Madrid, consistently with the surface projection of the causative faults, and unquestionably provide diagnostic elements for assessing an epicentral intensity equal to XI.

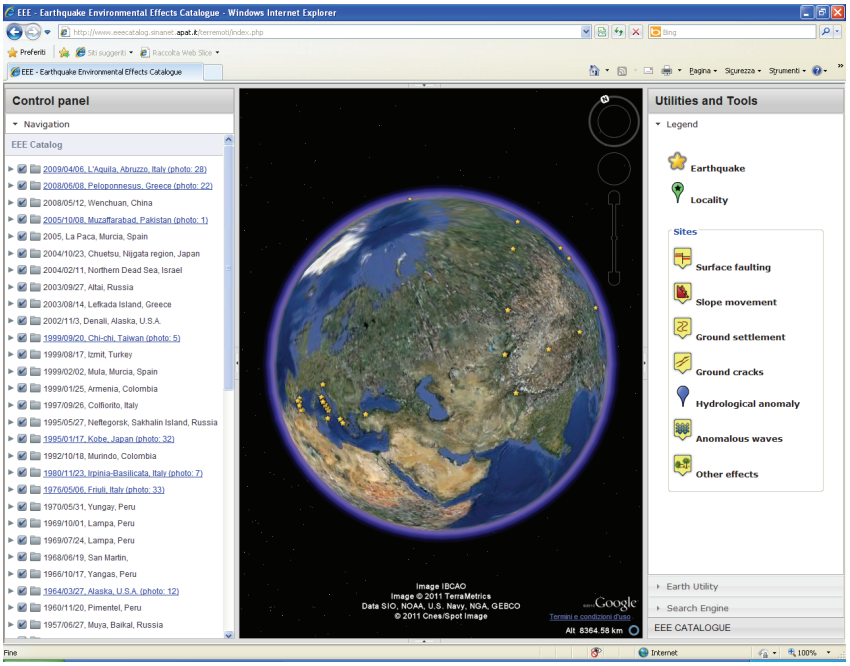

Fig. 2: The public interface of the EEE Catalogue, developed on Google Earth http://www.eeecatalog.sinanet.apat.it/terremoti/index.php.

Fig. 3: EEEs induced by the December 28, 1908 Messina Straits, Italy, earthquake in the area of the Messina harbour. If information from contemporary sources is very precise, it is possible to use the EEE Catalogue also for local seismic microzonation.

FINAL REMARKS

The recent catastrophic earthquakes occurred in Japan and New Zealand have clearly pointed out that traditional seismic hazard assessment based only on vibratory ground motion data need to be integrated with information about the local vulnerability of the territory to earthquake occurrence.
The collection of Earthquake Environmental Effects provided by the EEE Catalogue aims at identifying the areas most vulnerable to earthquake occurrence. This information must complement traditional SHA based on PGA maps.

Moreover, based on EEE characteristics, size and spatial distribution it is possible i) to assess the earthquake intensity through the ESI scale, and ii) to objectively compare the earthquake intensity of events occurred in different areas and/or in different periods.

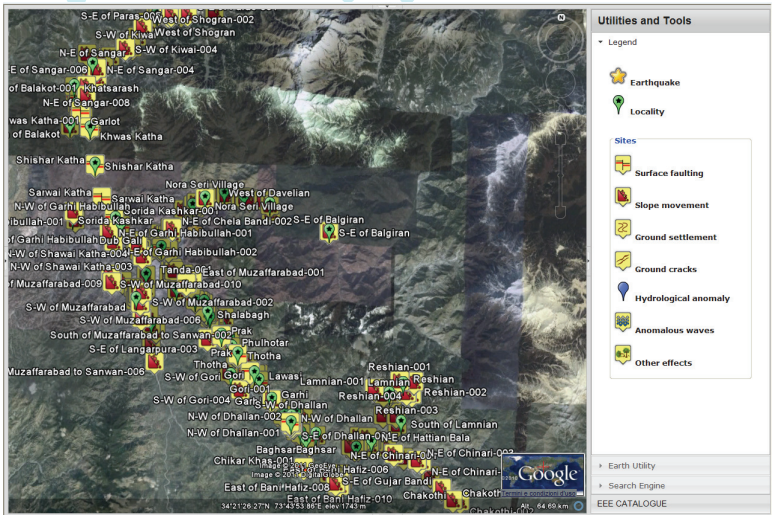

Fig. 4 :Surface faulting and slope movements induced by the October 8, 2005 Muzaffarabad earthquake.

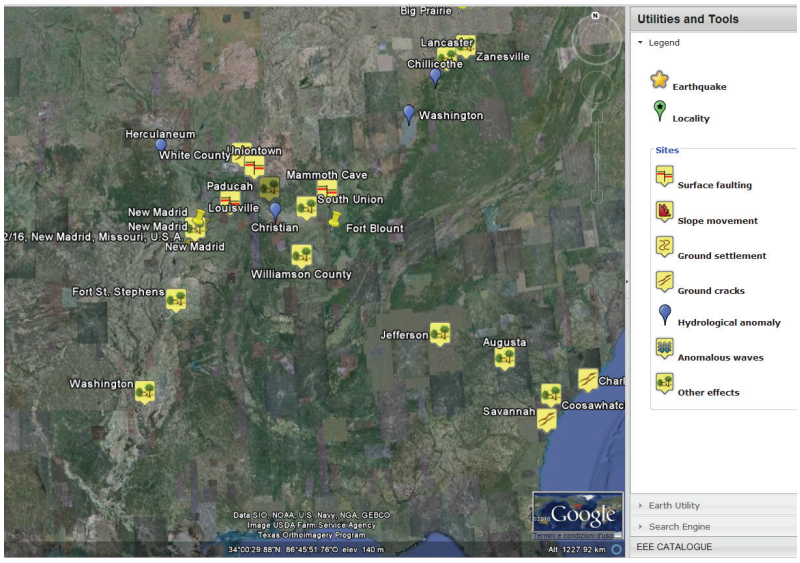

Fig. 5 : EEE induced by the December 16 1811 New Madrid, Missouri, earthquake. Primary and secondary effects indicative of intensity XI in the ESI 2007 scale are located in the epicentral area along the Mississippi Valley.

Acknowledgements:
Fabio Baiocco and Antonio Scaramella are acknowledged for their crucial support in building the infrastructure of the EEE Catalogue. We wish also to acknowledge all the people who has participated to the implementation of the EEE Catalogue in the frame of the #0418 INQUA TERPRO Project.

References

Ali Z., Qaisar M., Mahmood T., Ali Shah M., Iqbal T.,, Serva L., Michetti A.M.. and Burton P.W. (2009) - The Muzaffarabad, Pakistan, earthquake of 8 October 2005: surface faulting, environmental effects and macroseismic intensity Geological Society, London, Special Publications 2009, 316:155-172; doi:10.1144/SP316.9.

HERP (2009). Long-term assessment on seismic activity along Japan trench offshore Sanriku and offshore Boso Peninsular. *http://www.jishin.go.jp/main/chousa/09mar_sanriku/index.htm* [in Japanese with many figures].

Michetti, A. M., E. Esposito, L. Guerrieri, S. Porfido, L. Serva, R. Tatevossian, E. Vittori, F. Audemard, T. Azuma, J. Clague, V. Comerci, A. Gurpinar, J. McCalpin, B. Mohammadioun, N. A. Morner, Y. Ota, and E. Roghozin (2007). Intensity Scale ESI 2007. In *Memorie Descrittive Carta Geologica d'Italia* L. Guerrieri and E. Vittori (Editors), APAT, Servizio Geologico d'Italia—Dipartimento Difesa del Suolo, Roma, Italy, 74, 53 pp.

Sawai Y., Shishikura M., Okamura Y., Takada K., Matsu'ura T., Tin Aung T., Komatsubara J., Fuji Y., Fujiwara O., Satake K., Kamataki T., and Sato N. (2007). A study on paleotsunami using handy geoslicer in Sendai Plain (Sendai, Natori, Iwanuma, Watari and Yamamoto), Miyagi, Japan. N. 7, p. 47-80, 2007 *http://unit.aist.go.jp/actfault-eq/seika/h18seika/pdf/sawai.pdf* [In Japanese with English abstract and captions].

EARTHQUAKE ARCHAEOLOGY

INQUA PALEOSEISMOLOGY AND ACTIVE TECTONICS

ACTIVE TECTONICS OF ALBANIA INFERRED FROM FLUVIAL TERRACES GEOMETRIES

Guzman, Oswaldo (1,2), Jean-Louis Mugnier (1), Rexhep Koçi (3), Riccardo Vassallo (1), Julien Carcaillet (4), Francois Jouanne (1), Eric Fouache (5)

(1) Institut de sciences de la Terre. Université de Savoie, Bâtiment des Belledonnes, Campus Scientifique, 73376 Le Bourget du Lac Cedex, France. E-mail : Oswaldo-Jose.Guzman-Guitierrez@etu.univ-savoie.fr, Jean-Louis.Mugnier@univ-savoie.fr, Riccardo.Vassallo@univ-savoie.fr, Francois.Jouanne@univ-savoie.fr
(2) Dpto. Ciencias de La Tierra, Universidad Simon Bolivar, Edificio FE-II. Apartado 89000, Caracas 1081-A, Venezuela
(3) Institut de Sciences de la Terre. Université Joseph Fourier. Maison des Géosciences, 1381 rue de la Piscine, 38400 Saint Matin d'Hères, France. E-mail : Julien.Carcaillet@ujf-Grenoble.fr
(4) Institute of Seismology of the Academy of Science, Tirana, Albania. E-mail: rexhep.koci@yahoo.com
(5) University of Paris 10, Nanterre, UMR 8591, EA435 Gecko, France. E-mail: eric.g.fouache@wanadoo.fr

Abstract (Active Tectonics of Albania Inferred from Fluvial Terraces Geometries): *We studied four rivers of the southern Albanides in order to quantify the geodynamic control on the incision of alluvial terraces. The Vjosa, Osum, Devoll and Shkumbin rivers flow from north-western Greece and southern Albania across the active Dinaro-Hellenic Alpine fold belt to the west. From mapping and dating of terrace abandonment, we reconstructed spatial and temporal variations of incision rates along those rivers. These reconstructions allow a quantification of the fluvial evolution at a higher resolution than a glacial-inter-glacial cycle, and therefore an estimation of the effect of geodynamic uplift on river incision. We identified ten preserved terraces units developed since the "MIS-6" up to historic time. Uplift seems to produce two distinct effects: an overall increase of the incision rate from west to east related to regional bulging and local pulses of increasing incision generated by activation of faults.*

Key words*: Albania, Active Tectonics, Alluvial Terraces.*

INTRODUCTION

Active tectonics, eustatic and climatic variation are the forcing that controls the formations of fluvial terraces. In a tectonically active setting characterised by long term uplift, Pazzaglia (submitted) suggests that the incision rate equals ~~to~~ the long-term uplift rate. Nonetheless, the morphology of the rivers in this context is strongly climate-dependent: a change in downstream base level could have a profound impact on long profile shape (Merrits et al., 1994), and hydrologically-driven changes in discharge and sediment load induce periodically lateral incision processes that widen the channel bottom producing strath fluvial terraces (Hancock & Anderson 2002) or aggradation leading to the development of filled terraces (Ouchi, 1985)

The Albanide domain is rather small (less than 5. 10^4 km^2). We consider that the climatic evolutions of the different Albanide catchments are rather similar. Therefore differences in the evolution of the studied catchments would not be explained by local climate changes.

The active tectonics pattern in Albania is quite variable (*Fig. 1*), with a NE-SW shortening in the western part of the Albania, and a NW-SE extension in the inner part of the chain, it leads to spatially variable long term uplift (Aliaj, 2000). Therefore the comparison of the different catchments evolution would help to estimate the uplift rate in Albania and to outline the role of the variation of the tectonics rate in the sedimentation/erosion behaviour of the catchments.

GEOLOGICAL SETTING

The Dinaro-Hellenic Alpine fold belt constitutes a segment of the wide Circum-Mediterranean Peri-Tethyan thrust belt. This belt as a result of the Dinaric subduction. The Albanian foothills have been thrust westwards over the Adriatic foredeep during the Alpine orogeny (Roure et al., 2004).

The presenty-day geodynamic deformation results from the subduction of the Adriatic Sea floor beneath the foreland domain. This geodynamic setting produces contrasting relief with a flexural basin filled with Plio-Quaternary deposits and forming a flat costal plain in the foreland, a thin skinned fold and thrust belt in the midland, and a large basin and range zone in the hinterland, resulting from synorogenic Neogene-Quaternary grabens that crosscut the thrust system (Roure et al., 2004, Niewland, et al., 2001).

The area (*Fig.1*) is still tectonically active and produces permanent microseismicity and frequent earthquakes reaching intensities of IX. GPS data suggest that the western Albania is being affected by southwestward motions relative to Adriatic microplate, illustrating the ongoing collision of external Albanides, whereas inner Albanides present southward motion, increasing from north to south, relative to both Adriatic and stable Eurasia (Jouanne et al., submitted).

The neotectonics are controlled by NE-SW compressive stress in the western part connected to subduction of the Apulian lithosphere and extensional stress in the internal zones (Goldsworthy et al., 2002; Roure et al., 2004). The major extension direction varies from E-W close to the Ohrid and Prespa lakes

to NNW-SSE at the southern end of the Ersekë basins (Jouanne et al., submitted). On the regional scale the Albanides are governed by long-term uplift (Aliaj, 2000).

We concentrate our study on a zone located between two major transverse structures which cut the area: the Vlore-Fier-Elbasani-Dibra transfer zone in the central part of Albania (Roure et al., 2004), and the prolongation of the Keffalinia strike-slip zone at the northwestern border of Greece (Baker et al., 1997). The Vjosa, Osum, Devoll and Skhumbin rivers constitute four of the six main rivers of Albania. They are close to each other; therefore, their climatic settings are comparable.

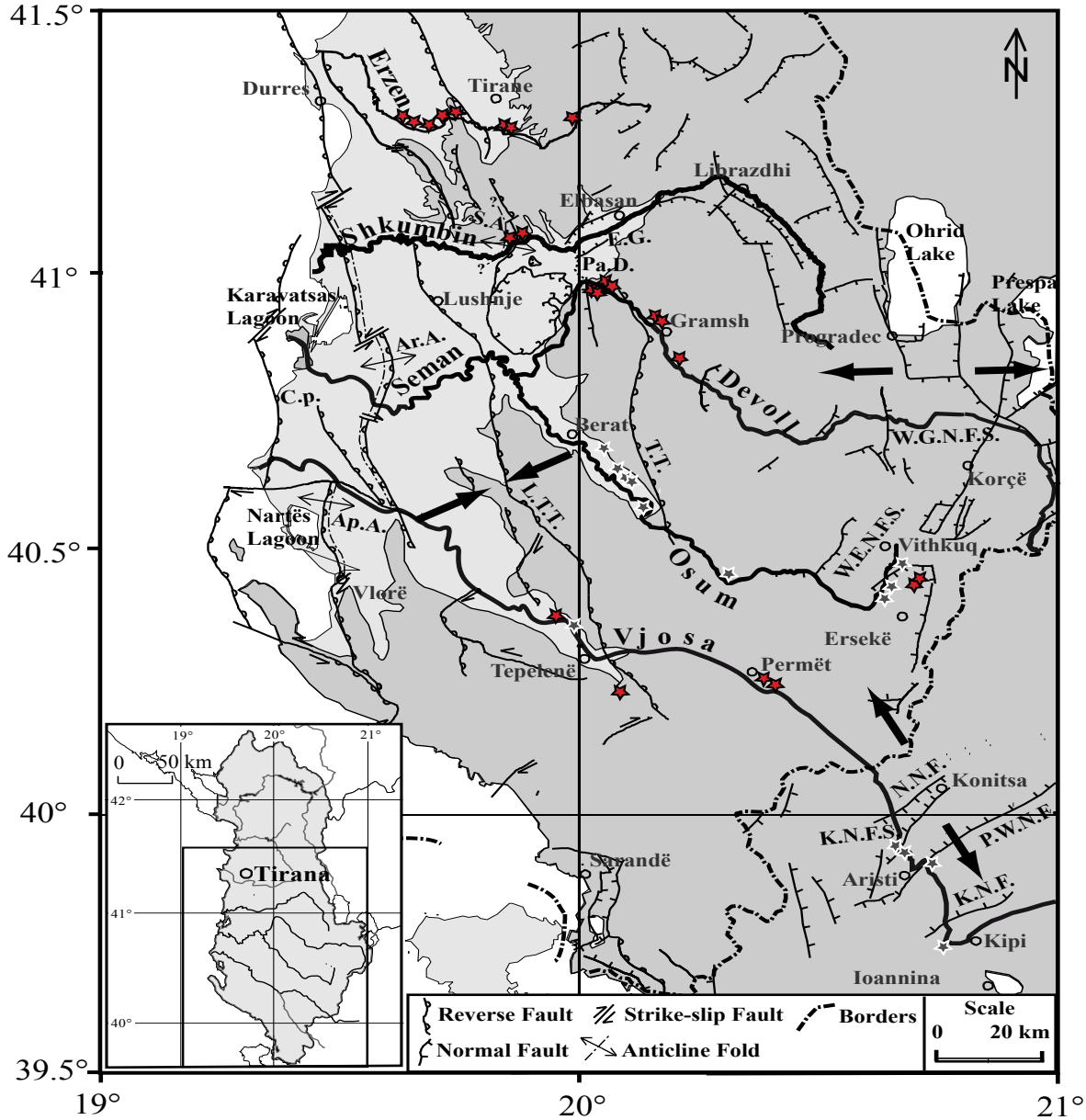

Figure 1. Neo-tectonic map of the Southern Albania and North-western Greece (Modified from Aliaj et al., 2000 and Carcaillet, et al, 2009). Areas located within 200 m above Sea level are in light grey. Dark grey stars indicate published data (Lewin et al., 1991; Hamlin et al., 2000; Woodward et al., 2001; Carcaillet et al., 2009) and red stars indicate data computed in the present study. Fault and fold types are described in the picture caption and the overall current tectonic deformation is represented by black arrows (from Jouanne et al., submitted). (C.p.) Coastal pop-up; (Ar.A.) Ardenica Anticline; (Ap.A.) Apollonia Anticline; (S.A.) Shkumbin Anticline; (T.T.) Tomorrica Thrust; (L.T.T.) Lushnje - Tepelenë Thrust; (B.N.F.) Bulcar Normal Fault; (E.G.) Elbasan Graben; (N.N.F.) Nerotrivi Normal Fault; (K.N.F.S.) Konitsa Normal Fault Systems; (P.W.N.F.) Papingo West Normal Fault; (K.N.F.) Kipi Normal Fault; (W.G.N.F.S.) West Graben Normal Fault Systems; (W.E.N.F.S.) West Ersekë Normal Fault Systems; (PaD) PaleoDevoll.

METHODS AND RESULTS

The terraces has been mapped from field work, satellite image and 1/25000 topo sheets. Terrace thicknesses and elevations above the present-day river bed have been measured using a laser range distancemeter. Terrace age control was obtained from data previously published by Lewin et al. (1991), Hamlin et al. (2000), Woodward et al. (2001) and Carcaillet et al. (2009) as well as from *in situ*

produced ^{10}Be and radiocarbon (^{14}C) dating specifically performed for this study.

We dated organic residues (thirteen ^{14}C ages) and quartz rich pebbles collected into layers developed during the last flooding event and considered the value as the age of abandonment of the alluvial terrace. This implies that the age of the terrace abandonment is contemporaneous to the age of deposition of the highest terrace layer. The samples for cosmonuclide (*in situ* produced ^{10}Be) age determinations have been collected on siliceous rich pebbles along depth-profiles of two terraces of the lower Skhumbin and one on the top of the upper Osum.

Incision rate has been calculated by dividing the elevation of the terraces above the river by the age of the upper surface of the terraces; the vertical motions of the faults have been deduced from the local change of the incision rates.

Our study has allowed estimating the vertical slip rate of actives structures in southern Albania (*Fig, 2, 3 and 4, Table 1*). These results confirm an important uplift rate, up to 2 mm/year (Carcaillet, et al. 2009), for the central Albania and the current activity of the Plio-Quaternary folds of external Albanides. They also show significant Quaternary displacement rates along normal faults of inner Albanides. Our results are in agreements with the E-W to N-S extension deduced from the GPS network.

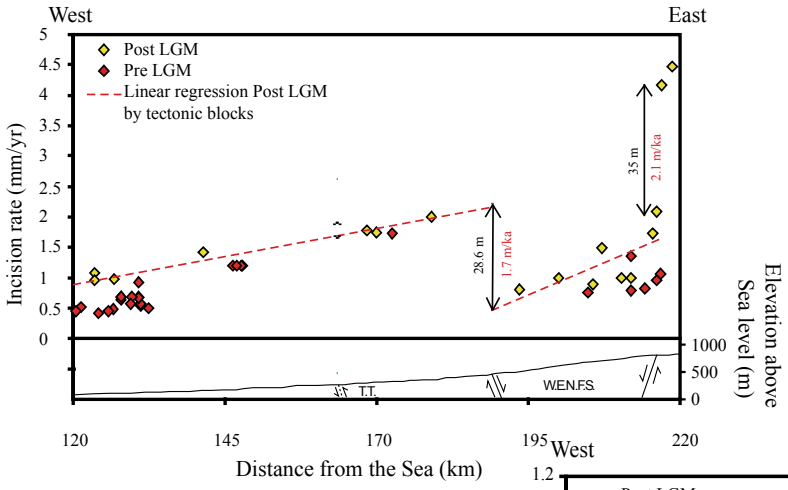

Figure 2. *Evolution of the incision rate along the river profile of the Osum. Left axis is the calculated incision rate; right axis is the the elevation of the present-day river bed. Colour of the diamonds refers to the different terraces units. Into the lower box, appear the actual river profile where are located the actives faults. Bold lines represent normal faults belong of West Ersekë Normal Fault Systems (W.E.N.F.S.) producing surface displacements and the dashed lines represent the Tomorrica Thrust (T.T.) which would not influence in the evolution of the river profile.*

Figure 3. *Evolution of the incision rate along the river profile of the Vjosa. bed. In the river profile are located the Lushnje - Tepelenë Thrust (L.T.T.), Nerotrivi Normal fault (N.N.F.), Konitsa Normal Fault Systems (K.N.F.S.) Papingo West Normal Fault (P.W.N.F.).*

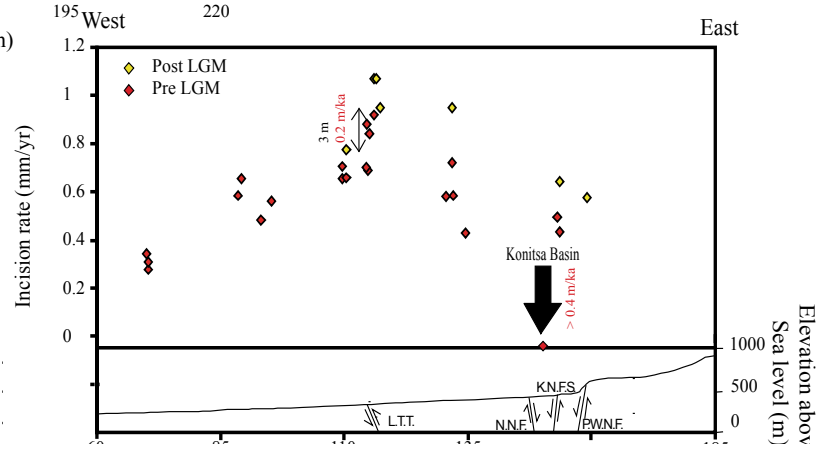

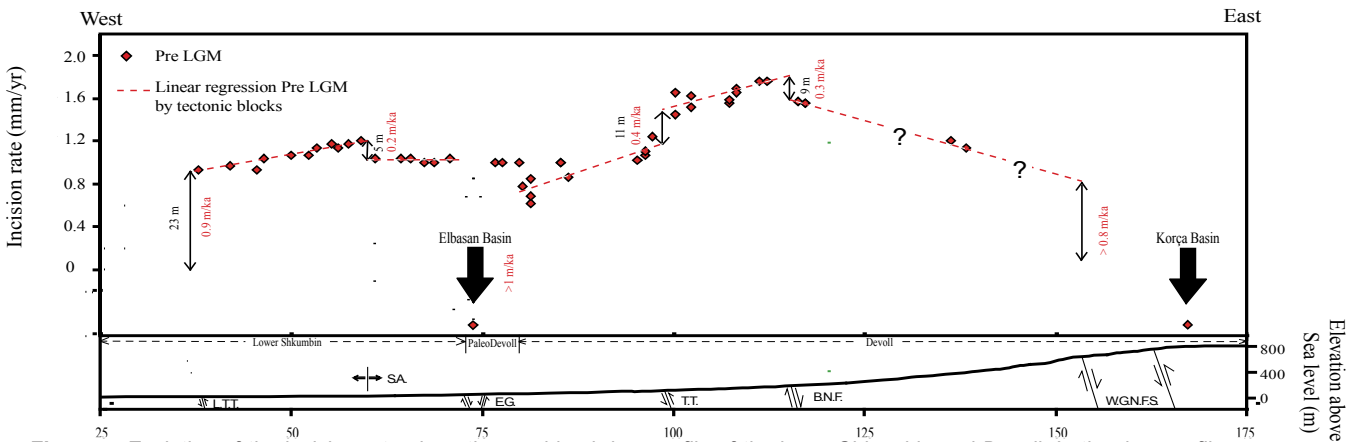

Figure 4. *Evolution of the incision rate along the combined river profile of the lower Shkumbin and Devoll. In the river profile are located the Lushnje - Tepelenë Thrust (L.T.T.), the Shkumbin Anticline (S.A.), Tomorrica Thrust (T.T.), the Burcal Normal Fault (B.N.F.) and the West Graben Normal Fault Systems (W.G.N.F.S.) producing surface displacements.*

Table 1. Kinematic of active structures active analyzed from the incision of the terraces levels of the Vjosa, Osum, Devoll and Shkumbin rivers.

Name Structure	River	Vertical slip rate (mm/yr)
Coastal pop - up	PaleoSeman	~ 0.1
Shkumbin Anticline	Shkumbin	~ 0.2
Elbasan Graben	Shkumbin	> 1
Lushnje - Tepelenë Thrust	Shkumbin	~ 0.9
Lushnje - Tepelenë Thrust	Vjosa	~ 0.2
Tomorrica Thrust	Devoll	~ 0.4
Burcal Normal Fault	Devoll	~ 0.3
Nerotrivi Normal Fault	Vjosa	> 0.4
Konitsa Normal Fault Systems	Vjosa	> 0.4
Papingo West Normal Fault	Vjosa	~1.8 between 25 and 17 Ka (Carcaillet, et al, 2009)
West Graben Normal Fault Systems	Devoll	> 0.8
West Ersekë Normal Fault Systems	Osum	1.7 – 2.1

SEISMICITY, PRESENT-DAY DEFORMATION AND ACTIVE TECTONICS

Current tectonics of Albania is characterized by an important microseismicity, small and medium size earthquake and a few large events as shown by the occurrence of earthquakes with magnitudes exceeding 6 during the last century (Jouanne et al., submitted), (e.g. 1905, Shkodra earthquakes Ms=6.6, 1911 Ohrid lake earthquake Ms = 6.7, 1920 Tepelena event Ms=6.4, 1926 Durres earthquake Ms=6., 1967 Dibra earthquake Ms=6.6and 1979 Montenegro earthquake Ms=6.9).

The strongest earthquakes occur in three well-defined seismic belts: a) The Ionian-Adriatic coastal earthquake belt at the eastern margin of the Adria microplate, which trends NW-SE represents the most seismically active zone in the country; b) The Peshkopia-Korça earthquake belt, which trends N-S, and c) The Elbasani-Dibra earthquake belt, which trends N-E, (Sulstarova et al. 2000; Aliaj, 2000).

Focal mechanisms (Sulstarova et al., 2000, Aliaj, 2000) and geodetic data (Jouanne et al., submitted), fit the geodynamics setting with a NE-SW compression across external Albanides and E-W to NNW-SSE extension in the internal Albanides.

The comparison of our results and the deformation deduced from the GPS network (jouanne et al., submitted) indicates that:

a) The horizontal shortening linked to the active thrust faults exceeds 2 mm/yr (assuming a mean dip of 30° for the thrusts) and is close to the deformation rates deduced from GPS ; b) the extension linked to normal fault system would be in the order of 1 mm/yr (assuming a dip of 60° for the normal faults) and is smaller than the deformation rates deduced from GPS; c) The normal faulting linked to the East Albanian graben systems seems more active than the normal faulting that affects the North West part of Greece.

Acknowledgements: The authors thank the NATO SFP 977993 and the Science for Peace team to have supported this work.

References

Aliaj, S. (2000). Neotectonics and seismicity in Albania, in: Geology of Albania, edited by: Meco, S., Aliaj, S., and Turku, I., Beitr. Regional. Geol. Erde, 28, 135–178.

Baker, C., Hatzfeld, D., Lyon-Caen, H., Papadimitriou, E., Rigo, A. (1997). Earthquake mechanisms of the Adriatic Sea and Western Greece: implications for the oceanic subduction-continental collision transition. Geophysical Journal International 131, 559-594.

Carcaillet, J., Mugnier, J.L., Koçi, R., Jouanne, F. (2009). Uplift and active tectonics of southern Albania inferred from incision of alluvial terraces. Quaternary Research 71, 465-476.

Goldsworthy, M., Jackson, J., Haines, J. (2002). The continuity of active fault systems in Greece. Geophysical Journal International 148(3), 596-618.

Hancock, G., Anderson, R. (2002). Numerical modeling of fluvial strath-terrace formation in response to oscillating climate. Geological Society of America Bulletin 114(9): 1131-1142

Hamlin, R.,Woodward, J., Black, S., Macklin, M.G. (2000). Sediment fingerprinting as 580 a tool for interpreting long-term river activity: the Voidomatis basin, NWGreece. In: 581 Foster, I.D.L. (Ed.), Tracers in Geomorphology. Wiley, Chichester, 473–501.

Jouanne, F., Bushati, S., Mugnier, J.L., Shinko, I., Pasha, M., Koci, R. (Submitted). GPS constrains on current tectonics of Albania. Geophysical Research Letters.

Lewin, J., Macklin, M.G., Woodward, J.C. (1991). Late Quaternary fluvial sedimentation in the Voidomatis basin, Epirus, Northwest Greece. Quaternary Research 35, 103-115.

Merritts, D.J., Vincent, K.R., Wohl, E.E. (1994). Long river profiles, tectonism, and eustasy: a guide to interpreting fluvial terraces. Journal of Geophysical research, 99, 14031-14050.

Niewland, D.A., Oudemayer, B.C., Valbona, U. (2001). The tectonic development of 616 Albania: explanation and prediction of structural styles. Marine and Petroleum 617 Geology 18, 161–177.

Ouchi, S. (1985) Response of alluvial rivers to slow active tectonics movements, Geol. Soc. Am. Bull., 96, 504-515.

Pazzaglia, F. J. River Terraces, in Wohl, E., ed., Treatise of Geomorphology, Elsevier. Submitted

Sulstarova, E., Peçi, V., Shuteriqi, P. (2000). Vlora-Elbasani-Dibra (Albania) transversal fault zone and its seismic activity. Journal of Seimology 4, 117-131.

Roure, F., Nazaj, S., Mushka, K., Fili, I., Cadet, J.P., Bonneau, M. (2004). Kinematic evolution and petroleum systems - An appraisal of the Outer Albanides. In: Mc Clay K.R. (Ed.), Thrust tectonics and hydrocarbon systems. AAPG memoir 82, 474-493.

EARTHQUAKE ARCHAEOLOGY

INQUA PALEOSEISMOLOGY AND ACTIVE TECTONICS

LECHAION, THE ANCIENT HARBOUR OF CORINTH (PELOPONNESE, GREECE) DESTROYED BY TSUNAMIGENIC IMPACT

Hadler, Hanna (1), Andreas Vött (1), Benjamin Koster (2), Margret Mathes-Schmidt (2), Torsten Mattern (3), Konstantin Ntageretzis (1), Klaus Reicherter (2), Dimitris Sakellariou (4), Timo Willershäuser (1)

(1) Institute for Geography, Johannes Gutenberg-Universität Mainz, Johann-Joachim-Becher-Weg 21, 55099 Mainz, GERMANY. E-mail: hadler@uni-mainz.de
(2) Neotectonics and Natural Hazards Group, RWTH Aachen, Lochnerstr. 4-20, 52056 Aachen, GERMANY.
(3) Faculty of Classical Archaeology, University of Trier, Universitätsring 15, 54296 Trier, GERMANY.
(4) Institute of Oceanography, Hellenic Centre for Marine Research, 47 km Athens-Sounio Ave., 19013 Anavyssos, GREECE.

Abstract: *Lechaion, the harbour of ancient Corinth, is situated at the south-eastern extension of the Gulf of Corinth (Peloponnese, Greece). Due to extensive fault systems dominating the gulf, seismic activity is frequent and often related to landslides or submarine mass movements. Thus, the study area is highly exposed to tsunami hazard. By means of geo-scientific studies comprising geomorphological, sedimentological and geophysical methods, evidence of multiple palaeotsunami impact was encountered at the Lechaion harbour site and the surrounding coastal area. The detected tsunami signatures include allochthonous marine sediments intersecting quiescent harbour deposits, extensive units of tsunamigenic beachrock and geo-archaeological destruction layers. Our results suggest that the harbour at Lechaion was finally destroyed in the 6th century AD by strong tsunami impact.*

Key words*: Palaeotsunami, beachrock, ancient harbours, Lechaion*

INTRODUCTION

Situated in the eastern Mediterranean, the Gulf of Corinth belongs to one of the seismically most active regions in the world. Due to ongoing continental rifting with high extension rates up to 16 mm/yr, this half-graben structure is surrounded by active on-shore and submarine faults (Papazachos & Dimitriu 1991; Sachpazi et al., 2003; Avallone et al., 2004). Strong earthquakes, often accompanied by coseismic displacement of the seafloor and/or inducing submarine slides are therefore common throughout the gulf. Water depths of maximum 900 m, steep submarine slopes and a narrow shelf additionally enhance the potential of strong tsunamis (Hasiotis et al., 2002; Stefatos et al., 2006). Accordingly, numerous tsunami catalogues for the Mediterranean and especially for Greece report on historical tsunami events that occurred within the Gulf of Corinth (Soloviev et al., 2000; Papadopoulos, 2003; Ambrasey & Synolakis, 2010). Solely for the 20th century, six tsunamis have been recorded; the most destructive occurred near Aeghio in 1963 (Papadopoulos, 2003).

The main objectives of our study were to (i) detect allochthonous high-energy event layers within the sedimentary record of the harbour basin at Lechaion and (ii) to reconstruct the late-Holocene coastal evolution of the study area.

LECHAION – THE ANCIENT HARBOUR OF CORINTH

Lechaion, the western harbour of ancient Corinth, is situated at the Isthmus of Corinth, which connects the Peloponnese with mainland Greece. The harbour was most probably founded around 600 BC when the Corinthians expanded their military and trading activities (Stiros et al., 1996). According to ancient sources, Lechaion served as a naval base from the 4th century BC and was connected to the city of Corinth by a harbour road protected by strong walls (Xen. Hell. 4.4.6-8 after Brownson, 1918). With the devastation of Corinth in 146 BC, Lechaion was abandoned but re-activated under Roman supremacy in 44 BC. In Roman times, the harbour underwent different phases of reconstruction and mainly served as trading base (Strab. Geogr. 8.6.20-23 after Hamilton & Falconer, 1903). The final abandonment of Roman Lechaion is reported to be associated with the destruction of ancient Corinth by a series of strong earthquakes in 521 or 551 AD. Though occasionally re-used in medieval times, the harbour never regained its former importance (Rothaus, 1995).

Today, certain harbour installations are still visible, including two outer moles, an entrance channel leading to an elongated inner harbour basin and the remains of an ancient quay wall (Paris, 1915). The present day topography is dominated by large mounds of sediments dredged from the harbour basin (Fig. 1). Between the inner harbour basin and the present beach the remains of an early Christian basilica, dating to the late 5th century AD, were

excavated. The basilica, 186 m long, represents the largest from this period and was completely destroyed by the 521 or 551 AD earthquake series (Krautheimer, 1989; Rothaus, 1995).

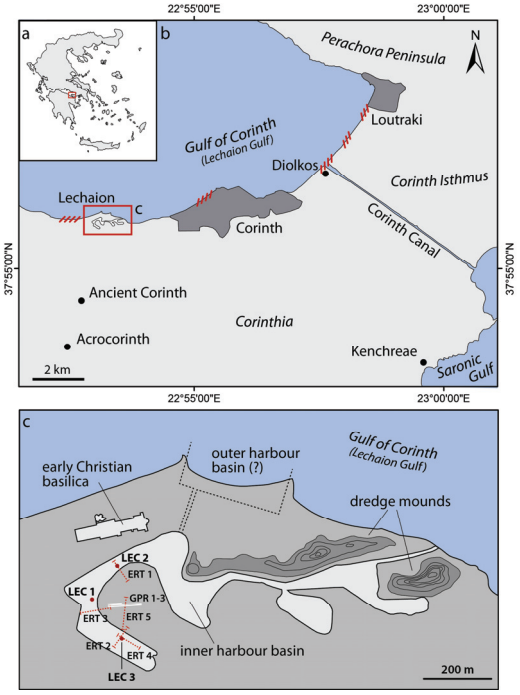

Fig. 1: (a) Location of study area in Greece. (b) Overview of the Corinthia. Red box indicates harbour site of Lechaion, red dashes indicate beachrock. (c) Map of the Lechaion harbour basin and adjacent area. Vibracores LEC 1-3 are indicated by red dots, ERT-measurements by red dashed lines and GRP-measurements by white lines (maps modified after Google Earth images, 2009).

TSUNAMI IMPACT AT THE LECHAION HARBOUR SITE

Sedimentary evidence from the harbour basin

As previous studies show, tsunami impact may be documented by layers of allochthonous coarse-grained sediment intersecting quiescent near-shore deposits (Vött et al. 2009). Low-energy environments such as harbour basins therefore represent excellent geological archives for palaeotsunami research.

Sedimentological, geochemical and micropalaeontological studies were carried out at the Lechaion harbour site (see Fig. 1 for location of vibracores). The local stratigraphy comprises shallow marine (pre-harbour) deposits overlain by harbour-related, quiescent lagoonal sediments followed by limnic to terrestrial deposits accumulated when the harbour was already out of use (Fig. 2). The stratigraphical record of all vibracores is repeatedly interrupted by layers of allochthonous coarse-grained sediment and shell debris, partly characterized by fining upward sequences. These ex situ-layers extend up to 450 m inland. Erosional unconformities at the base (Fig. 2b) and immediately re-established quiescent conditions on top of the event layers indicate short term high-energy interference of the Lechaion harbour site.

*Fig. 2: (a) Vibracore LEC 2 (N 37° 55' 58.6 E 22° 53' 03.5", -0.04 m a.s.l.) was drilled in the central Lechaion harbour basin. Here, two coarse-grained tsunami layers were found, intersecting the autochthonous, predominantly shallow-marine to lagoonal facies. Youngest tsunami deposit as encountered in core LEC 3 and covering early Christian basilica is dredged at site LEC 2 (see Δ). ^{14}C-samples are marked by *. (b) Detailed view of the younger event layer. The quiescent harbour environment was abruptly covered by allochthonous high-energy deposits (Photo by T. Willershäuser, 2010).*

The event-stratigraphical correlation of all vibracore profiles reveals three distinct tsunami layers. The geochronological framework is based on radiocarbon dating and age determination of diagnostic ceramic fragments. Tsunamigenic impact could be time-bracketed by radiocarbon dating to around 760 cal BC and 50 cal AD and to the 6th century AD by geoarchaeological findings. The youngest event correlates to the geoarchaeological destruction layer presented below.

Geoarchaeological destruction layers

Large sediment mounds adjacent to the inner harbour basin are generally referred to as natural dunes or sediments obtained from dredging activity (Frazer, 1965; Rothaus, 1995; Stiros, 1996). They consist of sand and gravel, intermingled with numerous ceramic fragments and marine macrofossils. The sediment composition and grain size distribution thus exclude natural dune formation. However, gravel is also completely atypical for the siltation of a quiescent harbour basin environment (Marriner & Morhange 2007). According to their grain size, the sediments provide evidence of high-energy influence. Incorporating marine as well as terrigeneous material, they indicate strong tsunamigenic inundation and backflow affecting the coastal plain at Lechaion. Since associated to dredging activities, the mounds therefore document tsunami influence burying the Lechaion harbour basin.

Widespread burial of the harbour site by high-energy influence must also be assumed regarding the ruins

of the 5th century AD Christian basilica. The entire foundation like the adjacent area is completely covered by an up to 2 m thick sediment layer. The surrounding topography as well as the sediment composition, however, exclude a colluvial, fluvial or mass denudative burial of the site. The deposits are also not related to the archaeological excavation of the site. A former door lintel used as a threshold after the destruction of the church attests that the entrance level was already elevated during historic times. Made up of a sandy matrix incorporating abundant gravel, numerous ceramic fragments and marine macrofossils, the high-energy sediment layer again reflects tsunami backflow.

Fig. 3: (a) Excavated remains of the 5th century AD Christian basilica erected to the north of the former harbour basin. (b) The present day ground surface overtops the basilica's original ground level by up to 2 m (in photo: ca. 1.2 m). (c) The sedimentary cover consists of sand and gravel with abundant ceramic fragments and marine shell debris.

Several earth resistivity transects were carried out around the ancient harbour basin (Fig. 1c). They revealed a sharp boundary between the allochthonous high-energy deposits and the underlying autochthonous fine-grained harbour sediments as well as a clear thinning landward of the event layer up to 450 m inland. Furthermore, ground penetrating radar profiles (Fig. 1c) revealed channel-like structures at their base. Orientated perpendicular towards the coastline, these incised channels indicate strong linear erosion in land-/seaward direction. Similar structures, created by strong backflow processes, were observed along the Chilean coast after the February 2010 Chile tsunami (Bahlburg & Spiske 2010).

In a summary view, our results give evidence for the influence of tsunami impact on the Lechaion harbour. According to Rothaus (1995), only few ceramic fragments younger than late Roman to early Byzantine times were found in the vicinity of the harbour basin and basilica. Thus, we consider tsunami landfall in the 6th century AD as the most probable cause for the final destruction and abandonment of the harbour.

Beachrock as indicator for tsunami impact

Along the Corinthian coastline, extensive beachrock formations dominate the present coastal geomorphology. As recently described by Vött et al. (2010), beachrock deposits may be of tsunamigenic origin. At the Corinth Canal at a distance of 7 km from Lechaion, the beachrock complex extends up to 300 m inland (Fig. 4a), while the maximum extension of the recent beach is less than 25 m. The deposits show a clearly laminated structure with multiple fining upward sequences reaching from gravel to fine sand. The inner structure reveals a landward orientated imbrication of the gravel components (Fig. 4b) documenting landward flow dynamics as may be induced during tsunami inundation. According to their sedimentary structure, these beachrock deposits must not automatically be regarded as lithified beach but may rather represent calcified tsunamigenic deposits (for further discussion see Vött et al. 2010). The "diolkos", an ancient slipway across the Isthmus of Corinth, is partly covered by beachrock; used until the early 1st century AD, the diolkos represents a *terminus post quem* for the tsunamigenic impact.

Fig. 4: (a) Extensive beachrock deposits at the Corinth Canal. (b) The internal structure shows a fining upward sequence as well as imbricated pieces of gravel.

CONCLUSION

Based on our studies, multiple tsunami impact was determined for the Lechaion harbour site and adjacent coastal areas. At least three distinct event layers were identified, the youngest and obviously most destructive event dating to the 6th century AD.

The spatial distribution and geomorphological variability of the encountered tsunami deposits require an event-stratigraphical approach to understand and reconstruct the chronology of events. Based on the combination of historical accounts with geomorphological, sedimentological, geophysical and geoarchaeological data we conclude that the ancient harbour of Lechaion, though influenced by tsunamis before, was finally destroyed by tsunami impact, most probably triggered during the 521 or 551 AD earthquake series. The present day topography of the harbour site is due to a latter re-activation of the

harbour in medieval or pre-modern times and thus only partly represents the ancient Corinthian harbour.

Acknowledgement: We acknowledge funding of the project by the German Research Foundation, DFG (Bonn, Gz. VO 938/3-1). Sincere thanks are due to the 37th Ephorate of Prehistoric and Classical Antiquities, Corinth, for support during field work and discussion.

References

Ambrasey, N. & C. Synolakis, (2010). Tsunami catalogs for the eastern Mediterranean, revisited. *Journal of Earthquake Engineering* 14, 309-330.

Avallone, A., P. Briole, A.M. Agatza-Balodimou, H. Billiris, O. Charade, C. Mitsakaki, A. Nercessian, K. Papazissi, D. Paradissis & G. Veis, (2004). Analysis of eleven years of deformation measured by GPS in the Corinth Rift Laboratory area. *Competes Rendus Geosciences* 336 (4-5), 301-311.

Bahlburg, H. & M. Spiske, (2010). The February 27, 2010 Chile Tsunami. Sedimentology of runup and backflow deposits at Isla Mocha. *American Geophysical Union, Abstract #OS42B-06*.

Brownson, C.L. (ed.), (1918). *Xenophon, Hellenica*. Harvard University Press. Cambridge.

Frazer, J.G., (1965). *Pausanias's description of Greece*. Biblo and Tannen. New York. 652 p.

Hamilton, H.C. & W. Falconer, (1903). *The Geography of Strabo*. George Bell & Sons. London.

Hasiotis, T., G. Papatheodorou, G. Bouckovalas, C. Corbau & G. Ferentinos, (2002). Earthquake-induced coastal sediment instabilities in the western Gulf of Corinth, Greece. *Marine Geology* 186, 319-335.

Krautheimer, R., (1989). Early Christian and Byzantine Architecture. Penguin Books. London. 556 p.

Marriner, N. & C. Morhange, (2007). Geoscience of ancient Mediterranean harbours. *Eart-Science Reviews* 80, 137-194.

Papadopoulos, G.A., (2003). Tsunami hazard in the eastern Mediterranean: strong earthquakes and tsunamis in the Corinth Gulf, Central Greece. *Natural Hazards* 29, 437-464.

Papazachos, B.C. & P.P. Dimitriu, (1991). Tsunamis in and near Greece and their relation to the earthquake focal mechanism. *Natural Hazards* 4, 161-170.

Paris, J., (1915). Contributions à l'étude des portes antiques du mond grec. Notes sur Lechaion. *Bulletin de Correspondance Hellénique* 39 (1), 5-16.

Rothaus, R., (1995). Lechaion, western port of Corinth: a preliminary archaeology and history. *Oxford Journal of Archaeology* 14 (3), 293-306.

Sachpazi, M., C. Clément, M. Laigle, A. Hirn & N. Roussos, (2003). Rift structure, evolution, and earthquakes in the Gulf of corinth, from reflection seismic images. *Earth and Planetary Science Letters* 216, 243-257.

Soloviev, S.L., O.N. Solovieva, C.N. Go, K.S. Kim & N.A. Shchetnikov, (2000). *Tsunamis in the Mediterranean Sea 2000 BC – 2000 AD*. Kluwer Academic Publishers. Dordrecht. 237 p.

Stefatos, A., M. Charalambakis, G. Papatheodorou & G. Ferentinos, (2006). Tsunamigenic sources in an antive European half-graben (Gulf of Corinth, Central Greece). *Marine Geology* 232, 35-47.

Stiros, S., P. Pirazolli, R. Rothaus, S. Papageorgiou, J. Laborel & M. Arnold, (1996). On the date of construction of Lechaion, western harbor of Ancient Corinth, Greece. *Geoarchaeology: An International Journal* 11 (3), 251-263.

Vött, A., H. Brückner, S.M. May, D. Sakellariou, O. Nelle, F. Lang, V. Kapsimalis, S. Jahns, R. Herd, M. Handl & I. Fountoulis, (2009). The Lake Voulkaria (Akarnania, NW Greece) palaeoenvironmental archive – a sediment trap for multiple tsunami impact since the mid-Holocene. *Zeitschrift für Geomorphologie N.F., Suppl. Issue* 53 (1), 1-37.

Vött, A., G. Bareth, H. Brückner, C. Curdt, I. Fountoulis, R. Grapmayer, H. Hadler, D. Hoffmeister, N. Klasen, F. Lang, P. Masberg, S.M. May, K. Ntageretzis, D. Sakellariou & T. Willershäuser, (2010). Beachrock-type calcarenitic tsunamites along the shores of the eastern Ionian Sea (western Greece) – case studies from Akarnania, the Ionian Islands and the western Peloponnese. *Zeitschrift für Geomorphologie N.F., Suppl. Issue* 54 (3), 1-50.

STRUCTURAL CHARACTERISTICS AND EVOLUTION OF THE YANGSAN-ULSAN FAULT SYSTEM, SE KOREA

S.-R. Han (1), M. Lee (1), J. Park (2), Y.-S., Kim (1)*

(1) Dept. of Environmental Geosciences, Pukyong National University, Busan 608-737, Korea. *Email: ysk7909@pknu.ac.kr
(2) GeoGeny Consultants Group Inc. 807-2 Bangbae-Dong Seocho-Gu, Seoul 137-831, Korea.

Abstract (Structural characteristics and evolution of the YangSAN-Ulan fault system, SE Korea): *The Yangsan-Ulsan Fault System (YUFS) is a major fault system in Korea. More than 40 Quaternary faults have been discovered around the YUFS. To understand the evolution and structural characteristics of the YUFS, we performed numerical modelling for the evolution of the YUFS and fault zone analysis on the eastern part of the Ulsan fault. The result of the modelling shows that the YUFS evolved into λ-fault, a low angle merging fault system. In a fault zone analysis, the hanging wall block of the fault shows relatively higher damage with higher fracture density and deformation structures compared with the footwall. This indicates that the hanging wall is more susceptible to deformation than the footwall during faulting events; this result is consistent with damage patterns in other Quaternary faults. Epicenters of recent earthquakes around the study area are also concentrated on the hanging wall of the Ulsan fault. This kind of study can help us to evaluate hazards resulting from future potential earthquakes in and around active fault systems.*

Key words*: Yangsna-Ulsan fault system, λ-fault , Quaternary faults*

INTRODUCTION

The Korean Peninsula is generally considered as a relatively safe region considering earthquake hazards, because it is located away from plate boundaries. However, many moderate and minor earthquakes occur around the Yangsan-Ulsan fault system (YUFS), in the southeastern part of the Korean Peninsula (Lee and Yang, 2006). Recently, more than 40 Quaternary faults were discovered near the YUFS (Jin et al., 2011).

There are two nuclear power plant sites near the YUFS (Fig.1). To prevent nuclear catastrophe due to a potential large scale earthquake, it is necessary to understand the deformation characteristics and future evolution of the YUFS. For this purpose, a numerical modelling related to the evolution of the YUFS and a detailed field investigation on a reactivated fault were carried out in this study.

STUDY AREA

The study area is located in the Cretaceous Gyeongsang Basin, SE Korea (Fig. 1). The basement of the study area is composed of Cretaceous sedimentary rocks with later igneous and volcanic rocks. The Yangsan fault is a NNE-SSW trending right-lateral dominant strike-slip fault, and the NNW-SSE trending Ulsan fault is interpreted as a strike-slip fault overprinted by later reverse-slip. Recently, more than 40 Quaternary faults have been discovered near the Yangsan and Ulsan faults. Historical records show many earthquakes in this region, with an earthquake producing over 100 casualties recorded in A.D. 779 (estimated M= 6.7), near the intersection of the two faults (Lee and Yang, 2006).

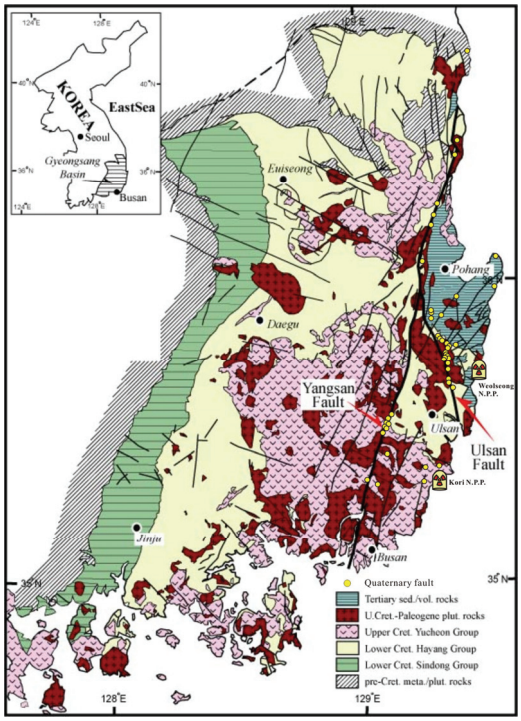

Fig. 1: Regional geologic map of Gyeongsang basin, the SE part of the Korean peninsula and Quaternary faults (circles) around the Yangsan and Ulsan faults. Two Nuclear Power plants are located near the YUFS (modified from Lee, 2000)

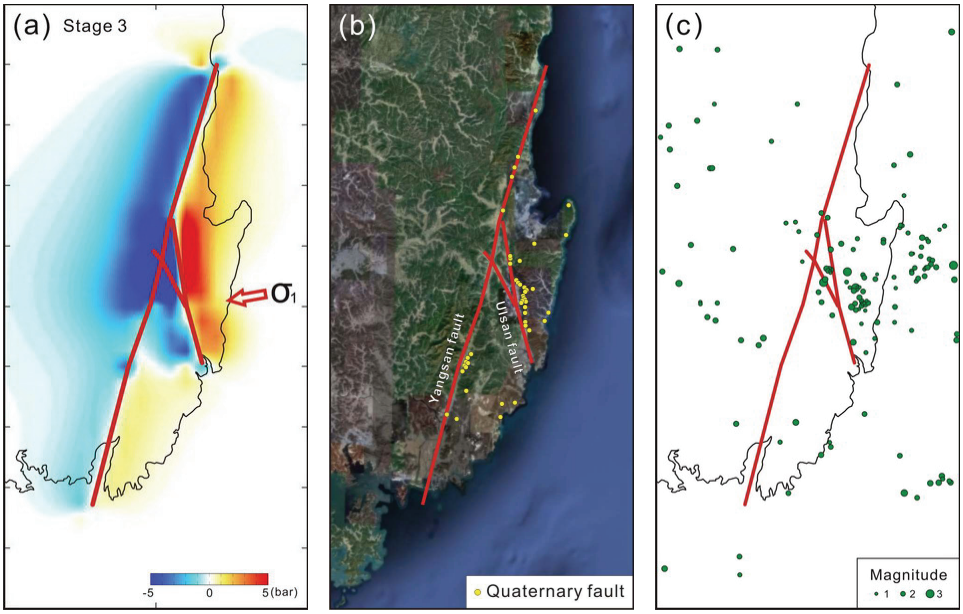

Fig. 2: Comparison between coulomb stress changes, distribution of Quaternary faults and epicenters of earthquakes around the Yangsan-Ulsan fault system (Han et al., 2009). (a) Coulomb stress changes are concentrated in the eastern and southeastern region of the Yangsan fault and eastern region of the Ulsan fault in Quaternary. (b) Locations of Quaternary faults around the Yangsan-Ulsan fault system. (c) Earthquake distributions around the southeastern part of the Korean peninsula (1994-1998). Green circles indicate the epicenters of the recent earthquakes. Earthquakes are concentrated in the eastern part (hanging wall) of the Ulsan fault.

EVOLUTION MODELLING OF THE YANGSAN-ULSAN FAULT SYSTEM

Analysis of lineaments and geomorphology of the YUFS indicate that the YUFS is analogous to the characteristics of λ-fault. The concept of λ-fault was suggested by Du and Aydin (1995). This is the geometric relationship between two intersecting strike-slip faults. When a strike-slip fault propagates into a pre-existing strike-slip fault, the orientation of the propagation depends on the angle between the maximum principal stress and propagating fault. To understand the evolution of the fault system, a numerical modelling on the YUFS with regards to stress changes with time was performed, using the USGS open program Coulomb 3 (http://earthquake.usgs.gov). This modelling was carried out based on a previously suggested tectonic evolution model for the YUFS (Park, 2004). The result of this numerical modelling indicates that the YUFS is a λ-fault. During the propagation of the Ulsan fault into the Yangsan fault in the late Miocene, coulomb stress increases at the north-western tip of the Ulsan fault. After the Ulsan fault connected to the Yangsan fault in Pliocene, a new segment was initiated at the northern part of the Ulsan fault due to stress changes. Since the penetration of the Ulsan fault into the Yangsan fault in Quaternary, coulomb stress increased in the north-eastern region of the Yangsan fault and the eastern region of the Ulsan fault. These regions are well consistent with the distribution of Quaternary faults and locations of epicenters of recent earthquakes around the YUFS (Fig. 2).

FAULT GEOMETRY AND SLIP ANALYSIS OF A FAULT ZONE IN THE WEOLSEONG AREA

In the SE part of Korea, two nuclear power plant (NPP) sites are located near the YUFS. In the new Weolseong NPP site located in the southeastern coast of Korea, an east dipping, N-S trending fault was discovered during construction. The main fault zone shows various different coloured fault gouge bands and shear fabrics indicating opposite slips (Fig. 3). These features indicate that there were discrete stages of normal and reverse faulting events along this fault zone. The analyzed kinematic indicators, such as lineations, cleavages, and slickenlines in the fault zone suggest that the fault was initiated as a normal fault and was reactivated as a reverse fault under NW-SE compression. The hanging wall block of the fault shows relatively higher damage indicating higher deformation in the hanging wall than the footwall.

CONCLUSION

It is common that earthquakes occur by reactivation of pre-existing faults (e.g. Chen, 2002; Ota et al., 2004; Ota et al., 2005). It is well known that most of the damage from earthquake is concentrated on the hanging wall block during the faulting (Ota et al., 2005). A N-S trending, east dipping fault zone was discovered in the construction site of the new Weolseong NPP.Detailed analysis was performed on this fault zone and the result indicates multiple faulting events. According to the analysis, this fault zone initiated as a normal slip fault and it was

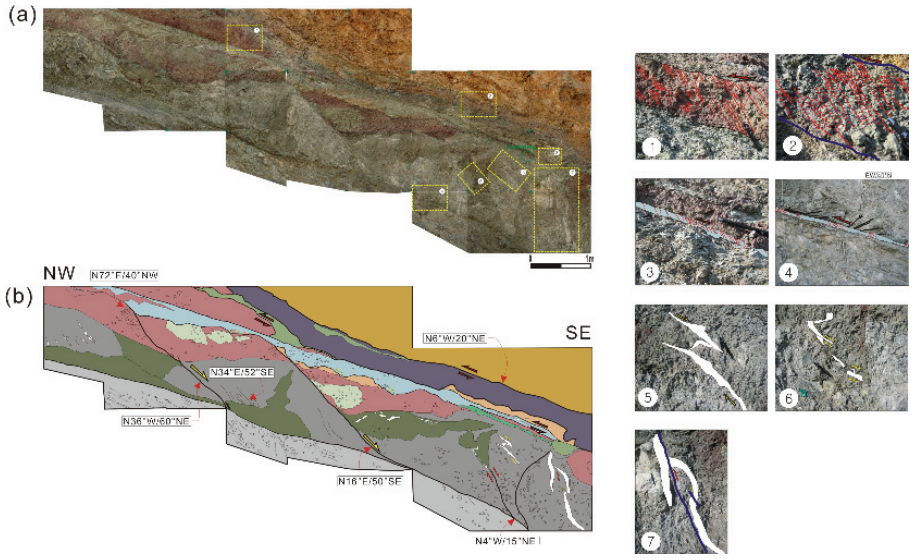

Fig. 3: Photomosaic (a), sketch (b) and sense indicators (c) of reactivated fault zone located at the new Weolseong nuclear power plant (Fig. 1).

reactivated as a reverse fault. The damages in the wall rocks of this fault were concentrated on the hanging wall block rather than footwall block. This result indicates that the hanging wall block is subject to higher deformation than footwall block during faulting. This result is well consistent with the result from larger scale deformation characteristics around the YUFS producing intense distribution of Quaternary faults and earthquakes in the hanging wall of the Ulsan fault. Therefore, detailed analysis of fault zone and fault evolution modelling can contribute to understanding of the deformation characteristics of a fault zone and the evaluation of earthquake hazards.

Therefore, the fault geometries and kinematics are important factors to evaluate conditions of important sites. Furthermore, fault damage zones (Kim et al., 2004) around faults are very important indications for the seismic hazard assessment due to secondary fractures and aftershocks (Kim and Sanderson, 2008).

Acknowledgements: This work was funded by Korea Institute of Nuclear Safety under Grant M20702070001-08M0207-00110.

References

Du, Y. and Aydin, A. (1995) Shear fracture patterns and connectivity at geometric complexities along strike-slip faults. Journal of Geophygical Research, 100, 18093-18102.

Han, S.-R., Park. J., Kim, Y.-S. (2009) Evolution modelling of the Yangsan-Ulsan fault system with stress changes. Journal of the Geological Society of Korea. 45, 361-377. (In Korean with English abstract)

Chen, Y.-G., Chen, W.S., Wang, Y., Lo, P.W., Lee, J.C., Liu, T.K.(b) (2002) Review of paleoseismological and active fault studies in Taiwan in the light of the Chichi earthquake of September 21, 1999.Tectonophysics 508, 63-77.

Lee, J.I. (2000) Provenance and thermal maturity of the lower Cretaceous Gyeongsang Supergroup, Korea. Ph.D. Thesis. Seoul National University.

Lee, K. and Na, S.H. (1983) A study of microearthquake activity of the Yangsan fault. Journal of the Geological Society of Korea, 19, 127-135.

Jin, K., Lee, M., Kim, Y.-S., Choi, J.-H. (2011). Archaeoseismological studies on historical heritage sites in the Gyeongju area, SE Korea. Quaternary International, doi:10.1016/j.quaint.2011.03.055.

Lee, M. S., Kang, P. C. (1964) Geological map of Yangsan area. Geological Survey of Korea. (In Korean with English abstract)

Lee, K., Yang, W.-S. (2006). Historical seismicity of Korea. Bulletin of the Seismo-logical Society of America 96, 846e855.Stiros, S. 1988b. Archaeology, a tool to study active tectonics – The Aegean as a case study. Eos, Transactions, American Geophysical Union 13, 1636-1639.

Ota, Y., Watanabe, M., Suzuki, Y., Sawa, H. (2004). Geomorphological identification of pre-exiting active Chelungpu Fault in central Taiwan, especially its relation to the location of the surface rupture by the 1999 Chichi earthquake. Quaternary International 115–166, 155– 166.

Ota, Y., Chen, Y.-G., Chen, W.-S., (2005). Review of paleoseismological and active fault studies in Taiwan in the light of the Chichi earthquake of September 21, 1999. Tectonophysics 508, 63-77.

Park. J. (2004) The structural characteristics of the Tertiary basin in Gyeongju region, Korea. Master thesis. Seoul National University. (In Korean with English abstract)

EARTHQUAKE ARCHAEOLOGY

INQUA PALEOSEISMOLOGY AND ACTIVE TECTONICS

WHERE LANDSLIDES REPRESENT THE MOST IMPORTANT EARTHQUAKE-RELATED HAZARDS: THE MOUNTAIN AREAS OF CENTRAL ASIA

Havenith, Hans-Balder (1)

(1) Georisks and Environment group, Department of Geology, University of Liege. B18. 4000 Liege. BELGIUM. Email: HB.Havenith@ulg.ac.be

***Abstract (Where landslides represent the most important earthquake-related hazards: the mountain areas of Central Asia)**: The goal of this paper is to show which areas are particularly prone to earthquake-induced slope failure. In this regard, the paper considers the short- and long-term effects of geological, tectonic, climatic and morphological conditions. Case histories related to five earthquake events in the Tien Shan and Pamir Mountains are outlined: the earthquakes of Kemin in 1911, Sarez in 1911, Khait in 1949, Gissar in 1989 and Suusamyr in 1992. The potential impact of seismically triggered mass movement affecting loess deposits is further pointed out through comparison with the 1920 Haiyuan (China) earthquake. One conclusion is that in semi-arid mountain regions marked by a strong seismic activity, such as those in Central Asia, seismogenic landslides and related long-term effects may represent the most important geohazards. Further, the susceptibility to seismic slope instability is highest along active fault zones and on convex slopes made of soft or fractured materials.*

***Key words**: landslides, co- and post-seismic effects, dynamics*

INTRODUCTION: THE PERCEPTION OF SEISMIC LANDSLIDE HAZARDS

During the last ten years, after a series of disastrous earthquake events in mountain regions in Taiwan (1999), El Salvador (2001), Pakistan (2005) and China (2008), increasing attention has been addressed to landslides triggered by earthquakes.

Previously, landslides have been considered as minor effects of earthquakes compared to the impact of the ground shaking itself. Schuster and Highland (2001) partly attributed the perception of the relatively small impact of earthquake-triggered mass movements to the fact that many related losses are often referred to as direct consequences of the earthquake. However, for the earthquake that hit the Kashmir mountains on October 8, 2005, Petley et al. (2006) estimated that about 30% of the total number of killed people (officially 87350), i.e. 26500, had been victims of co-seismic landslides. Less than three years later, on May 12, 2008, the Wenchuan earthquake hit the Sichuan and neighbouring provinces of China and caused 'more than 15000 geohazards in the form of landslides, rockfalls, and debris flows, which resulted in about 20000 deaths' (Yin et al. 2009). These casualties represent again almost 30 % of the official total number of fatalities of 69197 of this event.

In the remote areas of Central Asian mountains, M>6 earthquakes generally do not cause catastrophes – but if they do, they do it through mass movements, like in the case of the M=8.2 Kemin, 1911, M=7.4 Sarez, 1911, M=7.4 Khait, 1949, M=5.5 Gissar, 1989 and M=7.3 Suusamyr, 1992 earthquakes (see location in Fig. 1). These case histories show that both rapid flows (mainly) in loess deposits and massive rock avalanches created the greatest disasters. To highlight the important issue related to landslides triggered in loess deposits, a comparison is made with one of the worldwide most catastrophic seismic events involving landslides: the M=7.8 Haiyuan (or Gansu, 1920) earthquake in China.

Special attention must also to be paid to post-seismic increase of landslide activity. In this regard, we have to take into consideration so-called 'secondary or tertiary effects' of earthquakes, such as landslide dams and related flooding impacts. The 2008 Wenchuan earthquake clearly marked the importance of such effects – which could have killed another few thousands of people if efficient mitigation measures had not been taken by Chinese authorities.

GEOLOGICAL, TOPOGRAPHIC AND CLIMATIC SETTING OF EARTHQUAKE-INDUCED SLOPE FAILURE

Sassa (1996) observed that seismic landslide occurrence is strongly dependent on the proximity of the fault rupture. This observation is confirmed by many others made after the 1999 Taiwan, 2005 Pakistan and 2008 Sichuan earthquakes.

The geological factors have been extensively analysed by Keefer (1984) who concluded that any geological material with low geomechanical strength, be it soil or rock, may be susceptible to earthquake-induced slope instability. The low strength may be related to weak cementation, intense weathering or fracturing, high water saturation or poor compaction. Concerning the structural elements (bedding, foliation, sediment-rock contact), no clear trend can be outlined. Especially for seismic rock slope failure, e.g., it is not clear if cross-bedding joints or bedding contacts support the development of a sliding surface

or not. Here, clearly more research based on structural geology mapping is needed.

Further, earthquake-induced landslides may be triggered from any surface morphology, in flat areas, such as lateral spreads, or on steep cliffs, such as rock falls. Still, several particularities can be outlined. From observations after the 2005 Pakistan earthquake, Sato et al. (2007) inferred that 'there was a slight trend that large landslides occurred on vertically convex slopes rather than on concave slopes; furthermore, large landslides occurred on steeper (30° and more) slopes than on gentler slopes'. From my experience of earthquake-induced landslides in the Tien Shan (see below), it can be concluded that mainly the surface curvature has an influence on seismic slope stability at a global scale; particularly, hillcrests, higher parts of slopes and convex surface morphologies are prone to seismic slope failure. The influence of slope angle on seismic slope stability is not clear; in some cases, especially in rocks, steeper slopes are more prone to instability; in others, especially in soft sediments, gentle slopes produce most of the mass movements, indicating that the combined effect of slope and geology has to be taken into consideration.

The contribution of the climate to seismic slope failure has not yet been well investigated. According to our experience, the strongest contribution of earthquake-induced landslides to the total seismic and landslide hazards can be observed in semi-arid mountain regions marked by a high seismicity – such as the Tien Shan and the Pamir, but also the Hindu-Kush and others. Why semi-arid? If the climate is wet, the overall landslide hazards increase more than the specific hazard related to seismically triggered slope failure (e.g. Himalayas). On the contrary, if the climate is very dry – arid, the seismic hazards with direct impacts on building stability prevail (e.g. mountains in the Middle East, Southern Altai) since slope instability – also under seismic conditions - requires a certain amount of humidity in the top-soils to develop. In the Tien Shan, we observed that earthquakes, which occurred at the end of the dry summer season, caused relatively few slope failures (e.g., Ms=7.3 Suusamyr earthquake on August 19, 1992; Ms=6.7 Nura earthquake on October 5, 2008); while, for instance, the Ms=7.4 Khait earthquake of July 10, 1949 – at the beginning of the dry high-mountain summer - in northern Tajikistan triggered widespread slope instability.

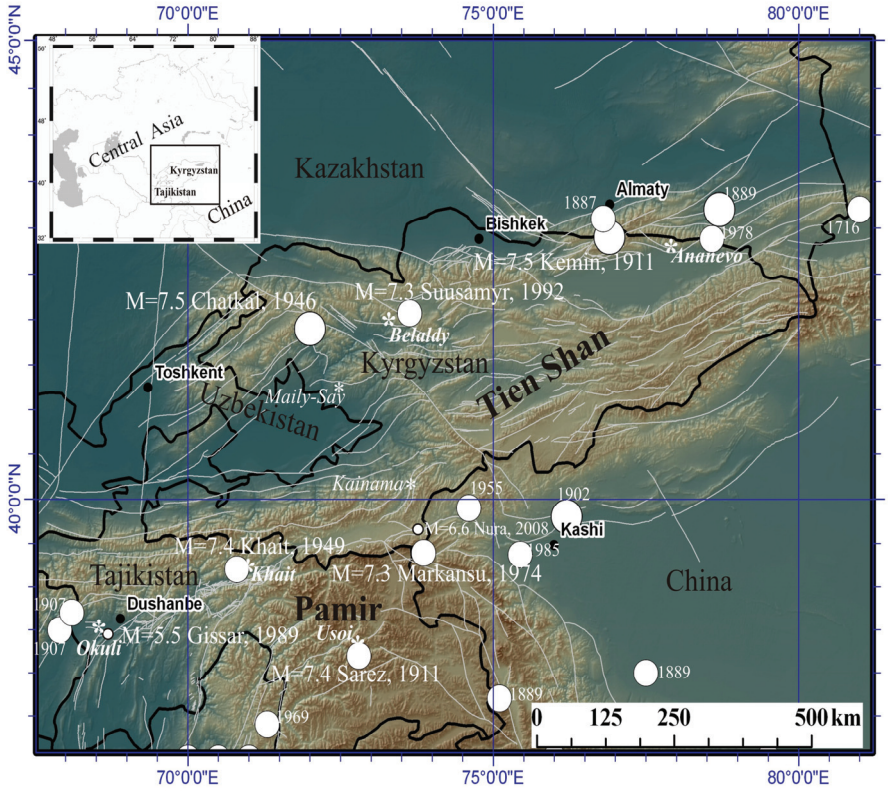

Fig. 1: Map of Tien Shan and Pamir Mountains in Central Asia with location of major faults and earthquakes (white filled circles show all recorded M>=7 earthquakes with the year of occurrence; the magnitude is indicated for analysed events) and related major mass movements (stars).

CASE HISTORIES FROM CENTRAL ASIA COMPARED WITH THE 1920 CHINA EVENT

Nadim et al. (2006) assessed landslide and avalanche occurrence probabilities worldwide on the basis of morphological, geological, meteorological and seismological data. They clearly showed that all landslide hotspots are located in seismically active mountain ranges. For Central Asia, they estimate that global landslide hazard can be rated as medium to very high. They further noted that some areas in

Tajikistan are marked by highest mortality risk due to landslides.

The following case histories document the landslide hazard and risk triggered by earthquakes in the Tien Shan and the Pamir Mountains. A comparison will be made with the 1920 Haiyuan (China) event to outline the most important factors contributing to landslide hazard and risk related to the presence of thick loess deposits in Central Asia.

The Kemin earthquake, 1911

The Kemin Ms=8.2 earthquake of 1911 (January 3) is one of the strongest events ever recorded in the Tien Shan. The earthquake caused extensive landsliding along the activated fault segments over a length of 200 km. The 'Ananevo' rockslide located in the north of lake Issyk Kul (at some 80 km east of the presumed epicentre) is one of the most prominent feature produced by the Kemin earthquake (Havenith et al., 2002, see Fig. 2). Failure took place at the southern end of a mountain ridge, just above the discontinuous Chon Aksu fault also activated by the 1911 Kemin earthquake. This section of the Chon Aksu fault is a thrust gently dipping towards the northeast into the collapsed slope. Evidence of the presence of the fault is the related scarp with a height of almost 10 m at 12 km to the WNW. On the site itself, outcrops at the foot of the southwest-oriented slope show particularly disintegrated and weathered granitic rocks within a 100-200 m thick fault zone.

Fig. 2: Photograph of the Ananevo rockslide. The horse-farm building (lower left corner) is 60 by 60 m.

The Sarez earthquake, 1911

The Sarez earthquake, Ms=7.6, struck the central Pamir Mountains, Tajikistan, on February 18, 1911. Such an earthquake is likely to have triggered hundreds or thousands of mass movements, but only one is well documented: the giant Usoi rockslide, which fell from a 4500 m high mountain down to an elevation of 2700 m in the valley (Schuster and Alford, 2004). This rockslide has formed a dam with a volume of about $2*10^9$ m^3 on Murgab River.

The Khait earthquake, 1949

According to Leonov (1960), the M=7.4 Khait earthquake that struck Northern Tajikistan on July 10, 1949, produced a very destructive mass movement that had buried the villages of Khait and Kusurak with thousands of inhabitants (Fig. 3) - the exact number of fatalities will never be known. This rock avalanche had been triggered from Borgulchak mountain at an altitude of about 2950 m and travelled more than 6 km before reaching the inhabited valley at an altitude of 1550 m. The volume is about $40*10^6$ m^3. A significant part of the mass movement was made of loess, which probably contributed to the mobility of the initial rockslide. In the Yasman valley, opposite to the Khait rock avalanche, massive loess earth-flows are believed to have buried about 20 villages. In total, the Khait rock avalanche and loess earth-flows are likely to have killed more than 5000 people during the 1949 event.

Fig. 3: Khait rock avalanche; view towards the East from Yasman valley (unpublished photograph of 2005 provided by A. Ischuk). The length of the scarp is about 1 km.

The Gissar earthquake, 1989

South of Dushanbe, in Gissar, Tajikistan, a Ms=5.5 earthquake on January 23, 1989 had triggered a series of earth-flows in loess. At least 200 people were killed and hundreds of houses were buried. According to Ishihara et al. (1990), those slides were all related to extensive liquefaction, which had developed for a horizontal acceleration of about 0.15g. Ishihara et al. (1990) associated the liquefaction to the 'collapsible nature' of the highly porous loess material (a silt-sized deposit with an average content of clay of 15 % and a low plasticity).

The Suusamyr earthquake, 1992

The most recent large seismic event hitting Central Asian mountain regions was the Ms=7.3 Suusamyr earthquake on August 19, 1992, triggering various types of ground failures in the Northern-Central Tien Shan (Bogachkin et al., 1997).

Most of the 50 people killed in the remote areas were victims of mass movements. Korjenkov et al. (2004) described a series of ground failures and also a great variety of gravitation cracks. Ground instability could be observed along the crest and southern slope of the Chet-Korumdy ridge – here, most landslides had developed from previously existing ground instabilities. The largest mass movement, a rock avalanche, had formed a landslide dam that partly failed in 1993, causing a long-runout debris flow and widespread flooding downstream.

The Haiyuan or Gansu earthquake, 1920

On December 16, 1920, a M=8.5 earthquake occurred near Ganyan Chi, Haiyuan County of the Ningxia Hui Autonomous Region in China (Zhang, 1995). Several hundreds of thousands of houses collapsed and officially 234.117 people died. Zhang (1995) noticed that particularly high intensities were recorded over areas covered by thick loess deposits and that in those deposits 'landslides were not only controlled by the intensity of the earthquake, but by the structure of the subsoil'. Zhang and Wang (2007) reported that about 100000 people were killed just by landslides in loess deposits. They observed that loess earth-flows triggered by the Haiyuan earthquake had developed on relatively gentle slopes compared to those triggered by rainfall in the same region. These observations highlight the particular susceptibility of loess areas to ground failure, such as it was clearly shown by Derbyshire et al. (2000) analysing geological hazards affecting the loess plateau of China.

CONCLUSIONS

A series of case histories of earthquake-induced landslides in Central Asia have been presented. These show that the most disastrous mass movements in Central Asia are long runout and rapid (>20 m/s) rock avalanches and loess earth-flows. While the giant rockslides are almost exclusively triggered by large magnitude seismic events (M≥7) in Central Asian mountain regions, loess earth-flows may also be triggered by smaller earthquakes – or even by climatic factors. Here, I presented some examples of fatal loess landslides triggered directly by a M=5.5 earthquake in Tajikistan. The comparison with the Haiyuan earthquake event of 1920 shows that such loess landslides can be very disastrous.

The importance of mid- and long-term effects is outlined for both rockslides and loess landslides. Several case histories showed that one important – if not the most important – long-term consequence of massive rockslides can be the formation of a dam and the impoundment of a natural reservoir. Actually, the largest still existing rockslide dam on earth had formed in 1911 in the Pamir Mountains.

I also wanted to show that similar earthquakes may not necessarily trigger the same number of landslides, due to different climatic conditions and groundwater level at the time of the earthquake.

Finally, it is important to note that landslides are not only instantaneous effects of earthquakes – some had already developed before the seismic shock and some continued or started moving well after the shaking. To better assess the short- to long-term effects earthquakes on slopes, landslides need to be monitored by geophysical, seismological and geotechnical systems, coupled to multi-temporal satellite imagery and numerical modeling of multi-event scenarios. In the frame of new projects on landslide problems in Central Asia, focus will be on the installation of such coupled monitoring–modeling systems.

Acknowledgements: This study was supported by the NATO science for Peace and Security Project LADATSHA 983289, 2009-2012.

References

Derbyshire, E., Meng, X. & T.A. Dijkstra, (2000). *Landslide in the Thick Loess Terrain of North-West China*. John Wiley, Chichester, U.K.

Havenith, H.B., Jongmans, D., Faccioli, E., Abdrakhmatov, K. & P.Y. Bard, (2002). Site effects analysis around the seismically induced Ananevo rockslide, Kyrgyzstan. *Bulletin of the Seismological Society of America*, 92, 3190-3209.

Ishihara, K., Okusa, S., Oyagi, N. & A. Ischuk, (1990). Liquefaction-induced flow slide in the collapsible deposit in the Soviet Tajik. *Soils and Foundations*, 30: 73-89.

Keefer, D.K., (1984). Landslides Caused by Earthquakes, *Geological Society of America Bulletin*, 95: 406–421.

Korjenkov, A.M., Mamyrov, E., Omuraliev, M., Kovalenko, V.A. & S.F. Usmanov, 2004. Rock Avalanches and Landslides Formed in Result of Strong Suusamyr (1992, M=7,4) Earthquake in the Northern Tien Shan. Test Structures for Mapping of Paleoseismic Deformations by Satellite Images. In *High Mountain Remote Sensing Cartography VII (HMRSC VII),* M. F. Buchroithner (ed.), Institute for Cartography of the Dresden University of Technology. Kartographische Bausteine, Band 23, Dresden, 19 p.

Leonov, N.N., (1960). The Khait, 1949 earthquake and geological conditions of its origin. In Proc. of Academy of Sciences of the USSR, *Geophysical Series*, 3: 409-424 (in Russian).

Nadim, F., Kjekstad, O., Peduzzi, P., Herold, C. & C. Jaedicke, (2006). Global landslide and avalanche hotspots. *Landslides*, 3: 159–173.

Petley, D., Dunning, S., Rosser, N. & A.B. Kausar, (2006). Incipient Landslides in the Jhelum Valley, Pakistan Following the 8th October 2005 Earthquake. *Disaster Mitigation of Debris Flows, Slope Failures and Landslides*, Universal Academy Press Inc./Tokyo, Japan: 47–55.

Sassa, K., (1996). Prediction of earthquake induced landslides. In Proc. *Landslides*, Senneset (ed.), 115-131.

Sato, H.P., Hasegawa, H., Fujiwara, S., Tobita, M., Koarai, M., Une, H. & J. IWAHASHI, (2007). Interpretation of landslide distribution triggered by the 2005 Northern Pakistan earthquake using SPOT5 imagery. *Landslides*, 4:113–122.

Schuster, R.L., L.M. Highland, (2001). Socioeconomic and environmental impacts of landslides in the western hemisphere. *USGS Open-File Report* 2001-0276.

Schuster, R.L., D. ALFORD, (2004). Usoi Landslide Dam and Lake Sarez, Pamir Mountains, Tajikistan. *Envir-onmental & Engineering Geoscience*, X, 2: 151–168.

Yin, Y., Wang, F. & P. Sun, (2009). Landslide hazards triggered by the 2008 Wenchuan earthquake, Sichuan, China. *Landslides*. DOI 10.1007/s10346-009-0148-5.

Zhang, Z., (1995). Geological Disasters in Loess Areas during the 1920 Haiyuan Earthquake, China. *GeoJournal*, 36.2, 3: 269-274.

Zhang, D., Wang, G., (2007). Study of the 1920 Haiyuan earthquake-induced landslides in loess (China). *Engineering Geology*, 94: 76–88.

A CASE STUDY OF EARTHQUAKES AND ROCKFALL - INDUCED DAMAGE TO A ROMAN MAUSOLEUM IN PINARA, SW TURKEY

Hinzen, Klaus-G. (1), Kehmeier, Helen (1), Schreiber, Stephan (1), Reamer, Sharon K. (1)

(1) Earthquake Geology and Archaeoseismology Group, Cologne University, Vinzenz-Pallotti-Str. 26, 51429 Bergisch Gladbach. GERMANY. Email hinzen@uni-koeln.de

Abstract (A Case Study of Earthquakes and Rockfall): *A Roman mausoleum located in the ancient city of Pınara, southwest Turkey, shows clear signs of damages due to dynamic loading. Considering the seismotectonic potential of the area, earthquake ground motions are a possible cause of the damages. However, the building is located at the foot of a 90 m high cliff with a significant rock fall hazard. We present a 3D discrete element model of the mausoleum based on a 3D laser scan. The range of impact velocities of blocks of different size and form and the actual slope of the cliff have been incorporated into 2D model calculations. The deformations caused by simulated rock impacts are compared to the actual displacements of blocks quantified from the laser scan. In addition, analytic ground motions signals are used to study the principal reaction of the building. The second damage scenario using earthquake strong ground motions shows that the damage is more likely caused by an earthquake than impacting rocks.*

Key words*: Quantitative Methods, Rockfall, Strong Ground Motion, Archaeoseismology.*

INTRODUCTION

A Roman mausoleum (Fig. 1) in the southwestern Turkey in the ancient city Pınara shows clear signs of dynamic loading that deformed the building. Its simple block structure and the fact that most parts of the building are still standing makes it an excellent test case for a quantitative archaeoseismic analysis. While collapsed structures usually allow at most an estimate of a minimum ground motion threshold, deformed but standing structures offer a deeper insight into the causes of the deformations.

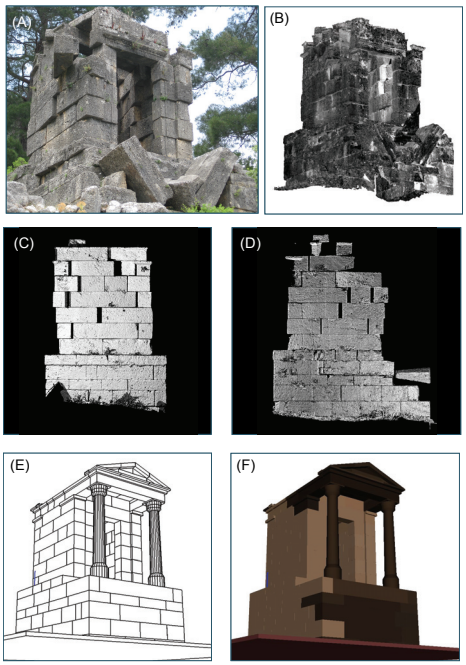

Fig. 1: (A) Photo with a view from SE of the Roman mausoleum in Pınara; (B) laserscan from the same perspective; (C) and (D) ortho-views of the scan of the west and south wall, respectively; (E) and (F) wireframe and rendered view of the discrete element model.

The suitability of the ancient city of Pınara in SW Turkey for archaeoseismic studies has been proven in several previous studies (Sintubin et al., 2003; Yerli et al., 2010; Yerli et al. 2009). Yerli et al. (2011) and Hinzen et al. (2010) provide detailed information about the seismicity and tectonic setting of the site.
The pronounced topography gives Pınara an unique character, but also introduces a rockfall risk for several exposed structures, including the Roman mausoleum.

ROMAN MAUSOLEUM

Laserscan Model
The mausoleum was surveyed with a 3D phase-laserscanner (Fleischer et al. 2010; Schreiber et al., 2010, Schreiber et al. 2009); nine individual scans (from in- and outside positions) were combined into a virtual model of 79 million 3D points (Fig. 1B-D). This model was used as the basis for a discrete element model (Fig. 1E and F) of the undamaged mausoleum and also to quantify the deformation of the still standing part of the structure.

A clear increase of the amount of deformation from bottom to top rows exists. Some parts of the sill and the pediment have fallen down. This also applies to the columns that are no longer found in situ. A part of the ceiling of the colonnade fell down and broke a

massive block of the front platform (Fig. 1 A and B). No fallen blocks are found inside the structure. On the western (back-) side of the structure the fallen pediment blocks are located in close proximity to the wall.

Discrete Element Model

Descriptions by Vitruvius (1796) and intact examples of a Roman mausoleum were used to reconstruct the missing front section of the Pınara mausoleum (shown in dark colour in Fig. 1F). The size of each construction block was measured from the 3D scan and transferred into a model of discrete rigid blocks (Fig. 1E). The model contains 180 blocks and with a density of the local conglomerate of 2.87 Mgm^{-3} it has a total mass of $1.8x10^5$ kg.

Rockfall

2D Cliff Model

A 2D model of the cliff and the slope on which the mausoleum is built was used to estimate impact velocities of rockfall material of different size and form. Boulders currently resting on the slope with sizes of several cubic meters and fresh fracture faces on the cliff indicate the persisting rockfall hazard at the site. Figure 2 shows the distribution of impact velocities of falling material on the mausoleum summarizing the results from numerous simulation calculations.

Impact to Mausoleum

Scenarios with rocks measuring 0.5 to 2.0 m with impact velocities between 10 m/s and 35 m/s and impacting the mausoleum at different height levels were tested.

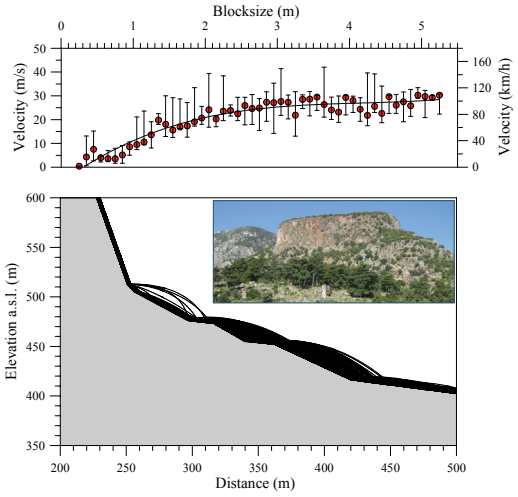

Fig. 2: (top) Red dots give median values of impact velocities of differently sized blocks at the location of the Roman mausoleum. (bottom) 2D model of the slope with trajectories of rocks of different size and form falling from the top of the cliff; a photo of which is shown in the insert.

Impacting rocks cause localized damage on the west wall of the structure. With rocks of 1 m size at velocities above 20 m/s blocks are being pushed inside the building. Above velocities of 30 m/s strong damage occurs if the rock impacts into the upper rows of blocks; however the rest of the structure is not significantly deformed (Fig. 3).

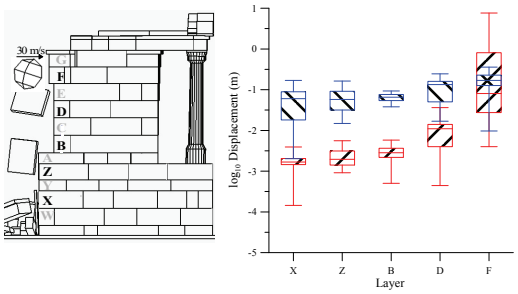

Fig. 3: (left) View of the mausoleum from south after the impact of a rock with 1 m edge length and 30 m/s impact velocity. Block layers of the structure are labelled with capital letters. (right): Boxplots of the distribution of the log of displacements of block corners in five layers. The upper boxes (hatched downwards and blue) show the displacements measured from the laserscan of the building; the lower boxes (hatched ascending and red) are the displacements after the rock impact.

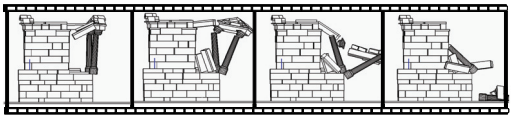

Fig. 4: Reaction of the Roman mausoleum to an analytic ground motion signal, a Morlet wavelet with 1 Hz main frequency and 10 s duration.

GROUND MOTION

Analytic Signals

Before using full 3D earthquake ground motions, a series of tests was carried out with analytic signals in the form of Morlet wavelets (Goupillaud et al., 1984). The colonnade of the structure is highly vulnerable to ground motion frequencies around 1 Hz (Fig. 4). At signals with main frequencies of 2 Hz and above, the typical corner expulsions and block shifts are observed.

Synthetic Seismograms

Site-specific Green's functions and an arbitrary number of rectangular dislocation planes were used to calculate synthetic seismograms using the method described by Wang (1999). A model of the local active faults is based on the work by Yerli et al. (2011).

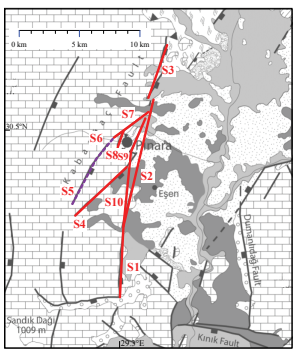

Fig. 5: Active faults in the vicinity of Pınara. Fault segments for different earthquake scenarios are labelled S1 to S10 (map from Yerli et al., 2011).

Impact to Mausoleum

An example of the deformation from a synthetic earthquake record is shown in Figure 6. In this scenario activation of segments S1, S10, S9, and S3 was assumed. The M_W 6.0 example earthquake did not topple the colonnade; however, the calculated displacements are very close to the actual ones with the exception of an underestimated F-layer. Test calculations with measured ground motions from the 2009 L'Aquila earthquake did also destroy the colonnade. As part of the ongoing work we will further quantify the ground motion parameters which caused the deformations.

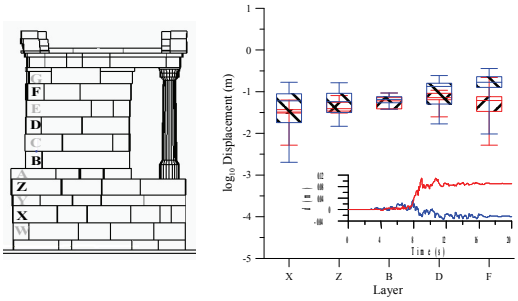

Fig. 6: Same layout as Fig. 3 for deformations of a synthetic earthquake with the ground motions shown in the insert; upper trace EW component lower trace NS component of ground motion.

CONCLUSIONS

The mausoleum located above the Roman *forum* of the ancient city of Pınara is heavily damaged; however, most of its simple block structure is still standing. Deformations indicate that the building suffered from dynamic loading and the location suggests rockfall and earthquake ground motion as possible causes.

Numeric modelling of rock fall impact indicates a different damage pattern from that one observed in the field. Impacting rocks tend to heavily deform the western wall facing the cliff; however, the rest of the building, especially block layers below the impact, are only insignificantly affected. Rocks with high impact velocities push blocks of the building to the inside; however, all fallen blocks from the top of the building were found outside of the structure.

Tests of the dynamic reaction of the mausoleum with analytic ground motion signals show a high vulnerability of the colonnade to horizontal movements with frequencies around 1 Hz. Ground motions with frequencies of 2 Hz and above initiate rocking of blocks with an increasing tendency from bottom to top. Morlet wavelets with main frequencies of 2 Hz dislocate the blocks in the same pattern as it is observed today. Synthetic ground motions of local earthquakes with M_W 5.6 to 6.0 also produce displacements similar to the observations.

Modeling of rock fall impacts and diverse earthquake scenarios indicate that the damages and displacements of building blocks of the Pınara mausoleum are more likely the result of an earthquake than being formed by rockfall. So far only a single earthquake has been used for the modeling. Further calculations are planned to test for the possibility of repeated earthquake action over the millennia since the construction of the mausoleum.

Acknowledgements: We are grateful for the help during the field work by Barish Yerli and Claus Fleischer. Part of the work was financially supported by Deutsche Forschungsgemeinschaft (DFG HI660/2-1).

References

Fleischer, C., K.-G. Hinzen & S. Schreiber (2010). Laser scanning eines roemischen Brunnens in der Archaeologischen Zone Koeln. *Allgemeine Vermessungs-Nachrichten* 5/2010, 176-180.

Goupillaud, P., A. Grossman & J. Morlet (1984). Cycle and related transforms in seismic signal analysis. *Geoexploration* 23, 85-102.

Hinzen, K.-G., S. Schreiber & B.Yerli, (2010). The Lycian Sarcophagus of Arttumpara, Pınara (Turkey) -Testing Seismogenic and Anthropogenic Damage Scenarios. *Bulletin of the Seismological Society of America* 100 (6), 3148-3164.

Schreiber, S., K. G. Hinzen & C. Fleischer (2010). Close-range Laserscanning in the Archaeological Zone Cologne, Germany, *Workshop on Remote Sensing Methods for Change Detection and Process Modelling, Cologne*, November 18-19 2010.

Schreiber, S., K. G. Hinzen & C. Fleischer (2009). An application of 3D laser scanning in archaeology and archaeoseismology: The medieval cesspit in the archaeological zone Cologne, Germany, *1st INQUA-IGCP-567 International Workshop on Earthquake Archaeology and Palaeoseismology, Baelo Claudia, Cadiz, Spain*, 7-13 September 2009, 136-138.

Sintubin, M., P. Muchez, D. Similox-Tohon, G. Verhaert, E. Paulissen & M. Waelkens (2003). Seismic catastrophes at the ancient city of Sagalassos (SW Turkey) and their implications for seismotectonics in the Burdur-Isparta area. *Geological Journal* 38 (3-4), 359-374.Vitruvius Pollio, M. & A. Rode (1796). Baukunst. Translated by August Rode, G. J. Goeschen (eds.), Leipzig, 10 Books.

Wang, R. (1999). A simple orthonormalization method for stable and efficient computation of Green's functions. *Bulletin of the Seismological Society of America* 89, 733-741.

Yerli, B., S. Schreiber & K.-G. Hinzen (2011). Seismotectonic background for archaeoseismologic studies in the Eşen Basin, SW Turkey. *Natural Hazards*, submitted.

Yerli, B., J. Ten Veen, M. Sintubin, C. Karabacak, C. Yaliciner & E. Altunel (2010). Assessment of seismically induced damage using LIDAR: the ancient city of Pinara (SW Turkey) as a case study. In: Ancient Earthquakes. *Geological Society of America, Special Paper 471*, M. Sintubin, I. Stewart, T. M. Niemi and E. Altunel (eds.), 157-170.

Yerli, B., S. Schreiber, K. G. Hinzen, J. H. t. Veen, M. Sintubin & M. Sintubin (2009). Testing the Hypothesis of earthquake-related damage in structures in the Lycian ancient City of Pinara, SW Turkey, *1st INQUA-IGCP-567 International Workshop on Earthquake Archaeology and Palaeoseismology, Baelo Claudia, Cadiz, Spain*, 7-13 September 2009, 173-176.

NEOTECTONICS OF GRACIOSA ISLAND (AZORES) – UNCERTAINTY IN SEISMIC HAZARD ASSESSMENT IN A VOLCANIC AREA WITH VARIABLE SLIP-RATES

Hipólito, Ana (1), José Madeira (2), Rita Carmo (1), João Luís Gaspar (1)

(1) Centro de Vulcanologia e Avaliação de Riscos Geológicos, Universidade dos Açores, Complexo Científico, 3º Piso – Ala Sul, Rua da Mãe de Deus, 9500-321 Ponta Delgada, Açores, PORTUGAL. Email: ana.rc.hipolito@azores.gov.pt
(2) Universidade de Lisboa, GeoFCUL, LATTEX/IDL-Laboratório Associado, Faculdade de Ciências das Universidade de Lisboa, Edifico C6, Campo Grande, 1749-016 Lisboa, PORTUGAL.Email: jmadeira@fc.ul.pt

***Abstract (Neotectonics of Graciosa Island (Azores) – uncertainty in seismic hazard assessment in a volcanic area with variable slip-rates)**: Graciosa is a mid-Pleistocene to Holocene volcanic island that lies on a complex plate boundary between the North American, Eurasian and Nubian plates. Large fault scarps displace the oldest volcanic units, but in the younger areas recent volcanism hides the surface expression of faulting, limiting neotectonic observations. Slip-rates deduced from neotectonic surveys are higher than those provided by kinematic plate motion models. This suggests a variability of deformation rates, alternating between high tectonic deformation periods, decreasing the recurrence interval of surface rupturing earthquakes, and phases of low slip-rate. Nevertheless, in historical time a few destructive earthquakes affected the island attesting for its seismic hazard.*

***Key words**: Neotectonics, Azores, Graciosa Island*

GEODYNAMIC AND VOLCANIC SETTING

The Azores archipelago lies on a complex geodynamic setting: the Eurasian (Eu), North American (NA) and Nubian (Nu) triple junction (Azores Triple Junction - ATJ) (*Fig.1*).

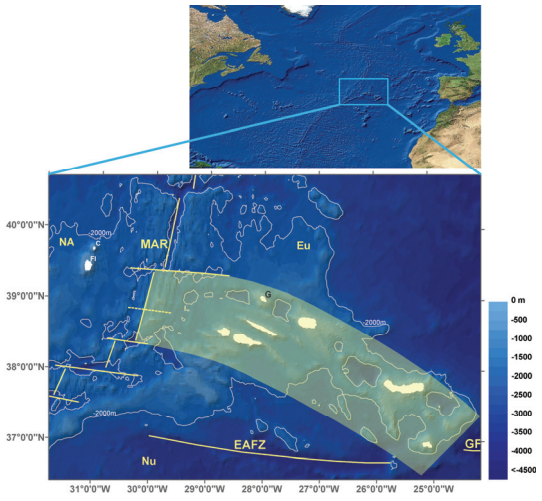

Fig. 1: Location of the Azores and main morphotectonic features of the region. The shaded area represents the sheared western segment of the Eu-Nu plate boundary; Plates: NA – North American; Eu – Eurasian; Nu – Nubian; Tectonic structures: MAR – Mid-Atlantic Ridge; EAFZ – East Azores Fracture Zone; GF – Gloria Fault; Islands: G – Graciosa Island. World topography and bathymetry from ESRI® (2008), Azores bathymetry adapted from Lourenço et al. (1997). Datum: WGS 1984 (modified from Hipólito, 2009).

Graciosa Island is located on the west segment of the Eu-Nu boundary, a diffuse and complex deformation zone (*Fig.1*) sheared by a dextral transtensile regime (*e.g.* Madeira & Brum da Silveira, 2003; Carmo, 2004; Hipólito, 2009).

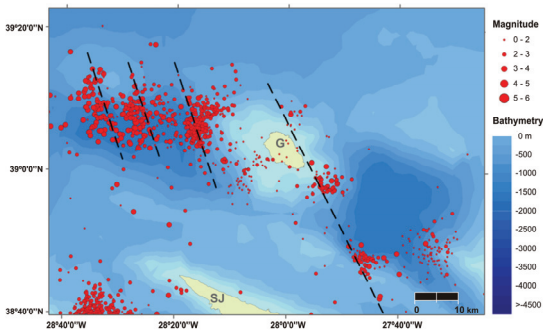

Fig. 2: Seismicity in and around Graciosa island from 2003 to 2009, defining three alignments in West Graciosa Basin and one at the western border of the East Graciosa Basin. Red dots mark earthquake epicenters and magnitudes (M_D). Data from CIVISA (Centro de Informação e Vigilância Sismovulcânica dos Açores), 2009.

This boundary acts as an ultra-slow oblique expansive center (Vogt and Jung, 2004) and a transfer zone accommodating the differential motion between Eu and Nu plates, due to the higher

spreading rates north of the Azores (*e.g.* DeMets, 1994; Fernandes *et al*., 2003).

Due to its geodynamic setting, the Azores archipelago presents frequent seismicity. Graciosa Island was affected by some significant earthquakes since its settlement in mid 15th century. One of them (1837) had probably its epicenter on land (Madeira, 1998; Silva, 2005). However, instrumental seismicity does not show significance seismic activity within the island (*Fig.2*). The epicenter distribution of the current activity reveals four NNW-SSE trending offshore alignments, one on the east flank of West Graciosa Basin, two crossing this basin floor to the west, and another alignment just east of the island (*Fig. 2*).

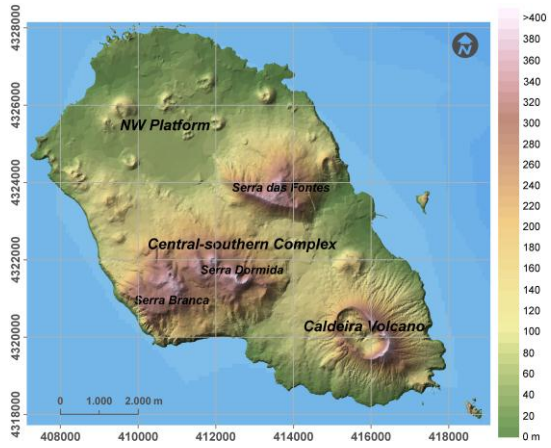

Fig. 3: Digital Elevation Model of Graciosa and the main morphologic regions. Based on Carta Militar de Portugal, Sheet 21 – Stª Cruz da Graciosa, Instituto Geográfico do Exército (2001); UTM Projection; Datum: WGS 1984.

Graciosa Island comprises one quiescent trachytic polygenetic volcano (the Caldera Volcano), an older volcanic complex (the Central-Southern Complex), resulting from the dismantling of an important central volcano, and several monogenetic eruptive centers included in the NW basaltic Platform that mantle the older units (Gaspar, 1996; *Fig.3*). The oldest volcanic-stratigraphic unit is around 620 ± 120 ka old (Féraud *et al*., 1980). The most recent volcanic event was a pre-settlement basaltic hawaiian-strombolian eruption at about 2 ka B.P. (Walker, unpublished data, in Gaspar, 1996). Currently the volcanic activity is just expressed by secondary manifestations, namely by thermal springs, fumarolic fields and diffuse degassing (*e.g.* Ferreira *et al*., 1993; Gaspar, 1996).

The island presents in general a smooth relief with maximum altitude of 402m (*Fig.3*). The central part is crossed by several NW-SE trending fault scarps parallel to the shape of the island (*Fig.4*). Those faults define a graben structure that is crossed in the SE by a NNE-SSW fault scarp which separates the older from the most recent volcanic units to the south.

STRUCTURAL DATA

Geometric and kinematic fault analysis

In Graciosa Island, neotectonic studies are limited by the absence of outcrops with well exposed fault planes. Tectonic features, corresponding to important fault scarps, several tens to hundreds of meters high, occur in the central region of the island. Unfortunately the faults producing these large features do not crop out and the small size of the island limits the observation of the full length of the faults. The thick and non-cohesive young volcanic fall deposits and the lava flows that mantle the topography were not tectonically displaced yet, hiding the trace of the faults in areas covered by recent volcanic units.

Therefore, paleoseismological studies were not made due the sheer size of the fault scarps and the absence of recent surface faulting with favorable conditions for trenching. The observed faults crop out either in quarry walls exploring cinder cones or in inaccessible sea cliffs. In the first case the nature of the deposits (homogeneous, coarse size and low cohesion) does not allow the generation of slickensides, hindering kinematic analyses.

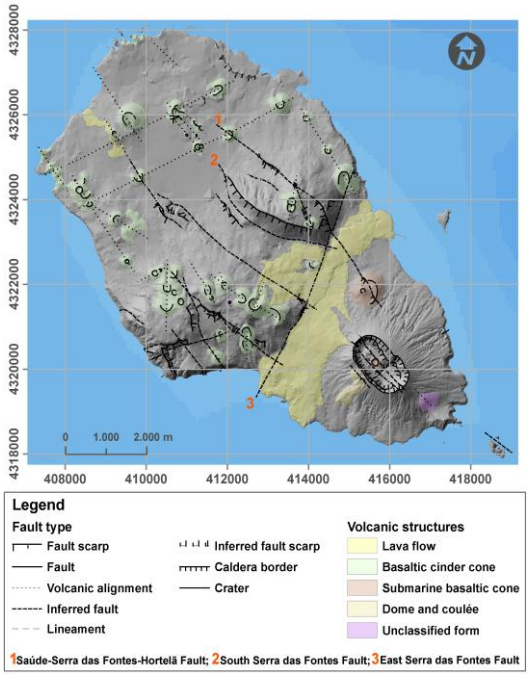

Fig. 4: Morphotectonic map of Graciosa Island. Based on Carta Militar de Portugal, Sheet 21 – Stª Cruz da Graciosa, Instituto Geográfico do Exército (2001); UTM Projection; Datum: WGS 1984.

Generally, the mapped structures are normal faults or present normal component. Although, in most cases it was difficult to recognize a strike-slip component, these structures may also have strike-slip component (dextral or sinistral) typical of a tectonic transtensile regime.

The tectonic map (*Fig.4;* Gaspar and Queiroz, 1995; Hipólito, 2009), the geometric (*Fig.5*) and kinematic (*Fig.6*) fault analysis (Hipólito, 2009) show the presence of two main fault systems: system A – composed of two sets of conjugated faults, one trending NW-SE, dipping to SW, presenting normal-dextral or dextral-normal oblique slip, and another striking NNE-SSW, dipping to ESE, with oblique normal-left lateral or left lateral-normal slip (*Fig. 6a*); system B – includes NNE-SSW to NE-SW trending faults, dipping to WNW or NW, presenting normal-dextral or dextral-normal oblique slip (*Fig. 6b*). A family of faults conjugated with these structures was not found. The strong fault dips (the 80º to 90º range dominate) also suggest oblique (normal/strike-slip) faulting (*Fig.5*).

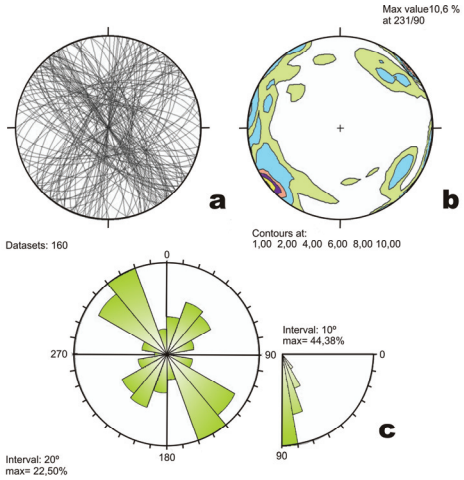

Fig. 5: Geometry of all analyzed faults: ***a)*** *stereographic plot of fault planes (lower hemisphere; Schmidt net) – β diagram;* ***b)*** *stereogram of fault poles density – π diagram;* ***c)*** *Circular histogram of unweighted frequencies of fault plane directions and dip angles. TectonicsFP software (Ortner et al., 2002).*

Paleostress analysis suggests that the region is affected by two different stress fields that can alternate in time and/or in space; variations of the local stress field may occur, which are responsible for the generation of new faults or reactivation of pre-existing structures (Hipólito, 2009).

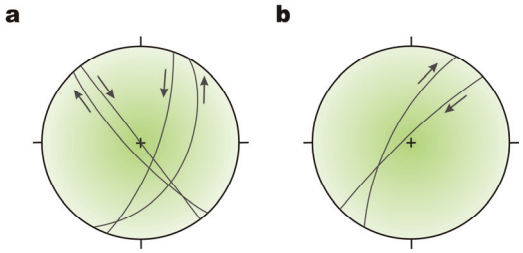

Fig. 6: Stereographic plot of two main fault systems (lower hemisphere; Schmidt net – β diagram). ***a****: system A - NW-SE to NNW-SSE faults, with normal-dextral oblique slip, conjugate of NNE-SSW to NE-SW normal-left lateral structures;* ***b****: system B - NNE-SSW to NE-SW faults with normal-dextral oblique slip. Black arrows: strike-slip sense. TectonicsFP software (Ortner et al., 2002).*

Slip-rates

Only three tectonic structures allowed slip-rate estimation: the Saúde-Serra das Fontes-Hortelã, the South Serra das Fontes and the East Serra das Fontes faults (*Fig. 4*). However, in two of them only the normal slip component was determined, while in the other only the strike-slip could be measured (*Table I*). The Saúde-Serra das Fontes-Hortelã Fault trace is marked by a 5750m-long south–facing scarp trending N306º to N328º producing 49m of dextral strike-slip displacement. The South Serra das Fontes Fault has a 200m-high south-facing scarp 3500m long, trending N282º to N327º. The East Serra das Fontes Fault trace is marked by a 4750m-long and 185m- maximum high east-southeast facing scarp, trending N20º. The total length of these faults is unknown because on-shore they are fossilized by younger units and there is no off-shore data allowing to trace them.

The estimated values indicate slip-rates somewhat higher than those provided by plate motion kinematic models (*Table II*) and contrasting with the present low seismicity and neotectonic deformation in the island (*Fig. 2*). These slip-rates could be over-estimated because the age of the used marker may not represent the whole deformation period. On the other hand, the real displacements may be greater than the measured ones due to infilling of tectonically depressed areas by younger deposits.

Table I: Slip-rates of three faults in Graciosa Island.

Structure	Displacement (m)		Age of marker (ka)	Slip rate (mm/year)	
	Normal	Strike slip		Normal	Strike slip
Saúde-Serra das Fontes-Hortelã fault	--	49	31, 407	--	**1,6**
South Serra das Fontes fault	200	--	31, 407	**6,4**	--
East Serra das Fontes fault	185	--	31, 407	**5,9**	--

Table II: Relative velocities and azimuth directions of slip vector for Eu and Nu plates and for those plates relatively to NA plate in ATJ zone, according to the NUVEL-1A (DeMets et al., 1994), REVEL (Sella et al., 2002) e DEOS2K (Fernandes et al., 2003) global kinematic models.

Plate pairs	Velocity (mm/year)	Azimuth (degrees)	Model
Eu-NA(stable)	~23	~97º	NUVEL-1A
	~25	~96º	REVEL
	~24	~94º	DEOS2K
Nu-NA(stable)	~20	~103º	NUVEL-1A
	~19	~151º	REVEL
	~19	~99º	DEOS2K
Eu-NU(stable)	~4	~66º	NUVEL-1A
	~6	~72º	REVEL
	~4	~80º	DEOS2K

DISCUSSION AND FINAL REMARKS

As in other zones in the Azores (Hipólito *et al*., 2011), several limitations prevent a more detailed neotectonic survey of Graciosa Island. Recent volcanic deposits, that mantle the topography, hide

the surface expression of major tectonic structures; basaltic lapilli deposits do not allow the generation of linear kinematic markers; there are no structures with scarp heights allowing paleoseismological studies, thus contributing to the assessment of seismic hazard. Nevertheless, the tectonic information from Graciosa Island is in agreement with the stress pattern proposed by other authors for the Azores region (*e.g.* Madeira, 1998, Lourenço *et al.*, 1988; Carmo, 2004).

The absence of seismic events producing surface rupture since settlement and the current low seismic activity in Graciosa Island, contrast with the youthful aspect of its tectonic morphology. The calculated slip-rates and the evident loss of geomorphic expression of fault scarps into the areas covered with the younger units (NW Platform and Caldeira Volcano) suggest that the occurrence of a period of important tectonic activity before 31 ka, with higher slip-rates than those observed in present times, responsible for the deformation of the central part of the island. That period was followed by a magmatic dominated phase, with the build-up of Caldeira Volcano and the installation of the fissural basaltic volcanism responsible for the formation of the NW Platform. During that period there was a reduction of fault slip-rates and consequent increase of the recurrence period of surface rupturing event. This is consistent with the occurrence of variations in deformation rates in the archipelago, with periods with slip-rates higher or lower than the average, as proposed by Madeira (1998).

Thus, the current tectonics in Graciosa Island is not particularly active. Nevertheless, as it is located between two important seismogenic sources (West and East Graciosa Basins) and on a complex geodynamic setting, seismic hazard cannot be disregarded.

Acknowledgements: Ana Hipólito and fieldwork were supported by CARIGE Project – Carta de Riscos Geológicos, Governo Regional da Região Autónoma dos Açores, Secretaria Regional da Habitação e Equipamentos.

References

Carmo, R. (2004). *Geologia estrutural da região Povoação - Nordeste (ilha de S. Miguel, Açores)*. MSc thesis, Azores Univ., 133 p.

DeMets, C., R. Gordon, D. Argus, S. Stein (1994). Effect of recent revisions to the geomagnetic reversal time scale on estimates of current plate motions. Geophys. *Res. Lett.* 21(20), pp. 2191-2194.

Féraud, G., I. Kaneoka, C.J. Allegre (1980). K-Ar Ages and Stress Pattern in the Azores - Geodynamic Implications. *Earth and Planet. Sci Lett.* 46(2), pp. 275-286.

Fernandes, R. M. S., B.A.C. Ambrosius, R. Noomen, L. Bastos, M.J.R. Wortel, W. Spakman, R. Govers (2003). The relative motion between Africa and Eurasia as derived from ITRF2000 and GPS data, *Geophys. Res. Lett.* 30 (16), 1828, pp. 1-1 - 1-5. doi: 10.1029/2003GL017089.

Ferreira, T., J. L. Gaspar, G. Queiroz (1993). Considerações sobre as emanações gasosas da Furna do Enxofre (Ilha Graciosa, Açores). Açoreana VII (4), pp. 603-612.

Gaspar, J.L.; G. Queiroz (1995). Carta Vulcanológica dos Açores, ilha Graciosa. Sheets A and B, scale 1:10000. Ed. Azores Univ. and Câmara Municipal de Santa Cruz da Graciosa.

Gaspar, J.L. (1996). *Ilha Graciosa (Açores): História Vulcanológica e Avaliação do Hazard*. PhD thesis, Azores Univ., 361p.

Hipólito, A. (2009). *Geologia Estrutural da ilha Graciosa – Enquadramento no âmbito da Junção Tripla dos Açores*. MSc thesis, Azores Univ., 155 p.

Hipólito, A., F. Viveiros, R. Carmo, C. Silva, N. Cabral, J. Cabral, V. Alfama, T. Ferreira, J.L. Gaspar (2011). Soil degassing surveys as a tool to identify hidden faults in volcanic areas: preliminary results at the Ribeira Grande graben (Fogo Volcano, S. Miguel Island, Azores). *Geophysical Research abstract*. 13, EGU2011-8992.

Lourenço, N., J. Miranda, J. Luís, A. Ribeiro, L. Mendes-Victor, J. Madeira, H. Needham (1998). Morpho-tectonic analysis of the Azores Volcanic Plateau from a new bathymetric compilation of the area. Marine *Geophys. Res.* 20, pp. 141-156.

Luís, J.F., J. M. Miranda (2008). Reevaluation of magnetic chrons in the North Atlantic between 35ºN and 47ºN: Implications for the formation of yhe Azores Triple Junction and associated plateau. *J. of Geophys. Res.* 113, B1o1o5. doi:10.1029/2007Jb005573.

Madeira, J. (1998). *Estudos de neotectónica nas ilhas do Faial, Pico e S. Jorge: uma contribuição para o conhecimento geodinâmico da junção tripla dos Açores*. PhD thesis, Lisbon Univ., 428 p.

Madeira, J., A. Brum da Silveira (2003). Active tectonics and first paleoseismological results in Faial, Pico and S. Jorge Islands (Azores, Portugal). *Annals of Geophysics* 46 (5), pp. 733-761.

Ortner, H., F. Reiter, P. Acs (2002). Easy handling of tectonic data: the programs TectonicVB for Mac and TectonicsFP for Windows. *Computers and Geosciences* 28, 1193-1200.

Sella, G., T. H. Dixon, A. Mao (2002). REVEL: a model for recent plate velocities from space geodesy. *J. Geophys. Res.* 107 (B4), 2081, pp. 11-1 – 11-12. doi: 10.1029/2000JB000033.

Silva, M. (2005). *Caracterização da sismiciade histórica dos Açores com base na reinterpretação de dados de macrossísmica: contribuição para a avaliação do risco sísmico nas ilhas do Grupo Central*. MSc thesis. Azores Univ., 163 p.

Vogt, P.R., W.Y. Jung (2004). The Terceira Rift as hyper-slow, hotspot dominated oblique spreading axis: A comparison with other slow-spreading plate boundaries. *Earth Planet. Sci. Lett.* 218, pp. 77–90. doi:10.10116/S0012-821X(03)00627-7.

EARTHQUAKE ARCHAEOLOGY

INQUA PALEOSEISMOLOGY AND ACTIVE TECTONICS

EVIDENCE FOR HOLOCENE TSUNAMI-IMPACT ALONG THE SHORELINE OF OMAN

Gösta Hoffmann (1), Klaus Reicherter (2), Thomas Wiatr (2), Christoph Grützner (2)

(1) Department of Applied Geosciences, German University of Technology in Oman, PO Box 1816, Athaibah, Muscat, PC 130, Sultanate of Oman, email: goesta.hoffmann@gutech.edu.om
(2) RWTH Aachen University, Inst. für Neotektonik und Georisiken, Aachen, 52056, Germany

Abstract (Evidence for Holocene tsunami-impact along the shoreline of Oman): *Three independent sets of evidence of past tsunami along the coastline of Oman are reported. The rocky coastline of the Sultanate of Oman between Fins and Sur is decorated by a number of large boulders and boulder accumulations forming ramparts. The boulders occur as individual blocks of almost 50 tons weight, as imbricated sets and "boulder trains". The coast is made up of folded Tertiary limestones and beach rock of Quaternary age. The transport distance from the fractured cliff front of 6-10 m height above mean sea level varies between several meters up to 70 m inland. We found individual blocks of recent corals and overturned blocks with oysters and pools. T-LIDAR was used to analyse geomorphologic features and for volumetric estimates of boulder weight. Tropical cyclones such as Gonu in 2007 or Phet in 2010 as well as historical tsunamis are known to have affected Oman's coastline in the past. Coastal changes by cyclones are known to have been negligible; therefore, we interpret the boulder ridges as tsunamigenic deposits. Additionally, fine grained lagoonal sediments were analyzed. A distinct shell layer with allochthonous species is documented. A tsunamigenic origin is most likely. Although no dating evidence of the observed boulder and lagoon deposits is available at the moment we conclude that the 1945 Makran tsunami affected Oman's coastline. This conclusion is based on interviews with local people.*

Key words*: Oman, tsunami, boulder deposits, T-LiDAR*

INTRODUCTION

Recent tsunami events like the Indian Ocean tsunami on 26th December 2004 and the Tôhoku earthquake and tsunami on 11th March 2011 resulted in large numbers of casualties and immense damage to infrastructure. These events underline the need for tsunami hazard research and assessment for any potentially vulnerable region. In most cases this can only be done by studying past tsunami records. The coastlines of the Sultanate of Oman are prone to various natural hazards such as tropical cyclones, landslides and tsunamis. The devastating effects of the cyclone Gonu, caused by flash floods and landslides in June 2007 illustrated the need to investigate the recurrence intervals of such events in order to assess the vulnerability and to mitigate damages. So far no scientific research concerning recurrence intervals of natural hazards has been carried out. However, studies published by Heidarzadeh et al. (2008a, 2008b, 2009) and Jordan (2008) reveal past tsunami events in the Indian Ocean with possible effects on the coastline of Oman (Fig. 1). As the population of Oman and the neighboring countries is concentrated along the coastline and large infrastructure projects are planned or already completed a holistic scientific approach to decipher the geological record of past extreme events is overdue. On 27th November 1945 an earthquake occurred in the Makran Subduction Zone offshore Pakistan and triggered a tsunami (Jaiswal et al., 2009). Up to 4000 casualties were reported along the coastlines of NW India and Pakistan, including 5 m run-up along the coastlines of the Sultanate of Oman. Donato et al. (2008, 2009) analysed shallow sediment cores from the lagoon in Sur and recorded a 5-25 cm thick shell bed close to the surface. Based on the taphonomy and fragmentation a tsunamigenic origin is discussed as the most likely form of deposition related to the 1945 tsunami. However, there are almost no historical documents available for Oman for this period as the country was isolated with no international contacts until the 1970s, living conditions were poor and no modern technology was in use. We report geological and historical evidence for the tsunami along Oman's coastline. These evidence are: (a) fine grained lagoon sediments, which show distinct layers with allochthonous, offshore species (mollusks and foraminifera); (b) boulder deposits encountered along cliff-coastlines and (c) eyewitness-reports of old people we interviewed.

OBSERVATIONS

The coastal area under investigation is situated in the eastern part of Oman between the cities Quariat and Sur. The area is sparsely populated as most of the country; small fishing villages are scattered along the coast. Only since 2008 there is a paved road connecting the cities Quariat in the north and Sur in the south.

The geology of the area is dominated by Paleogene to Neogene limestone formations, which rise from the coast up to 1500 m to form the Selma Plateau. Geomorphologic evidence of Quaternary land-uplift is obvious along the entire coastline: coast-parallel, wave-cut terraces are encountered up to elevations of 300 m. Within the study area these terraces are

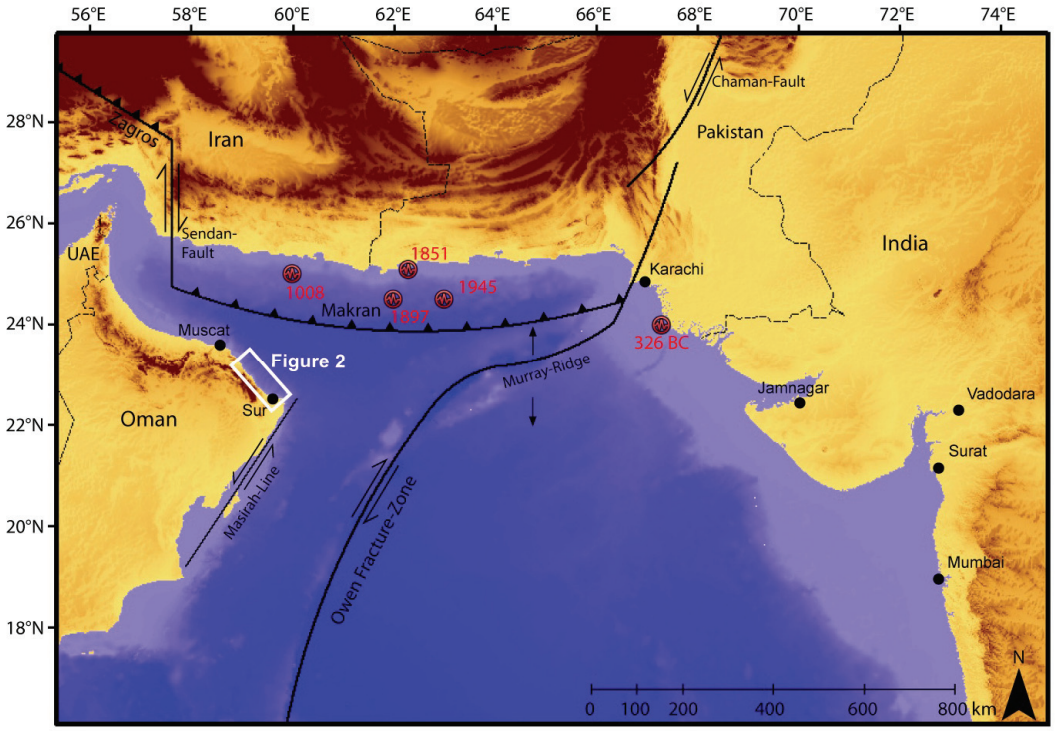

Fig. 1: Historical tsunamis in the Indian Ocean and working area in the Sultanate of Oman.

cut into Paleocene-Early Eocene limestone formations. Quaternary deposits are either of fluvial origin or ancient to subrecent littoral deposits, usually preserved as beachrock. In most cases only erosional remnants of the beachrock are found and the underlying older strata dominate along the cliff coast. Several intertidal lagoons exist in the vicinity of Sur and Ras al Hadd. These lagoons serve as geological archives with a preservation potential for palaeo-tsunami and were investigated during several field campaigns in 2010.

We collected seven sediment cores at various locations within Sur lagoon. The deepest core reaches 10 m below the present surface. The sequence is characterized by silty fine sand in the lower part (10-6 m) and fine-sand in the upper part (6 – 0 m). Within the uppermost meter several distinct shell beds were identified. The shell and foraminifera assemblage contains allochthonous species living in the subtidal zone and offshore. Additionally, we collected 4 sediment cores in the lagoon of Ras al Hadd. The longest core is 3 m long. The base of the sequence is made up of sandy gravel partly

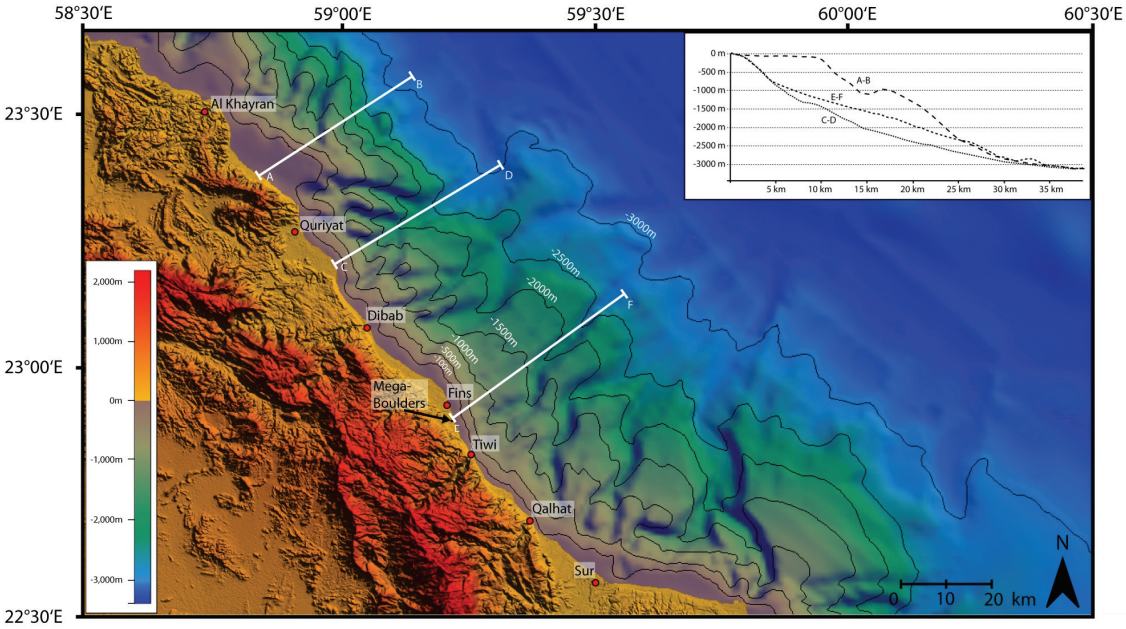

Fig. 2: Study area along the east coast of the Sultanate of Oman. Inset shows bathymetric sections.

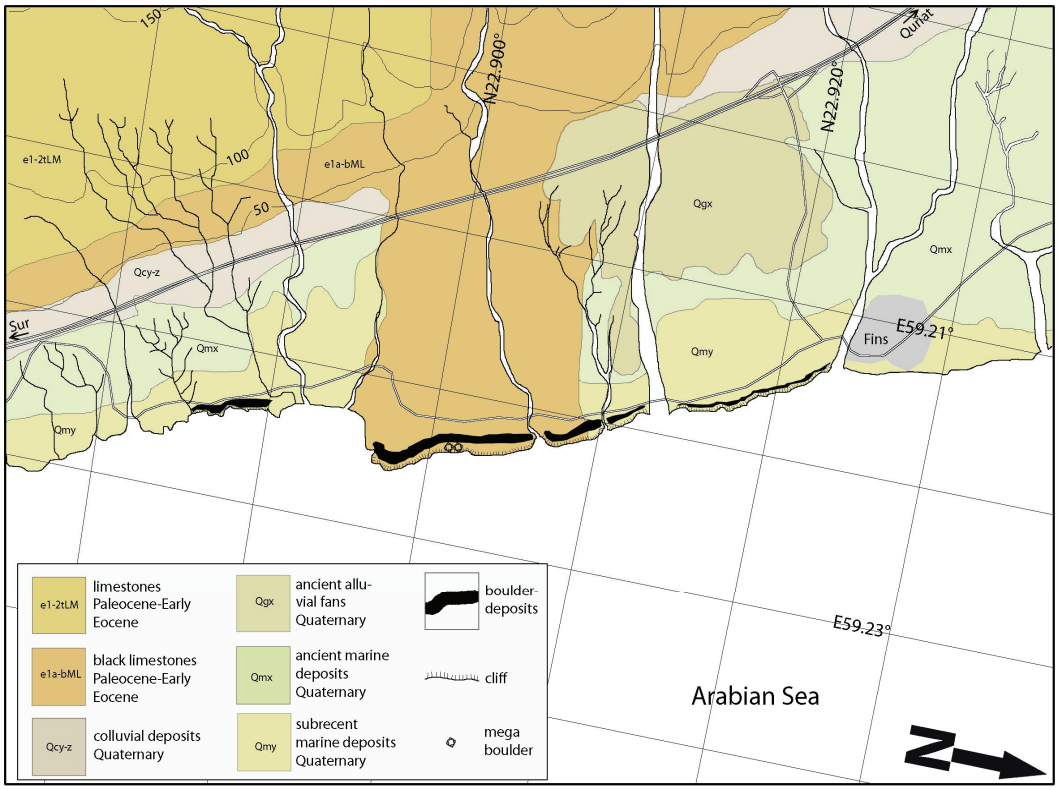

Fig. 3: Study area along the east coast of the Sultanate of Oman with the observed ramparts.

cemented as beachrock, overlain by fine to medium sand. The mollusk and foraminifera assemblages in the upper 100 cm show a variety of species. Especially some bivalve species within this layer are allochthonous as their habitat is characterized as subtidal and offshore.

In our 2011 survey we found boulder deposits south of the village of Fins (Fig. 2) and more distal finer-grained deposits yielding shells and coral blocks on the cliff top and to approx. 60-70 m inland (Fig. 3). The blocks are partly imbricated and reach volumes of more than 20 m^3 (determined with terrestrial LiDAR scanning), corresponding to a weight of almost 50 tons. Also, we found so called tsunami boulder trains, where blocks are aligned in a row (Fig. 3). Some blocks are toppled or upright with hit marks on the surface, erosional pot holes, *Lithophaga* borings and attached oysters (which provide dating material, dating is in progress). The boulders form ramparts and have a wavy, lobe-like pattern. Most blocks have a platy shape, which origins in layer thickness of reworked material, mainly beach rock and Tertiary limestones. We measured the long axis (a-axis) of 60 boulders, a vast majority is oriented N30, possibly pointing towards the wave direction. The cliff tops are "cleaned", however, drift wood of the tropical cyclone Phet in 2010 is found in height of approximately 6 m above mean sea level. Inland, boulders are found in a gravel/sand matrix with various fossil remains like shell and corals (Fig. 4). The finer-grained layers show fining-up cycles. We also interviewed old people living in the towns of Sur and Tiwi. An old man in Sur recalled an event that happened most probably during the 1940s: first the sea retreated, then, two waves washed onshore. The event took place at 02:00 am.

Another old man of the village of Tiwi reported from hearsay, as he was born in 1946. He heard about an event that destroyed the local graveyard in the 1940s. He described that the graveyard was located much further inland. Furthermore, he gave an account of fish (sardines) and mollusks (oysters) being washed into the Wadi Shab. The women who used to get freshwater from the wadi could not walk there anymore, but boats had to be used. The marine fishes lived in the wadi after the event.

DISCUSSION

The uppermost ~1m in the lagoon of Sur as well as in the lagoon of Ras al Hadd clearly indicates an event-layer which can be either storm- or tsunami-generated (see Kortekaas and Dawson 2007). As the lagoons are intertidal, reworking and bioturbation of the sediments is a common phenomenon that hampers a clear stratification. Boulders deposits along the east coast of the Sultanate of Oman form ramparts between Fins and Sur. Inland, boulder deposits are incorporated in finer-grained sediments. Observations of the coastline changes and modifications of the last two very strong tropical cyclones Gonu and Phet rather exclude tropical cyclones a "moving agent" for the large 50 tons boulders. This was also proven by comparing time series of Google Earth, where blocks are detectable, but remained in the position (before and after).

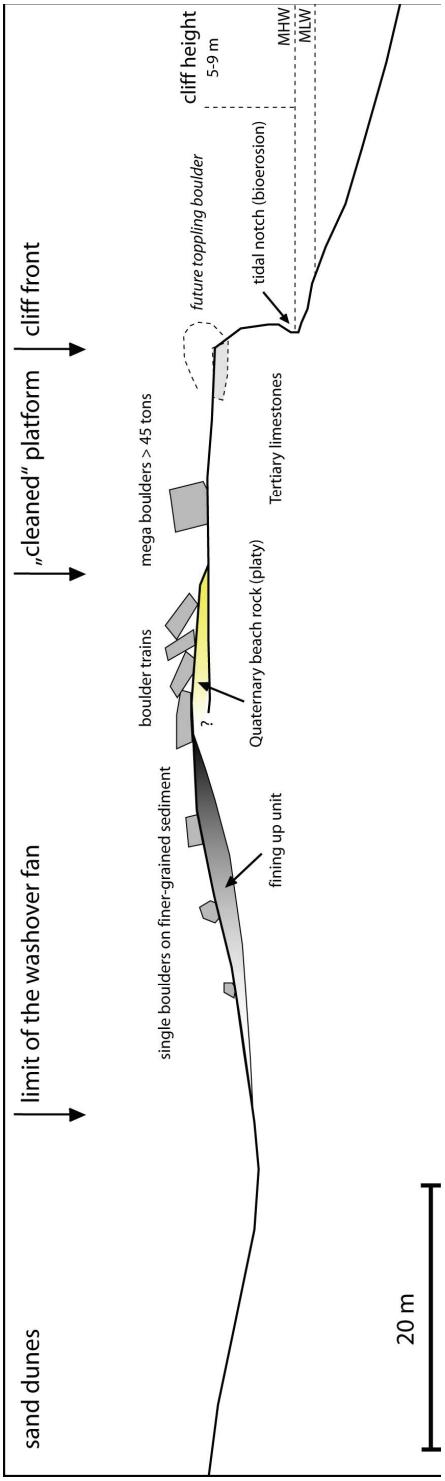

Fig. 4: Sketch of the possible tsunamigenic deposits.

Hence, we propose a tsunamigenic event being responsible for the rampart formation and the boulder deposits along this part of the coast. Dating of oysters, which have grown on the blocks and died during the deposition, is in progress.

The information gained from the interview in Sur is very helpful. The timing of an event resulting in sea-water entering the house was given with 02:00 am which is 22.00 GMT (local time zone is GMT +4). This fits quite well with the time of the Makran earthquake on 27.11.1945 which is reported by Pendse (1948) as 21:57 GMT. The modeled travel time of the tsunami wave is 20-30 minutes (Heidarzadeh and Kijko. 2011). The description of a retreating sea fits general tsunami descriptions. The arrival of two separate waves fits observations in India (see Rajendran et al. 2008) where also two waves with disparity in arrival time are reported. A submarine landslide is assumed for the second wave. The descriptions given in the interview in Tiwi cannot unambiguously be related to any know event. However, the accounts are more likely to be the effect of a tsunami wave rather than wadi-flooding.

Acknowledgements: This study was financially supported by the German Research Foundation (DFG-project Re 1361/14-1) and GUTech in Mascat. Our students Sina Rausch, Kathrin Wagner and Tobias Rausch are thanked for field and lab support, and Tobias also for graphic design.

References

Donato, S. V., Reinhardt, E.G., Boyce, J.I., Rothaus, R., Vosmer, T. (2008). Identifying tsunami deposits using bivalve shell taphonomy, Geology, 36, 199-202.

Donato, S. V., Reinhardt, E. G., Boyce, J. I., Pilarczyk, J. E., Jupp, B. P. (2009) Particle-size distribution of inferred tsunami deposits in Sur lagoon, Sultanate of Oman, Mar. Geol., 257, 54-64.

Heidarzadeh, M., Pirooz, M., Zaker, N. H., Yalciner, A. C., Mokhtari, M., Esmaeily, A. (2008a) Historical tsunami in the Makran subduction zone off the southern coasts of Iran and Pakistan and results of numerical modeling, Ocean Eng., 35, 774-786.

Heidarzadeh, M., Pirooz, M., Zaker, N. H., Synolakis, C. (2008b). Evaluating tsunami hazard in the northwestern Indian Ocean, Pure Appl. Geophys., 165, 2045-2058, Doi:10.1007/s00024-008-0415-8.

Heidarzadeh, M., Pirooz, M., Zaker, N. H., Yalciner, A. C. (2009). Preliminary estimation of the tsunami hazards associated with the Makran subduction zone at the northwestern Indian Ocean, Nat. Hazards, 48, 229-243, Doi:10.1007/s11069-008-9259-x.

Heidarzadeh, M., Kijko, A. (2011). A probabilistic tsunami hazard assessment for the Makran subduction zone at the northwestern Indian Ocean, Nat. Hazards 56, 577-593.

Jaiswal, R., Singh, A., Rastogi, B. (2009). Simulation of the Arabian Sea tsunami propagation generated due to 1945 Makran earthquake and its effect on western parts of Gujarat (India), Nat. Hazards, 48, 245-258, Doi:10.1007/s11069-008-9261-3.

Jordan, B. R. (2008). Tsunamis of the Arabian Peninsula - a guide of historic events, Science of Tsunami Hazards, 27, 31-46.

Kortekaas, S., Dawson, A. G. (2007). Distinguishing tsunami and storm deposits: An example from Martinhal, SW Portugal, Sed. Geol. 200, 208-221.

Pendse, C. G. (1948). The Makran earthquake of the 28th of November, 1945, Scientific Notes, Indian Meteorological Dept. 10, 141-145.

Rajendran, C. P., Ramanamurthy, M.V., Reddy, N.T., Rajendran, K. (2008). Hazard implications of the late arrival of the 1945 Makran tsunami, Current Science 95, 1739-1743.

EARTHQUAKE ARCHAEOLOGY

INQUA PALEOSEISMOLOGY AND ACTIVE TECTONICS

MONITORING COASTAL CHANGES ON THE IONIAN ISLANDS (NW-GREECE) BY MULTI-TEMPORAL TERRESTRIAL LASER SCANNING

Hoffmeister, Dirk (1), Ntageretzis, Konstantin (2), Tilly, Nora (1), Curdt, Constanze (1), Bareth, Georg (1), Brückner, Helmut (1), Andreas Vött (2)

(1) Institute for Geography, University of Cologne, Albertus-Magnus-Platz, 50923 Cologne. GERMANY. Email: dirk.hoffmeister@uni-koeln.de
(2) Institute for Geography, Johannes Gutenberg-Universität Mainz. Johann-Joachim-Becher-Weg 21, 55099 Mainz. GERMANY. Email: konstantin.ntageretzis@uni-mainz.de

Abstract: *This study deals with the application of terrestrial laser scanning (TLS) for monitoring both gradual and abrupt coastal changes, the latter for example associated to seismic events. TLS is a widely-used method for accurate measurements and monitoring of surface changes over time. Several sites in northwestern Greece were surveyed during TLS campaigns in 2009 and 2010. Our main objectives were (i) to measure the present configuration and geometry of a mushroom rock at Poros (Cefalonia Island), which repeatedly experienced co-seismic uplift and (ii) to monitor annual coastal changes of selected shoreline sections on Lefkada Island. At the Poros mushroom rock, up-to-date 3D data of different generations of notches, which were uplifted by palaeoseismic events offer a solid base for evaluating future event-related uplifts. At Lefkada, TLS datasets of different years were compared with each other, resulting in a net balance of elevation changes. Results are checked by photographs taken by a camera on top of the TLS. Comparing the years 2009 and 2010, clear differences in the grain size distribution on beach sediments can be observed as well as slight changes in the coastline configuration. However, shadowing effects of the complex surface and noise caused by sea water represent lead to considerable problems analysing the data.*

Key words*: terrestrial laser scanning, coseismic uplift, coastal change, Ionian Islands*

INTRODUCTION

Western Greece, especially the Ionian Islands, belong to the most active seismic regions in the Mediterranean Sea as they are directly exposed to the Hellenic Trench system and the Cefalonia transform fault (Cocard et al. 1999, Hollenstein et al. 2008). Transform faulting, collision, and subduction can be found within less than 100 km distance (Sachpazi et al. 2000).

The tectonic setting of Cefalonia Island, located at the northwestern edge of the Hellenic Trench, consists of E dipping and NW/NNW-SE/SSE striking thrust sheets (Stiros et al. 1994). The vertical movement of Cefalonia Island is dominated by gradual subsidence interrupted by co-seismic uplifts (Hollenstein et al. 2008).

In the southeastern part of Cefalonia, a mushroom rock (Fig. 1) in the harbour of Poros is well known for two uplifted Holocene notches at +0.6 m and +1.2 m above present sea level (a.s.l.), respectively (Pirazzoli et al. 1994, Stiros et al. 1994). The lower notch was co-seismically uplifted during the 1953 earthquake, and the upper notch during a seismic event around 1.500 yr BP (Stiros et al. 1994, Pirazzoli et al. 1994). Due to the high seismic activity of the region, further uplift due to future earthquakes can be expected.

For measuring the dimensions and for monitoring geomorphological features which are moved, due to co-seismic crustal movements, laser scanning is an ideal approach, easy to realize by multi-temporal surveys. Laser scanning is an active remote sensing technique, also known as Light Detection and Ranging (LIDAR).

Fig. 1: Mushroom rock with two elevated notches in the harbour of Poros (southeastern Cefalonia) (Photo: K. Ntageretzis 2009).

Direct measurement of distances and angles between the sensor and reflecting targets provides highly accurate 3D point clouds. LIDAR can be applied from the ground surface as terrestrial laser scanning (TLS) (Heritage & Large 2009). The interpretation of 3D point clouds is used within the framework of various applications (Vosselmann & Maas 2010). For example, TLS is used to study erosion and denudation processes along cliffs (Lim et

al. 2010) and hillslopes, such as landslides and rock fall (Abellan et al. 2011, Nguyen et al. 2011). Richter et al. (2011) quantified the erosion of a dune cliff and the change of beach width by multi-temporal airborne laser scanning. Rosser et al. (2005) used terrestrial laser scanning for dune cliff erosion monitoring. Also, the rapidly changing geomorphology of fluvial systems can be monitored by laser scanning approaches (Heritage & Milan 2009).

In this study, we used TLS to retrieve high-resolution data of the introduced mushroom rock of Poros (Cefalonia Island), which provides a reliable base for long-term monitoring of uplifting movements by seismic events. Furthermore, a recent notch at Kaminia Beach (Lefkada Island) was scanned to monitor annual changes in the coastal sedimentary system by gradual sediment transport and the influence of storms.

LOCATIONS

Several sites were surveyed by TLS along the shores of the eastern Ionian Sea within the framework of an interdisciplinary research project on palaeo-tsunami impacts (Vött et al. 2010). TLS field campaigns were carried out in 2009 and 2010. In this paper, we focus on the sites of Poros (Cefalonia Island) and Kaminia Beach (Lefkada Island) (see Fig. 2).

Fig. 2: Map of the study areas in the Ionian Sea (NW Greece). Poros lies on Cefalonia Island and Kaminia Beach on the Island of Lefkada. Map based on Modis and ASTER GDEM.

METHODS

We used a TLS LMS-Z420i Riegl instrument for this survey. The time-of-flight range measurements have an accuracy of 0.6 cm with a range between 2 m and 1,000 m. A high-resolution digital Nikon D200 camera mounted on the head of the laser scanner took RGB-photos which were used to colourize the TLS point clouds and to control the results. For data acquisition and first post-processing steps, the RiSCAN PRO Riegl-software was applied.

For the mushroom rock at Poros four scan positions were chosen to retrieve a good coverage. For the area of Kaminia Beach, two scan positions were selected, which cover the whole site. At one of these two scan positions, the scanner was tilted to obtain a view of the entire study area. The resolution for a detailed scan was around 0.8 cm at a distance of 10m.

A Topcon HiPer Pro DGPS instrument was used to measure the different scan positions with a relative accuracy of 1 cm. Positions were recorded in the WGS84 system, UTM Zone 34 N. Furthermore, positions of cylindrical reflectors on ranging poles were recorded.

For the annual measurements, the base point of the local DGPS net was marked by a metal mark and measured 500 times to achieve a mean, enhanced position. All measurements in relation to this base point were within the stated accuracy. Additionally, in each year the similar scan positions were chosen.

Point clouds were subsequently georeferenced by the DGPS points of the scan positions and the reflectors. Afterwards, the registration was enhanced by the ICP-algorithm. The mushroom rock at Poros was reconstructed using the Geomagic Studio 12 software and textured according to the photographs. The results of the two campaigns at Kaminia Beach were clipped and high resolution digital elevation models (HRDEMs) for each year were established. In a first step, the results of the HRDEM comparison were checked visually by the pictures of mounted camera.

RESULTS AND DISCUSSION

The mushroom rock at Poros with the two generations of uplifted notches were reconstructed as an 3D-object and textured by photographs for a near-realistic model (Fig. 3). The data set of Fig. 3 is a valuable tool to precisely measure the present situation as well as the amount of uplift by palaeoseismic events. It also provides a reliable base for monitoring after future events.

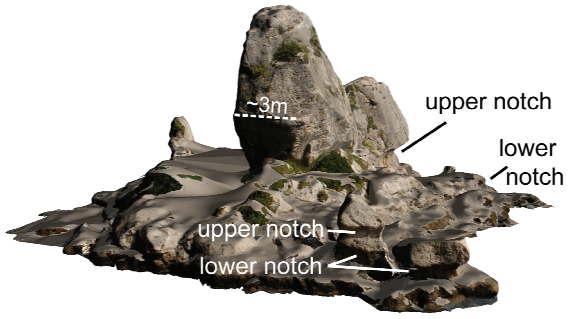

Fig. 3: Perspective view of the mushroom rock model at Poros (Cefalonia Island).

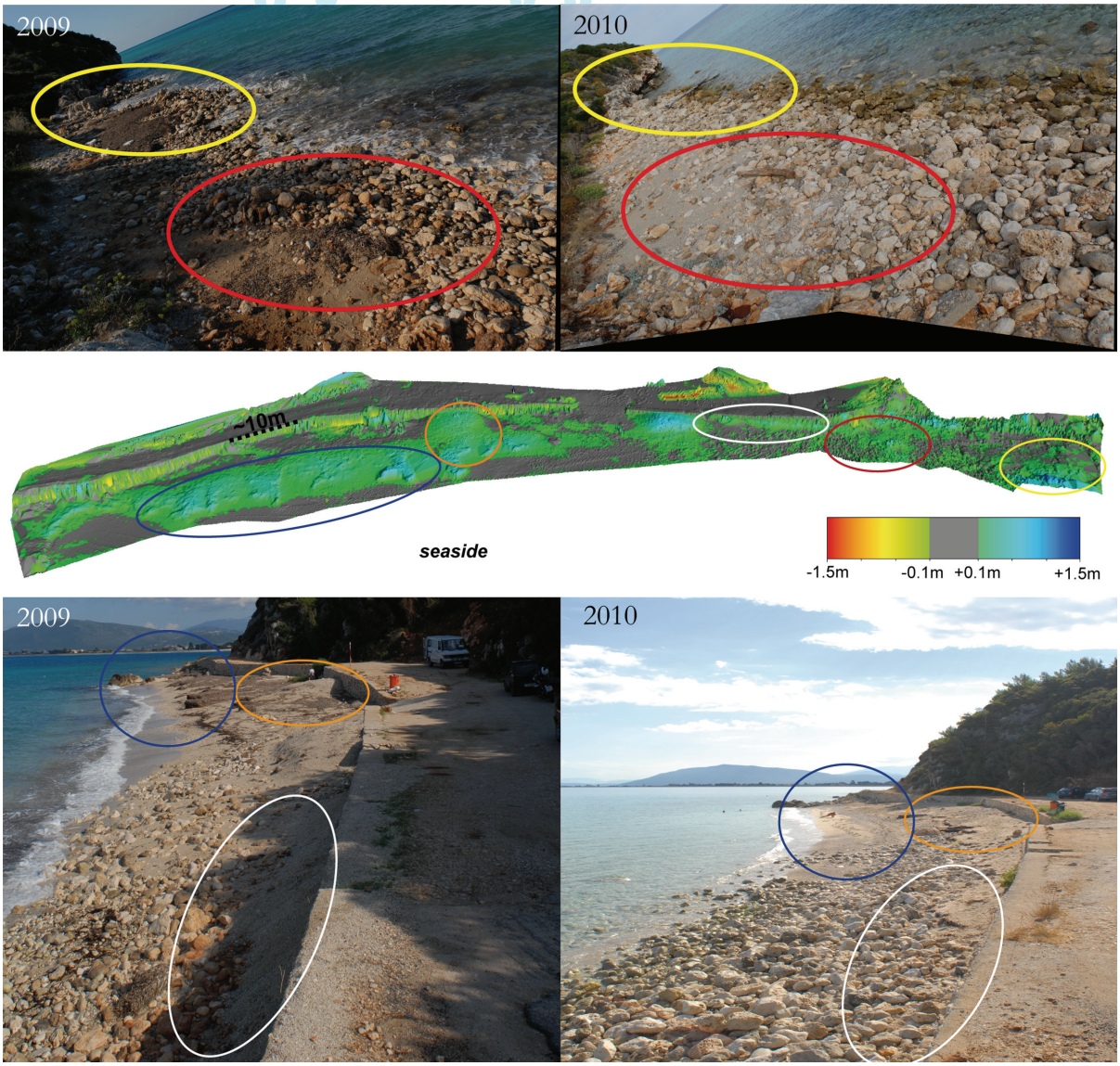

Fig. 4: Morphological net elevation changes of the shoreline at Kaminia Beach between 2009 and 2010 calculated from TLS data (center). Elevation changes go hand in hand with changes in the sedimentary structure along the shoreline (top and bottom photos); exemplary areas are marked by ellipses and discussed in the text.

Comparing the point clouds from the years 2009 and 2010 regarding the notch at Kaminia Beach no changes were observed. However, comparing the beach morphology of 2009 with the one of 2010 considerable changes in the littoral zone can be observed.

Results of the net elevation differences calculated from multi-temporal TLS data with according photographs are illustrated in Fig. 4. The sea weed, which in 2009 covered a large part of the beach has mostly disappeared in 2010 (yellow and blue ellipses). At the same time, a deposit of sandy sediments (orange ellipse) was considerably reduced up to 1 m in size. Another sand cover close to a wall (white ellipse) was replaced by coarse-grained material in 2010. The yellow ellipse marks an area close to the Kaminia notch where gravel was accumulated inland and the coast line was smoothened. This proves active littoral abrasion and documents that the present notch is formed by wave erosion and not by bio-erosion. The red ellipse shows an area where a sand cover was partly erroded and underlying gravel exhumed. However, some pieces of gravel with 30-50 cm diameter seem to have also been displaced. We assume that the observed changes in the sedimentary budget are mainly due to winter storm events.

Post-processing of point clouds turned out to be difficult due to noise caused by water and shadow effects at places where dense gravel occurs (Fig. 5). A major problem, especially at Kaminia beach, is that measurements from the seaside are not possible.

CONCLUSIONS AND OUTLOOK

Our studies show that the application of TLS in different littoral settings is an appropriate tool for monitoring both abrupt and gradual coastal changes.

With regard to palaeoseismic research, TLS based high-resolution 3D models of geomorphologic features moved by co-seismical uplift yield detailed and precise data, for instance at Poros (Cefalonia Island). Moreover, the 3D model may be used to quantify effects from future earthquakes. Furthermore, multi-temporal TLS datasets allows to detect and to monitor gradual coastal changes.

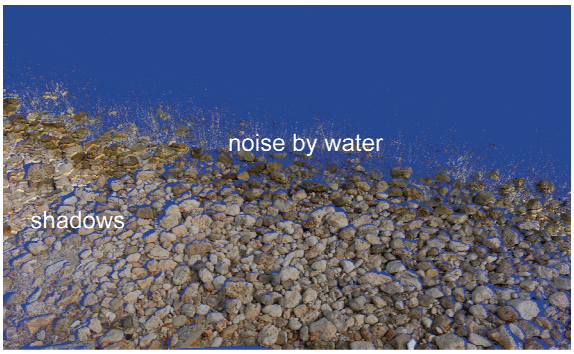

Fig. 5: Two major methodological problems arose in coastal monitoring using TLS in littoral zones: noise caused by water and shadowing effects by coarse material in the upper littoral zone.

The results in this paper represent an essential progress in coastal monitoring by calculating a net balance of sediment budget achieved by a comparison of HRDEMs from different years, generated by TLS data .

Acknowledgements: We gratefully acknowledge financial support by the German Research Foundation (DFG, VO 938/3-1).

References

Abellan, A., J. M. Vilaplana, J. Calvet, D. Garcia-Selles & E. Asensio (2011). Rockfall monitoring by Terrestrial Laser Scanning a case study of the basaltic rock face at Castellfollit de la Roca (Catalonia, Spain). *Nat. Hazards Earth Syst. Sci*. 11, 829-841.

Cocard, M., H.-G. Kahle, Y. Peter, A. Geiger, G. Veis, S. Felekis, D. Paradissis & H. Billiris (1999). New constraints on the rapid crustal motion of the Aegean region: Recent results inferred from GPS measurements (1993-1998) across the West Hellenic Arc, Greece. *Earth Planetary Science Letters* 172, 39–47.

Heritage, G. L. & A.R.G. Large (Eds.) (2009). *Laser Scanning for the Environmental Sciences*. 1. ed., Wiley-Blackwell, Chichester, UK. 278 p.

Heritage, G. L. & D.J. Milan (2009). Terrestrial Laser Scanning of grain roughness in a gravel-bed river. *Geomorphology* 113 (1-2), 4-11. doi: 10.1016/j.geomorph.2009.03.021

Hollenstein, C., M.D. Müller, A. Geiger & H.G. KAHLE (2008). Crustal motion and deformation in Greece from a decade of GPS measurements, 1993-2003. *Tectonophysics* 449, 17-40.

Lim, M., N.J. Rosser, D.N. Petley & M. Keen (2011). Quantifying the Controls and Influence of Tide and Wave Impacts on Coastal Rock Cliff Erosion. *Journal of Coastal Research* 27 (1), 46-56. doi: 10.2112/jcoastres-d-09-00061.1

Nguyen, H. T., T.M. Fernandez-Steeger, T. Wiatr, D. Rodrigues, D. & R. Azzam (2011). Use of terrestrial laser scanning for engineering geological applications on volcanic rock slopes - an example from Madeira island (Portugal). *Nat. Hazards Earth Syst. Sci*. 11 (3), 807-817. doi: 10.5194/nhess-11-807-2011

Pirazzoli, P.A., S.C. Stiros, J. Laborel, F. Laborel-Deguen, M. Arnold, S. Papageorgiou & C. Morhange (1994). Late-Holocene shoreline changes related to paleoseismic events in the Ionian Islands, Greece. *The Holocene* 4 (4), 397-405.

Richter, A., D. Faust & H.G. Maas (2011, in press). Dune cliff erosion and beach width change at the northern and southern spits of Sylt detected with multi-temporal Lidar. *Catena*.

Rosser, N. J., D. N. Petley, M. Lim, S. A. Dunning & R. J. Allison (2005). Terrestrial laser scanning for monitoring the process of hard rock coastal cliff erosion. *Quarterly Journal of Engineering Geology and Hydrogeology* 38(4), 363-375. doi: 10.1144/1470-9236/05-008

Sachpazi, A., C. Hirn, M. Clement, F. Laigle, E. Haslinger, P. Kissling, Y. Charvis, J.C. Hello, M. Lepine, M. Sapin, & J. Ansorge (2000). Western Hellenic subduction and Cephalonia transform: local earthquakes and plate transport and strain. *Tectonophysics* 319 (4), 301-319.

Stiros, S.C., P. A. Pirazzoli, J. Laborel & F. Laborel-Deguen (1994): The 1953 earthquake in Cephalonia (Western Hellenic Arc): coastal uplift and halotectonic faulting. *Geophysical Journal International* 117, 834-849.

Vött, A., G. Bareth, H. Brückner, C. Curdt, I. Fountoulis, R. Grapmayer, H. Hadler, D. Hoffmeister, N. Klasen, F. Lang, P. Masberg, S. M. May, K. Ntageretzis, D. Sakellariou & T. Willershäuser (2010). Beachrock-type calcarenitic tsunamites along the shores of the eastern Ionian Sea (western Greece) – case studies from Akarnania the Ionian Islands and the western Peloponnese. *Zeitschrift für Geomorphologie N.F.,* Suppl. Issue 54 (3), 1-50.

Vosselmann, G. & H.-G. Maas (Eds.) (2010). *Airborne and terrestrial laser scanning*. 1st ed., Whittles Publishing, Dunbeath, UK. 311 p.

PRELIMINARY REPORT ON THE VODICE FAULT ACTIVITY AND ITS POTENTIAL FOR SEISMIC HAZARD IN THE LJUBLJANA BASIN, SLOVENIA

Jamšek, Petra (1), Lucilla Benedetti (2), Miloš Bavec (1), Jure Atanackov (1), Marko Vrabec (3), Andrej Gosar (4,3)

(1) Geological Survey of Slovenia. Dimičeva 14. SI-1000 Ljubljana. SLOVENIA. Email: petra.jamsek@geo-zs.si
(2) Centre Européen de Recherche et d'Enseignement des Géosciences de l'Environnement. BP 80, Europôle Méditerranéen de l'Arbois. 13545 Aix-en-Provence Cedex 4. FRANCE.
(3) University of Ljubljana, Faculty of Natural Sciences and Engineering, Department of Geology. Aškerčeva 12. SI-1000 Ljubljana. SLOVENIA.
(4) Slovenian Environment Agency, Seismology and Geology Office. Dunajska 47. SI-1000 Ljubljana. SLOVENIA.

Abstract (Preliminary report on the Vodice fault activity and its potential for seismic hazard in the Ljubljana Basin, Slovenia): *In Ljubljana Basin (Slovenia) the Vodice fault was investigated to decipher its recent activity and seismic hazard potential for the densely populated central part of Slovenia. Preliminary geomorphological analysis and field observations suggest it may have been recently reversely active. Moreover, using preliminary optical stimulation ages we estimated a slip-rate along the Vodice fault at about 0.2 – 0.4 mm/yr over the last 115 ± 32 ka. An earthquake of magnitude 6.2 – 6.3 could be expected on this fault which may have been the source of the Ljubljana 1895 magnitude 6.1 earthquake. Further analysis will follow to better constrain characteristics of this fault and seismic hazard of the area.*

Key words*: active fault, seismic hazard, Ljubljana Basin, Slovenia*

INTRODUCTION

The Ljubljana Basin (Fig. 1), the most densely populated and urbanized area of Slovenia, experiences constant seismic activity and has been the site of strong historical seismic events with magnitude as high as 6.1 (intensity VIII–IX EMS-98, Ljubljana earthquake 1895 (Ribarič, 1982)). The basin is filled with Quaternary sediments reaching a thickness of up to 280 m in some parts, which may significantly enhance site effects and therefore increase the earthquake hazard in the area (Gosar et al., 2010). However, active faults capable of producing strong magnitude earthquakes in this area are poorly known.

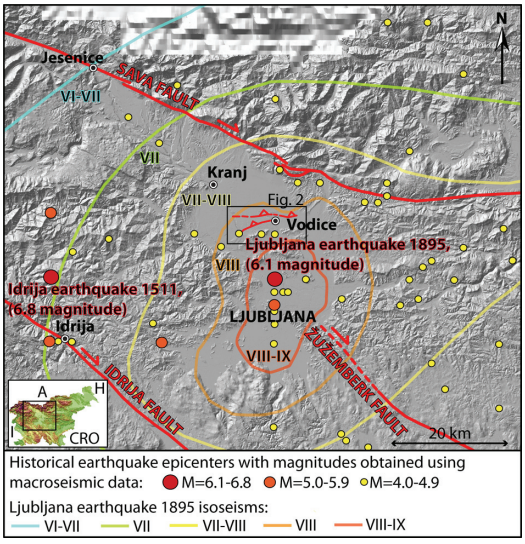

Fig. 1: The Ljubljana Basin map with main active structures (modified according to Buser, 2009), historical earthquake epicentres with magnitude above 3.9 (according to Živčič, 2009; note that earthquakes magnitudes are obtained from macroseismic data and that locations of historical earthquake epicentres are not well constrained), and isoseisms of the Ljubljana earthquake 1895 (according to Lapajne, 1989).

The Ljubljana Basin probably results from transpression with dextral strike-slip movement along NE-SW faults and thrusting along smaller scale E-W structures (Vrabec, 2001; Bavec et al., 2003; Benedetti et al., 2000). In this report we focus on the Vodice fault escarpment, located 15 km north of Ljubljana, the capital city located within the Quaternary basin infill. This escarpment is offsetting Quaternary surfaces for 5 to 25 m along a length of 10 – 11 km. This feature was previously described as a terrace riser of the Sava river (Žlebnik, 1971), and later as a reverse fault (Bavec et al., 2004; Verbič, 2006). To decipher whether the Vodice fault has been recently active and to asses its potential for seismic hazard we performed a detailed study of its morphology and topography. Herein, we present our preliminary interpretations.

METHODS

We investigated its surface expression trough geomorphological analysis of topographical maps (1 : 5.000 and 1 : 10.000 scale), digital elevation model (resolution 5 m), aerial images, and 2.5 m resolution SPOT images in stereo pairs. Each alluvial surface was carefully mapped and a series of topographical profiles were extracted across, and parallel to the scarp from 5 m resolution digital elevation model.

Based on analysis of topographical profiles, detailed mapping and field observations we were able to evidence recent movement along the fault. Based on preliminary optical stimulation luminescence ages (Bavec et al., 2005) we evaluated the slip-rate along the Vodice fault, possible earthquake magnitude and average displacement per event.

VODICE FAULT SURFACE EXPRESSION

The flat Ljubljana Basin surface resulting from Quaternary deposition is perturbed in the area of Vodice by an unusual linear feature, ENE-WSW oriented, 10-11 km long scarp between Pšata river on the east and Sava river on the west (Fig. 2). East of Vodice, the scarp splays into two branches. A series of detailed topographic profiles levelled across, and parallel to the scarp show that the height of the scarp varies from 25 to 5 m for the southern branch and from 18 to 3 m for the northern branch (Figs. 2 and 3). Evidence of ongoing uplift is attested by the presence of abandoned streams across the structure and perched valleys (Fig. 3). Active streams strongly incise the northern, hanging wall compartment, this upper surface being clearly older as shown by its degradation mostly due to dolines. These observations lead us to interpret the Vodice scarp as the surface expression of an active reverse fault. The latter suggests that the scarp can not be interpreted as a terrace riser of a former course of the Sava river.

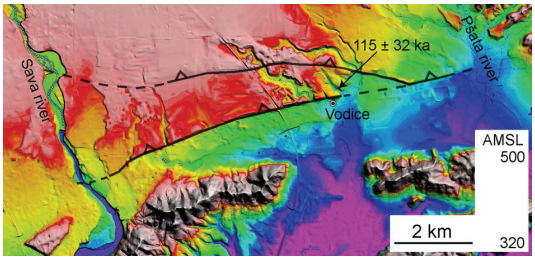

Fig. 2: The Vodice fault surface expression.

SUBSURFACE DEFORMATIONS

Further evidences of the fault activity are provided from subsurface deformations. Folding was reported in a clay pit at the eastern end of the scarp (Fig. 4, Drobne et al., 1960; Šifrer, 1961). Westward, where the fault cuts the N-S running Sava River, Quaternary conglomerates are also folded and offset (Fig. 5). In both cases the deformations are consistent with a reverse fault interpretation.

FIRST EVALUATION OF SEISMIC HAZARD POTENTIAL

Preliminary optical stimulation luminescence ages of deformed sediments, located at the eastern tip of the fault (Bavec et al., 2005), suggest an age of 115 ± 32 ka for the upper alluvial surface (Fig. 2). Using this age and assuming a northward dip of 35 – 45°, we estimated a minimum slip-rate along the Vodice fault at about 0.2 – 0.4 mm/yr over the last 115 ± 32 ka.

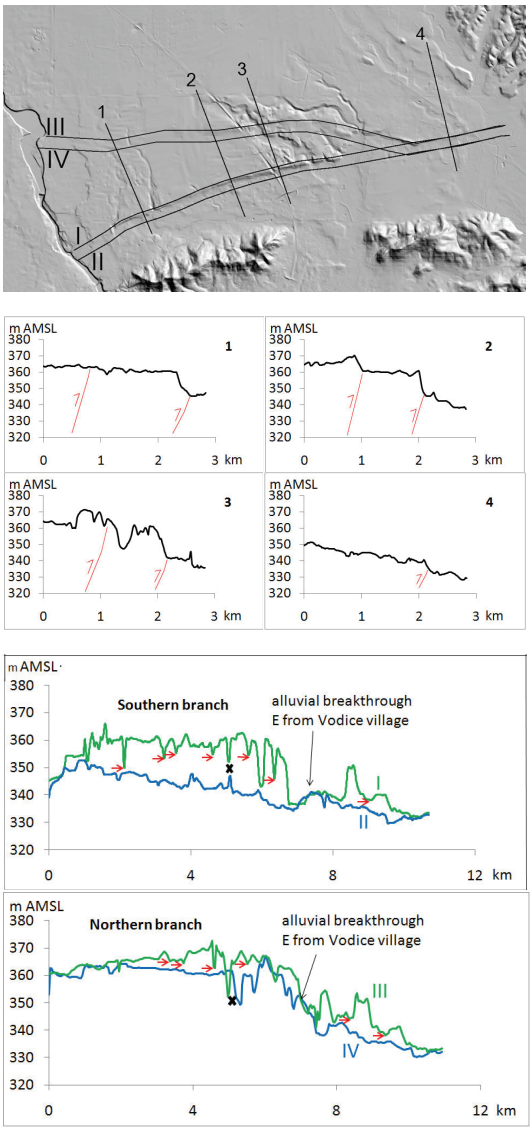

Fig. 3: The series of topographic profiles across, and parallel to the Vodice fault scarp (red arrows = perched valeys). Note that the profile in the image is showing two fault branches because it is shalow, but in the depth the two branches are most probably joined into one fault.

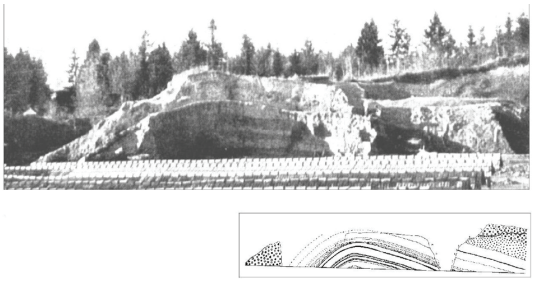

Fig. 4: Folded Quaternary sediments at the eastern end of the scarp reported by Šifrer (1961).

On a 10 – 11 km long reverse fault, an earthquake of magnitude 6.2 – 6.3 could be expected. Such earthquake could trigger an average displacement of ~ 0.5 m with an average recurrence time of 1200 – 3000 yr (Wells & Coppersmith, 1994).

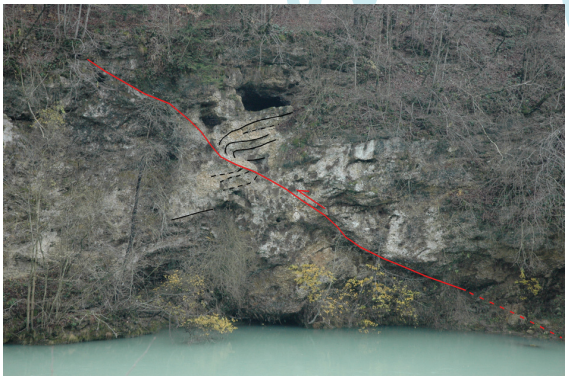

Fig. 5: One of the Vodice fault outcrops. Fault plane (red line) dips towards NNW for 35°. Features that may also be interpreted as near surface expression of faulting are marked in black.

DISCUSSION

This preliminary geomorphological analysis and field observations suggest recent activity along E-W trending 10-11 km long Vodice reverse fault and correlates well with results of previous studies (Bavec et al., 2004; Verbič, 2006). However, to further prove Vodice scarp as the surface expression of a reverse fault the geophysical investigations are planned. Also, to better constrain the Vodice fault displacements and its slip-rate, further accurate quantitative analysis of the morphology are warranted (levelling survey using theodolite or diferential GPS) and Quaternary geochronology to date the offset surfaces.

A first approximation suggests the Vodice fault could trigger magnitude 6.2 – 6.3 earthquake events. Considering its location and proximity to Ljubljana, the Vodice fault is a candidate to be the source of the Ljubljana earthquake 1895. To better assess the seismic hazard of this area further analysis will follow, such as geophysical investigations of the fault geometry (high-resolution seismic reflection and ground penetrating radar profiling) and paleoseismological investigations along the fault to define its seismic behaviour and decipher its seismic history.

Recognition of seismic hazard is crucial in areas such as Ljubljana Basin, where destructive earthquakes can represent a huge danger for population and infrastructure. Investigations in active tectonics are the first step towards seismic hazard assessment, leading to protection of human lives as well as to a decrease of economical damage in case of a destructive seismic event. To determine the seismic hazard in the Ljubljana Basin we will also extend our investigations to other presumably active faults bounding the basin.

Acknowledgements: This work is funded by the Slovenian Research Agency, through 1) The project L1–2383 Seismotectonic model of the Ljubljana Basin (cofounded by the Slovenian Environment Agency), 2) The programme P1 – 0011 Regional geology, and 3) The support for young researcher (contract 1000-09-310068).

References

Bavec, M., B. Celarc, M. Demšar, M. Poljak, D. Rajver, I. Rižnar, F. Preusser, M. Toman, J. Žibrat, M. Novak & K. Hribernik, (2005*). Izdelava geoloških kart: letno poročilo za leto 2005.* Geological Survey of Slovenia. Ljubljana.

Bavec, M., B. Celarc, M. Poljak, M. Demšar, D. Rajver, D. Skaberne, T. Verbič, I. Rižnar, F. Preusser & M. Culiberg, (2004). *Izdelava geoloških kart. Karta aktivnih prelomov v Sloveniji: letno poročilo za leto 2004.* Geological Survey of Slovenia. Ljubljana.

Bavec, M., M. Poljak, M. Demšar, D. Rajver, M. Komac, M. Toman, S. Stojanova, B. Mušič, M. Vrabec, T. Verbič & I. Rižnar, (2003). *Izdelava geoloških kart. Karta aktivnih prelomov v Sloveniji : letno poročilo za leto 2003. 1. del : Raziskave na območju Ljubljansko-kranjske kotline.* Geological Survey of Slovenia. Ljubljana. 56 f.

Benedetti, L., P. Tapponnier, G. C. P. King, B. Meyer & I. Manighetti, (2000). Growth folding and active thrusting in the Montello region, Veneto, northern Italy. *Journal of Geophysical Research – Solid Earth* 105, 739–766.

Buser, S. (2009). *Geological map of Slovenia 1:250.000.* Geological Survey of Slovenia. Ljubljana.

Drobne, F., R. Pavlovec & A. Šercelj, (1960). Some analyses and problems of Pleistocene sediments at Lokarji near Vodice. *Kamniški zbornik* 6, 163–194.

Gosar, A., J. Rošer, B. Šket Motnikar, P. Zupančič, (2010). Microtremor study of site effects and soil-structure resonance in the city of Ljubljana (central Slovenia). *Bulletin of earthquake engineering* 8 (3), 571–592.

Lapajne, J. (1989). Veliki potresi na Slovenskem – III.: potres v Ljubljani leta 1895. *Ujma* 3, 55–61.

Ribarič, V. (1982). *Seismicity of Slovenia. Catalogue of earthquakes (792 A.D.–1981).* Seismological Survey of Slovenia. Ljubljana. 649 p.

Šifrer, M. (1961). *The basin of Kamniška Bistrica during the Pleistocene period.* Slovenian Academy of Sciences and Arts. Ljubljana. 211 p.

Verbič, T. (2006). Quaternary-active reverse faults between Ljubljana and Kranj, central Slovenia. *Razprave IV. razreda SAZU* 47 (2), 101–142.

Vrabec, M. (2001). *Structural analysis of the Sava Fault zone between Trstenik and Stahovica. PhD thesis.* University of Ljubljana. Faculty of Natural Sciences and Engineering. Department of Geology. 94 f.

Wells, D. L. & K. J. Coppersmith, (1994). New Empirical Relationships among Magnitude, Rupture Length, Rupture Width, Rupture Area, and Surface Displacement. *Bulletin of the Seismological Society of America* 84 (4), 974–1002.

Živčić, M. (2009). *Catalogue of earthquakes in Slovenia.* Internal documentation. ARSO – Slovenian Environment Agency. Ljubljana.

Žlebnik, L. (1971). Pleistocene Deposits of the Kranj, Sora and Ljubljana Fields. *Geologija* 14, 5–51.

DISTRIBUTION AND SEDIMENTARY CHARACTERISTICS OF TSUNAMI DEPOSITS ON PHRA THONG ISLAND, THAILAND

Jankaew, Kruawun (1), Dominik Brill (2), Maria E. Martin (3), Yuki Sawai (4)

(1) Department of Geology, Faculty of Science, Chulalongkorn University, Bangkok, 10330 THAILAND
Email:kruawun.j@chula.ac.th
(2) Department of Geography, University of Cologne, GERMANY
(3) Department of Earth and Space Sciences, University of Washington, Seattle, USA
(4) Geological Survey of Japan, National Institute of Advanced Industrial Science and Technology (AIST), Tsukuba, JAPAN

Abstract (Paleotsunami): *Phra Thong Island is located along the western coast of Thailand directly facing the source area of the 2004 Indian Ocean tsunami. Here we report a distribution of paleotsunami sand layers on Phra Thong Island, collected during four years of field work (2007-2011). Sedimentary characteristics of paleotsunami deposits are compared with those of the 2004 tsunami. Thicknesses of the 2004 and paleotsunamis sand layers are controlled by micro-topography and subjected to post-depositional alteration. Sand layers of 2004 and paleotsunami layers contain fining upward sequence(s), which suggest deposition from suspension, with similar grain size distribution. The sedimentary structures of the 2004 tsunami, where present, are already obliterated six years after the event, making it difficult to interpret the flow direction and to differentiate between deposits from inflow and outflow of tsunami. This will affect accuracy of future work in estimating flow characteristics of past tsunamis based on the depositional record in the vegetated area such as Thailand.*

Key words*: Paleotsunami, tsunami deposits, Indian Ocean, Thailand*

INTRODUCTION

Phra Thong Island is located about 580 km southwest of Bangkok and about 120 km north of Phuket (Fig.1). It is about 15 km in length and 9 km in width, with the long axis in an approximate N-S direction and the western side directly facing the Andaman Sea. The island composes of beach-ridge plain on the western side and the mangrove-fringed tidal inlet to the east. The 2004 tsunami severely struck the island and completely wiped out one of the only three villages on the island. Paleotsunami deposits on Phra Thong Island were reported by Jankaew et al. (2008) and Fujino et al. (2009).

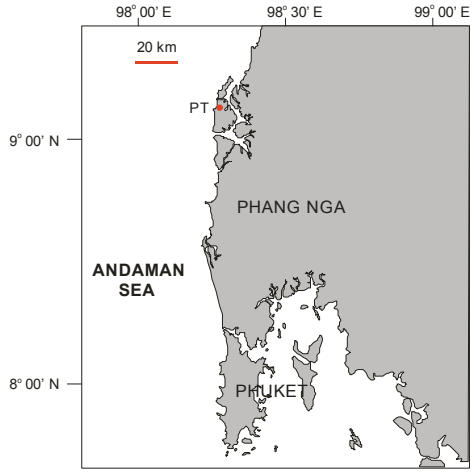

Fig. 1: Map showing location of Phra Thong Island (PT).

Apart from the frequency, a magnitude of large tsunamis is important information needed to be established in certain coastal area in order have better mitigation measure in place for possible future catastrophic events. The magnitudes of tsunamis responsible for the sand layers at Phra Thong, can be assessed using numerical models with help from tsunami deposits to validate the model results. Because of its relatively flat terrain, Phra Thong offers a suitable site to study velocity and tsunami flow depth from characteristics of the deposits. Thickness and grain size distribution of tsunami deposits can be used in sediment transport models (Jaffe & Gelfenbaum, 2002; Jaffe & Gelfenbaum, 2007) to derive estimates of flow velocity and water depth (Peters et al., 2007), which are important in building design and in planning evacuation route.

We present distribution of paleotsunami deposits on Phra Thong Island and sedimentary characteristics of 2004 and paleotsunamis.

METHOD

We dug shallow pits and trenches to observe sedimentary characteristics of tsunami sediments (both 2004 tsunami and paleotsunamis) and to collect samples for grain size analyses. In order to better observe and to be able to make a meaningful conclusion of the deposit thickness and grain size variation, observed in the 2004 and paleotsunami deposits, we collected samples along two transects parallel to the tsunami flow (Fig. 2). Sediment samples were collected to the end of the 2004

tsunami sedimentation limit. Total length of the two transects are 1.5 km and 2 km, respectively. Along these transects wherever the paleotsunami sand layer is present, we also collected samples for grain size analyses. The samples were collected at 0.5 cm interval, and analysed using settling tube, measuring size range from 0-5 ϕ with 0.1 ϕ intervals.

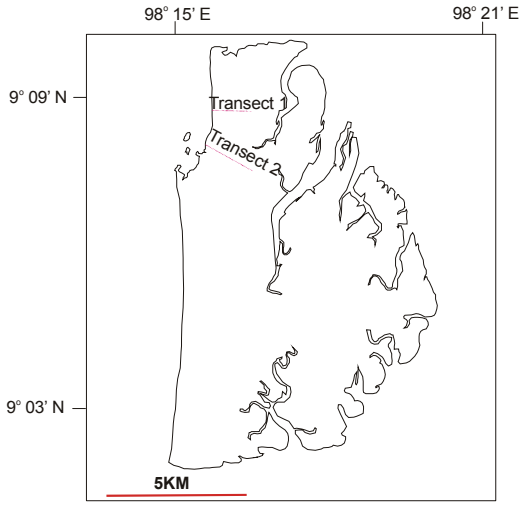

Fig. 2: Sediment samples were collected from two transect from the northern part of the island.

RESULT

The thickness of deposits of the 2004 tsunami and its predecessors varies across the beach-ridge plain and is primarily controlled by local topography. Thickness tends to be greatest in a low-lying swale (as much as 30 cm). On ridges and higher ground it tends to be thinner (few cm, 10 cm at most). Fig. 3 shows a variation in thickness of the 2004 tsunami deposit along transect 2 (in Fig. 2). A thicker, and sometimes coarser, deposit in topographic lows is a response of the flow to the deeper water depth, which slows the flow and drive deposition (Apotsos et al., 2009). In the case of Phra Thong, if the swale is located on a path of back flow, which is often channelized, thickness is much higher. Back flow deposits contain both sediments eroded from

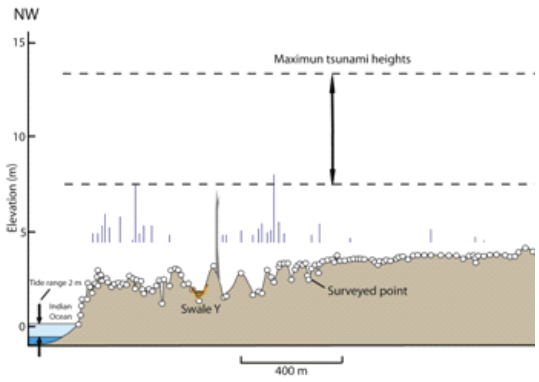

Fig. 3: Thicknesses of 2004 tsunami deposit along transect 2 (blue vertical line: VE x10).

landward location and sediments remaining in suspension. The 2004 tsunami deposits contain up to

Fig. 4: Thick 2004 tsunami deposit (almost 30 cm thick) in a swale. Sedimentary structures indicating flow direction are clearly visible in this picture. The sea is to the right of the picture.

4 fining-upward sequences. Fig. 4 is an example of 2004 tsunami deposit in the swale located on a path of the back flow. In Fig. 4, the lowest fining-upward sequence was probably deposited out of the first tsunami wave. Above this sequence, a continuous dark gray layer of fine silt-clay which was probably deposited when the tsunami flow was still and between the two main waves. Above this silty clay layer there are 2-3 fining upward sequences, which were possibly deposited from back flow of the first or second wave. Sets of cross bedding in these upper sequences indicate a flow direction towards the sea. Revisiting the sites allow us to observe that dense vegetation in the tropics, especially in the low lying fresh water swales, already destroy most of these cross bedding sets. This will complicate the interpretation of flow depths and velocities based on the deposit thickness.

On high ground of Phra Thong Island (about 4 m above msl.), with less vegetation cover, the 2004 tsunami deposit lies above the sand ridge sediments with faint soil in between them. It is still possible to identify the 2004 tsunami deposits in the high ground 6 years after the event, but allowing more time differentiating it from the sand ridge below will be problematic. At many locations, distinguishing the 2004 tsunami laid sand and the underlying ridge sand was already difficult due to the lack of organic soil formation on top of the ridge sand. On the high ground immediately next to the swale, after the tsunami dumped a majority of sediments in the swale, the 2004 tsunami deposit composes mainly of silt which fell out of suspension (Fig. 5). The tsunami flow then picked up more sediment from the ridge area along its flow path. As a result, grain size of 2004 tsunami on high ground is composed mainly of silt in contrast to sand and silt in the swale deposit. The thicknesses of the 2004 deposits at different locations are also shown.

Fig. 5: Thin 2004 tsunami deposit (about 5 cm thick) on high ground. The deposit contains mainly silt and very fine sand with no sedimentary structure. The sea is to the left of the picture.

Apart from variation in the thickness of the deposit, internal characteristics of 2004 deposit on Phra Thong also varies greatly from one place to another. Often the deposits show no internal structure or layering. Typically the deposits appear as a massive bed or faintly normally graded. In locations close to the sea, some deposits are coarsened upward.

The 2004 tsunami sediments range in grain size from coarse sand to coarse silt, with distinctive bimodal distribution with the first mode in fine-sized range (2 ϕ), and the second and highest mode in very fine-size range (3.3 ϕ). The coarser sediments are composed of coarse sands, derived from beach berm and possibly from offshore areas, and broken shell fragments, large foraminiferas and other macrofossils, whereas the finer sediments were possibly derived from the subtidal zone. The 2004 sediment composes about 85% of clear to white quartz grains, 8% of shell fragments and microfossils, 4% of muscovite and 3% of heavy minerals - mostly small grains of tin. Although typically 2004 tsunami deposits at Phra Thong appear as a massive bed or faintly normally graded, detailed grain size analyses show that they can contain 2-3 fining-upward sequences. The mean grain size of the 2004 tsunami is slightly bigger than that of the paleotsunami sand. The 2004 tsunami layer contains 2-3 fining-upward sequences while paleotsunami deposits contain 2 fining-upward sequences.

Paleotsunami deposits at Phra Thong Island are composed of grains ranging in size from coarse sand to coarse silt, with bimodal distribution. A small first mode in fine-sized range (2.3 phi), and second and the highest mode in very fine-size range (3.2 phi). Grains compose of about 91% of clear to white quartz grains, 7% of muscovite and 2% of heavy minerals - mostly small grains of tin. The shell fragments and microfossils are absent in the paleo-sand layer. Phra Thong paleotsunami deposits appear as a massive bed or faintly normally graded, more so than the 2004 deposits, but mean grain size at 0.5 cm thickness intervals show that they contain up to two fining-upward sequences

DISCUSSION

Deposition of tsunami sediment, although generally has a sheet-like geometry, is greatly controlled by the local topography with thicker deposit in the low-lying area. The thickness of tsunami deposit is further altered by post-depositional processes such as human and animal disturbances, erosion and bioturbation. However, the thick deposits in the low-lying area have a greater tendency to be preserved and remained as a geological record. Dense vegetation in a study area quickly destroy most of the sedimentary structures contain in the deposit which may complicate differentiation between inflow and outflow deposits, leading to over or under estimation of the thicknesses of tsunami deposited by each wave. Sedimentation limit of the paleo-event is also difficult to define, especially in the case of Phra Thong Island where deposits are mainly preserved in the swales and are subjected to bioturbation.

CONCLUSION

Future work in estimating hydrodynamic properties of past tsunamis from sediment deposits in the tropics should not be dependent on thickness of the deposits.

Acknowledgements: This work was supported by Japan Society for the Promotion of Science (to YS and KJ), DFG grant numbers BR 877/27 and KE 190/26 (to DB and KJ) and NRCT grant number GE3/2554 (to KJ).

References

Apotsos, A.; B. Jaffe, G. Gelfenbaum, and E. Elias, (2009). Modeling time-varying tsunami sediment deposition. *Proceedings of Coastal Dynamics 2009*, 1-15.

Fujino, S., H. Naruse, D. Matsumoto, T. Jarupongsakul, A. Sphawajruksakul, and N. Sakakura, (2009). Stratigraphic evidence for pre-2004 tsunamis in southwestern Thailand. *Marine Geology* 262, 25-28.

Jaffe, B. E. and G. Gelfenbaum, (2002). Using tsunami deposits to improve assessment of tsunami risk. *Solutions to Coastal Disasters'02, Conference Proceedings, ASCE*, 836-847.

Jaffe, B. E. and G. Gelfenbaum, (2007). A simple model for calculating tsunami flow speed from tsunami deposits, *Sedimentary Geology* 200, 347-361.

Jankaew, K., B.F. Atwater, Y. Sawai, M. Choowong, T. Charoentitirat, M.E. Martin, and A. Prendergast, (2008). Medieval forewarning of the 2004 Indian Ocean tsunami in Thailand. *Nature* 455, 1228–1231.

Peters, R.; Jaffe, B. & Gelfenbaum, G. (2007). Distribution and sedimentary characteristics of tsunami deposits along the Cascadia margin of western North America, *Sedimentary Geology* 200, 372-386.

ARCHAEOSEISMOLOGY OF THE AD 1545 EARTHQUAKE IN CHIANG MAI, NORTHERN THAILAND

Kázmér, M. (1), Kamol Sanittham (2), Punya Charusiri (3), Santi Pailoplee (3)

(1) Department of Palaeontology, Eötvös University, Pázmány sétány 1/c, Hungary. Email: mkazmer@gmail.com
(2). Department of Mathematics and Statistics, Chiangmai Rajabhat University, Chiang Mai, Thailand
(3) Department of Geology, Chulalongkorn University, Bangkok, Thailand

Abstract (Archaeoseismology of the A.D. 1545 earthquake in Chiang Mai, northern Thailand): *The A.D. 1545 Chiang Mai earthquake in northern Thailand was studied by historical and archaeological sources.The temple Wat Chedi Luang has lost about half of the original 80-metres height due to southward-directed collapse. Twenty-one temple sites – out of 74 visited – has tilted pagodas, up to 5° in various directions, dominated by a SE trend. All damaged temples were built before the 1545 earthquake. We suggest that a city-wide liquefaction event caused tilting. The responsible earthquake possibly occurred along the Doi Suthep Fault within city limits. Possible activity of distant faults is assessed.*

Key words*: palaeoseismology, Thailand, liquefaction, Wat Chedi Luang*

INTRODUCTION

An important obstacle to the assessment of earthquake hazard at present is the lack of information about old earthquakes (Ambraseys, 2009: xii). The locations of larger historical earthquakes have been found to be known well enough to guide field studies for further in situ investigations. Properly run field studies provide reliable observations for the assessment of damage, intensity, and its distribution, ground effects and surface faulting. Field studies of old earthquakes are time-consuming and often present subtle problems but they are essential (Ambraseys 2009: 16). Here we provide a brief description of traces of a significant earthquake in Northern Thailand, and provide assessment of seismic parameters of the event.

Fig. 1: Wat Chedi Luang in Chiang Mai, Thailand, seen from the southeast. Damaged during the AD 1546 earthquake, the upper half of the stupa fell to the south.

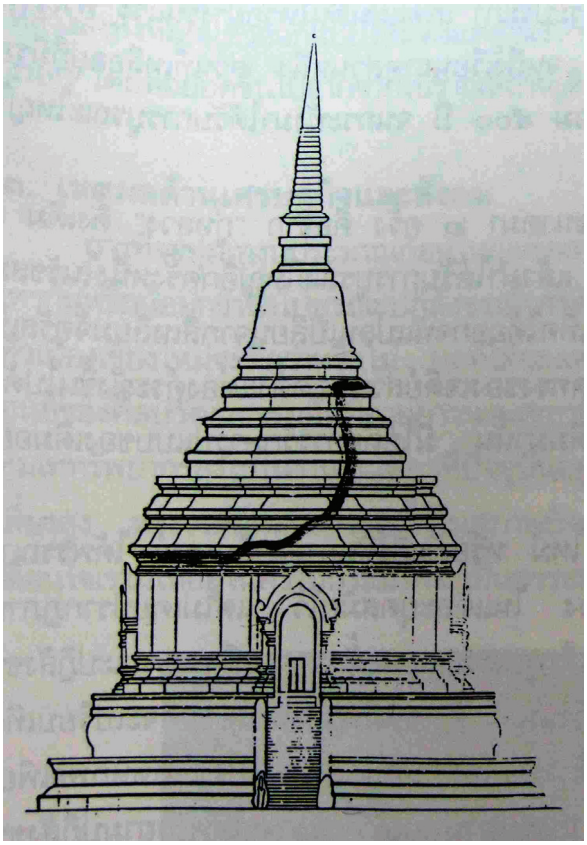

Fig. 2: Archaeological reconstruction of the pre-earthquake dimensions of Wat Chedi Luang as seen from the east. Total height was approx. 80 m. The portion above the heavy line is the art historian's vision about its looks.

Both historical documents and archaeological data are available describing the A.D. 1545 earthquake in Northern Thailand. We studied the Buddhist temples in and around the old city of Chiang Mai (Kázmér &

Sanittham, 2011) to identify possible earthquake-induced damages preserved in the buildings' structure and orientation.

Currenty earthquake activity in northern Thailand is interpreted within the framework of Thoen Fault (Chiang Saen, May 2007, M_L = 6.3), Mae Tha and Pha Youv fault zones tens of kilometres away (Pailoplee et al., 2010). Since recurrence time of major earthquakes seems to be longer than the instrumental period of 50 years, archaeoseismology is a necessary tool to extend the observation period to centuries.

METHODS

Historical, archaeological, and geological-geophysical data are combined to understand the Chiang Mai earthquake of AD 1545. The published historical description was cross-checked with archaeological data of the site of Wat Chedi Luang and elsewhere. We visited 74 temples of Chiang Mai city. While recording earthquake archaeological effects (Rodriguez-Pascua et al. 2011), we measured the angle and direction of tilt of the chedi (stupa) by a stonemason's tiltmeter and a compass, respectively.

Coordinates of chedi location were taken from the digital map of Northern Thailland (ThinkNet 2010). Construction ages were drawn from Thai-language publications. When no printed source was available, we accepted the dating of tourist information tablets in the monasteries.

There is no official English transliteration system for the Thai language. English spelling of Thai names is inconsistent to the extent that one's own name is written differently on subsequent occasions. In this paper we use names as found on the electronic map of ThinkNet (2010), which is neither official, nor better than any other spelling.

HISTORICAL DATA

There was a damaging earthquake in Chiang Mai city (Northern Thailand) on 28 July 1545 in the afternoon hours between 4.30 and 6.00 pm. *„The earth trembled and shook, groaned and moaned, very intensely. The finials,* (top parts) *yòt, of the Jedi Luang and of the jedi in Wat Phra Sing broke off and fell down, and also the finials of many other jedis"*, recorded the contemporary Chiang Mai Chronicle in Lanna language (translated by Penth, 2006).

WAT CHEDI LUANG IN CHIANG MAI

The largest chedi (stupa, pagoda) ever built in what is Thailand today is the Wat Chedi Luang, standing in the monastery of the same name in the centre of old Chiang Mai city (Fig. 1). Built in 1391, it has been reconstructed and enlarged several times, A huge chedi, 56 x 56 m rectangular basement, approx. 80 m high was built in 1479-1481. The base was enlarged and strengthened in 1512 (Podjarawaraporn, 2547).

On 28 July 1545 there was a huge rainstorm and an earthquake, which caused the chedi to topple, leaving only half if its structure to stand (Fig. 2). The power and richness of the Medieval Lanna Empire already in the decline, no funds have ever been available to restore the damaged building to its former glory. The chedi was left in this damaged condition for more than four centuries. A cosmetic restoration in 1992 completed the strengthening by a 60 x 60 m base, .

TILTED BUILDINGS CITYWIDE

In addition to the famous damaged chedi, numerous religious and secular monuments in and around the old city bear evidence for some kind of earthquake damage. The most obvious evidence is tilting of chedis: the pointed top part of the monument clearly deviates from the vertical by a few degrees (Fig. 3). (The lightweight metal decoration at the very top is almost always heavily tilted; we did not take these into account, only the brick portion below.) Historical data on construction time of the chedis indicate that all of them were built in the 14-15th century AD, before the A.D. 1545 earthquake (Fig. 4). Locations and tilt directions are mapped on Fig. 5.

Tilt directions are dominated by a conspicuous SE trend (Fig. 6).

Fig. 3: Tilted buildings citywide

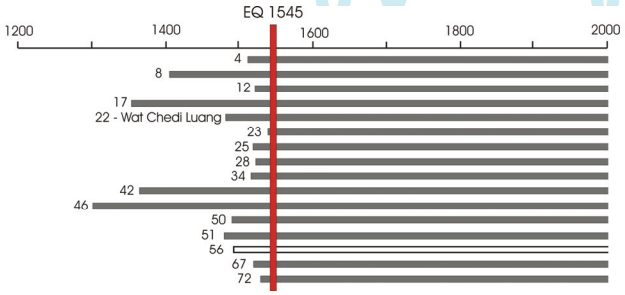

Fig. 4: All tilted chedis (stupas) were built before the AD 1545 earthquake. 4 – Wat Chiang Yeun, 8 – Wat Hua Khuang, 12 – Wat Lok Mo Li, 17 – Wat Phra SIngh, 23 – Wat Chai Prakiat, 28 – Wat Phuak Hong, 34 – Wat Chet Rim, 42 – Wat Umong, 46 – Wat Chiang Man, 50 – Wat Srisupan, 51 – Wat Nantharam, 56 – Wat Daowadueng (no tilting was observed), 67 – Wat Bupharam, 72 – Wat Chomphu.

SUBSOIL

The tilted chedis are all on the alluvial plain of the Ping River, extending over at least 4 km^2. Groundwater lever was high during our survey in August 2010, about 70 to 100 cm below ground, as seen in several wells within the temple compounds. Historical data indicate a rainy summer season for 1545, too.

We suggest that a city-wide liquefaction event, caused uneven settlement and subsidence of the buildings in the saturated soil. The dominant SE-ward tilt direction possibly reflects strong motion directionality.

INTENSITY

While modified Mercalli intensity VII is the damage threshold for many archaeological sites (Kovach and Nur, 2006), we assume that damages to Wat Chedi Luang related to the 1545 earthquake require a larger intensity due to the especially compact construction of the building. The pagoda, built like a pyramid, is certainly a more earthquake-resistant structure than any ordinary city house, even palace. Intensity IX or higher (good masonry damaged seriously, in areas of loose sediment, sand, mud, and water ejected – Rapp, 1986) seems more probable.

Intensity VIII to IX (heavily damaging to destructive) is assumed on the ESI 2007 environmental intensity scale (Michetti et al., 2007): liquefaction with settlement up to 30 cm or more. The total affected area was in the order of 1000 to 5000 km^2 (Reicherter et al., 2009), i.e. all of the Chiang Mai-Lamphun Basin.

EPICENTER AND MAGNITUDE

Known and possibly active faults were assessed for source of the earthquake, and the minimum magnitude for liquefaction calculated after Obermeier (1996, Fig. 42).

The Doi Suthep fault, the master fault of the half-graben of the Chiang Mai Basin is 3 km away. It is not known to be active: a minimum M 5.5 seismic event here could cause liquefaction.

The SW-NE trending, left-lateral Mae Kuang Fault 32 km to the NE is possibly inactive since the Tertiary, althought the fault trace is particularly conspicuous in the landscape (Rhodes et al. 2004). A minimum M 6.3 seismic even would have been sufficient to cause liquefaction in Chiang Mai.

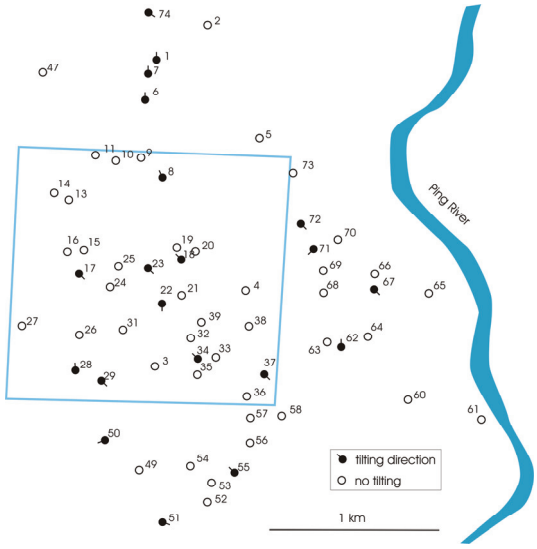

Fig. 5: Tilted chedis (Fig. 4) (black dots) on the alluvial plain of Ping River (Margane & Tatong, 1999). Ticks towards direction of tilting. Untilted chedis are marked with empty circles. Rectangle indicates walled city of old Chiang Mai.

The Lampang-Thoen fault zone 120 km to the SE is active (Chiang Saen, May 2007, M_L = 6.3). The segments are long enough to produce M 7 earthquakes (Pailoplee et al., 2009). A minimum M 7 seismic event is needed to cause liquefaction in Chiang Mai city.

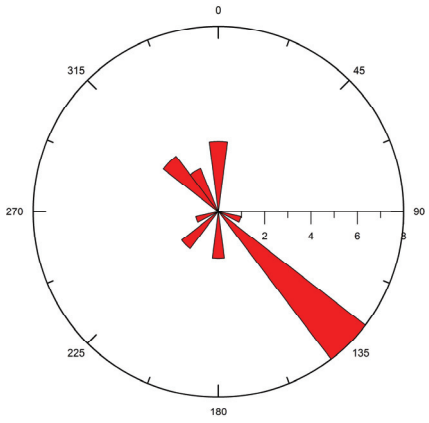

Fig. 6:Tilt directions plotted in polar bar chart. Horizontal axis – number of pagodas tilted in a certain direction. Note the prominent southeastward tilting of several chedis.

The Sagaing Fault in Myanmar, forming the boundary between the Sunda and Burma plates is 200 km to the W. It regularly produces M > 7 earthquakes (M 7.0-7.4) (Hurukawa & Maung, 2011). However, the M 7.5 earthquake on December 3, 1930, did not cause any liquefaction event in Chiang Mai we are aware of. A lack of proper attenuation model for Thailand (Chintanapakdee et al., 2008) prevents formulating a suitable explanation. There is local model developed for Chiang Mai (Kannika & Takada, 2009), although for rock sites, not for alluvium. We suggest that earthquake intensities display a strong directionality along the right-lateral Sagaing Fault: higher intensities occurring parallel and lower intensities perpendicular to the fault, thus protecting Chiang Mai from major plate-boundary events.

Whether any of the above or another fault is resonsible for the AD 1545 earthquake is an open question as yet. Studies on strong motion direction causing the major damages (see, for example. Korjenkov & Mazor, 1999, 2003; Kázmér & Major, 2010; Hinzen, 2008, 2009) may help tor resolve some of the open questions.

Acknowledgements: Our thanks are due to the staff of Mahamakat Buddhist University, Lanna Campus library for their help in accessing relevant literature in the Thai language. Financial help from Hungarian National Science Foundation (OTKA) grant K 67.583 and and an IGCP 567 travel grant are sincerely acknowledged here. Raúl Pérez López is thanked for his comments, which improved this manuscript.

References

Publication dates of Thai-published books in Thai only are given as of the Thai calendar. Deduce 543 for conversion to western, Gregorian years.

Ambraseys, N.N. (2009). *Earthquakes in the Mediterranean and Middle East. A Multidisciplinary Study of Seismicity up to 1900.* Cambridge, Cambridge University Press. 968 p.

Chintanapakdee, C., Naguit, M.E. & Charoenyuth, M. (2008). Suitable attenuation model for Thailand. – *14th World Conference on Earthquake Engineering: Innovation Practice Safety*, Beijing, 2008. [8 p.] Download: http://www.14wcee.org/Proceedings/files/02-0088.PDF (accessed 25 June 2011)

Hinzen, K.-G. (2008). Can ruins indicate a back azimuth?: *Seismological Research Letters*, 79 (2), 290.

Hinzen, K.-G. (2009). Simulation of toppling columns in archaeoseismology. *Bulletin of the Seismological Society of America* 99 (5), 2855–2875.

Hurukawa, N. & Maung, P.M. (2011). Two seismic gaps on the Sagaing Fault, Myanmar, derived from relocation of historical earthquakes since 1918. – *Geophysical Research Letters* 38, L01310, 5 PP., doi:10.1029/2010GL046099

Kannika, P. & Takada, T. (2009). *Updating framework for site-specific attenuation relation of seismic ground motion in Thailand.* MSc thesis, Building Research Institute, Tsukuba, Japan, 70 p.

Kázmér, M., & Major, B. (2010). Distinguishing damages of two earthquakes – archeoseismology of a Crusader castle (Al-Marqab citadel, Syria). In: *Ancient Earthquakes*. (Stewart, I., Sintubin, M., Niemi, T., Altunel, E. eds). Geological Society of America Special Paper, 471, 186 –199.

Kázmér, M. & Sanittham, K. (2011). Archeoseismology of the A.D. 1545 earthquake in Chiang Mai, northern Thailand. In: *International Symposium on the 2001 Bhuj Earthquake and Advances in Earthquake Science*, AES 2011. 22-24 January 2011, Institute of Seismological Research, Raisan, Gandhinagar, India. Abstract Volume AES 2011, 117-118.

Korjenkov, A.M. & Mazor, E. (1999). Seismogenic origin of the ancient Avdat Ruins, Negev Desert, Israel. *Natural Hazards* 18, 193–226.

Korjenkov, A.M. c Mazor, E. (2003). Archaeoseismology in Mamshit (southern Israel): Cracking a millennia-old code of earthquakes preserved in ancient ruins: *Archäologischer Anzeiger*, 2003 (2), 51–82.

Kovach, R.L & Nur, A. (2006). Earthquakes and archeology: Neocatastrophism or science?: *Eos, Transactions, American Geophysical Union* 87 (32), 317.

Margane, A. & Tatong, T. (1999): Aspects of the hydrogeology of the Chiang Mai-Lamphun Basin, Thailand that are important for the groundwater management. – *Zeitschrift für angewandte Geologie* 45, 188-197.

Michetti, A.M., Esposito, E. et al. (2007). Environmental Seismic Intensity Scale 2007 – ESI 2007. In: Vittori, E:, Guerreri, L. eds. *Memorie Descrittive della Carta Geologica d'Italia.* LXXIV. Servizio Geologico d'Italia, Roma, 7–54.

Obermeier, S.F. (1996): Use of liquefaction-induced features for paleoseismic analysis. – *Engineering Geology* 44, 1-76.

Pailoplee, S., Takashima, I., Kosuwan, S. & Charusiri, P. (2009). Earthquake activities along the Lampang-Theon fault zone, northern Thailand: evidence from paleoseismological and seismicity data. – *Journal of Applied Science Research* 5 (2), 168-180.

Pailoplee, S., Sugiyama, Y. & Charusiri, P. (2010). Probabilistic seismic hazard analysis in Thailand and adjacent areas by using regional seismic source zones. – *Terestrial, Atmospheric and Ocean Sciences* 21, 757–766.

Penth, H. (2006). Earthquakes in Old Lan Na: part of natural catastrophes. *Chiang Mai University CMU Journal* 5 (2), 255-265.

Podjarawaraporn (2547). *Pra wad Wat Chedi Luang wor ra wi harn.* [History of Wat Chedi Luang.] Text by Pra Bhuda Podjanawaraporn (Chan Kusato), pictures by Pra Kro Soponkaweewat (Thanachan Suramanee). Published by Wat Chedi Luang, Chiang Mai, Thailand, 160 p. ISBN 974-92159-8-2 (In Thai)

Rapp, G., Jr. (1986). Assessing archaeological evidence for seismic catastrophes. *Geoarchaeology* 1, 365–379.

Reicherter, K., Michetti, A.M. & Silva Barroso P.G. (2009). Palaeoseismology: historical and prehistorical records of earthquake ground effects for seismic hazard assessment. *Geological Society, London, Special Publication* 316, 1-10.

Rhodes, B.P., Perez, R., Lamjuan, A. & S. Kosuwan, S. (2004). Kinematics and tectonic implications of the Mae Kuang Fault, northern Thailand. *Journal of Asian Earth Sciences* 24 (1): 79-89.

Rodríguez-Pascua M.A., R. Pérez-López, J.L. Giner-Robles, P.G. Silva, V.H. Garduño-Monroy and K. Reicherter (2011). A Comprehensive Classification of Earthquake Archaeological Effects (EAE) in Archaeoseismology: application to ancient remains of Roman and Mexican cultures. *Quaternary International.* DOI: 10.1016/j.quaint.2011.04.044.

ThinkNet (2010). *Map of 14 northern provinces of Thailand* + CD. Bilingual Mapping Software. ThinkNet Co., Ltd, Bangkok, Thailand. (In Thai and English)

OUTLINE OF THE 3.11 TOHOKU EARTHQUAKE IN JAPAN

Yoshihiro Kinugasa (1)

(1) Association for the Development of Earthquake Prediction, Tokyo, Japan. Email: king@8f.adep.or.jp

Abstract (Outline of the 3.11 Tohoku earthquake in Japan): *Author will discuss the following subjects on the 3.11 Tohoku Earthquake (Mw=9.0), based on the published data by the time of the Corinth2011 workshop.*

1. *Seismological Characteristics of the Earthquake; Location, Magnitudes, Focal Mechanism, Intensity Distribution, etc.*
2. *Tsunami*
3. *Ground Deformations*
4. *Re-activation of Normal Fault*
5. *Paleoseismology along the Tohoku Coast*
6. *Impacts on the Fukushima NPPs.*

Key words*: Tohoku Earthquake, Tsunami, Paleoseismology, Fukushima NPPs*

THE EVIDENCE OF TSUNAMIGENIC DEPOSITS IN THE GULF OF CORINTH (GREECE) WITH GEOPHYSICAL METHODS FOR SPATIAL DISTRIBUTION

Koster, Benjamin (1), Klaus Reicherter (1), Andreas Vött (2), Christoph Grützner (1)

(1) Neotectonics and Natural Hazards Group, RWTH Aachen University, Lochnerstr. 4 - 20, 52056 Aachen, Germany. Email: b.koster@nug.rwth-aachen.de
(2) Natural Hazard Research and Geoarchaeology, Institute for Geography, Johannes Gutenberg-Universität Mainz, Johann-Joachim-Becher-Weg 21, 55099 Mainz, Germany

The evidence of tsunamigenic deposits in the Gulf of Corinth (Greece) with geophysical methods for spatial distribution: *Drill core sampling in coastal areas in the Mediterranean proved evidence for tsunamis. Sedimentary analyses were conducted to identify tsunamigenic deposits, but did not reveal larger scale sedimentary structures or spatial distribution of tsunamites in a regional scale. We used ground penetrating radar (GPR) in combination with electrical resistivity tomography (ERT) measurements and sedimentological research methods in different areas. The combination of these three methods allows us to generate 3D visualizations, which give clues for tsunamite distribution and sediment architecture. GPR data indicate unconformable thicknesses of tsunamigenic layers, channel-like structures of backwash deposits, in some extent non-planar erosion basement, as well as abrasion-scours in various places, and boulder accumulation inside the deposits.*

Key words*: tsunami, GPR, ERT, Greece*

INTRODUCTION

Former studies of various authors on tsunamis mainly focused on a hydromechanical analysis of specific tsunami events (e.g., Bondevik et al., 2005) or sedimentary analyses of drill cores (e.g., Reicherter et al., 2010; Shiki et al., 2008; Vött et al., 2009). The latter method encompasses sieve curves as well as magnetic susceptibility measurements and micropaleontology to prove tsunamigenic features. Characteristics of the sediments, such as fining-upward sequences, coarse shell debris, upward rising magnetic susceptibility and marine foraminifera in sandy sediments, give amongst others evidence for tsunami events. X-ray fluorescence spectroscopy measurements (XRF) were performed in some cases. OSL and ^{14}C-dating can be used for dating.

All of these studies defined characteristics of the deposits (e.g., Bryant et al., 2005; Shiki et al., 2008), but do not show the spatial distribution of an event or the larger scale sediment structures of tsunami deposits. With the knowledge of spatial distribution and extent of erosion due to tsunamis it would be easier to understand processes during a tsunami event and to estimate the possible damage by a future tsunami. Since drilling is time-intensive and expensive (depending on extend), this method can by far not cover an entire coastal area. As the distribution and preservation of tsunamigenic deposits is highly variable according to several studies (e.g., Dawson & Stewart, 2007), there is a strong interest in a low-cost and easy to use imaging technique.

Only one published study dealt with GPR for detecting tsunami deposits. Switzer et al. (2006) investigated a wash-over fan, but did not validate the data by other geophysical methods. Therefore, it is still not clear whether or not the detected sediments were deposited by a tsunami. Furthermore, a limiting factor of GPR measurements is a wet environment. A shallow ground water table or even sea water intrusions close to the ocean can reduce data quality significantly. Relative dielectric permittivity ε_r and the conductivity σ of tsunamigenic deposits are unknown. However, we can show that GPR has the ability to distinguish between tsunami deposits made up of marine sands, boulders and shells and clayey background sediments although this is an ambitious challenge.

STUDY AREA

Our study area is located near Lechaion, one of the ancient harbors of Corinth (Fig. 1). It was probably the most important harbor of this type in antiquity, and one of the most important harbors in Greece for more than one millennium (Rothaus, 1995). Today it is partially buried by up to 2 meters of sediment.

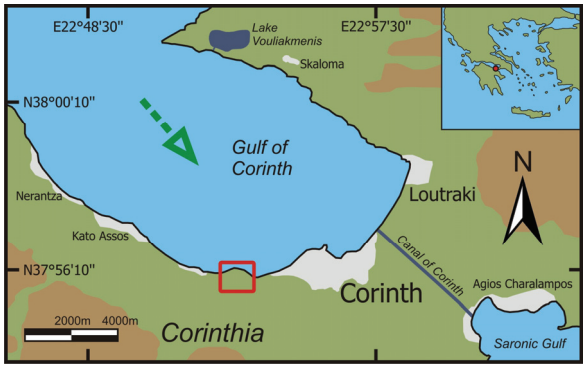

Fig. 1: Study area in Greece, Lechaion close to Corinth, brown areas illustrate topographic elevation; red box indicates area of GPR measurements (see Fig. 2 for details); green arrow displays possible tsunami propagation

Lechaion may very well have been affected by a series of seismic events and possible tsunami in late fourth century after Christ. Reconstruction of the

harbor in AD 353 - 358 (Stiros et al., 1996) contingently supports this idea.

We collect GPR data in combination with drill cores and electrical resistivity tomography (ERT) in order to test our method in an extraordinary environment, an ancient harbor which could have been affected by a tsunami (Soloviev, 1990).

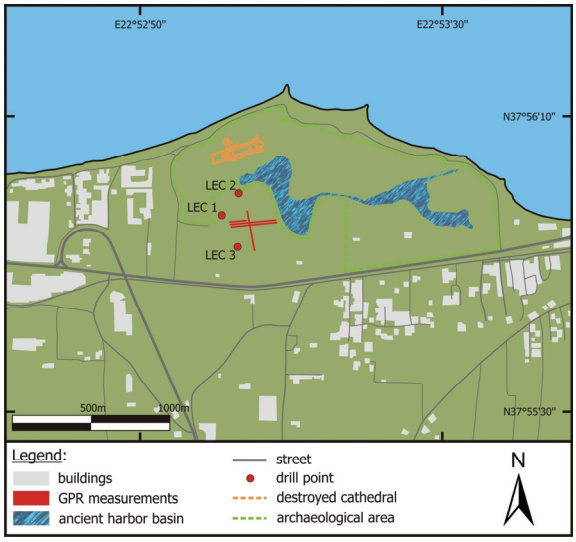

Fig. 2: Map of the study area with locations of drill points and GPR measurements

METHODS

GPR measurements were performed in patterns directly adjacent to drilling locations and ERT profiles. We used the GSSI 400 MHz antenna with a survey wheel, the SIR-3000 unit, and a handheld GPS (Fig. 3).

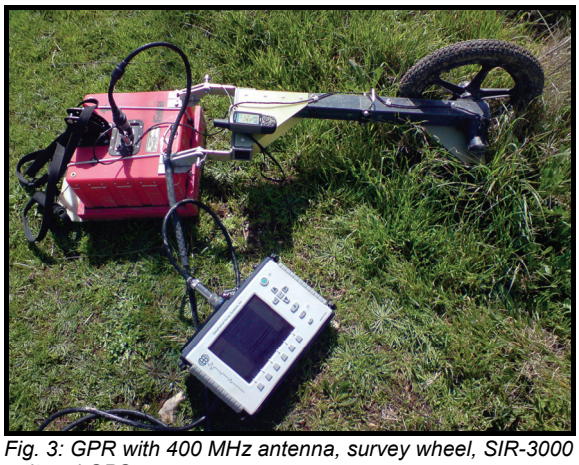

Fig. 3: GPR with 400 MHz antenna, survey wheel, SIR-3000 unit and GPS

Trace increment was set to 0.02 m for detailed investigation, the range was set to 120 ns TWT and the sample rate to 512. From drillings and field observations a target depths up to 3.50 m could be assumed. The thickness of the assumed tsunami sediment layer reaches up to 2.00 m, so the 400 MHz antenna promised the best compromise. Data processing included static correction, background removal, gain adjustment and velocity adaption for depth calculations based on a hyperbola analysis. Boulders were detected due to hyperbolic features in the data. Results of sedimentary drill cores (Fig. 4) and ERT profiles in the study area give evidence for three tsunami events (Hadler et al., this volume).

VISUALIZATION & RESULTS

Three GPR profiles were taken parallel to the coast, one profile was recorded perpendicular to the shoreline (Fig. 2). Three drill cores (Fig. 4) were taken between 50 and 150 meters away from GPR profiles in the ancient inner harbor. All GPR measurements took place on the top of the ancient harbor facility, which is buried under a possible third tsunami event layer. The base and inner structures of the possible tsunami deposits could be imaged in all the profiles.

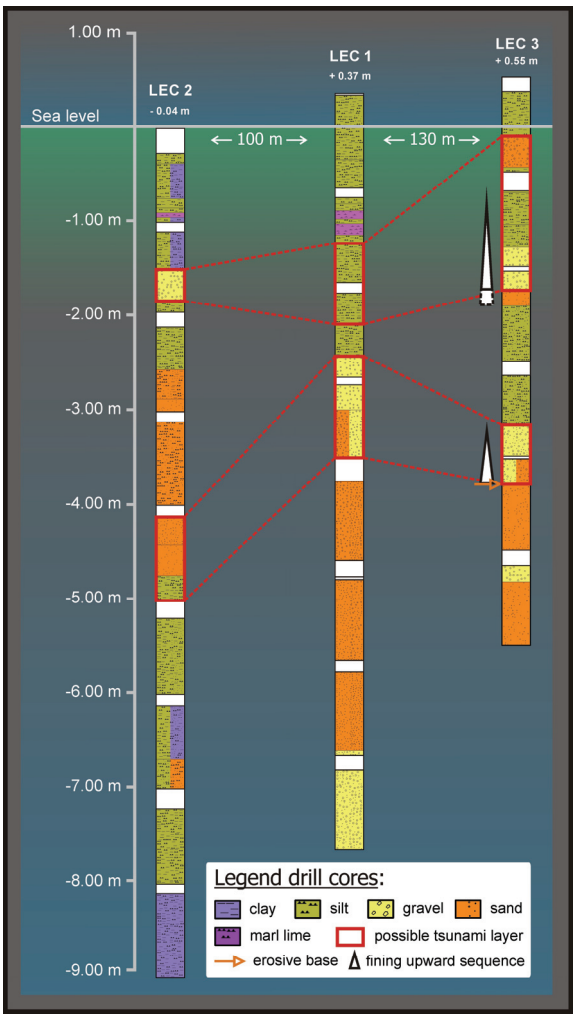

Fig. 4: Correlation of drill cores in the study area of Lechaion; two possible tsunami layers were detected (red boxes with red dashed lines for correlation); these layers include fining-upward sequences as well as erosive bases

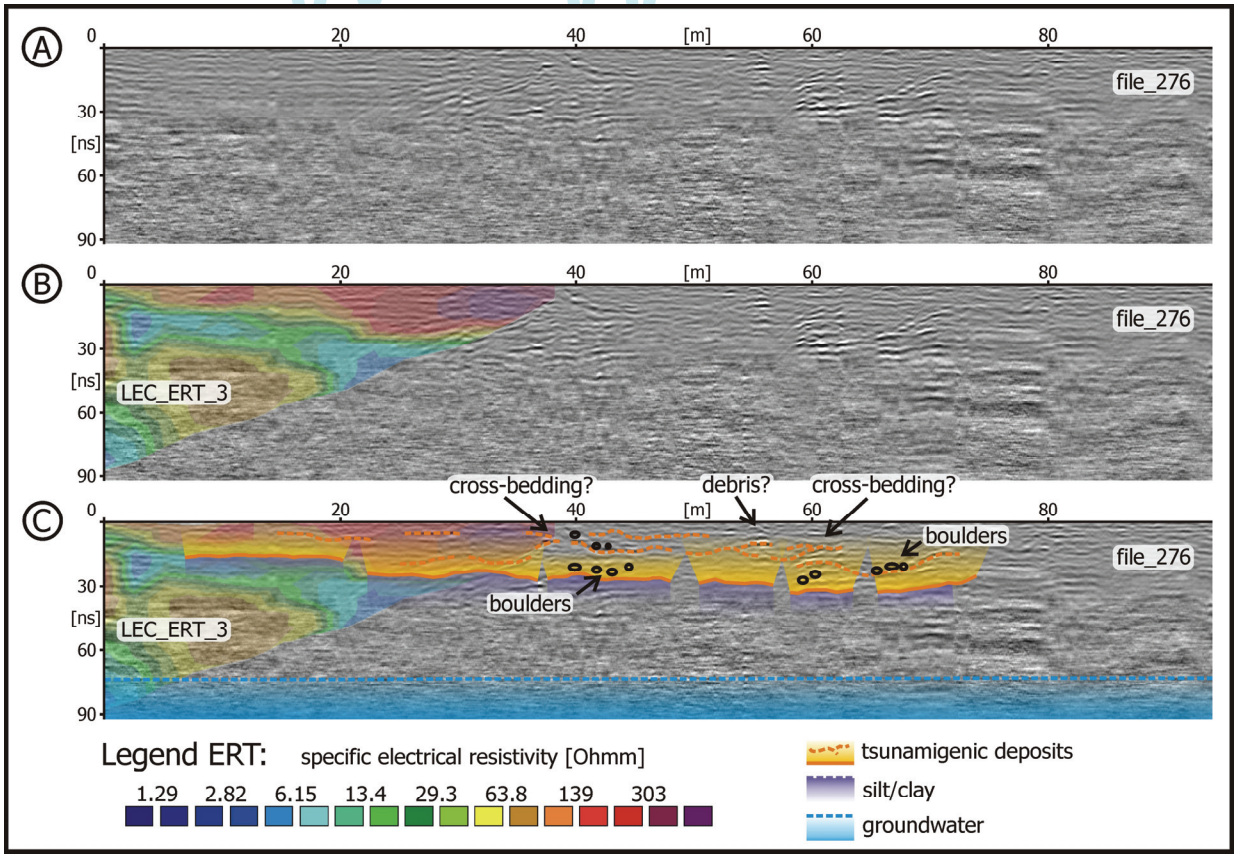

Fig. 5: GPR profile 276 taken parallel to the coastline at the ancient harbor Lechaion (Greece) in combination with ERT profile LEC_ERT_3: A) processed GPR data, B) processed GPR and ERT data; C) processed and combined analyzed data; yellow colored areas show tsunamigenic deposits; the base is illustrated by orange line; dashed orange lines refers to inner structures

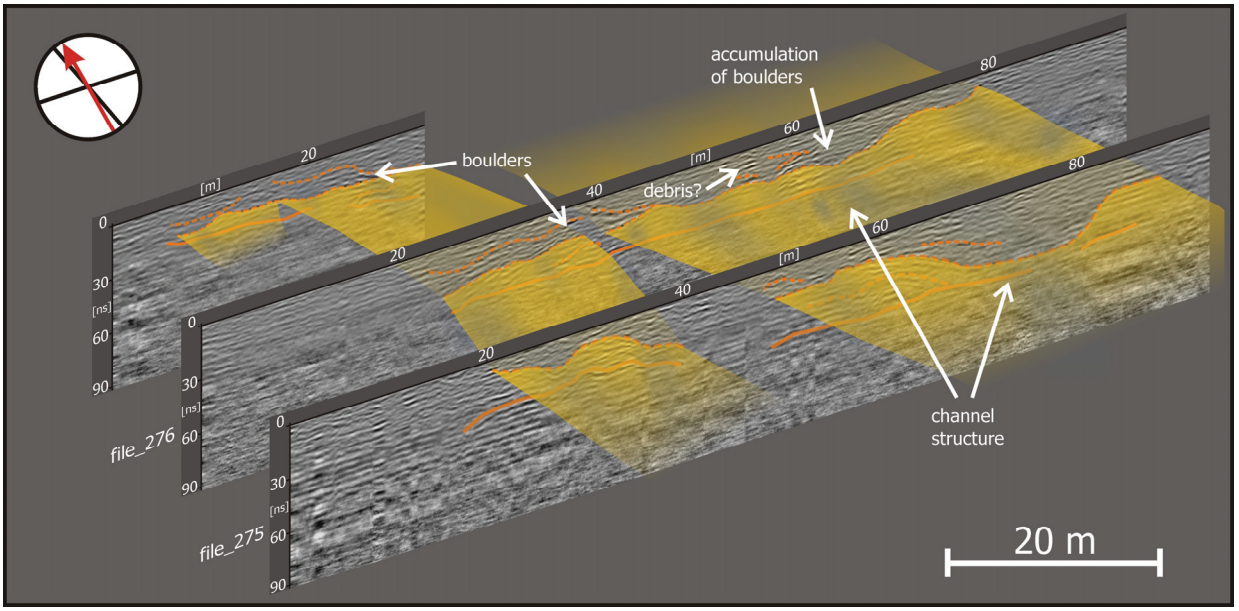

Fig. 6: GPR profiles 275, 276 & 277 taken parallel to the coastline at the ancient harbor Lechaion (Greece); direction of profiles is plotted in the circle on top left (red arrow is north; both black linings show x- and y-direction of ground surface); the yellow plain is a visualized inner structure of the possible upper tsunamigenic deposit; orange lines on the GPR data underline the reflected boundaries of layers or inner structures (dashed orange line); big channel structures within the possible tsunamite are clearly visible with accumulation of boulders in depressions; as well some smaller channels could be construed as abrasion-scours

The combination of ERT and GPR measurements in the study area suggests that there are bigger channel structures with erosive bases and boulder deposits inside these channels (Fig. 5 & 6). They point toward the ocean and are not part of the buried harbor. The channels can be part of a flow-system during the backwash processes after a tsunami (Dawson & Stewart, 2007). In some cases, channel-

like structures could also be interpreted as abrasion-scours, which can originate by backwash processes with high backflow velocities. Some kind of cross-bedding is visible in the GPR data as well (Fig. 5). The tsunamigenic deposits reaches depths up to 2.00 m. The sedimentary evidence from the drill cores could not be verified due to high attenuation in lower depths (>2.50 m). The inner layer-structures of the tsunamites (maybe due to multiple waves) show an unconformable thickness (Fig. 5). Boulders in the sediments appear as hyperbolas (v = 0.12 m/ns). Boulders with diameters larger than the resolution limit of the 400 MHz GPR antenna are located inside the deposits and could be detected by GPR. ERT profiles show as well electrical resistivity contrasts at the boundary between the tsunamigenic deposits and underlying harbor sediments. For the other GPR profiles the correlation with ERT data has been done similarly, if ERT profiles were available.

CONCLUSIONS

Due to highly variable sedimentation processes and materials (gravels, sand or silt/clay to some extend with boulders) in the Mediterranean and worldwide in the context of a tsunami event, deposited sediments differ extremely. Therefore, no specific values for relative dielectric permittivity ε_r or the conductivity σ can be declared for these variable sediments. Drill cores or outcrops are always necessary to prove tsunami characteristics and to correlate these results with the GPR data. Distinctive contrast changes in the GPR data help proving the spatial distribution of tsunami deposition interfaces. Only the combination of the presented methods is the key for conclusions on detailed spatial distribution of tsunamites.

The main result is the visualization of channelized structures in the tsunamigenic horizon. The structures most likely originate from backwash processes. Our data lead us to conclude that the topography of an effected area plays an important role for the expansion of the channels, since we observed different channel types as well e. g., in Spain. It is possible to detect the upper and lower boundary of the tsunamite in some cases, depending on the grain size of the tsunamigenic material in contrast to the background sedimentation.

With the 400 MHz GPR antenna it is also possible to detect bigger structures like abrasion-scours, unconformable thicknesses of tsunamigenic beddings, in some extent non-planar erosion basement and boulder accumulations inside the deposits. Typical thinning-inland structures (Dawson, 1994) could not be detected in this case within the GPR profile perpendicular to the coast. A GPR with higher resolution should be useful to detect further sedimentary structures in tsunamigenic deposits in the future.

OUTLOOK

In the future, GPR and other shallow geophysical methods will be used to detect run-up distances and for creating large-scale models considering topography to detect sediment thickness and volume. With these data it would be possible to calculate the physical power and the possible damage of the tsunami wave and typical sediment structures. Due to account on spatial distribution information it could be possible the reconstruct the topography of the landscape before and after a paleo-tsunami.

Another aim is to get detailed information of the deposits by trenching and using methods like LiDAR, multispectrometry, magnetic susceptibility and the documentation commonly used in archeological excavations.3-dimensional data or block-plots can be generated based on these methods to evaluate new features and characteristics of tsunamigenic deposits.

References

Bondevik, S., F. Løvholt, C. Harbitz, J. Mangerud, A. Dawson & J.I. Svendsen, (2005). The Storegga Slide tsunami – comparing field observations with numerical simulations. *Marine and Petroleum Geology* 22, 195-208.

Bryant E., R.L. Wiegel, F.P. Shepard & D. Myles, (2005). *Natural hazards*. Cambridge University Press, 2nd edition, 214-225.

Dawson, A.G. & I. Stewart, (2007). Tsunami deposits in the geological record. *Sedimentary Geology* (200), 166-183.

Dawson, A. G. (1994). Geomorphological effects of tsunami run-up and backwash. *Geomorphology* 10, 83-94.

Hadler, H., A. Vött, B. Koster, M. Mathes-Schmidt, T. Mattern, K. Ntageretzis, K. Reicherter, D. Sakellariou, T. Willershäuser, (2011). Lechaion, the ancient harbour of Corinth (Peloponnese, Greece) destroyed by tsunamigenic impact. 2nd INQUA-IGCP-567 International Workshop on Active Tectonics, Earthquake Geology, Archaeology and Engineering, Corinth, Greece. This volume.

Reicherter, K., D. Vonberg, B. Koster, T. Fernández-Steeger, C. Grützner & M. Mathes-Schmidt, (2010). The sedimentary inventory of the 1755 Lisbon tsunami along the southern Gulf of Cádiz (southwestern Spain). *Zeitschrift für Geomorphologie N.F., Suppl. Issue* 54 (3), 147-173.

Rothaus, R., (1995). Lechaion, western port of Corinth: a preliminary archaeology and history. *Oxford Journal of Archaeology* 14 (3), 293-306.

Shiki, T., T. Tachibana, O. Fujiwara, K. Goto, F. Nanayama & T. Yamazaki, (2008). Characteristic features of tsunamiites. In: *Tsunamiites – Features and Implications* (T. Shiki, Y. Tsuji, T. Yamakazi & K. Minoura eds). Elsevier Scientific Publishing Company, 319-336.

Soloviev, S.L., (1990). Tsunamigenic Zones in the Mediterranean Sea. *Natural Hazards* (3), 183-202.

Stiros, S., P. Pirazzoli, R. Rothaus, S. Papageorgiou, J. Laborel & M. Arnold, (1996). On the Date of Construction of Lechaion, Western Harbor of Ancient Corinth, Greece. *Geoarchaeology* 11 (3), 251-263.

Switzer A.D., C.S. Bristow & B.G. Jones, (2006). Investigation of large-scale washover of a small barrier system on the southeast Australian coast using ground penetrating radar. *Sedimentary Geology* 183, 145-156.

Vött, A., H. Brückner, S.M. May, D. Sakellariou, O. Nelle, F. Lang, V. Kapsimalis, S. Jahns, R. Herd, M. Handl & I. Fountoulis, (2009). The Lake Voulkaria (Akarnania, NW Greece) palaeoenvironmental archive - a sediment trap for multiple tsunami impact since the mid-Holocene. *Zeitschrift für Geomorphologie N.F., Suppl. Issue* 53 (1), 1-3.

EARTHQUAKE ARCHAEOLOGY

INQUA PALEOSEISMOLOGY AND ACTIVE TECTONICS

COSEISMIC SURFACE RUPTURING IN THE EPICENTRAL AREA OF GERMANY'S STRONGEST HISTORICAL EARTHQUAKE

S. Kübler(1), A. M. Friedrich(1), M. R. Strecker(2)

(1) Ludwig-Maximilians-University Munich, Department of Earth and Environmental Sciences, Luisenstr. 37, 80333 Munich, Germany, Email: kuebler@iaag.geo.uni-muenchen.de
(2) University of Potsdam, Institute of Geosciences, Karl-Liebknecht-Str. 24, 14476 Potsdam, Germany

Abstract (Coseismic surface rupturing in the epicentral area of Germany's strongest historical earthquake): *The Lower Rhine Embayment is one of the most seismically active regions in intraplate Europe. A trenching investigation carried out south of the city of Düren near the estimated epicenter of Germany's largest historical event (1756 AD, M_L 6.2 ± 0.2) revealed evidence of significant coseismic deformation of the earth's surface. Deformation is expressed by co-planar sets of fractured and rotated pebbles as well as liquefaction of fine-sand deposits. Two event horizons indicate an older rupturing event that occurred presumably in the Early to Mid Holocene and a younger rupturing event that occurred in the Latest Holocene, and may correspond to the 1756 Düren earthquake.*

Key words*: paleoseismology, historical earthquake, coseismic rupture, Germany*

DISCUSSION

Based on historical documents and instrumental data the Lower Rhine Embayment is currently one of the most seismically active regions in intraplate Europe. At least 21 M > 5 instrumental and historical earthquake events have been recorded and documented, respectively, for western Germany, eastern Belgium and southern Netherlands (Leydecker, 2002). One of the largest of these events was the earthquake of February 18th 1756 near the city of Düren at the western border of the LRE. Damage related to this event included triggered landslides and destroyed buildings and castles, but the occurrence of surface ruptures has not been reported for this or any other historic event in this region.

The LRE is characterized by NW-SE striking normal faults. Fault plane solutions indicate an extensional normal faulting regime (Hinzen, 2003). Several paleoseismic studies in the LRE indicate that strong, surface-rupturing events may have repeatedly occurred in this region since the Late Pleistocene (e.g., Camelbeeck & Meghraoui, 1998; Vanneste et al., 2001; Vanneste & Verbeeck, 2001), but there has been (Ahorner, 1996) and continues to be (Houtgast et al., 2003, 2005) controversy about whether faults in the LRE mainly move by creep, or whether earthquakes that are large enough to break the surface commonly occur in this region. The 1756 Düren earthquake had a local magnitude of 6.2 ± 0.2 based on empirical studies (Meidow, 1994), the total moment for this event was estimated at 1.6 x 10^{17} Nm (M_W 6.1; Hinzen & Reamer, 2007). Events of this magnitude are commonly associated with surface ruptures, but there is still great uncertainty in the reliability of historic documents for estimating the correct magnitude of historic events. Therefore, the identification of a surface rupture related to the Düren event would be important to better understand the mechanical behaviour of faulting in this tectonically active region.

In contrast to paleoseismic and geomorphic studies in arid regions, where fault scarps are exposed for many kilometers along strike and their preservation potential is excellent, the recognition and characterization of potentially active faults is much more difficult in the moderately humid Lower Rhine area. The dense vegetation cover and intense agricultural landuse hamper the recognition of seismogenic surface ruptures in the densely populated region. Low displacement rates on individual faults, and hence a sparse earthquake record due to long recurrence intervals of large seismic events, additionally aggravate seismic hazard evaluation. Thus, multidisciplinary paleoseismic studies are important to identify seismically active fault segments in the LRE.

In order to search for a potential surface rupture related to the 1756 Düren event, we carried out multidisciplinary reconnaissance studies including geomorphic mapping, shallow drilling and shallow geophysical prospecting in the vicinity of Düren, wherever we could find late Holocene fluvial deposits covering the projection of potentially active faults. At one location, we identified two gentle 0.5 and 0.6 m high surface scarp in late Holocene deposits in prolongation of the E-dipping, 16-km long Schafberg fault. The trends of the two scarps differ: the south-

western step strikes 125° and is slightly curved, whereas the north-eastern step is perfectly straight and strikes 155°. The study site is situated a few kilometres W of Untermaubach, where the Schafberg fault crosses the Rur river valley. Geophysical prospecting identified two anomalous zones characterized by resistivity minima, high near-surface conductivity, and offset radar reflectors that coincide with the two 0.5 and 0.6 m high surface scarps (Streich, 2003).

We excavated the fault along an up to 5 m deep and 85 m long trench approximately 200 m west of the current Rur river course. At the trench site, the Schafberg fault is covered by < 5 m thick, scarcely to moderately well layered Holocene sandy gravel deposits and fine-grained flood deposits overlaying Lower Devonian shale and sandstone. The trench exposes two asymmetric channels that coincide with the position of the observed surface scarps. The channel fill consists of sandy silt and clay-rich layers. At the base of both channels, we detected a high concentration of organic material including trees and branches. We mapped various types of soft-sediment deformation in the gravel deposits including tilted and rotated clasts as well as fractured clasts that show offsets on a millimeter to centimeter scale. We further detected liquefaction features in sand and silt deposits.

Our mapping revealed a narrow zone of localized deformation below the north-eastern scarp expressed by abundant fractures with aligned and broken clasts extending vertically throughout the entire gravel unit. We carried out detailed gravel analysis including mapping of 237 fractured clasts and the long-axis orientation of ~ 10.000 clasts. Results define a ~ 10 m wide fault zone that coincides with the surface offset and an almost 40 m wide deformation zone where gravel deformation is still prominent. In contrast, gravel below the south-western scarp exhibits no indicators of coseismic deformation and is therefore most likely a fluvial channel. Liquefaction occurs 20 m east and 50 m west of the suspected rupture zone. As the overlaying flood deposits do not show signs for seismogenic deformation, the contact between the gravel and overlaying silt and clay appears to mark the most recent event horizon. An older event horizon – a paleosoil with high amounts of organic material – is preserved at a depth of 2.5 m within the gravel deposits. Here, underlying gravel deposits show clear deformation features while gravel above this marker horizon is undisturbed. The maximum vertical displacement across the fault appears to range between 0.8 and 1.2 m based on two offset marker horizons. This is in accordance with estimates derived from borehole data, geophysical prospecting and morphometric analysis.

We interpret the observed deformation features, especially the co-planar sets of rotated and fractured clasts, as the result of coseismic deformation at the near-surface end of the rupture, and we rule out slow deformation due to aseismic creep as governing process to cause rupturing of pebbles this close to the surface. Preliminary radiocarbon data bracket the younger event horizon to Latest Holocene age, which rules out periglacial processes as cause for the observed sediment deformation. Age results also imply that this fault may be a possible source for the 1756 earthquake. Further analyses are in progress.
We identified coseismic deformation at the trench site, because special conditions produced a number of features not normally observed in other fault exposures. The thin sedimentary cover (< 5 m) above basement rocks and the high water table may have played an important role in producing this unusual deformation pattern. However, this newly investigated trench site yields the first evidence for Late Holocene seismogenic surface rupturing in the German part of the LRE, and thus confirms the importance of paleoseismic studies for seismic hazard analysis in humid low-strain intraplate regions.

Acknowledgements: Trench excavation and geological field work was financed by the DFG, research grant awarded to Friedrich and Strecker (AF 6513).

References

Ahorner, L., 1996, How reliable are speculations about large paleo-earthquakes at the western border fault of the Roer Valley Graben near Bree, In: *Bonatz, M., ed., Comptes-Rendus des 81ièmes Journées Luxembourgeoises de Géodynamique*, Walferdange, Grand Duchy of Luxemburg, p. 39-57.

Camelbeeck, T. and M. Meghraoui (1998). Geological and geophysical evidence for large paleoearthquakes with surface faulting in the Roer Graben (northwest Europe). *Geophys. J. Int.*, 132, 347 - 362.

Hinzen, K. G. (2003). Stress field in the Northern Rhine area, Central Europe, from earthquake fault plane solutions, Tectonophysics, 377, 325 - 356.

Hinzen, K. G., and S. K. Reamer (2007). Seismicity, seismotectonics, and seismic hazard in the Northern Rhine Area, In: *Intraplate Seismicity* (Stein, S. and Mazzotti, S. eds). GSA Books, 225-243.

Houtgast, R.F., R. T. van Balen, K. Kasse, and J. Vandenberghe (2003). Late Quaternary tectonic evolution and postseismic near surface fault displacements along the Geleen fault (Feldbiss fault zone-Roer valley rift system, the Netherlands), based on trenching, *Geologie en Mijnbouw*, 82(2), 177-196.

Houtgast, R.F., R. T. van Balen, and C. Kasse (2005). Late Quaternary evolution of the Feldbiss fault (Roer valley rift system, the Netherlands) based on trenching, and its potential relation to glacial unloading, *Quaternary Science Reviews*, 24(3-4), 489-508.

Leydecker, G. (2002). Earthquake Catalogue for the Federal Republic of Germany and Adjacent Areas for the Years 800 - 2001. *Datafile*, Federal Institute for Geosciences and Natural Resources, Hannover, Germany.

Meidow, H. (1994). Comparison of the macroseismic field of the 1992 Roermond earthquake, the Netherlands, with those of large historical earthquakes in the Lower Rhine Embayment and its vicinity, *Geologie en Mijnbouw*, 73(2-4), 282-289.

Streich, R (2003). Geophysical prospecting of suspected Holocene fault activity in the Lower Rhine Embayment, Germany, *MSc Thesis.* University of Potsdam, Germany.

Vanneste, K. and Verbeeck, K. (2001). Paleoseismological analysis of the Rurrand fault near Jülich, Roer Valley graben, Germany: coseismic or aseismic faulting history? *Geologie enMijnbouw*, 80, 155-169.

Vanneste, K., Verbeeck, K., Camelbeeck, T., Paulissen, E., Meghraoui, M., Renardy, F., Jongmans, D. and Frechen, M. (2001). Surface-rupturing history of the Bree fault scarp, Roer Valley graben: evidence for six events since late Pleistocene. *Jour. Seism.*, 5, 329-359.

SEISMOTECTONIC AND SEISMIC HAZARD MAPS OF LITHUANIA (BALTIC REGION) – RECENT IMPLICATIONS OF INTRACRATONIC SEISMICITY

Lazauskiene, Jurga (1) and Pacesa, Andrius (2)

(1) Lithuanian Geological Survey under the Ministry of Environment. S. Konarskio 35; Vilnius University, M.K. Čiurlionio 21/27, LT-03123 Vilnius, Lithuania. Email: jurga.lazauskiene@lgt.lt,
(2) Lithuanian Geological Survey under the Ministry of Environment. S. Konarskio 35, LT-03123 Vilnius, Lithuania. Institute of Geology and Geography, T.Ševčenkos, 13, LT-03123 Vilnius, Lithuania. Email: andrius.pacesa@lgt.lt,

Abstract (Seismotectonic and seismic hazard maps of Lithuania (Baltic region) – recent implications of intracratonic seismicity): *Lithuania, situated in the western part of the East European Craton, is regarded as an intracratonic area of low seismicity. Several dozens of earthquakes of intensity up to VII (MSK-64) were recorded since 1616 implying the possible occurrence of stronger earthquakes. The northern part of in the Baltic region is seismically more active than the southern, but the Kaliningrad earthquakes of 2004 showed the necessity to re-assess the seismicity of the region. The identification of seismogenic faults in the Baltic region is rather complicated due to the small scale of tectonic structures and significant errors of location of seismic events and even faults. Still, recently the seismic hazard and seismotectonic maps of Lithuania were compiled implying the highest seismic hazard of 32,6 cm/s^2 PGA in eastern and 25-30 cm/s^2 in northern Lithuania. The majority of the territory is described by PGAs of 10-20 cm/s^2.*

Key words*: intracratonic seismicity, Baltic region, seismic hazard, seismotectonic framework,*

INTRODUCTION

The territory of Lithuania comprises a part of the Baltic sedimentary basin situated in the western part of the East European Craton that is characterised by low seismic activity - the historical sources since 1616 to 1964 record only a few tens of weak or moderate earthquakes (Pačėsa et al., 2005). The historical seismic activity in the eastern Baltic region is significantly lower comparing with seismicity of the Fennoscandian shield. High seismic activity of the Fennoscandian shield and adjacent Baltic Sea territories during the Late Glacial and Holocene (last 13 000 years) is also well documented by numerous paleoseismic investigations and corresponding publications. The earthquakes caused landslides in glacial till, seismically-induced soft sediment deformation structures, “seismites”, are common in trench exposures in the vicinity of the faults in northern Sweden and even with tsunami events reported in the Baltic Sea (Mörner, 2005, 2008).

Still, the eastern Baltic region is more seismically active comparing with the more “inland” aseismic territories of the craton. Several tens (~ 40) of earthquakes of intensities of VI-VII (MSK-64 scale) and local magnitudes up to M_L = 5 are recorded in the Baltic region and neighbouring since 1616 (*fig. 1*) The strongest instrumentally registered earthquakes are Ossmussare (Estonia) earthquake of 1976 (with maximal magnitude up to M_L = 4,75) and the Kaliningrad (Russia) earthquakes of 2004 of magnitudes, respectively, M_L = 4.75 and M_L = 5.0 (M_w = 5.2, *table 1*). The other more significant earthquakes in the region are:

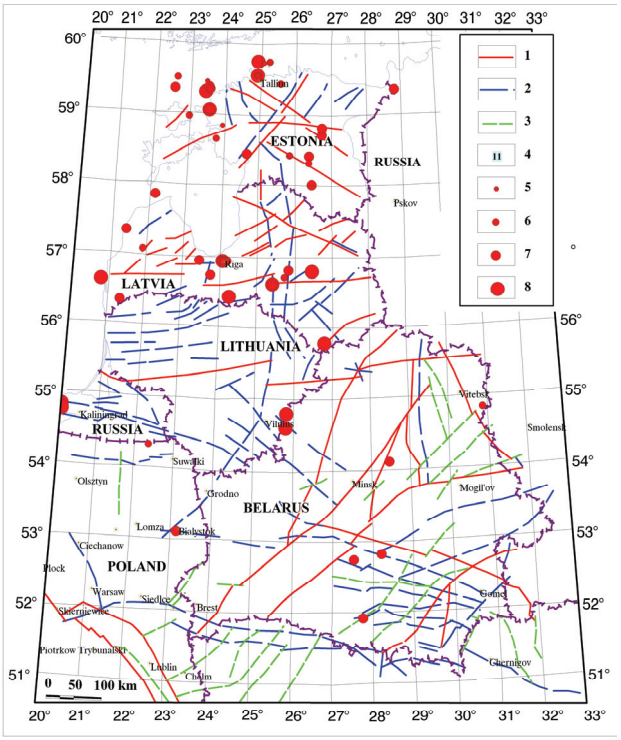

Fig. 1: Main tectonic faults and seismic events in the Baltic region (after Sharov (ed.) et al., 2007; Pačėsa et al., 2005). 1–3 faults: 1 – superregional, 2 – regional, 3 – subregional; 5–8 – epicentres of earthquakes with local magnitudes: 5 – M_L = 1-2, 6 – M_L = 2-3, 7 –M_L = 3-4, 8 – M_L = 4-5.

February 22, 1821, Kokneses (Estonia), M_L = 4.5; December 28, 1908, Gudogai (Belarus), M_L = 4.5;

December 29, 1908, Madona (Latvia); M_L = 4.5 (Boborikin et al., 1993). All the mentioned earthquakes within the same Baltic sedimentary basin in the same tectonic setting show the recent seismic activity of the Baltic region.

INTRACRATONIC SEISMICITY OF THE BALTIC REGION

The seismic activity in the Baltic region has an irregular distribution - the northern part of the region is more seismically active than the southern one (*fig. 1*). The maximum activity is recorded in Latvia that is characterized by most intense faulting of the sediment layers. Seismic activity is slightly lower in Estonia, while the territory of Lithuania seems to be the most quite. The boundary between two areas of different seismicity approximately coincides with the northern state border of Lithuania. A quite similar boundary between northern and southern parts of the region was established in previous global seismic hazard assessment studies e.g. WSHAP (Giardini, 1999) and European–Mediterranean Seismic Hazard Map (Jimenez et al., 2003).

No earthquakes are registered instrumentally or reliably recorded historically in the territory of Lithuania. Peter of Duisburg, a 14th Century chronicler of the Teutonian Knights (Chronicon Terrae Prussiae) reported “a ground shaking which was felt in Skirsnemune castle” (south-western part of Lithuania) in 1328; after the event the castle was abandoned. However, this historical record causes some doubts and is considered controversially:

A. Nikonov (personal communication) includes this seismic event of 1328 (and one of 1303 in Prussia; (Chronicon Terrae Prussiae)) into revised seismological catalogue of the South-East Baltic region, while Grunthal and Riedel (2007) strongly deny the existence of these events. Thus, this event was not included to the complete catalogue of seismic events of Eastern Baltic Region. There are also three records about the ground shaking during the years 1908-1909 in western and central part of Lithuania, but the primary sources rises some doubts and could not be considered as reliable. The first local seismic event with magnitude of M = 2.1 presumably of tectonic origin was instrumentally registered 4-th of September, 2001 by one of short period seismic station, located in the NE part of Lithuania. The seismic signal of this seismic event was the typical one for tectonic events (Pačėsa et al., 2002). Still, as it was registered only in one station, no accurate location of this event was possible and the epicentre of the earthquake could have been located in a distance of ~80 km from the station. The passive seismic experiment PASSEQ was carried out in the eastern part of Europe, including territory of Lithuania in 2006–2007. The preliminary data received from the project indicated some possibility of tectonic seismic event in the middle Lithuania 4-th July, 2007 (*coordinates - 55,053; 24,264*) and one more event in Kaliningrad offshore of the Baltic Sea, 14-th June, 2007 (*coordinates - 54,796; 19,232*) (Kozlovskaya et al., 2010). The coordinates of the epicentre of the onshore Lithuania event were identified near Kaunas town, located within the Middle Lithuanian Suture zone (the zone between two different Precambrian domains) with possibly increased tectonic activity. Both onshore and the Baltic Sea offshore events have occurred at the night-time. The seismic signals have the characteristics of tectonic events, but the quality of data is too poor to define magnitudes and depths of epicentres of these seismic events and, respectively, too poor for the reliable conclusions. Also, it must be noted, that the network of local seismic stations in the eastern Baltic region, especially Lithuania, is rather sparse and the instrumental seismological information is quite poor.

No doubts, the seismic events in Kaliningrad area showed the necessity to review the understanding of the seismicity of the Baltic region - earlier it was considered that the maximum magnitude of the earthquakes in this part of region might be M_L = 4.8; but the magnitude of the Kaliningrad earthquake was M_L = 5.0 (M_w = 5.2; *table 1*). Thus, taking into consideration the accepted margin of 0.5 (based on common agreement), the maximum magnitude could be assumed to be as high as M_w = 5.7 that implies the possibility of occurrence of some stronger earthquakes in the Baltic region.

Date	Time	Lat	Long	Magn	Depth
10/25/1976	8:39:00	59.2	23.58	4.7 M_L	15 - 18
9/21/2004	11:05:04	54.908	20.029	5.0 M_w	16 ± 9
9/21/2004	13:32:31	54.849	20.088	5.2 M_w	20 ± 10

Table 1. The strongest seismic events of Eastern Baltic region with magnitude M>4 (compiled by A. Pačėsa: the first one - Ossmussare (Estonia) earthquake, the other two – Kaliningrad (Russia) earthquakes. Magnitude types: M_L *– local magnitude,* M_w *– moment magnitude. Coordinates of epicentres are provided in geographical system of coordinates: Lat - latitude (North), Long – longitude (East); time – in GMT; Magn – magnitude; Depth - in km. After: Gregersen et al., 2007.*

The seismotectonic framework of the study areas has been outlined several times during the last decades (Sharov et al., 2007; Suveizdis, 2003). A number of faults and fault zones have been distinguished in the Baltic region and adjacent territories based on geological and geophysical data. Still, different authors provide quite different tectonic and seismotectonic maps of the eastern Baltic region and there is no single commonly accepted tectonic map of this region currently; location, orientation, length or the other parameters of the same fault might be interpreted differently. No doubts, summarizing different maps one can infer some dominating fault zones, directions and spacing (*fig. 1*).

DISCUSSIONS

As it was mentioned, majority of seismic events in the eastern Baltic region are historical ones. The primary sources of information do not provide any evaluations of errors of epicentre locations for historical events, but, most likely, the errors vary from ten to several

tens of kilometres. Even the epicentres for the two strongest Kaliningrad earthquakes were scattered in the area with a diameter of about 30 km (Pačėsa et al., 2005). It is very hard to associate single earthquakes with some certain faults unambiguously due to significant errors of location of seismic events and even location of faults. Additionally, the identification of the seismogenic faults in the region is rather complicated due to the small scale of tectonic structures located within an intracratonic area. It must also be pointed out that not all the earthquakes in the Baltic region are related to fault zones. Moreover, the majority of the previous global seismogenic and seismic hazard studies (Grünthal et al., 1999; Jimenez et al., 2003) that included also the territory of the Baltic region, strongly implied the local seismogenic sources with diffused seismicity. Thus, it was rather complicated to understand the geodynamic control on the seismicity of the relatively seismotectonically non-active cratonic area.

Accordingly, until recently, no any seismic hazard map has been compiled neither for the territory of Lithuania, nor for the wider Baltic region. Finally, in year 2011, on request of the Lithuanian Geological Survey, the seismic hazard and seismotectonic maps (Šliaupa, 2011) have been compiled for the territory of Lithuania. The complex analysis of the geological, geophysical, geodetic, structural, seismic and geodynamic data allowed to distinguish 5 active seismogenic zones and 5 potentially active seismogenic zones in the territory of Lithuania. The maximal seismic potential has been implied for the W-E trending Silute-Polock and Northern Prieglius–Birstonas fault zones (Northern Prieglius has „hosted" Kaliningrad earthquakes), transecting the central and southern part of Lithuania, with a maximum magnitude up to M = 5,5 of the possible earthquake predicted. It is implied that possible seismic activity of the faults is related to the regional stress field that affects the lithosphere of the Baltic region. No uniform stress pattern can be found for Baltic countries. Two stress provinces are suggested in Lithuania: NW-SE horizontal compression in the western part, whereas the main horizontal stress in the eastern part is NE-SW oriented. The western zone is attributed to the North Atlantic stress province, while the eastern is possibly a part of the Mediterranean stress province (Šliaupa, 2011; *fig. 2*). Therefore, as the seismic stresses are rather variable within the territory of Lithuania this might influence the character of the fault activation.

The newly compiled seismic hazard map of Lithuania (Šliaupa, 2011) shows that the highest seismic hazard with peak ground acceleration equal to 32,6 cm/s^2 (0,025 g) with 10% probability of exceedance within 50 years could be expected in the eastern part of Lithuania; also, the increased seismic hazard (peak ground acceleration being equal to 25-30 cm/s^2 (0,030 g) with 10% probability of exceedance within 50 years) also is estimated in the northern part of Lithuania. Therefore, the majority of the territory of Lithuania is described by rather law seismic hazard - peak ground acceleration values varies in a range of 10-20 cm/s^2 with 10% probability of exceedance within 50 years.

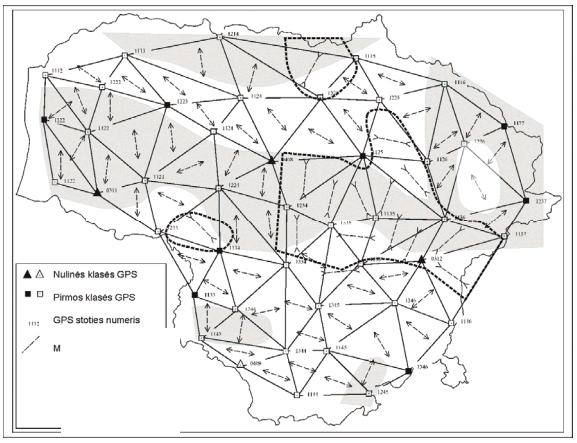

Fig. 2. Directions of maximum dilatation in the territory of Lithuania (Sliaupa, 2011). Grey areas roughly indicate N-S maximum dilatation, blank – NW-SE maximum dilatation; areas subjected to bi-axial compression are bounded by dotted countures.Triangules indicates GPS points of the zero class; squares – GPS points if the first class; numbers -the numbers of GPS stations; dotted lines – maximal dilatation.

The results of the new seismic hazard assessment show good coincidence with the results of previous global seismic hazard assessment - according to the results of Global Seismic Hazard Assessment Program (Grünthal et al., 1999) seismic level in the territory of Lithuania was estimated in the range of 10–30 cm/s^2 for the standard seismic level of civil engineering (10% probability of exceedance within 50 years or for a return period of 475 years) and according to the European map of seismic hazard (ESC-SESAME project, (Jimenez et al., 2003) the standard seismic level of civil engineering (return period of 475 years) was estimated as high as 20cm/s^2.

References

Boborikin, A..M., Avotinia, I.Y., Yemelianov, A. P., Sildvee, N. N., Suveizdis, P. (1993). Catalogue of historical earthquakes of Belarus and the Baltic Region. Seismological report of seismic stations of Minsk–Pleshchenitsi and Naroch for 1988. Minsk. 126–137.

Kozlovskaya, E., Budraitis, M., Janutyte, I., Motuza, G., Lazauskiene, J. and PASSEQ-Working Group, (2010). 3-D crustal velocity model for Lithuania and its application to local event studies. EGU General Assembly 2010, Vienna, Austria, 02-07 May, 2010, *Abstract and programme book*, Abstract No. EGU2010-10625.

Giardini, D. (Ed.). 1999. The Global Seismic Hazard Assessment Program 1992–1999. *Annali Geofis.* 42 (6) Special Issue.

Gregersen S., P. Wiejacz, W. Debski, B. Domanski, B. Assinovskaya, B. Gutterch, P. Mantiniemi, V.G. Nikulin, A. Pacesa, V. Puura, A.G. Aronov, T.I.Aronova, G. Grunthal, E.S. Husebye, S. Sliaupa. (2007). The exceptional earthquakes in Kaliningrad district, Russia on September 21, 2004. *Physics of the Earth and planetatry interiors 164*, 63-74.

Grünthal, G. and GSHAP Region 3 Working Group. (1999). Seismic Hazard Assessment for Central, North and Northwest Europe: GSHAP Region 3. *Annali di Geofisica* 42 (6), 999–1011.

Grünthal, G., Riedel, P. (2007). Zwei angebliche Erdbeben in den Jahren 1303 und 1328 im heutigen Raum Kaliningrad. *Zeitschrift für Geologische Wissenschaften*. Berlin, 35 (3). 157–163 (in Germany with English summary).

Jiménez, M. J., Giardini, D. and Grünthal, G. (2003). The ESC-SESAME Unified Hazard Model for the European–Mediterranean Region. *EMSC/CSEM Newsletter*. 19, 2–4.

Mörner, N.A. (2005). An interpretation and catalogue of Paleoseismicity in Sweden. *Tectonophysics* 408, 265-307.

Mörner, N.A. (2008). Tsunami events within Baltic. *Polish Geological Institute Special Papers*, 23. 71-76.

Pačėsa, A., Šliaupa, S., Satkūnas J. (2005). Recent earthquake activity in the Baltic region and seismological monitoring in Lithuania. *Geologija* 50, 8-18. (in Lithuanian).

Pačėsa, A., Narbuntas, J., Nemcovas, G. (2002). The annual bulletin of the seismological monitoring in Lithuania. 2001. Vilnius. 40 p. (internal report in Lithuanian with English summary).

Sharov N. V., Malovichko A. A., Schukin Ju. K. (eds.). (2007). Earthquakes and microseismicity of Eats European Platform – recent geodynamic approach. Book 1 Earthquakes. *Petrozavodsk: KarNC RAN*, 381 p. (in Russian).

Suveizdis (ed.). (2003). Tectonic structure of Lithuania. Institute of Geology and Geography, Vilnius. 160 p. (in Lithuanian).

Šliaupa, S. (2011). Assessment of the seismic observations in the territory of Lithuania. Book 2 - Seismic hazard map of Lithuania. 136 p. (internal report, in Lithuanian).

PRELIMINARY STUDY ON DAMAGED STONE MONUMENTS IN GYEONGJU, SE KOREA

Minjung Lee (1), Young-Seog Kim (1,)*

(1) GSGR, Dept. of Earth Environmental Sciences, Pukyong National University, Daeyeon3-dong, Busan 608-737, Korea.
*Email: ysk7909@pknu.ac.kr

Abstract (Preliminary study on damaged stone monuments in Gyeongju, SE Korea): *Concerns over the possibility of future earthquakes are high in Eastern Asia, since the catastrophic earthquake in north-eastern Japan on the 11th of March, 2011. The Korean peninsula is regarded as a relatively safe area from earthquakes because it is located within the Eurasian intracontinental region. According to historical records, the Gyeongju area was struck by many large earthquakes. Recently a long crack was discovered on the east facing exterior surface of Seokgatap, a famous pagoda in Gyeongju. The crack length is 132 cm and its width is 5 mm. During the investigation into the cause of the damage, we performed kinematic analysis of the cracks on the pagoda. We cannot find any consistency between the damage of the pagoda and earthquakes, recently cracks were found within the pagoda, which was most probably developed by a prolonged continuous force. Other probable earthquake damage can, however, be seen in other historical heritage sites within this city and its surrounding regions. Some of the damage at this and other sites are also recorded in historical references. Therefore, more careful studies are necessary to identify and distinguish the origins of the damage.*

Key words*: stone heritage, physical damage, Gyeongju, paleoseismology.*

INTRODUCTION

The Korean peninsula is located within the relatively safe Eurasian intracontinental region. In some neighbouring countries around Korea such as Japan and Taiwan, big earthquakes occur frequently. Over forty Quaternary faults were recently discovered along the Yangsan and Ulsan faults which are major tectonic features in SE Korea (Fig. 1). According to Korean historical records (e.g. Samguksagi, Mukseojipyeon), several relatively strong seismic events, greater than intensity VII, have affected the Korean peninsula in the past (Lee and Yang, 2006). Gyeongju is a good place to study damage of stone heritages, because it has many stone artefacts at its heritage sites and it was the capital city of the Silla Dynasty for almost 1000 years from 57 BC to 935 AD. During this time, many large seismic events (over intensity VII) affected the Gyeongju and Ulsan areas destroying many heritage sites. In AD 779, a huge seismic event was recorded and resulted in about 100 casualties. A number of buildings were destroyed due to this earthquake. It is inferred to be a destructive earthquake with a magnitude of 6.7 (Lee & Yang, 1983, 2006). The purpose of this study is to examine stone heritage sites and to distinguish and interpret the affects of recorded paleoseismological events at cultural heritage sites in the Gyeongju area.

GENERAL GEOLOGY

The basement of the study area consists of Cretaceous sedimentary rocks, the Taegu Formation, which forms part of the Gyeongsang Basin. This formation is discordantly intruded by Cretaceous and Tertiary igneous rocks (Fig. 1). In recent years, more than forty Quaternary faults have been reported near the Yangsan and Ulsan fault systems, which are the major fault systems in and around the Gyeongsang Basin (Lee and Jin, 1991; Kyung & Okada, 1995; Chang, 2001; Kim and Jin, 2006). The geometry of the intersection zone between the Yangsan and Ulsan faults is similar to simulated λ-faults (a low angle merging fault system; Du & Aydin, 1995, Kim et al., 2000).

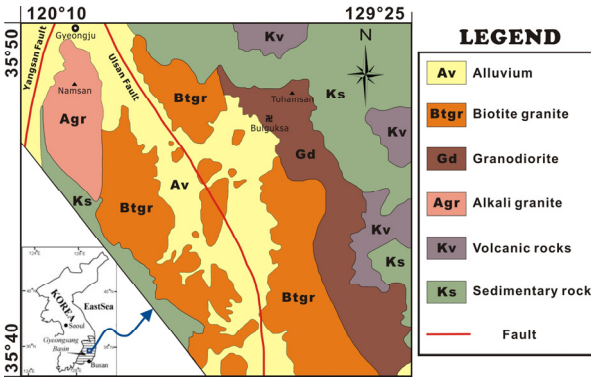

Fig. 1: Location map and geological map of the study area (modified from Lee et al., 1995).

EARTHQUAKE RECORDS

Instrumental recording of earthquakes in Korea began in 1905, and about one thousand earthquakes of mostly small magnitude ($<M_L = 4$), have been detected on or near the Korean Peninsula. However, 94 historical earthquakes were recorded above a magnitude of 5 around Gyeongju in historical records

between 2 to 1904 AD (Jin et al., in press, Lee & Yang, 2006).

Based on the compiled earthquake catalogue (Fig. 2), more reliable records were reported after the Koryeo Dynasty. We have identified 3 clusters and their respective recurrence intervals. We observed that after the first cluster there was a recurrence interval of 368 years. After this recurrence interval, earthquakes occurred frequently over a period of 193 years. This was followed by another recurrence interval of 53 years which was in turn followed by a 110 year period of repeated earthquakes. We are now 200 years into a period without earthquake events.

DESCRIPTION OF THE SEOKGATAP

Bulguksa temple was built in AD 751 and is one of the most famous temples in Korea. There are two main pagodas in the temple site. The three-story Seokgatap which stands at 8.2 m is a traditional Korean-style granite pagoda with simple lines and minimal detailing. Seokgatap is over 13 centuries old. The other one - Dabotap - is 10.4 m tall. In contrast to Seokgatap, Dabotap is famous for its highly ornate structure.

The temple was renovated during the Koryeo Dynasty (AD 918 – 1392) and the early Joseon Dynasty (AD 1392 – 1910). Historical records say that the Seokgatap was destroyed twice, in 1024 and in 1036 by big earthquakes (National Museum of Korea, 1997). After 1604, reconstruction and the expansion of Bulguksa started, this was followed by about 40 renovations leading up to 1805. During the Colonization of Korea between 1910 and 1945, the Japanese conducted restoration, but there were no records of the work done, and many known treasures disappeared during this time. After World War Ⅱ and the Korean War, partial restoration was conducted and completed in 1966. Upon an expansive archeological investigation, major restoration was conducted between 1969 and 1973, bringing Bulguksa to its current form. These stone pagodas are now preserved in their original Silla style.

To interpret the factors related to fracturing and the instability of the pagoda, we performed a kinematic analysis on the developed cracks. Cracks on the structure demonstrate the factors that control crack creation and spreading. We can use crosscutting relationship, kinematic indicators, inferring stress and damage zone theory to interpret the conditions that the pagoda has been subjected to.

According to an engineering survey for the Seokgatap, the following problems of structural stability are observed. The pagoda is tilled 0.9° to the Northwest. Foundation stones are dislocated with respect to each other by about 4 cm (Fig. 3). The center of the pagoda has subsided by about 3 cm. Also, we observed that there are cracks in the flat stones that are laid on other stones ranging in length between 1 and 6.5 cm. Some blocks have a gap between each other ranging from 3 to 4.5 cm. Also, a long crack of 132 cm in length and width of 5 mm have recently been detected on the eastern side of the pagoda. By comparing these results with previous state, the structural stability of the upper part of the pagoda is not safe and damage currently occurring.

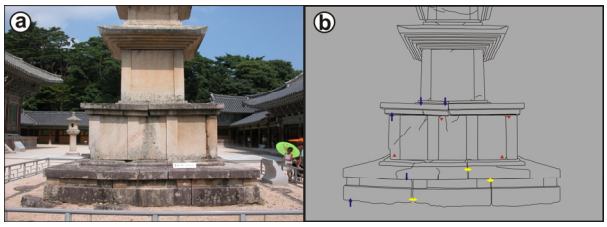

Fig. 3: (a) Photograph of western part of Seokgatap (b) sketch of western part of Seokgatap.

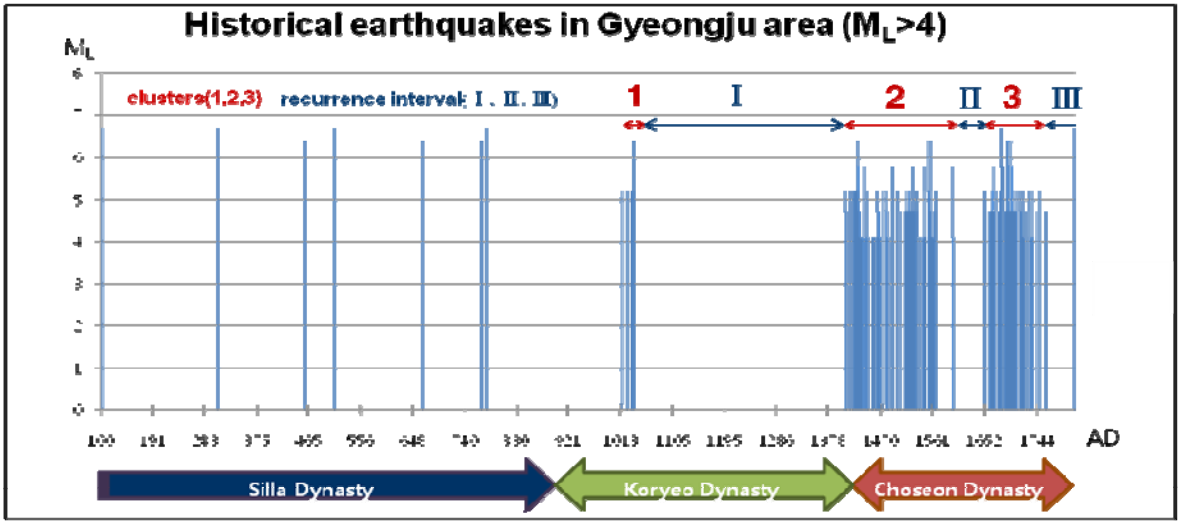

Fig. 2: Histogram of historic earthquake catalogue from 2 AD to 1810 AD for >ML = 4. It shows three earthquake clusters from 1013 AD and various recurrence intervals in the study area (modified from Jin et al., in press).

DISCUSSION

Quaternary faults have mainly been focused on the subject of paleoseismological studies in Korea. Recently, an archaeoseismological approach was used to infer the causes of the falling of a Buddha statue in Gyeongju area (Jin et al., in press). Archaeoseismological research in Gyeongju is important because deformed man-made structures with known age and original state offer supplementary information on past seismic events. Studying damaged monuments such as Seokgatap, Cheomseongdae and Sukbinggo suggest different major factors contributed to the damage at each site. The Cheomseongdae was built as an observatory and leans to the north by about 4° and it shows a horizontal shift in its large ashlars (Fig. 4), which may have been caused by episodic forces. If we carry out a similar engineering survey and a kinematic analysis (slip sense, opening and tilting etc.) in order to know how the cracks and gaps are developed in the pagoda at Cheomseongdae as we did at Seokgatap, we could be able to estimate the reason of the damage.

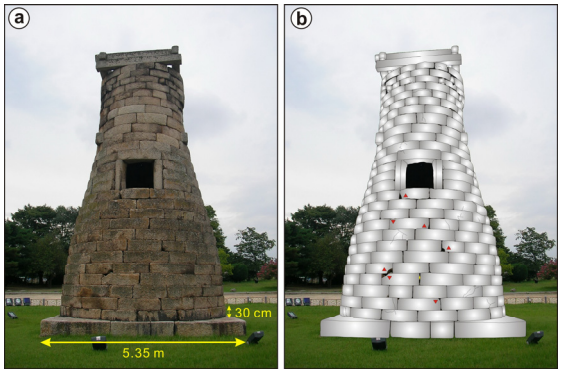

Fig. 4: (a) Overview of the damaged Cheomseongdae observatory in Gyeongju. (b) Sketch of southern part of Cheomseongdae.

CONCLUSIONS

Gyeongju is located around the junction between the Yangsan and Ulsan faults. Recently many Quaternary faults have been reported along the Yangsan and Ulsan faults. This has encouraged research on fault activities such as Quaternary faults and related paleoseismicities. According to historical records, the study area was significantly affected by earthquakes. Large seismic events produced heavy casualties and destroyed historical property. To identify the reason for the damage, we have performed kinematic analysis on the Seokgatap, in Gyeongju. Comparing previous report of structural stability with its present state, it is being destroyed by anonymous forces and movements such as foundation subsidence. Further detailed research on other destroyed stone monuments in Gyeongju would be helpful to clarifying the relationship between damage and historical earthquakes. So this study can give some valuable information to heritage preservation and earthquake hazard study in Korea.

Acknowledgements: This work was funded by the Korea Meteorological Administration Research and Development Program under Grant CATER 2008-5502

References

Chang, T.W. (2001). Quaternary tectonic activity at the Eastern Block of the Ulsan Fault. *Journal of the Geological Society of Korea*, 37, 431-444 (in Korean with English abstract).

Du, Y and Aydin, A., (1995). Shear fracture patterns and connectivity at geometric complexities along strike-slip faults. Journal of Geophysical Research, 100, 18093-18102.

Jin, K., Lee, M., Kim, Y.-S., Choi, J.-H. (2011). Archaeoseismological studies on historical heritage sites in the Gyeongju area, SE Korea. Quaternary International, doi:10.1016/j.quaint.2011.03.055.

Kim, Y.-S., Andrews, J.R., Sanderson, D.J. (2000). Damage zones around strike-slip fault systems and strike-slip fault evolution, Cracking Haven, southwest England. *Geoscience Journal*, 4, 53-72.

Kim, Y.-S., Jin, K. (2006). Estimated earthquake magnitude from the Yugye Fault displacement on a trench section in Pohang, SE Korea. *Journal of the Geological Society of Korea*, 42, 79-94 (in Korean with English abstract).

Kyung, J.G., Okada, A. (1995). Liquefaction phenomena due to the occurrences of great earthquakes; some cases in central Japan and Korea. *Journal of the Geological Society of Korea*, 31, 237-250.

Lee, K. and Na, S. H. (1983). A study of microearthquake activity of the Yangsan fault. Journal of the Geological Society of Korea, 19, 127-135.

Lee, K., Jin, Y.G. (1991). Segmentation of the Yangsan fault system: geophysical studies on major faults in the Kyeongsang basin. *Journal of the Geological Society of Korea*, 27, 434-449.

Lee, K. (1998). Historical earthquake data of Korean, Journal of the Korea Geophysical Society, 1, 3-22.

Lee, K., Yang, W.-S. (2006). Historical seismicity of Korea. Bulletin of the Seismo-logical Society of America 96, 846e855.Stiros, S. 1988b. Archaeology, a tool to study active tectonics – The Aegean as a case study. *Eos, Transactions, American Geophysical Union* 13, 1636-1639.

National Museum of Korea (1997). News.

Kim, B.-S. (1145) Samguksagi.

EARTHQUAKE ARCHAEOLOGY

INQUA PALEOSEISMOLOGY AND ACTIVE TECTONICS

EARTHQUAKE GEOLOGY AND RELATED HAZARD IN KACHCHH, GUJARAT, WESTERN INDIA

Malik, Javed N.(1), Michio Morino (2), Mahendra S. Gadhavi (3,4), Khalid Ansari (1), Chiranjeeb Banerjee (1), B. K. Rastogi (3),Fumio Kaneko (2), Falguni Bhattacharjee (3), Ashok. K. Singhvi (5)

(1) Department of Civil Engineering, IIT Kanpur. Kanpur 208016. UP. INDIA. Email: javed@iitk.ac.in
(2) OYO International Corporation Yushima 1-Chome Bldg. 4F, 1-6-3 Yushima, Bunkyo-ku, Tokyo 113-0034, JAPAN. Email: morino@oyointer.com; kaneko@oyointer.com
(3) Institute of Seismological Research, Gandhinagar 382018, Gujarat, INDIA. Email: mahendrasinh@gmail.com; brastogi@yahoo.com; falguni.geo@gmail.com
(4) L. D. College of Engineering, Ahmedabad, Gujarat. INDIA
(5) Physical Research Laboratory, Ahmedabad. INDIA. Email: aksprl@yahoo.com

Abstract: *The Kachchh falls under seismic zone V outside the Himalaya. It is marked by several E-W striking longitudinal faults viz. the Allah Bund Fault (ABF), Island Belt Fault (IBF), South Wagdh Fault (SWF), Kachchh Mainland Fault (KMF), and Katrol Hill Fault (KHF). Several large to moderate magnitude earthquakes have struck this area during last 300 years, viz. 893 AD, 1668 Indus Delta (M7); 1819 Allah Bund (M7.8), 1956 Anjar earthquake (Ms6.1), and the recent 2001 Bhuj earthquake (Mw7.6). The rupture of 2001 remained concealed, suggestive of occurrence on blind fault. We carried out active fault identification, mapping and paleoseismic studies along ABF, KMF and KHF. CORONA satellite photos were used for identification of active fault traces. Ground Penetrating Radar (GPR) profiling helped us in locating appropriate site for trenching across KMF and KHF. Our study suggests that all three fault are active and were ruptured during recent historic past.*

Key words*: Kachchh, active faults, paleoseismic studies, Western India.*

INTRODUCTION

The state of Gujarat has two fold hazard posed by earthquakes, one on-land along the active faults in Kachchh region and its neighbourhood, and another offshore along the Makran Subduction Zone (MSZ) located in the west (Figure 1). The entire coastline is highly vulnerable from the tsunami triggered by an earthquake occurring along the MSZ. Two such tsunami events have been recorded during historic and recent times by earthquakes along MSZ, i.e., during 325 BC and 1945 AD. Apart from this the Kachchh region has been struck by several large to moderate magnitude earthquakes during last 300 years, viz. 893 AD, 1668 Indus Delta (M7); 1819 Allah Bund (M7.8), 1956 Anjar earthquake (Ms6.1), and the recent 2001 Bhuj earthquake (Mw7.6) (Malik et al., 1999a; Bilham, 1999). From these events, only 1819 Allah Bund earthquake has been reported to have accompanied with 80-90 km long surface rupture and uplift resulting into formation of about 4-6 m high scarp (Quittmeyer and Jacob, 1979; Johnstan and Kanter, 1990). The recent 2001 Bhuj earthqukae with magnitude Mw7.6, the rupture remained concealed below the ground at a depth of 7-10 km, suggestive of occurrence on blind fault (Mandal and Horton, 2007). It is a matter of concern that if movements on a blind fault are capable of producing large magnitude earthquakes, than having earthquakes of similar magnitude or larger on active faults with surface rupture cannot be ruled out (Malik et al., 2008; Morino et al., 2008). Active faults are considered to be the source for large magnitude earthquakes in seismically active regions. Their proper identification and distribution significantly help in knowing the seismic potential and associated hazard in the region. The landscape of Kachchh is marked by several E-W striking longitudinal faults viz. the Allah Bund Fault (ABF), Island Belt Fault (IBF), South Wagdh Fault (SWF), Kachchh Mainland Fault (KMF), and Katrol Hill Fault (KHF). Under the project sponsored by Gujarat State Disaster Management Authority (GSDMA) on Seismic Microzonation of Gandhidham, Kachchh, we carried out active fault mapping and paleoseismic investigations along ABF, KMF and KHF. In this paper we highlight in brief our findings based on detailed satellite data interpretation for identification of active faults and related geomorphic features as well as paleo-earthquake signatures preserved in sediment succession (Figures 1).

Active fault and paleoseismic investigations:

Katrol Hill Fault:

Several new active fault traces were identified along Katrol Hill Fault (KHF) (Figure 1). These fault traces were identified based on satellite photo interpretation and field survey. Trenches were excavated to identify the paleoseismic events, pattern of faulting and the nature of deformation. Active fault traces were recognized about 1km north of the topographic boundary between the Katrol Hill and the plain area.

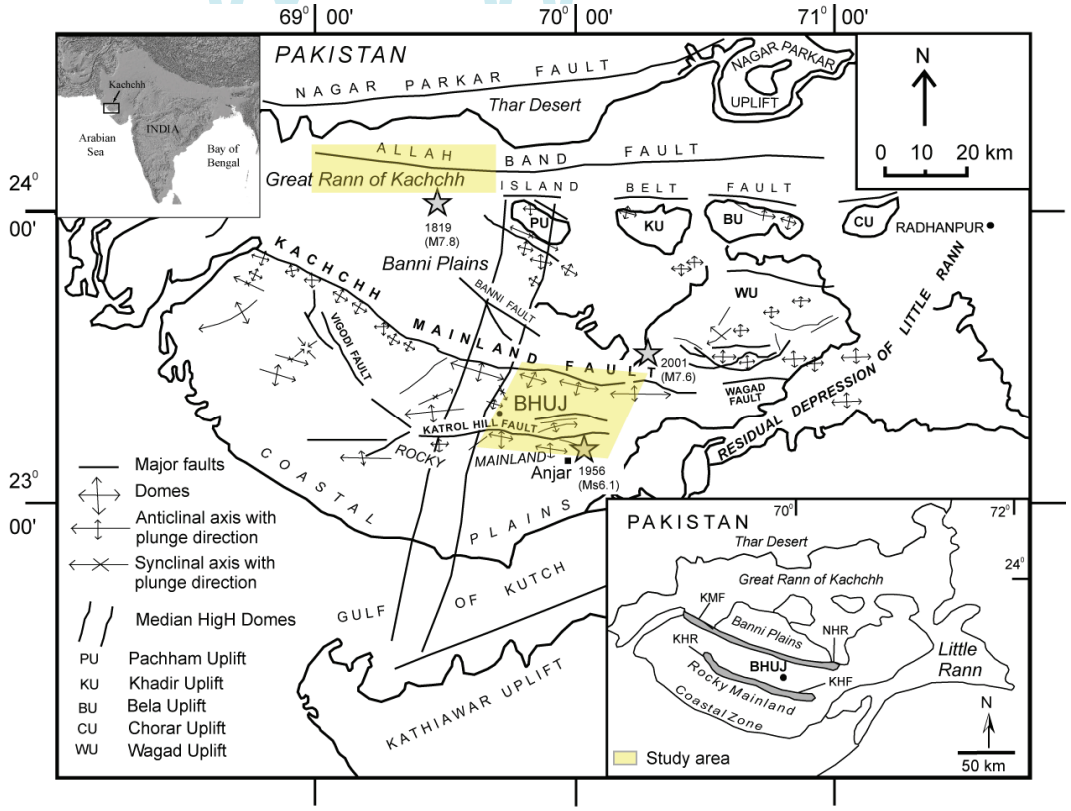

Figure 1. *Generalized structural map of Kachchh region (after Biswas and Deshpande, 1970). Inset at the left top show DEM of India highlight the location of Kachchh peninsula and Makran Subduction Zone (MSZ). Inset at the lower right shows major geomorphic zones of Kachchh. Yellow box marks the study area along Kachchh Mainland Fault and Katrol Hill Fault, and along Allah Bund Fault. NHR- Northern Hill Range, KHR- Katrol Hill Range, KMF Kachchh Mainland Fault and KHF- Katrol Hill Fault.*

The fault exposure along the left bank of Khari River with 10m wide shear zone in the Mesozoic rocks and showing displacement of the overlying Quaternary deposits is indicative of continued tectonic activity along the ancient fault. The E-W trending active fault traces along the KHF in the western part changes to NE-SW or ENE-WSW near Wandhay village. Trenching survey across a low scarp near Wandhay village reveals three major fault strands F1, F2, and F3 (Figures 2a & b). These fault strands displaced the older terrace deposits comprising Sand, Silt and Gravel units along with overlying younger deposits from units 1 to 5 made of gravel, sand and silt. Stratigraphic relationship indicates at least three large magnitude earthquakes along KHF during Late Holocene or recent historic past.

Kachchh Mainland Fault:

Two trenches were dug along the KMF, one near Jhura and another near Lodai villages. We reported first identified active fault exposure from Kachchh region along the Kachchh Mainland Fault (KMF) other than the 1819 Allah Bund earthquake. The active fault scarps striking E-W were identified near Lodai village along KMF. North facing scarps with height from 10-15 m are the manifestation of the displaced alluvial fan surface along this fault. Occurrence of discontinuous linear mound ranging in height from 3-5 m aligned along the strike about 100 m north of the main scarp are suggestive of younger tectonic movement and progressive shift of tectonic activity towards north along new imbricated fault (Figure 3). Three low to high angle reverse fault strands (F1, F2 and F3) displacing young Quaternary deposits (late Pleistocene-Holocene?) classified as A to F units comprising gravel and sand-silt facies were identified in a trench excavated at the base of the linear mound along KMF (Figure 3). Our preliminary observations revealed occurrence of at least two large magnitude earthquakes along the F3 fault, and may be older events along the F1 and F2. Latest event (Event-I) occurred along F3 after the deposition of unit B registering the displacement of ~33 cm, penultimate event (Event-II) occurred after the deposition of unit C with ~40 cm of displacement. The maximum displacement of about 73 cm along F3 indicates cumulative displacement accommodated during more than one event. The total displacement of ~98 cm along F2 strand displacing the E and F units is the result of more than one event, and since the F2 probably displaced the unit C suggests that the movements occurred during penultimate (Event II) and during the Event III, older than penultimate. Displacement of Mesozoic succession during older events and unit B during the latest Event I along F1 suggests repetitive movement along this fault. The fragile nature of ~3-4 m wide shear zone formed in Mesozoic rocks (shale+sandstone) also point towards repetitive tectonic movement along KMF.

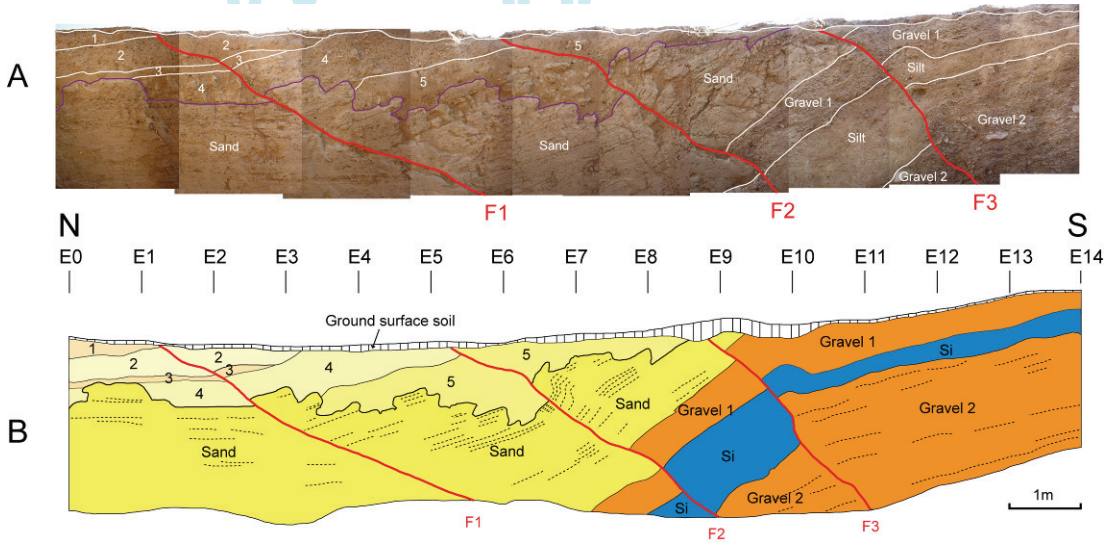

Figure 2a. *Photo-mosaic of the eastern wall of Wandhay trench exposed across the Katrol Hill Fault near Wandhay Dam. The trench was excavated across a very low fault scarp (refer Figure 2, for location). Three strands of thrust faults (F1, F2 and F3) dipping towards south were identified registering the latest event along F1, the penultimate as well as latest event along F2 and the older event along F3.* ***2b.****Trench log of eastern wall of Wandhay trench. Terrace deposits are composed of Sand, Gravel-1, Silt, and Gravel- 2. These terrace deposits are covered by units 1 to 5 (after Morino et al., 2008).*

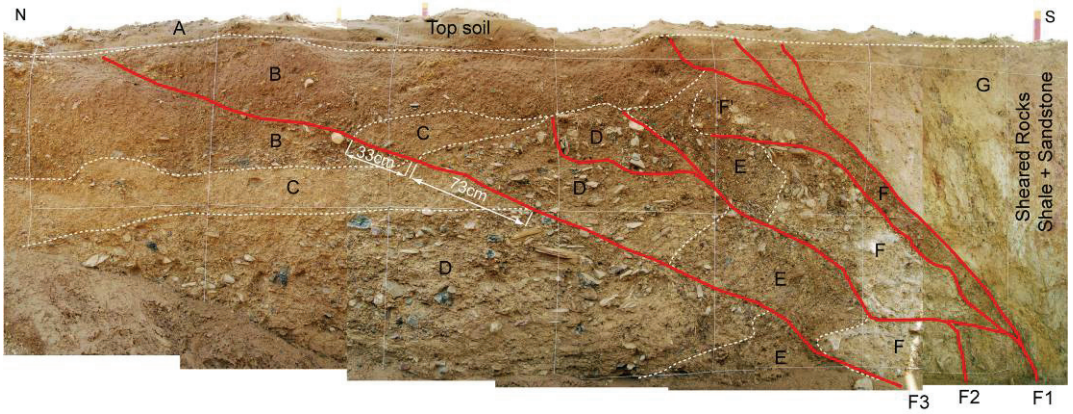

Figure 3. *East wall view of trench excavated across active fault scarp near Lodai village along Kachchh Mainland Fault (KMF). Three main fault strands F1, F2 and F3 shows reverse faulting with variable dip ranging from 10°-55° towards south.*

To confirm further active faulting along the KMF, paleoseismic investigation near Jhura Village about 30 km west of Lodai revealed an active fault displacing overbank deposits of Kaila River (Figure 2 and 6). Two fault strands F1 and F2 were identified in the trench. The northern F1 shows a low-angle reverse fault with inclination of 15° towards the south. At least two faulting events were inferred on the basis of upward fault termination with clear angular unconformity. The net-slip during a single faulting event considering deformation on the hanging wall of F1 fault is over 5 m, suggestive of a large magnitude event during late Holocene period.

Allah Bund Fault in Great Rann of Kachchh:

The Kachchh region is not only well known for the occurrence of large magnitude earthquakes, but also for having a major Harappan (4000-4500 year) and historical sites. One of such major sites was Dholavira located on Khadir Island (Figure 1). Few sites in Great Rann of Kachchh (GRK), probably flourished until 1819 Allah Bund earthquake (?). Till date it is not fully understood as whether these sites were affected by the major seismic events in the past and also the presently evolved landscape was influenced by tectonic movements. The geologists, archaeologists, and scholars of ancient Indian history have mentioned the existence of numerous mighty southwest flowing rivers viz. the Sindhu (Indus), Shatadru or Nara (Sutlej) and Sarasvati, during Pre-Vedic and Vedic times (~4000 yr). These rivers flowed into then existing Arabian Sea, presently the GRK.

We excavated 6-8 trenches in Allah Bund region GRK. Study reveals occurrence of at least 3 major events during recent past, which were probably responsible for the disruption of major channels (?), changing the landscape and destruction of the settlements (Figure 4). Trenches on the hanging wall of ABF shows thick massive yellowish medium-fine sand overlain by 1-1.5 m thick laminated sequence of

silty-sand and clay. This suggests change in depositional environment from fluvial to fluvial-marine or tidal environment (high sea-level during 4000-6000 yr?). Trench at Vigukot revealed prominent sand-sheets at three levels indicative of 3 major liquefaction events, triggered by near source earthquakes (Figure 4), the latest event probably be the 1819 Allah Bund. Preliminary OSL ages of the sediments dated from the sand blow, soft sediment deformational structures, faulted sedimentary units from the trenches excavated on the hanging wall and across the Allah Bund Fault suggests occurrence of at least 2-3 events during 2.0-3.0 ka, with the most recent event during 2.0 ka.

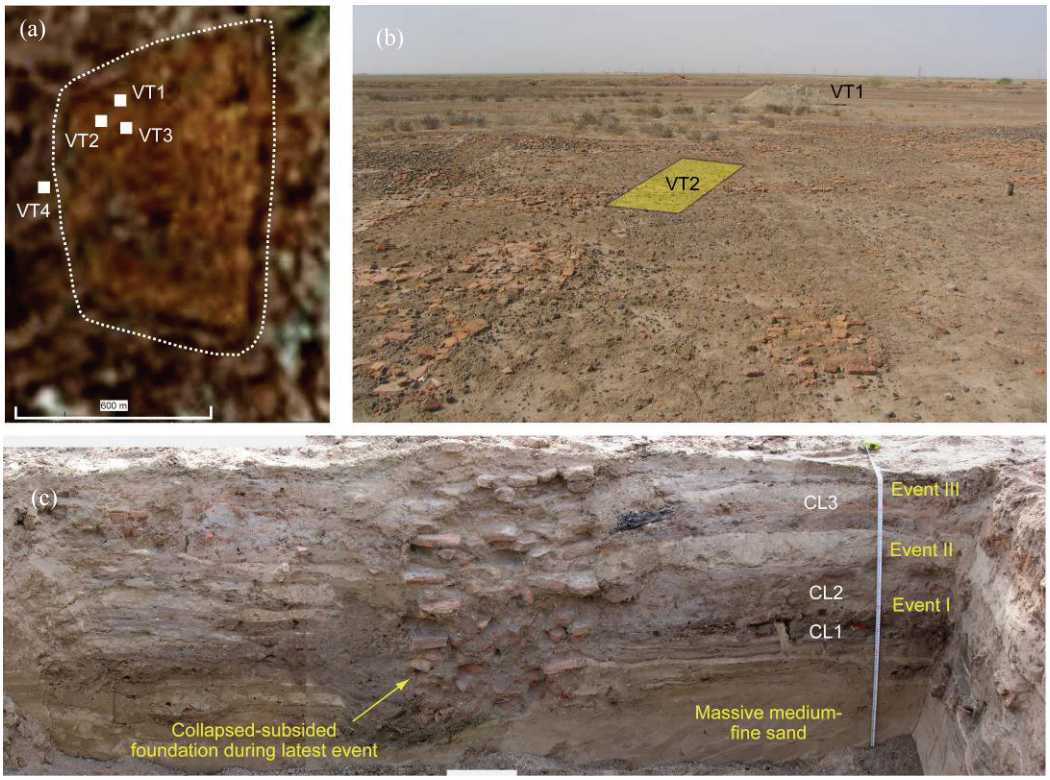

Figure 4. (a) Vigukot Fort in GRK, fortification area is marked by broken while line. VT1, VT2, VT3 and VT4 are the locations of trenches excavated in and around Vigukot Fort, **(b)** field-*photo showing location of trench VT1 and VT3. Location of VT3 is marked by yellow-box. Oriented bricks on the surface represents remnant of old foundation and* **(c)** *east wall view of 1.2 m deep and 3.5 m long trench excavated across a 80 cm thick wall (for location refer figure* ***4b)****. Exposed succession exhibits massive medium to fine sand at the base – suggestive of fluvial environment, capped by 1 m thick laminated succession – indicative of tidal environment. Preliminary interpretations suggests occurrence of at least three major event marked by prominent liquefied sand embedded in form of sand-sheet. CL1, CL2 and CL3 mark three cultural or occupation levels, the foundation in the centre of the trench belongs to the latest cultural level (CL3), which got severely affected during latest event, most likely the 1819 Allah Bund event(?).*

Acknowledgements: The authors are thankful to GSDMA, Gujarat, for funding this project. We are grateful to Prof. S. K. Jain, IIT Kanpur, now at IIT Gandhinagar and Dr. Alpa Sheth, VMS Consultants Private Limited, for their constant encouragement, support and discussion during this work.

References

Bilham, R. (1999). Slip parameters for the Rann of Kachchh, India, 16 June 1819 earthquake quantified from contemporary ccounts. Coastal Tectonics. Stewart, I. S., and Vita-Finzi, C. (eds.). *Geological Society of London* 146, 295-318.

Biswas, S. K. (1980): Structure of Kutch-Kathiawar Region, W. India.- Proc. 3rd Ind. *Geol. Congr., Pune*, 255-272. Biswas, S. K., and Deshpande, S. V. (1970): Geological and tectonic maps of Kutch. - In: , 7, 115-116

Johnston, A. C. and Kanter, L. R. (1990). Earthquakes in stable continental crust. *Scientific American*, 68-75. Malik, J. N., Sohoni, P. S., Karanth, R. V. and Merh, S. S. (1999a). Modern and Historic seismicity of Kachchh

Malik, J. N., Morino, M., Mishra, P., Bhuiyan, C., and Kaneko, F. (2008). First active fault exposure identified along Kachchh Mainland Fault: Evidence from trench excavation near Lodai village, Gujarat, Western India. Journal Geological Society of India, 71, 201-208.

Morino, M., Malik, J. N., Gadhavi, M. S., Ansari, K., Mishra, P., Bhuiyan, C., and Kaneko, F. (2008). Active Low-Angle Reverse Fault and Wide Quaternary Deformation Identified in Jhura Trench across Kachchh Mainland Fault, Kachchh, Gujarat, India. Journal of Active Fault Research, Japan, 29, 71-79.

Morino, M., Malik, J. N., Mishra, P., Bhuiyan, C., and Kaneko, F. (2008). Active fault traces along Bhuj Fault and Katrol Hill Fault, and trenching survey at Wandhay, Kachchh, Gujarat, India. Journal of Earth System Sciences, 117(3),181–188.

Quittmeyer, R. C. and Jacob, K. H. (1979). Historical and modern seismicity of Pakistan, Afghanistan, Northwestern India and South-eastern Iran. Bull. Seism. Soc. of America, 69, 773-823.

EARTHQUAKE ARCHAEOLOGY

INQUA PALEOSEISMOLOGY AND ACTIVE TECTONICS

SEISMOGENIC SLUMPS IN PALAEO-DEAD SEA SEDIMENTS

Marco, Shmuel (1) and G. Ian Alsop (2)

(1) Department of Geophysics and Planetary Sciences, Tel Aviv Univesity. Ramat-Aviv, Tel-Aviv 69978, ISRAEL (shmulikm@tau.ac.il)
(2) Department of Geology and Petroleum Geology, School of Geosciences, University of Aberdeen, Aberdeen AB24 3UE, UK (ian.alsop@abdn.ac.uk)

Abstract (Seismogenic slumps in palaeo-Dead Sea sediments): *We analyze a series of slumps in lake sediments overlying the Dead Sea Fault. The slumps are interpreted as seismites that have been triggered by earthquakes, thus providing a palaeoseismic record for the DSF. The direction of slumping inferred from the geometry and orientations of folds and thrusts varies systematically along the entire ~100 km length of the western Dead Sea Basin. They are interpreted to form part of a large-scale radial slump system directed towards the depocentre of the precursor to the Dead Sea. The recognition that slumps may be reworked by younger seismically-triggered events suggests that in some cases the seismic recurrence interval may be shorter than previously anticipated.*

Key words*: paleoseismology; seismites; slumps; Dead Sea Fault*

DISCUSSION

Seismites found in sediments of lakes that straddled the Dead Sea Fault have provided a 70-kyr-long palaeoseismic record, one of the longest on Earth (e.g., Ferry et al., 2011; Kagan et al., 2011; Ken-Tor et al., 2001; Marco et al., 1996; Migowski et al., 2004). Still, questions concerning the significance of their detailed shapes and the physical process that governed the formation of these seismites remain open. Understanding the seismites evolution and the underlying physics are tools for reconstructing the properties of past earthquakes on the basis of the observed deformations. These could also be useful in detecting and understanding off-fault earthquake indicators in other submarine environments.

The Rayleigh-Taylor instability can explain mushroom-like symmetric deformation of inversed-density stratification, where heavy strata overlay lighter strata (Figure 1a). However, stable stratification and asymmetric folds predominate the seismites in the Lisan Formation, which was deposited during the last glacial period in Lake Lisan (the precursor to the Dead Sea). Seismites in stably stratified lacustrine marls favor a mechanism of earthquake-triggered shear known as the “Kelvin-Helmholtz Instability” (Heifetz et al., 2005). Field observations and numerical simulations show that the deformation begins as moderate wave-like folds due to shear at the water-sediment interface (Wetzler et al., 2010). It evolves into asymmetric folds, then reclining folds, and in cases of backwash and/or vertical relaxation we observe backward-oriented folds (Fig. 1). If the flow becomes turbulent the layers are fragmented, re-suspended, and ultimately re-deposited as breccia. During past earthquakes this process stopped at different stages, depending on the strength and duration of the shaking.

Our detailed analysis of the seismites (Alsop and Marco, 2011b) reveals that some of them were affected by later events. Failure to recognize reworked seismites would reduce the number of earthquakes inferred from simple counting. In cases of incomplete reworking careful scrutiny can distinguish two earthquakes represented in one seismite. For example, we observe breccia layers that are folded as part of slumps, which we interpret as multiple event seismites (Fig. 2).

We recognize that the direction of slumping inferred from the folds and thrusts varies systematically along the entire ~100 km length of the western Dead Sea Basin (Fig. 3). Hence the asymmetry of the folds represents the sense of shear, which was determined by very subtle slope of less than 1°. In the case of Lake Lisan coherent pattern of the fold vergence indicates that the location of the depocenter dictated the flow (Alsop and Marco, 2011a).

Acknowledgments: We thank Mr. John Levy, together with the Carnegie Trust and the Royal Society of Edinburgh for travel grants to IA, and the Israel Science Foundation for grant 1539/08 to SM.

References

Alsop, G. I., and Marco, S., 2011a, A large-scale radial pattern of seismogenic slumping towards the Dead Sea Basin: Journal of the Geological Society. Accepted.

Alsop, G. I., and Marco, S., 2011b, Soft-sediment deformation within seismogenic slumps of the Dead Sea Basin: Journal of Structural Geology, v. 33, no. 4, p. 433-457.

El-Isa, Z. H., and Mustafa, H., 1986, Earthquake deformations in the Lisan deposits and seismotectonic implications: Geophys. J. R. Astron. Soc., v. 86, p. 413-424.

Ferry, M., Meghraoui, M., Abou Karaki, N., Al-Taj, M., and Khalil, L., 2011, Episodic Behavior of the Jordan Valley

Section of the Dead Sea Fault Inferred from a 14-ka-Long Integrated Catalog of Large Earthquakes: Bulletin of the Seismological Society of America, v. 101, no. 1, p. 39-67.

Hall, J. K., 1996, Digital topography and bathymetry of the area of the Dead Sea Depression: Teconophysics, v. 266, p. 177-185.

Heifetz, E., Agnon, A., and Marco, S., 2005, Soft sediment deformation by Kelvin Helmholtz Instability: A case from Dead Sea earthquakes: Earth Planet. Sci. Lett., v. 236, p. 497-504.

Kagan, E., Stein, M., Agnon, A., and Neumann, F., 2011, Intrabasin paleoearthquake and quiescence correlation of the late Holocene Dead Sea: J. Geophys. Res., v. 116, no. B4, p. B04311.

Ken-Tor, R., Agnon, A., Enzel, Y., Marco, S., Negendank, J. F. W., and Stein, M., 2001, High-resolution geological record of historic earthquakes in the Dead Sea basin: J. Geophys. Res., v. 106, no. B2, p. 2221-2234.

Marco, S., Stein, M., Agnon, A., and Ron, H., 1996, Long term earthquake clustering: a 50,000 year paleoseismic record in the Dead Sea Graben: J. Geophys. Res., v. 101, no. B3, p. 6179-6192.

Migowski, C., Agnon, A., Bookman, R., Negendank, J. F. W., and Stein, M., 2004, Recurrence pattern of Holocene earthquakes along the Dead Sea transform revealed by varve-counting and radiocarbon dating of lacustrine sediments: Earth and Planetary Science Letters, v. 222, no. 1, p. 301-314.

Wetzler, N., Marco, S., and Heifetz, E., 2010, Quantitative analysis of seismogenic shear-induced turbulence in lake sediments: Geology, v. 38, no. 4, p. 303-306.

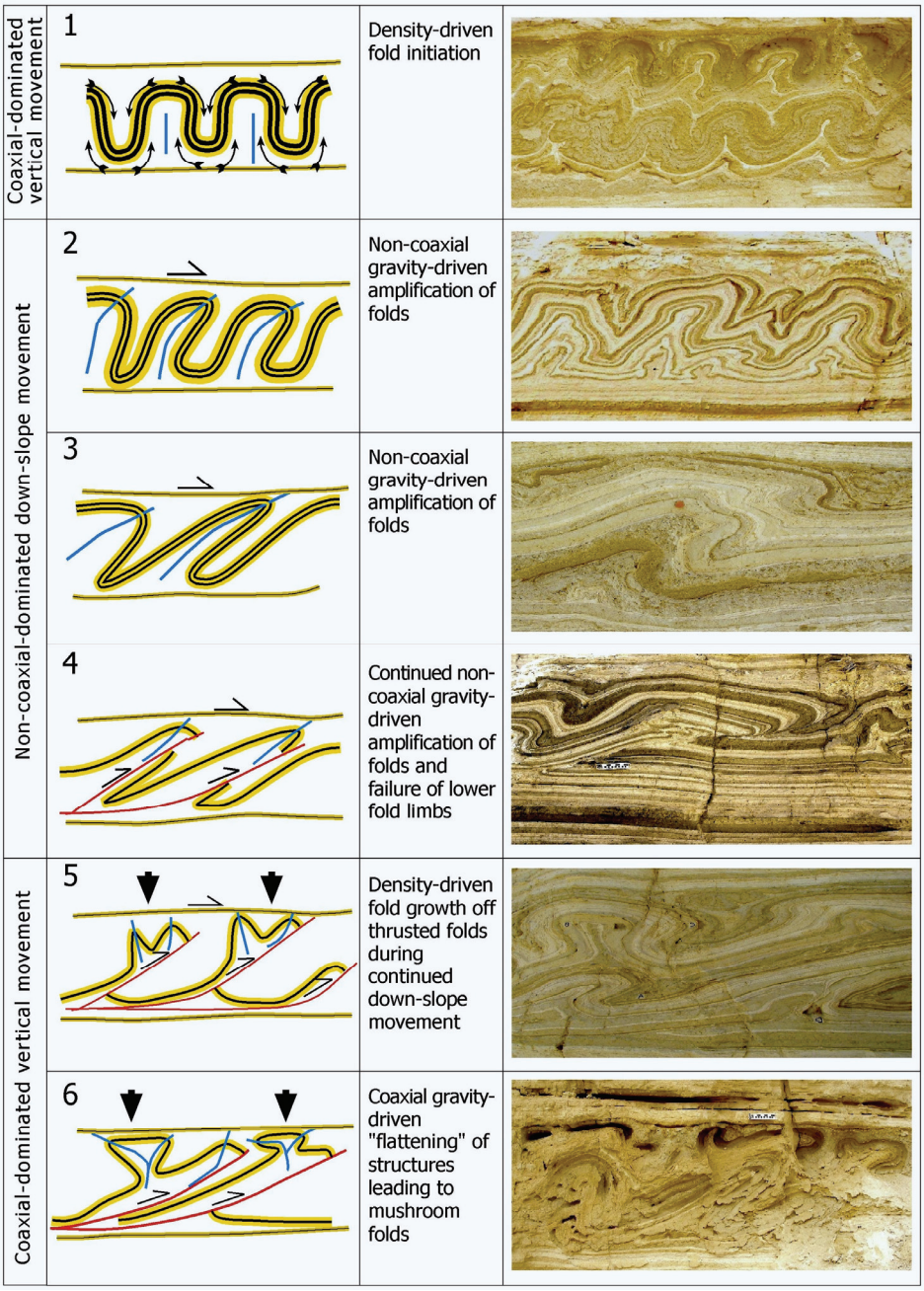

Figure 1. Schematic line drawings and photographic examples of structures generated during slump sheet initiation (a), translation (b, c), cessation (d), relaxation (e) and compaction (f). Folded beds are shown in yellow, while axial planes (blue) and thrusts (red) are also highlighted together with possible deformation styles. Not all slump sheets will show the full range and evolution of structures depicted here. Northeast is on the right of photographs (Figure from Alsop and Marco, 2011b).

Figure 2. Seismites 1 and 2 that are recognized as breccia layers are included in a seismogenic slump. Note that the upper part of the slump is also brecciated. We therefore interpret the sequence as containing evidence for three seismic events. Coin diameter is 20 mm.

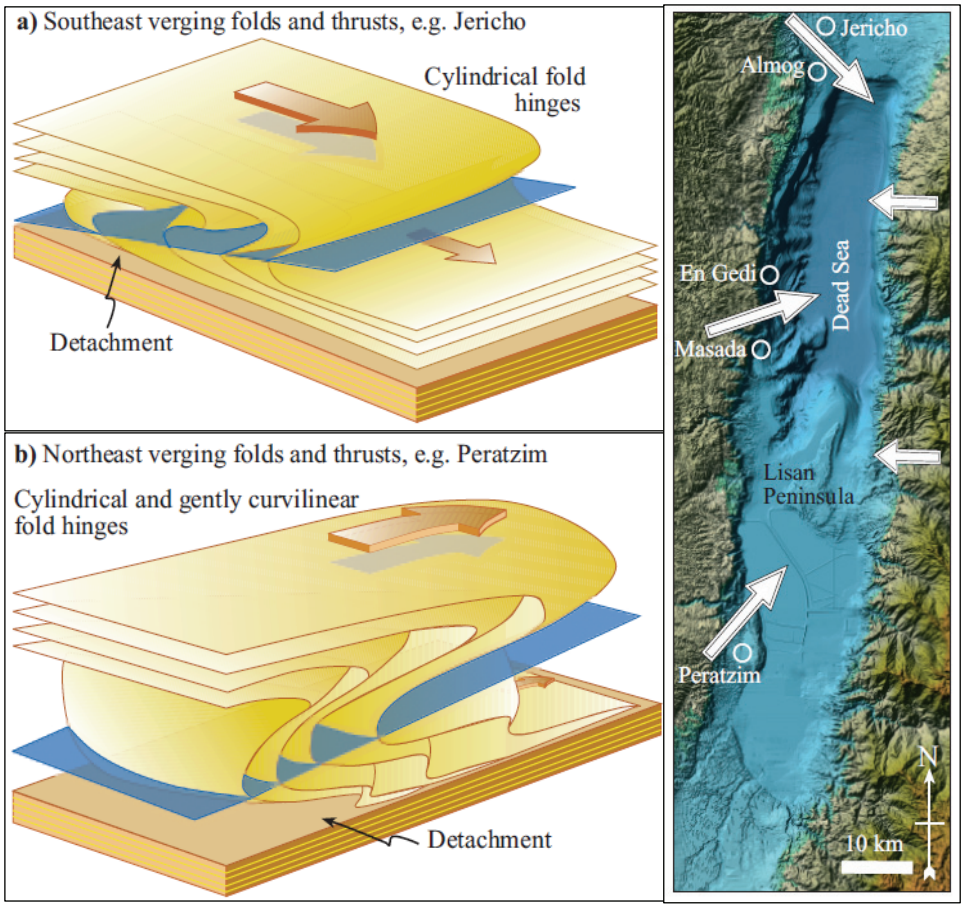

Figure 3. Schematic illustrations of slump structures showing radial vergence directions. We show the mean vergence directions of over 350 measured folds on the west and slump directions from El-Isa and Mustafa (1986) on the east, suggesting the control of the depocenter on the slump transport (Alsop and Marco, 2011a). Map from Hall (1996).

EARTHQUAKE ARCHAEOLOGY

INQUA PALEOSEISMOLOGY AND ACTIVE TECTONICS

MAPPING AND MEASURING HOLOCENE FAULT SCARPS IN DENSE FORESTS WITH LIDAR

McCalpin, James P.

GEO-HAZ Consulting, Inc., P.O. Box 837, Crestone, Colorado 81131 USA. Email: mccalpin@geohaz.com

Abstract (Mapping and Measuring Holocene Fault Scarps in Dense Forests with Lidar): *In the past decade new fault scarps have been discovered in the forests of North America by the use of Lidar DEMs. Most of the surveyed regions had been examined previously with aerial photographs, but no scarps were seen through the tree canopy. Lidar in those same areas shows obvious fault scarps. The scarp heights and slope angles can be accurately measured directly from the DEM, and compare favourably to field measurements at the same sites. We describe several case histories in the USA where Lidar-detected scarps have been trenched and analyzed for their seismic source characteristics.*

Key words*: fault scarps, Holocene, Lidar*

INTRODUCTION: THE PROBLEM OF FINDING FAULT SCARPS IN DENSE FORESTS

The identification and mapping of Quaternary fault scarps is well advanced in arid and semi-arid regions that contain little vegetation. Sub-humid and humid regions, in contrast, are often heavily forested and the ground surface cannot be seen in aerial photographs. Until recently the only way to locate and map fault scarps in forested areas was to enter the forest on foot and begin searching, but without a previously-identified target, a search would be random and extremely time-consuming. As a result, the density of fault scarps mapped to date in forested areas is a small fraction of that mapped in open areas. The scarcity of mapped Quaternary faults in forested areas has, in turn, translated into lower predicted seismic hazards, particularly in areas with low historic seismicity. This low predicted seismic hazard may be incorrect for many regions, resulting mainly from the lack of a reliable technique for finding Quaternary faults in forests.

The advent of light detection and ranging (LiDAR) in the 1990s has changed the situation dramatically. In this paper I describe four case histories where new fault scarps have been discovered in dense forests of the western USA and Alaska.

LiDAR Basics

LiDAR is also known by the more descriptive phrase "Laser altimeter terrain mapping." An airborne scanning laser rangefinder collects millions of distance measurements between the airplane and the ground, as many as 30,000 points per second at ~15 cm accuracy. The plane's position is measured by differential GPS and an inertial navigation system. Each laser pulse measures multiple returns (distance measurements) along a single beam, with the first return from the top of local vegetation, and the last return from the ground surface. The last returns are amalgamated into a "bare earth" digital elevation model (DEM) which shows the shape of the ground surface beneath the forest canopy (virtual deforestation). The current cost of a LiDAR survey and bare-earth DEM is ca. $150–$400/km2.

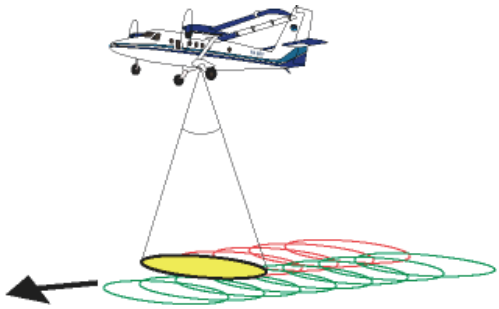

Fig. 1: Schematic diagram of LiDAR data acquisition

The Puget Sound area in Washington State: The Seattle Fault and its Backthrusts

The first LiDAR survey of the Puget Sound area in 2000 revealed two previously unsuspected late Quaternary faults, the Toe Jam and Waterman Point faults. The Toe Jam fault scarp on Bainbridge Island was trenched by US Geological Survey in 1998 and 1999 (Nelson et al., 2003). Trenching confirmed that the scarp records at least one, and probably more, large earthquakes since the latest glacial maximum (LGM, ca. 18 ka). A fossil beach terrace that surrounds this part of Bainbridge Island was uplifted about 7 meters in a single large earthquake about 1,100 years ago. Likewise, trenching in August 2001 confirmed that the Waterman Point scarp, like the Toe Jam scarp, follows a south-verging thrust fault that has moved since the Latest Glacial Maximum.

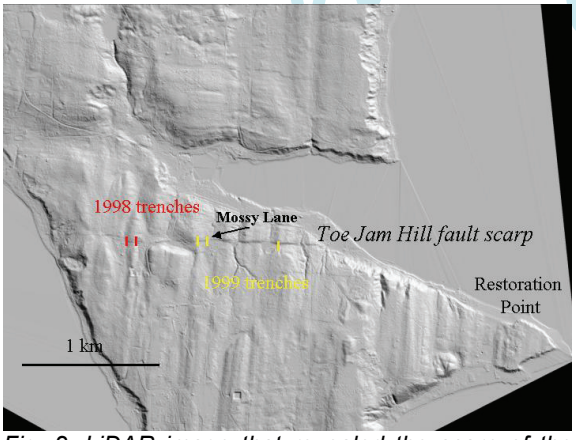

Fig. 2. LiDAR image that revealed the scarp of the Toe Jam fault on Bainbridge Island, west of downtown Seattle, Washington, USA. The fault is an east-west-trending, north-dipping reverse fault.

Western USA; The Upper Rio Grande Rift, Colorado

The 1000 km-long Rio Grande rift traverses the desert state of New Mexico and much of the state of Colorado. In the desert Quaternary fault scarps are unobscured by vegetation, but as the rift floor gradually rises northward to 2500 m and ultimately 3000 m in central Colorado, the rift margins become densely forested. Fault scarps higher than about 10 m can be seen on aerial photographs (i.e., about half as high as the average tree height of 20-25 m). Smaller scarps cannot be seen on airphotos, but can be seen on LiDAR.

The Williams Fork normal fault was discovered in 2002 in a dense pine forest at the foot of the Williams Fork Mountains in central Colorado. Even though the aerial photographs did not show any fault scarps in the dense forest, Kirkham (2004) walked to the range front and discovered multiple-event Quaternary fault scarps there. That fault is now the northernmost known Quaternary fault associated with the Rio Grande rift zone, where scarps are clearly late Quaternary in age, and trenches show displacement of late Quaternary strata.

This discovery encouraged the collection of 2400 km2 of additional LiDAR of the rift margins in 2010 by the Colorado Geological Survey and USGS. The new LiDAR DEMs show numerous previously unknown fault scarps on the forested rift margins. These fault scarps fill in large gaps in the maps of the Quaternary Fault and Fold Database of the USA.

Alaska: The Yakutat Microplate, Reverse Faults and Sackungen

The Yakutat microplate lies in south coastal Alaska, comprising a small plate fragment caught between the North American plate and the Pacific Plate (Fig. 3). The northward plate convergence of 55 mm/yr has created a spectacular barrier of coastal hills and mountains. These mountains intercept Pacific storms and lead to an annual precipitation of about 2000 mm/yr. Due to the high precipitation the terrain is blanketed by a dense coastal rain forest, which has defeated past attempts to unravel its neotectonics.

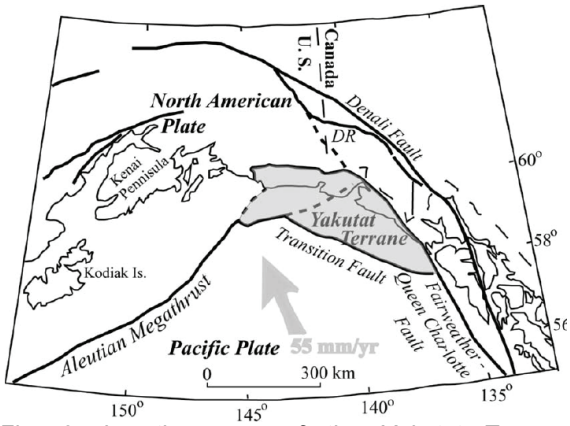

Fig. 3. Location map of the Yakutat Terrane (microplate) in south coastal Alaska.

Re-folding of foreland fold and thrust belt structures has created Holocene fault scarps in mountain blocks throughout the western part of the microplate. The morphology of the fold belt is atypical of classical foreland fold belts, where valleys and ridges are typically elongated parallel to fold axes. The Yakutat landscape is composed by irregular to elongated, north to northeast trending mountain blocks separated by flat-floored valleys filled with alluvial and glacial deposits. This morphology reflects Quaternary re-folding of foreland folds about plunging hinge-lines and vigorous erosion by glaciers and rivers. The mountain blocks are covered with swarms of discontinuous scarps (Fig. 4), mainly formed by displacement along bedding during second-phase folding of Tertiary strata.

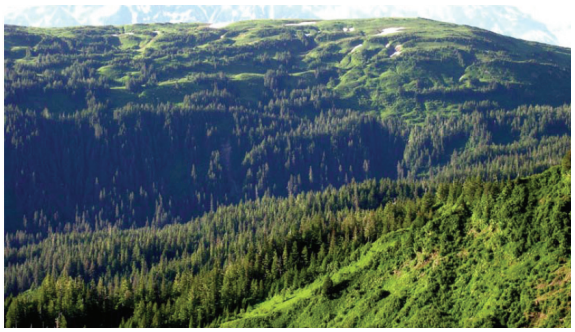

Fig. 4. Photograph of flexural-slip scarps on a typical mountain ridge in the Yakutat microplate.

Flexural-slip scarps occur in a variety of orientations with respect to hill slopes and ridge crests; parallel to ridge crests, cutting across ridge crests, and extending across alpine valleys. Scarps forming by flexural-slip folding are tens to hundreds of meters in length, have vertical offsets up to several meters, most face 'up-slope', and some have a dominant lateral slip component (Li et al., 2010). Ratios of fault scarp displacement to length (D/L) range between 0.1 to 0.001, overlapping with, but generally larger than, D/L for discrete tectonic faults. Distances between scarps measured normal to bedding are tens of meters. The fundamental controls on

localization of bedding parallel scarps are the mechanical competence of bedding and mechanical anisotropy imparted by the first-phase structures (Li et al., 2010). Other factors may include complex stress distributions within steep-sided mountain blocks, and stress transients generated by ground motion during large to great magnitude earthquakes.

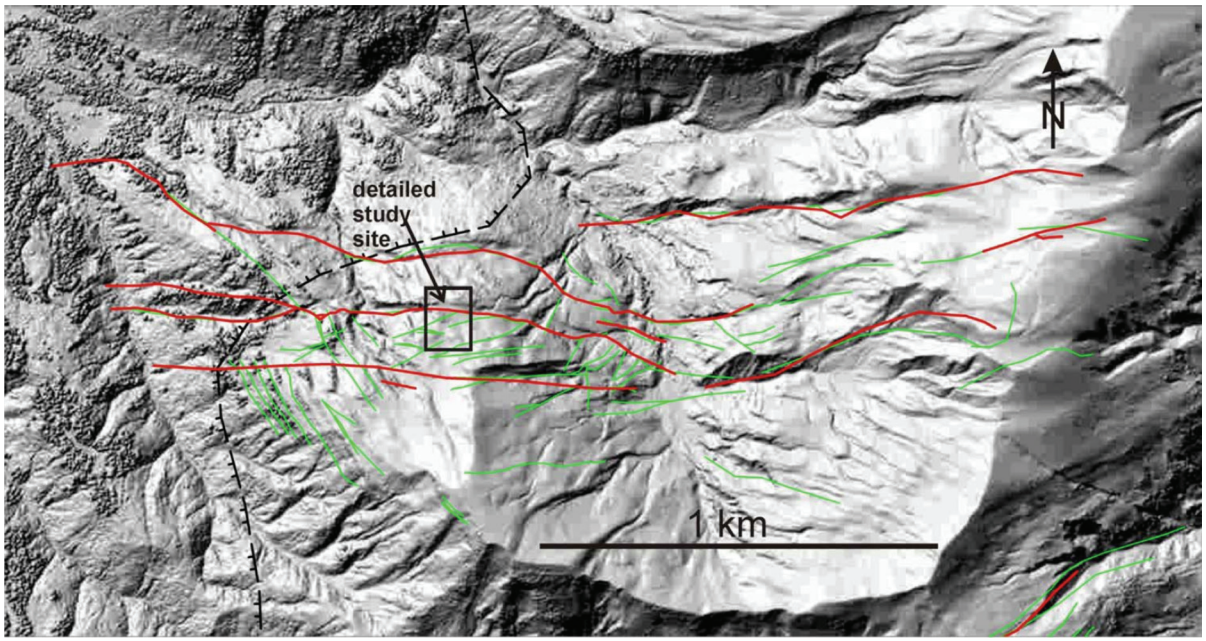

Fig. 5. Faults (red) and gravitational scarps (green) shown by LiDAR around the Martin Lake detailed study site, in the western Yakutat microplate. Black dashed line with hachures shows the LGM glacial trimline. From McCalpin et al., in press.

Alaska: The Foothills Fault Zone

The Foothills fault zone is a zone of north-verging thrusts and interconnecting strike-slip faults on the north side of the Alaska Range in central Alaska. Some alternative routes for the proposed Alaska-Canada Gas Pipeline cross the fault zone. Recent neotectonic studies in the crossing areas (Carver et al., 2008; 2010) have discovered fault scarps along the densely-forested range front, visible on LiDAR imagery but not detectable on aerial photographs.

DISCUSSION

LiDAR DEMs promise to change the way neotectonic-paleoseismic investigations are performed in forested regions. LiDAR should be the standard tool used for the critical step of identifying and mapping Quaternary fault scarps (Fig. 6). The success of this step determines the success of the remaining steps in the investigation.

Acknowledgements: I thank the St. Elias Erosion-Tectonics Project (STEEP) and the National Science Foundation for funding the neotectonic work in the Yakutat microplate.

References

Carver, G.A., Bemis, S.P., Solie, D.N., and Obermiller, K.E. (2008). Active and potentially active faults in or near the Alaska Highway corridor, Delta Junction to Dot Lake, Alaska: Preliminary Interpretive Report 2008-3d, Alaska Division of Geological and Geophysical Surveys, Fairbanks, AK, 32 p

Carver, G.A., Bemis, S.P., Solie, D.N., Castonguay, S. and Obermiller, K.E. (2010). Active and potentially active faults in or near the Alaska Highway corridor, Dot Lake to Tetlin Junction, Alaska: Preliminary Interpretive Report 2010-1, Alaska Division of Geological and Geophysical Surveys, Fairbanks, AK, 41 p.

Kirkham, R.K. (2004) Quaternary faulting in the Williams Fork Valley graben, north-central Colorado, and comparison with late Quaternary deformation near Spinney Mountain, central Colorado. Unpublished Final Technical Report submitted to the U.S. Geological Survey, NEHRP Program, Grant 02HQGR0102, revised 09-JAN-2004, 50 p.

Li, Z., Bruhn, R.L., Pavlis, T.L., Vorkink, M. and Zeng, Z. (2010). Origin of sackung uphill-facing scarps in the Saint Elias orogen, Alaska: LIDAR data visualization and stress modeling. Geol. Soc. Amer. Bull., 122 (9-10), 1585-1599.

McCalpin, J.P. (ed). (2009). Paleosesmology, 2nd Edition: Academic Press-Elsevier, 848 p.

McCalpin, J.P., Bruhn, R.L., Pavlis, T.L., Gutierrez, F., Guerrero, J and Lucha, P., in press, Antislope scarps, gravitational spreading, and tectonic faulting in the western Yakutat microplate, south coastal Alaska. Geosphere., 2011.

Nelson, A. R., Johnson, S. Y., Kelsey, H. M., Wells, R. E., Sherrod, B. L., Pezzopane, S. K., Bradley, L. A., Koehler, R. D., and Bucknam, R. C. (2003). Late Holocene earthquakes on the Toe Jam fault, Seattle fault zone, Bainbridge Island, Washington. Geol. Soc. Am. Bull. 115(11), 1388–1403.

Pavlis, T. L. and Bruhn, R. L. (2011). Application of LIDAR to resolving bedrock structure in areas of poor exposure: An example from the STEEP study area, southern Alaska, Geological Society of America Bulletin, v. 123, p. 206-217, doi: 10.1130/B30132.1.

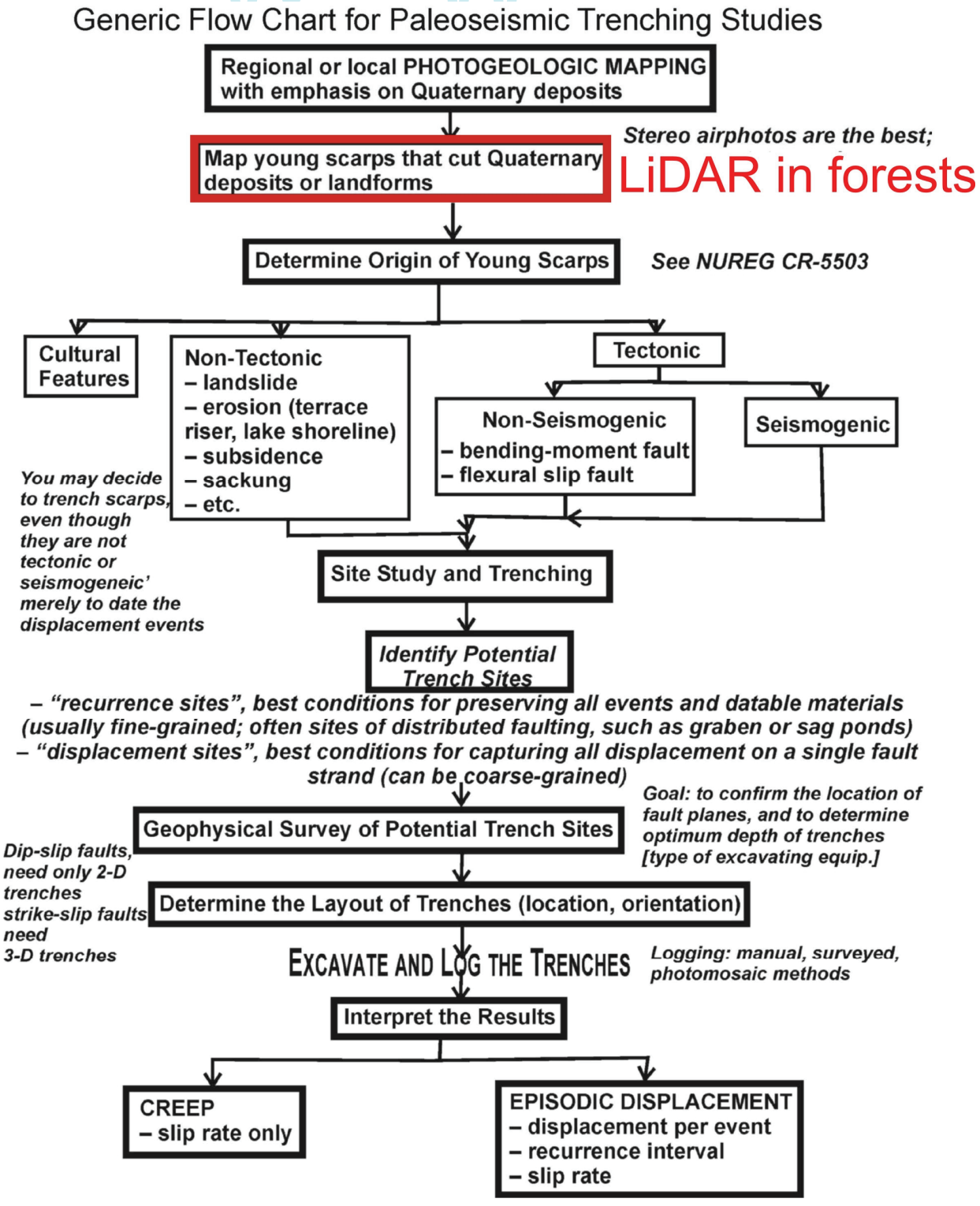

Fig. 6. Flow chart of a typical paleoseismic investigation that includes fault trenching, showing the early need for LiDAR surveys in forested areas. You cannot trench a fault scarp if you never find it. Adapted from McCalpin (2009).

EARTHQUAKE ARCHAEOLOGY

INQUA PALEOSEISMOLOGY AND ACTIVE TECTONICS

CHANGES ON THE GEOMORPHIC SETTINGS OF SAND-POOR ENVIRONMENT COAST OF BANDA ACEH, INDONESIA SUBJECT TO TECTONIC AND TSUNAMI EVENTS

Meilianda, Ella (1), Ben Maathuis (2), Marjolein Dohmen-Janssen (3)

(1) INTERCOAST, University of Bremen, MARUM - Leobener Strasse D-28359 Bremen, GERMANY. Email: emeilianda@marum.de
(2) Water Resource Department, Faculty of Geo□Information Science and Earth Observation (ITC), The Netherlands.+31 53 487 4391; Email: maathuis@itc.nl
(3) Water Engineering & Management (WEM), University of Twente, PO Box 217, 7500 AE Enschede, NETHERLANDS, email: c.m.dohmen-janssen@utwente.nl

Abstract: *Geomorphic settings before and after the December 2004 tsunami of the Banda Aceh coast, Sumatra, Indonesia were investigated in this study. The coast of Banda Aceh is a sand-poor environment contains thin layer of mobile sand perched on top of a consolidated Holocene prograding delta. Changes on the coastal shoreface morphology as the response to the tsunami waves were varying subject to the difference of geomorphic settings. The seawater inundated to the coastal plain as far inland as the shoreline position of 0.6 ky BP, during which a comparable magnitude of tsunami confirmed to have occurred in this region. This study demonstrates that such huge tsunami event occurred abruptly, but led to changes of the geomorphology developed in the Holocene.*

Key words*: tsunami, tectonic, geomorphic setting, Holocene*

INTRODUCTION

Despite the growth of tsunami-related studies since December 2004's tsunami event, there was little discussion on the geomorphological adjustment and development of the affected coast. Given the fact that such a powerful earthquake leading to an extraordinary magnitude of tsunami is a rare event in human-life time history, there are ample knowledge gaps that hinder thorough investigations towards this level. In addition, even before the tsunami of December 2004 occurred, that the topic of paleotsunami requires inevitable sedimentological and geomorphological research, since such extreme event effects on sedimentary transport or considerable alterations of the coastal configuration. In spite of this, only 5% of the existing tsunami literature is related to such issues (Scheffers & Kelletat, 2003).

The geomorphological state and development of the coast in pre-tsunami time is essential to investigate the extent of the environmental damage of the coast after being hit by such a huge catastrophe. In the absence of this knowledge for the coastal management practice, it is impossible, to forecast or to set-up future scenarios of the geomorphological development of the affected coasts.

In terms of sedimentary transport and geomorphological research, our main challenge is the lack of readily available data of the pre-existing geomorphology of the affected coast, particularly in the less-investigated study location of Banda Aceh, Sumatra Island, Indonesia. Pragmatically, the investigation on the coastal geomorphological development using various types of available information such as literature, historical maps, satellite images, bathymetric charts and in-situ sample data are tailored to construct the geomorphological interpretation. The objective of the present study is therefore to qualitatively measure the impact of the December 2004 tsunami on the coastal geomorphology based on the reconstruction of geomorphology of the Banda Aceh coast in the past.

The work in this study rests on the notion that each older geomorphological unit provides a boundary for the more recent units and therefore co-determines more recent geomorphological developments. Some preliminary studies after the tsunami event revealed that the extent of the tsunami inundation on the Banda Aceh coastal plain reached as far as about 5 km away from the coastline (Dohmen-Janssen et al., 2006).

Given the lack of geological data to support the quantification of the coastal destruction, we use data on the Holocene sea-level fluctuation of the region as a proxy and combined it with a Digital Elevation Model (DEM) of the coastal plain to interpret the geomorphological development of the coastal area. Additionally, this study also uses the generic knowledge of geomorphology and sediment stratification from bore hole samples to support the geomorphological interpretation. The geomorphic settings of the coastal area are also given by synthesizing the various but very limited geological and geomorphological studies of the coastal region. Overall, the study was aimed to answer the following research questions: 1) Which geomorphological units

can we distinguish at the Banda Aceh coast and how do they respond to the earthquake and tsunami?; 2) To what extent have the earthquake and tsunami of 26 December 2004 affected this coastal system?

STUDY SITE, DATA SETS AND METHODS

Banda Aceh is located at the northwestern tip of Sumatra Island, Indonesia (Fig. 1). The coastal plain has elevations from -0.5 m to +11 m relative to present sea level and occupies 125 square km of the northwest valley of the Barisan mountain range, which is the backbone of Sumatra Island. Krueng Aceh River is the main river crossing this low-lying coastal plain. In the 1990s, the middle reach of the river was bifurcated by a floodway channel, as a means to divert the surplus discharge of the river which caused annual flooding of the city. The coastline is dissected by parallel lagoon inlets in between some of the beach ridges sections.

This study interpreted the geomorphology of the Banda Aceh coast from various types of maps and satellite images covering the past century and from literature covering the geological and geomorphological evolution of the surrounding region. All maps, images and charts were geo-referenced to a master map (i.e. ortho-rectified aerial photo of 2005) which was processed in ArcGIS™. The nautical charts, bathymetric data and a post-tsunami's topographic map of the coastal plain were transformed into Digital Elevation Models (DEMs) using Triangulation Irregular Network (TIN).

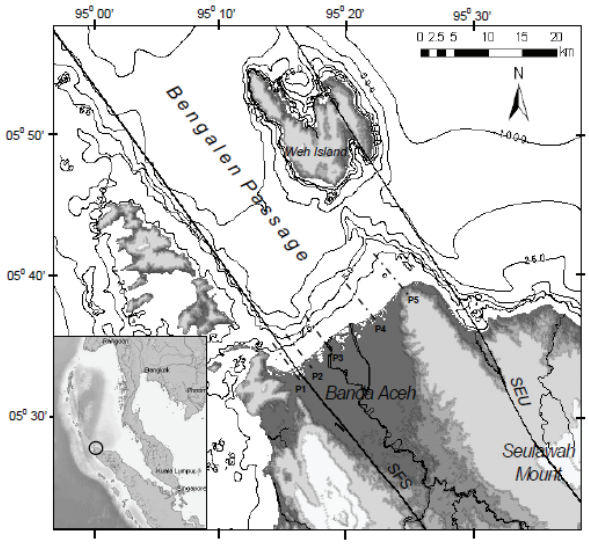

Fig. 1: Topographic map of Banda Aceh coastal plain, Sumatra, Indonesia derived from DEM (RSTM™ 2003 for the land part and nautical chart 1978 by BAKOSURTANAL, Indonesia).

The Holocene sea-level fluctuation curves produced by Tjia & Fujii (1989) were used in our study to reconstruct the Holocene shoreline changes and the development of the Banda Aceh coastal plain towards the modern shoreline position. Overall, we use the results of these various studies in combination with the analysis of satellite images, topographic maps, bathymetric charts and bore hole samples as the proxy to the non-existing data (e.g. from core sampling, etc.) to reconstruct the development of the geomorphic settings of Banda Aceh.

GEOMORPHIC SETTINGS OF BANDA ACEH

Similar to the low latitude regions in the world, Banda Aceh (5° N) experienced a sea-level fall during the late Holocene (e.g. since 6.0 ky BP). Sea-level raised in Malacca Strait from -13 m in 8.0 ky BP to about +5 m around 5.5 ky BP and then declined towards the present level (Geyh et al., 1979). Similar phenomena were also observed in Australia (Woodroffe and Horton, 2005), Singapore (Hesp *et al.* 1998) and Thailand (Sinsakul, 1990) for the same period.

Tjia & Fujii (1989) suggested that at the west coast of Malaysian Peninsula the sea level reached its maximum of about 5 metres above present sea-level at approximately 5.0 ky BP. They used the carbon dating technique to investigate Holocene shoreline of the coasts of Malaysian Peninsula using abrasional and biogenic indicators. The sampled location at the west coast of Langkawi Island which is situated in the same tectonic region as to Banda Aceh and both locations are situated in the solitary Andaman Sea environment. In the present study, the sea-level fluctuation indicated by Tjia and Fujii (1989) was compared with the elevations as well as the units of morphology identified from the DEM of Banda Aceh coastal plain, which was derived from the 0.5-m-contour-interval topographic map. In this way, the shorelines associated with different phase of transgression and regression of sea-level during the Holocene were extracted. At the same time, the pre-dominant process leads to the coastal morphology can be interpreted.

Geomorphic settings of Banda Aceh coast

Banda Aceh coastal plain and shoreface region consists of two distinctive geomorphic settings. The northeastern part is a tilted coastal zone (during the Pleistocene) which developments during the Holocene was influenced by the marine regression process. During this period, broad parallel coastal ridges and swales were developed over the modern coastal plain, and the shoreface has a concave - shape profile with sandy surface, indicating the pre-dominant influence of the marine regression. On the other hand, the southwestern part consists of a broad alluvial flat-plain over a depression zone associated with the Sumatran Fault zone. The shoreface stratigraphic layers mainly consisted of silty-clay structures which profile is convex-shape, indicating an alluvial progradation which was developed during the Holocene (Meilianda, 2009).

From the shoreline reconstruction using this method we analyse that the shoreline response to sea level fluctuations at Banda Aceh during the Holocene was highly influenced by the mechanisms of repeated changes of river mouths position and intermittent beach-ridge formation caused by periods of above

average onshore winds; a similar climate condition of Jakarta Bay in Java Island according to Verstappen (1973).

Modern coastal geomorphic settings and changes after December 2004's tsunami

Parallel to the completion of this study, several new findings about the recurrence of tsunami events in the Indian Ocean region have emerged. Monecke, et al. (2008) suggested that the three sediment coring samples at Meulaboh (west coast of Aceh), Simeulue (offshore west coast of Aceh) and Phra Thong (west coast of Thailand) show sediment deposit layers unconformity which age range are correlated with the historic tsunami occurrences in this region.

Two sample units in Meulaboh and Phra Trong suggested the ranges of age of the deposit of AD 1290 to 1400 (or 660 to 550 y BP) and AD 1300 to 1450 (or 650 to 500 y BP), respectively (Monecke et al., 2008). In their report, they used the age estimates of coastal terraces in the Andaman Islands region by Rajendran, et al. (2008) to confirm their interpretation as evidence for subduction earthquakes. The problem with estimates made by Rajendran, et al. (2008) was that the range of age they provide was considerably large. The marine terrace of Andaman Islands was suggested to age of AD 1170-1600 and AD 550-1330 (or equal to 750-350 y BP and 1400-620 y BP). In this study, we produced an alternative proxy to that provides comparable confirmation to the analysis of great tsunami recurrence studied by Monecke, et al. (2008).

In the 2004 tsunami, the inundation by seawater reached as far as 5 km inland, crossing the entire coastal plain of Banda Aceh that was already established since 3.5 ky BP (compare the tsunami inundation with the shoreline position of 2.8 ky BP in Fig. 1). It left deposits of various thickness and texture among the ruins and debris. The outer belt of beach ridge was mostly breached and even completely disappeared. After four days, the inundation reduced to about 50% from its initial extent (see also Dohmen-Janssen et al., 2006), which changed the low-lying housing areas, wetland and lagoon system behind the barrier islands into submerged areas. These areas are somehow associated with the one that geomorphologically modified by the last marine transgression (i.e. tsunami) in 0.6 ky BP. This shows that a huge tsunami event occurs only in a very short time-scale, but it leads to changes in geomorphology that has developed in a long-term scale, i.e. in centuries to millennia.

The Banda Aceh coast in the recent pre-tsunami time consisted of a narrow sandy beach perched on top of the toe of the beach ridges from the previous coastal development (Pleistocene and Holocene morphological units). The preceding development has made the modern coast of Banda Aceh to be highly dissected within a 25-km coastal stretch. Figure 2 shows the five representative cross-shore shoreface profiles at Banda Aceh (P1, P2, P3, P4 and P5 in Fig. 2). Each profile shows the elevation changes of three points in time within the recent century, i.e., before the tsunami (1893 and 1924), and after the tsunami (2006).

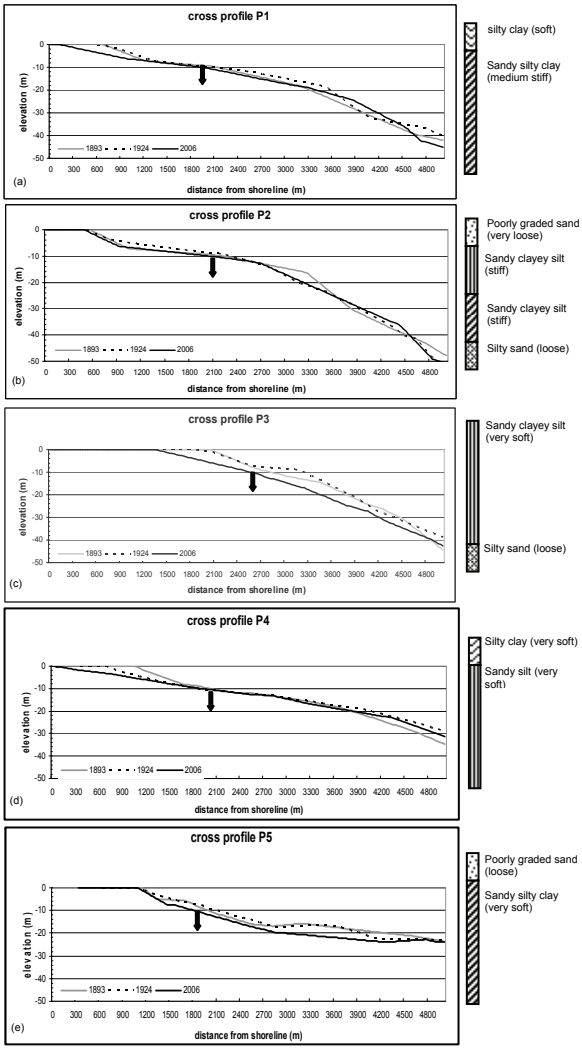

Fig. 2: Shoreface profile development in the past century and the associated bore hole samples. The downward arrows point at the sampling location at a depth ca. 10 m from mean sea level using rotational machine bore drilling log technique. The right panels of each profile display the stratification of the samples. Profile locations are in Fig. 1.

From the borehole samples shown in Fig. 2 it can be observed that most of the intercalated layers underneath the top layers of each profile on the southwestern part of the coast (P1 and P2) consist of stiff deposits. These layers were associated with the alluvial delta progradation during the last Holocene. Furthermore, we suppose that the intercalating layers found near the Sumatran Fault zone (e.g. P2) were influenced by some tectonic-related event (e.g. land subsidence or tsunami). Mobile fine sediments were subsequently perched on top of these Holocene deposits. The deposits associated with the prograding delta process consist of very fine sediments (e.g. silty clay or clayey silt) which eventually become stiff structure of deposit layers in

a long time and becomes the basement of the subsequent development (marine regression).
The shoreface profile of Banda Aceh in response to the tsunami can be seen in cross shore profiles in 1924 and 2006 shown in Fig. 2. The amount of eroded shoreface sediments varied from one profile to another. Interestingly, each shoreface profile maintained its convexity or concavity upon being eroded by the tsunami. The upper layer of the shoreface consists of young loose sediments underlain by the more consolidated morphological units (see bore hole data in Fig. 2) which indicate the combination between alluvial and regression processes during the Holocene. As a result, the upper layer were easily eroded during the tsunami (e.g. soft clay or silty layer deposit at the upper shoreface of profile P1 and the entire profile P3), while the shoreface composed by older deposits were less eroded (e.g. profiles center part of profile P1, profile P2 and P4). The shoreface erosion has modified the shoreface profiles of the entire coast and therefore has eventually modified the hydrodynamics of the coastal system.

DISCUSSION

The shoreface profile changes in Figure 2 show that the convex shoreface was influenced by the pre-dominant alluvial progradation during sea-level regression, whilst the concave shoreface was influenced by sea-level regression process during the Holocene. In addition, the resistance of the shoreface against severe erosion by the tsunami waves may depend on the degree of consolidation or the rate of weathering of the shoreface deposits. On the other hand tectonic intensity must be influential in the consolidation processes (e.g. liquefaction or compaction) on a specific coastal section preceding the December 2004 tsunami. In particular, tectonics and extreme waves such as tsunami have left their signature in the present geomorphology.

Regarding the complexity of the processes involved and the resulting geomorphology, proper attention should therefore be given to the boundary conditions which are imposed by the development of older geomorphological units. The complex geomorphology underlying the Banda Aceh coastal plain resulted from various processes in history and ultimately determines the shoreface geomorphic settings and the morphological development, composition and texture of beach sediments, and the rates of shoreline position changes. This case demonstrated that it is essential to understand the geomorphic settings of a coast before attempting to model the large-scale behaviour of these types of coastal systems.

This study was aimed to establish the general framework for future research on this specific study location which deserves attention to gain knowledge on the tectono-tsunami process and its impact on the coastal system. Borehole samples and reviews from other studies about this study area incorporated in the analysis in the present study fairly ascertain our interpretations on the geomorphic settings inherited from various morphological developments in history. Further study on the stratification of sediment deposit layers, carbon-dating, and side-looking radar may be utilized in future to support the overall interpretations of the present study.

Acknowledgements: This study was conducted in the Water Engineering and Management Group of University of Twente, Enschede, The Netherlands, in collaboration with the International Institute for Geo-Information Science and Earth Observation (ITC), Enschede, The Netherlands. The project is co-funded by the Syiah Kuala University of Banda Aceh, Indonesia and the University of Twente, Enschede, The Netherlands. Data sets was provided by BRR-Nias/NAD Banda Aceh.

References

Dohmen-Janssen, C.M., Meilianda, E., Maathuis, B.H.P. & Wong, P.P. (2006). State of Banda Aceh beach before and after the tsunami. *Proceeding of 30th International Conference on Coastal Engineering*, ASCE, Sand Diego, California.

Geyh, M.A., Kudrass, H.R. & Streif, H., (1979). Sea-level changes during the late Pleistocene and Holocene in the Strait of Malacca. *Nature* 278(5703), 441 – 443.

Hesp, P.A., Hung, C.C., Hilton, M. , Ming, C.L., Turner, I.M., 1998. A first tentative Holocene sea-level curve for Singapore. *Journal of Coastal Research* 14(1), 308-314.

Meilianda, E., (2009). *Past, present and future morphological development of a tsunami-affected coast: A case study of Banda Aceh.* Ph D Thesis, University of Twente, Enschede, The Netherlands.

Monecke, K., Finger, W., Klarer, D., Kongko, W., McAdoo, B.G., Moore, A.L. & Sudrajat, S.U., (2008). A 1000-year sediment record of tsunami recurrence in northern Sumatra. *Nature (Letter)* 455, 1232-1234.

Rajendran, K., Rajendran, C.P., Earnest, A., Ravi Prasad, G.V., Dutta, K., Ray, D.K. & Anu, R., (2008). Age estimates of coastal terraces in the Andaman and Nicobar islands and their tectonic implications. *Tectonophysics* 455, 53-60.

Scheffers, A. & Kelletat, D., (2003). Sedimentologic and geomorphologic tsunami imprints worldwide – a review. *Earth-Science Reviews* 63, 83-92.

Sinsakul, S., 1990. Evidence of sea-level changes in the coastal area of Thailand: A review. In: *Proceedings IEM/ICE Joint Conference on Coastal Engineering in National Development* (1991), pp. B1-B30.

Tjia, H.D., (1992). Holocene sea-level changes in the Malay-Thai Peninsula, a tectonically stable environment. *Geology Society of Malaysia* 31, 157-176.

Tjia, H. D. & Fujii, S., (1989). Late Quaternary shorelines in Peninsular Malaysia. In: *Spafa Final Report Seminar in Prehistory of Southeast Asia* 1987, 239–257.

Verstappen, H. Th., (1973). *A geomorphological reconnaissance of Sumatra and adjacent islands*. Wolters-Noordhof Publication, Groningen.

Woodroffe, S.A. & Horton, B.P., (2005). Holocene sea-level changes in the Indo-Pacific. *Journal of Asian Earth Science* 25, 29-43.

SEISMIC ANALYSIS OF LIQUID STORAGE TANKS

Konstantin Meskouris, Britta Holtschoppen, Christoph Butenweg, Julia Rosin (1)

(1) Chair of Structural Statics and Dynamics, Mies-van-der-Rohe Strasse 1, 52074 Aachen, GERMANY.
Email: meskouris@rwth-aachen.de

Abstract (Tank design for seismic loading): *In the event of strong earthquakes, it is important that the structural integrity of tanks containing liquids is maintained in order to not jeopardize the population's supply with essential goods. The continuous operation of tanks after strong earthquakes requires safe and effective design rules. The overall seismic behaviour of tanks is, however, quite complex, since the dynamic interaction effects between tank wall and liquid must be considered. The interaction can be simplified with the concept of generalized single-degree-of-systems representing the convective, rigid impulsive and flexible impulsive vibration modes of tank and liquid. This concept is well accepted for anchored tanks with a fix connection to a rigid foundation. This paper presents the state of the art of tank design with special focus on the practicability of the available design rules. Analytical and numerical calculation approaches are compared on the example of a typical tank geometry, taken the relevant interaction effects into account.*

Key words*: liquid filled tank, seismic design, impulsive vibration mode, critical facilities*

INTRODUCTION

Recent earthquake events showed that heavy seismic damages of tanks may lead to environmental hazards, fire following earthquakes and temporary loss of essential facilities. The vibration of liquid filled tanks subject to seismic loading depends on the inertia of the liquid and on the interaction effects between the liquid and the tank shell. Different calculation methods are available for describing the vibration behaviour and the earthquake loads. These methods are either quite simple (Housner, 1963) or very accurate but complex (Fischer et al., 1991). Therefore a well comprehensive and feasible method is needed, that provides realistic results for the seismic behaviour of tanks with an acceptable computing time. The following considerations apply to cylindrical, anchored tanks with a fix connection to a rigid foundation.

SEISMICALLY INDUCED LOAD COMPONENTS OF LIQUID FILLED TANKS

The seismic loads acting on wall and bottom of cylindrical tanks (Figure 1) can be divided into the following components (Meskouris et al., 2010):

- the convective load component; the fluid vibration in the rigid tank (sloshing),
- the impulsive rigid load component; caused by the inertia of the liquid, if the rigid tank moves together with the foundation,
- the impulsive flexible load component; representing the combined vibration of the flexibile tank shell (e.g. steel tanks) with the liquid.

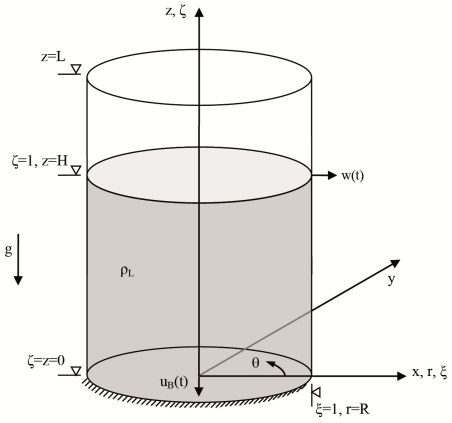

Fig. 1: Cylindrical tank

Convective pressure

Figure 2 shows the mode of vibration and the pressure distribution corresponding to the convective pressure component.

The pressure distribution is defined as:

$$p_k(\xi, \zeta, \theta, t) = \sum_{n=1}^{\infty} \frac{2 \cdot R \cdot \rho_L}{(\lambda_n^2 - 1)} \left[\frac{J_1(\lambda_n \cdot \xi)}{J_1(\lambda_n)}\right] \left[\frac{\cosh(\lambda_n \cdot \gamma \cdot \zeta)}{\cosh(\lambda_n \cdot \gamma)}\right] \cdot [\cos(\theta)] \, [a_{kn}(t) \cdot \Gamma_{kn}] \quad (1)$$

with

p_k convective pressure component due to horizontal excitation
n summation index; number of considered sloshing modes (here: n = 1)
R inner tank radius
ρ_L liquid density

J_1 first order Bessel function:

$$J_1(\lambda_n \cdot \xi) = \sum_{k=0}^{\infty} \frac{(-1)^k}{k! \cdot \Gamma(1+k+1)} \cdot \left(\frac{\lambda_n \cdot \xi}{2}\right)^{2k+1}$$

λ_n null derivation of Bessel function:
$\lambda_1 = 1{,}841$, $\lambda_2 = 5{,}331$, $\lambda_3 = 8{,}536$

ξ dimensionless radius: $\xi = r/R$

ζ dimensionless height: $\zeta = z/H$

θ angle of circumference

γ tank slenderness: $\gamma = H/R$

$a_{kn}(t)$ horizontal acceleration-time history as a result of an equivalent single-degree-of-freedom system with a period T_{kn} for the n^{th}-eigenmode of the sloshing wave. By using the response spectrum analysis the spectral accelerations corresponding to the natural periods T_{kn} should be calculated based on the elastic response spectrum.

Γ_{kn} participation factor for the convective pressure component for the n^{th}-eigenmode.

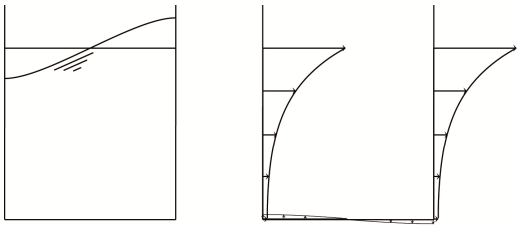

Fig. 2: Convective pressure - mode of vibration and pressure distribution

Taking into account the first sloshing eigenmode (n = 1) and the pressure distribution of the tank shell (ξ = 1), equation (1) can be simplified to:

$$p_k(\xi = 1, \zeta, \theta, t) = R \cdot \rho_L \left[0{,}837 \cdot \frac{\cosh(1{,}841 \cdot \gamma \cdot \zeta)}{\cosh(1{,}841 \cdot \gamma)}\right] \cdot [\cos(\theta)][a_{k1}(t) \cdot \Gamma_{k1}] \quad (2)$$

The natural period T_{kn} for the n^{th}-eigenmode of the sloshing wave is calculated with:

$$T_{kn} = \frac{2\pi}{\sqrt{\frac{g \cdot \lambda_n \cdot \tanh(\lambda_n \cdot \gamma)}{R}}} \quad (3)$$

Rigid impulsive pressure

Figure 3 shows the mode of vibration and the pressure distribution corresponding to the rigid impulsive pressure component.

The pressure distribution is given by the expression:

$$p_{is,h}(\xi, \zeta, \theta, t) = \sum_{n=0}^{\infty} \frac{2 \cdot R \cdot \gamma \cdot \rho_L \cdot (-1)^n}{v_n^2} \left[\frac{I_1\left(\frac{v_n}{\gamma} \cdot \xi\right)}{I_1'\left(\frac{v_n}{\gamma}\right)}\right] \cdot [\cos(v_n \cdot \zeta)][\cos(\theta)][a_{is,h}(t) \cdot \Gamma_{is,h}] \quad (4)$$

with:

$p_{is,h}$ rigid impulsive pressure component due to horizontal excitation

v_n $v_n = \frac{2n+1}{2}\pi$

I_1 modified first order Bessel function:

$$I_1\left(\frac{v_n}{\gamma} \cdot \xi\right) = \frac{J_1\left(i \cdot \frac{v_n}{\gamma} \cdot \xi\right)}{i^n} = \sum_{k=0}^{\infty} \frac{1}{k! \cdot \Gamma(1+k+1)} \cdot \left(\frac{\frac{v_n}{\gamma} \cdot \xi}{2}\right)^{2k+1}$$

I_1' Derivation of the modified Bessel function regarding to DIN EN 1998-4 (2007)

$$I_1'\left(\frac{v_n}{\gamma} \cdot \xi\right) = I_0\left(\frac{v_n}{\gamma} \cdot \xi\right) - \frac{I_1\left(\frac{v_n}{\gamma} \cdot \xi\right)}{\left(\frac{v_n}{\gamma} \cdot \xi\right)}$$

$$I_1' = \sum_{k=0}^{\infty} \frac{1}{k! \cdot \Gamma(0+k+1)} \cdot \left(\frac{\frac{v_n}{\gamma} \cdot \xi}{2}\right)^{2k+0} - \frac{\sum_{k=0}^{\infty} \frac{1}{k! \cdot \Gamma(1+k+1)} \cdot \left(\frac{\frac{v_n}{\gamma} \cdot \xi}{2}\right)^{2k+1}}{\frac{v_n}{\gamma} \cdot \xi}$$

$a_{is,h}(t)$ horizontal acceleration-time history. By using the response spectrum analysis $a_{is,h}(t)$ should be replaced by the spectral acceleration S_a corresponding to T = 0 s.

a_{gR} reference peak ground acceleration on type A ground

S soil factor

γ_I importance factor according to DIN EN 1998-1 (2010) or DIN EN 1998-4 (2007)

$\Gamma_{is,h}$ participation factor for the rigid impulsive pressure component: $\Gamma_{is,h} = 1{,}0$, because the rigid tank is moving together with the foundation.

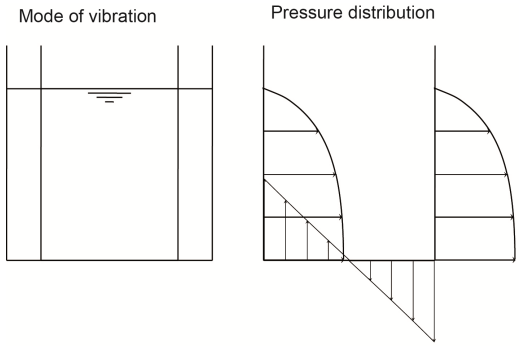

Fig. 3: Rigid impulsive pressure - Mode of vibration and pressure distribution

Taking into account the pressure distribution of the tank shell (ξ = 1), equation (4) is simplified to:

$$p_{is,h}(\xi = 1, \zeta, \theta, t) = R \cdot \rho_L \sum_{n=0}^{\infty} \left[\frac{2 \cdot \gamma \cdot (-1)^n}{v_n^2} \frac{I_1\left(\frac{v_n}{\gamma}\right)}{I_1'\left(\frac{v_n}{\gamma}\right)} \cos(v_n \cdot \zeta)\right] \cdot [\cos(\theta)][a_{is,h}(t) \cdot \Gamma_{is,h}] \quad (5)$$

The corresponding natural period is T = 0.

Flexible impulsive pressure

Figure 4 shows the mode of vibration and the pressure distribution corresponding to the flexible impulsive pressure component.

The flexible impulsive pressure component is calculated in an iterative procedure using the added-mass-model according to DIN EN 1998-4 (2007), Annex A. Within the framework of the procedure the tank wall is loaded with iterative calculated additional mass portions of the activated fluid. The pressure distribution is given by the expression:

$$p_{if,h}(\xi, \zeta, \theta, t) = \sum_{n=0}^{\infty} 2R\,\rho_L \left[\frac{I_1\left(\frac{v_n}{\gamma}\cdot\xi\right)}{\frac{v_n}{\gamma}\cdot I_1'\left(\frac{v_n}{\gamma}\right)}\right]\left[\cos(v_n\cdot\zeta)\int_0^1 f(\zeta)\cdot\cos(v_n\cdot\zeta)\,d\zeta\right] \cdot [\cos(\theta)]\,[a_{if,h}(t)\cdot\Gamma_{if,h}] \quad (6)$$

with:

$p_{if,h}$ flexible impulsive pressure component due to horizontal excitation

$f(\zeta)$ deflection curve of the first (anti-symmetric) mode of oscillation of the tank-fluid combination

$a_{if,h}(t)$ horizontal acceleration-time history as a result of an equivalent single-degree-of-freedom system. By using the response spectrum analysis the spectral accelerations corresponding to the first natural period $T_{if,h,1}$ should be used.

$\Gamma_{if,h}$ participation factor for the flexible impulsive pressure component due to horizontal excitation

The participation factor $\Gamma_{if,h}$ for the flexible impulsive pressure component is calculated as follows:

$$\Gamma_{if,h} = \frac{\int_0^1 p_{if,h}(\zeta)\,d\zeta}{\int_0^1 f(\zeta)\cdot p_{if,h}(\zeta)\,d\zeta}, \quad s(\zeta) = \text{const.} \quad (7)$$

with:

$p_{if,h}(\zeta)$ pressure function of the flexible impulsive pressure component as a function of the filling height

$s(\zeta)$ wall thickness of the tank

Taking into account the pressure distribution of the tank shell ($\xi = 1$), equation (6) can be simplified to:

$$p_{if,h}(\xi = 1, \zeta, \theta, t) = = R\cdot\rho_L \sum_{n=0}^{\infty}\left[2\cdot\frac{I_1\left(\frac{v_n}{\gamma}\right)}{\frac{v_n}{\gamma}\,I_1'\left(\frac{v_n}{\gamma}\right)}\cdot\cos(v_n\cdot\zeta)\int_0^1 f(\zeta)\cdot\cos(v_n\cdot\zeta)\,d\zeta\right] [\cos(\theta)]\,[a_{if,h}(t)\cdot\Gamma_{if,h}] \quad (8)$$

The first natural period $T_{if,h,1}$ is calculated as follows:

$$T_{if,h,1} = 2\cdot F(\gamma)\sqrt{\frac{W_L}{\pi\cdot g\cdot E\cdot s(\zeta = 1/3)}} = 2\cdot R\cdot F(\gamma)\sqrt{\frac{H\cdot\rho_L}{E\cdot s(\zeta = 1/3)}} \quad (9)$$

with:

W_L fluid weight: $W_L = \pi\cdot R^2\cdot H\cdot\rho_L\cdot g$

$F(\gamma)$ correction factor: $F(\gamma) = 0{,}157\cdot\gamma^2 + \gamma + 1{,}49$

$s(\zeta = 1/3)$ wall thickness of the tank at 1/3 filling height

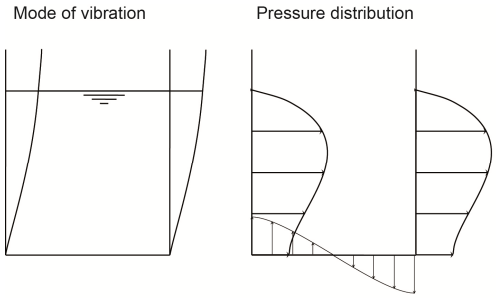

Fig. 4: Flexible impulsive pressure - Mode of vibration and pressure distribution.

The function curve of $f(\zeta)$ in (8) is generally not known. It depends on the impact of the liquid onto the tank, in other words the aforementioned pressure function $p_{if,h}$. Thus the joint bending form must be correctly determined iteratively. In DIN EN 1998-4 (2007), Annex A the "added-mass concept" is proposed. According to this the resonating fluid, activated with the first bending shape, is added to the tank wall density. Then with the new "dry" tank model, the more accurate bending form is determined (Fischer et. al., 1991).

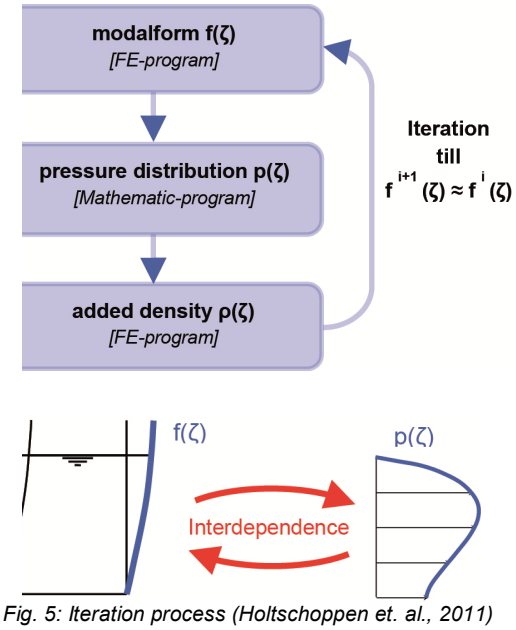

Fig. 5: Iteration process (Holtschoppen et. al., 2011)

However as Figure 5 shows, even this iterative process is impractical because the calculation is based on a complex mathematical pressure function (6) which requires a coupling of a mathematical software tool with a finite element program.

Though, with comprehensive parameter studies it is shown that the bending form of any tank can be described by using a parameterized sine wave which

can be mapped correctly to the natural frequencies for all common geometric and material configurations (Cornelissen, 2010):

$$f(\zeta)=a\cdot \sin\left(\frac{\pi}{2}\cdot(\zeta-b)\cdot c+d\right) \quad (10)$$

The bending form of the combined vibration – and with this the parameters a, b, c, d – depends on

- the tank slenderness (γ = H/R),
- the Poisson's ratio ν,
- the ratio fluid mass to tank mass and
- a changing wall thickness along the tank heigh.

However, the last named influences are comparatively small. By using the sine function (10) it is possible to determine the flexible impulsive pressure without iteration. For practical use and to represent the pressure the equation

$$p_{if,h}(\xi,\zeta,\theta,t)=R\cdot\rho_L\cdot\cos(\theta)\cdot\Gamma_{if,h}\cdot a_{if,h}(t)\cdot C_{if,h}(\xi,\zeta) \quad (11)$$

is suitable. $C_{if,h}(\xi,\zeta)$ corresponds to the normalized pressure at θ=0. Figure 6 shows the variation of the factor $C_{if,h}(\xi=1,\zeta)$ for the tank shell (ξ = 1) for different tank slendernesses.
For simplicity, the formulations of all pressure functions are also provided in a standardized, tabulated form (Meskouris et. al., 2011).

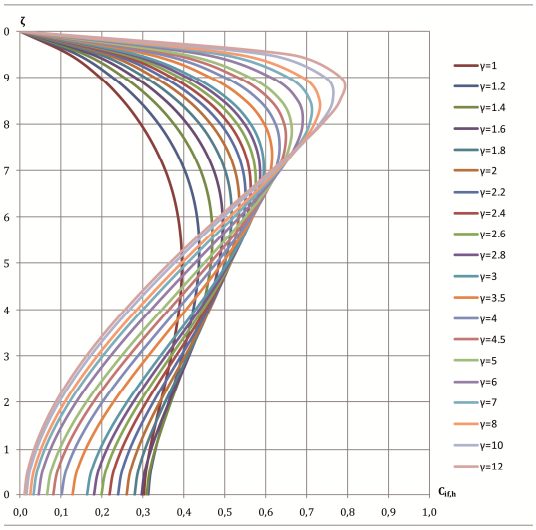

Fig. 6: Normalized flexible impulsive pressure $C_{if,h}$.

The participation factor for the flexible impulsive pressure $\Gamma_{if,h}$, which is specified in equation (7), can be tabulated as well, assuming that the tank wall is constant and the tank mass is insignificant.

CONCLUSION

This paper provides guidance for the implementation of normative demands for the seismic design of liquid filled tanks. With the tabulation of different factors the cumbersome mathematical formulas for calculating the load components are avoidable, which allows an easy load generation for finite element analysis.

References

Cornelissen, P., (2010). Erarbeitung eines vereinfachten impulsiv-flexiblen Lastansatzes für die Berechnung von Tankbauwerken unter Erdbebenlast. Diplomarbeit, Fakultät für Bauingenieurwesen, RWTH Aachen

DIN EN 1998-1, (2010). Auslegung von Bauwerken gegen Erdbeben – Teil 1: Grundlagen, Erdbebeneinwirkungen und Regeln für Hochbauten, Deutsche Fassung EN 1998-1:2004+AC:2009, Deutsches Institut für Normung (DIN), Berlin

DIN EN 1998-4, (2007). Auslegung von Bauwerken gegen Erdbeben – Teil 4: Silos, Tanks und Pipelines, Deutsche Fassung EN 1998-4:2006, Deutsches Institut für Normung (DIN), Berlin

Fischer, F.D., Rammerstorfer, F.G., Scharf, K., (1991). Earthquake Resistant Design of Anchored and Unanchored, Liquid Storage Tanks under Three-Dimensional Earthquake Excitation. In: *Structural Dynamics* (G.I.). Springer Verlag, 317-371, ISBN 3-540-53593-4

Holtschoppen, B., Cornelissen P., Butenweg, C., Meskouris, K., (2011). Vereinfachtes Berechnungsverfahren zur Berücksichtigung der Interaktionsschwingung bei flüssigkeitsgefüllten Tankbauwerken unter seismischer Belastung. Baustatik Baupraxis 11, Institut für Baustatik, Technische Universität Graz, ISBN 978-3-85125-115-9

Housner, G.W., (1963). The dynamic behaviour of water tanks, Bulletin of the Seismological Society of America, Vol. 53, 381-387

Meskouris, K., Holtschoppen B., Butenweg, C., Park, J., (2010). Seismische Auslegung von Silo- und Tankbauwerken. Festschrift für Prof. Dr.-Ing. Mangering, Universität der Bundeswehr München

Meskouris, K., Hintzen, K.-G., Butenweg, C., Mistler, M., (2011). Bauwerke und Erdbeben. Vieweg und Teubner Verlag

EARTHQUAKE ARCHAEOLOGY

INQUA PALEOSEISMOLOGY AND ACTIVE TECTONICS

GEOLOGICAL CRITERIA FOR EVALUATING SEISMICITY: LESSONS LEARNED FROM THE PO PLAIN, NORTHERN ITALY

Michetti, Alessandro M. (1), Leonello Serva (1), Andrea Berlusconi (1), Livio Bonadeo (1), Fabio Brunamonte (1), Francesca Ferrario (1), Gianfranco Fioraso (2), Franz Livio (1), Giancanio Sileo (1), Eutizio Vittori (3)

(1) Dipartimento di Scienze Chimiche e Ambientali, Università dell'Insubria, Via Valleggio 11, 22100, Como. ITALY. Email: alessandro.michetti@uninsubria.it
(2). CNR, Istituto di Geoscienze e Georisorse, Via Valperga Caluso, 35,10125, Torino. ITALY. E-mail: g.fioraso@csg.to.cnr.it
(3). Dipartimento Difesa del Suolo, Servizio Geologico d'Italia, ISPRA, Via V. Brancati 48, 00144 Roma, ITALY. Email: eutizio.vittori@isprambiente.it

Abstract (Geological criteria for evaluating seismicity: lessons learned from the Po Plain, N Italy): *We compare available literature and new geological and paleoseismological data, in particular from the Monte Netto - Brescia site, to maintain that A) strong earthquakes similar to the intensity IX to X MCS - M6.5 to 7 - historical events occurred in 1117 and 1222, though very rare, must be considered unlikely but credible events along virtually all the Quaternary faults throughout the whole Po Plain Foredeep, at least until we learn from geological and geophysical studies how/if the Quaternary tectonic structures near Lake Garda are truly different from those in other areas such as, for example, the Turin Hills, Monferrato, Insubria or around Piacenza, B) the late Quaternary (and especially Holocene) history of deformation and the local seismic landscape are far more valuable tools in estimating seismic hazard than has generally been appreciated until now in Italy – as well as in most parts of the world. The lack of significant earthquakes for 8 centuries in the Garda region and for longer elsewhere must prompt an effort to much deeper understanding of the actual seismic potential in one of the most populated and economically developed areas of Europe.*

Key words*: Paleoseismology, late Quaternary tectonics, Po Plain, Seismic Hazard*

INTRODUCTION

In the field of paleoseismology and earthquake hazard assessment, the year 2011 has been characterized by two "unexpected" destructive events, the Christchurch eq. in New Zealand and the Tohoku eq. in Japan. In particular, the devastating impact from the March 11, 2011, M9 Tohoku coseismic environmental effects – and of course in particular the massive tsunami – is definitely bound to deeply influence the standards for seismic hazard assessment worldwide for decades.

In fact, these events have clearly shown that "the most important contribution to the understanding of long term seismicity, which is critical to the siting and design of safe structures and to the establishment of realistic building codes, is to learn more – region by region – of the late Quaternary history of deformation". This of course includes the evidence for paleoseismicity. This is a quote from Allen (1975), a paper that has inspired also the title of this note. A retrospective look to the origin of the science of Paleoseismology is surprisingly instructive today, while we are still shocked by the effects of the 2011 catastrophic seismic crises.

The purpose of the present note is to argue that the approach discussed by Allen (1975), and further developed – among others – by Serva (1996) and Michetti et al. (2005) with the introduction of the notion of seismic landscape, is definitely validated not only by the investigations conducted before and after the 2011 events in New Zealand and Japan, which are seismically very active countries, but also by the lessons learned during the 4 decades of seismotectonic studies in the Po Plain, in Northern Italy, one of the most populated and developed areas of Europe, hosting a substantial portion of the Italian industrial production, many infrastructures and a number of high risk plants.

From historical seismicity studies we know that the Po Plain, near Lake Garda, has been hit by two strong earthquakes in the XII – XIII centuries, the January 13, 1117, Verona, and Christmas 1222, Brescia, events, both in the range of intensity IX-X MCS, equivalent to M6.5 to 7 (Fig. 1). No other comparable earthquakes have occurred since than in the Central-Western Po Plain region.

We use available literature and new geological and paleoseismological data to maintain that A) strong earthquakes similar to the Verona and Brescia must be considered credible events – though unlikely – along virtually all the Quaternary faults throughout the Po Plain Foredeep, at least until we understand from geological and geophysical studies if/how the Quaternary tectonic structures near Lake Garda are truly different from those in other areas such as in the Turin Hills, Monferrato, Insubria or around Piacenza (Figs. 1 and 2), B) the late Quaternary (and especially Holocene) history of deformation and the local seismic landscape are far more valuable tools in estimating seismicity and associated seismic hazard than has generally been appreciated until now in Italy - like in most parts of the world, and C) the "absence of evidence" for historical or instrumental strong/large

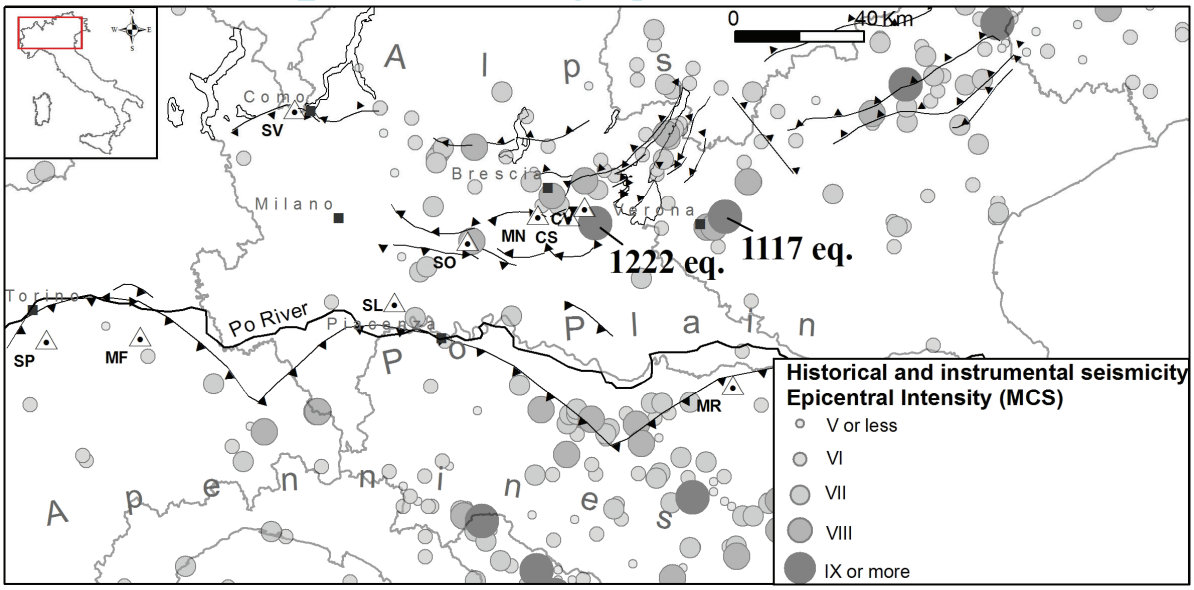

Fig. 1: Historical and instrumental earthquakes catalogue (modified from CPTI, 2004) and map of Quaternary capable faults in the Po Plain (after Livio et al., 2009). SP, Superga; MF, Monferrato; SV, Spina Verde; SL, San Colombano al Lambro; MN, Monte Netto; CV, Ciliverghe; CS, Castenedolo; MR, Mirandola; SO, Soncino.

seismic events within a region should never be construed as "evidence of absence" of seismic hazard, unless systematic and specific paleoseismic analyses have been conducted in that region.

Indeed, in the past decade our knowledge about the magnitude and rates of the key geomorphic agents which control the late Quaternary landscape evolution of the Po Plain and surrounding piedmont belts (along the margins of the Apennines to the S, and the Southern Alps to the N), has greatly improved. In particular, due to the large amount of novel information on the active tectonics and seismic potential of this region, it has become increasingly clear the role played by strong seismic events in this process.

As already pointed out in the literature (e.g., Desio, 1965; Carraro et al., 1995), both the Apennines and the Southern Alps piedmont belts are characterized by Quaternary tectonic features, i.e. drainage anomalies, isolated hills (e.g., Superga, Spina Verde,

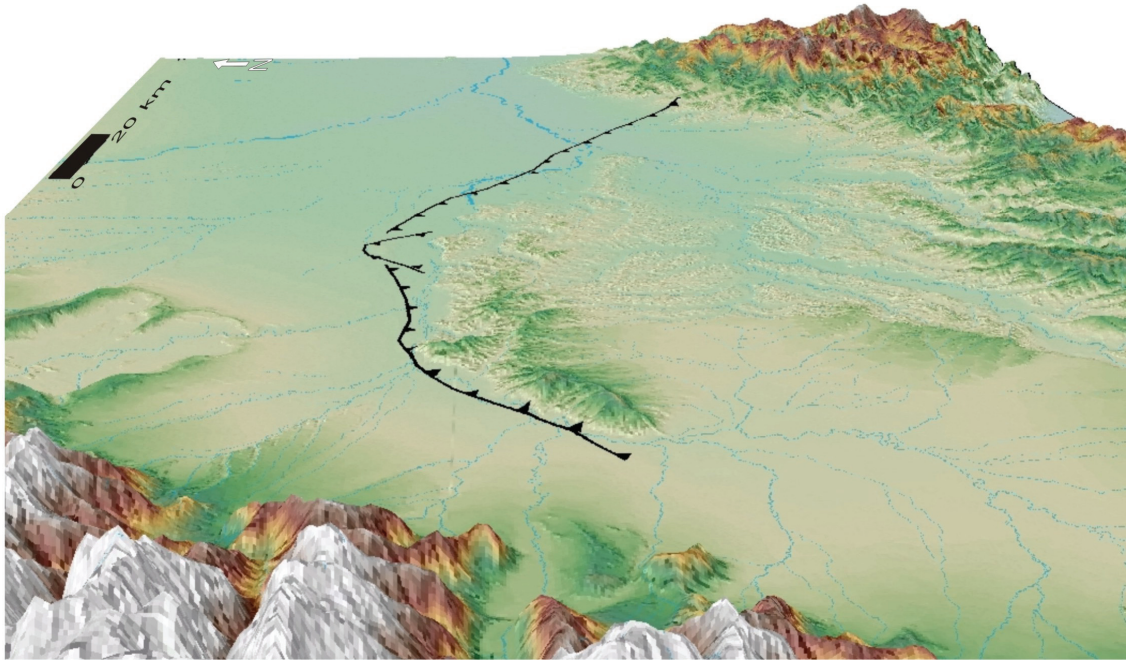

Fig. 2: Digital Elevation Model of the Superga and Monferrato Hills (vertical exaggeration 5x).

San Colombano, Figs. 1 and 2), and buried structural highs (e.g., Soncino, Mirandola), evidence of the Quaternary growth of the two mountain belts beneath the Po Plain. However, only in the past decade, thanks to the integrated research conducted by the University of Insubria and partners (ISPRA-Geological Survey of Italy, ENI E&P, UCL London, Colorado University-Boulder, Innsbruck University, Università Statale di Milano, Università di Brescia, INGV, CNR Torino, Regione Lombardia) it has been possible to study the first paleoseismic site showing evidence for repeated latest Pleistocene to Holocene compressional surface faulting earthquakes along the Monte Netto Backthrust, Brescia (Livio et al., 2009; Figs. 3 and 4). At this site, 3 paleoseismic events have been recorded in the past ca. 40 kyr B.P. Based on trench data and geomorphic investigations, the magnitude estimated for these events is consistent with the earthquake size of the Christmas 1222 Brescia event (M6.2 to 6.8; e.g., Serva, 1990; Guidoboni & Comastri, 2005).

It is important to note that this result has been possible only due to the availability of extensive oil exploration subsurface data (seismic reflection and deep stratigraphic boreholes, courtesy of ENI E&P); and large quarry excavations at Monte Netto site, which provided outstanding exposures of late Quaternary growth anticlines, bending moment surface faulting, and coseismic liquefaction (data and site access courtesy of Fornaci Laterizi Danesi SpA).

In fact, the Monte Netto structure is a unique case study in the Po Plain. Which is logic in a sense, due to i) the moderate seismicity level of this tectonic province, ii) the local high erosional and depositional rates compared to slip rates of capable faults, iii) the need for expensive investigations (seismic reflection profiles, boreholes, trenching, dating) due to the reverse style of faulting, and a geomorphic and human environment unfavorable to paleoseismic analyses.

Literature data and our ongoing research strongly suggest that several Quaternary structures in the Po Plain share the same tectonic and geomorphic features of the Monte Netto Backthrust. However, virtually no comparable paleoseismic information and detailed structural characterization is available for these structures.

DISCUSSION

We are systematically investigating the structural features and evidence for capability along the Quaternary faults in Figure 1; to be scientifically prudent, at present we cannot rule out that many of these faults are able to generate earthquakes similar to the Verona and Brescia Middle Age events. So, in view of the difficulties in interpreting the historic record from Middle Age events, and the lack of detailed paleoseismic information for most of the structures showing some evidence for capability, we stress the need to be exceedingly conservative in estimating the probability of major damaging earthquakes in the Po Plain. “We have been surprised too often in the past, and we cannot afford to be surprised too many times in the future” (Allen, 1975); this must be the case for the Po Plain, point made even more clear after the Japan and New Zealand experience in 2011, where, it must be said, the basic knowledge was seemingly much better.

The Po Plain hosts one of the most industrially developed areas in the world, and like in many other “megacities” located in seismically active regions, every year the seismic risk keeps growing up, with more and more serious societal effects to be expected. The Po Plain has not been the subject of an intensive seismotectonic research effort since the end of the Italian Nuclear Program more than 20 years ago (e.g., Serva, 1990). The state of the art in paleoseismology, and the seismic events of 2011, demonstrate that our conservatism is scientifically sound. The lack of events in the last 8 centuries in

Fig. 3: Decametric Late Quaternary growth anticline at the Monte Netto site. Note the gravity graben due to due to bending moment normal faulting on the fold crest; new exploratory trenching across this graben revealed 3 paleoseismic surface faulting events in the past 40 kyr B.P. The coseismic liquefaction shown in Figure 4 is located near the core of the anticline, indicated by the person for scale.

the Garda region and longer (how much?) elsewhere must not indulge us to optimism, but, on the contrary, warn us to get prepared, how unlikely a M6-7 seismic event can be. As a matter of fact, siting and design of safe structures, and realistic building codes for the Po Plain should be based on a much better understanding of the long term seismicity, that is on the detailed knowledge of the late Quaternary history of deformation and Holocene paleoseismicity. This is the kind of knowledge revealed by the new data collected at the Monte Netto site, as of yet basically the only paleoseismic site available in the region.

Fig. 4: Monet Netto site, liquefaction feature near the core of the anticline described in Figure 3.

Acknowledgements: This work has been partly funded by Project S1 INGV-DPC 2007-2009; and by grants from the Operational Programme Cross Border Cooperation IT / CH 2007-2013 – project "SITINET: census, networking and development of geological and archaeological sites" ID 7621984.

References

Allen, C., (1975), Geological criteria for evaluating seismicity. *Geological Society of America Bulletin*; 86 (8), 1041-1057; DOI: 10.1130/0016-7606

Desio, A., (1965), I rilievi isolati della Pianura Lombarda ed i movimenti tettonici del Quaternario. *Rendiconti Istituto Lombardo Accademia Scienze e Lettere, Sez. A*, 99, 881-894.

Carraro, F., G. Collo, M.G. Forno, M. Giardino, F. Maraga, A. Perotto & D. Tropeano, (1995), L'evoluzione del reticolato idrografico del Piemonte centrale in relazione alla mobilità quaternaria. In: R. Polino & R. Sacchi, Eds., Atti del Convegno Rapporti Alpi-Appennino e guide alle escursioni, Peveragno (CN), 31 maggio - 1 giugno 1994, Accademia Nazionale delle Scienze detta dei 40, 1995 - XII, 441-465.

Guidoboni, E. & A. Comastri, (2005), Catalogue of earthquakes and tsunamis in the Mediterrean area from the 11th to the 15th century. 1037 pp., SGA Storia Geofisica Ambiente srl, Bologna.

Livio, F., A. Berlusconi, A.M. Michetti, G. Sileo, A. Zerboni, L. Trombino, M. Cremaschi, K. Mueller, E. Vittori, C. Carcano, & S. Rogledi, (2009), Active fault-related folding in the epicentral area of the December 25, 1222 (Io = IX MCS) Brescia earthquake (Northern Italy): seismotectonic implications. *Tectonophysics*, 476 (1-2), 320-335, doi:10.1016/j.tecto.2009.03.019

Michetti A.M., F. Audemard & S. Marco, (2005), Future trends in paleoseismology: Integrated study of the seismic landscape as a vital tool in seismic hazard analyses. Tectonophysics, 408 (1-4), 3-21.

Serva, L., (1990). Il ruolo delle Scienze della Terra nelle analisi di sicurezza di un sito per alcune tipologie di impianti ad alto rischio. Il terremoto di riferimento per il sito di Viadana (MN). *Bollettino Società Geologica Italiana*, 109 (3), 375-411.

Serva, L., (1996), Criteri geologici per la valutazione della sismicità: considerazioni e proposte. *Atti dei Convegni Lincei* 122, "Terremoti in Italia", Accademia Nazionale dei Lincei, 1-2 Dicembre 1994, Roma, pp. 103-116.

ANCIENT SEISMITES AS GEODYNAMICAL INDICATOR: APPROACH TO CONSTRUCT A REACTIVATION EVENT ON THE MAIN BOUNDARY THRUST IN THE HIMALAYAN REGION

Mishra, Anurag (1), D.C. Srivastava (2), Jyoti Shah (3)

(1) Department of Earth Sciences, Indian Institute of Technology, Roorkee, Haridwar, Uttarakhand-247667.
Email: anurag2009iitr@gmail.com

Abstract: *Diversified soft-sediment deformation structures exposed in the nearest vicinity of the Main Boundary Thrust in the South-eastern Kumaun Himalaya, show progressive increase in abundance and complexity towards the thrust. After establishing liquidization as dominant deformation mechanism, a whole to part study has been done to identify most possible triggering process, excluding all the other probable processes, integrating criteria based approaches in combination. The structures show their development due to seismic origin, hence called as seismites, define a clear relationship with the Main Boundary Thrust. Magnetostratigraphic dates of the associated sediments show 4-5 Ma as the age of development of the structures. Hence these structures, acting as geodynamical indicator, show paleoseismicity of the area, and dates back a reactivation event on the Main Boundary Thrust in the Kumaun Himalaya around 4-5 Ma, when established age for the formation of this thrust is around 11 Ma.*

Key words*: Soft-sediment deformation structures, seismites, Main Boundary Thrust*

INTRODUCTION

The Alpine-Himalayan orogeny originating in the late period of the Mesozoic era led to development of a series of orogen scale detachment boundaries, named as the South Tibet Detachment Zone, the Main Central Thrust, the Main Boundary Thrust and the Main Frontal Thrust *(Fig. 1a*) from North to South (Jackson and Bilham, 1994).

The Main Boundary Thrust gains importance due to recent active seismicity of the thrust causing catastrophic earthquakes and accommodation of large scale crustal shortening along the thrust (Nakata, 1989). But the dating of the Main Boundary Thrust has not been given much consideration in previous works in comparison to all the other boundary thrusts, perhaps due to poor exposures and lack of cross-cutting relationships. The available dates for the formation of thrust do not converge perhaps due to ambiguous relation between the activity of the thrust and applied methods, such as one of the date suggest it's development before 11 Ma whereas another younger than 5 Ma (Yin, 2006). Most of the available dates for the activity of the Main Boundary Thrust are largely based on study of change in depositional pattern in the Himalayan Foreland and study of exhumation based on rate of subsidence of the Himalayan Foreland. It is presumed that exhumation is directly incorporated with the uplift in the hanging wall of the Main Boundary Thrust. But the Main Boundary Thrust is Southerly of the Thrusts cutting through the Himalaya, and exhumation can be related with any of the Northerly thrust cutting through the rocks.

The soft-sediment deformation structures of seismic origin are called as seismites (Seilacher, 1969). They have been used for understanding geodynamic activity of causative seismogenic faults and paleoseismicity of an area.

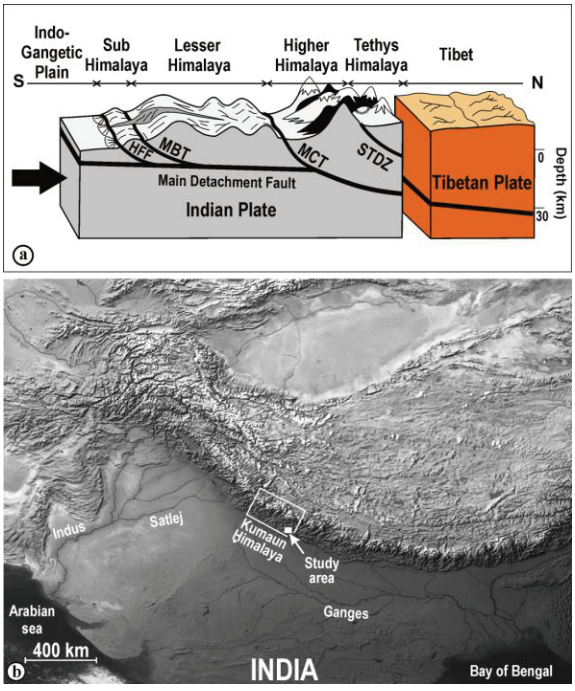

Fig. 1: (a) Litho-tectonic units and demarcating boundaries in the Himalayan terrain. (b) Satellite imagery showing Himalayan terrain, location of Kumaun Himalaya and our study area.

We use the soft-sediment deformation structures exposed in the vicinity of the Main Boundary Thrust for constraining one of the movement events along the thrust, in case they are seismites and show an undisputed relationship with the Main Boundary

Thrust. We follow a 3 fold-process: To classify these structures, to understand their origin in terms of deformation mechanism, driving force system and triggering agent, and finally finding out possible relationship with the Main Boundary Thrust.

OBSERVATIONS

A large variety of the soft-sediment deformation structures are abundantly exposed in the vicinity of the Main Boundary Thrust in the southeastern Kumaun Himalaya *(Fig. 1b*). The structures identified in the area are the deformed cross-stratifications, the liquefaction pockets, the slump folds, the mushroom structures, the convolute laminations, the sand dykes, the synsedimentary faults, the fluid-escape structures and the flame structures.

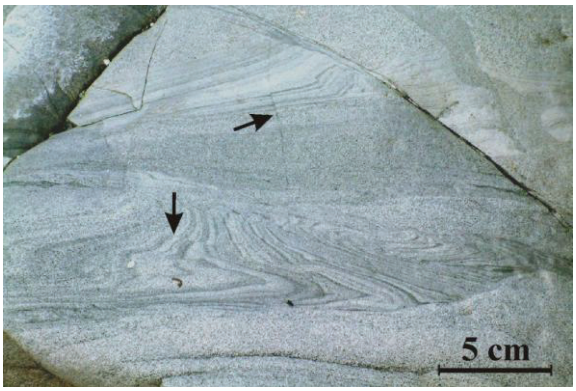

Fig. 2: Recumbent cross-stratification in sandstone. Arrows point to minor faults cutting through the liquefied laminations. Note the fluid-escape structure in the right-upper part originating from the liquefied bed below.

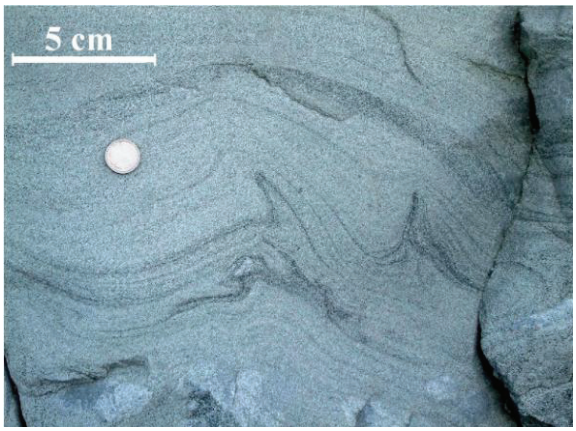

Fig. 3: Typical convolute laminations in sandstone

The recumbent cross-stratifications show well preserved laminations and thickness of individual laminae varies throughout the structure *(Fig. 2*). Most plausible explanation for their development is deformation of liquefied sediments due to current drag, as foresets are folded towards paleocurrent direction (Allen and Banks, 1972, Allen, 1982). The minor faults are developed due to cohesive nature of sediments, when grain to grain packing established after liquefaction (Owen, 1987, 1996).

The convolute laminations developed in medium to fine grained sandstone lithology *(Fig. 3).* Folded laminations, thicker at the crest and thinner at the trough show that sediments became hydro-plastic in nature during development of these structures *(Fig. 4).* At the crest, the laminations are blurred and show homogenization of sediments *(Fig. 4).*

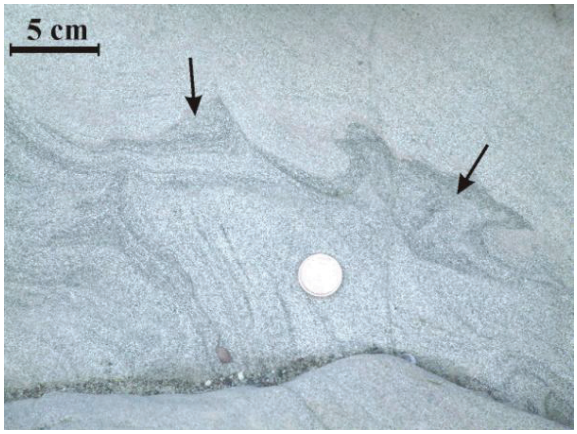

Fig.4: Convolute lamination in relatively medium grained sandstone. Arrows show blurring of laminations and homogenization of sediments.

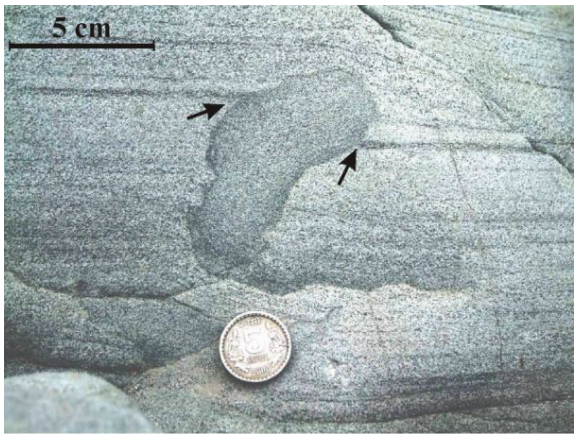

Fig. 5. Liquefaction pocket in sandstone. Arrows mark the offset in laminations.

Liquefaction pockets are developed due to complete homogenization of sediments and obliteration of primary structures *(Fig. 5)* by liquefaction within the local pockets of few centimeters (Lowe, 1975). Laminations are offset along these pockets *(Fig. 5).*

Sand dykes developed due to intrusion of coarse-grained sandstone upward, originated by drag force of fluids *(Fig 6 and Fig. 7)*. Their origin is well established and related to fluidization.

Mushroom structures developed due to fluidization in the upward regime, called as elutriation, by which a plume type *(Fig. 8)* of forceful injection took place, aligning clay minerals in the neck connected to the clay enriched dome shaped main body (Lowe, 1975, Allen, 1982).

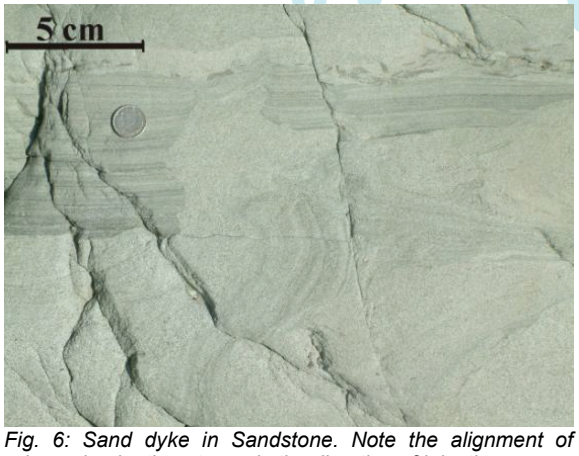

Fig. 6: Sand dyke in Sandstone. Note the alignment of primary laminations towards the direction of injection.

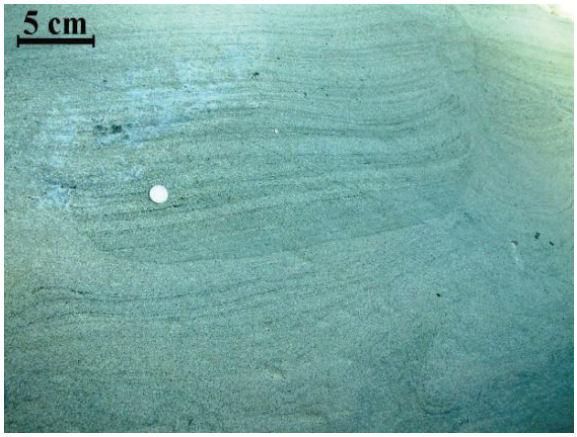

Fig. 7. Multiple sand dyke system in medium-grained sandstone. Note the reorientation of parallel laminations due to drag of upward sand injection. A synsedimentary fault is cutting through the parallel laminated sandstone and sand dyke.

Fig. 8. Two classes of mushroom structures in medium grained sandstone. In left photograph, the upper domal part is detached from the main body, whereas in the right one it is connected through a narrow neck. Notice the darkening of structure in compared to surrounding lithology and warping and folding of surrounding laminations (shown by arrow)

Their development indicates requirement of instant force, so that elutriation and sudden expulsion could take place. The best possible originating force for these structures is seismic shaking, as there is no difference in grain size between injecting and injected body, and these structures are confined within undeformed horizons.

Fluid escape structures *(Fig. 9)* are developed due to expulsion of fluids to surrounding beds of same comparable lithology due to any of the processes that causes extraction of fluids from the beds such as liquefaction, fluidization or compaction of sediments.

Fig. 9. Fluid escape structures in sandstone

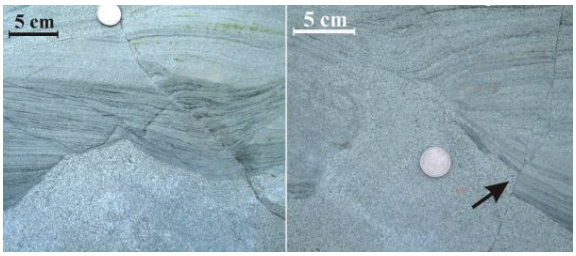

Fig. 10. Syn-sedimentary faults in sandstone. Notice the geometry of faults.

Several variably oriented planar or listric synsedimentary faults *(Fig. 10)* developed that cut through the soft-sedimentary deformation structures. Compaction may be one of the plausible mechanisms for the development of these structures, but observing the insufficient thickness of overburden, large scale offset of many faults and superposition on earlier phases of fluidized structures, seismic activity seems to be most possible cause.

DISCUSSION

Liquefaction and fluidization are the most dominant deformation mechanisms for development of these structures. Triggers such as groundwater movement, rapid sediment deposition, storm waves, meteoritic impact and earthquake shocks can be responsible for the development of the soft-sediment deformation structures (Van Loon and Brodzikowski, 1987). We follow the criteria given by Sims (1973), Owen and Moretti (2011) and Owen et al. (2011) for identifying the trigger of these structures. These structures are confined within rocks of varied lithology such as, in several varieties of sandstone and in mudstone-marlstone beds. This indicates the probability of out

of system, allogenic trigger for the development of these structures. Rapid sedimentation cannot be a cause of development as magnetostratigraphic dating reveals same rate of sedimentation throughout the area (Kotalia et al., 2001). Storm waves can be neglected due to established fluviatile origin of these sediments (Tandon, 1976). We suggest seismic origin, after excluding all the probable triggers. Our inference gets more strength as it fits on criteria based approaches and gives several evidences for approval, given in the following lines:

1) The structures confined within the same stratigraphic horizons, follow these beds for a sufficient lateral extent of about more than 2 km in linear tract in the nearest vicinity of the Main Boundary Thrust.
2) These are confined within cohesionless loose and friable sediments that are potentially liquefiable.
3) These structures are comparable with the structures developed in seismic shaking experiments.
4) The structures are exposed in the vicinity of the Main Boundary Thrust that is one of the most seismically active thrusts in the Himalayan Terrain.
5) Several small scale structures such as minor faults in the recumbent-cross stratification are developed.
6) Mushroom structures are very suggestive for seismic trigger.
7) Frequent occurrence of faults with liquefied structures indicates need of instant shaking as soon as the grain to grain contact develops that suggest possible seismic origin.

It is generally agreed that seismic activity of not less than 5.5 magnitude on Richter scale can possibly be recorded in sediments, as seismites (Ambraseys, 1988). Hence this event shows an earthquake event of at least 5.5 magnitude on Richter scale. Two phases of seismic trigger has been established on the basis of overprinting of structures. The sand dyke representing the fluidization of one phase must has been developed earlier than synsedimentary fault of second phase cutting through it, that shows brittle nature of origin *(Fig. 10)*.

Confined within the 4-5 Ma horizon (Kotalia et al., 2001), the soft-sedimentary deformation structures increase in abundance and, towards the Main Boundary Thrust. As the development of the Main

Boundary Thrust occurred c. 10-11 Ma. (Miegs et al., 1995). Hence, it is evident that the ancient seismites, discussed in this article, are related to the 4-5 Ma old reactivation event on the Main Boundary Thrust.

Acknowledgements: I express my thanks to conference organizers for giving me chance to present my work.

References

Allen, J.R.L., Banks, N.L., 1972. An interpretation and analysis of recumbent-folded deformed cross-bedding. Sedimentology 19, 257-283.

Allen, J.R.L., 1982. Sedimentary Structures: their character and physical basis. Development in Sedimentology. Vol. 30. Elsevier, Amsterdem. 663 pp.

Ambraseys, N.N., 1988. Engineering seismology. Earthquake Engineering Structural Dynamics 17, 1–105.

Jackson, B., Bilham, R., 1994. Constraints on Himalayan Deformation Inferred from the vertical velocity fields in the Nepal and Tibet. Journal of Geophysical Research 99 (B7), 13897-13,912.

Kotalia, B.S., Nakayama, K., Bhalla, M.S., Phartiyal, B., T. Kosake, 2001. Lithology and magnetic stratigraphy of Lower-Middle Siwalik succession between Kathgodam and Ranibagh, Kumaun Himalaya. Journal Geological Society of India 58, 411-423.

Lowe, D.R., 1975. Water escape structures in coarse-grained sediments. Sedimentology 22, 157–204.

Miegs, A. J., Burbank, D. W., Beck, R. A., 1995. Middle late-Miocene (>10 ma) formation of the main boundary thrust in the western Himalaya. Geology. 23, 423-426.

Nakata, T., 1989. Active faults of the Himalaya of India and Nepal. Geological Society of America. Special paper. 232, 243-264.

Owen, G., 1987. Deformation processes in unconsolidated sands. In: Jones, M.E., Preston, R.M.F. (Eds.), Deformation of Sediments and Sedimentary Rocks, Geological Society of (London) Special Publication. No. 29, pp. 11–24.

Owen, G., 1996. Experimental soft-sediment deformation structures formed by the liquefaction of unconsolidated sands and some ancient examples. Sedimentology 43, 279–293.

Owen, G., Moretti, M., 2011. Identifying triggers for liquefaction-induced soft-sediment deformation in sands. Sedimentary Geology 235, 141-147.

Owen, G., Moretti, M., Alfaro, P., 2011. Recognising triggers for soft-sediment deformation: current understanding and future directions. Sedimentary Geology 235, 133-140.

Seilacher, A., 1969. Fault-graded beds interpreted as seismites. Sedimentology 13, 155–159.

Sims, J.D., 1973. Earthquake-induced structures in sediments in Van Norman Lake, San Fernando, California. Science 182, 161–163.

Tandon, S.K., 1976. Siwalik sedimentation in a part of Kumaun Himalaya. Sedimentary Geology 16, 131–154.

Van Loon, A.J., Brodzikowski, K., 1987. Problems and progress in the research on soft sediment deformations. Sedimentary Geology 50, 167–193.

Yin, A., 2006. Cenozoic evolution of the Himalayan orogen as constrained by along-strike variation of structural geometry, exhumation history, foreland sedimentation. Earth Sciences Reviews 76, 1-131.

SAMPLING BIASES IN THE PALEOSEISMOLOGICAL DATA

Mouslopoulou Vasiliki (1,2), Andrew Nicol (3), John J. Walsh (1), John G. Begg (3), Dougal B. Townsend (3), Dionissios T. Hristopulos (2)

(1) Fault Analysis Group, University College Dublin, Dublin 4, Ireland. Email: vasiliki@mred.tuc.gr, john@fag.ucd.ie
(2) Dpt. of Mineral Resources Engineering, Technical University of Crete, 73100, Greece. Email: dionisi@mred.tuc.gr
(3) GNS Science, PO Box 30368, New Zealand. Email: a.nicol@gns.cri.nz ; j.begg@gns.cri.nz ; d.townsend@gns.cri.nz

Abstract (Sampling biases in the paleoseismological data): *The recent earthquakes in Christchurch, New Zealand, show that active faults, capable of generating large-magnitude earthquakes, can be hidden beneath the Earth's surface. Here we combine near-surface paleoseismic data with deep (<5 km) onshore seismic-reflection lines to identify sub-resolution active faults and to explore the relations between fault growth over short (<27kyr) and long (>1Ma) timescales in the Taranaki Rift, New Zealand. Displacement rates vary temporally on individual faults by in excess of an order of magnitude over timescales of thousands to millions of years. These changes are attributed to fault interactions rather than to changes in regional strain rates. During the Holocene fault displacement rates were both faster (~50%) and slower (~50%) than their million-year averages. The short-term fault data are incomplete and biased towards the faults that have moved fastest during the Holocene. The integration of different timescale datasets provides a basis for identifying active faults not observed at the ground surface, estimating maximum fault-rupture lengths, inferring maximum short-term displacement rates and improving earthquake hazard assessment.*

Key words*: rift, paleoearthquakes, fault-trenching, seismic-reflection data*

INTRODUCTION

Analysis of active faulting at, or near, the ground surface may provide a useful record of surface-rupturing earthquakes on individual faults. This record can be incomplete for faults with low displacement rates (<0.5 mm/yr), and where the time-window of observation is similar to, or less than, the time intervals between large earthquakes. Assessing the level of completeness may have implications for earthquake hazard assessment and for determining whether longer-term displacement rates are representative of the paleoearthquake record.

Characterising a small fraction (e.g., < 20 kyr) of the growth history of a single fault is common (e.g., Schwartz & Coppersmith, 1984; Weldon et al., 2004; Palumbo et al., 2004; Nicol et al., 2006), however, assessing both its short- (<27 kyr) and long-term (>1 Ma) growth patterns is rare. The Taranaki Rift, New Zealand, provides a unique opportunity to quantify and compare displacements accumulated on individual faults over timescales that range from individual earthquakes to millions of years. In this paper, we compare high-quality trench (short-term) and seismic-reflection (long-term) data for faults in the rift. This information has been used to examine temporal changes in displacement rates and sampling biases in short-term (<27 kyr) paleoseismic data. The implications of these temporal changes in rates and the sampling biases for seismic hazard assessment are considered.

GEOLOGICAL SETTING AND FAULT DATA

The Taranaki Rift extends for about 350 km within the Taranaki Basin, which is mainly west of the North Island, New Zealand (Fig. 1, inset) (Townsend et al., 2010). The rift is part of a back-arc basin, forming in association with subduction of the Pacific Plate beneath the Australian Plate along the Hikurangi margin (Fig. 1, inset) (Giba et al., 2010). The Taranaki Rift traverses Taranaki Peninsula where it comprises multiple active fault traces at the ground surface that strike NE-SW (Fig. 1). The rift is 30-50 km wide and accommodates extension rates of 1-2 mm/yr. The present rifting phase commenced in the

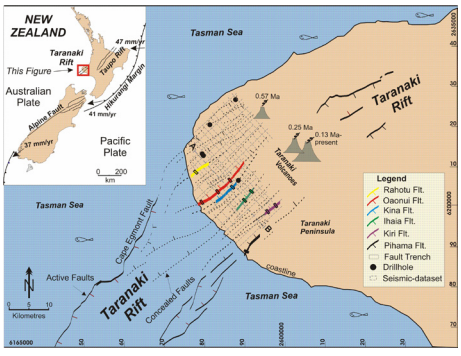

Fig. 1: Fault-map of the Taranaki Rift. Onshore faults that rupture the ground surface are colour-coded and offshore active faults are indicated with black solid lines. Concealed faults onshore are also shown by black dashed lines. The seismic-reflection lines and five wells used in this study are indicated with grey dashed lines and black filled circles, respectively. The locations of fault-trenches are indicated by the black rectangles. Late Quaternary volcanic activity on the peninsula is highlighted. Inset: shows study area location and subducting Pacific Plate east of the North Island of New Zealand.

Pliocene (3-4 Ma) and has produced kilometre-scale cumulative displacements on normal faults (Nicol et al., 2007; Giba et al., 2010; Mouslopoulou et al., In review), active faulting at the ground surface (Townsend et al., 2010; Mouslopoulou et al., in review) and historical seismicity (Sherburn & White, 2006).

Crustal extension is also accompanied by widespread Late Quaternary (≤0.57 Ma) volcanism on the Taranaki Peninsula. The most recent phase of volcanic activity started about 100 ka (last eruption ca. 250 years ago) and resulted in the formation of the impressive volcanic cone of Mt. Taranaki. Although Mt. Taranaki rises to 2518 m above sea-level (a.s.l.) and dominates the landscape, studies show no direct link between the timing of prehistoric large-magnitude earthquakes in the rift and volcanic eruptions or episodes of cone collapse (Townsend et al., 2010).

Here we combine seismic-reflection and trench data for individual faults to chart their growth in displacement through time. Two-dimensional (2D) seismic-reflection lines occupying the southwest of Mt. Taranaki, extend across the entire onshore width of the rift and in a rift-parallel direction for about 20 km (Fig. 1). The 2D seismic survey comprises a total of 21 fault-perpendicular and 17 fault-parallel lines spaced at 0.5 to 5 km. These seismic lines image all of the known active faults and provide estimates of ≥0.5 Ma cumulative throws at each of ten trench sites. Seismic reflectors extending to depths of up to ca. 5 km have been tied to five wells (Figs 1 and 2a) in which the stratigraphy was dated using micropaleontology (King & Thrasher, 1996). The six youngest of these seismic reflectors (ca. 0.5, 2, 3, 3.6, 5.5 and 10 Ma) were traced along and across the faults around the grid of seismic lines and provide information on the accumulation of fault displacements during the Plio-Pleistocene. For individual faults in the area of study fault vertical displacements are up to ca. 1.5 km and decrease with reduction in horizon age from 3.6 Ma (Fig. 3a).

The paleoearthquake history of the six active faults with resolvable surface traces is defined by constraints from 10 excavated trenches. Associated trench data permit identification of a total of 23 large paleoearthquakes (M>5.5) that ruptured the ground surface since 27 ka (Fig. 2b). The earthquake record is complete since 5 ka on all six active faults and for 27 kyr on two of these faults. Vertical displacements measured in the trenches range from 0.1 m to 4 m (e.g., Townsend et al., 2010; Fig. 2b) and accrued from earthquakes with single-event displacements of up to 1.2 m. These displacements, which represent point measurements on fault traces (accrued during one or more earthquakes), are supplemented by scarp heights recorded along the lengths of each active trace. Paleoearthquake ages are primarily constrained by ^{14}C dating of near-surface (< 6 m deep) stratigraphy displaced by active faults (Fig. 2b). Further details of the trenching are documented by Townsend et al. (2010).

SAMPLING BIASES

Seismic-reflection lines record many more faults than can be inferred from field mapping of active traces. Thirteen faults displace the 0.5 Ma horizon and clearly extend upwards towards the ground surface (Fig. 2a). Field mapping and interpretation of aerial ortho-photographs suggest that six of these faults have surface scarps up to 4 m high and displace a diachronous landscape mainly ranging in age from ~8 to 27 ka (Fig. 1) (Townsend et al., 2010; Mouslopoulou et al., in review). Trench data confirm that these faults are active and have ruptured the ground surface during large-magnitude prehistoric earthquakes (Figs. 2b) (Townsend et al., 2010). The remaining seven faults that displace the 0.5 Ma horizon generally have large cumulative displacements (>1000 m throw) and also displace near-surface horizons (<50m below the ground surface), but yet have no resolvable surface trace and probably last ruptured within the last 100-200 kyr (Fig. 2a). These faults are considered to be active and capable of generating future large-magnitude earthquakes.

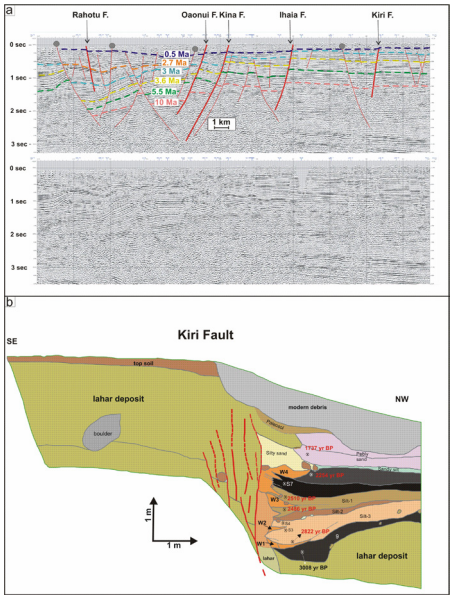

Fig. 2: a) Interpreted (above) and uninterpreted (below) seismic-reflection profile across the transect A-B (for location see Fig.1). Twenty-four normal faults are identified to displace up to six horizons of 0.5-10 Ma in age. The active faults with surface traces and inferred active faults that displace the 0.5 Ma horizon are indicated by arrows and grey circles, respectively. b) Example of trench-log from the Kiri Fault, which has been the fastest moving fault in the Taranaki Rift during Holocene. From the trench-log five earthquakes are inferred to have ruptured the ground surface during the last 3 kyr (see formation of successive colluvial wedges 'W$_i$'). The timing of the earthquakes is constrained by nine radiocarbon (^{14}C)

The lengths of faults in the sub-surface are generally much greater than their equivalent surface-trace lengths. Surface trace lengths for the six active faults range from 1.4 to 13.2 km, while their sub-surface

lengths are generally between 20 and 30 km. Analysis of individual faults suggests that the sub-surface fault lengths are about 2-8 times larger than their equivalent surface traces. Some of this discrepancy arises because fault scarps <1m in height are typically sub-resolution, particularly in areas where local topography is in excess of 1 m, resulting in undersampling of these low fault scarps.

FAULT DISPLACEMENT RATES

Displacement rates in the Taranaki Rift system since 27 ka varies significantly between faults. This variability exceeds one order of magnitude, i.e. from ca. < 0.1 mm/yr on the Oaonui Fault to ca. 1.6 mm/yr on the Kiri Fault. In addition to rates being variable between faults, displacement rates also appear to vary with time on some faults. The Pihama Fault, for example, has undergone two periods of accelerated growth (22-27 and 0-13 ka) which are separated by a ~10 kyr time interval of relative seismic quiescence.

Million-year displacement rates range from ca. 0.025 to 0.2 mm/yr for the active faults. On individual faults these rates varied temporally since their inception at ~3.6 Ma. The majority of active faults in the rift experienced accelerated displacement rates between 3.6 and 2.7 Ma up to four times faster than their subsequent rates. This ~1 Myr increase in displacements rates on most onshore faults in the rift is interpreted to reflect an increase in regional strain rates.

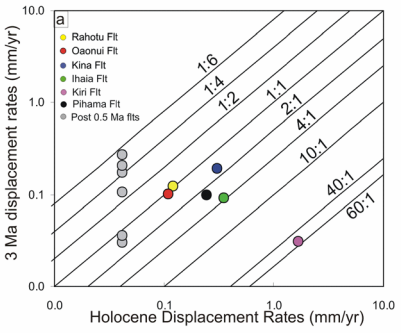

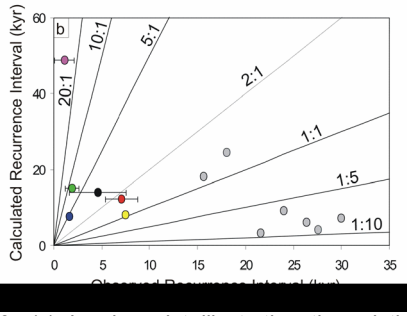

Fig. 3: (a) Log-log plot illustrating the relationship between post-27 kyr and 3.6 Ma displacement rates for each fault in the rift that ruptured the ground surface and the 0.5 Ma horizon. Maximum post-27 kyr rates for the latter faults are calculated assuming that they have displaced the ground surface by 1 m (maximum possible sub-resolution throw) divided by the maximum age of the ground surface (i.e., 27 kyr). (b) Plot comparing the observed (in trenches) earthquake recurrence interval with that calculated for each active fault in the system based on the Wells & Coppersmith (1994) relation. Faults that displace the 0.5 Ma horizon are also included for comparison.

Comparison of tens of thousand years (<27 kyr) and million-year (e.g., averaged since 3.6 Ma) displacement rates for each fault with a resolvable active trace suggests that they all accrued displacement more rapidly in the short-term (Fig. 3a). Most faults with active traces accumulated displacements between two and four times faster during 0 to 27 ka than averaged since 3.6 Ma. The Kiri Fault, which has the lowest displacement rate averaged since the inception of faulting (ca. 3.6 Ma), has moved up to 50 times faster recently compared to its million-year rate (Fig. 3a). By contrast, the Oaonui Fault, which appears to be the slowest moving fault in the system since 27 ka, has an average long-term rate at about 72% of the short-term rate (Fig. 3a).

The increase in displacement rates on active faults since 27 ka could be due to increasing single-event displacement and/or to decreasing recurrence intervals between events. Million-year displacement profiles suggest that fault lengths have not changed significantly since 2.7 Ma (Mouslopoulou et al., in review) and, as maximum earthquake slip increases proportionally with length (e.g., Wells & Coppersmith, 1994), maximum slip has probably also remained constant. Therefore, the increase in short-term rate for active faults with observable scarps cannot be attributed to fault propagation with associated increases in single-event displacement.

Comparison of recurrence intervals measured from trench data with estimates based on the long-term average suggests that a decrease in recurrence intervals may contribute to the increase in rates (Fig. 3b). Long-term average recurrence interval estimates were calculated from equation $RI=L*10^{-5}/DR$ of Wells and Coppersmith (1994), assuming characteristic slip per event (DR= average displacement rate since 3.6 Ma; L= subsurface fault length). Data show that for up to 27 ka, earthquakes have ruptured the ground surface along active faults in the rift much more frequently than the estimates based on the million-year displacements, displacement rates and lengths (Fig. 3b). Indeed, trench data suggest that the observed earthquakes have occurred on the active faults in the system up to 30 times (Fig. 3b) more frequently than would be inferred from long-term fault displacement rates.

We suggest that these elevated short-term displacement rates are developed by temporal clustering of earthquakes on individual faults combined with a sampling bias towards faults with the shortest recurrence intervals during the Holocene (Nicol et al., 2009). Earthquake clustering has been documented on many faults globally (Coppersmith, 1989; Sieh et al., 1989; Marco et al., 1996; Weldon et al., 2004; Nicol et al., 2006), and may chiefly result from fault interactions coupled with the inherent complexity of earthquake occurrence on faults (Nicol et al., 2006; Mouslopoulou et al., 2009). Sampling bias arises from our tendency to mainly sample those faults which are better preserved in the landscape,

often through impressive fault scarps (Nicol et al., 2009). These faults are likely to be those which have recently accommodated successive earthquakes (e.g. during the Holocene). This view is supported by seismic reflection lines which show that the number of surface-rupturing faults in the rift is significantly less than the total number of faults in the rift (Figs 1 and 2a). Examination of the buried faults indicates that, in addition to the six ground-rupturing faults, there are at least a further seven faults, including the larger faults in the system, that reach within ~50 m of the modern ground surface and are probably active (i.e. still accruing displacement and capable of producing future ground-rupturing earthquakes). For these additional seven active faults, long-term displacement rates are greater than Holocene rates by up to a factor of five (Fig. 3a). Thus, faults with increased and decreased displacement rates in the Holocene could be present in approximately equal proportions. As a result of these temporal rate changes, the sums of long-term rates on all faults in the system and Holocene displacement rates on the 13 active faults identified are similar (i.e. long-term 3.4±0.5 mm/yr and Holocene 3.1±0.5 mm/yr). This similarity in the sum of the rates over each time interval supports the view that regional rates of extension may not have changed, and that the temporal clustering of earthquakes reflects migration of the locus of fault activity from one fault to another. An important consequence of this migration is that faults which are currently in a relatively quiescent phase of earthquake activity may in the next 10 kyr, for example, become relatively active. Earthquake hazard analysis must take account of these relatively quiescent faults.

CONCLUSIONS

In the Taranaki Rift displacement rates vary temporally on individual faults by in excess of an order of magnitude over timescales of thousands to millions of years. These changes are attributed to fault interactions rather than to changes in regional strain rates. During the Holocene fault displacement rates were both faster (~50%) and slower (~50%) than their million-year averages. Faults moving faster than the long-term average can be identified in the landscape, while those moving slower cannot. The numbers of active faults and their active trace lengths are underestimated by at least 50% using geomorphic mapping of the scarps. Therefore, the number of potential earthquake sources may be significantly higher than it is represented in seismic hazard models. As a result, some future earthquakes will occur on faults that were not previously known to be active. Integration of seismic-reflection with paleoseismic data provides a basis for identifying active faults not observed at the ground surface, estimating maximum fault-rupture lengths and improving earthquake hazard assessment.

Acknowledgements: This research was funded by an IIF Marie Curie Fellowship of the European Community's 7th Framework Program (contract no. PIIF-GA-2009-235931) and an IRCSET (Irish) Postdoctoral Fellowship.

References

Coppersmith, K.J., (1989). On spatial and temporal clustering of paleoseismic events. *Seismological Research Letters* 59, 299-230.

Giba, M., A. Nicol & J.J. Walsh, (2010). Evolution of faulting and volcanism in a back-arc basin and its implications for subduction processes. *Tectonics* 29, doi:10.1029/2009TC002634.

King, P.R. & G.P. Thrasher, (1996). Cretaceous and Cenozoic geology and petroleum systems of the Taranaki Basin, New Zealand. *Institute of Geological & Nuclear Sciences Monograph* 13, 243 p.

Marco, S., M. Stein & A. Agnon, (1996). Long-term earthquake clustering: a 50 000-year paleoseismic record in Dead Sea Graben. *Journal of Geophysical Research* 101, 6179-6191.

Mouslopoulou, V., J.J. Walsh & A. Nicol, (2009). Fault displacement rates on a range of timescales. *Earth and Planetary Science Letters* 278, 186-197.

Mouslopoulou, V., A. Nicol, J.J. Walsh, J.G. Begg, D.B. Townsend & D.T. Hristopulos, (in review). Relations between paleoearthquakes and million year fault growth in an active rift. *Journal of Structural Geology*, 2011.

Nicol, A., J.J. Walsh, K. Berryman, P. Villamor, (2006). Interdependence of fault displacement rates and paleoearthquakes in an active rift. *Geology* 34, 865-868.

Nicol, A., C. Mazengarb, F. Chanier, G. Rait, C. Uruski & L. Wallace, (2007). Tectonic evolution of the Hikurangi subduction margin, New Zealand, since the Oligocene. *Tectonics* 26(4), TC4002. doi:10.1029/2006TC002090.

Nicol, A., J.J. Walsh, V. Mouslopoulou, & P. Villamor, (2009). Earthquake histories and Holocene acceleration of fault displacement rates. *Geology* 37, 911–914.

Palumbo, L., L. Benedetti, D. Bourles, A. Cinque & R. Finkel, (2004). Slip history of the magnolia fault (Apennines, Central Italy) from 36Cl surface exposure dating: evidence for strong earthquakes in the Holocene. *Earth and Planetary Science Letters* 225, 163–176.

Schwartz, D.P. & K.J. Coppersmith, (1984). Fault behavior and characteristic earthquakes: examples from the Wasatch and San Andreas fault zones. *Journal of Geophysical Research* 89, 5681–5698.

Sherburn, S. & R.S. White, (2006). Tectonics of the Taranaki region, New Zealand: earthquake focal mechanisms and stress axes. *New Zealand Journal of Geology and Geophysics* 49, 269–279.

Sieh, K., M. Stuiver & D. Brillinger, (1989). A more precise chronology of earthquakes produced by the San Andreas Fault in Southern California. *Journal of Geophysical Research* 94, 603-623.

Townsend, D., A. Nicol, V. Mouslopoulou, J.G. Begg, R.D. Beetham, D. Clark, M. Giba, D. Heron, B. Lukovic, A. McPherson, H. Seebeck & J.J. Walsh, (2010). Paleoearthquake histories across a normal fault system in the southwestern Taranaki Peninsula, New Zealand. *New Zealand Journal of Geology and Geophysics* 53, 1-20.

Weldon, R., K. Scharer, T. Fumal, G. Biasi, (2004). Wrightwood and the earthquake cycle: what a long recurrence record tells us about how faults work. *GSA Today* 14, 9, 4-10.

Wells, D.L. & K.J. Coppersmith, (1994). New empirical relationships among magnitude, rupture length, rupture width, rupture area and surface displacement. *Bulletin of the Seismological Society of America* 8, 974-1002.

EARTHQUAKES IN AQABA, JORDAN OVER THE PAST 2,000 YEARS: EVIDENCE FROM HISTORICAL, GEOLOGICAL, AND ARCHAEOLOGICAL DATA

Tina M. Niemi (1)

(1) Department of Geosciences, University of Missouri-Kansas City, 5100 Rockhill Road, Flarsheim Hall 420, Kansas City, MO 64110 U.S.A. Email: niemit@umkc.edu

Abstract (Earthquakes in Aqaba, Jordan Over the Past 2,000 Years: Evidence from Historical, Geological, and Archaeological Data): *Aqaba lies at the boundary between the Gulf of Aqaba and Wadi 'Arabah segments of the Dead Sea Fault Zone (DSFZ) and is therefore situated to sustain earthquake damage from rupture of either segment. The rupture history of these fault segments remains rather enigmatic because of the low population density around them throughout history. This paper presents a synthesis of paleoseismic trenching, archaeological excavations, and historicl data and provides a model for the recurrence of earthquakes along the southern DSFZ. Significant periods of active seismicity in the 4th, 7th-8th, 11th-13th, and 15-16th centuries suggest a three- to five-century recurrence rate of faulting of the Gulf of Aqaba and Wadi 'Arabah segments of the DSFZ. It is interesting to note that earthquakes have been coincident with major political transitions that have occurred in this region and thus are likely to have played a significant role in these cultural shifts.*

Key words*: Archaeoseismology, Dead Sea Transform, Jordan, Earthquakes*

INTRODUCTION

The Dead Sea fault zone (DSFZ) is an left-lateral, strike-slip transform plate boundary between the Arabian and Sinai plates (Fig. 1). Earthquakes in the southern 'Arabah and Gulf of Aqaba of Jordan and Israel are created by motion along the DST. The Mw 7.2 Nuweiba earthquake of November 22, 1995 that ruptured a submarine fault in the Gulf of Aqaba (Gulf of Eilat) was the largest earthquake in the modern instrumented era (Hofstetter *et al.,* 2003) along the Dead Sea fault. Most of the significant damage was concentrated in cities in the Sinai Peninsula near the epicenter, but damage was also reported from the Saudi Arabian coastline and the cities of Aqaba, Jordan and Eilat, Israel; both about 70 km north of the epicenter.

Historical earthquake data reported in recent catalogues (Guidoboni, 1994; Guidoboni and Comastri, 2005; Ambraseys, 2009) suggest that the seismic events in A.D. 110-114?, 363, 749, 1068, 1212, 1458, and 1588 likely caused damage in the region of southern Jordan and Aqaba. It is unclear whether events recorded in the Dead Sea region or Jerusalem, such as the earthquakes of A.D. 419, 597, 634, 659, 1293, and 1546, could have also caused damage in Aqaba. Data from earlier catalogues have largely been superseded by more recent catalogue compilations.

The city of Aqaba is situated at the northern end of Gulf of Aqaba along the southern part of the Dead Sea Transform fault system that separates the Sinai and Arabian tectonic plates. Furthermore, Aqaba lies

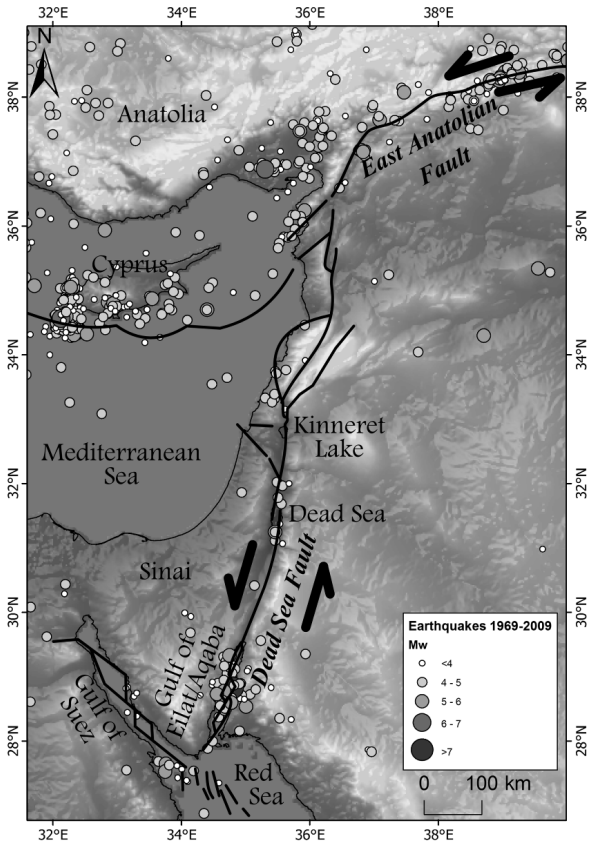

Fig. 1: Regional setting o the Dead Sea fault system showing recent location of recent earthquake foci. Map after Hartman (2011).

along the transition from the marine to the continental Eilat/Aqaba sedimentary basins. Faults controlling the structurally dynamics of sedimentation as well as the seismic activity lie both onshore and offshore. In order to understand the history of earthquakes in the region, an understanding of the seismogenic faults in both the marine and continental environments is thus essential.

ACTIVE FAULTING

Offshore geophysical surveys have recently identified four submarine fault zones in the northern Gulf of Aqaba (Tibor *et al.,* 2010). Two fault zones flank the margins of the gulf (the Eilat fault and Aqaba fault) and continue onland as faults that truncate the distal portions of alluvial fan systems. Both the onshore and offshore Eilat marginal faults have normal fault displacement (*e.g.,* Ben-Avraham 1985; Bowman & Gerson, 1986). Along the eastern margin of the gulf lie the Aqaba and west Aqaba fault zones. The very steep bathymetric escarpment with granitic bedrock truncated at the eastern shoreline indicates that a significant amount of vertical offset is accommodated on faults of the Aqaba fault zone. The zone is wide with three offshore strands. Hartman (2011) mapped strands of a "West Aqaba" fault that may also accommodate strike-slip motion. In the middle of the basin, the Ayla fault zone that appears to bound subsidence across a localized basin was apparently active in the early Holocene. The main offshore strike-slip fault continues northward as the Evrona fault in Israel. This fault extends into Jordan where it crosses the Wadi Muhtadi alluvial fan and continues northward to the Dead Sea. The fault in Jordan is called the Wadi 'Arabah fault. Faulting in the 1068 earthquake has been documented on this fault in the Evrona *sabkha* (Amit *et al.,* 1999, 2002; Zilberman *et al.* 2005).

In Aqaba a concerted effort has been made to map the onshore continuation of the Aqaba fault zone. Due to the dense urbanization, mapping the northward continuation of faults has been difficult. Air photo interpretation of the Aqaba regional surficial geology suggests that the Aqaba fault emerges from the gulf and that slip is transferred to northwest-trending cross faults (Niemi and Smith 1999; Slater and Niemi 2003; Mansoor *et al*. 2004). Because the cross faults are linear and not offset, this geometry constrains the location of the Aqaba fault to lie south and/or east of the cross faults and at the toe of the eastern alluvial fan surfaces.

Geological trenches (T-1 through T-5) were excavated across four NW-trending cross-faults (Fig. 2) that produce active tectonic subsidence at the head of the Gulf (Mansoor, 2002; Slater and Niemi, 2003). Mapping of alluvial fan and buried soil horizons in the trenches reveal multiple fault ruptures on the highest scarps and fewer distinct ruptures on the lowest scarp (Mansoor, 2002). The scarp heights range from 25 cm across the youngest Qf3 surface to 1.3 m across the older Qf1 and Qf2 surfaces. These data indicate that scarp heights reflect cumulative slip events. The most recent scarp-forming event fault occurred after A.D. 1045-1278 based on a corrected, calibrated radiocarbon age from charcoal collected from a buried campfire at the base of the scarp in Trench T-1. This likely represents fault motion in one of the historical earthquakes affecting southern Jordan (*e.g.* 1068, 1212, 1458, or 1588).

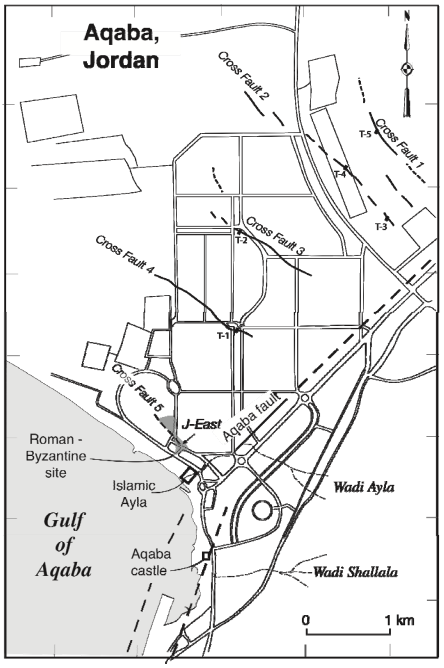

Fig. 2: Map of the city of Aqaba showing the location of major archaeological sites. Active cross faults (CF) mapped from aerial photos and in the archaeological excavations of J-East are also shown (Thomas et al., 2007).

ARCHAEOSEISMOLOGY

Aqaba has a rich cultural history. The earliest evidence of sedentary occupation found are the Late Chalcolithic sites of Tell Magass, and Tell Hujayrat al-Ghuzlan located 3-4 km northeast of the gulf (Khalil & Schmidt, 2009). An Iron through Hellenistic period (8th - 4th centuries B.C.) site called Tell el-Kheleifeh (Pratico, 1993) is located along the Jordan-Israel border. Along the coast and extending underneath the modern city, the remains of the early Roman-Byzantine (1st century B.C.-7th century A.D.), Early Islamic (7th-12th century), and Mamluk through Ottoman (13th-early 20th century) cities of Aila (or al 'Aqabah) have been partially excavated (e.g. Whitcomb, 1994; Parker, 2007; De Meulemeester & al-Shqour, 2008).

Excavation of the Aila ruins from the 1st to the 8th centuries in Area J-East of the Roman Aqaba Project exposed a monumental mudbrick structure heavily damaged by successive earthquakes. Nine faults were mapped across the site (Thomas *et al.,* 2007). Based on subsidence across the fault locations,

changes in floor elevations, and layers of collapsed mudbrick, the archaeological data suggest that the site was ruptured in an early 2nd century earthquake, an early 4th century earthquake, and the 363 A.D. earthquake. The monumental use of the structure was converted to domestic use in the late 4th to early 5th century.

We also have evidence for primary ground rupture for at least four post-date 363 A.D. earthquakes that fault the ruins in the J-East area of Aila. Primary fault rupture is documented in stratigraphic sections and plan maps of walls of various construction ages. Two earthquakes occurred during the Byzantine to Umayyad period (sixth to eighth centuries). There is a hiatus of deposition at this location between the Umayyad and the modern age. The two most recent earthquakes, with 42 and 35 cm of dip slip, occurred some time after the 8th century and likely correlate to the historical earthquakes after the 11th century. No stratified materials were found at this site that could be used to further refine the timing of these seismic events.

The early Islamic (8th-11th centuries A.D) site of Ayla was excavated in 1986-1995. Whitcomb hypothesized that the drainage running through the ancient site originated in erosion along the structural weakness of a fault and placed such a fault on the site plan map (Whitcomb, 1994). However, excavations by Rucker and Niemi (2005) of the NE corner tower of the walled city in the wadi and interpretation of 1918, 1945, and 1953 air photos indicate the wadi is man-made. There is evidence at Islamic Ayla for damage as a result of the 749 (or 746 or 757? See Ambraseys 2005; 2009) earthquake followed by extensive reconstruction at the beginning of the Abbasid period. Major damage occurred in the town of Ayla in the March 18, 1068 earthquake. One contemporary source living in Baghdad, Ibn al-Banna, wrote “As for Aila, its inhabitants all perished except for 12 persons who had gone fishing at sea, thus escaping death.” (Guidoboni and Comastri, 2005, p. 53). The site of Islamic Ayla was apparently never reoccupied to any significant degree after the earthquake.

The site of Early Islamic Ayla was not rebuilt, but a new castle or caravan station was built about 1 km to the southeast. Excavations in and around the Aqaba castle from 2000-2008 have revealed three different phases in the “khan” or castle from the late 12th to 16th centuries (De Meulemeester and Al-Shqour, 2008). The extant castle was built in 1515 and rebuilt in 1587/8, probably after the Gulf of Aqaba earthquake of January 4, 1588 which, based on historical accounts, was felt in NW Arabia, Aqaba, and Sinai (Guidoboni and Comastri, 2005; Ambraseys, 2009). The archaeological data from the Aqaba castle (De Meulemeester and Al-Shqour, 2008) also appear to support rupture of the Gulf of Aqaba fault segment in the earthquake of 1212 and possibly of the Wadi ‘Arabah fault segment in 1458.

Our data suggest significant periods of active seismicity in the 4th, 7th-8th, 11th-13th, and 15-16th Centuries. These data suggest a recurrence rate of faulting and damaging earthquakes either from the Gulf of Aqaba segment or the Wadi ‘Arabah segment of the Dead Sea fault system of about every three to four centuries. It is interesting to note that earthquakes have been coincident with major political transitions that occurred in the region. Seismic activity is thus likely to have played a significant role in these cultural shifts.

Acknowledgements: The Wadi ‘Arabah Earthquake Project has been supported by the Roman Aqaba Project, the American School of Oriental Research, a UMKC Faculty Research grant, the University of Missouri Research Board, and two grants from the Committee on Research and Exploration of the National Geographic Society. I am grateful for the assistance of Dr. Fawwaz al Khraysheh, former General Director, and Dr. Sawsan Fakhri, Aqaba Region director of the Department of Antiquities of Jordan, who granted permission to work in Aqaba.

References

Ambraseys, N.N. (2005). The seismic activity in Syria and Palestine during the middle of the 8th century; an amalgamation of historical earthquakes. *Journal of Seismology* 9, 115-125.

Ambraseys, N. (2009). *Earthquakes in the Mediterranean and Middle East: A Multidisciplinary Study of Seismicity up to 1900*. Cambridge University Press. Cambridge, U.K. 947 p.

Amit, R., E. Zilberman, N. Porat, N. & Y. Enzel, (1999). Relief inversion in the Avrona playa as evidence of large-magnitude historical earthquakes, southern Arava valley, Dead Sea rift. *Quaternary Research* 52, 76-91

Amit, R., E. Zilberman, Y. Enzel & N. Porat, (2002). Paleoseismic evidence for time dependency of seismic response on a fault system in the southern Arava Valley, Dead Sea rift, Israel. *Geological Society of America Bulletin* 114 (2), 192-206.

Ben-Avraham, Z. (1985). Structural framework of the Gulf of Eilat (Aqaba), Northern Red Sea. *Journal of Geophysical Research* 90, 703-726.

Bowman, D. & R. Gerson, (1986). Morphology of the Latest Quaternary Surface Faulting in the Gulf of Elat Region, Eastern Sinai. *Tectonophysics* 128, 97-119.

De Meulemeester, J. & Al-Shqour, R. (2008). *The Islamic Aqaba Project 2008*: Preliminary Unpublished Report. Ghent University, Belgium, 48 p.

Guidoboni, E. (1994). *Catalogue of Ancient Earthquakes and Tsunamis in the Mediterranean Area from the 11th to the 15th Century*. Istituto Nazionale di Geofisica. Roma, Italy. 504 p.

Guidoboni, E., & A. Comastri, (2005). *Catalogue of Ancient Earthquakes in the Mediterranean Area up to the 10th Century*. Istituto Nazionale di Geofisica. Roma, Italy. 1037 p.

Hartman, G. (2011). *Quaternary Evolution of a Transform Basin: The Northern Gulf of Eilat/Aqaba*. Dissertation. Tel Aviv University, Israel. 100 p.

Hofstetter, R., Y. Gitterman, V. Pinksy, N. Kraeva, & L. Feldman, (2008). Seismological observations of the northern Dead Sea basin earthquake on 11 February 2004 and its associated activity. *Israel Journal of Earth Sciences* 57 (2), 101-124.

Khalil, L., & Schmidt, K. (2009). *Prehistoric ‘Aqaba I.* Orient-Archäologie Band 23, Rahden/Westf., Germany, Verlag Marie Leidorf. 419 p.

SWATH BATHYMETRY AND MORPHOLOGICAL SLOPE ANALYSIS OF THE CORINTH GULF

Nomikou, P. (1), Alexandri M. (2), Lykousis V. (2), Sakellariou D. (2), Ballas D. (2)

(1) University of Athens, Department of Geology and Geoenvironment, Panepistimioupoli Zografou, 15784 Athens, Greece, evi@ath.hcmr.gr

(2) Institute of Oceanography, Hellenic Centre for Marine Research, POBox 712, 19013 Anavyssos, Greece, matina@ath.hcmr.gr, vlikou@ath.hcmr.gr, sakell@ath.hcmr.gr, dballas@ath.hcmr.gr

***Abstract (*Swath Bathymetry and Morphological Slope Analysis of Corinth Gulf):** The swath bathymetric survey of the Gulf of Corinth has been conducted during multiple campaigns of HCMR's vessel R/V "AEGAEO" between March 2001 and November 2004, using the 20 kHz, SEABEAM 2120 system. The bathymetric map was produced using a 20 meter grid interval and plotted with a Mercator projection at 1:300.000 scale with 20 m contours. The major part of the central Gulf is a 800-870 m deep, 40km long, 9-12km wide, WNW-ESE elongate flat area. West of Aigio, the basin is shrinking towards its central run off axis, and finally diminishes at Rio-Antirrio straight. Eastwards the central basin terminates at the Alkyonides islets, east of which a sub-basin with maximum depth of 350 m is formed. The steep (30–40%) southern margin of the basin between Kiato to Aigio, is incised by numerous small canyons. The northern margin dips gently till the 400m isobaths and becomes steeper between 400-800m. The very detailed illustration of the Gulf's bathymetry and morphology reflects the offshore active tectonics and faulting of the seafloor and the deformation during Quaternary.

***Key words**: Swath Bathymetry, Sea Bed Morphology, Corinth Gulf*

INTRODUCTION

The Corinth Rift, which separates the Peloponese from continental Greece, is a N100°E oriented elongate graben, 105 km long, bounded by systems of very recent normal faults (less than 2 my old). The Corinth Gulf reflects the modification of the geomorphology and crustal structure formed during the alpine orogenesis by the extension tectonics and the resulted deformation of the Aegean region during Miocene-to-Quaternary. The rift transects obliquely the Pindos mountain chain resulted from the alpine nap tectonics.

This structure is the most seismically active zone in Europe, and the fastest opening area of continental break-up, with up to 1.5 cm yr-1 of north-south extension rate (Clarke et al, 1998), and more than 1 mm yr-1 of uplift rate of the southern margin and 0.7-1 mm yr-1 subsidence of the northern margin (Lykousis et al., 2009). The high rates of tectonic faulting and uplift lead to the outcropping of very recent fault planes with large offsets.

Offshore active faulting on the seafloor of the Gulf of Corinth has been studied in detail during dozens of offshore campaigns led by Greek and international research teams (Sakellariou et al, 2001; 2004; 2007; Stefatos et al, 2002; Moreti et al, 2004; Zelt et al, 2004; McNeill et al, 2005; Lykousis et al, 2006; 2008; 2007a,b; 2009; Bell et al, 2008; Taylor et al, 2011).

The tectonic graben of the Corinth Gulf has been filled up by gravitational deposits (turbidity flows, debris flows, mudflows etc.), while fun delta prograding deposits during Pleistocene sea-level changes, coupled by extensive slumping are the predominant sedimentary processes in the steep flanks of the gulf (Heezen *et al.* 1966; Ferentinos *et al.* 1988; Papatheodorou & Ferentinos 1997; Lykousis *et al.* 1998; Perisoratis et al. 2000; Lykousis *et al.* 2007a).

SURVEY AND SYSTEM DEPLOYMENT

The multibeam bathymetric surveys were carried out by the R/V AEGAEO of the Hellenic Centre for Marine Research, using a SEABEAM 2120 swath system during 2001-2004 within the frame of various EU and National projects like ASSEM (Lykousis et. al., 2006) (Fig.1). The SEABEAM 2120 is a hull-mounted swath system operating at 20 kHz in water depths not exceeding 6000 m. It has an angular coverage sector of 150^0 with 149 beams, covering a swath width from 7.5 to 11.5 times the water depth for depths from 20 m to 5 km. The maximum swath coverage can reach 9 km at maximum depth and gives satisfactory data quality at speeds up to 11 knots. During some cruises we perform high resolution 3.5kHz and Air Gun profiling, side scan sonar imaging, gravity and box coring, deployment of a current-meter and CTD measurements.

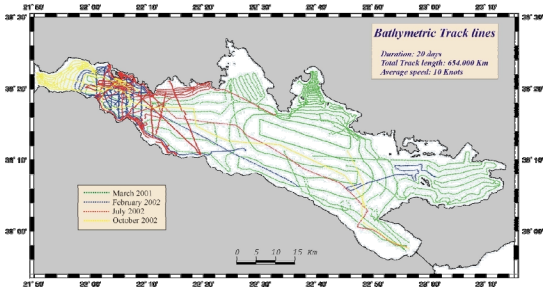

Fig.1: Bathymetric Track lines during 2001-2004 oceanographic cruises with R/V AEGAEO.

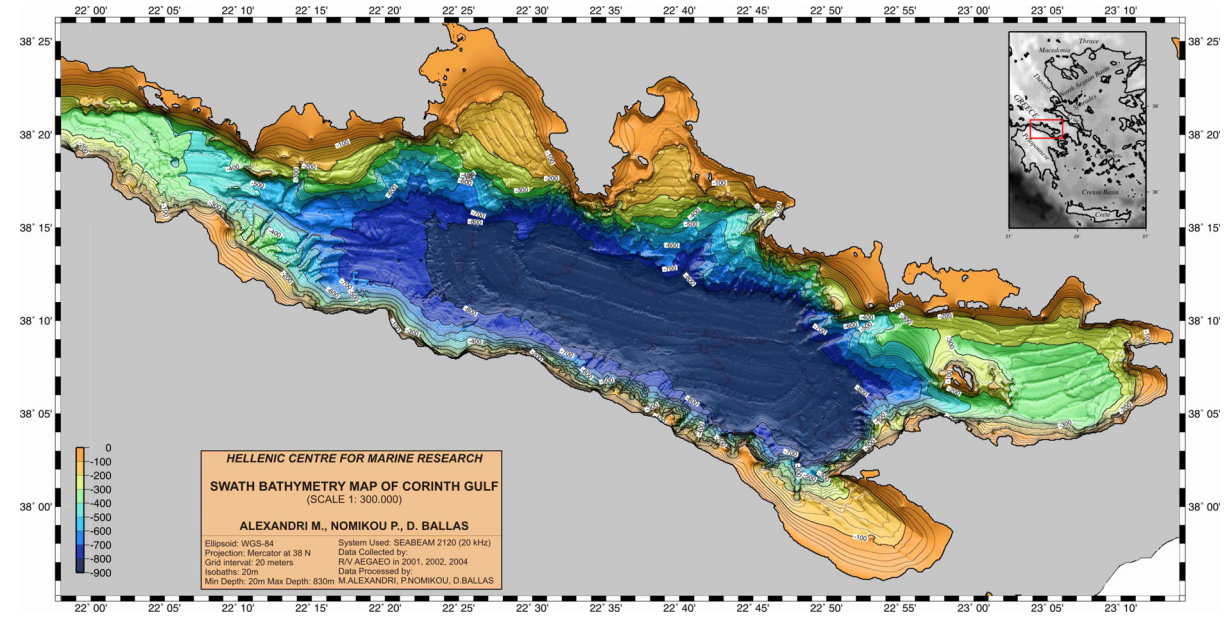

Fig.2: Multibeam Bathymetric Map of Corinth Gulf using 20m isobaths

SWATH BATHYMETRY

The multibeam data have been extensively processed by means of data editing, cleaning of erroneous beams, filtering of noise, processing of navigation data and interpolation of missing beams. The resulting bathymetric map of Corinth Gulf was originally compiled at 1/300.000 scale, which was greatly reduced for publication with 9 different colors corresponding to 100 m depth intervals and with additional isobaths of 20 m (Fig.2). This map permits the first detailed description of the overall topography of the sea floor as well as the mapping of the major morphotectonic structures within this area.

Most of the central part of the Gulf from 800 up to 870 m depth is a very wide flat area forming an extensive WNW-ESE elongated basin of 40km length and a width of 9 km at the west up to 12 km at the east (Alexandri et al., 2003) (Fig. 2).

West of Aigio, the basin is shrinking towards its central run off axis, and finally diminishes at Rio-Antirio straight. Eastwards the central basin is reaching the Alkyonides islets where a sub-basin with maximum depth of 350 m is formed. The steep southern margin, that reaches the 800m isobath is scored, from Kiato to Aigio by numerous small canyons trending NE-SW transversal to the main direction of the gulf (Fig. 3). In contrast, the northern margin spans up to 400m depth where abruptly drops to 800 m creating the northern border of the central basin.

MORPHOLOGICAL ANALYSIS

The bathymetric map of the area was analyzed from the perspective of slope distribution and the results are presented as a slope distribution map (Fig.5). This map shows that the distribution of slope values within the studied area can be subdivided into five categories: (1) areas of mean morphological slope 0-5%, (2) areas of 5-15%, (3) areas of 15-25%, (4) areas of 15-25% and (5) areas of 35-50%.

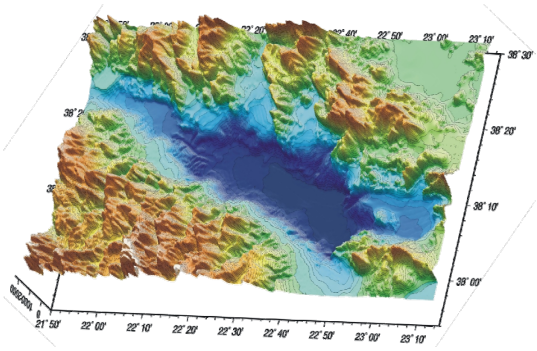

Fig. 3: 3D view of Corinth Gulf combined offshore and onshore data.

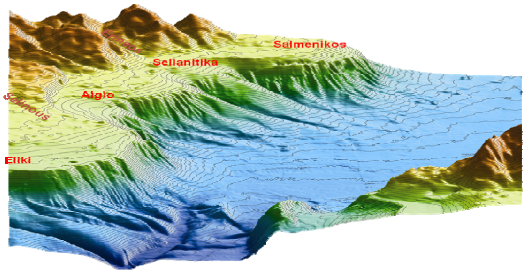

Fig. 4: 3D view of fan delta failures (debris flows) along the southern flanks of Western Gulf of Corinth (imaged from ENE) (Lykousis et al., 2009).

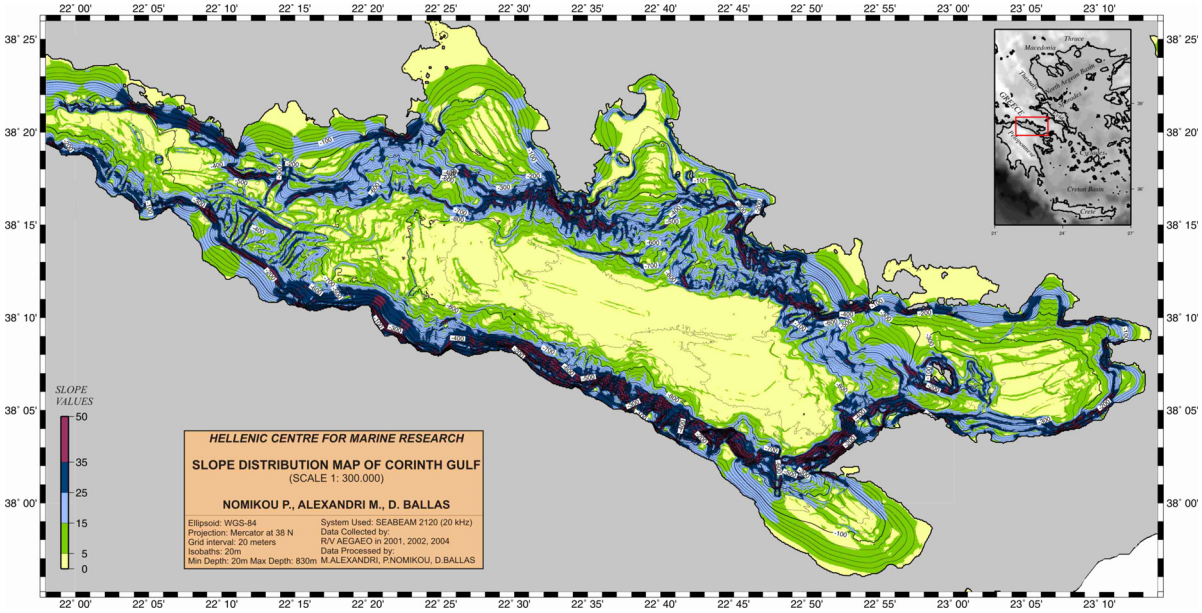

Fig.5: Slope distribution Map of Corinth Gulf

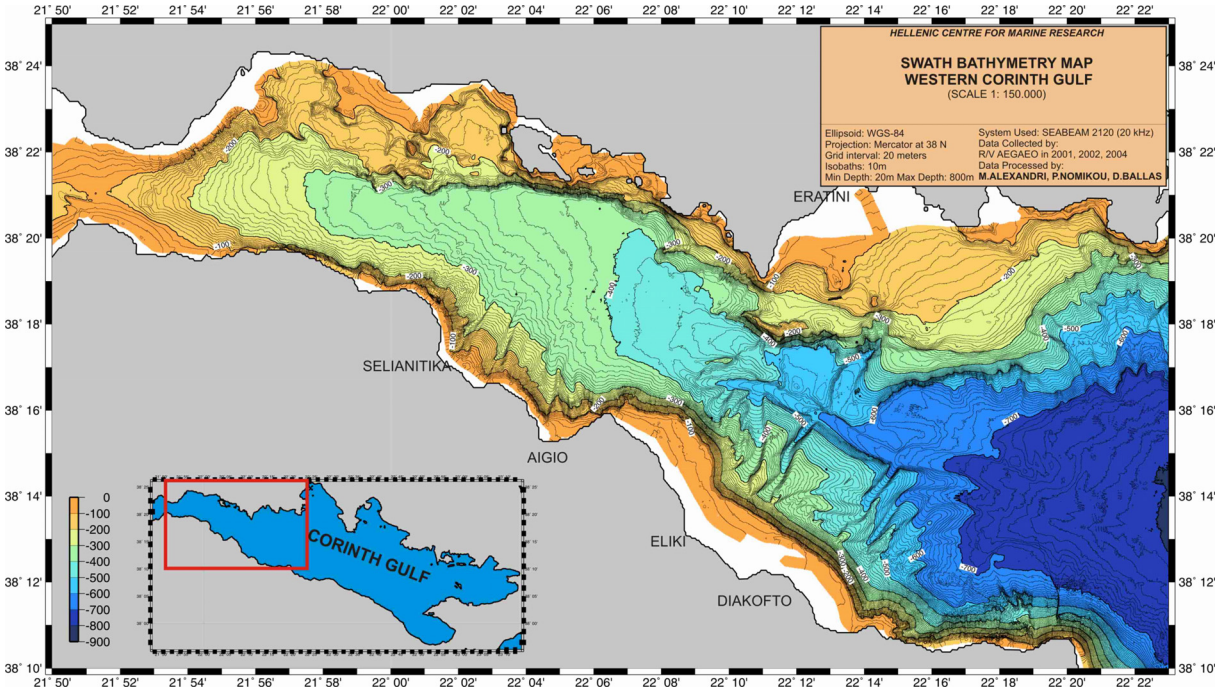

Fig.6: Detailed swath bathymetry map of the Western Corinth Gulf using 10m isobaths

This classification of the slope magnitudes clearly illustrates the zones where there is an abrupt change of slope, which usually reflects the position of active tectonic structures or steep slopes.

The highest slope values (35-50%) are observed in the southern margin from Kiato to Aigio due to numerous small canyons. The northern margin of the gulf if characterized mostly by morphological slopes up to 25% showing a smooth transition to the basin. On the contrary, the central part of the gulf is characterized by a flat bottom of the basin with low morphological slopes from 0-5%.

WEST CORINTH GULF

The western Gulf of Corinth is the currently most active part of the Gulf and has been the site of the Aegion M:6 earthquake in 1995 and many other strong tremors during the last century.

The seabed morphology of the western Gulf of Corinth is dominated by slope canyon systems feeding an axial channel which is only present within this part of the gulf (Fig. 6). Canyons prevail the southern margin but are rare on the northern margin of the gulf. The basin floor reaches a maximum depth of 800m towards the east. Slope failures are abundant in the southern margin and are related to prodelta sediment instabilities and to a minor degree in the northern margin (Eratini area, etc.). A couple of sites were related to historical tsunarnis and are expected to be the potential tsunarnigenic sites íη the W. Corinth Gulf in the future (Lykousis et al., 2007a; Lykousis et al., 2009). Infinite slope stability analysis indicated that slopes steeper than 2-3 degrees are capable to induce slope failures taken account the expected (seismic) ground accelerations for the next 50 years (Lykousis et al., 2009). The northern margin is dominated by a basement horst uplifted by the North (N) and South (S) Eratini faults (Stefatos et al., 2002). The horst is most prominent near the Psaromita Peninsula and is progressively buried and reduced in topography to the east and west, with faults as long as 15 km (McNeil et al., 2005).

DISCUSSION

The swath bathymetric survey of the Gulf of Corinth provides insight into morphological expression of the active seafloor processes, like faulting and submarine sliding, erosions and sediment deposition and enables detailed mapping of the offshore structural elements.

The major part of the central Gulf is a 800-870 m deep, 40km long, 9-12km wide, WNW-ESE elongate flat area. West of Aigio, the basin is shrinking towards its central run off axis, and finally diminishes at Rio-Antirio straight. Eastwards, the central basin terminates at the Alkyonides islets, east of which a sub-basin with maximum depth of 350 m is formed. Both, the steep (30–40%) southern margin and the gentler dipping north margin of the basin are fault controlled. The steep margins are incised by numerous small canyons.

References

Alexandri M., Nomikou P., Ballas D., Lykousis V. & Sakellariou D. (2003): Swath bathymetry map of Gulf of Corinth. Geoph. Res. Abstracts, Vol. 5, 14268, EGS 2003.

Bell, R., McNeill, L.C., Bull, J.M., and Henstock, T.J., 2008. Evolution of the western Gulf of Corinth continental rift, Greece. Geological Society of America Bulletin, 120, 156-178.

Clarke, P.J., Davies, R.R., England, P.C., Parson, B., Billiris, H., Paradissis, D., Veis, G., Cross, P.A., Denys, P.H., Ashkenazi, V., Bingley, R., Kahle, H.-G., Muller, M.-V., and Briole, P., 1998, Crustal strain in central Greece from repeated GPS measurements in the interval 1989-1997: Geophysical Journal International, 135, 195-214.

Ferentinos, G., Papatheodorou, G. & Collins,M.B., 1988. Sediment transport processes on an active submarine fault escarpment: Gulf of Corinth, Greece, *Mar. Geol.,* 83, 43–61.

Heezen, B.C., Ewing, M. & Johnson, G.L., 1966. The Gulf of Corinth floor, *Deep-Sea Res.,* 13, 381–411.

Lykousis V., Sakellariou D., Blandin J., Person R., Etiope G., Alexandri M., Nomikou P., Rousakis G., 2006, The ASSEM sea bed observatory for long term multihazard monitoring: Gulf of Corinth experiment. 8ο Πανελ. Συμπ. Ωκεανογρ. & Αλιείας, σελ. 151-154.

Lykousis, V., Sakellariou, D., Papanikolaou, D., 1998. Sequence stratigraphy in the northern margin of the Gulf of Corinth: implications to upper Quaternary basin evolution, *Bull. Geol. Soc. Greece,* 32, 157–164.

Lykousis V., Sakellariou D., Rousakis G., Alexandri S., Kaberi H., Nomikou P., Georgiou P., Balas D. ,2007a. Sediment failure processes in active grabens: the Western Gulf of Corinth (Greece). In: Lykousis V., Sakellariou D., Locat J. (eds.), Submarine Mass Movements and their Consequences, 297-305, Springer.

Lykousis V., Sakellariou D., Moretti, I., Kaberi H. ,2007b. Late Quaternary basin evolution of the Gulf of Corinth: Sequence stratigraphy, sedimentation, fault–slip and subsidence rates. Tectoniphysics, 440, 29-51.

Lykousis, V., G. Roussakis , D. Sakellariou, 2009. Slope failures and stability analysis of shallow water prodeltas in the active margins of Western Greece, northeastern Mediterranean Sea. J. Earth Sciences, 98, 807–822.

McNeill, L., Cotterill, C., Stefatos, A., Henstock, T., Bull, J., Collier, R., Papatheoderou, G., Ferentinos G., and Hicks, S. 2005, Active faulting within the offshore western Gulf of Corinth, Greece: implications for models of continental rift deformation: Geology, 33, 241-244.

Moretti, I., Lykousis, V., Sakellariou, D., Reynaud, J.-Y., Benziane, B., and Prinzhoffer, A., 2004, Sedimentation and subsidence rate in the Gulf of Corinth: what we learn from Marion Dufresne's long-piston coring: Comptes Rendus Geoscience, 336, 291-299.

Papatheodorou, G. & Ferentinos, G., 1997. Submarine and coastal sediment failure triggered by the 1995, Ms = 6.1 Aegion earthquake, Gulf of Corinth, Greece, *Mar. Geol.,* 137, 287–304.

Perissoratis C., Piper D.J.W. and Lykousis V., 2000. Alternating marine and lacustrine sedimentation during late Quaternary in the Gulf of Corinth rift basin, central Greece. Mar. Geol. 167: 391-411.

Sakellariou, D., Lykousis,V. & Papanikolaou, D. (2001) Active faulting in the Gulf of Corinth, Greece. In: 36th CIESM Congress Proceedings, 36 pp. 43.

Sakellariou, D.,Kaberi, H. & Lykousis,V. (2004) Infuence of active tectonics on the recent sedimentation of the Gulf of Corinth basin. In: 10th International Congress of Greek Geological Society, Abstracts 15-17 April, p. 232-233, Thessaloniki.

Sakellariou D., Lykousis V., Alexandri S., Kaberi H., Rousakis G., Nomikou P., Georgiou, P., Ballas D., (2007): Faulting, seismic-stratigraphic architecture and Late Quaternary evolution of the Gulf of Alkyonides basin – East Gulf of Corinth, Central Greece. Basin Research, 19/2, p. 273-295.

Stefatos, A., Papatheoderou, G., Ferentinos, G., Leeder, M., and Collier, R., 2002, Active offshore faults in the Gulf of Corinth, Greece: Their seismotectonic significance: Basin Research, 14, 487-502.

Taylor, B., Weiss, J.R., Goodliffe, A. M., Sachpazi, M., Laigle, M. & Hirn, A., 2011. The structures, stratigraphy and evolution of the Gulf of Corinth rift, Greece *Geophys. J. Int.* (2011) 185, 1189–1219

Zelt, B.C., Taylor, B., Weiss, J.R., Goodliffe, A.M., Sachpazi, M., and Hirn, A., 2004. Streamer tomography velocity models for the Gulf of Corinth and Gulf of Itea, Greece. Geophys. J. Int., 159, 333-346.

EARTHQUAKE ARCHAEOLOGY

INQUA PALEOSEISMOLOGY AND ACTIVE TECTONICS

IS THE DECADENCE OF LEPTIS MAGNA (LYBIA) THE CONSEQUENCE OF A DESTRUCTIVE EARTHQUAKE?

Pantosti, Daniela (1), Stefano Pucci (1), Paolo Marco De Martini (1), Alessandra Smedile (1)

(1) Istituto Nazionale di Geofisica e Vulcanologia. Via di Vigna Murata, 605. 00143- Roma. ITALY.
Email: daniela.pantosti@ingv.it, stefano.pucci@ingv.it, paolomarco.demartini@ingv.it, alessandra.smedile@ingv.it

Abstract (Is the decadence of Leptis Magna (Lybia) the consequence of a destructive earthquake?): *The relationships between human modification of the environment and natural events in the Roman city of Leptis Magna are analyzed. Historical and archaeological sources indicate extreme natural events as the cause of the town's decline: earthquakes, flooding, and tsunamis. Stratigraphical and geomorphological surveys investigated history and dynamics of the depositional and erosional systems of the settlement area by integrating independent constraints as archaeological and absolute radiocarbon dating. The results highlighted that once the Romans society could no longer guarantee the maintenance of defensive structures, destructive floods affected the town. Conversely, large earthquakes or tsunami have been discarded as primary cause of the town decline.*

Key words*: Natural Hazards, Flooding, Earthquakes, AD 365 Crete earthquake and tsunami*

The Roman city of Leptis Magna (UNESCO world heritage) in western Libya was a magnificent, flourishing, strategic town in Tripolitania reaching its maximum expansion during the Empire of Septimius Severus (193-211 A.D.). The town is built on a wide alluvial fan fed by wadi (creek in Arabic) Lebda whose outlet served as a harbor since Phoenician times (Figure 1). An ingenious hydraulic system composed by a dam and an artificial channel diverting the wadi water was built by the Romans to prevent the town from flooding. The decline of Leptis Magna irreversibly started in the 4th Century. Historical and archaeological sources suggest that the town decadence is related to the fact that the harbor became inefficient and was abandoned due to its complete sediment infill. Several causes are taken in consideration to explain this infilling, these are: i) violent flooding following the collapse of a dam built to regulate the course of the wadi because of the large 365 A.D. Crete earthquake (Salza Prina Ricotti, 1995; Di Vita, 1990); ii) lack of maintenance due to the decline of the settlement induced by severe damage after the 365 A.D. earthquake (Di Vita, 1990 and 1995), or other local seismic sources (Guidoboni et al., 1994; Stiros, 2001); iii) inundation of a tsunami wave caused by the 365 A.D. earthquake that left a huge amount of debris and modified the local coastal morphology (Guidoboni et al., 1994; Ambraseys et al., 1994; Lorito et al., 2007, Shaw et al., 2008); iv) bad orientation and geometry of the harbor structures with respect to the local marine currents that were bringing sediments inside (Salza Prina Ricotti, 1972-1973). Most of these hypotheses are connected to the M8.5, 365 A.D. Crete event that, being the largest historical earthquake and tsunami ever occurred in the Mediterranean, has certainly stimulated the formulation of many hypothesis that put in connection any critical situation recognized in the mid of the 4th Century. with the occurrence of this catastrophe.

We studied in detail the geomorphology and the stratigraphy of Leptis Magna to understand if the causes of the decline of the town can be deciphered in the natural events recorded in the local geology (Pucci et al., 2011). To build up a consistent chronological record of significant natural events and their interaction with human history, geomorphological analyses (the study of cores and natural/artificial exposures), and the reconstruction of the different depositional environments based on the palaeontological content, were integrated to radiometric dating and archaeological knowledge.

Given the strategic role of the harbor in the flourishing/decline of the town, this is certainly a key site to study to understand the history and men-nature interactions but, to fully understand the functioning of the natural and human system and equilibrium besides the harbor, we investigated the wadi, along with its hydraulic system built to control flooding (dam and aegere), the town, and the surrounding coastal area.
At the same time we have surveyed the buildings in town to check for evidence of seismically induced collapses.

The integration of all these observations allowed us to reconstruct the following history for the site (Pucci et al., 2011 - Figure 2):
1) Building of hydraulic protections (dam and a channel diverting the wadi along a defensive aegere) to prevent flooding and have at disposal a water reserve, 32-131 A.D. No deposition in the lower reach of wadi (north of the dam), in town and in the harbor (B in figure 2).
2) Functioning of the hydraulic system, expansion of the town toward the lower reach into the dry wadi bed and on its lower terraces. Enlargement of the harbor into the Severian monumental structure allowed by the lack of sediment/water discharge at the wadi outlet. Efficiency at least up to the time of Septimius Severus

(193-211 A.D.). Deposition only in the upper reach of the wadi (south of the dam), siltation effects cleared by artificial sweeping of the dam basin (C in figure 2).
3) Maintenance (sweeping) of the hydraulic protections start to fail during the 3rd Century; onset of the dam siltation and beginning of the decadence of the town. In about 100 yrs the reservoir is completely filled; the wadi starts to spill out from the dam with the first alluvial deposits passing again the lower wadi reach and harbor area and with beginning of erosion at the base of the right shoulder of the dam (D in figure 2).
4) Collapse of the right shoulder of the dam, entrenchment of the siltation body, restoration of the natural equilibrium of the wadi longitudinal profile by remobilization of a large amount of deposits that were previously stored in the dam basin. At 320-440 A.D. the wadi floods again the alluvial plain, begins to bury the town with alluvial sediments and to discharge large amounts of sediments into the harbor (E in figure 2).

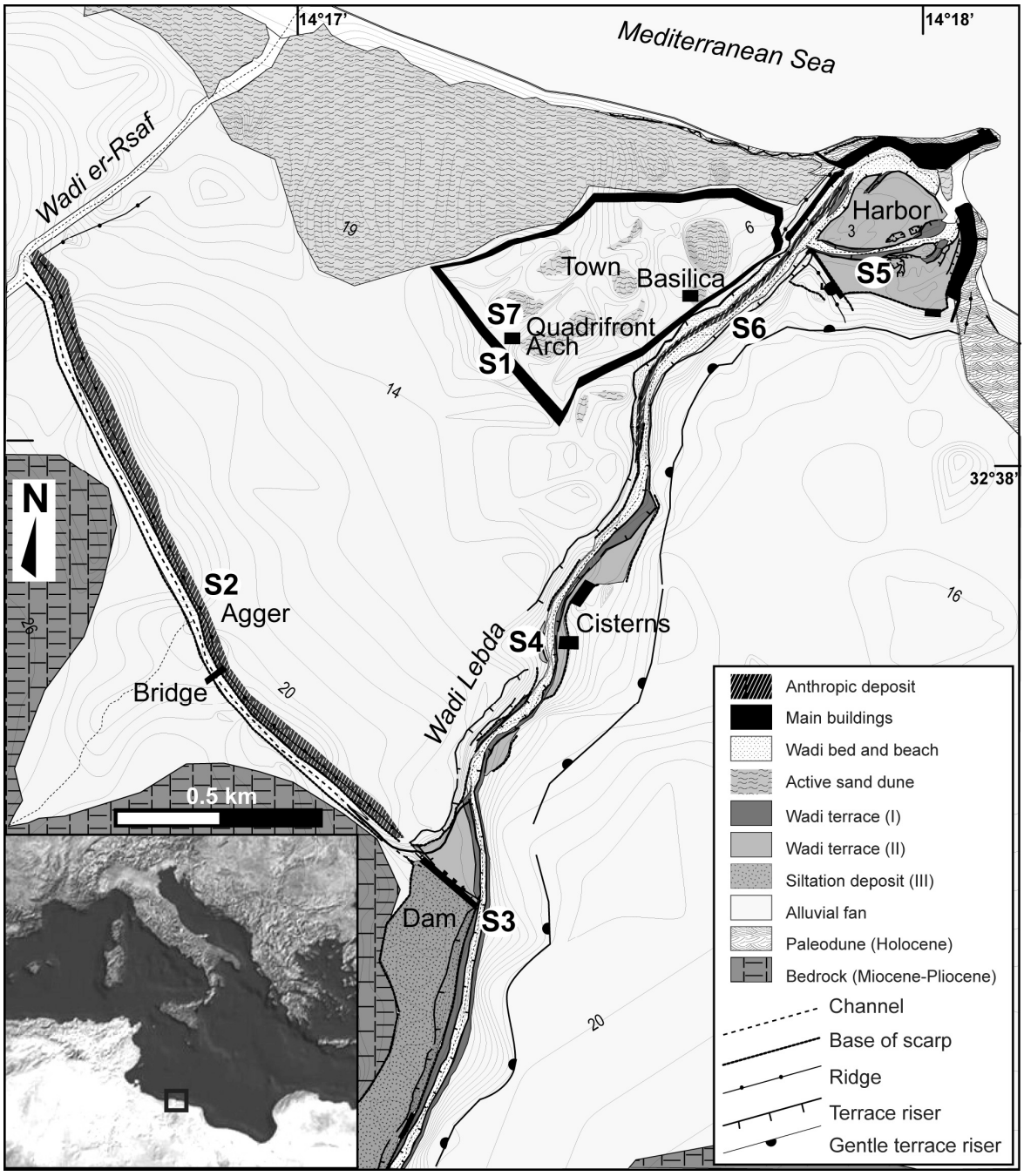

Figure 1. Geological and geomorphological map of the area of Leptis Magna. Locations S1-S7 are those studied in detail through stratigraphic and laboratory analyses. Inset in the lower left locates the study area on the north African coast (modified from Pucci et al., 2011).

5) Harbor is completely infilled by wadi sediments at the 6th Century (F in figure 2).
6) No evidence for important seismic collapses or damage was found by inspecting the buildings, as they appear today and the dam. Unfortunately, there was no possibility to check the original documents related to the early archaeological excavations to confirm the lack of major shaking effects. A wall in a recent excavation (Prof. F. Tommasello, pers. comm.), collapsed on top of 1 m-thick alluvium burying already the town, may be evidence for an earthquake. If seismic, this collapse occurred well after that repeated flooding draped the town with a thick layer of alluvium and thus post-dates 320-440 A.D.

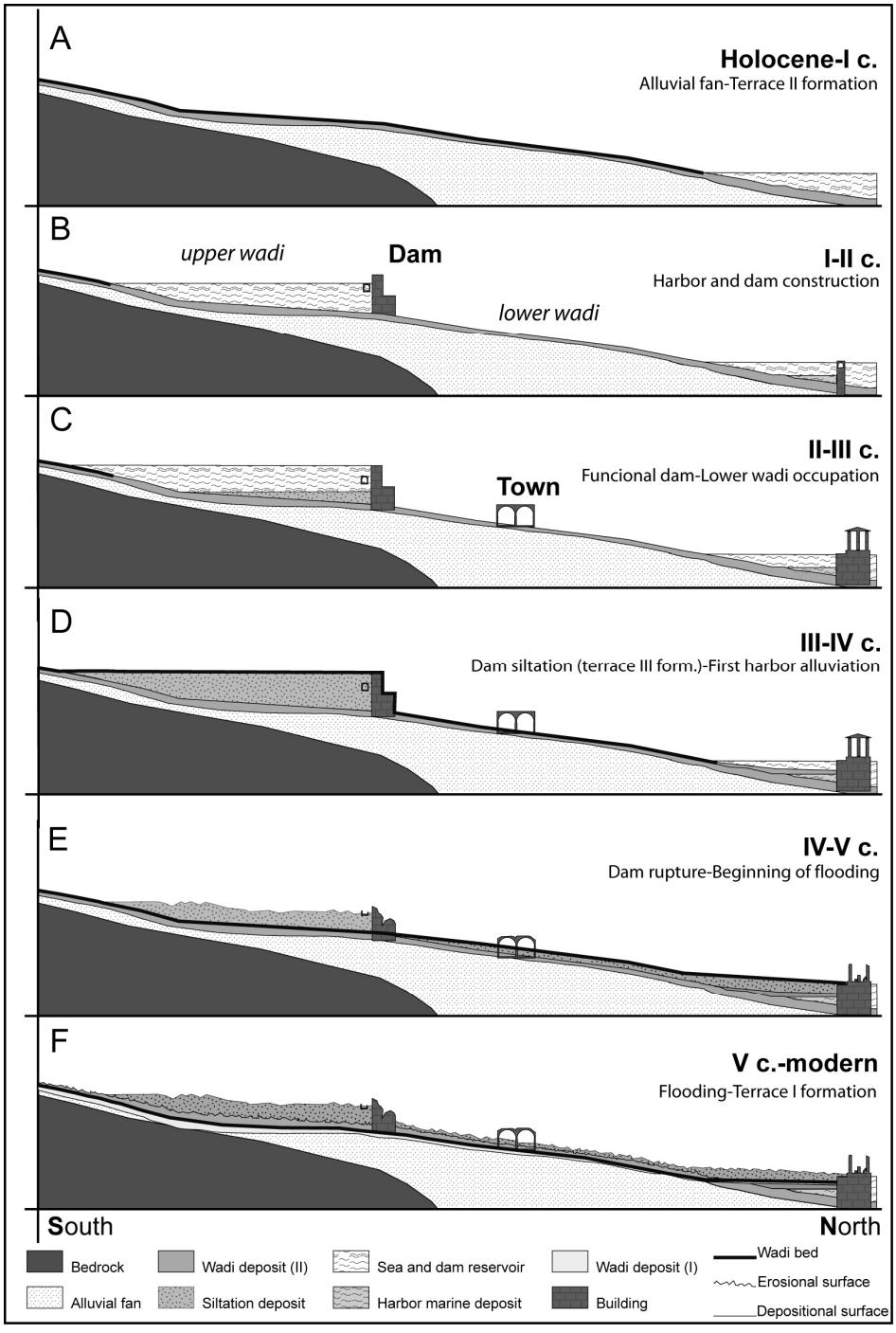

Figure 2. Conceptual sketch of the evolution of the wadi Lebda longitudinal profile, from the dam to the harbor, and its depositional history in relation with the different studied locations (upper wadi, lower wadi, harbor, town - modified from Pucci et al., 2011).

The data collected, although not definitive to characterize the true cause for the decline of Leptis Magna, allow evaluating the initial hypotheses (Pucci et al., 2011).

1) Flooding due to the collapse of the dam because of the 365 A.D. earthquake is discarded. This is because no traces for earthquake effects were found in the existing structures (including the dam), but also because no water was present in the dam basin at the time of the dam shoulder collapse. In fact, as it is today, the basin should have been completely filled with sediments due to the siltation process incepted by lack of dam sweeping. Should the dam shoulder have collapsed when the basin was still containing water (to produce the violent flooding) no siltation would have ever occurred as the dam was no more efficient and the wadi would have re-gained its course and profile.

2) Lack of maintenance due to severe damage to the town after the 365 A.D. This hypothesis is partly correct. In fact, lack of maintenance is the primary cause for siltation in the dam and for all the consequent effects (flooding in town and sediments infilling in the harbor) that made the initial (economic?) decline irreversible. However, the reason for this lack of maintenance does not seem related to the damage from an earthquake (and certainly not the 365 A.D. Crete event) as no serious evidence for seismically induced damage was found.

3) 365 A.D. tsunami harbor inundation is discarded as well. Coring in the harbor we reconstructed the whole history of the sedimentation in that area, from marine to continental. No evidence for such a violent event was found. A possible layer representing the deposit from a paleotsunami was found in the upper part of harbor stratigraphy, when alluvium was already deposited in the harbor after the 6th Century.

4) Bad orientation and geometry of the harbor as the cause of debris deposition from marine currents is clearly discarded because the reconstruction of the depositional environments in the harbor has shown initial marine conditions (up to the 3rd Century) that gradually had a continental input to become purely alluvial (5th Century). If the initial hypothesis was correct, the harbor infill would have only a marine origin.

In conclusion, we can rule out the hypothesis that an earthquake, and particularly the Crete 365 A.D., was the cause for the decadence of Leptis Magna. On the contrary, from the analyses of the recent geological history of the site it is likely that social and economic criticalities (possibly related to the continuous robberies and attacks from the Austurians) are the primary cause for this decadence that made the Lepticians unable to cope with natural hazards and preserve their “risk management plans”. The fact that nature took up the place again, causing widespread flooding and huge sediments remobilization made it too difficult for the Lepticians to recover and the initial decline of the town became irreversible.

Acknowledgements: This work was funded by Istituto Nazionale di Geofisica e Geofisica e Vulcanologia — INGV with contribution of the EU Transfer project. We are thankful to the Italian Archaeological Mission leaded by L. Musso for hosting us and for the fruitful discussions and collaboration.

References

Ambraseys, N.N., Melville, C.P., Adams, R.D., (1994). *The Seismicity of Egypt, Arabia and the Red Sea: a Historical Review*. Cambridge Univ. Press, Cambridge.

Di Vita, A., (1990). Sismi, urbanistica e cronologia assoluta. Terremoti e urbanistica nella città di Tripolitania tra il I secolo a.C. ed il IV d.C. In: *L’Afrique dans L’Occident Romani (Ier Siècle Av. J.-C.- IVe Siècle Ap. J.- C.)*, Actes du Colloque Organisé par l’Ècrole Français de Rome sous le Patronage de l’Institut National d’Archéologie et d’Art de Tunis (Rome, 3-5 décembre 1987), Roma, pp. 425e494.

Di Vita, A., (1995). Archaeologists and earthquakes: the case of 365 AD. *Annali di Geofisica* 38, 971-976.

Guidoboni, E., Comastri, A., Traina, G., (1994). *Catalogue of Ancient Earthquakes in the Mediterranean Area up to the 10th Century*. ING SGA, Rome.

Lorito, S., Tiberti, M.M., Basili, R., Piatanesi, A., Valensise, G., (2007). Earthquake generated tsunamis in the Mediterranean Sea: scenarios of potential threats to Southern Italy. *Journal of Geophysical Research*, doi:10.1029/2007JB004943.

Pucci, S., D. Pantosti, P.M. De Martini, A. Smedile, M. Munzi, E. Cirelli, M. Pentiricci, L. Musso, (2011). Environment-man relationships in historical times: The balance between urban development and natural forces at Leptis Magna (Libya), *Quaternary International*, doi:10.1016/j.quaint.2011.03.050

Salza Prina Ricotti, E., (1972-1973). I porti della zona di Leptis Magna. *Rendiconti della Pontificia Accademia di Archeologia* 45, 75-103.

Salza Prina Ricotti, E., (1995). Leptis Magna la città delle ombre bianche. *Archeo* 9 (127), 50-91.

Shaw, B., Ambraseys, N.N., England, P.C., Floyd, M.A., Gorman, G.J., Higham, T.F.G., Jackson, J.A., Nocquet, J.M., Pain, C.C., Piggott, M.D., (2008). Eastern Mediterranean tectonics and tsunami hazard inferred from the AD 365 earthquake.*Nature Geoscience* 1, 268-276. doi:10.1038/ngeo151.

Stiros, S.C., (2001). The AD 365 Crete earthquake and possible seismic clusteringduring the fourth to sixth centuries AD in the Eastern Mediterranean: a reviewof historical and archaeological data. *Journal of Structural Geology* 23, 545-562.

EARTHQUAKE ARCHAEOLOGY

INQUA PALEOSEISMOLOGY AND ACTIVE TECTONICS

ON-SHORE PROLONGATION OF BATHYMETRICALLY RECOGNIZED FAULT ZONES BASED ON GEODETIC GPS OBSERVATIONS ALONG SANTORINI VOLCANO

Papageorgiou, Elena (1), Nomikou, Paraskevi (2)

(1) University of Athens, Department of Geophysics and Geothermy, Zografou 15784, Greece, Email: epapageo@geol.uoa.gr
(2) University of Athens, Department of Dynamic, Tectonic and Applied Geology, Zografou 15784, Greece, Email: evi@ath.hcmr.gr

Abstract (On-shore prolongation of bathymetrically recognized fault zones based on geodetic GPS observations along Santorini volcano): *Ground deformation monitoring on Santorini Volcanic Complex (SVC) revealed different horizontal kinematics in several parts of the volcano. However, in the current reposed state of SVC, ground deformation is primarily the result of tectonic activity. This work aims to combine and interpret the results of both GPS measurements and bathymetric survey conducted at SVC. The GPS data were intermittently collected during numerous campaigns between 1994 and 2005, while bathymetric survey was completed by the Hellenic vessel R/V 'AEGAEO' in November 2001, using the 20 kHz, SEABEAM 2120 swath system and mapping a total area of 2480 km². In this attempt a correlation between the morpho-tectonic features exposed on the seabed by the bathymetric survey, and the surface displacements observed by the GPS measurements could be finally achieved. An interpretation will be held, on whether these submarine tectonic features continue and intersect the volcanic island, especially in the areas where the surface displacements enable the plausible existence of contemporary tectonics.*

Key words*: Tectonics, Bathymetry data, GPS Displacements, Santorini Volcano*

INTRODUCTION

Santorini Volcanic Complex (SVC) lies in an area of complex extensional and subduction-related tectonics in a continental environment (Le Pichon & Angelier, 1979; Fytikas et al., 1984; Papanikolaou, 1993; Jackson, 1994). The development of the volcanic field has been strongly influenced by regional faults.The current geodynamic state of SVC is controlled by two major volcanoes, the Nea Kammeni Volcano built up in the central caldera and the submarine Columbo Volcano, NE of Cape Columbo. Two major faulting zones Kammeni and Columbo (KFZ, CFZ, respectively) cross the volcanoes in a NE-SW direction, for several km, forming vents through which the magma ascend to the surface (Fouqué 1879; Reck 1936). Generally, the major structural features in Santorini are striking in a NE direction (Heiken & McCoy 1984; Druitt et al., 1989, 1999; Jackson 1994; Mountrakis et al., 1998; Pe-Piper & Piper, 2005).

Seismic data (Bohnhoff et al., 2006; Dimitriadis et al. 2009) indicate that the main volcanic centers of the Santorini volcanic field (Christiana, Santorini, Columbo and minor volcanic cones) are aligned along the NE-SW trending Santorini-Columbo volcano-tectonic line, a deep-seated, strike-slip feature (Sakellariou et al., 2010; Nomikou et al., 2011a) which served as conduit for the rising magma.

Herein, we present the joint data interpretation of GPS measurements and bathymetry survey of the surrounding area of Santorini, in an attempt to relate the submarine rupture system, with its onshore continuation as deduced from surface displacement variations on either side of the possible prolonged faults.

GPS OBSERVATIONS

DGPS has proven to be an important tool for intermediate and long-term monitoring of active volcanoes, as it provides high resolution 3-D information about the deformation field (e.g. Dvorak & Dzurisin, 1997; Fernandez et al., 1999 and many others). At the SVC, DGPS measurements conducted during the period 1994-2005 have detected non-trivial amounts of ground displacement, in both the horizontal and vertical axes (e.g. Papageorgiou et al., 2007). This enabled the identification of several domains with different kinematic characteristics. The interested reader may find details about the field measurement and data reduction procedures in Papageorgiou et al. (2007, 2010).

In particular, the GPS analysis presents several distinct domains with different horizontal kinematics, which could be defined most possibly by the major tectonic fault zones of the area. Thus, areas with uniform GPS displacements both in rate and orientation that characterize homogeneous regions were separated among others with considerable changes in their kinematic pattern. The observed differential deformation between these deforming domains is thought primarily to be the result of differential motion across faulting structures located at the boundaries. For the purpose of this paper, a synthetic map was constructed showing the above mentioned homogeneous regions, based merely on

their kinematics, as well as the areas/zones which may correspond to the major regional faults, as they still affect the tectonic–volcanic evolution of the SVC, as has already been observed in the past (Fig. 1).

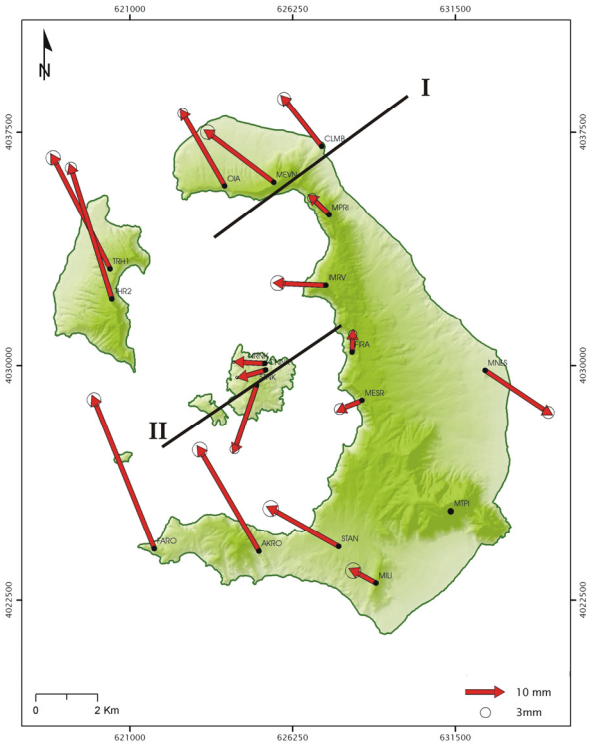

Fig. 1: Horizontal displacements relative to MTPI (NE Thera) for the period 1994-2005 (Papageorgiou et al., 2010).

In Northern Thera, in between the GPS stations 33 and 43 a different kinematic pattern is observed, indicating the possible existence of an area/zone (case I) of kinematic change (Fig. 1). Similarly, in central caldera, at Nea Kammeni Volcano, a second kinematic differentiation is observed, between the northern GPS stations 15 and 22 and the central GPS station 45 (case II). In both cases (I and II), fault zones are implicated to consist the boundary of the different homogeneous deforming domains, where in either side of which the horizontal GPS displacements change both in rate and orientation (Fig. 1).

This is a very complex pattern and certainly difficult to interpret. Nevertheless, the observed deformation pattern enables the drafting of a qualitative model of contemporary tectonics, which is also presented and discussed in detail in Papageorgiou et al. (2010). However, the most important differences of surface displacements which are observed for the time interval 1994-2005 are thought to be explained with the existence of tectonic features. As it appears, these features coincide with the major fault zones in the area, the Kammeni, and Columbo Fault Zones (Fig. 2).

BATHYMETRIC SURVEY

The multibeam bathymetric survey was completed by the Hellenic vessel R/V 'AEGAEO' in November 2001, using the 20 kHz, SEABEAM 2120 swath system and mapping a total area of 2480 km². The bathymetric map was produced using a 50 meter grid interval and plotted with a Mercator projection at a scale of 1:100.000 with 10m contours (Alexandri et al., 2003; Nomikou et al., 2011a). What comes out from the bathymetric map (Fig. 2) is the identification of several morphological discontinuities that finally correspond to fault zones as indicated from seismic profiling data (Fig. 3) (Sakellariou et al., 2010; Nomikou et al., 2011). The volcanic cones in the regional area of the SVC presented in Fig. 3 show linear distribution which is controlled by strike-slip faults that run parallel to the long axis of the Anydhros basin.

Furthermore, the CFZ is an active, possibly right-lateral, 40 km long, strike-slip fault-zone, which has enabled the upward migration of magmatic fluids, the creation of dikes and the development of submarine volcanic cones, with Columbo submarine volcano as the most productive among them (Sakellariou et al., 2010). The KFZ in addition, passing through Nea Kammeni volcano, in the centre of the caldera is directly related to CFZ and displays similar characteristics.
A particularly noteworthy feature that should be mentioned is a hydrothermal vent field at the northern caldera that is located in line with the normal fault system of the Columbo rift, and also near the margin of a shallow intrusion that occurs within the sediments of the north caldera (Sigurdsoon et al., 2006; Nomikou et al., 2011).

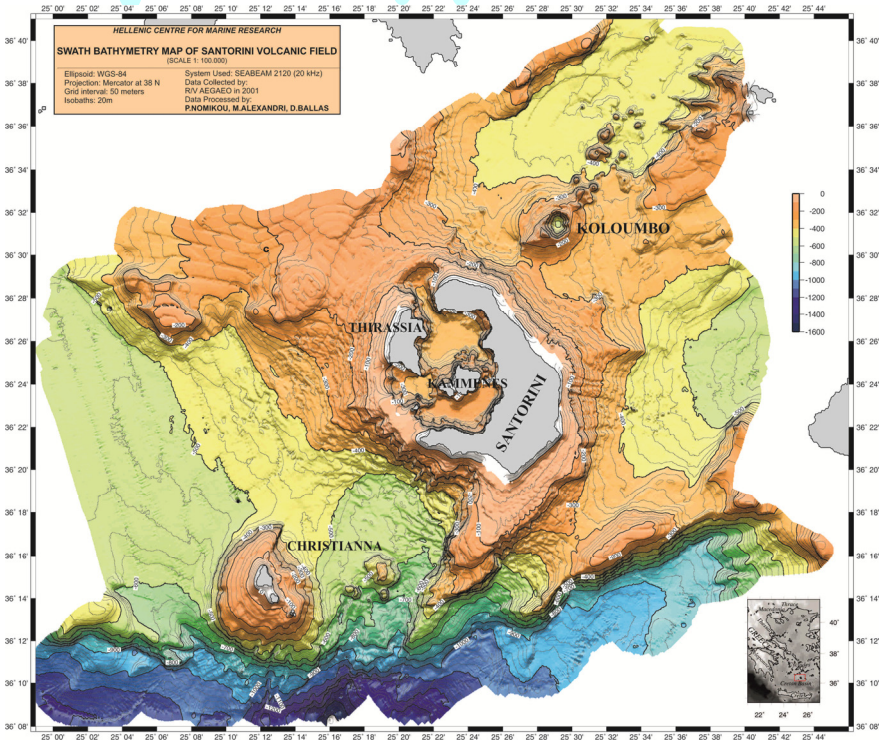

Fig. 2: Multibeam Bathymetric Map of Santorini Volcanic Field using 20m isobaths (Nomikou et al., 2011).

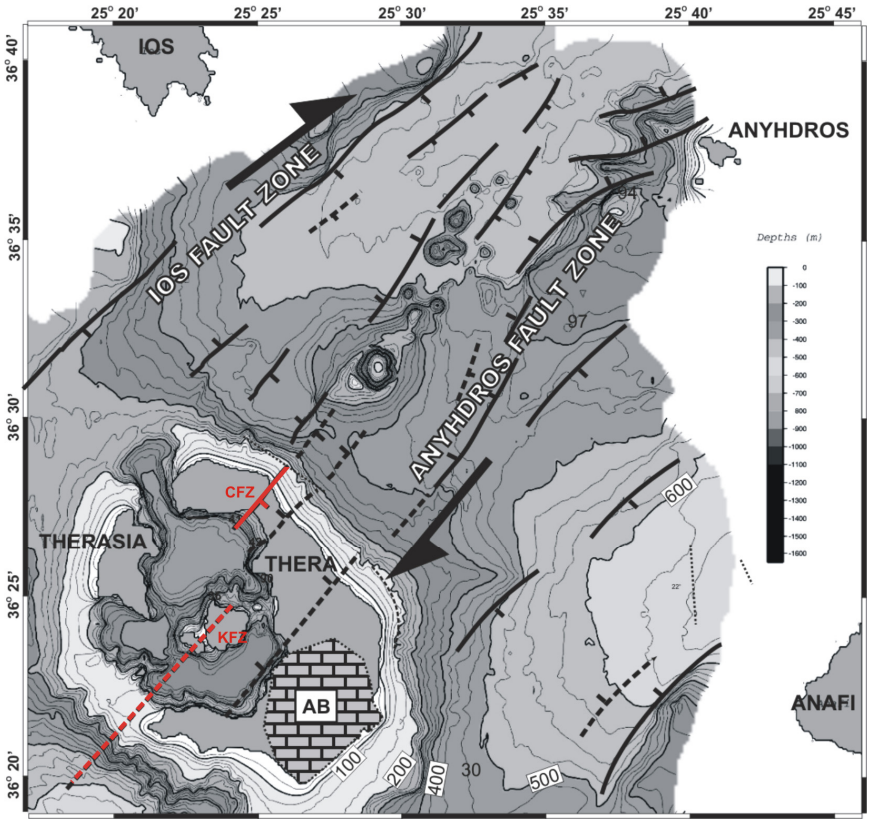

Fig. 3: Tectonic map of Santorini-Columbo volcanic field (Sakellariou et al., 2010).

DISCUSSION

The results of GPS measurements agree with the swath bathymetry data, as the observed submarine tectonic fault zones seem to prolongate onshore crosscutting the whole of the volcanic edifice. This phenomenon is more obvious in Northern Thera with the continuation of the Columbus Fault Zone up to the northern part of the Santorini caldera. The GPS horizontal displacements vectors show evidently different kinematic pattern on both sides of the CFZ, agreeing for the distinct existence of the CFZ and its continuation on land. However, a consideration should be taken into account on whether the GPS data reflect the existence of two different tectonic blocks on both sides of the CFZ, or whether it may indicate an updoming due to ascending magma along the fault zone which at the same time is used by the volcanic dikes.

This is also evident in other parts of the SVC. The displacement field in Nea Kammeni volcano, is differentiating in each side of the Kammeni Fault Zone (KFZ), indicating primarily two kinematic blocks bounded by the KFZ, and secondly its onshore prolongation at Nea Kammeni.

However, the GPS results show a more complex kinematic model of the SVC and further numerical modelling should be considered in order to get a more representative tectonic regime. Yet, this study enabled the combination of two different methods, as is the GPS observations and bathymetric data, in order to successfully certify the existence of major fault zones on the surface.

Acknowledgements: Part of the GPS raw data was given by Prof. E. Lagios. Part of the collection and analysis of GPS data was financed by (i) The European Union (75%), (ii) The General Secretariat for Research & Technology (25%), and (iii) Terramentor E.E.I.G. Funding for offshore work at Santorini Volcanic Field was provided by GEOWARN project. The European Commission is acknowledged for their financial contribution to the project. The officers and the crew of the R/V AEGAEO are gratefully acknowledged for their important and effective contribution to the field work.

References

Alexandri, M., D. Papanikolaou & P. Nomikou (2003). Santorini volcanic field - new insights based on swath bathymetry. Abstracts IUGG, 30 June-11July 2003, Sapporo, Japan.

Bohnhoff, M., M. Rische, Th. Meier, D. Becker, G. Stavrakakis & H-P. Harjes (2006). Microseismic activity in the Hellenic Volcanic Arc, Greece, with emphasis on the seismotectonic setting of the Santorini–Amorgos zone. Tectonophysics, 423, 17–33.

Dimitriadis, I., E. Karagianni, D. Panagiotopoulos, C. Papazachos, P. Hatzidimitriou, M. Bohnhoff, M. Rische, & T. Meier (2009). Seismicity and active tectonics at Coloumbo Reef (Aegean Sea, Greece): Monitoring an active volcano at Santorini Volcanic Center using a temporary seismic network. Tectonophysics, 465, 136-149.

Druitt, T.H., R.A. Mellors, D.M. Pyle, & R.S.J. Sparks (1989). Explosive volcanism on Santorini, Greece. Geol. Mag., 126, 95-126.

Druitt, T.H., L. Edwards, R.A. Mellors, D.M. Pyle, R.S.J. Sparks, M. Lanphere, M. Davies, & B. Barreirio (1999). Santorini Volcano. Geol. Soc. Mem., 19, 165.

Dvorak, J.J., & D. Dzurisin (1997). Volcano geodesy; the search for magma reservoirs and the formation of eruptive event. Rev. Geophys., 35, 343–384.

Fernández, J., J.M. Carrasco, J.B. Rundle, & V. Aránа (1999). Geodetic methods for detecting volcanic unrest: A theoretical approach. Bull. Volcanol., 60, 534–544.

Fouqué, F., 1879. Santorin et ses eruptions. Masson et Cie., Paris, 440p.

Fytikas, M., F. Innocenti, P. Manetti, R. Mazuoli, A. Peccerilo & L. Vilari (1984). Tertiary to Quaternary evolution of the volcanism in the Aegean Region. In Dixon J.E. & Robertson A.H.F. (eds.). The Geological Evolution of the Eastern Mediterranean. Geol. Soc. London, Spec. Pub., 17, 687-699.

Heiken, G., & F. McCoy (1984). Caldera development during the Minoan eruption, Thera, Cyclades, Greece. J. Geophys. Res., 89, 8441-8462.

Jackson, J.A. (1994). Active tectonics of the Aegean region. Annual Reviews of Earth and Planetary Sciences, 22, 239-271.

Le Pichon, X., & J. Angelier (1979). The Hellenic Arc and trench system: a key to the Neotectonic evolution of the Eastern Mediterranean area. Tectonophysics, 60, 1-42.

Mountrakis, D., S. Pavlides, A. Chatzipetros, S. Meletidis, M. Tranos, G. Vougioukalakis & A. Kilias (1998). Active deformation in Santorini. In: Casale R., Fytikas M., Sigvaldarsson, G., & G. Vougioukalakis (eds): The European laboratory volcanoes. European Commission, EUR 18161, 13-22.

Nomikou, P., S. N. Carey, D. Papanikolaou, K.L.C Bell, D. Sakellariou, M. Alexandri, & K. Bejelou (2011a). Exploration of the submarine cones in the Kolumbo Submarine Volcanic Zone of the Hellenic Arc (Aegean Sea, Greece). Journal of Global and Planetary Change, In review.

Nomikou, P., D. Papanikolaou, M. Alexandri,& D. Sakellariou (2011b). Submarine Volcanoes along the Agean Volcanic Arc. Tectonophysics, In review.

Papanikolaou, D. (1993). Geotectonic evolution of the Aegean. Bull. Geol. Soc. Greece, XXVII, 33-48.

Papageorgiou, E., E. Lagios, S. Vassilopoulou & V. Sakkas, (2007). Vertical & Horizontal Ground Deformation of Santorini Island deduced by DGPS measurements. Proceedings of the 11th International Conference Geol. Soc. Greece, Athens, Greece. Bull. Geol. Soc. Greece, 40 (3), 1219-1225.

Papageorgiou E., A. Tzanis, P. Sotiropoulos, & E. Lagios (2010). DGPS and magnetotelluric constraints on the contemporary tectonics of Thera Island, Greece. Bull. Geol. Soc. Greece, XLIII, 1,344-356.

Pe-Piper, G. & D.J.W. Piper (2005). The South Aegean active volcanic arc: relationships between magmatism and tectonics. Develop. in Volc., 7, 113-133.

Sakellariou D., H. Sigurdsson, M. Alexandri, S. Carey, G. Rousakis, P. Nomikou, P. Georgiou & D. Ballas (2010). Active tectonics in the Hellenic volcanic arc: The Kolumbo submarine volcanic zone. Bull. Geol. Soc. Greece, XLIII, 2,1056-1063.

Sigurdsson, H., S. Carey, M. Alexandri, G. Vougioukalakis, K. L. Croff, C. Roman, D. Sakellariou, C. Anagnostou, G. Rousakis, C. Ioakim, A. Gogou, D. Ballas, T. Misaridis, and P. Nomikou 2006. Marine investigations of Greece's Santorini volcanic field. EOS, 87(34):337, 342.

Reck, H. (1936). Santorini. –Der Werdergang eines Inselvulcans und sein Ausbruch 1925-1928. Dietrich Reimer, Berlin, 3 vols. MANCA.

THE DYNAMIC ANALYSIS OF MULTI-DRUM ANCIENT STRUCTURES UNDER EARTHQUAKE EXCITATIONS

Loizos Papaloizou (1), Petros Komodromos (2)

(1) University of Cyprus, Department of Civil and Environmental Engineering, School of Engineering, University of Cyprus 75 Kallipoleos Street, PO Box 20537, 1678 Nicosia, Cyprus. Email: loizop@ucy.ac.cy
(2). University of Cyprus, Department of Civil and Environmental Engineering, School of Engineering, University of Cyprus 75 Kallipoleos Street, PO Box 20537, 1678 Nicosia, Cyprus. Email: komodromos@ucy.ac.cy

Abstract (The dynamic analysis of multi-drum ancient structures under earthquake excitations): *The seismic behaviour of ancient monumental structures with monolithic or multi-drum classical columns and colonnade systems in two rows is investigated. In particular, the Discrete Element Method (DEM) is utilized in the study of ancient columns under strong ground excitations, by simulating the individual rock blocks as distinct bodies. A specialized software application is developed, using a modern object-oriented programming language, in order to enable the effective simulation of multi-drum columns and colonnades. A number of parametric studies is performed in order to investigate the effect of excitation characteristics on the behaviour of multi-drum columns under harmonic and earthquake excitations. The simulations reveal that the columns and colonnades have the capacity to successfully withstand earthquakes excitations that were selected from regions where these monuments are often built.*

Key words*: Ancient Columns, Earthquake, DEM.*

INTRODUCTION

Strong earthquakes are common causes of destruction of ancient monuments, such as classical columns and colonnades. Ancient classical columns of great archaeological significance can be abundantly found in high seismicity areas in the Eastern Mediterranean. Multi-drum columns are constructed of stone blocks that are placed on top of each other, with or without connecting material between the individual blocks. The seismic behaviour of these structures exhibits complicated rocking and sliding phenomena between the individual blocks of the structure that very rarely appear in modern structures.

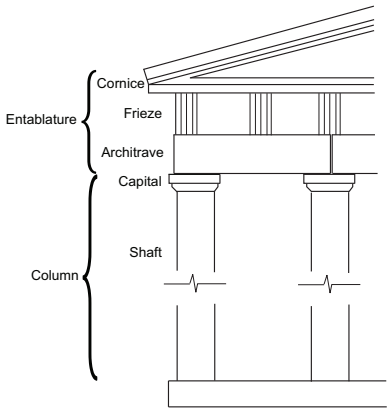

Fig. 1: Architecture of a typical classical monument.

In ancient Greece the temples formed the most important class of buildings erected during that era and can be classified into three "Orders of Architecture", the Doric, Ionic and Corinthian order. An "order" in Greek architecture consists of the column, including the base and the capital, and the entablature (Fig. 1). The entablature is divided into the architrave (lower part), the frieze (middle part) and the cornice (upper part). The differences among these three orders refer on the dimensions, proportions, mouldings and decorations of the various parts.

Today, the remains of most of these temples are often limited to series of columns with an entablature or only an architrave, and in some cases only standalone columns. The investigation of the seismic behaviour of such monuments is scientifically interesting, as it involves complicated rocking and sliding responses of the individual rock blocks. The understanding of the seismic behaviour of these structures contributes to the rational assessment of efforts for their structural rehabilitation and may also reveal some information about past earthquakes that had struck the respective region.

Ancient monuments, compared to modern structures, have been exposed to large numbers of strong seismic events throughout the many centuries of their life spans. Those that survived have successfully withstood a natural seismic testing that lasted for several centuries. Thus, it is important to understand the mechanisms that enabled them to avoid structural collapse and destruction during strong earthquakes. Since analytical study of such multi-block structures under strong earthquake excitations is practically difficult, if not impossible for large numbers of blocks, while laboratory tests are very difficult and costly, numerical methods can be used to simulate their seismic response.

A very extensive review of the literature on the usage of numerical methods for the analysis of monuments until 1993 was published by Beskos (1993). The dynamic behaviour of infinitely rigid bodies during horizontal excitations was studied by Housner (1963), while, later on, other researchers (Psycharis et al., 2003, Pompei et al., 1998, Makris & Zhang, 1998, Manos et al., 2001, Komodromos et al., 2008) investigated further, both analytically and experimentally, the required conditions to overturn rigid bodies. Such structures can be simulated utilizing the Discrete Element Methods (DEM), which have been specifically developed for systems with distinct bodies that can move freely in space and interact with each other with contact forces through an automatic and efficient recognition of contacts.

Research efforts to use the DEM in the simulation of ancient structures have already shown promising results, motivating further utilization of this method. Recent research work based on commercial DEM software applications (Psycharis et al., 2003, Papantonopoulos, 2002), demonstrated that the DEM can be reliably used for the analysis of such structures, although they reported a sensitivity of the response to small perturbations of the characteristics of the structure or the excitation. However, similar sensitivity has also been observed in experiments with classical columns (Mouzakis et al., 2002). Hence, it is important to perform large numbers of simulations with varying earthquake characteristics and design parameters to properly assess and interpret the simulation results.

Latest research studies in the fields of paleoseismology and archaeoseismology (Hinzen et al., 2010, Caputo et al., 2011) investigate the damage in ancient monument structures and propose various quantitative models to test the seismogenic hypothesis of observed damage. Papaloizou and Komodromos (2011) used the Discrete Element Method (DEM) as well as a modern object-oriented design and programming approach, in order to examine the simulation of multi-drum columns and colonnades under harmonic and earthquake excitations.

A custom-made DEM software has been specifically designed (Papaloizou and Komodromos, 2011) and implemented to enable efficient performance of large numbers of numerical simulations with varying parameters, modelling these structures with independent distinct bodies, as they are constructed in practice. Such simulations allow us to assess the influence of different earthquake characteristics as well as the various mechanical and geometrical parameters of these structures on their seismic responses.

NUMERICAL ANALYSIS

A large number of parametric studies is performed in order to investigate the effect of excitation characteristics as well as the influence of geometrical and mechanical characteristics of multi-drum columns on their behaviour and response under harmonic and earthquake excitations. Colonnade systems with two rows of columns, one over the other, are examined with earthquake ground motions.

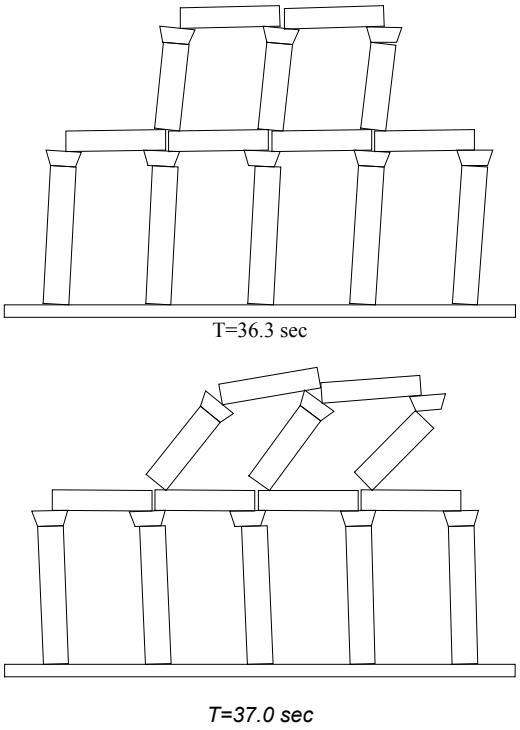

Fig. 2: Mexico City Earthquake (scaled 1.5 Times).

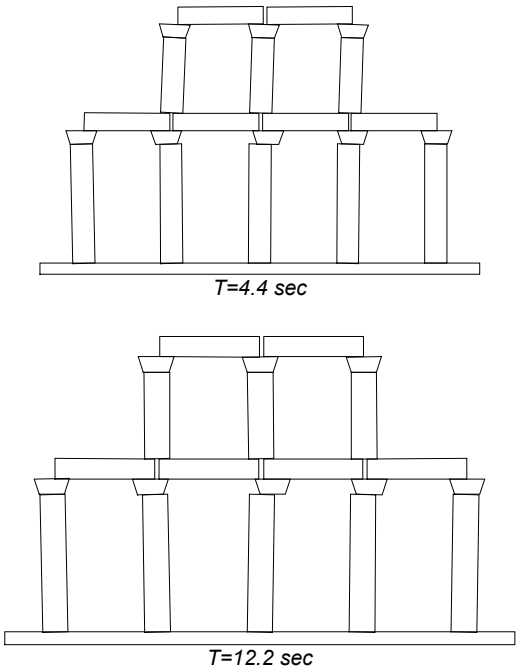

Fig. 3: Athens Earthquake (scaled 9 Times).

Parametric studies have been performed by varying the excitation frequency and acceleration, as well as the friction coefficient and the geometric

characteristics of the simulated columns and colonnades in order to assess the influence of these parameters in the seismic response of the structure.

Fig. 2 and Fig. 3 show snapshots (in different time steps) of the response of such structural systems for the Mexico City and the Athens Earthquakes, respectively (Table 1). The results show that the frequency content of the ground motion affects significantly the response. The displacements of the upper level columns in respect to the displacements of the lower level column are affected by the frequency content of the excitation.

Specifically, for the Mexico City earthquake, which has low predominant frequencies, the upper level columns overturn. For the Athens Earthquake, which has higher predominant frequencies, and for a much larger maximum ground acceleration the upper level columns are not affected by the seismic excitation.

Date and Time	Earthquake Component	PGA (m/sec2)	Predominant Frequencies (Hz)
9/19/1995 (13:19CT)	Mexico City (270)	0.98	0.45-0.53
9/7/1999 (11:56:50)	Athens (N46)	3.01	4.1-8.3

Table 1. List of earthquake records that have been used in the analyses.

Moreover, for low frequency harmonic excitations, the exhibited response is dominated by rocking, while sliding prevails in cases of excitations with very high frequencies. In between the two extremes, the response contains both rocking and sliding phenomena.

Furthermore, the results indicate that the required acceleration to initiate rocking or sliding decreases as the excitation frequency increases. The acceleration that is needed to overturn the column also increases as the frequency increases.

By examining the stability of multi-drum columns and colonnades for earthquakes that were selected from regions, where these monuments are often built, such as the Eastern Mediterranean regions, the simulations reveal that the columns have the capacity to successfully withstand strong earthquakes. The required acceleration to overturn a column decreases as the predominant frequency of the earthquake decreases.

The investigation of the dynamic response of such monumental structures, combined with the research fields of paleoseismology and archaeoseismology, may reveal certain information from past strong earthquakes that have struck the respective regions. The investigation of the response of multi-drum structures under different ground motions can help in defining the frequency content of old destructive earthquakes.

Acknowledgements: The authors would like to thank the Cyprus Research Promotion Foundation for funding the active research project entitled “Investigation for the protection of ancient multi-drum columns and colonnades from strong earthquakes (ΑΝΘΡΩΠΙΣΤΙΚΕΣ/ΑΝΘΡΩ/0609(BE)/23)”.

References

Beskos D. (1993), “Use of finite and boundary elements in the analysis of monuments and special structures”, Association of Civil Engineers of Greece, 217.

Caputo, R., Hinzen, K.-G., Liberatore, D., Schreiber, S., Helly, B., Tziafalias, A., (2011), “Quantitative archaeoseismological investigation of the Great Theatre of Larissa, Greece “Bulletin of Earthquake Engineering. 9 (2), pp. 347-366.

Hinzen, K.-G., Fleischer, C., Reamer, S.K., Schreiber, S., Schütte, S., Yerli, B., (2010), “Quantitative methods in archaeoseismology” Quaternary International, DOI: 10.1016/j.quaint.2010.11.006.

Housner G.W (1963), ‘The behavior of inverted pendulum structures during earthquakes”. Bulletin of seismological Society of America, 53, 403-417.

Komodromos P., Papaloizou L., Polycarpou P., (2008) “Simulation of the response of ancient columns under harmonic and earthquake excitations”, Engineering Structures 30(8), 2154-2164.

Makris N. and Zhang J., (2001) “Rocking response of anchored blocks under pulse-type motions”, Engineering Mechanics 127, 484-493.

Manos G.C., Demosthenous M., Kourtides V., Hatzigeorgiou A., (2001) “Dynamic and earthquake behavior of models of ancient columns and colonnades with or without energy absorbtions systems”, Proceedings of Second Greek National Conference on Earthquake Engineering and Seismology, 1, 257-276.

Mouzakis H., Psycharis I., Papastamatiou D., Carydis P., Papantonopoulos C., and Zambas C., (2002). “Experimental investigation of the earthquake response of a model of a marble classical column”, Earthquake Engineering and Structural Dynamics 31, 1681-1698.

Papaloizou, L., Komodromos, P., (2011) “Investigating the seismic response of ancient multi-drum colonnades with two rows of columns using an object-oriented designed software”, Advances in Engineering Software, DOI: 10.1016/j.advengsoft.2011.05.030.

Papantonopoulos C., Psycharis I., Papastamatiou D., Lemos J. and Mouzakis H., (2002). “Numerical prediction of the earthquake response of classical columns using the distinct element method”, Earthquake Engineering and Structural Dynamics 31, 1699-1717.

Pompei A., Scalia A. and Sumbatyan M.A. (1998), “Dynamics of Rigid Block due to Horizontal Ground Motion”, Engineering Mechanics 124, 713-717.

Psycharis I., Lemos J., Papastamatiou D., Zambas C. and Papantonopoulos C. (2003), “Numerical study of the seismic behaviour of a part of the Parthenon Pronaos”, Earthquake Engineering & Structural Dynamics 32, 2063-2084.

EARTHQUAKE ARCHAEOLOGY

INQUA PALEOSEISMOLOGY AND ACTIVE TECTONICS

NEOTECTONIC AND ACTIVE DIVERGING RATES OF EXTENSION IN THE NORTHERN AND SOUTHERN HELLENIDES ACROSS THE CENTRAL HELLENIC SHEAR ZONE

Papanikolaou, Dimitrios (1), Royden, Leigh (2), Vassilakis, Emmanuel (1)

(1) School of Geology and Geoenvironment, Department of Dynamics, Tectonics and Applied Geology, National and Kapodistrian University of Athens, 15784, Greece. Email: dpapan@geol.uoa.gr

(2) Department of Earth, Atmospheric and Planetary Sciences, Massachusetts Institute of Technology, 54-826, Cambridge, MA 02139, USA

Abstract (Neotectonic and active diverging rates of extension in the Northern and Southern Hellenides across the Central Hellenic Shear Zone): *Present day location and geometry of the Hellenic arc and trench system is only a small portion of the previously developed Hellenic arc that created the Hellenides orogenic system. The timing of differentiation is constrained in Late Miocene, when the arc was divided in a northern and a southern segment. This is based on: a) the dating of the last compressive structures observed all along the Hellenides during Oligocene to Middle-Late Miocene, b) on the time of initiation of the Kephalonia transform fault, c) on the time of opening of the North Aegean Basin and d) on the time of opening of new arc parallel basins in the south and new transverse basins in the central shear zone, separating the rapidly moving southwestward Hellenic subduction system from the slowly converging system of the Northern Hellenides. The driving mechanism of the arc differentiation is the heterogeneity produced by the different subducting slabs in the north (continental) and in the south (oceanic) and the resulted shear zone because of the retreating plate boundary producing a roll back mechanism in the present arc and trench system. The extension produced in the upper plate has resulted in the subsidence of the Aegean Sea and the creation of several neotectonic basins in southern continental Greece in contrast to the absence of new basins in the northern segment since Late Miocene. Crustal thickness, structural profiles, earthquake mechanisms and GPS rates are compared in the two segments, showing significant extension in the Southern Hellenides.*

Key words*: Hellenides, neotectonic extension, slab roll-back*

INTRODUCTION

The active portion of the Hellenic orogen is an arcuate belt reaching from the central Adriatic Sea southwards and eastwards to western Anatolia (McKenzie, 1978; Le Pichon and Angelier, 1979; Picha, 2002; Reilinger et. al., 2006). Within the northwest-trending portion of the Hellenic belt, two segments can be distinguished by subduction rate (slow in the northwest, fast in the southeast) and water depth of the foreland lithosphere (shallow in the northwest, deep in the southeast; e.g. Dewey and Sengor, 1979; Finetti, 1982; McKenzie, 1978; Le Pichon and Angelier, 1979, Fig. 1). These segments, dextrally offset from one another near the island of Kephalonia, have been referred as the Northern and Southern Hellenides (Papanikolaou and Royden, 2007; Royden and Papanikolaou, 2011).

THE SEPARATION OF THE NORTHERN AND SOUTHERN HELLENIDES BY THE CENTRAL HELLENIC SHEAR ZONE

Several years of GPS measurements indicate a convergence rate of ~5-10 mm/yr across the Northern Hellenic subduction boundary, as measured between stations on the subducting plate (Apulia) and on the over-riding plate in northern Greece (Hollenstein et al., 2008; Bennett et al., 2008; Vassilakis et al., 2011) and seismic activity and focal solutions for local earthquakes attest to continuing convergence in this region (e.g. Louvari et al., 1999; Papazachos et al., 2000). Based on evidence from seismology, morphology and industry seismic data, the active thrust front of the Northern Hellenides lies just west of the Ionian islands of Corfu and Paxos (Monopolis & Bruneton, 1982; Vassilakis et al., 2011) (Fig. 1).

Even though gravity data indicate that the basement is flexed downward beneath the thrust front and the resulting depression filled with sedimentary foredeep deposits (Moretti and Royden, 1988), no trench is present in the bathymetry along the Northern Hellenides. For ease of reference we will refer to this zone of convergence as the Northern Hellenic trench, despite the fact that the trench has been entirely filled with sediments. The lithosphere entering the Northern Hellenic trench is continental or transitional in character, with a crustal thickness of ~25-30 km (Morelli et al, 1975; Marone et al, 2003, Cassinis et. al., 2003). Modern water depths near the thrust belt are generally ~1 km or less and overlie a shallow water sedimentary sequence of Triassic through Pliocene age (Jacobshagen et al., 1978).

On the contrary the same GPS data indicate a convergence rate of ~35 mm/yr across the Southern Hellenides, as measured between Africa and points in the over-riding (Aegean) domain (McClusky et al., 2000; Reilinger et al., 2006). Behind the Southern Hellenides, a Benioff zone reaches to ~150 km depth (e.g. Papazachos et al., 2000) and an active volcanic arc is present ~200 km behind the trench (Fytikas et al., 1984). The zone along which basement is subducted beneath the Hellenides lies ~50 km west

of the southwestern coast of the Peloponnesus, passing beneath the deepest portions of the Hellenic trench (Fig. 1). Here, earthquake hypocenters and gravity data indicate that the depth to basement is ~12-15 km depth (Royden 1993; Hirn et al., 1997; Clément et al., 2000; Sachpazi et al., 2000). Thrust faults and folds also occur within the accretionary prism outboard of the trench, over a width of several hundred kilometers to the Mediterranean ridge (Kopf et al., 2003), but thrusting here involves only sedimentary cover detached above the basement. The crust beneath the Ionian Sea is almost certainly oceanic, probably Triassic or Jurassic in age, and consists of approximately 8 km of crystalline crust overlain by 6-10 km of sedimentary cover (Makris, 1985; Kopf et al., 2003). The water depth throughout much of the Ionian Sea region is 3-4 km, with the deepest depths of up to 5 km occurring along the Southern Hellenic Trench.

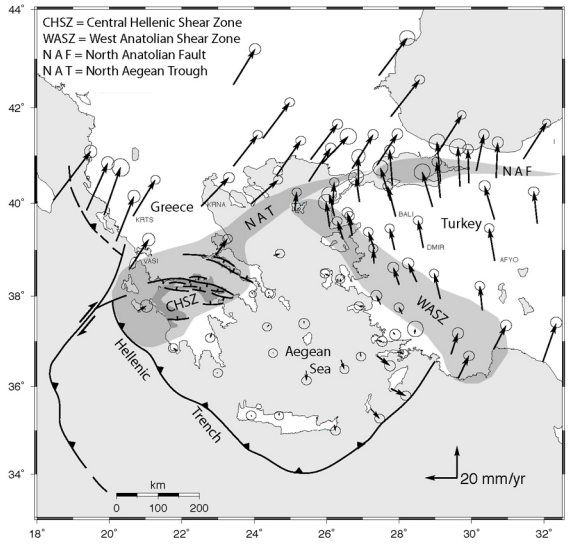

Fig. 1: Selected GPS velocities from McClusky et al. [2000] in a reference frame that minimizes velocities in the Aegean region. Some data were omitted in areas where high data density obscured the velocity pattern, mainly near the North Anatolian Fault zone. Shading indicates the zones of active oblique extension that bound the northwestern and northeastern margins of the largely undeforming Aegean domain.

The northern and southern segments of the Hellenic subduction boundary are separated by the Kephalonia transform zone (e.g. Dewey and Sengor, 1979; Finetti, 1982; Kahle and Muller, 1998; Kahle et al., 1995; Hollenstein et al., 2008), across which GPS data indicate ~25 mm/yr of dextral motion (Fig. 1). The Kephalonia transform separates the slowly subducting, continental foreland of the northern Hellenides from the rapidly moving upper plate of the southern Hellenides. Focal solutions from earthquakes located along the Kephalonia transform show right-slip on steep southwest-striking fault planes and also thrust faulting along northeast-striking fault planes.

The Kephalonia transform coincides closely with a change in foreland water depth from ~1 km in front of the Northern Hellenides to ~3-4 km in front of the Southern Hellenides, particularly near the west coast of mainland Greece (Fig. 1). Here the Hellenic subduction boundary (trench) appears to be dextrally offset by ~100-150 km across the Kephalonia transform zone, although the precise offset is difficult to determine due to north-south variations in water depth and sediment thickness and due to the fact that some of the offset of the northern and southern segments is taken up by clockwise rotation of crustal units adjacent to the south side of the transform (Vassilakis et al., 2011). Northeastward, the Kephalonia transform zone extends into mainland Greece to merge with the broadly defined zone of dextral and extensional deformation in the Central Hellenic Shear Zone (Papanikolaou and Royden, 2007; see also discussions by Goldsworthy et al., 2002; Armijo et al., 1996; Roberts and Jackson, 1991).

Global P-wave tomography indicates a northeast-dipping zone of high P-wave speeds beneath the Southern and Northern Hellenides (Spakman et al., 1993; van der Hilst et al., 1997; Karason and van der Hilst, 2001; Wortel and Spakman, 2000; Suckale et al., 2009). Behind the Southern Hellenides, the subducted lithosphere appears to reach to the base of the upper mantle, perhaps deeper. A northeast-dipping zone of high P-wave speed also exists north of the Kephalonia transform zone, but here the velocity contrast with the surrounding mantle is not as large as beneath the Southern Hellenides.

COMPARISON OF TECTONIC STRUCTURES AND DEFORMATION RATES BETWEEN THE NORTHERN AND SOUTHERN HELLENIDES

The difference of the tectonic structure and of the deformation rates in the Northern and Southern Hellenides can be studied in two time periods: the recent neotectonic period of the last 5 million years during the Pliocene-Pleistocene and the active deformation of the last 14000 years during the Holocene incorporating also the actual observations and measurements. The main points showing the diverging rates of extension in the two segments of the Hellenides are the following.

1) The width of the Hellenic peninsula from the Ionian sea at the west to the Aegean Sea at the east, is longer approximately by 60 km across the southern profile which corresponds to the offset of the trench across the Kephalonia transform since the Aegean coast is rather rectilinear from the Olympus foothills to the Southern Evia and Andros-Tinos-Mykonos Cycladic islands.

2) The crustal thickness in the Southern Hellenides is much thinner (less than 25 km) than in the Northern Hellenides (up to 45 km) (Makris, 1977; 1985).

3) The tectonic structure of the Southern Hellenides is characterised by the occurrence of the External Tectonometamorphic Belt in Peloponnesus in the form of tectonic windows, which resulted from extensional detachments during Miocene

(Papanikolaou and Royden, 2007; Papanikolaou et al., 2009). Thus, the structure in the Northern Hellenides is rather simple with a regular nappe emplacement from the area west of the Olympus tectonic window up to the Ionian Sea in contrast to the more complex structure in the Southern Hellenides, where there are new metamorphic geotectonic units (such as the Mani and Arna units) appearing below the non metamorphosed nappes (such as the Tripolis and Pindos units) (Papanikolaou and Vassilakis, 2010).

4) A number of arc parallel extensional neotectonic basins oriented NW-SE occur along the transverse profile of the Southern Hellenides (e.g. in Southern Peloponnesus) as described by Papanikolaou et al. 1988 (Fig. 2). In contrast, no neotectonic basins are developed in the transverse profile of the Northern Hellenides with the exception of the Ioannina basin (the only extensive Plio-Quaternary structure west of the Oligo-Miocene Mesohellenic basin). The difference of extension in the two segments within the upper plate is more than 20%.

5) The last onshore compressive structures in the Northern Hellenides are observed in Corfu and Parga areas, involving Late Miocene and early Pliocene sedimentary formations (including the Messinian evaporites) and in Kephalonia and Zakynthos islands in the Southern Hellenides with a dextral offset similar to the Kephalonia transform but somewhat smaller.

6) The transition from compression to extension as determined by earthquake mechanisms occurs in central Epirus in the Northern Hellenides and in the shallow marine zone between the Ionian islands and mainland Greece in the Southern Hellenides.

7) The rate of upper plate extension across the belt is ~3-5mm/yr in the Northern Hellenides and more than 30mm/yr in the Southern Hellenides.

EPILOGUE

All arguments displayed above point to the same conclusion of differentiation between the northern and southern Hellenides, regarding the amount of the extension both during the neotectonic period and the present day deformation. In many cases this differentiation can be quantified and the results are quite impressive showing that a major complex structure such as the Central Hellenic Shear Zone is acting as an oblique transform structure of the Hellenides by dividing the Hellenic peninsula and changing the present morphology.

Acknowledgements: This research was supported by the Continental Dynamics Program at NSF, grant EAR-0409373.

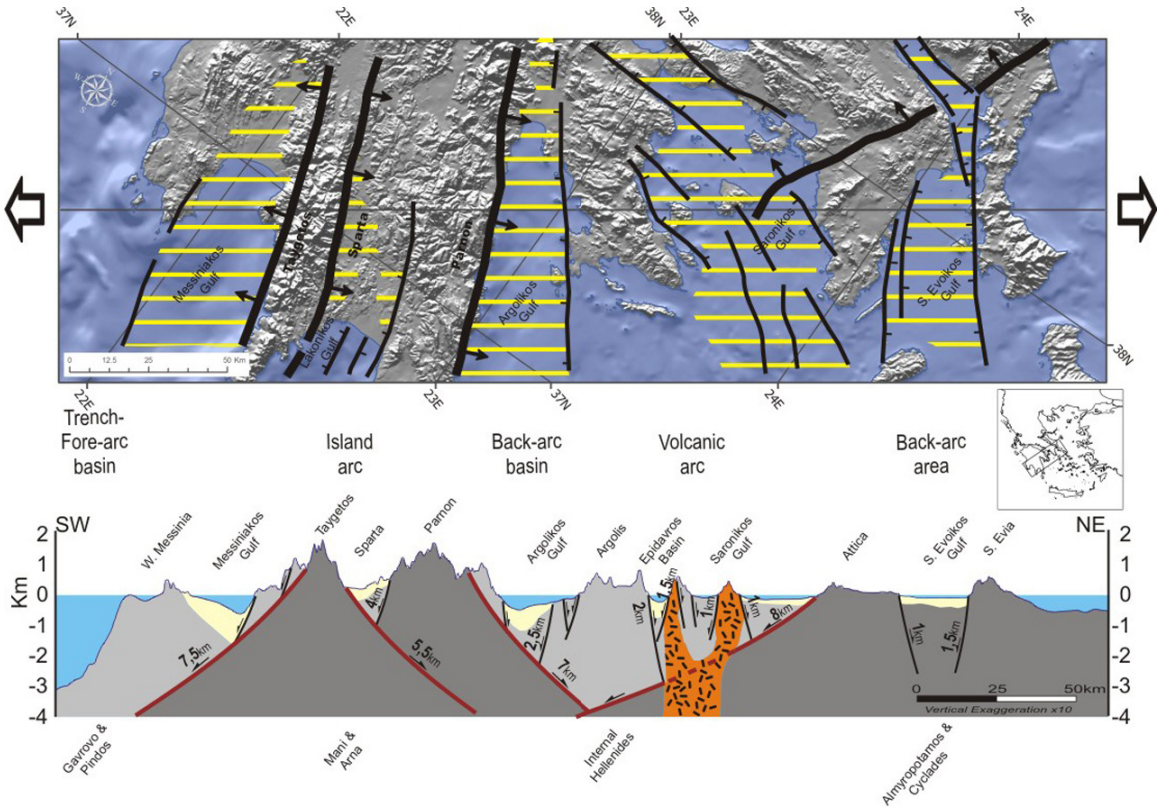

Fig. 2: In this vertically exaggerated (x10) SW-NE section across the Southern Hellenides the post-nappestacking extensional structures are indicated.

References

Armijo, R., et al. (1996), Quaternary evolution of the Corinth Rift and its implications for the late Cenozoic evolution of the Aegean, *Geophys. J. Int*, *126*, 11-53.

Bennett, R. A., et al. (2008), Eocene to present subduction of southern Adria mantle lithosphere beneath the Dinarides, *Geology*, *36*(1), 3-6.

Cassinis, R., et al. (2003), The deep crustal structure of Italy and surrounding areas from seismic refraction data: a new synthesis, *Bollettino di Geofisica Teorica ed Applicata*, *122*, 365-375.

Clément, C., et al. (2000), Seismic structure and the active Hellenic subduction in the Ionian islands, *Tectonophysics*, *329*(1-4), 141-156.

Dewey, J. F., and C. Şengör (1979), Aegean and surrounding regions: Complex multiplate and continuum tectonics in a convergent zone, *Geological Society of America Bulletin*, *90*(1), 84-92.

Finetti, I. (1982), Structure, stratigraphy and evolution of central Mediterranean (Pelagian Sea, Ionian Sea), *Bollettino di Geofisica Teorica ed Applicata*, *24*(96), 247-312.

Fytikas, M., et al. (1984), Tertiary to Quaternary evolution of volcanism in the Aegean region, in *The geological evolution of the eastern Mediterranean*, edited by J. Dixon and A. Robertson, pp. 687-701, Geological Society of London, London.

Goldsworthy, M., et al. (2002), The continuity of active fault systems in Greece, *Geophysical Journal International*, *148*(3), 596-618.

Hirn, A., et al. (1997), Increase in melt fraction along a south-north traverse below the Tibetan Plateau: evidence from seismology, *Tectonophysics*, *273*(1-2), 17-30.

Hollenstein, C., et al. (2008), Crustal motion and deformation in Greece from a decade of GPS measurements, 1993-2003, *Tectonophysics*, *449*(1-4), 17-40.

Jacobshagen, V. (1986), *Geologie von Griechenland*, 363 pp.

Kahle, H. G., and S. Mueller (1998), Structure and dynamics of the Eurasian-African/Arabian plate boundary system: Objectives, tasks and resources of the WEGENER group, *Journal of Geodynamics*, *25*(3-4), 303-325.

Kahle, H. G., et al. (1995), The strain field in northwestern Greece and the Ionian Islands: results inferred from GPS measurements, *Tectonophysics*, *249*, 41-52.

Kopf, A., et al. (2003), The Mediterranean Ridge: A mass balance across the fastest growing accretionary complex on Earth, *J. Geophys. Res.*, *108*(B8), 2372.

Le Pichon, X., and J. Angelier (1979), The Hellenic arc and trench system: a key to the neotectonic evolution of the eastern Mediterranean area, *Tectonophysics*, *60*, 1-42.

Louvari, E., et al. (1999), The Cephalonia Transform Fault and its extension to western Lefkada Island (Greece), *Tectonophysics*, *308*, 223-236.

Makris, J. (1976), A dynamic model of the Hellenic Arc deduced from Geophysical data, *Tectonophysics*, *36*, 339-346.

Makris, J. (1985), Geophysics and geodynamic implications for the evolution of the Hellenides, in *Geological Evolution of the Mediterranean Basin*, edited by D. J. Stanley and F. Wezel, pp. 231–248, Springer, Berlin

Marone, F., et al. (2003), Joint inversion of local, regional and teleseismic data for crustal thickness in the Eurasia-Africa plate boundary region, *Geophysical Journal International*, *154*(2), 499-514.

McClusky, S., et al. (2000), Global Positioning System constraints on plate kinematics and dynamic in the eastern Mediterranean and Caucasus, *Journal of Geophysical Research*, *105*(B3), 5695-5719.

McKenzie, D. (1978), Active tectonics of the Alpine-Himalayan belt: the Aegean Sea and surrounding regions, *Geophysical Journal of the Royal Astronomical Society*, *55*(1), 217-254.

Monopolis, D., and A. Bruneton (1982), Ionian sea (Western Greece): Its structural outline deduced from drilling and geophysical data, *Tectonophysics*, *83*(3-4), 227-242.

Morelli, C., et al. (1975), Bathymetry, gravity and magnetism in the Strait of Sicily and in the Ionian Sea, *Bollettino di Geofisica Teorica ed Applicata*, *17*, 39-58.

Moretti, I., and L. Royden (1988), Deflection, Gravity-Anomalies and Tectonics of Doubly Subducted Continental Lithosphere - Adriatic and Ionian Seas, *Tectonics*, *7*(4), 875-893.

Papanikolaou, D., (2010), Major palaeogeographic, tectonic and geodynamic changes from the last stage of the Hellenides to the actual Hellenic arc and trench system, *Bulletin Geological Society of Greece, XLIII(1)*, 72-85.

Papanikolaou, D., and E. Vassilakis (2010), Thrust faults and extensional detachment faults in Cretan tectono-stratigraphy: Implications for Middle Miocene extension, *Tectonophysics*, *488*(1-4), 233-247.

Papanikolaou, D., and L. Royden (2007), Disruption of the Hellenic arc: Late Miocene extensional detachment faults and steep Pliocene-Quaternary normal faults - Or what happened at Corinth?, *Tectonics*, *26* (TC5003).

Papanikolaou, D., et al. (1988), A comparative study of neotectonic basins across the Hellenic Arc: The Messiniakos, Argolikos, Saronikos and Southern Evoikos Gulfs, *Basin Research, 1*, 167-176.

Papanikolaou, D., et al. (2009), The Itea-Amfissa detachment: a pre-Corinth rift Miocene extensional structure in central Greece, *Geological Society, London, Special Publications*, *311*(1), 293-310.

Papazachos, B. C., et al. (2000), The geometry of the Wadati-Benioff zone and lithospheric kinematics in the Hellenic arc, *Tectonophysics*, *319*, 275-300.

Picha, F. J. (2002), Late Orogenic Strike-Slip Faulting and Escape Tectonics in Frontal Dinarides-Hellenides, Croatia, Yugoslavia, Albania, and Greece, *AAPG Bulletin*, *86*(9), 1659-1671.

Reilinger, R., et al. (2006), GPS constraints on continental deformation in the Africa-Arabia-Eurasia continental collision zone and implications for the dynamics of plate interactions, *J. Geophys. Res.*, *111*.

Roberts, S., and J. Jackson (1991), Active normal faulting in central Greece: an overview, *Geological Society, London, Special Publications*, *56*(1), 125-142.

Royden, L. H. (1993), Evolution of retreating subduction boundaries formed during continental collision, *Tectonics*, *12*(3), 629-638.

Royden, L., and D. Papanikolaou (2011), Slab segmentation and late Cenozoic disruption of the Hellenic arc, *Geochem. Geophys. Geosyst.*, *12*(3), Q03010.

Sachpazi, M., et al. (2000), Western Hellenic subduction and Cephalonia Transform: local earthquakes and plate transport and strain, *Tectonophysics*, *319*(4), 301-319.

Spakman, W., et al. (1993), Travel-time tomography of the European-Mediterranean mantle down to 1400 km, *Physics of The Earth and Planetary Interiors*, *79*(1-2), 3-74.

Suckale, J., et al. (2009), High-resolution seismic imaging of the western Hellenic subduction zone using teleseismic scattered waves, *Geophysical Journal International*, *178*(2), 775-791.

van der Hilst, R. D., et al. (1997), Evidence for deep mantle circulation from global tomography, *Nature*, *386*(6625), 578-584.

Vassilakis, Emm., et al. (2011), Kinematic Links from the Hellenic Trench to the Western Gulf of Corinth. *Earth & Planetary Science Letters, 303,* 108-120.

Wortel, M. J. R., and W. Spakman (2000), Subduction and Slab Detachment in the Mediterranean-Carpathian Region, *Science*, *290*(5498), 1910-1917.

CLUSTERING AND ANTICLUSTERING IN THE SOUTHERN APENNINES AS EVIDENCED FROM GEOLOGICAL FAULT SLIP-RATE SEISMIC HAZARD MAPS AND THE HISTORICAL RECORD

Papanikolaou Ioannis D. (1,2), Gerald Roberts (2)

(1) Mineralogy-Geology Laboratory, Department of Earth and Atmoshperic Sciences, Agricultural University of Athens, Iera Odos 75, 118-55, Athens, Greece
(2) Department of Earth and Planetary Sciences, Birkbeck and University College London, Gower Street, WC1E 7HX. UK.
i.papanikolaou@ucl.ac.uk, gerald.roberts@ucl.ac.uk

Abstract (Clustering and anticlustering in the Southern Apennines as evidenced from geological fault slip-rate seismic hazard maps and the historical record): *Geological fault slip rate seismic hazard maps were constructed in the area of the southern Apennines. By comparing short-term throw-rates (e.g. historical record) with longer-term throw-rates (e.g. offset postglacial geomorphic features), one might be able to differentiate areas that are currently in a cluster of earthquakes from areas that are currently in an anticluster, providing important insights into seismic hazards. In the southern Apennines, there seems to be an inconsistency between the historical record and the longer-term rates extracted from the geological fault slip-rate hazard maps, implying that the historical record is not representative of the longer-term throw-rates. This occurs because the northern part of the study area (Irpinia, northern Basilicata) appears to be ahead of its longer-term seismicity rate, thus perhaps in a temporal clustering period, whereas the southern part (Pollino, southern Basilicata) appears to be below its longer-term rate, implying that it is in a temporal anticlustering period. The latter agrees with the so-called Pollino seismic gap.*

Key words*: Southern Italy, Pollino, active faults*

INTRODUCTION

Gaps on seismicity maps are areas that constantly attract the interest of the scientific community. One fundamental question that puzzles scientists worldwide is whether a seismic gap on a seismicity map that is based on instrumental/historical data, could represent: a) an area of genuinely low long-term seismicity, leading to a correct low hazard interpretation; or b) a poor or incomplete historical record, suggesting that the region has experienced large earthquakes in the past, but they have not been recorded because the catalogues were either too short or incomplete; or c) a quiescent period in an area characterised by temporal clustering followed by a long recurrence interval (e.g. Marco et al. 1996).

Scenario a suggests a low hazard whereas, scenarios b and c imply a high hazard potential. In particular, in scenario b the time elapsed since the last event, exceeds the duration of historic catalogues, implying that the region could probably have entered the last stage of the seismic cycle. In scenario c, if a perceived seismic gap coincides with a quiescent interval, then the region sooner or later will enter a period of earthquake spatial and temporal clustering, implying a very high potential hazard.

However, without knowledge of the long-term seismicity record scenarios b and c are difficult to differentiate from scenario a. Geological data have the potential to extend the history of slip on a fault back many thousands of years, a time span that generally encompasses a large number of earthquake cycles (e.g. Yeats and Prentice, 1996), and thus elucidates the long-term pattern of fault-slip. As a result, multi-cycle seismic hazard maps based on geological fault slip-rate data provide a way to visualize this by depicting the long-term deformation pattern of slip.

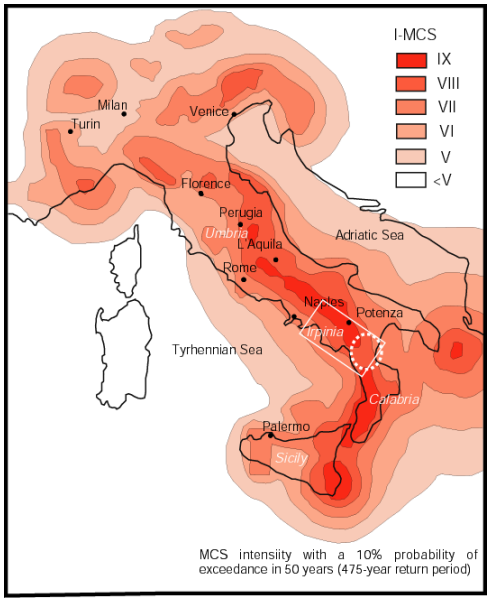

Fig.1.Seismic hazard map of Italy derived from the historical earthquake record (GNDT-SSN, 2001). This map shows intensities that have a 90% probability of not being exceeded in a certain time period (e.g. 50 years) assuming a 475-year return period. White box shows the area of the seismic hazard map constructed during this study, whereas the dash white circle shows the Pollino seismic gap.

In this paper we present such hazard maps for the region of the southern Apennines. Then we weigh our map against the historical record by comparing

the number of recorded earthquakes in the last 5-7 centuries with that implied by slip-rates on active normal faults averaged over 18 kyrs, a time period which contains numerous seismic cycles. This comparison demonstrates that the long history of earthquakes in the Italian Apennines, which is certainly complete for 5-7 centuries (Boschi et al. 1995) may indeed contain evidence for earthquake clustering, implying that the historical record is unrepresentative of the long-term deformation pattern.

THE AREA OF THE SOUTHERN APPENNINES AND THE POLLINO SEISMIC GAP

A so-called “seismic gap” appears on a historical seismicity map in the Pollino region in the southern Italy (Fig.1). In the Pollino area where several active faults exist, no large magnitude historical earthquakes are known, but palaeoseismological studies clearly demonstrate the occurrence of surface faulting events (Michetti et al., 1997; Cinti et al., 1997; Michetti et al. 2000). However, seismic hazard and probabilistic maps based on the historical record (Slejko et al., 1998; Faenza and Pierdominici, 2007) regard this area as an area of genuinely low hazard, disregarding the geological evidence. We suggest that knowledge of the long-term rates of surface faulting derived from offset geology is essential before such an area can be defined as low or high hazard.

SEISMIC HAZARD MAP FROM GEOLOGICAL FAULT SLIP-RATE DATA

Methodology

Fault throw-rates are firstly converted into earthquake frequencies, assuming that each fault ruptures in "floating" earthquakes, which are distributed around a mean magnitude of fixed size. Then, this information is turned into a hazard map after using: i) empirical relationships between coseismic slip values, rupture lengths and earthquake magnitudes (Wells and Coppersmith 1994), ii) empirical relationships between earthquake magnitudes and intensity distributions that define the shapes and sizes of IX and VIII isoseismals (Grandori et al. 1991, D’ Amico et al. 1999) and iii) a simple attenuation/amplification functions for seismic shaking on bedrock compared to flysch and basin-filling sediments. The final product is a high spatial resolution seismic hazard map showing how many times each location has been shaken at a certain intensity value (e.g. intensity IX) over a fixed time period (e.g. since the last glaciation), which can be easily transformed into a map of recurrence intervals (see Papanikolaou 2003 and Roberts et al., 2004).

Data input

Fault geometry and fault throw-rates have been extracted from Papanikolaou and Roberts (2007) and references therein (Fig.2). Throw rates are mainly extracted from post-glacial fault scarps, using as a reference the last major glacial retreat phase that initiated 18,000 years ago and left a clear imprint in the topography (Palmentola et al. 1990); other input data from published trench-site palaeoseismic data were also utilised (e.g. Pantosti et al. 1993, Michetti et al. 1997). In these maps each fault ruptures in "floating" earthquakes (e.g. WGCEP 2002), which are distributed around a mean magnitude of Ms=6.5.

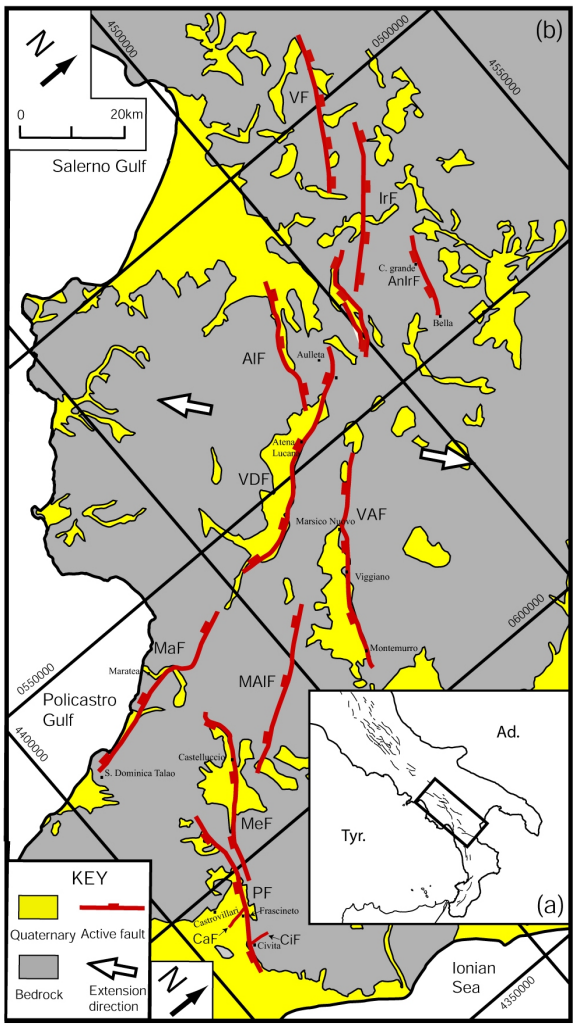

Fig. 2: (a) Location map of the study area, showing active faults that have displaced Holocene deposits, (b) Map of major active faults of the Southern Apennines in UTM coordinate frame (Papanikolaou and Roberts 2007). The bedrock map was modified and simplified from the CNR (1990) map. VF - Volturara Fault; IrF - Irpinia Fault; AntIrF - Antithetic Irpinia Fault; SGrF - San Gregorio Fault; AlF - Alburni Fault; VDF - Vallo di Diano Fault; VAF - Val' D Agri Fault; MaF - Maratea Fault; MAF - Monte Alpi Fault; MeF - Mercure Fault; PF - Pollino Fault, CaF – Castrovillari fault (from Cinti et al., 2002), CiF – Civita fault (from Michetti et al., 1997).

Results

Figure 3 shows the frequency of shaking for intensity VIII assuming homogeneous bedrock geology, a circular pattern of energy release and a 25 km radius for the VIII intensity. The highest hazard is observed in the centre of the map which receives enough energy to shake at intensity VIII or higher about 80 times and decreases smoothly towards the tips of the fault array (about 20-30 times).

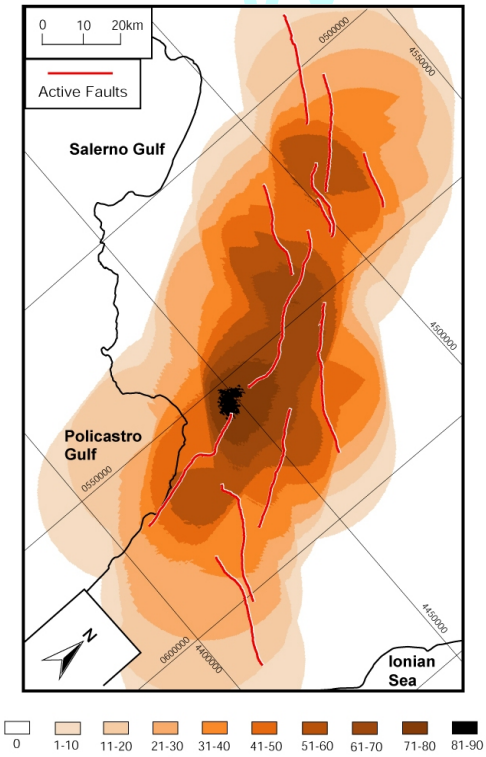

Fig. 3: Seismic hazard map showing the frequency of shaking for intensity VIII assuming homogeneous bedrock geology, a circular pattern of energy release and a 25 km radius for the VIII isoseismal.

Figure 4 shows how many times a locality receives enough energy to shake at intensities ≥IX in 18 kyrs, assuming a 12.5 km radius of isoseismal IX and a simple attenuation/amplification function, where bedrock Mesozoic-Cenozoic limestones shake at a single intensity value less than the Quaternary/flysch/foredeep deposits at the same epicentral distance. In particular, the area of highest shaking frequency is located in the hangingwall centre of the Val' D' Agri fault, which will receive enough energy to shake at intensity IX or higher up to 36 times in 18 kyrs. On the other hand, the hangingwall centres of the Volturara and the Pollino distal faults will shake only about 10-15 times at intensities ≥IX because these faults have lower slip-rates. Therefore, the recurrence interval for intensity IX or higher is estimated to be as short as 500 yrs for localities in the hangingwall centre of the Val' D' Agri fault and as long as 1200-1800 yrs in the hangingwall centres of the Pollino and the Volturara faults.

COMPARISON WITH THE HISTORICAL RECORD

To investigate whether rates of earthquake occurrence measured using the historical record (e.g. 442 years) are representative of longer time periods (18 kyrs) where the effects of clustering may be averaged out, the recurrence intervals extracted from these maps are compared with the historical record. Overall, 24 towns were chosen that are uniformly distributed in the entire area and most of them have numerous records of earthquake shaking dating back to the sixteenth and seventeenth century (Table 1). There is no correlation (R^2<0.1) between the normalised long-term shaking values and the historical record both for intensities IX and VIII. Instead, there is a geographic variation, where earthquake shaking from historical seismicity for towns in the north area is ahead of the rate expected given modeling of the 18 kyrs record of fault slip, with the opposite relationship in the south close to the so-called "Pollino Gap". This suggests earthquakes have been clustered in time in the north during historical times and anticlustered in the south (Scenario c of the Introduction).

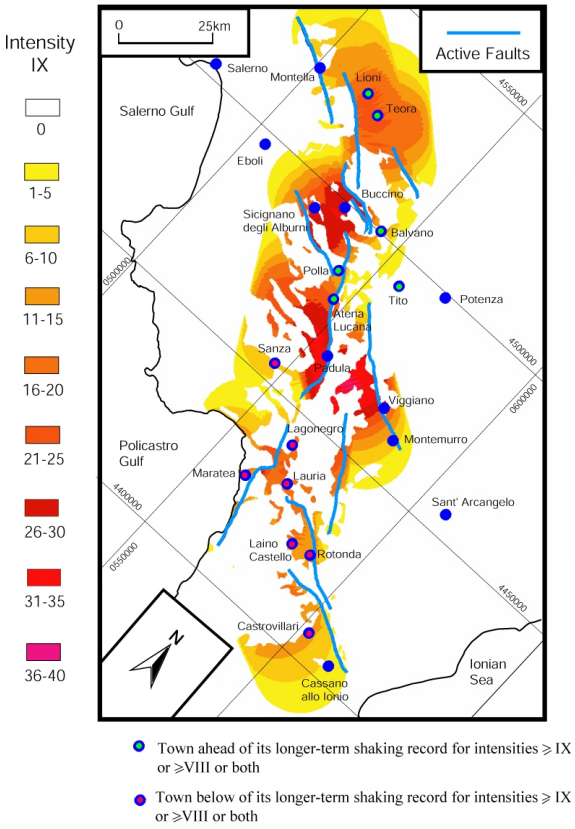

Fig.4: Map showing the locations of the towns presented in Table 1. It also shows how many times a locality receives enough energy to shake at intensities ≥IX in 18 kyrs, assuming a 12.5 km radius of isoseismal IX and a simple attenuation/amplification function where bedrock Mesozoic-Cenozoic limestones shake at a single intensity value less than the Quaternary/flysch/foredeep deposits at the same epicentral distance.

DISCUSSION- CONCLUSIONS

By comparing short-term throw-rates (e.g. historical record) with longer-term throw-rates (e.g. offset postglacial geomorphic features), one can differentiate areas that are currently in a cluster of earthquakes from areas that are currently in an anticluster, providing important insights into seismic hazards. In the southern Apennines, there seems to be an inconsistency between the historical record and the longer-term rates extracted from the hazard maps. This shows that a 442 or even a 654 year-period is too short for a complete pattern of hazard to have emerged because many low throw-rate faults (e.g. Pollino, Volturara, Mercure) will probably have

not ruptured during this time period and other faults that could be in a temporal clustering period.

Table 1

Town (see also Fig. 3)	Predictions from Fig.3 and Fig.4: Number of times in 18 kyrs		Normalised values Number of times				Historical Record (Number of times each locality was shaken at stated intensity)	
			In 442 yrs		In 654yrs			
	IX	VIII	IX	VIII	IX	VIII	≤IX	VIII
Buccino	28	49	1	1	1	2	1	3
Balvano	12	44	0	1	0	2	3	1
Padula	31	68	1	2	1	2	1	0
Atena Lucana	20	70	1	2	1	3	2	2
Tito	0	25	0	1	0	1	4	0
Salerno	0	0	0	0	0	0	0	0
Potenza	0	0	0	0	0	0	0	3
Sicignano d' Alburni	25	45	1	1	1	2	1	1
Eboli	0	10	0	0	0	0	0	0
Cassano allo Ionio	3	15	0	0	0	1	0	0
Maratea	18	48	0	1	1	2	0	1
Laino Castello	18	37	0	1	1	1	0	0
Rotonda	13	37	0	1	0	1	0	0
Castrovillari	12	22	0	1	0	1	0	0
Sant' Arcangelo	0	0	0	0	0	0	1	0
Montemurro	8	42	0	1	0	2	1	0
Sanza	8	65	0	2	0	2	0	1
Lagonegro	18	70	0	2	1	3	1	0
Lauria	20	55	1	1	1	2	0	2
Lioni	23	32	1	1	1	1	3	1
Teora	23	35	1	1	1	1	4	0
Viggiano	21	46	1	1	1	2	1	0
Montella	0	15	0	0	0	1	0	3
Polla	15	65	0	2	1	2	2	2

It is evident that the northwestern part of the study area (Irpinia and northern Basilicata) is ahead of its longer-term shaking record, indicating that this area may be in a temporal earthquake cluster. Towns like the Balvano, Atena Lucana, Tito, Lioni, Teora, Polla have experienced more intensity IX (in particular) and VIII events during the last five to seven centuries compared to their longer-term shaking record derived from the maps (Table 1, Fig. 4). On the other hand, the southeastern part of the study area (Pollino, southern Basilicata) may be in a temporary anticlustering process. Towns like the Lauria, Lagonegro, Sanza, Castrovillari, Rotonda, Laino Castello and Maratea have experienced less events (particularly for intensity VIII) compared to the longer-term shaking record (Table 1, Fig.3, Fig. 4). The latter can potentially explain why paleoseismic data extracted from the Pollino region (Michetti et al., 1997; Cinti et al., 1997) are in conflict with the historical record, with paleo surface ruptures found in a region with no major recorded historical events.

References

Boschi, E., et al. (1995). Catalogo dei forti terremoti in Italia dal 461 a.C. al 1980, Istituto Nazionale di Geofisica - SGA Storia Geofisica Ambiente, printed by Grafica Ragno, Ozzano Emilia, BO, Italy, 973 pp.

Cinti, F., L. Cucci, D. Pantosti, G. D'Addezio and M. Meghraoui (1997). A major seismogenic fault in a "silent area": the Castrovillari fault (southern Italy), Geophysical Journal International, 130, 595-605.

CNR (1990). Structural model of Italy, 1:500000, edited by Bigi,G., Cosentino, D., Parotto, M., Sartori, R., and Scandone, P., Consiglio Nazionale delle Richerche. S.E.L.C.A. Florence.

D'Amico, V., Albarello, D. and Mantovani, E. (1999). A distribution-Free Analysis of Magnitude-Intensity Relationships: an Application to the Mediterranean Region. Phys. Chem. Earth 24, 517-521.

GNDT-SSN Albarello, D.et al. (2001). New seismic hazard maps of the Italian territory. Gruppo Nazionale per la Difesa dai Terremoti- Servizio Seismico Nazionale Website:http://www.dstn.it/ssn/PROG/2000/carte_pericolosita/mcs_e.gif.

Grandori, G., Drei, A., Perotti, F. and Tagliani, A. (1991). Macroseismic intensity versus epicentral distance: the case of Central Italy. Tectonophysics 193, 165-171.

Faenza, L. and Pierdominici, S. (2007). Statistical occurrence analysis and spatio-temporal distribution of earthquakes in the Apennines (Italy). Tectonophysics 439, 13-31.

Marco, S., Stein, M., Agnon, A., and Ron, H. (1996). Long-term earthquake clustering: a 50000 year paleoseimic record in the Dead Sea Graben. Journal of Geophysical Research 101, 6179-6191.

Michetti, A.M., L. Ferreli, L. Serva and E. Vittori (1997). Geological evidence for strong historical earthquakes in an "aseismic" region: the Pollino case (Southern Italy), Journal of Geodynamics 24, 1-4, 67-86.

Michetti. A.M., Ferreli, L., Esposito, E., Porfido, S., Blumetti, A-M, Vittori, E., Serva, L., and Roberts, G.P. (2000). Ground effects during the 9 September 1998, Mw=5.6, Lauria earthquake and the seismic potential of the "Aseismic" Pollino region in Southern Italy. Seismological Research Letters 71, 31-46.

Palmentola, G., Acquafredda, and Fiore, S. (1990). A new correlation of the Glacial Moraines in the Southern Apennines, Italy. Geomorphology 3, 1-8.

Pantosti, D., Schwartz, D.P., and Valensise, G. (1993). Paleoseismology along the 1980 surface rupture of the Irpinia fault: implications for the Earthquake recurrence in the Southern Apennines, Italy. Journal of Geophysical Research 98, 6561-6577.

Papanikolaou, I.D., (2003). Generation of high resolution seismic hazard maps through integration of earthquake geology, fault mechanics theory and GIS techniques in extensional tectonic settings. Unpublished Ph.D thesis, University of London, 437pp.

Papanikolaou, I.D., and Roberts, G.P. (2007). Geometry, kinematics and deformation rates along the active normal fault system in the southern Apennines: Implications for fault growth. Journal of Structural Geology 29, 166-188.

Roberts, G.P., Cowie, P., Papanikolaou, I., and Michetti, A.M., (2004). Fault scaling relationships, deformation rates and seismic hazards: An example from the Lazio-Abruzzo Apennines, central Italy. Journal of Structural Geology 26, 377-398.

Slejko, D., Peruzza, L., and Rebez, A. (1998). Seismic hazard maps of Italy. Annali di Geofisica 41, 183-214.

Yeats, R.S., and Prentice, C.S. (1996). Introduction to special section: Paleoseismology. Journal of Geophysical Research 101, 5847-5853.

Working Group on California Earthquake Probabilities, (2002). Earthquake probabilities in the San Francisco bay region: 2002-2031. USGS Open-File Report 03-214.

Wells, D.L., Coppersmith, K., (1994). New Empirical Relationships among Magnitude, Rupture Length, Rupture Width, Rupture Area, and Surface Displacement. Bull. Seismological Society of America 84, 974-1002.

THE SPARTA FAULT, SOUTHERN GREECE: TECTONIC GEOMORPHOLOGY, SEISMIC HAZARD MAPPING AND CONDITIONAL PROBABILITIES

Papanikolaou Ioannis D. (1,2), Gerald Roberts (2), Georgios Deligiannakis (1,3), Athina Sakellariou (1), Emmanuel Vassilakis (3)

(1) Mineralogy-Geology Laboratory, Department of Earth and Atmoshperic Sciences, Agricultural University of Athens, Iera Odos 75, 118-55, Athens, Greece
(2) AON Benfield UCL Hazard Research Centre, Department of Earth Sciences Birkbeck College and University College London, WC 1E 6BT,London UK, Email: (i.papanikolaou@ucl.ac.uk)
(3) Laboratory of Natural Hazards, Faculty of Geology and Geoenvironment, National and Kapodistrian University of Athens, Panepistimioupolis, 15784, Athens, Greece

Abstract (The Sparta fault, southern Greece: Tectonic geomorphology, seismic hazard mapping and conditional probabilities): *The Sparta Fault system is a major structure approximately 64km long that bounds the eastern flanks of the Taygetos Mountain front (2.400m) and shapes the present-day Sparta basin. This fault is examined and described in terms of its geometry, segmentation, drainage pattern and postglacial finite throw, emphasizing also how these parameters vary along strike the fault. Based on fault throw-rates and the bedrock geology, geological data can offer both a qualitative and quantitative approach of the expected hazard distribution. This is achieved by the construction of a seismic hazard map based on fault throw-rates that shows the number of times a locality receives enough energy to shake at a certain intensity value, extracting a locality specific long-term earthquake recurrence record. The Sparta fault was activated in 464 B.C., devastating the city of Sparta. Since no other major earthquake has been generated by this system since 464 B.C., a future event could be imminent. As a result, not only time-independent but also time-dependent probabilities, which follow the concept of the seismic cycle, have been calculated for the city of Sparta.*

Key words*: Lakonia, slip-rates, time-dependent probabilities, Taygetos,*

INTRODUCTION

In 464 B.C. a large earthquake devastated the city of Sparta (~20000 fatalities), causing great social unrest (Papazachos and Papazachou, 1997). This event is regarded as the oldest well-defined event in the Hellenic historical record (Papazachos and Papazachou, 1997). However, the area is characterized by low seismicity over the last 25 centuries (Papanastassiou, 1999) and no other major event has occurred in the town of Sparta since 464 B.C, suggesting that a future event could be imminent. This is also supported by cosmogenic dating techniques applied on the Sparta bedrock scarp showing that this fault ruptured repeatedly (six times over the last 13kyrs), with time intervals ranging from 500-4500yrs (Benedetti et al., 2002). This fault is studied in detail based on its postglacial scarp, the analysis of the drainage network and the major catchments that are influenced by footwall uplift.

THE SPARTA FAULT SYSTEM

The Sparta fault system (Fig. 1), bounds the eastern part of the Taygetos Mt (2.407m) and shapes the western boundary of the Sparta basin (Fig.2). It trends NNW-SSE and has a length of 64km. Its southern tip is located close to the Gerakari catchment approximately 2-3km SW from the Potamia village, whereas its northern tip towards the Alfios river, a couple of km westwards from the Kamaritsa village in the Megalopolis basin. Two major faults are traced within this structure (Fig.1). The northern segment is about 14 km long and characterized by lower slip-rates. On the other hand, the southern segment is 50km long and leaves the most impressive imprint in the topography showing sings of recent intense activity. The southern segment can be divided into two patches that in the past were probably two individual structures that are now hard-linked. This fault exhibits an impressive postglacial scarp that can be traced for many km (Fig.3). In particular, from the village of Anogia up to the area of Mystras, it is continuous and has an 8-12m high scarp (Fig.4).

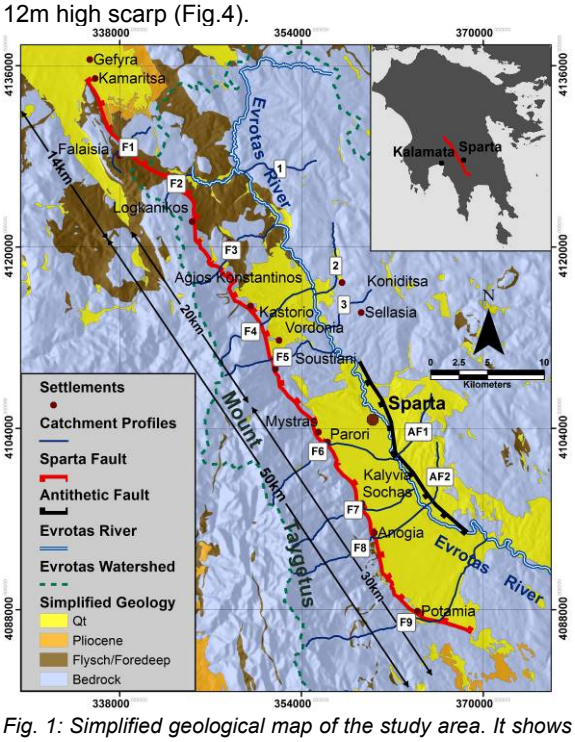

Fig. 1: Simplified geological map of the study area. It shows the segmentation pattern as well as the localities of the studied catchments profiles.

Fig.2: Distant view of the Sparta fault. It uplifts the Taygetos Mt on its footwall and shapes the basin of Sparta towards its hanging wall.

Fig.3: View of the post-glacial scarp of the Sparta fault in the Kalyvia-Sochas locality.

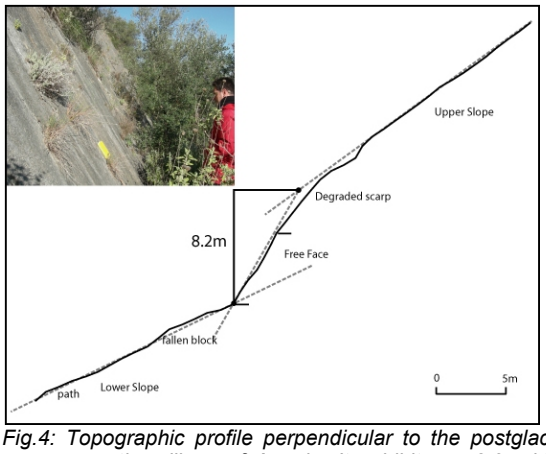

Fig.4: Topographic profile perpendicular to the postglacial scarp near the village of Anogia. It exhibits an 8.2m high scarp.

TECTONIC GEOMORPHOLOGICAL ANALYSIS; CATCHMENTS AND TECTONIC UPLIFT

The Evrotas river flows through the Sparta Basin, parallel to the Sparta Fault, trending NNW-SSE, while the secondary branches of this fluvial system consist of transient rivers which flow perpendicular to the main structure, indicating a strong tectonic influence to the drainage pattern. The combination of fault parallel and fault perpendicular flow is characteristic of active normal faulting settings.

Kirby & Whipple (2003) demonstrated that tectonically unperturbed "equilibrium" fluvial long profiles are typically smooth and concave-up. However, upland rivers are also sensitive to along-stream variations in differential uplift (potentially leading to changes in the profile concavity or steepness index) and also to changes in uplift rate through time. Whittaker et al. (2008) showed that rivers with drainage areas greater than 10km^2 and crossing faults that have undergone an increase in throw rate within the last 1Myrs have significant long-profile convexities. They also established that this relationship holds for throw rate variation along strike the same fault segment, as well as between faults. Moreover, Boulton & Whittaker (2009) suggested that rivers crossing active faults are undergoing a transient response to ongoing tectonic uplift and this interpretation is supported by typical signals of transience such as gorge formation and hill slope rejuvenation within the convex reach.

Nine fluvial long profiles of the transient rivers crossing different segments of the Sparta fault were studied in order to examine the longitudinal convexity and its variation along strike. Such profiles were also compared to the longitudinal profiles of rivers that are not influenced by any fault. Furthermore, in order to examine the transience of the streams across the Sparta fault, cross sections perpendicular to the river flow in the headwaters and within the downstream convex reach were analyzed.

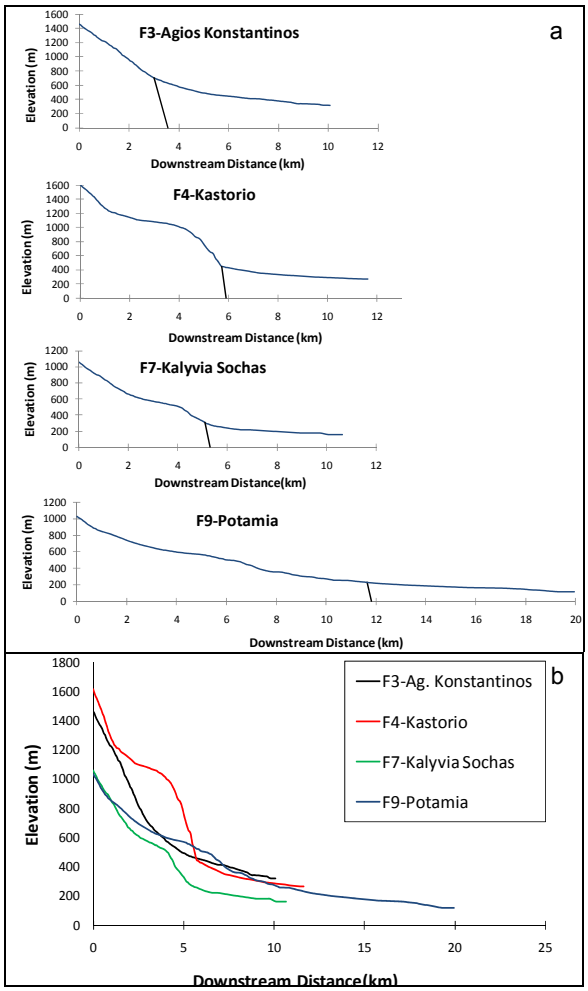

Fig.5: a) Long profiles of catchments crossing perpendicular the Sparta Fault. Locality names are shown geographically in Fig.1. b) Comparison of long profiles in the same graph of the above catchments showing significant differences in longitudinal convexities along strike the faults.

While river long profile convexities can lead to the observation of the ongoing tectonic uplift, differential erosion of geological formations may also cause the same pattern. Thus, in order to exclude the latter phenomena and emphasize the tectonic uplift, the rivers to be examined must fulfill some restrictions. Whittaker, et al. (2008) suggest that the selected rivers should discharge a drainage basin larger than 10km^2 above fault and the upstream length should be at least 5km. These restrictions are applicable in the south and central segments of Sparta fault. However, in the northern segment of Sparta fault the streams are not long enough to fulfill these criteria, due to the proximity of the watershed of Evrotas Basin to the SW segment of the fault.

Catchments crossing the North, Central and South parts of the Sparta Fault were grouped and studied separately. Qualitative analysis of long profiles showed a significant difference in longitudinal convexity between the Central and both the South and North parts of the fault, leading to the conclusion of varying uplift rate along strike. A convex reach of 205m height in Potamia catchment long profile (southeast part of the Sparta Fault) can be observed although it seems to have propagated upstream in relation to the fault. This could happen as the channel successively adjusts to the imposed uplift field (Whipple & Tucker, 2002). Moreover, Kalyvia Sochas fan deposits were extensively examined by Pope et al. (2003). Kalyvia Sochas catchment long profile revealed a convex reach of 246m height, which is in contact with the Sparta fault, in contrast to Potamia catchment's convex reach. Agios Konstantinos catchment seems to have a concave-up channel profile, possibly indicating a constant slip rate (Whittaker, et al. 2008). On the other hand, towards the central part of the Sparta fault, were no fan deposits and talus cones appear and the finite throw is smaller, the Kastorio catchment's convex reach height outreaches 590m, as measured from the fault (Fig. 5a,5b).

In addition, the normalized steepness index, k_{sn}, using a reference concavity of 0.45, was calculated for six catchments crossing all Sparta fault parts, as well as for the two catchments crossing the antithetic structure and two catchments that cross no fault (localities shown in Figure 1). The k_{sn} rates for the catchments closer to the tips of the Sparta fault (F3-Agios Konstantinos and F9-Potamia) were 81 and 82.7 respectively, while in the central part the steepness rates are higher and vary from 98.5 to 114 ($98.5<k_{sn}<114$). Along-strike variations of this scale show that the central part of the Sparta Fault appears to have undergone an increase in relative uplift rate compared to the other two parts. Moreover, the height of the convex reach in Kastorio channel profile could also indicate that the Sparta Fault has been tectonically active as one hard-linked structure only for the last couple of hundred of thousand years. Prior to this linkage there were two separate segments with different lengths and displacements. This can explain the absence of Upper Pleistocene sediments and alluvial fans and the smaller finite throw of the Kastorio-Soustiani segment.

SEISMIC HAZARD MAP FROM GEOLOGICAL FAULT SLIP-RATE DATA

Methodology

Fault throw-rates are firstly converted into earthquake frequencies, assuming that each fault ruptures in "floating" earthquakes, which are distributed around a mean magnitude of fixed size. Then, this information is turned into a hazard map after using: i) empirical relationships between coseismic slip values, rupture lengths and earthquake magnitudes, and ii) empirical relationships between earthquake magnitudes and intensity distributions (see Papanikolaou 2003 and Roberts et al., 2004). The final product is a high spatial resolution seismic hazard map showing how many times each location has been shaken at a certain intensity value (e.g. intensity IX) over a fixed time period (e.g. since the last glaciation), which can be easily transformed into a map of recurrence intervals.

Empirical relationships

For the Greek territory, magnitude-intensity laws and attenuation relationships are extracted from statistical elaboration of historical and instrumental data. However, there are significant differences between published data regarding the relationship between Magnitude, epicentral intensity and its attenuation with distance (Papaioannou 1984, Theodoulidis 1991, Papazachos & Papaioannou 1997). More importantly, for an M=7.0 earthquake, that a structure similar to the Sparta fault is able to generate (Wells & Coppersmith, 1994; Benedetti et al., 2002), only Theodoulidis's (1991) equations result in an epicentral intensity X, as has been clearly demonstrated by the Sparta 464 B.C. macroseismic field (Papazachos & Papaioannou 1997). Theodoulidis (1991) proposes that an earthquake with epicentral intensity X has a mean radius of 6-7km for the X isoseismal and a mean radius of 16-18km, for the isoseismal IX depending of which variable is used.

Results

Figure 6 shows how many times a locality receives enough energy to shake at intensities ≥IX in 15±3kyrs. Highest hazard is observed, as expected, towards the hangingwall centre of the Sparta fault and diminishes towards the tips, following the slip-rate variability. The town of Sparta lies closer to the hangingwall centre and is founded on Quaternary sediments, whereas surrounding villages are founded on alluvial fans and triangular facets. Therefore, it will receive enough energy to shake at intensity X, 8 or 9 times (lies on the boundary) over 15±3kyrs. The latter implies that it experiences a destructive event similar to the 464 B.C. approximately every 1792±458yrs years.

TIME INDEPENDENT AND TIME DEPENDENT PROBABILITIES FOR THE TOWN OF SPARTA

Following the results above a time-independent probability of 1,66% over the next 30 years and 2,75% over the next 50 years is calculated for the

town of Sparta. A considerably higher time-dependent probability of 2,14% over the next 30 years and 3,55% over the next 50 years has been calculated. The time dependent probability follows the seismic cycle concept (WGCEP 2002) and exhibits higher values because the elapsed time since the last event (2475yrs) has exceeded the mean recurrence interval (1792±458yrs). However, due to the irregularity of earthquake time intervals of the Sparta fault (Benedetti et al. 2002) and the introduction of a high sigma value (σ=0.64) this difference is noteworthy, but not substantial.

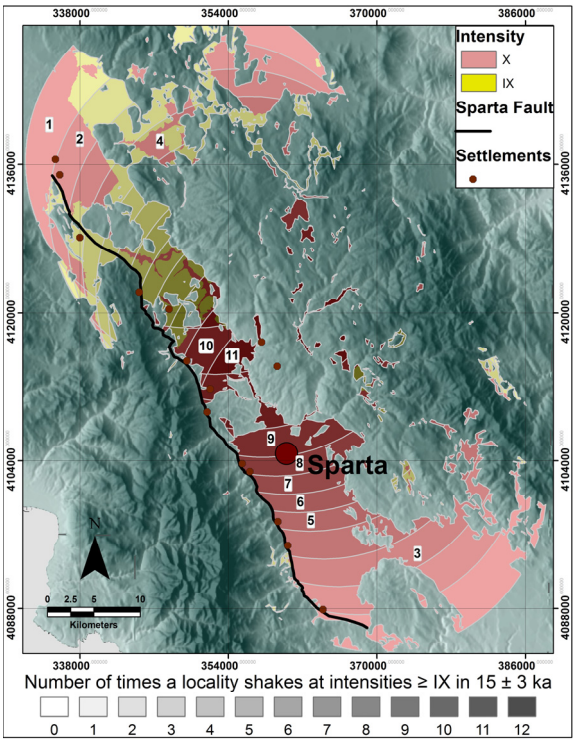

Fig.6: Seismic hazard map for the Sparta Basin, showing how many times a locality receives enough energy to shake at intensities ≥IX in 15±3kyrs, after considering the bedrock geology and assuming a circular pattern of energy release, with a 18 km radius of isoseismal IX.

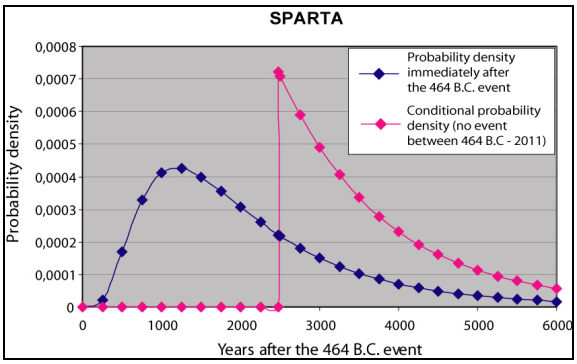

Fig. 7: Diagram showing the probability density for the town of Sparta immediately after the 464 B.C. event and the conditional probability density considering that no event occurred since 2011. A sigma value of 0.64 is used.

Acknowledgements: The Institution of State Scholarships of Greece is thanked for support.

References

Benedetti, L, et al. (2002). Post-glacial slip history of the Sparta fault (Greece) determined by ^{36}Cl cosmogenic dating: Evidence for non-periodic earthquakes. Geophys. Res. Letters 29, 10.1029/2001GL014510.

Boulton, S.J., Whittaker, A.C., (2009). Quantifying the slip rates, spatial distribution and evolution of active normal faults from geomorphic analysis: Field examples from an oblique-extensional graben, southern Turkey. Geomorphology 104, 299-316.

Kirby, E., Whipple K.X., (2003). Distribution of active rock uplift along the eastern margin of the Tibetan Plateau: Inferences from bedrock channel longitudinal profiles. Journal of Geophysical Research, 108(B4/2217), pp.1-24

Papaioannou, Ch., (1984). Attenuation of seismic intensities and seismic hazard in the area of Greece. Ph.D. Thesis, University of Thessaloniki, 200pp.

Papanastassiou, D. (1999). Seismic hazard assessment in the area of Mystras-Sparta, south Peloponnesus, Greece, based on local seismotectonic, seismic, geologic information and on different models of rupture propagation. Natural Hazards 18, 237-251.

Papanikolaou, I.D., (2003). Generation of high resolution seismic hazard maps through integration of earthquake geology, fault mechanics theory and GIS techniques in extensional tectonic settings. Unpublished Ph.D thesis, University of London, 437pp.

Papazachos, B. C., Papaioannou, (1997). The macroseismic field of the Balkan area. Journal of Seismology 1, 181-201.

Papazachos B. C. and Papazachou C., (1997). *The earthquakes of Greece*. Thessaloniki: Ziti Publications.

Pope, R.J., Wilkinson, K.N., and Millington, A.C. (2003). Human and climatic impact on Late Quaternary deposition in the Sparta basin piedmont: Evidence from alluvial fan systems. Geoarcheology: An International Journal 18, 685-724.

Psonis, K., Latsoudas, C., (1983). 1:50000 Geological Map "Xirokampion", IGME.

Psonis, K., (1990). 1:50000 Geological Map "Sparti", IGME.

Roberts, G.P., Cowie, P., Papanikolaou, I., and Michetti, A.M., (2004). Fault scaling relationships, deformation rates and seismic hazards: An example from the Lazio-Abruzzo Apennines, central Italy. Journal of Structural Geology 26, 377-398.

Theodoulidis, N.P. (1991). Contribution to the study of strong motion in Greece. Ph.D. Thesis, University of Thessaloniki, 500pp.

Whipple, K.X., Tucker, G.E., (2002). Implications of sediment-flux-dependent river incision models for landscape evolution. Journal of Geophysical Research, 107(B2), pp.1-20.

Whittaker, A.C., Attal, M., Cowie, P.A., Tucker, G.E. & Roberts, G., (2008). Decoding temporal and spatial patterns of fault uplift using transient river long profiles. Geomorphology 100, 506-526.

Working Group on California Earthquake Probabilities, (2002). Earthquake probabilities in the San Francisco bay region: 2002-2031. USGS Open-File Report 03-214.

Wells, D.L., Coppersmith, K. (1994). New Empirical Relationships among Magnitude, Rupture Length, Rupture Width, Rupture Area, and Surface Displacement. Bull. Seismological Society of America 84, 974-1002.

Zindros, G., Exindavelonis, P. (2002). 1:50000 Geological Map "Kollinae", IGME.

ACTIVE FAULTING TOWARDS THE EASTERN TIP OF THE CORINTH CANAL: STUDIED THROUGH SURFACE OBSERVATIONS, BOREHOLE DATA AND PALEOENVIRONMENTAL INTERPRETATIONS

Papanikolaou Ioannis D. (1, 4), Maria Triantaphyllou (2), Aggelos Pallikarakis (1,3), Georgios Migiros (1)

(1) Mineralogy-Geology Laboratory, Department of Earth and Atmoshperic Sciences, Agricultural University of Athens, Iera Odos 75, 118-55, Athens, Greece
(2) Hist. Geology-Paleontology Department, Faculty of Geology and Geoenvironment, National and Kapodistrian University of Athens, Panepistimiopolis 15784, Athens, Greece
(3) Laboratory of Natural Hazards, Faculty of Geology and Geoenvironment, National and Kapodistrian University of Athens, Panepistimioupolis, 15784, Athens, Greece
(4) AON Benfield UCL Hazard Research Centre, Department of Earth Sciences, University College London, WC 1E 6BT, London UK, Email: i.papanikolaou@ucl.ac.uk

Abstract (Active faulting towards the Eastern tip of the Corinth Canal: Studied through surface observations, borehole data and paleoenvironmental interpretations): *The most important active fault that crosses the eastern tip of the Corinth Canal is studied in detail, involving surface observations, borehole data and peleoenvironmental interpretations. This fault intersects and/or is parallel and at short distances with major infrastructure facilities such as the Athens-Corinth highway, the railway and the Corinth Canal. A positive remark referring to the seismic hazard assessment is that this fault has a limited length (~5km) and thus it can not produce extensive and large displacement (>20cm) from primary surfaces ruptures. Moreover, borehole data and correlation between the footwall and hangingwall horizons, show no significant offset over the last 200ka, confirming that no significant displacements have been accumulated and/or has a very low slip-rate. Paleoenvironmental interpretations based on borehole data show a very complex sedimentation history during the Upper Pleistocene that involves subaerial exposure, backshore, paralic, lagoonal, shallow marine environments and possibly even some lake sediments.*

Key words*: Isthmus, Saronic Gulf, seismic hazards, Isthmia - Kalamaki*

INTRODUCTION

The Gulf of Corinth is one of the fastest extending regions worldwide with up to 20mm/yr that diminishes to 8 and 4 mm/yr towards its eastern end (Billiris et al. 1991; Briole et al. 2000). Our study area lies eastwards from the major active faults that shape the present-day eastern part of the Corinth Gulf, towards the Corinth Isthmus. In particular, it lies towards the eastern tip of the Corinth Canal (Fig.1). The area of the Isthmus divides the Corinth and Saronic Gulfs. The Corinth Canal is a major infrastructure project 6.3km long, 8m deep and with up to 60m high slopes that often experience landslides (Marinos and Tsiambaos 2008, Papantoniou et al. 2008).

The Canal was constructed 120 years ago and offers a unique opportunity to visualise the faults, forming an impressive mega-trench. More than 40 faults can be recognised, most of them normal and oblique normal (Freyberg 1973). Some of them are overlain by undeformed late Pleistocene strata and are clearly not a hazard threat. The majority of them do not displace the topography and are of limited length, therefore are considered as secondary structures with low slip-rates. However, towards the eastern tip of the Canal we traced a significant ENE-WSW trending fault that downthrows towards the SSE and appears to displace the modern ground surface. The hazard potential of this fault is studied in detail based on surface observations and the analysis of borehole data and discussed in this paper.

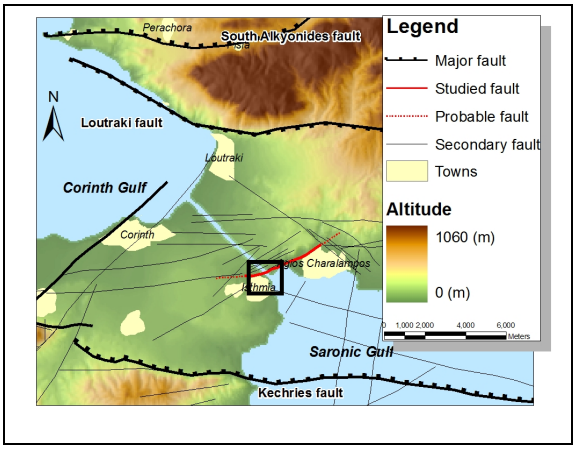

Fig.1: Digital elevation map showing the major and secondary faults in the study area (modified from Bornovas et al. 1972, Gaitanakis et al. 1985, Papanikolaou et al. 1989, Papanikolaou et al. 1996, Roberts et al. 2009).

FAULT MAPPING AND SURFACE OBSERVATIONS

This fault lies in the hangingwall of the Kechries and Loutraki faults and in the footwall of the South Alkyonides fault that was activated during the 1981 earthquake sequence. Our 1:5000 mapping shows that the study fault is extended for at least 1km southwards and 4km northwards of the Canal (Fig.1, Fig.2). This fault controls the topography of the area, producing 150m of topographic variation towards its

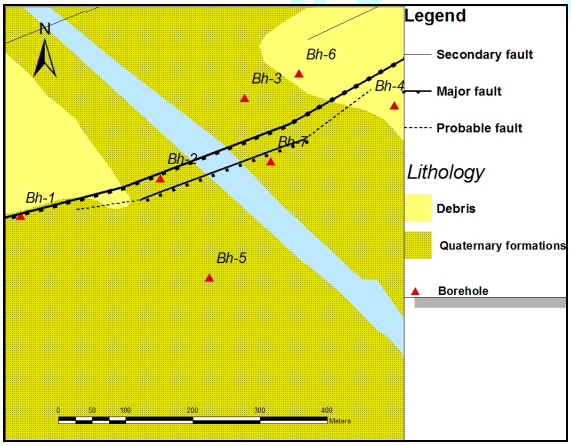

Fig.2 Simplified geological map showing the studied fault. A detailed map showing the main and secondary fault planes and the boreholes near the Canal crossing.

Fig. 3: View of the main fault plane about 50m northwards the Canal (right). Close up view of the free face and the striations developed on the fault plane (left). This is a high angle normal fault dipping 65° towards the SSE.

centre, between the footwall and the hangingwall, and bounds recent alluvial sediments. Moreover, it offsets Upper Pleistocene sediments, exhibits a clear fault plane and a free face with striations (Fig.3), indicating recent activation. It strikes at 075°-255° (ENE-WSW trending) and is a high angle normal fault dipping at 65° towards the SSE. Striations measured on the fault plane are plunging at 55° towards the SE (145°), confirming that it is an almost pure normal fault. Strata exposed on the immediate footwall are Upper Pleistocene sediments, dipping about 10-20° to the NNW, indicating also that this tilt is due to the recent fault activity.

The fault plane has also been traced about 650m southwards the Canal where it trends at 070°-250° and dips 70° towards the SSE (Fig.5). The crossing of the Isthmus and its intersection with the fault, is characterized by the presence of semicohesive Upper Pleistocene sediments of variable grain sizes (from cm thick pebbles to clay) with an abundance of ostracods that indicate a recent brackish marine shallow water environment (e.g. Krstic & Dermitzakis, 1981). In addition, to the NW of the main fault plane and over a 350m distance we identified several fault planes parallel to the main fault trace. Based on their characteristics we suggest that the fault activity has progressively migrated eastwards towards our studied fault, which forms the predominant present day structure that influences the topography. Moreover, we identified some secondary active fault planes of the studied fault in the immediate hangingwall that offset the entire sedimentary column (Fig.2, Fig.4). These secondary fault planes outcropping in the immediate hangingwall, extend the width of the fault zone up to 50m.

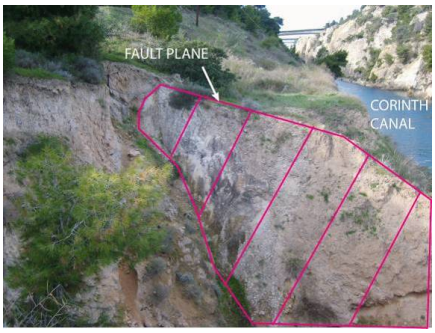

Fig.4: View of the secondary fault plane of the principal fault on the southern part of the Canal. It also created a landslide in the past.

Fig. 5: View of the fault about 650m southwards the Canal. Arrows point to the fault plane displayed in the photo towards the right. It trends 070°-250° and dips 70° towards the SSE.

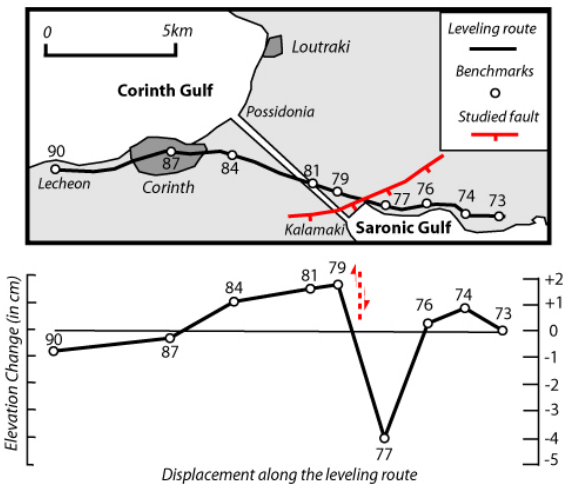

Fig. 6: Location map showing the levelling route, the benchmarks and their post-1981 displacements (redrawn from Mariolakos and Stiros 1987). Benchmark 77 the only one that subsided by 4cm, lies at the immediate hangingwall of the fault and benchmark 79 that was uplifted by 2cm on its immediate footwall, implying that our studied fault may have been passively ruptured during the 1981 earthquake.

It is interesting to note that the area of the Canal uplifted by approximately 2cm from the 1981 earthquake based on a levelling campaign (Mariolakos and Stiros 1987) except for one benchmark that subsided by 4cm and lies at the immediate hangingwall of our studied fault (Fig. 6). The latter implies that our studied fault may have been passively ruptured during the 1981 earthquake.

PALEOENVIRONMENTAL INTERPRETATIONS

Borehole data

Seven boreholes have been recovered on the easterm side of the Corinth Canal; three of them at the hanging wall up to 70 m deep and four at the footwall up to 57 m deep (Figure 2). Two of the longest boreholes were selected for detailed micropaleontological-paleoenvironmental analyses, while the rest were maintained for geotechnical analyses. Approximately 100 samples were collected from these boreholes (45 from borehole Bh-3 and 57 from borehole Bh-7). Each sample (20 gr dry weight) was treated with H_2O_2 to remove the organic matter, and subsequently was washed through a 125μm sieve and dried at 60°C. A subset of each sample was obtained using an Otto microsplitter to obtain aliquots of at least 200 benthic foraminifers. The microfauna were identified under a Leica APO S8 stereoscope. A scanning electron microscope analysis (SEM Jeol JSM 6360, Dept. of Hist. Geology-Paleontology) was used for taxonomical purposes.

Lithostratigraphic units

In each borehole lithological alterations of sand, clay, clayey sand, conglomerate, marl, fractions of limestone, even topsoil have been recognized. It is important that among these layers no significant correlation was found except for a conglomerate horizon that lies on top of a coral colony. The latter strongly indicates that there are major lateral alterations and stratigraphic variations. Between the two boreholes we identified a layer that can be easily correlated in both of them. This is a conglomerate layer 5.5 m thick in Bh-3 and 3 m thick in Bh-7.

Micropaleontological analysis

Samples from Bh-3 and Bh-7 were analyzed in order to identify foraminiferal assemblages (Figure 7). The studied benthic foraminiferal assemblages are relatively abundant and moderately preserved. The identified foraminiferal species were grouped in euryhaline forms mainly represented by *Ammonia* spp. large and small sized, *Elphidium* spp., *Haynesina* spp., *Aubignyna perlucida* and marine foraminiferal indicators, mostly including miliolids, and in a lesser degree full-marine species grouping *Asterigerinata, Neoconorbina*, *Rosalina* spp., *Planorbulina mediterranensis*. A series of different depositional environments were recognized through micropaleontological analysis of the benthic foraminiferal fauna (e.g. Triantaphyllou et al., 2003; Goiran et al., 2011) in both boreholes. In Bh-3 and in Bh-7 we found approximately the same pattern of alternations, but with slight differences.

In Bh- 3 the microfauna indicates a shallow marine environment within the upper 10 m thick layer, partially influenced by fresh water, that turns to an open lagoon. Beneath this layer, the next 6 m were described as a paralic or even a backshore environment, with no or few broken foraminiferal specimens. The underlying layers were characterized as shallow marine to open lagoon environment, indicating that sea level had changed once more. In these sediments apart from foraminiferal fauna, a colony of *Cladocora* corals was found. This layer is approximately 6 m thick. Beneath these sediments the environment changes to paralic-backshore for the next 9 m and beneath them, again a 6 m thick layer is described as shallow marine. Down to the base of Bh-3 at 70 m depth, we encounter two more alternations of the depositional environment from shallow marine to coastal.

At the top layers of Bh-7 the microfauna indicates a shallow marine to paralic environment. These sediments were 4 m thick while beneath them we encountered a 3 m thick layer with no microfauna at all; indicating the presence of a paralic or backshore environment. Below this layer we determine a 6 m thick layer described as shallow marine/paralic. The micropaleontological analysis provides clear evidence for the presence of a closed lagoon in the underlying 1 m thick layer. In the following 10 m we encountered at least 4 alternations between the depositional environment, from shallow marine to closed lagoon and back to shallow marine-paralic conditions. At approx. 23 m depth the environment changed again to closed lagoon, that followed once more by shallow marine with fresh water input, that turned to a closed lagoon for a short interval. Below this point no microfauna was found indicating a paralic/backshore environment. It is significant that at 18m depth we found a colony of *Cladocora* corals, occurring approximately at the same height as in Bh-3. The beginning of fault's deformation zone was observed at ca. 33m depth and ended at approximately 45m depth. In the following 12m, dense alternations of cataclastites and fragments of limestones occur. From that point until the end of Bh-7 at 56 m depth, no foraminifera specimens are traced, indicating the lack of full marine conditions. The presence of ostracods (*Cyprideis* spp.) at this level implies a brackish –oligohaline paleoenvironment.

Presence of corals and other shallow marine foraminifera shows that marine sediments were deposited at glacioeustatic sea level highstands. Thus, we try to correlate these with the global glacioeustatic sea level curve and the known uplift rate from neighbouring corals (0.3mm/yr uplift rate from 200ka corals in the centre of the Canal about 2 km westwards from our locality based on Collier et al. 1992). Within our boreholes we have a succession of lowstand and highstand deposits. Lowstand deposits such as subaerial deposits and top soil, are marking unconforminites with marine highstand deposits. Relative dates for these lowstand and highstand deposits can be derived from the sea level

curve. Therefore, it is clear from our records that the marine to subaerial transitions form when the location emerges above sea level either due to uplift and/or due to falling global sea level. As a result, marine sediments are expected at 125ka for several thousand years, then possibly during a short period at 175ka and then at a prolong period at 200ka (Fig.8).

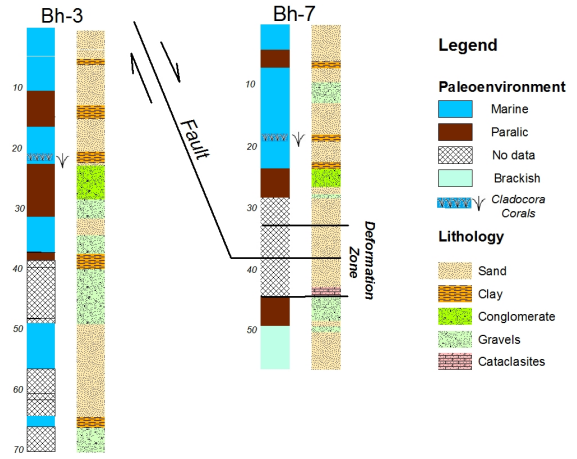

Fig.7: View of the stratigraphic columns and the depositional environment of the two boreholes (Bh3 located on the immediate footwall and Bh7 located on the immediate hangingwall of the studied fault).

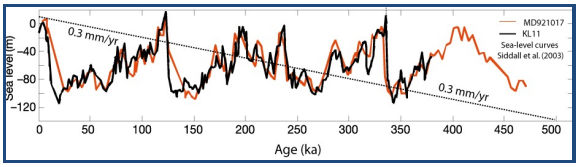

Fig.8: Sea level curve from Sidall et al. 2003 and the expected depositional environment based on the 0.3mm/yr uplift rate from the neighbouring dated corals of Collier et al. (1992).

DISCUSSION- CONCLUSIONS

We have studied a normal fault that trends ENE-WSW and downthrows towards the SSE. The current study confirms that the studied fault is active and forms a secondary structure that accommodates displacement between major E-W trending faults. This fault crosses an area, where major infrastructure facilities are based, such as the Corinth Canal, the highway and the railway. A positive remark referring to the seismic hazard assessment and design is that this fault has a limited length (~5km) and thus it can not produce extensive primary surfaces ruptures. Primary surface ruptures from this fault are not expected to exceed 20cm of displacement. In addition, correlation of the same horizons based on borehole data from the footwall and hanging wall of the fault, show an offset of 4±2m of the corals that based on the expected depositional environment are probably 200kyrs old. Therefore, no significant displacements have been accumulated over the last 200kyrs, implying that it is a very low slip-rate fault. Finally, borehole data exhibit a complex paleoenvironment with major lateral and temporal alterations and stratigraphic variations as a result of the interplay between the sea level fluctuations and the tectonic activity that resembles to the nearby Perachora peninsula (Roberts et al. 2009).

References

Billiris, H., et al. (1991), Geodetic determination of tectonic deformation in central Greece from 1900 to 1988. Nature, 350, 124– 129, doi:10.1038/350124a0.

Bornovas, J., Lalechos, N. and Filipakis, N. (1972). 1:50.000 scale geological map, Sheet "Korinthos". Institute of Geology and Mineral Exploration

Briole, P., A. Rigo, H. Lyon-Caen, J. C. Ruegg, K. Papazissi, C. Mitsakaki, A. Balodimou, G. Veis, D. Hatzfeld, and A. Deschamps, Active deformation of the Corinth rift, Greece: Results from repeated Global Positioning System surveys between 1990 and 1995, J. Geophys. Res., Solid Earth, 21, 25,605– 25,625, 2000.

Collier, R.E.L., Leeder, R.M., Rowe, P. and Atkinson, T. (1992). Rates of tectonic uplift in the Corinth and Megara basins, Central Greece, Tectonics, 1159-1167.

Gaitanakis, P., Mettos, A., and Fytikas, M. (1985). 1:50.000 scale geological map, Sheet "Sofikon". Institute of Geology and Mineral Exploration.

Goiran, J.P., Pavlopoulos, K., Fouache, E., Triantaphyllou, M.V., Etienne, R., 2011. Piraeus, the ancient island of Athens: Evidence from Holocene sediments and historical archives. Geology, doi:10.1130/G31818.1.

Freyberg, V. (1973). Geologie des Isthmus von Korinth, Erlangen Geologische Ablhandlungen, Heft 95, Junge und Sohn, Universitats Buchdruckerei Erlangen, 183pp.

Krstic, N., Dermitzakis, M.D., (1981). Pleistocene Fauna from a section in the channel of Corinth (Greece). Ann. Geol. du Pays Hellen. 30 (2): 473-499.

Mariolakos, I. and Stiros, S.C. (1987). Quaternary deformation of the Isthmus and Gulf of Corinth (Greece). Geology 15, 225-228.

Marinos, P. and Tsiambaos, G. (2008). The Geotechnics of Corinth Canal: A review. Bulletin of the Geological Society of Greece XXXXI/I, 7-15.

Papanikolaou, D., Chronis, G., Lykousis, V., Pavlakis, P., Roussakis, G., and Syskakis, D. (1989). 1:100.000 scale, Offshore Neotectonic Map the Saronic Gulf. Earthquake Planning and Protection Organization, National Centre for Marine Research, University of Athens.

Papanikolaou, D., Logos, E., Lozios, S. and Sideris, Ch. (1996). 1:100.000 Neotectonic Map of Korinthos Sheet, Earthquake Planning and Protection Organization, Athens.

Papantoniou, L., Rozos, D., Migiros, G. (2008). Engineering geological conditions and slope failures along the Corinth Canal. Bull. Geol. Soc. Greece, Vol. XXXVI/I, 17-24.

Roberts, G. P., S. L. Houghton, C. Underwood, I. Papanikolaou, P. A. Cowie, P. van Calsteren, T. Wigley, F. J. Cooper, and J. M. McArthur (2009). Localization of Quaternary slip rates in an active rift in 10^5 years: An example from central Greece constrained by 234U-230Th coral dates from uplifted paleoshorelines, Journal of Geophys. Res. 114, B10406, doi:10.1029/2008JB0058

Triantaphyllou, M.V., Pavlopoulos, K., Tsourou, Th. & Dermitzakis M.D., 2003. Brackish marsh benthic microfauna and paleoenvironmental changes during the last 6.000 years on the coastal plain of Marathon (SE Greece). Rivista Italiana Paleontologia et Stratigafia, 109 (3), 539-547.

Siddall, M., E. J. Rohling, A. Almogi-Labin, C. Hemleben, D. Meischner, Schmelzer, and D. A. Smeed (2003), Sea-level fluctuations during the last glacial cycle. Nature 423, 853 – 858.

ROMAN AQUEDUCTS AS INDICATORS OF HISTORICALLY ACTIVE FAULTS IN THE MEDITERRANEAN BASIN

Passchier, Cees W. (1), Gilbert Wiplinger (2), Gül Sürmelihindi (1), Paul Kessener (3), Talip Güngör (4)

(1) Department of Earth Sciences, Gutenberg University , 55099 Mainz, Germany. Email: cpasschi@uni-mainz.de, surmelih@uni-mainz.de
(2) Österreichisches Archäologisches Institut, Vienna, Austria. Email: gilbert.wiplinger@gmail.com
(3) van Slichtenhorststraat 13, NL 6524 JH Nijmegen, Netherlands. Email: lenl@euronet.nl
(4) Department of Geological Engineering, Dokuz Eylül University, Izmir, Turkey. Email: talip.gungor@deu.edu.tr

Abstract (Roman aqueducts as indicators of historically active faults in the Mediterranean Basin): *Roman aqueducts are a potential source of information on infrequently active faults in the Mediterranean Basin. We have localised more than 1300 such aqueducts from the literature. Carbonate deposits in aqueduct channels can help to date and characterise fault activity in detail. As an example, the Değirmendere aqueduct near Ephesos, Turkey is described, which was apparently displaced and tilted by up to 2 metres a short time after it came into use. The aqueduct was subsequently repaired by constructing a second channel at the correct elevation running next to the original one over a length of several km.*

Key words*: roman aqueduct, sinter, carbonate deposits, fault, fault scarp*

INTRODUCTION

Major fault zones such as the San Andreas and North Anatolian fault systems have been extensively studied, and the local risk of earthquakes and their frequency is understood to some extend. Smaller faults, however, which may produce strong earthquakes at very long time intervals, may go undetected and may pose a similar or greater risk, as local building regulations are not adapted. Examples are the Basel earthquake of 1356 (Lambert et al. 2005) and the Lisbon earthquake of 1755 (Mendez-Victor 2008). For a better understanding of earthquake risks and neotectonic processes, it is useful to determine which faults show this kind of long-term activity.

Several attempts have been made in the past to localize infrequently active faults mainly by the study of historical records and paleoseismic events. Here, Roman aqueducts[1] are presented as a new tool for earthquake studies to enhance our knowledge of infrequently active faults in the Mediterranean Basin.

ANCIENT AQUEDUCTS

Ancient aqueducts are gravity driven water transport systems consisting of roofed masonry channels or piped conduits running from perannial springs to cities, villages or farms (Fig. 1,2). Meandering along the contour lines of the terrain, they gradually descend from source to destination (Hodge 1992, Wikander 2000, Grewe 1986). Aqueducts that served large cities frequently acquired considerable lengths, the 250 km Constantinople aqueduct at the top of the list (Grewe 1986, Hodge 1992, Çeçen 1996).

Fig. 1. Presently known roman aqueducts in central Italy, showing the dense network of long channels, several of which cross major faults. ROMAQ Database.

Aqueducts can be valuable for the study of historically active faults for several reasons:
(1) they are long, anastomosing objects that cover a large area, and are much more likely to be cut by an active fault than any other structure; (2) they comprise bridges, inverted siphons and tunnels which are vulnerable to earthquake damage; (3) they may serve as an earthquake recording device for over 2000 years, i.e. from the construction date to present day; (4) they generally slope down with a minor and rather constant gradient allowing a detailed reconstruction of the uplift pattern produced by movement on faults; (5) since most aqueducts are linked with cities where archaeological work is in progress or has been done, the building and operation of the aqueduct can usually be dated

[1] We use the term “aqueduct” to represent the entire water transporting system of channel, piped conduit, intermediate basins, tunnels and substructures, not just the bridges.

with an accuracy of decades or less; (6) many aqueducts contain carbonate deposits (Fig. 2) which record seasonal and abrupt changes in water chemistry, temperature and depth. Even if an aqueduct is not directly cut by an active fault, a seismic event can leave traces in the carbonate deposits that can be dated.

Ancient aqueducts are found on all continents, including the Aztec and Inca Empires of South America (Wright et al. 2006), but the largest concentration is in the Mediterranean Basin. Most are of Roman Imperial age (50-300 AD) when hundreds of aqueducts were built within a short period of time, often close together (Fig. 1)(Bedon 1997; Hodge 1992; Wikander 2000). More than 1300 Greek and Roman aqueducts are known from the literature.

Fig. 2. Cross section of the roman aqueduct channel of Cologne, showing typical elements. The buried masonry channel is covered on the inside by a red layer of waterproof cement ("opus signinum"). Carbonate on the walls tapers upwards because of variable and gradually rising water level. In the Cologne case, the deposits indicate that the aqueduct ran for approximately 170 years (Fig. 3).

A number of aqueducts are known to have been damaged by earthquakes. An aqueduct near Venafro (Italy) was apparently damaged by three major earthquakes on what seemed to be a minor fault (Galli and Naso 2009; Galli et al. 2010); the major 1349 earthquake that damaged many cities in central Italy, known from medieval records, can now be traced to this fault (Galli et al. 2010). The aqueduct of Nimes (France) was damaged by an earthquake in the third or fourth century in a zone that was thought to be free of recent tectonic activity (Levret et al. 2008; Volant et al. 2009). Marra et al. (2004) reported on a small aqueduct near Rome that was deformed by an earthquake. Damage to the aqueducts of Petra (Jordan) could be attributed to an earthquake of AD 363 (Bellwald et al. 2003). The aqueduct at Aphamea (Syria) was destroyed by earthquakes in 526 and 528 AD and subsequently repaired (Balty 1987). At Al Hativ (Syria) the Dead Sea fault displaced an aqueduct by up to 13 metres in several seismic events (Meghraoui et al. 2003; Sbeinati et al. 2010).

Fig. 3. *Sinter from the Cologne aqueduct. Note typical laminated deposition. Height of sample 12 cm.*

THE ROLE OF CARBONATE DEPOSITS

Many aqueducts were damaged by earthquakes during or after their active life, but it is usually hard to date these events, or to understand how many times the channels were damaged and repaired (cf. Meghraoui et al. 2003; Sbeinati et al. 2010). In such cases, carbonate deposits in roman aqueducts may give clues.

Many aqueducts carried water from karstic aquafers containing carbonates, which deposited on the walls of the channel. (Fig. 3)(Grewe 1986, Guendon & Vaudoir 2000, Garczynski et al. 2005, Guendon & Leveau 2005, Dubar 2006). This travertine like material, also known as *sinter,*

could, over time, acquire considerable thickness corresponding to the period that the aqueduct was running, from decades to as long as 800 years (Sbeinati et al. 2010*)*. Earthquakes have interfered with these deposits in several ways.

1 – Fault motion when an aqueduct is running.
In the most dramatic case, the channel is cut by the fault and water flow is interrupted. Even if the channel was not destroyed, fracturing of the walls and sinter deposits could occur, with subsequent growth of new sinter over the fractures (Carbon et al. 2005). In this way, the seismic event can be precisely localised in the sinter stratigraphy. Careful examination of the damaged site can reveal much about earthquake displacement and dating (Meghraoui et al. 2003*;* Volant et al. 2009; Galli et al. 2010; Carbon et al. 2005*)*. Volant et al. (2009) found deformation twins in calcite in sinter of the Nimes aqueduct, which they attribute to earthquake damage.

Seismic events may also leave marks in sinter away from the damaged site, or where the active fault did not cross the aqueduct. Local damage to the channel or to bridges can lead to water loss and thinner deposits downstream after the earthquake (Levret et al. 2008; Carbon et al. 2005). In case a section of aqueduct was ruptured and subsequently repaired, sinter deposits in this section will differ from those upstream from the damaged site. Fragments of building material and speleothems fallen into the channel, and clastic sediments may be covered by sinter. Commonly, a new layer of waterproof cement is put on top of the deposits when repairing the channel. If the rupture site is lost due to later destruction or erosion, deposits downstream from the site may still differ from those upstream, and a relative dating of the earthquake can thus be established. A further item to be explored is the possibility that an earthquake may temporarily or permanently cause changes in the chemical composition of the water due to alterations in the cave aquifer system that fed the aqueduct.

Fig. 4. Double channel of the Değirmendere aqueduct looking north. The lower channel is the older one and was partly demolished to build the upper channel on the right. Location shown in Figure 5.

2 – Fault motion after the aqueduct has stopped running.
If faults cut an aqueduct after it ceased to operate, dating of the event is possible by classical trenching and dating techniques used for active faults (Sbeinati et al. 2010). In this case, the aqueduct serves to give a minimum age for fault slip, and careful geodetic survey of the deformed channel can give information about vertical ground motion on both sides of the fault.

THE DEĞIRMENDERE AQUEDUCT OF EPHESOS

In recent years Gilbert Wiplinger of the Österreichisches Archaeologisches Institut (ÖAI) and an international team of researchers investigated the Değirmendere aqueduct of Ephesos, Turkey. This aqueduct, one of seven that served the ancient city, took its waters from a spring along a nappe contact to the SE (Fig. 4; Wiplinger 2008). The 37,5 km aqueduct was built as a masonry vaulted channel 80 cm wide and over 240 cm high and was equipped with tunnels and bridges. For a stretch of over 10 km, two channels appeared to run parallel to each other (Figs. 4,5). It was found that the channels were not built simultaneously but one some years after the other, the younger channel being partly built on top of the older one, so that both channels cannot have carried water at the same time. Halfway this 10 km stretch the aqueduct crosses a valley by means of the two story Bahçecikboğaz bridge, where the level of both channels coincide. However, at the upstream end the younger channel's floor is positioned 2 meters *above* the older one, while at the downstream end, close to where an extended tunnel section starts, it is 2 meters *below* it. (Wiplinger 2008, Figs. 4,5).

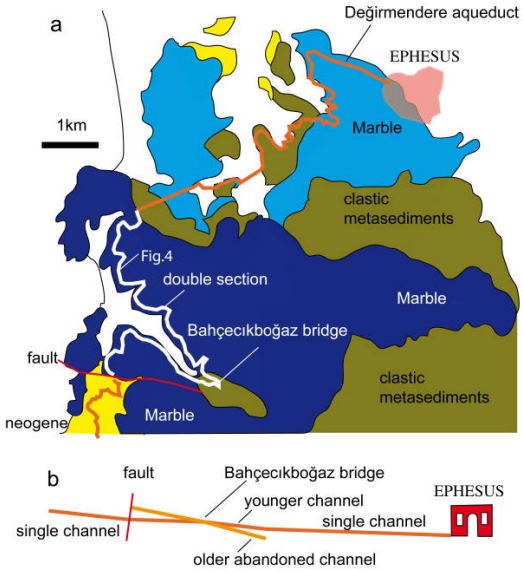

Fig. 5. a - Schematic geological map of the area south of Ephesos. The double channel section lies in the central marble unit; b - schematic height profile of the Değirmendere aqueduct showing the section with two channels. Geology after Çetınkaplan (2002).

Initially it was thought that survey errors by the Roman engineers would explain this feature (Wiplinger 2008). However, recent work has shown that the earlier channel has a layer of sinter several mm wide, which indicates that it must have carried water for several years. This makes survey errors unlikely. The younger channel has carbonate deposits up to 30 cm wide accounting for many decades of running water up to the final stage of the aqueduct. Geological reconaissance early 2011 has localised a major fault scarp near the upstream starting point of the twin section. Whether the northern, downstream end of the twin section also coincides with a fault is currently under investigation. We presently think of the following scenario.

The Değirmendere aqueduct was cut by at least one major fault after it has been in operation for only a few years, probably in the second half of the second century AD. The fault produced a scarp of approximately 2 metres high, interrupting the water flow and altering the slope of the aqueduct over a stretch of 10 km (Fig. 5). To restore the aqueduct, a new channel parallel to the disrupted one had to be built at the proper level. The aqueduct channel and the geology surrounding the Değirmendere aqueduct will be further investigated in 2011.

Acknowledgements: The authors thank the Geocycles Cluster and the University of Mainz for financial support. The Österreichisches Archaeologisches Institut provided crucial logistic and general support.

References

Balty, J. C., (1987). Problèmes de l'eau a Apamée de Syrie. In: Les Travaux de la Maison de l'Orient. *L'Homme et l'eau en Mediterranée et au Proche Orient*. (Louis, P, Métral, F., Métral , J. eds). 4, 9-23.

Bedon, R., (1997). Les aqueducs de la gaule romaine et des regions voisines. Pulim, Limoges.

Bellwald,U., M. Al-Huneidi, A. Salihi, D. Keller, R. Naser, & D. Al-Eisawi, (2003). *The Petra Siq, Nabataean hydrology uncovered*. Petra National Trust.

Carbon, D., G. Fabre, P. Volant, J.-L. Fiches, A. Levret & P. Combes, (2005). L'aqueduc de Nîmes dans la haute Vistrenque: analyse interdisciplinaire d'un tronçon souterrain. *Gallia* 62, 69-86.

Çeçen, K., (1996). Roma su yollarının en uzunu (The Longest Roman Water Supply Line).

Çetınkaplan, M., (2002). Tertiary high pressure / low temperature metamorphism in the Mesozoic cover series of the Menderes massif and correlation with the cycladic crystalline complex. Unpublished PhD. Thesis, Izmir.

Dubar, M., (2006). Recherche et interprétation climatique des microcycles du concrétionnement travertineux de l'aqueduc romain de fréjus (var, France) *Quaternaire* 17, 79-85

Galli, P.A.C., Naso J.A., (2009), Unmasking the 1349 earthquake source (southern Italy); paleoseismological and archaeoseismological indications from the Aquae Iuliae Fault, *Journal of Structural Geology* 31,128–149.

Galli, P.A.C., Giocoli, A., Naso, J.A., Piscitelli, S., Rizzo, E., Capini, S. & Scaroina, L., (2010). Faulting of the Roman aqueduct of Venafrum (southern Italy): Methods of investigation, results, and seismotectonic implications. In: Ancient Earthquakes (Sintubin, M., Stewart, I.S., Niemi, T.M., Altunel, E. eds). *Geological Society of America Special Paper* 471, 233-242.

Garczynski, P, J. Foucras & M. Dubar, (2005). L´aqueduc d´Antipolis dit de la Boullide (Alpes Maritimes). *Gallia* 62, 13-34

Grewe, K., (1986). *Atlas der römischen Wasserleitungen nach Köln*. Rheinland Verlag, Koeln.

Guendon, J-L., Vaudoir, J., (2000). Concrétions et fonctionement de l´aqueduc: étude morpho-stratigraphique. In: *L´aqueduc de Nîmes et le Pont du Gard*. (Fabré, G., Fiches, J-L., Paillet, J-L. eds). CNRS Editions. 263-271

Guendon, J-L., Leveau, Ph., (2005). Dépots carbonatés et fonctionement des aqueducs romains. *Gallia*, 62, 87-96

Hodge, A. T., (1992). *Roman aqueducts and water supply*, Duckworth, London.

Lambert J., T. Winter, T.J. Dewez & P. Sabourault, (2005). New hypotheses on the maximum damage area of the 1356 Basel earthquake (Switzerland), *Quaternary Science Reviews*, 24, 383–401.

Levret, A, Ph. Volant, D. Carbon, D Combescure, T. Verdel, A. Piant, O. Scotti & Ph. Laurent, (2008). L' aqueduc romain de Nimes (France): nouveaux résultats en archéosimicité. In: *Archéosismicité et Vulnérabilité: patrimoine bâti et société*. (Levret, A. ed),165-188

Marra, F., P. Montone, M. Pirro & E. Boschi, (2004). Evidence of tectonics on a Roman aqueduct system (II-III century AD) near Rome, Italy. *Journal of Structural Geology* 26, 679-690.

Meghraoui, M., F. Gomez, R. Sbeinati, J. Van der Woerd, M. Mouty, A. Nasser Darkal, Y. Radwan, I. Layyous, H. Al Najjar, R. Darawcheh, F. Hijazi, R. Al-Ghazzi & M. Barazangi, (2003). Evidence for 830 years of seismic quiescence from palaeoseismology, archaeoseismology and historical seismicity along the Dead Sea fault in Syria. *Earth and Planetary Science Letters* 210, 35-52.

Mendez-Victor, L. A., C. S. Oliveira & J. Azevedo, (2008). *The 1755 Lisbon Earthquake: revisited*. Springer Verlag.

ROMAQ. Unpublished database. Passchier, C. W., Van Opstal, D., Schram, W. (eds.) Internet publication pending.

Sbeinati, M., M. Meghraoui, G. Suleyman, F. Gomez, P. Grootes, M. Nadeau, H. Al Najjar & R. Al Ghazzi, (2010). Timing of earthquake ruptures at the Al Harif Roman aqueduct (Dead Sea fault, Syria) from archaeoseismology and paleoseismology. G*eological Society of America Special Papers* 471, 243-267.

Volant, Ph., A. Levret, D. Carbon, O. Scotti, D. Combescure, T. Verdel, A. Piant, Ph. Laurent, (2009). An archaeo-seismological study of the Nîmes Roman aqueduct, France: indirect evidence for an M6 seismic event? *Natural Hazards* 49, 53-77.

Wikander, O., (2000). Handbook of ancient water technology. Brill, Leiden.

Wiplinger, G., (2008). The Değirmendere Aqueduct to Ephesus. *Anodos* 8, 393-400.

Wright, K. R.,G. F. McEwan & R. M. Wright, (2006). *Tipon: water engineering masterpiece of the Inca empire*. ASCE Press.

TESTING ARCHAEOSEISMOLOGICAL TECHNIQUES WITH INSTRUMENTAL SEISMIC DATA CAUSED BY THE Mw 5.1 LORCA EARTHQUAKE (5-11-2011, SE OF SPAIN)

Pérez-López (1), R., J.L. Giner-Robles(2), M.A. Rodríguez-Pascua (1), F. Martín-González(3), J. García Mayordomo (1) J.A. Álvarez-Gómez(4)(5), M.J. Rodríguez-Peces(4), J.M. Insua-Árévalo (4), J. J. Martínez-Díaz (4) and P.G. Silva(6)*

(1) IGME – Instituto Geológico y Minero de España, Área de Investigación en Riesgos Geológicos. Madrid, SPAIN. Email: r.perez@igme.es , m.rodríguez@igme.es, julian.garcia@igme.es
(2) Departamento de Geología. UAM, Universidad Autónoma de Madrid. SPAIN. Jorge.giner@uam.es
(3) Universidad Rey Juan Carlos I, Madrid. SPAIN
(4) Departamento de Geodinámica. Facultad de Ciencias Geológicas. Universidad Complutense de Madrid. SPAIN. Email: jmartinez@geo.ucm.es
(5) Instituto de Hidráulica Ambiental "IH-Cantabria", E.T.S.I. Caminos, Canales y Puertos, Universidad de Cantabria. Spain.
(6) Departamento de Geología. Universidad de Salamanca. Email: pgsilva@usal.es
* Corresponding author

Abstract (Testing archaeoseismological techniques with instrumental seismic data caused by the Mw 5.1 Lorca Earthquake, 5-11-2011, SE of Spain): *the earthquake of the 11th of May of 2011 was located near of the village of Lorca (SE of Spain) and with a magnitude (Mw) of 5.1. Despite of the small sized- earthquake, it generated a relative high seismic intensity (VII EMS), nine people were killed and almost 14,000 were left from their homes. The total estimated cost of this earthquake is 75 millions of Euros. A systematic analysis of damaged ancient buildings was performed with the aim to check archaeoseismological new techniques. Namely, we have described different Earthquake Archaeological Effects (EAE) affecting both monumental buildings as modern edifices. The interest is the possibility to compare EAEs with focal parameters of the earthquake and the geometry of the seismic source, the Alhama de Murcia Fault (FAM).The preliminary results displays an almost N-S seismic wave anysotropy obtained from different EAE recorded at eight different monumental buildings.*

Key words*: archaeoseismology, instrumental earthquake, EAE, Lorca, SE of Spain*

THE LORCA EARTHQUAKE OF THE 5-11-2011

The 11th of May, 2011, a small and shallow earthquake struck the village of Lorca (92,000 inhabitants approximately). This earthquake hit the city at 18:50 h (local time), such as you can see in the broken clock of the tower of the San Francisco church (also so-called the church of "El Paso Azúl"). The recorded magnitude by the Spanish *Instituto Geográfico Nacional*, IGN, was 5.1 Mw (www.ign.es). Nevertheless, the maximum value of the peak ground acceleration (PGA) was 0.41g, recorded at the basement of the ancient jailhouse of the city. Also, 5 mm of GPS movement northward was recorded in the basement of the Fireman Station. Outliers values for this small magnitude.

Unfortunately, this small earthquake killed nine people, two from the collapse of one modern building located at *La Viña* neighbourhood, southward of the city, and the others due to the falling of the hanging decoration from the outer façade. Besides, almost 14,000 people were moved from their homes and 300 of them still live in camp sites. The city was dramatically collapsed and during the following twelve hours the fatality ruled the city.

A few hours after the main shock, a group of earthquake geologists grew up from diverse Spanish institutions, and they went to the disaster zone with the aim of finding answers to these questions: (1) what was the seismic source of this earthquake? Or better, which is the causative fault of the earthquake? (2) Is there evidence of surface rupture for such a minor event?

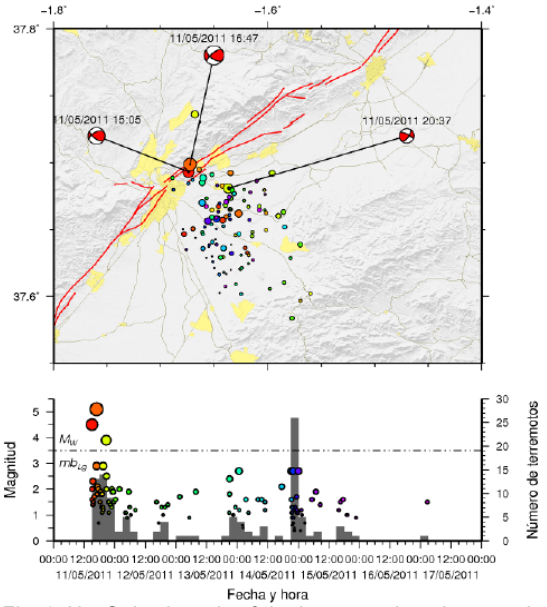

Fig. 1: Up. Seismic serie of the Lorca earthquake recorded by the IGN. The size of the point is related to the earthquake magnitude. The colour indicates the day of the occurrence. The focal mechanism solutions show two strike-slips with reverse component. The red lines indicate the main active faults. The FAM (Alhama de Murcia major Fault) is a NE-SW reverse fault with oblique component, with a total length of ca 90 km (Martínez-Díaz, 2002). Down: frequency grey bars indicate the number of earthquakes recorded in 3 h.

Empirical models predict small rupture area (i.e. ca 12 km^2, Wells & Coppersmith, 1994), (3) Can we compile an Earthquake Environmental Effect

catalogue from this shaking? Rock fall, ground cracks affecting soils and rocks, changes of temperature in hot springs and thermal aquifers, liquefactions, and so, and finally, (4) Can we do an *archaeoseismic-type* analysis from the monumental building damage within the village? In this case we tried to make a compilation of the maximum number of the Earthquake Archaeological Effects (see Rodríguez-Pascua et al., 2011 for a comprehensive description of EAEs). The interest of this last analysis is the correlation between EAEs and focal and geometrical parameters of the earthquake.

Despite the low magnitude of the earthquake, we have enough geological and seismological data to find a preliminary answer to these questions: high seismic intensity (VII EMS, www.ign.es), high building damage (almost 200 damaged buildings are catalogued), we have an active fault with different outstanding palaeoseismic studies (the Alhama de Murcia Fault, FAM)(Silva et al., 1997, Martínez-Díaz 1998)(see location in Fig.1).

Consequently, the aim of this work is to check EAEs usefulness by comparing the damage anisotropy caused by the main shock of the earthquake (Mw 5.1), and performed along the old town of the historic village of Lorca. The technique used here is widely described in Giner-Robles et al. (2009).

SEISMOTECTONICS OF THE EARTHQUAKE

A precursor event of Mw 4.5 (www.ign.es) occurred 3 hours before of the main shock of 5.1. The epicentre location of both earthquakes coincides with the mapped active fault of Alhama de Murcia (FAM)(Bousquet & Montenat, 1974))(Fig.1). The location of the epicentres on the FAM suggests that a small segment of 3 x 3 km could have broken. Moreover, the focal mechanism solutions indicate either a NE-SW fault plane (in coincidence with the FAM trending) or NW-SE fault plane. The geometry of both mechanisms shows an oblique fault with reverse component. This geometry is in agreement with the geology and palaeoseismological studies on the FAM (Silva et al., 1997; Martínez Díaz et al., 2001). The estimated depth of the earthquake lies between 3 and 5 km (www.ign.es).

In the following six days, more than 100 aftershocks with a maximum magnitude of 3.9 were recorded (www.ign.es). The temporal occurrence of aftershocks shows cluster behaviour in small groups instead of a slight decay of the number of aftershocks from the main shock (Fig. 1).

GEOLOGICAL EFFECTS (EEE) OF THE EARTHQUAKE

A shallow earthquake (2 km deep) and high seismic intensity (VII EMS) suggested the possibility to have a surface rupture associated to the earthquake. With this aim, we performed a field trip across the fault trace of FAM to catalogue Earthquake Environmental Effects (EEE) according to the ESI 07 scale (Michetti et al., 2007).

Fig. 2. Rock fall triggered by the Lorca earthquake and located at Las Estancias Sierra, southwestwardly of the epicentre location.

The main effect was rock falling located in steep carbonatic cliffs in the nearby (<7 km) (Fig. 2). In summary, the earthquake geological effects were the following: neither surface rupture (Fig. 3), nor permanent ground dislocation. Also no relevant changes of the water temperature were observed. Temperature data measured, hours after the main shock, at the Carraclaca hot spring showed an increasing of 0.7ºC from the averaged temperature. Taking in mind that the accuracy of the thermocouple device is 0.3ºC and the reference value is a media, is hard to assume a significant temperature change. Besides, this hot point is the nearest to the epicentre, few hundred meters away, and the water upwelling is directly related to the FAM fault plane. A few natural springs along the Las Estancias Range experimented a significant caudal increasing just after the seismic event.

Regarding the slope instabilities, in general these are of a small size and distribute in a localized area. However, this assertion has to be contrasted with aerial imaginary taken after the main shocks. The ground instabilities produced by the earthquakes are basically rock-falls of very different size, single rock-falls and collapses of sections of the external wall of Lorca's castle. Few of the instabilities produced by the earthquake can be referred as significative in the sense that they have produced some damage in buildings and temporal road-cuts.

In particular, at the easternmost point of Lorca's Castle cliff (Fig. 3), a fallen rocky block has destroyed part of the wall enclosing the patio of a house. Alike, on the road up-the-hill to the castle few rock-falls have badly damaged the pavement. A similar situation has taken place on the road to the *Pantano de Puentes*, which was temporarily closed to traffic. It is remarkable that on Friday 13th.

It is highlighted that the stability measures deployed on the southern slope of the castle cliff have performed adequately, avoiding what it would have been an aggravation of the damage produced by the earthquake and may be a larger number of

casualties, particularly on the habitations located right under the cliff. A quick visual inspection suggested the perfect state of the measures, although this observation should be confirmed after a systematic and detailed inspection. The approximate volume of rock falling blocks is lesser than 10^3 m^3.

Fig. 3. Partial collapse of the easternmost point of Lorca's castle cliff. A detached rock-block produced damage in a near house.

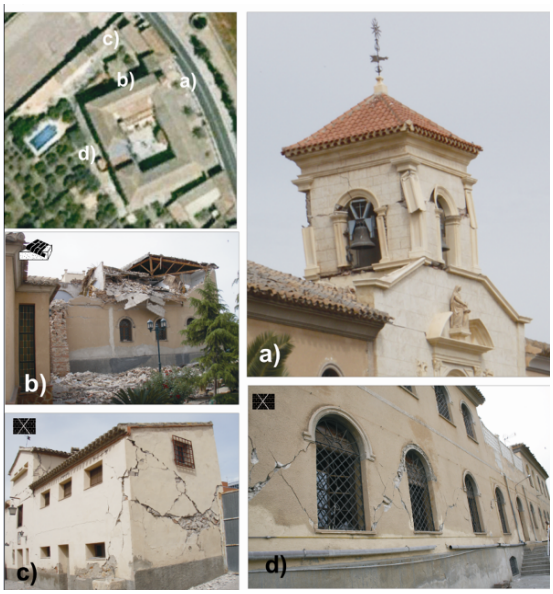

Fig. 4. Damage in the tower and main buildings of the Clarisas´ Convent. (a) Destroyed tower, (b), collapsed roof of the main edifice, (c) and (d) X-fractures in the East and West sides of the annexed building.

ANALISIS OF EAE: DAMAGE DESCRIPTION

The earthquake of Lorca (SE Spain) was responsible for a large amount of damage and seismic intensity on a wide range of buildings in the city of Lorca, including the historical buildings. Aerial view shows a concentration of damage in the highest towers, mainly affecting the arches, buttresses canopies, bollards etc. Rotations also appear in decorative elements such as bollards and obelisks, like the obelisk in the San Francisco church.

The most relevant key of this archaeoseismic study is the correlation between the instrumental information of this earthquake with damage in historical and modern buildings. This information also can be correlated with seismic and geological parameters, such as the magnitude and focal mechanism of earthquake, the seismogenic fault and site effects related to the geology of Lorca.

Lorca's earthquake has not produced widespread buildings collapses (only two buildings collapsed), during the inspection we have recognized, classified and described more than one hundred effects of the earthquake on buildings and structures, similar to those described in the work of Giner-Robles et al., 2009, Rodríguez-Pascua et al., 2011. These authors defined the Earthquake Archaeological Effects, (commonly known as EAE).

The EAE describes and quantifies the coseismic deformation in archaeological sites and historic buildings. After Giner-Robles et al., 2009 and Rodríguez-Pascua et al., 2011, they classified according to EAE: (1) permanent deformation of the surface (2) temporary deformation by the seismic shaking during the earthquake.

Figure 4 shows an example of the type of analysis that we have performed in the village. We have located the damaged building and we have described all of EAEs recognized. In this case, the Clarisas's Convent displayed two types of EAEs: collapsed roof and walls, and penetrative conjugated faults affecting oriented sides of annexed buildings. Other type of study involves the orientation of fallen key stones in arches. Fig. 5 is a clear example of arches showing evidence of damage anisotropy obeying the mechanism proposed by Giner et al., 2009.

All this preliminary information has been represented in a rose diagram (Fig. 6), showing the main orientation in a NW-SE trend, N150º-160ºE. We interpret these direction NW-SE with azimuth from the SE.

PRELIMINARY RESULTS

- Alhama-Murcia Fault (FAM) is the structure with greater evidence of Quaternary activity in the area: paleoseismic activity (Mw > 6.0) over the last 1000 years, associated with thermal springs and a well-recognized surface trace. Destructive historical seismicity located along the trace during the XVII, XVIII and XIX centuries were reported in chronicles. FAM has a trace that it is parallel to one of the nodal planes of focal mechanisms obtained for the earthquake. The oblique (reverse - sinistral movement) movement of the fault is consistent with the focal mechanism solution.

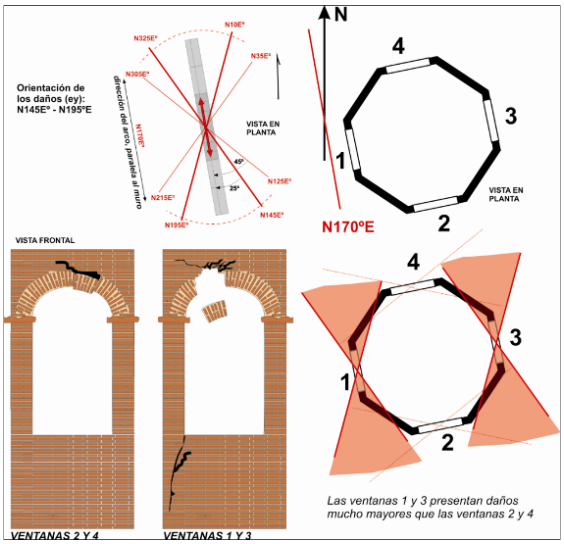

Fig. 5. Example of analysis of deformation structures and the results of the orientation assessment of the strain (San Juan's Church) (After Martínez-Díaz et al., 2011).

- The high seismic intensity experienced by the town of Lorca (intensity VII EMS-98 scale, data IGN) associated with a magnitude 5.1 Mw, may be due to the earthquake spread from the Sierra de la Tercia (epicentral area) to the SW. The lack of geological effects to the east of the epicenter (La tercia Range and Lower Guadalentin Valley) support the possible existence of rupture directivity southwest.
-The seismic wave propagation supports the directionality of the FAM rupture spread from the epicentral area, crossing the city of Lorca. This reason associated with the shallowness of the earthquake, would explain the high seismic intensity and peak accelerations of 0.36 g (IGN data) recorded in the accelerometer of the old prison of Lorca (located in the downtown). However, the high value of PGA could be also related to site effects.
- The archaeoseismic data (more than a hundred values) suggest an origin of the deformation associated with a nearby seismic field, implying that the main earthquake rupture occurred beneath the historic city of Lorca because the faulting subsurface rupturing runs below the Lorca village.
- The ESI 07 macroseismic classification (Michetti et al. 2007) for this earthquake is between VI and VII, according to the features observed. Hence, the interest of this small-sized earthquake is that it could be used as a lower limit for the instrumental calibration of the scale ESI 07.

Acknowledgements: Thanks are given to the Spanish Instituto Geografico Nacional (IGN) for providing instrumental data of the earthquake. Also a special mention to the people of Lorca which helped us even with their homes collapsed and all people which showed friendly and kindness against the earthquake disaster.

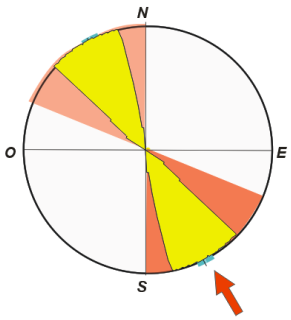

Fig. 6. Rose diagram of the seismic shaking, using the EAEs. Preliminary results (After Martínez-Díaz et al., 2011).

References

Bousquet, J.C. y Montenat, C. (1974). Presence décrochements NE-SW plio-quaternaires dans les Cordillères Bétiques Orientales (Espagne). Extension et signification général. C. R. Acad. Sci. Paris 278: 2617-2620.

Giner-Robles, J.L. M.A. Rodríguez-Pascua, R. Pérez-López, P.G. Silva, T. Bardají, C. Grützner and K. Reicherter. (2009). Structural Analysis of Earthquake Archaeological Effects (EAE): Baelo Claudia Examples (Cádiz, South Spain), vol. 2,130p. Instituto Geológico y Minero de España, Madrid. Dep. Leg. M-27206-2009.

Martínez Díaz, J.J., E. Masana , J.L. Hernández-Enrile & P. Santanach. (2001). Evidence for coseismic events of recurrent prehistoric deformation along the Alhama de Murcia Fault, Southeastern Spain. Geol. Acta. 36 (3-4): 315-327.

Martínez Díaz, J.J. (1998). Neotectónica y Tectónica Activa del Oeste de Murcia y sur de Almería (Cordillera Bética). Tesis Doctoral. Universidad Complutense Madrid. 470p.

Martínez-Díaz, J. J. (2002). Stress field variety related to fault interaction in a reverse oblique-slip fault: the Alhama de Murcia Fault, Betic Cordillera, Spain. Tectonophysics, 356: 291-305.

Martínez Díaz J. J.; et al. (2011). Geological Preliminary Field Report of The Lorca Earthquake (5.1 Mw, 11th May 2011). Instituto Geológico y Minero de España (IGME), Spanish Group of Active Tectonics, Paleosismicity and Risks, Universidad Complutense de Madrid (UCM), Universidad Autónoma de Madrid (UAM) and Universidad Rey Juan Carlos de Madrid (URJC). 45p.

Michetti A.M., Esposito E., Guerrieri L., Porfido S., Serva L., Tatevossian R., Vittori E., Audemard F., Azuma T., Clague J., Comerci V., Gurpinar A., Mc Calpin J., Mohammadioun B., Morner N.A., Ota Y. & Roghozin E. (2007). Intensity Scale ESI 2007. In. Guerrieri L. & Vittori E. (Eds.): Memorie Descrittive Carta Geologica. d'Italia., vol. 74, Servizio Geologico d'Italia – Dipartimento Difesa del Suolo, APAT, Roma, 53 p.

Rodríguez-Pascua M.A., R. Pérez-López, J.L. Giner-Robles, P.G. Silva, V.H. Garduño-Monroy and K. Reicherter. (2011). A Comprehensive Classification of Earthquake Archaeological Effects (EAE) in Archaeoseismology: application to ancient remains of Roman and Mesoamerican cultures. Quaternary International, doi:10.1016/j.quaint.2011.04.044.

Silva, P.G., Goy, J.L., Zazo, C., Lario, J., Bardají, T. (1997). Paleoseismic indications along "aseismic" fault segments in the Guadalentín depresion (SE Spain). J. Geodynamics 24(1-4), 105-115.

Wells, D.L. & Coppersmith, K.J. (1994). New empirical relationships among magnitude, rupture length, rupture width, rupture area, and surface displacement. Bull. Seismol. Soc. Amer. 84, 974-1002.

FRONTIERS OF EARTHQUAKE ARCHAEOLOGY: THE OLYMPIA AND SAMICUM CASES (PELOPONNESE, GREECE)

Reicherter, Klaus (1)

(1) RWTH Aachen University, Inst. of Neotectonics and Natural Hazards, Aachen, 52056, Germany, email: k.reicherter@nug.rwth-aachen.de

Abstract (Frontiers of earthquake archaeology: the Olympia and Samicum cases (Peloponnese, Greece)): *The ancient Olympia on the western Peloponnese/Greece is worldwide known as the place where for 1170 years the classical Olympic Games took place. Furthermore, to domino-like toppled column drums of the Zeus temple are famous and widely accepted as earthquake-related structural damage the 522/551 AD events. The Peloponnese peninsula is characterized by frequent seismicity within the Euroasian-African convergence zone (Hellenic arc and backarc system) by mainly E-W trending normal faults.*
Herein, some examples of the heterogeneous structural deformation are given observed in the ancient Olympia including an interpretation. Also, we show deformation patterns at Samicum, a Hellenistic fortified village (acropolis) with a cyclopean masonry situated on top of the coastal Lapithas mountain ridge, close to Olympia. Both examples may be interpreted as archaeoseismic evidence, however, an on-fault palaeoseismological approach and assessment is missing in this part of Greece.

Key words*: earthquake geology and archaeology, Olympia, Samicum, structural deformation*

INTRODUCTION

This paper deals with the combination of well-known historic sites and their earthquake-related damage. By a number of ancient historians (see references) we know about the destruction of ancient Olympia by several earthquakes (early 4th cent. AD, 522 AD, 551 AD) and by warfare and vandalism. On the other hand, the close-by fortified village Samicum was described as abandoned by Pausanias in the 2nd cent. AD (Fig. 1). This seems rather strange taking into account the strategic position of the village on top of the mountain Lapithas. We apply the classification of Earthquake Archaeological Effects of Rodríguez-Pascua et al. (2011; EAE) to describe and classify the observed damage. The investigation of past earthquakes is commonly split into several disciplines, which cover Instrumental Seismology, Historical Seismology, Archaeoseismology and Earthquake Geology or Palaeoseismology depending on information available (e.g. Caputo and Helly, 2008). However, the ambiguity of data and results of distinct disciplines (Niemi, 2008), e.g. of written sources and recent observations, results in limitations of the seismic hazard assessment of an area (Nur, 2008).
The Elis region is characterized by a huge number of neotectonic faults, which have been intensely studied (Fig. 2; Lekkas et al., 1993; Lekkas et al., 2000, Papanikolaou et al., 2007; Fountoulis and Mariolakos, 2008). The seismicity in the study area on the western Peloponnese peninsula is high. The last earthquake with M 5.5 struck the Pyrgos area on the 23rd of March in 1993 with maximum intensities of VIII (e.g. Lekkas et al., 2000) associated with EEE (Earthquake Environmental Effects on the INQUA ESI-scale, Papanikolaou et al., 2009) like liquefaction, landslides, ground fractures and changes in the aquifer level.

STUDY AREAS

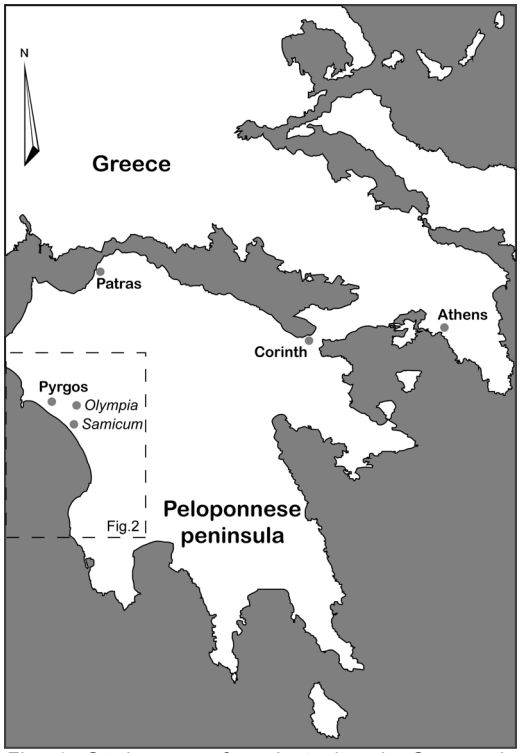

Fig. 1: Study area of ancient sites in Greece, inset shows location of Fig. 2.

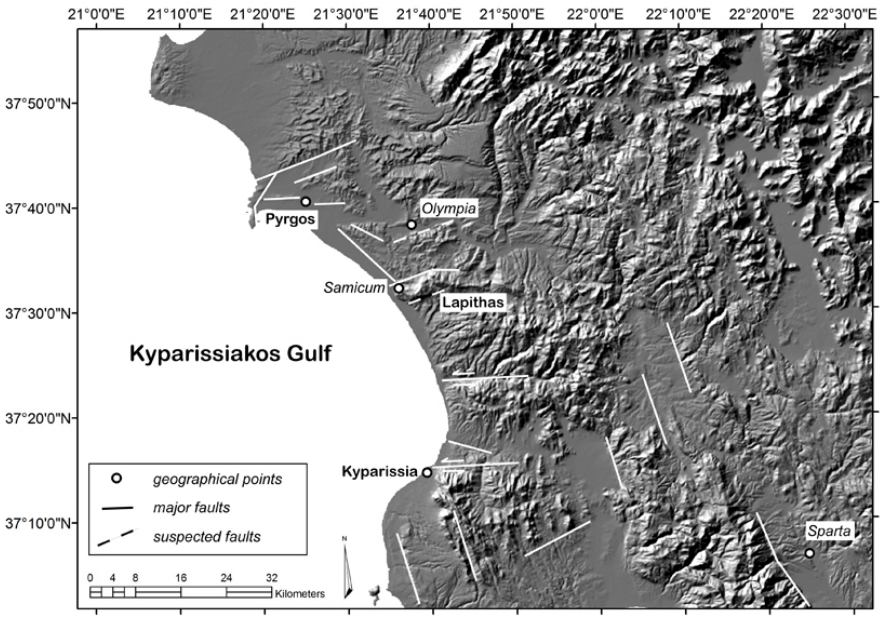

Fig. 2: Study area of ancient sites on the Peloponnese peninsula, Greece, with major faults (compiled from Lekkas et al., 1993; Lekkas et al., 2000, Papanikolaou et al., 2007; Fountoulis and Mariolakos, 2008).

Ancient Olympia

The ancient Olympia is a famous World Heritage site located in the Peloponnesian province of Elis in the west of the peninsula (Figs.1 and 2). Known as the place of the classical Olympic Games, the sanctuary (Altis) consists of several buildings, which spread between the Kladeos creek and Mount Kronos. The Altis resembles a variety of buildings of different use and age during more than 3000 years (since c. 2500 BP until 6th cent. AD). Finally, the area was flooded and covered by sediments of the Kladeos creek and Alfeios river (Fouache and Pavlopoulos, 2010) and was forgotten by people until 1829 AD. One of the most famous examples of EAE are the domino-style fallen columns of the Temple of Zeus (5th cent. BC), which made it on the cover of a book entitled "Archaeoseismology" (see Stiros, 1996). The former Temple of Zeus, today known as Temple of Hera (it was rededicated in the 5th cent. BC), is reported to have been destroyed by an earthquake in the early 4th cent. AD, and was never rebuilt. Table 1 sums the construction and destruction events of the Zeus and Hera temples, several dates of possible destruction are ambiguous and not stated by exact dating, furthermore the causative fault(s) are not known.

Date	Event
590-580 BC	Construction of the Temple of Hera
472-456 BC	Construction of the Temple of Zeus
c. 175 BC	Earthquake? and repair of the Zeus statue, roof and columns (Pausanias, IV,31,6 and Dinsmoor, 1941) sculptures of the Temple of Zeus (Dinsmoor, 1941), which are replaced
36 BC	Earthquake? Second-hand roof tile – repair work (Dinsmoor, 1941)
3th cent. AD	Series of earthquakes?
early 4th cent. AD	Earthquake (destroys Temple of Hera)
394 AD	Pillage of Olympia by the Goths
426 AD	Theodosius orders destruction of the Temple of Zeus
522 AD	Earthquake (destroys Temple of Zeus) in combination with floods of the Alfeios and Kladeos, and landslide from the Kronos hill? (date unclear could be 551 AD)
551 AD	Earthquake (destroys Temple of Zeus) in combination with floods of the Alfeios and Kladeos, and landslide from the Kronos hill?

Tab. 1: Timetable of con-/ and destruction observed in Olympia (compiled with different sources)

Fig. 3: Fallen columns of the Temple of Zeus, Olympia (Classical period)

Samicum

The fortified village of Samicum (or Macistus, ancient Kato Samia, however there is discussion, Pausanias and Polybius mention only Samicum, and Xenophon only Macistus) is situated in the southern part of the Elis region (Ilia, Triphylia) on top of the Lapithas mountain ridge, south of mouth of the Alfeios river

(Perseus Digital Library, 2011). Most probably Samicum was founded in the last 5th cent. BC (classical Hellenistic period) and was occupied until the 2nd cent. AD (Roman period). Samicum was occupied by the Aetolian Polysperchon against the Arcadians in 244 BC, and was later taken by Philip, in 219 BC. According to archaeologists the Samicum site has to be considered as one of the most important cities in Elis because of the strategic position on the mountain top, controlling the Kaiafas pass, lagoons and springs.
The village is surrounded by a so-called pseudo-polygonal wall of c. 1500 m length in a trapezoid shape with several towers, thus forming an acropolis. The cyclopean masonry of the wall surrounding Samicum is characterized by polygonal limestones, which fit each other with precision and minimal clearance between the stones and no use of mortar, little gaps are filled with shaped small stones.

OBSERVATIONS

Ancient Olympia
Walking around in the Altis of Ancient Olympia reveals a good opportunity to also study earthquake-related structural damage. On the other hand, a lot of reconstruction work and replacement limits full pleasure, which is further diminished by "slow" deformation due to landslides in the Kronos hill area.
The most prominent features are the domino-like fallen columns of the Temple of Zeus (Fig. 3). Already Stiros (1996) stated that one of the columns is known to have been fallen during a storm (possibly after its reconstruction in the 19th cent. AD). Another peculiar observation is that the colonnade columns fell towards the N- and the S-side of the temple´s long axis. The spaces between individual column drums are filled with sediment yielding ceramics.

Fig. 4: Vaulted entrance to the stadium Olympia (Crypt), approx. 200 BC (Hellenistic period)

Dinsmoor (1941) observed to different styles of column drum beds, on which the connection to each other is observable: one with Lewis Holes, one without (but with the Empolion, the central hole). Of 175 drums analyzed only 30 drums yielded Lewis Holes (Dinsmoor, 1941). This and repair work at columns as well as repair clamps at the western corners, lead Dinsmoor (1941) to postulate a 175 BC earthquake damage. Further on, entering the stadium via the vaulted archway of c. 200 BC, dropped key stones can be observed (Fig. 4).
Finally, the Phillipeion, a 338 BC construction, shows nice corner breakouts (Fig. 5), described as "dipping corners" by Rodríguez-Pascua et al. (2010) in the EAE.

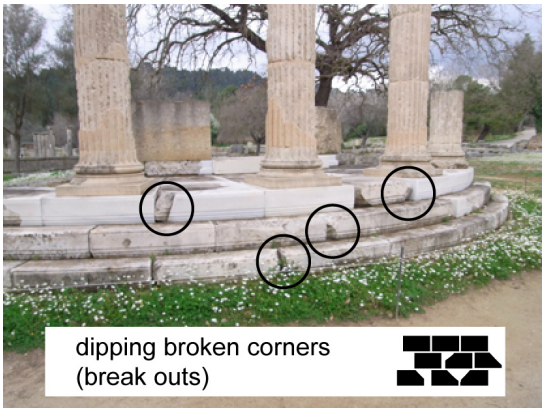

Fig. 5: Phillipeion, Olympia, c. 338 BC (Hellenistic period)

However it is remarkable that the Roman ruins do not show such peculiar features of deformation. After an earthquake in the early Byzantine period (6th cent. AD), the Altis was covered by a "mass of yellow earth spread over the entire area after a cloudburst perhaps in the 7th cent. AD" (Dinsmoor, 1973).

Samicum
After reaching the ruins of Samicum on the Lapithas mountain enjoy the nice view around including the Volax and Kaifas lagoons. Little of the central part is excavated, the most impressive feature of Samicum is the cyclopean masonry of the city wall with several fallen towers and gates. Towards the south a steep cliff frames the fortified village. The wall and its blocks show various indicators of seismic damage. Among them are moved and rotated blocks, corner break-outs, collapsed watch towers (Figs. 6 and 7).
Up to now these damages are not described and related to earthquakes, also there is no historic account for earthquake damage in Samicum. But Pausanias refers to his journey to Samicum, where

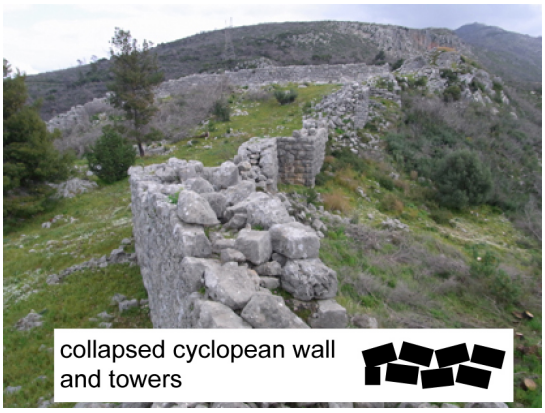

Fig. 6: Samicum, wall damage (Hellenistic period)

he found the village abandoned and destroyed in the 2nd cent. AD.

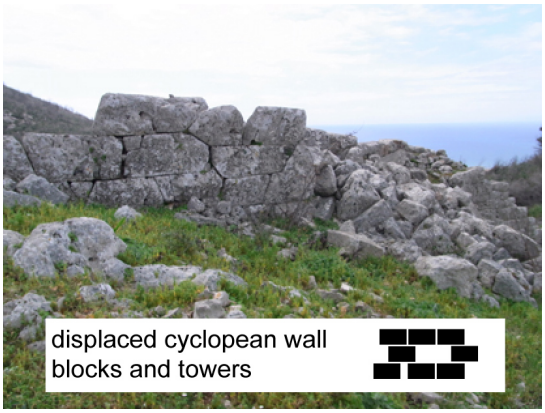

Fig. 7: Samicum, wall damage and tower collapse (Hellenistic period)

CONCLUSIONS

We presented EAE of the ancient Greek sites of Olympia and Samicum, both have in common that the structural damage up to now has not been mapped, characterized and catalogued in detail. Also, the structural damage has not been classified and differentiated in the cause of damage. The Samicum case is most probably a "one-event" earthquake deformation. Whereas Ancient Olympia has obviously suffered from several earthquakes and other destructions (pillage, landslides and flooding). Both cases have also in common that the causative fault(s) for the earthquakes have not been detected yet, palaeoseismological studies are missing. Recent seismicity, such as the 1993 Pyrgos event (EEE description in Papanikolaou et al., 2009) shows that even moderate earthquakes (M ≤ 6.5) can cause severe structural damage and secondary effects as landslides and liquefaction. So, as a conclusion both cases reveal clearly the frontiers of archaeoseismology, and are at the moment that what Sintubin et al. (2008) pointed out: just a good story.

References

Caputo, R., Helly, B. (2008). The use of distinct disciplines to investigate past earthquakes. Tectonophysics, 453(1-4), 7-19.

Dinsmoor, W.B. (1941). An archaeological earthquake at Olympia. Am. J. Archaeol., 45/3, 399-427.

Dinsmoor, W.B. (1973). The architecture of Ancient Greece. An account of its historic development. Biblio and Tannen, 424 pp.

Fouache, E., Pavlopoulos, K. (2010). The interplay between environment and people from Neolithic to Classical times in Greece and Albania. In: Martini, I.P. (ed.). Landscapes and Societies: Selected Cases, Chapter 10, 155-166.

Fountoulis, I., Mariolakos, I. (2008). Neotectonic folds in the central-western Peloponnese, Greece. Z. dt. Ges. Geowiss., 159/3, 485-494.

Lekkas, E., Papanikolaou, D., Fountoulis, L. (1993). Neotectonic map of Greece, Pyrgos-Tropaia sheets, scale 1:100.000, Research Project of eth Univ. of Athens, Dept. of Geology, Division of Dynamic, Tectonic and Applied Geology, Athens. Available online at: http://elekkas.gr/en/research/mapping.html

Lekkas, E., Fountoulis, I., Papanikolaou, D. (2000). Intensity distribution and neotectonic macrostructure Pyrgos Earthquake data (26 March 1993, Greece). Nat. Haz., 21, 19-33.

Niemi, T. (2008). Historical Earthquake Catalogues and Archaeological Data: Avoiding Circular Reasoning. Seismological Research Letters, 79(2), 289.

Nur, A. (2008). Apocalypse. Earthquakes, Archaeology, and the Wrath of God. Princeton University Press, Princeton.

Papanikolaou, D., Fountoulis, I., Metaxas, C. (2007): Active faults, deformation rates and Quaternary paleogeography at Kyparissiakos Gulf (SW Greece) deduced from onshore and offshore data. Quat. Int., 171-172, 14–30.

Papanikolaou, I.D., Papanikolaou, D.I., Lekkas, E. (2009). Advances and limitations of the Environmental Seismic Intensity scale (ESI 2007) regarding near-field and far-filed effects from recent earthquakes in Greece: implication for the seismic hazard assessment. In: Reicherter, K., Michetti, A.M., Silva, P.G. (eds.). Paleoseismology: Historical and prehistorical records of earthquake ground effects for seismic hazard assessment. J. Geol. Soc. London Spec. Publ., 316: 11-30.

Pausanias (c. 115-180 AD). Pausanias Description of Greece with an English Translation by W.H.S. Jones, Litt.D., and H.A. Ormerod, M.A., in 4 Volumes. Cambridge, MA, Harvard University Press; London, William Heinemann Ltd. 1918. Online at http://www.perseus.tufts.edu.

Perseus Digital Library, lasted visit 5/2011: http://www.perseus.tufts.edu

Polybius (c. 200 – 120 BC). Histories. Evelyn S. Shuckburgh (translator). London, New York. Macmillan. 1889. Reprint Bloomington 1962. Online at http://www.perseus.tufts.edu.

Rodríguez-Pascua, M.A., Pérez-López, R., Giner-Robles, J.L., Silva, P.G., Garduño-Monroy, V.H., Reicherter, K. (2011, in press). A comprehensive classification of Earthquake Archaeological Effects (EAE) in Archaeoseismology: application to ancient remains of Roman and Mesoamerican cultures. Quat. Int.

Sintubin, M., Stewart, I. S., Niemi, T. and Altunel, E. (2008). Earthquake Archaeology - Just a Good Story? Seismological Research Letters, 79(6), 767-768.

Stiros, S.C. (1996). Identification of Earthquakes from Archaeological Data: Methodology, Criteria and Limitations. In: Archaeoseismology (edited by Stiros, S. C. and Jones, R. E.). Fitch Laboratory Occasional Paper 7. Institute of Geology and Mineral Exploration and the British School at Athens, Athens, 129-152.

Strabo (c. 63 BC - 29 AD), Geography. Online at http://www.perseus.tufts.edu.

Xenophon (c. 430-354 BC), Hellenica, 3.2. Online at http://www.perseus.tufts.edu.

REGIONAL STRAIN-RATES ON ACTIVE NORMAL FAULTS AND VARIABILITY IN THE SEISMIC CYCLE: AN EXAMPLE FROM THE ITALIAN APENNINES

Roberts, Gerald (1), Joanna Faure Walker (1), Patience Cowie (2), Richard Phillips (3), Ken McCaffrey (4), Ioannis Papanikolaou (5), Max Wilkinson (4), Alessandro Michetti (6), Peter Sammonds (1).

(1) Department of Earth and Planetary Sciences, Birkbeck/UCL, University of London, Gower Street, WC1E 7HX. UK.
gerald.roberts@ucl.ac.uk
(2) Department of Earth Sciences, University of Bergen, Postboks 7800, NO-5020 BERGEN
(3) Institute of Geophysics and Tectonics, School of Earth and Environment, University of Leeds, LS2 9LT, UK
(4) Department of Earth Sciences, Durham University, Science Labs, Durham DH1 3LE. UK.
(5) Mineralogy-Geology Lab of the Agricultural University of Athens, Greece.
(6) Università degli Studi dell'Insubria - Sede di Como, Facoltà di Scienze MM. FF. NN., Dipartimento di Scienze Chimiche e Ambientali, Via Valleggio, 11 - 22100 Como – Italy.

Abstract(Regional strain-rates on active normal faults and variability in the seismic cycle: an example from the Italian Apennines): *The rate at which a fault slips fundamentally determines the seismic hazard because average earthquake recurrence intervals tend to decrease as slip rates increase. Slip-rates on different faults within a growing fault system are not distributed randomly in space and time, because slip-rates must accommodate the regional strain-rate. Here we show how slip-rates vary temporally and spatially along the Italian Apennines, constrained by offsets across fault scarps dated with ^{36}Cl in situ cosmogenic dating. We map regional variations in strain-rate, investigating natural variability in the seismic cycle.*

Key words*: Fault scarps, regional strain-rates, cosmogenic dating, seismic-cycle.*

INTRODUCTION

Palaeoseismologists and earthquake geologists should try to move forward from simply characterising slip on single faults. Instead, they should try to characterise slip across systems of faults as it is clear that faults interact through stress transfer, and this controls regional patterns of slip-rate (the geography of seismic hazard), and the recurrence intervals for earthquakes on specific faults. The regional approach is needed to complement the regional strain-rate databases provided through GPS geodesy and instrumental seismicity. We should attempt to constrain how the geography of seismic hazard implied over 10^2-10^3 years (palaeoseismology and earthquake geology) compares with that over 10-100 years (geodesy and instrumental seismicity). We expect differences between data from these different timescales to reveal temporal and spatial variability in the seismic cycle (e.g. Faure Walker et al. 2010).

Fault scarps and ^{36}Cl cosmogenic dating

The Italian Apennines are characterised by fault scarps that offset and deform deposits and landforms formed during the last glacial maximum. The offsets have accumulated since 15 ±3 ka shown by studies of tephrachronology and ^{14}C dating (Giraudi and Frezzotti 1995, 1997) and this is confirmed by ^{36}Cl *in situ* cosmogenic dating (Palumbo *et al.* Schlagenhauf 2009, Schlagenhauf *et al.* 2010), and our own ongoing cosmogenic dating. The scarps are widespread and allow a regional study of strain rates and natural variability in the seismic cycle.

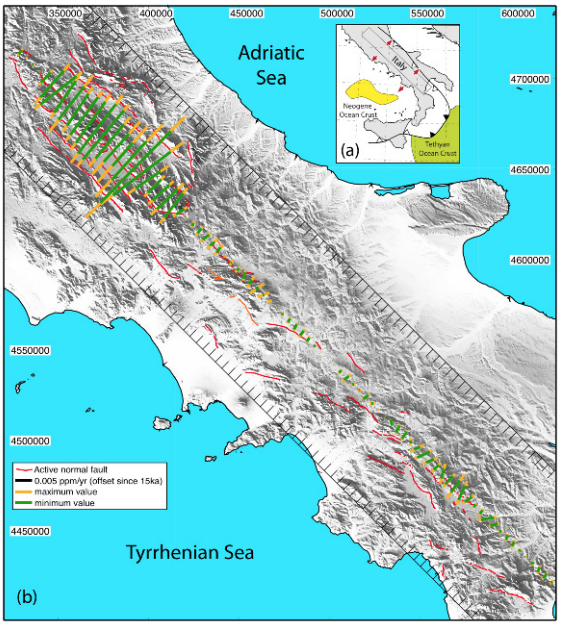

Figure 1. A regional strain-rate map for the Italian Apennines constrained by offsets of 15 ±3 ka features across fault scarps.

Regional Strain rates

A key unknown is how far a fault can stray from its long-term slip rate, both at a timescale equivalent to the interseismic period (10^2-10^3 years), and over timescales equivalent to several seismic cycles (10^3-10^4 years). The lack of such knowledge impedes our ability to perform probabilistic seismic hazard

assessments and understand the underlying physics that controls repeated earthquake slip. In order to study the existence of possible deficits or surpluses of geodetic and earthquake strain in the Italian Apennines compared to 15 ±3 kyr multi-seismic-cycle strain-rates, horizontal strain-rates are calculated using slip-vectors from striated faults and offsets of Late Pleistocene-Holocene landforms and sediments, using an adaptation of the Kostrov equations (Faure Walker 2010).

Strain-rates calculated over 15 ±3 kyr within 5km x 5km grid squares vary from zero up to 2.34 ±0.54 x 10^{-7} yr^{-1}, 3.69 ±1.33 x 10^{-8} yr^{-1}, and 1.20 ±0.41 x 10^{-7} yr^{-1} in the central Apennines Lazio-Abruzzo region, the Molise-North Campania region, and the southern Apennines South Campania-Basilicata region, respectively. The data resolve variations in strain orientations and magnitudes along the strike of individual faults. Strain-rates over a time period of 15 ±3 kyrs from 5km x 5km grid squares integrated over an area of 1.28 x 10^4 km^2 (80 km x 160 km), show the horizontal strain-rate of the central Apennines is 1.18 (+0.12/-0.04) x 10^{-8} yr^{-1} parallel to the regional principal strain direction (043-223° ±1°). In Molise and North Campania, the horizontal principal strain-rate calculated over an area of 5 x 10^3 km^2 (50 km x 100 km) is 2.11 (+1:14/-0:16) x 10^{-9} yr^{-1} along the principal horizontal strain direction (039-219° ±3°). Within the southern Apennines region within an area of 8 x 10^3 km^2 (50 km x 160 km), the average horizontal principal strain-rate is 3.70 ±0:26 x 10^{-9} yr^{-1} along the horizontal principal strain direction (044-224° ±2°).

Strain-rates calculated within 5 x 5 km and 20 x 20 km grid squares, and at a regional scale, are highest in the central Apennines, medial in the southern Apennines and lowest Molise and North Campania. At the regional length-scale, the strain-rates are comparable in direction and magnitude to strain-rates calculated using GPS. Smaller areas (~2000-7000 km^2), corresponding to polygons defined by geodesy campaigns (126 years) and seismic moment summations (700 years) show higher 10^2 yr strain-rates than 10^4 yr strain-rates in some areas, with the opposite situation in other areas where seismic moment release rates in large (> Ms 6.0) magnitude historical earthquakes have been reported to be as low as zero. High strain-rates over 15 ±3 kyr in places occur where instrumental seismicity rates have been low. This demonstrates that strain-rates vary spatially on the length-scale of 10-100 km and on a timescale between 10-100 yrs and 10^4 yrs in the Italian Apennines.

The multi seismic cycle strain-rates are used to calculate earthquake recurrence intervals for a given earthquake slip magnitude, at the scale of individual seismic sources; these value are compared to palaeoseismic data. The results are used to discuss spatial and temporal earthquake clustering and the natural variability of the seismic cycle.

Acknowledgements: We thank the Natural Environment Research Council for funding. NERC Urgency Grant NE/H003266/1. A LiDAR and field study of surface rupture and post-seismic slip for the 6th April 2009 L'Aquila Earthquake (M6.3). Dr. K. McCaffrey, Dr. G. P. Roberts, Prof. P. Cowie. (April 2009-May 2010). NERC Standard Grant NE/E01545X/1. Testing Theoretical models for Earthquake Clustering using ^{36}Cl Cosmogenic Exposure Dating of Active Normal Faults in Central Italy. Prof. P. Cowie, Dr. G. P. Roberts, Dr. K. McCaffrey (October 2007-2010).

References

Faure Walker, J., Mechanics of continental extension from Quaternary strain field in the Italian Apennines. Unpublished PhD Thesis, University College London. 2010.

Faure Walker, J., Roberts, G. P., Sammonds, P., Cowie, P. A., Comparison of earthquakes strains over 10^2 and 10^4 year timescales: insights into variability in the seismic cycle in the central Apennines, Italy. *Journal of Geophysical Research* VOL.115, B10418, doi:10.1029/2009JB006462, 2010

Giraudi, C., Frezzotti, M., 1995. Paleoseismicity in the Gran Sasso Massif (Abruzzo, Central Italy). Quaternary International, 25, 81-93.

Giraudi, C., Frezzotti, M., 1997. Late Pleistocene glacial events in the central Apennines, Italy. Quaternary Research, 48, 280-290.

Palumbo, L., L. Benedetti, D. Bourles, A. Cinque, R. Finkel, 2004. Slip history of the Magnola fault (Apennines, Central Italy) from ^{36}Cl surface exposure dating: evidence for strong earthquakes over the Holocene, Earth and Planetary Science Letters, 225, 163-176.

Schlagenhauf, A., Identification des forts seismes passes sur les failles normales actives de la region Lazio-Abruzzo (Italie centrale) par "datations cosmogeniques" (36Cl) de leurs escarpments. These, Docteur de l'Universite Joseph Fourier, Grenoble, France. 2009.

Schlagenhauf, A., et al. Using Chlorine-36 cosmonuclides to recover earthquake histories on limestone normal fault scarps : a reappraisal of methodology and interpretations. Geophys. J. Int., doi:10.1111/j.1365-246X.2010.04622.x 2010.

EARTHQUAKE ARCHAEOLOGY

INQUA PALEOSEISMOLOGY AND ACTIVE TECTONICS

THE VARIABILITY OF ALONG-STRIKE CO-SEISMIC SLIP: A NEW EXAMPLE FROM THE IMPERIAL FAULT OF SOUTHERN CALIFORNIA

Rockwell, Thomas K., (1,2), Yann Klinger (2)

(1) Geological Sciences, San Diego State University, San Diego, CA 92182 USA, trockwell@geology.sdsu.edu
(2) Institute du Physique du Globe, Paris

Abstract (The variability of along–strike co-seismic slip: A new example from the Imperial Fault of Southern California): *The 1940 M7 earthquake on the Imperial fault in southern California and northern Baja California produced 70 km of surface rupture along a N37W striking right lateral fault. This rupture crossed cultivated fields with long alignments of crop and tree rows, along with an orthogonal pattern of canals and roads, and 15 km of the rupture was photographed from the air in high-resolution stereo immediately after the earthquake. We determined the precise scale of these vintage aerial photographs and used them to assess the short spatial variability of slip along strike. We also analyzed 3 km of very high-resolution aerial photography taken the day after the 1979 rupture of the northern half of the Imperial fault. We find that lateral slip varies substantially along strike by more than 30% over distances of tens to hundreds of meters. These results are similar to the variability determined after the 1999 Izmit and Duzce ruptures in Turkey, and the 2010 El Mayor-Cucapah rupture in northern Baja California.*
Key words*: surface rupture, Imperial Fault, rupture variability, rupture distribution*

INTRODUCTION

The short spatial variability of co-seismic slip along strike for large strike-slip fault ruptures has generally been attributed to the inability of geologists to measure off-fault deformation. However, after the 1999 Izmit and Duzce earthquakes in Turkey, Rockwell et al. (2002) demonstrated from offset groves of trees that both off-fault near-field deformation and lateral variations of co-seismic slip along fault strike were significant variables in making field measurements of displacement after large earthquakes. New optical correlation techniques applied to the 2010 El Mayor-Cucapah surface rupture in northern Baja California (Hudnut et al., 2010) confirm that there are both short and long wavelength along-strike variations in lateral slip as well as substantial off-fault deformation such that field measurements of lateral slip consistently underestimated the amount of strike-slip, even where basement rock is close to the surface and alluvial cover is thin.

In this work, we present new measurements for the 1940 and 1979 surface ruptures along the Imperial fault in southern California (Figure 1), made from high-resolution aerial photography. We measured over 600 new displacements along 15 km of the 1940 rupture, and over 300 new displacements along 3 km of the 1979 rupture, which are the extents of high-resolution aerial photography for these ruptures. Measurements are mostly on long, linear cultural features and crop rows, and are spaced between one to tens of meters apart, allowing for resolution of variations in lateral slip. We present these new measurements and conclude that slip variations are real aspects of co-seismic slip along large strike-slip faults. We also show that the slip distribution reported for the 1940 earthquake underestimates the maximum displacement, as field measurements after the earthquake were made on widely spaced cultural features, such as roads and canals, and the zone of maximum displacement was not visited.

These observations point to the need for field geologists to over sample displacement data after an earthquake, rather then make random, widely spaced measurements that may not represent the actual co-seismic slip distribution.

DETERMINATION OF SCALE OF THE AERIAL PHOTOGRAPHY

We determined the scale for the aerial photographs by measuring the distance between field boundaries (~400 m) and other man-made structures and then comparing them to the identical features in Google Earth. We made measurements only in the central (50%) portion of the stereo pairs, as the affects of parallax are minimal in this part of the imagery. We then constructed a scale that is accurate to within 1%. We then used the scaling tool in Adobe Illustrator to construct a smaller scale to measure offset cultural features.

The largest uncertainty in both the 1940 and 1979 data sets is the determination of the alignment of a crop row, tree row, road, canal, or other feature. We used a straight-line segment to place along a feature on one side of the fault, and copied the segment to maintain a parallel line for the same feature across the fault. The line width is about 10 cm, which is about the smallest increment of displacement that could be measured for the 1940 imagery. For the 1979 photography, we could commonly measure to about 5 cm. A significant source of uncertainty is the actual placement of the line along a feature, which is dependent on how straight the feature was, and how far it could be extended beyond the near-field fault zone. In most cases with crop rows, the plow lines were found to be remarkably straight outward from the fault for tens to hundreds of meters, and straight line segments were easy to place along the middle or

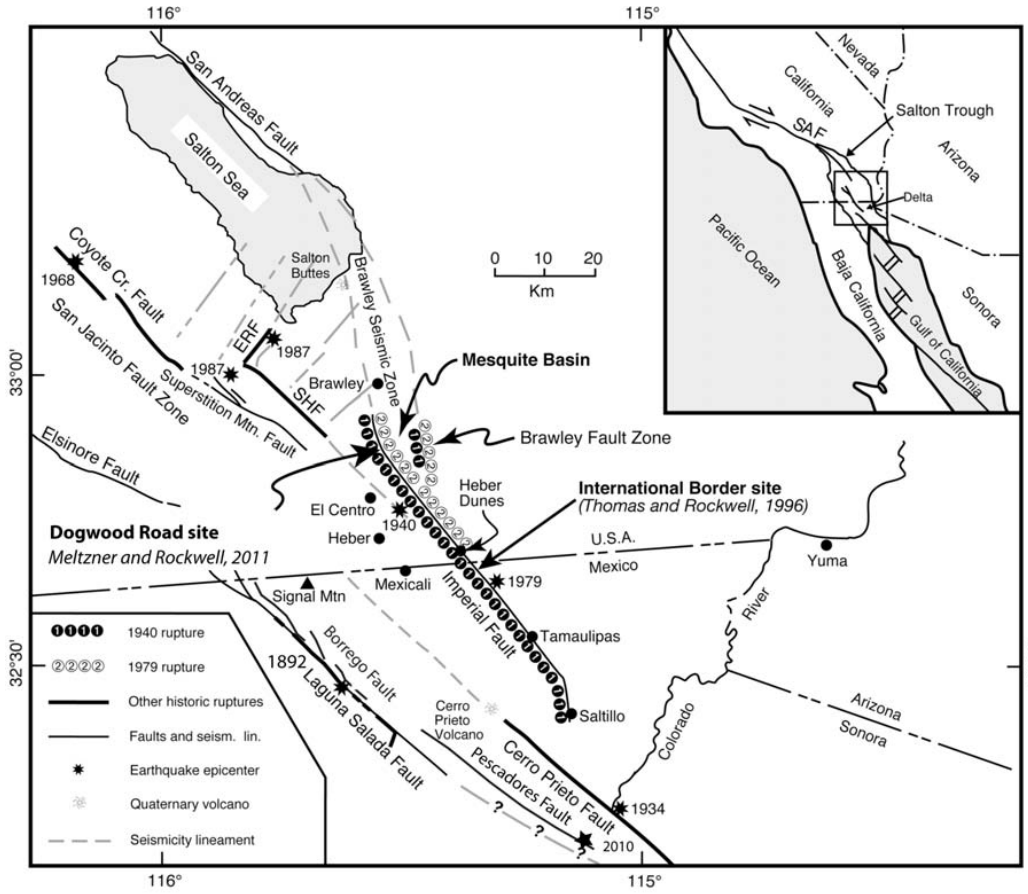

Fig. 1: Location map of the Imperial fault in southern California and northern Baja California. Note that the 1940 earthquake ruptured the entire length of the Imperial fault, whereas the 1979 earthquake only ruptured the northern half. Also note the paleoseismic sites along the fault, and the other historical surface ruptures.

edge of a crop row. For the 1979 imagery, we estimate that small crop rows had placement uncertainties of only 10-15 cm, whereas for the 1940 imagery, the uncertainties are larger and perhaps as much as 0.5 m. In affect, this provided hundreds of alignment arrays to be measured along the strike of the fault to assess lateral slip variability, with reasonably small uncertainty estimates.

OBSERVATIONS

Comparison to J.P. Buwalda's field measurements from his field notes

As a first test of our methods, we located the sites of Buwalda's field measurements that were made immediately after the 1940 rupture, of which there were only six along the 15 km of rupture captured in the aerial photography. Figure 2 shows our slip estimates versus Buwalda's field measurements; they are in close agreement except for the All American Canal (site B1a) where Buwalda reports only a single strand, whereas two strands are clearly evident in the imagery and cause displacement of the canal, resulting in our larger estimate.

Maximum Displacement

Maximum displacement for the 1940 earthquake exceeded the reported 6 m of lateral displacement by about a meter. In the same general vicinity as Sharp's 6 m measurement, we determined that both edges of a road adjacent to a field was offset about 7 m (Figure 3). Slip decreased
in both directions to between 5 and 6.5 m, similar to the variability in lateral displacement that we observed along the entire photographed portion of the rupture.

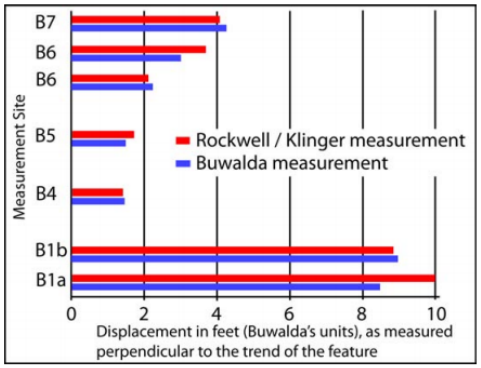

Fig. 2: Comparison of J.P. Buwalda's field measurements with our estimates from analysis of aerial photography.

Slip Distribution

Figure 4 shows the slip distribution for the 1940 earthquake from our new measurements, along with

J.P. Buwalda's 1940 field measurements in red (corrected to a bearing of 323°). We also include measurements by R.V. Sharp on preserved features north and south of the international border (black

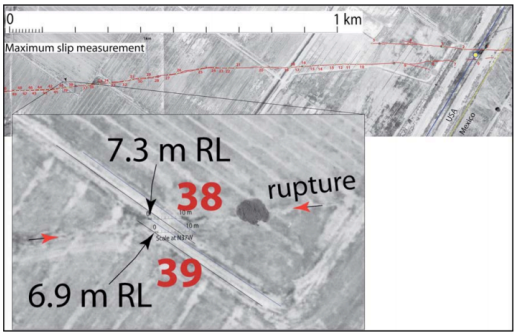

Fig. 3: The 1940 rupture along the Imperial fault north of the international border. The All American Canal is just meters north of the border. About 2 km NW from the border, a road/field boundary is offset about 7 m, the maximum displacement that we found along the 1940 rupture. R.V. Sharp measure about 6 m near the border, whereas J.P. Buwalda measured only about 5 m across one of two strands. The detail shows the offset, with scale included, at our measurement points 38 and 39.

dots). Finally, we surveyed a line of telephone poles that were established prior to the 1940 earthquake at Tamaulipas (formerly Cucapa) and resolved 2.7 m of right-lateral strike-slip (blue star). Our new observations increase the number of slip observations for the 1940 surface rupture by over an order of magnitude, although the majority are on a section of the fault that represents only 20-25% of the full length of the rupture.

An important observation on slip distribution is that there are significant lateral variations in displacement over short spatial dimensions, similar to that reported by Rockwell et al. (2002) for the 1999 Izmit and Duzce earthquakes. This degree of variability has been observed for many previous earthquakes, including the 1999 Hector Mine earthquake (Treiman et al., 2002), the 1992 Landers earthquake (Sieh et al., 1993), the 1987 Superstition Hills earthquake (Sharp et al., 1989), and many others. However, in most previous cases, slip measurements were made on small geomorphic features such as channel margins, channel thalwegs, alluvial bars, canyon walls, etc., none of which were linear for any distance from the fault. Consequently, near-field off-fault deformation could not be assessed and it was generally assumed that some of the variability was the result of non-quantified offset. In contrast, measurement of long crop rows, tree lines, roads, fences and other long cultural features along the 1940 surface rupture demonstrates that significant lateral variations in displacement are real, and that they occur over short spatial dimensions. For instance, we determined displacement for adjacent rows of trees and crops for entire fields. In some cases, as in figure 5, the variability occurs at about our estimated resolution of displacement uncertainty, a half meter. In this case, we measured offset of individual tree lines to vary by about 1 m over a lateral distance of a few hundred meters, similar to the variability on offset tree lines in the Izmit earthquake, but one could argue that within the stated uncertainty, these measurements agree. However, other examples, such as the offset crop rows in figure 6, we measured the offsets to ±10 cm, and estimate the uncertainty to about ±20 cm. In this case, lateral slip varied from zero to over a meter along a several hundred meter section of rupture.

The overall degree of variability along strike is evident in the slip distribution curve in figure 4. Areas

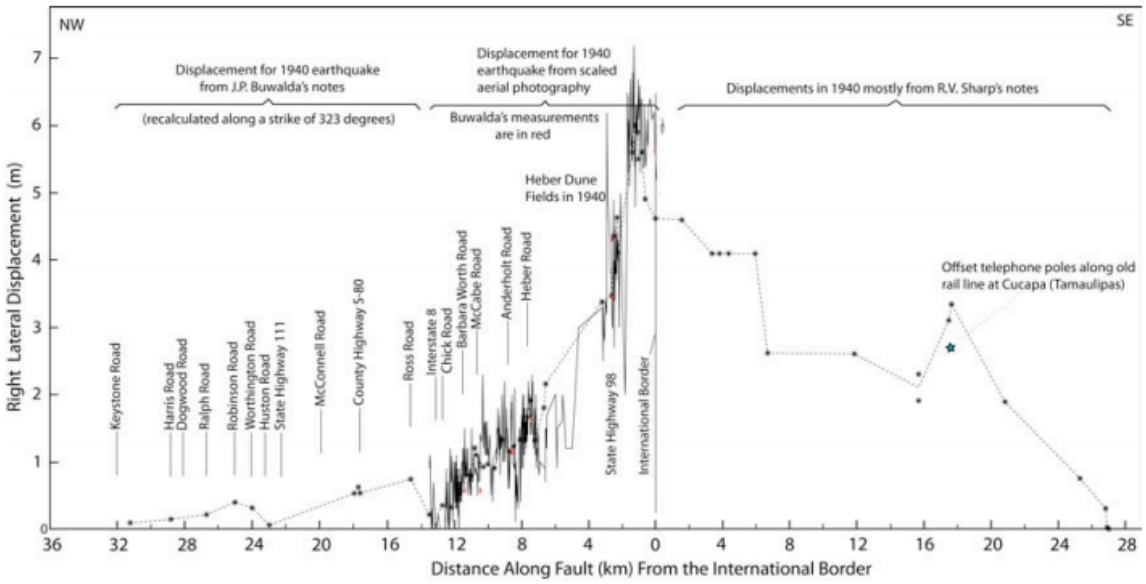

Fig. 4: Slip distribution for the 1940 Imperial fault rupture. Our new observations are between the international border (zero point) and about km 14 north of the border. J.P. Buwalda's field measurements are plotted in red, R.V. Sharp's estimates of displacement are plotted as black dots, and our measurement of an offset telephone line is the blue star.

of larger offset tend to have greater variations in displacement, even though resolution of displaced features and estimates of uncertainty remain about the same. From these observations, we conclude

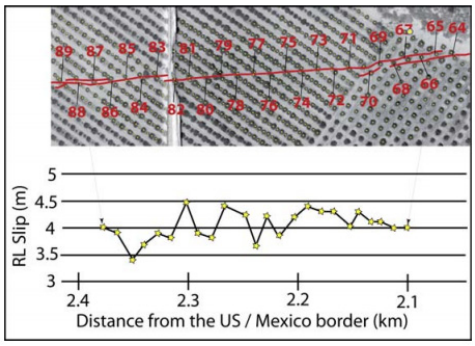

Fig. 5: Offset grove of trees between 2.1 and 2.4 km NW of the international border. A dot was placed on the center of each tree, and the dots were regressed to resolve lateral displacement. Uncertainty is estimated at about 0.5 m.

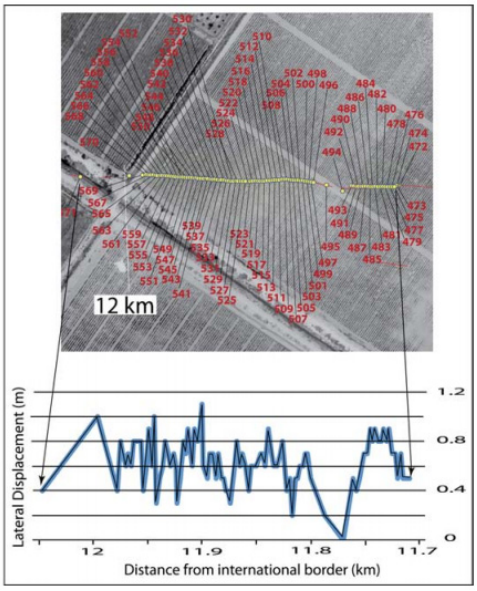

Fig. 6: Offset crop rows between 11.7 and 12 km NW of the international border. Crops rows could be measured to 10-15 cm resolution, but offsets vary by over a meter.

that lateral variability of displacement typically varies by as much as 30% along a section of rupture.

DISCUSSION AND CONCLUSIONS

Until the advent of pre- and post-earthquake comparisons of LiDAR and optical imagery data, most measurements of lateral displacement along strike-slip faults after large earthquakes were conducted on nearfield, non-linear features such as rills, stream channels, channel margins, bars, and other common geomorphic features (Clark et al., 1972; Sharp, 1982; Sieh et al., 1993; Treiman et al., 2002; Barka et al., 2002). Surveying of long cultural features such as tree rows, telephone pole arrays, and fence lines demonstrate that significant off-fault warping can account for a substantial amount of the near-field strike slip (Rockwell et al., 2002), and much of this is rarely accounted for in the measurement of non-linear geomorphic features but it is clearly evident for the Imperial ruptures.

Based on the collection of nearly 1000 new displacement measurements from the 1940 and 1979 surface ruptures along the Imperial fault, several generalizations can be made. First, the sparse field data from the 1940 earthquake, nearly all of which was collected at convenient road crossings, missed the maximum displacement of about 7m, as well as the maximum displacement along strike, although most of the field observations fall near the average displacement for a section of fault. It is evident from this analysis that dense collection of displacement data is required to quantify the maximum displacement along a rupture, and that sparse data likely miss such displacement peaks and other details of the rupture.

Second, lateral variations along strike are substantial and show similar variability to that documented with survey data after several recent earthquakes. Off-fault warping is evident in the bending of crop rows, and some of this bending may be missed in near-field field mapping of a rupture after an earthquake. Using long agricultural features as closely spaced alignment arrays allows for both the assessment of total slip at a point along the fault, as well as the lateral variability of displacement along the fault. The variability that we document here is similar in magnitude and spatial scales to that documented after the Izmit and Duzce earthquakes, as well as more recently with optical imaging techniques after the 2010 El Mayor-Cucapah earthquake in northern Baja California (Hudnut et al., 2010).

References

Barka, A., Akyuz, H. S. et al. 2002. The surface rupture and slip distribution of the 17 August 1999 Izmit earthquake (M7.4), North Anatolian fault. Bulletin of the Seismological Society of America (Special Issue on the 1999 Izmit and Duzce, Turkey, Earthquakes, N. Toksoz (ed.)), 92(1), 43–60.

Clark, M.M., 1972, Surface rupture along the Coyote Creek fault, in The Borrego Mountain Earthquake of April 9, 1968, U.S. Geol. Sur. Prof. Pap. 787, p. 55-87.

Hudnut, K.W., J.M. Fletcher, T.K. Rockwell, J.J. Gonzalez-Garcia, O. Teran, and S.O. Akciz, 2010, Earthquake rupture complexity evidence from field observations. EOS Transactions, Fall AGU, T51E-02.

Rockwell, T. K., S. Lindvall, T. Dawson, R. Langridge, W. Lettis, Y. Klinger, 2002, Lateral offsets on surveyed cultural features resulting from the 1999 Izmit and Duzce earthquakes, Turkey. Bulletin of the Seismological Society of America, v. 92, no. 1, pp. 79-94.

Sharp, R.V., 1982, Comparison of 1979 surface faulting with earlier displacements in the Imperial Valley, *in* The Imperial Valley, California earthquake of October 15, 1979: U.S. Geological Survey Professional Paper 1254, p. 213-221.

Sieh, K., L. Jones, et al., 1993, Near-field investigations of the Landers earthquake sequence, April to July 1992, *Science v.* 260, pp. 171–176.

Treiman, J.A., Kendrick, K.J., Bryant, W.A., Rockwell, T.K., and McGill, S.F., 2002, Primary surface rupture associated with the Mw 7.1 16 October 1999 Hector Mine earthquake, San Bernardino County, California. Bulletin of the Seismological Society of America, v. 92, no. 4, pp. 1171-1191.

EARTHQUAKE ARCHAEOLOGICAL EFFECTS GENERATED BY THE LISBON EARTHQUAKE (FIRST OF NOVEMBER 1755) IN THE CORIA´S CATHEDRAL (CÁCERES, WESTERN SPAIN)

Rodríguez-Pascua M.A. (1), P.G. Silva (2), Perucha Atienza, M.A. (1), J.L. Giner-Robles (3), R. Pérez-López (1)

(1) Instituto Geológico y Minero de España. Street Ríos Rosas, 23. 28003-Madrid. SPAIN. E-mail: ma.rodriguez@igme.es, ma.perucha@igme.es ; r.perez@igme.es
(2) Dpto. Geología, Escuela Politécnica Superior de Ávila, Universidad de Salamanca. Avda. Hornos Caleros, 50. 05003-Ávila. pgsilva@usal.es
(3) Dpto. Geología. Facultad de Ciencias. Universidad Autónoma de Madrid. Cantoblanco. Tres Cantos. Madrid. SPAIN. E-mail: jlginer@gmail.es

Abstract (Earthquake Archaeological Effects generated by the Lisbon Earthquake (first of November 1755) in the Coria´s Cathedral (Cáceres, western Spain): *The Lisbon Earthquake was the most destructive earthquake in the Western European history. This earthquake affected the entire Iberian Peninsula and the city of Lisbon completely collapsed. The intensity of this earthquake was X (EMS-1998) and damaged the historical buildings of Spain. These effects are preserved in historical buildings, like the Coria's Cathedral. The damage observed in this cathedral is described by using the new classification of Earthquake Archaeological Effects (EAE), with the aim to study both strain structures and the seismic wave pattern.*

Key words*: Lisbon Earthquake (1755), Coria´s Cathedral, Earthquake Archaeological Effects (EAE).*

INTRODUCTION

The Lisbon earthquake (November 1st, 1755) is the largest earthquake that struck Western Europe in historic times. This earthquake affected the population in a physical sense and also changed the knowledge of the scientific origin of earthquakes. This date was the starting point of foundation of modern seismology. The Lisbon earthquake affected the entire Iberian Peninsula and North Africa. Its shaking was felt in Central European countries like Germany (Martínez Solares, 2001). Nowadays the epicentre of the earthquake is still the subject of scientific debate (Gutscher, 2005), although the approximate location is widely assumed at the southwest of San Vicente Cape, regardless of the exact fault that produced it. The maximum intensity of this earthquake was X (EMS-1998) (Martínez Solares and Mezcua, 2002), being located in southern Portugal (Algarve Coast). Some of those seismic intensity effects from the earthquake are still visible in the historic heritage all around the Iberian Peninsula, such as churches and cathedrals. This is the case study of the Coria´s Cathedral (Cáceres, central part of Spain). The building suffered structural damage, even collapse the cupola of the tower.

GEOGRAPHICAL SETTING

The town of Coria is located to the NW of the city of Caceres in the central Western part of Spain and near of the border with Portugal. The isoseismal map of the Lisbon Earthquake (Martínez-Solares, 2001) suggests that Coria and surroundings were affected by a seism intensity VI (Fig. 1). The main damage in the city was produced in the cathedral, in which the collapse of the cupola of the tower killed thirteen people.

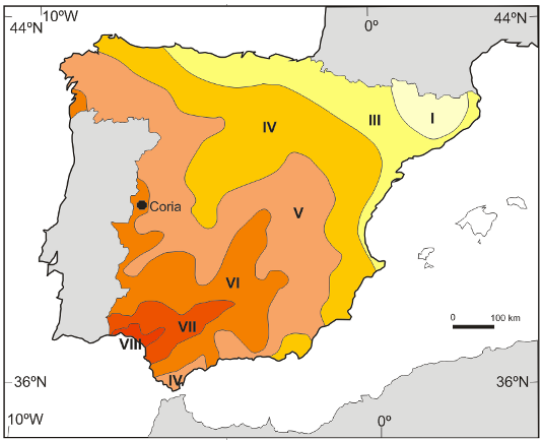

Fig. 1: Location of the town of Coria on the isoseismal map of the 1755 Lisbon earthquake (Intensity scale EMS-1998) (after Martínez Solares, 2001).

METHODOLOGY

Some of the effects of the earthquake in the cathedral of Coria were documented by the Dean of the Cathedral (Martínez-Vázquez, 1999) and are available for public consult in the archive of the Cathedral. Hence, we have elaborated a list of structural damage using the classification of Earthquake Archaeological Effects (EAE) (Rodríguez-Pascua et al., 2011). However, we have to bear in mind that the Cathedral is also affected by geotechnical problems that could mask the effects of the earthquake of Lisbon. Those have to be discriminated by using existing documentation, both the earthquake and previous geotechnical studies (Martínez-Vázquez, 1999).

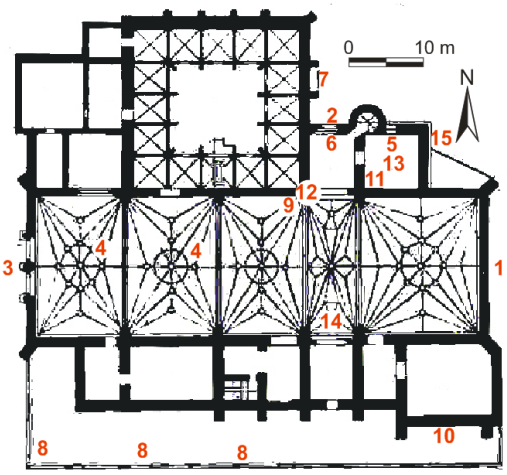

Fig. 2: Plan of the Coria´s Cathedral. The red numbers are the location of the different EAEs (see the text for further explanation).

DATA

According to the classification of damage proposed by the EAE scale (Rodríguez-Pascua et al., 2011), the effects of the Lisbon earthquake catalogued in the Cathedral of Coria are the following (see Fig 2 for spatial location):

Penetrative fractures in masonry blocks:

1- Cracks in the East front. Existing prior to the earthquake and enhanced by this.
2- Cracks in the lintel of the north entrance and in the north front of the Cathedral.
3- Cracks in the west main front separated by the central column which differentiates the two entrance arches of the door (Fig. 3).
4- Cracks in the ceilings and vaults of the central nave of the building.

Dropped key stones in arches or lintels in windows and doors:

5- Arches of the bell tower with horizontal displacement of key stones in the segments to the arcs of the N front of the tower.
6- Arch of the north entrance with dropped lintel.

Collapsed walls or balustrades:

7- Collapsed balustrade and pinnacles of the "Relics Balcony" (Fig. 4).
8- Fall down of the balustrade's pinnacles in the south terrace of the Cathedral (Fig. 5A).
9- Fall down of the balustrade's pinnacles in the north and south front of the Cathedral (Fig. 5B).
10- Collapsed balustrades of the balconies in the south front subsequently repaired with bricks.
11- Fall down of the tower's pinnacles.

Rotated and displaced drums in columns and pinnacles:

12- Clockwise rotations of the pinnacles (hexagonal pyramidal base) of the north front of the Cathedral (Fig. 6).
13- Collapse of the tower's cupola.

Displaced masonry blocks:

14- Sinistral displacement of masonry blocks in the columns of the organ (Fig. 7).
15- Displacement of masonry blocks in the tower's balcony.

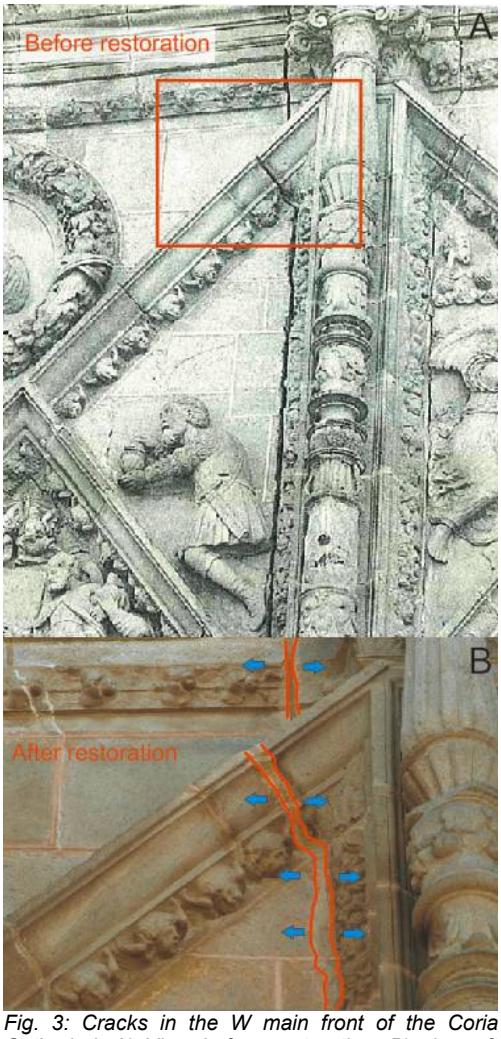

Fig. 3: Cracks in the W main front of the Coria´s Cathedral. A) View before restoration; B) view after restoration in 2009.

DISCUSSION AND CONCLUSIONS

The intense seismic damage of the Coria Cathedral could be attributed to its topographic location: on the cliff edge overlooking the Alagón River's flood plain.

The average orientation of cracks (NE-SW) to about 45° to the central axis of the building, suggest a sinistral shear in the building. All of this data (checked by epoch documents) could be applied in other buildings affected by the Lisbon Earthquake.

As a principal geological effect of the Lisbon Earthquake within the area, the river modified his course and changed the channel by moving to the south. Consequently, the medieval "Stone Bridge" was out of use and today you can ask yourself why medieval people had built a heavy stone bridge in the middle of the cultivation land?

Fig. 4: Collapsed balustrade and pinnacles of the "Relics Balcony".

Acknowledgements: Thanks are given to the project ACI2009-1037 (MICINN).

References

Gutscher, M.A. 2005. What caused the Great Lisbon Earthquake? Science, 305: 1247-1248.

Martínez-Solares, J.M. 2001. Los efectos en España del terremoto de Lisboa. Instituto Geográfico Nacional. Ministerio de Fomento. 756 pp.

Martínez-Solares, J.M. & Mezcua, J. 2002. Catálogo sísmico de la Península Ibérica (880 a.C.-1900). Instituto Geográfico Nacional. Ministerio de Fomento. 756 pp.

Martínez-Vázquez, F. 1999. El terremoto de Lisboa y la Catedral de Coria (Vicisitudes del Cabildo) 1755-1759. Colección Temas Cauriaciences. Vol. V. Ed. Ayuntamiento de Coria. 187 pp.

Rodríguez-Pascua, M.A.; Pérez-López, R.; Giner-Robles, J.L.; Silva, P.G.; Garduño-Monroy, V.H. & Reicherter, K. 2011. A comprehensive classification of Earthquake Archaeological Effects (EAE) in archaeoseismology: Application to ancient remains of Roman and Mesoamerican cultures. Quaternary International, DOI: 10.1016/j.quaint.2011.04.044.

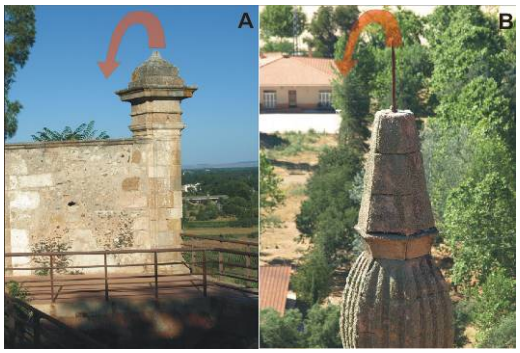

Fig. 5: A) Fall down of the balustrade´s pinnacles in the south terrace of the Cathedral B) decapitated pinnacles in the north front of the Cathedral.

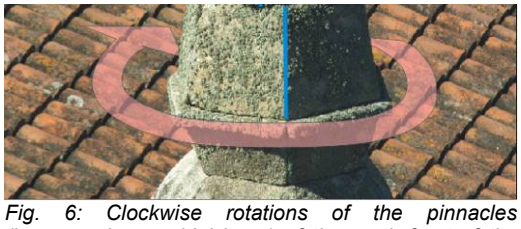

Fig. 6: Clockwise rotations of the pinnacles (hexagonal pyramidal base) of the north front of the Cathedral.

Fig. 7: Sinistral displacement of masonry blocks in the columns of the organ.

NEOTECTONIC OF THE LONGITUDINAL FAULT SYSTEM IN SOUTHERN COSTA RICA

Rojas, Wilfredo (1), Nury Simfors-Morales (2), Luis Sanez (3), Åke Sivertun (4)

(1, 3) Escuela Centroamericana de Geología, University of Costa Rica. Email: wrojas@geologia.ucr.ac.cr
(2, 4) Department of Computer Science, University of Linköping, Sweden. Email: nury.simfors2@comhem.se

Abstract (Neotectonic of the longitudinal fault system in Southern Costa Rica): *Southern Costa Rica is one of the most seismically active areas in Costa Rica because the subduction between Cocos, Caribbean and Nazca Plates. Several active fault zones go also across the study area. One of this fault zones is the WNW-ESE Longitudinal fault system (LFS) which is the longest fault in southern Costa Rica. The goal of this study is to find a suitable place to use it as a sanitary landfill site. The results indicate that there are several geological structures in the study area that indicate deformation due active faulting but more detail studies are necessary in order to understand better the seismogenic potential of this fault. Future work in southern Costa Rica will take into account these issues.*

Keywords*: Trenching, Neotectonics, Longitudinal, Subduction*

INTRODUCTION

Most of the seismic activity in southern Costa Rica is due to the subduction between Cocos, the Caribbean and the Nazca Plates. However, the area is also characterized by several active fault systems which cut across southern Costa Rica, causing also seismic activity and serious damage during strong earthquakes. The Longitudinal Fault System (LFS) is the longest fault system in southern Costa Rica with a length of about 167.2 km (Mann & Corrigan, 1990), (Kolarsky et. al., 1995), (Cowan et al., 2001) and (Montero, 1998) (Fig. 1). It is an ESE-striking oblique-reverse fault, parallel to the volcanic arc in Costa Rica and western Panama (Montero, 1994). The recurrence of earthquake events of this fault is not well known, while the fault slip rate may be roughly estimated at 15 mm/year in Costa Rica and 10 mm/year in Panamá (Cowan et al., 2001).

The objective of this preliminary work is to find a suitable place to use it as a sanitary landfill site. Two trenches were open on the outskirts of Rio Claro, southern Costa Rica (Fig. 1). The results indicate that there are several geological structures in one of the excavated trenches that indicate deformation due to active faulting. Two other fault scarps on the way to Ciudad Nelly cited in this work were also visited. They could be potential trenching targets in case more studies will be done in the future. Taking into account the importance of this fault in southern Costa Rica and western Panama is recommended to do more studies and apply dating techniques in order to better understand the seismogenic potential of the fault and the damage it could pose to the communities. The University of Costa Rica (UCR) has a seismic monitoring project in southern Costa Rica which is studying the spatial and temporal seismicity and earthquake rupture processes in the region. The LFZ and other important faults in the region will be studied in more detail in a close future.

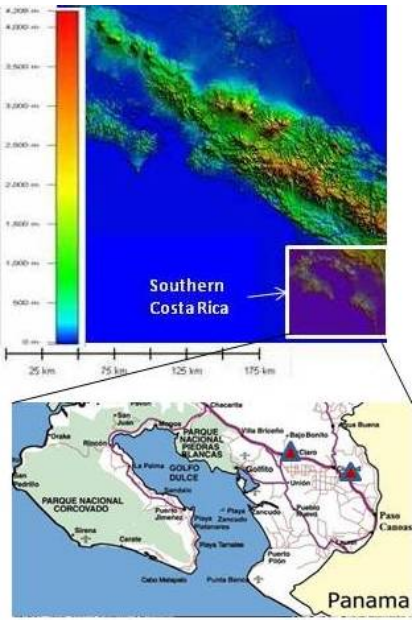

Fig. 1: *Digital Elevation Model of Costa Rica showing the location of southern Costa Rica. In the map two triangles show the location of Rio Claro and Ciudad Nelly. The trenches were excavated in Rio Claro (see: Fig.3). The fault scarp follows toward the NE and ca. 1 kilometer from the trench side the fault scarp can be seen clearly along the smooth plain of southern Costa Rica (Fig. 4 and 5). On the outskirts of Ciudad Nelly was also found two interesting places where the LFZ could be studied in the near future (Fig. 6). (Map courtesy of University of Costa Rica).*

HISTORIC SEISMICITY IN SOUTHERN COSTA RICA

The spatial distribution of the main historical subduction related earthquakes (1803, 1854, 1904, 1941 and 1983) which have affected southern Costa Rica over the past 200 years have been generated by the subduction of the Cocos plate along its interface with Panama Microplate. Although most of the historic earthquakes are subduction related, few of them are due to faulting. Subduction earthquakes rupture at shallow focal depths between 28 and 34 km and magnitudes around 7.0 to 7.5 (Rojas et al., 1993) and (Morales-Simfors et al., submitted). According to the historic earthquakes there is a medium-term probability of a strong earthquake Mw 7.3 in the cited area in the near future. The recurrence interval of strong events (Mw ≥ 7.0) is in the order of 45 years. In case a big earthquake occurs in southern Costa Rica, damage is expected with a Mercalli Intensity of VIII (Rojas 2008) and this may cause significant casualties in the communities.

THE LONGITUDINAL FAULT SYSTEM (LFZ)

The WNW-ESE trending Longitudinal fault system extends from western Panama to central Costa Rica in the west (Mann & Corrigan, 1990) (Fig.2). The slip rate of the Longitudinal fault zone may be <1 mm/yr in Panama and there is clear evidence of late Holocene rupture from radiocarbon dating of charcoal (Beta-117478, 2,580±60 yr B.P.) and pottery that are offset by the fault zone in a trench at Rio Abrojo, Costa Rica (Cowan et al. 2001). Fisher et al. (2001) dated also a wood from a raised wavecut platform along the LFZ front; the radiocarbon dated wood was 5540 yrs.

During this study we visited three places along the LFZ. The first place was the site where two trenches were excavated some weeks before our visit, in order to see if it was a suitable place for a sanitary landfill site in Rio Claro (Coordinates: 569.491 and 291.356, Piedras Blancas topographic sheet, 1.50000). The fault scarp in the trench site is of approximately 4 meters high, it has steep faces but it is difficult to see the stratigraphy due to the vegetation. The trench was excavated in the toe of the scarp. The photos taking in the site show a deformed grey-blue clay layer (Fig. 3). Correlation of the stratigraphic units was problematic but however it was possible to see a marked competence contrast between the different stratigraphic layers which have been cut and deformed by at least for two thrust faulting events. Secondary normal faulting has also cut the layers in the area.

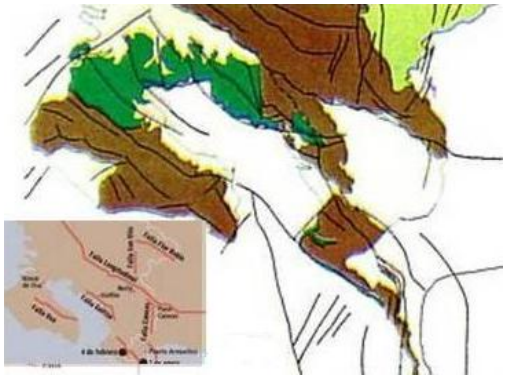

Fig. 2: Simplified geological map of southern Costa Rica. It shows sedimentary rocks in brown (Mesozoic-Paleozoic), Volcanic Rocks in green (Miocene-Pliocene), Volcanic Quaternary rocks in dark green. The small map in the left corner shows the major fault zones in the study area (Maps courtesy of UCR).

Fig. 3: Trench site in Rio Claro. A. The trench was 44 meters long. Close to the digging machine (A) the trench exposed an 8 meters zone of a dark blue, deformed and faulted clay. This clay has been faulted at least by two fault episodes. (The photos are courtesy of RSN).

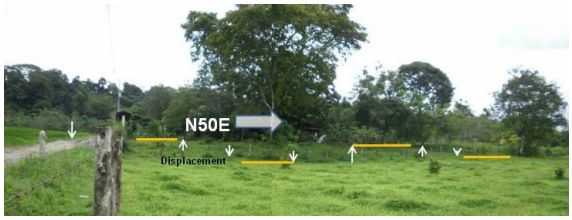

Fig. 4: View of the fault scarp at 1 kilometer NE from the trench site (Coordinates: 569.405 291.319, Piedras Blancas Sheet, 1.50000). This fault scarp trends N50 E and it extends along the smooth plain in Rio Claro.

Fig. 5: A. View of the fault scarp at NE of the trench site at Rio Claro (Coordinates: 569.405 291.319, Piedras Blancas Sheet, 1.50000). B. The scarp is smaller than the scarp close to the trench in figure 2. This fault scarp is ca. 2 meters high and it extends several kilometers along the plain in Rio Claro. C. The fault trace goes almost perpendicular across the road. It is possible to see a narrow change in the dip of the road.

Fig. 6: View of fault scarp at Abrojo, Costa Rica (Coordinates: 582.785 and 286146, Canoas topographic sheet, 1 50000). The scarp goes almost parallel to the highway from Costa Rica to Panama.

The second place was 1 kilometer away from the trench site, where the fault scarp can be seen clearly and follows towards the NE several kilometers along the smooth plains in southern Costa Rica (Fig. 4). The displacement of this scarp is ca. 2 meters (Fig. 5). The third point was outside Ciudad Nelly 30 kilometers to the SE of the trench side where it is possible to see several geological structures from the main highway that communicate Costa Rica with Panama. In this site the scarp is ca 2 meters high (Fig. 6).

RESULTS AND RECOMMENDATIONS

Two trenches were excavated in the study area in order to find a suitable site for a sanitary landfill site. One of the trenches presents a clear evidence of geological structures due to active faulting.

The Fig. 3B and C shows a close view of the gray-blue deformed clay layer in the trench which is overturned and faulted by two thrust faults and other secondary normal faults but in order to do a better interpretation of the tectono-stratigraphic sequence of this site, a detail study of the fault is necessary. The LFZ and other faults in the region appears to be in obvious proximity with important infrastructure such as hospitals, schools, roads, highways etc. in southern Costa Rica and western Panama, In order to understand the active tectonics in the area, more detail studies are necessary to evaluate the seismogenic potential of the fault and answer other questions about the age of the fault scarps, earthquake recurrence and seismic hazard in southern Costa Rica.

Acknowledgements: The authors thank Peter Bryer for helping us with the English manuscript. We are also grateful to the Municipality of Golfito, southern Costa Rica and the Osa-Golfo Dulce Research Program (PIOSA), University of Costa Rica

References

Cowan H, M., N. Machette., K.M. Haller & R.L. Dart (2001). Map and Database of Quaternary Faults and Folds in Panama and Its Offshore Regions. *Open-File Report 98-779*. 41 pp.

Fisher, D. M., T.W, P. Gardner., P. Sak; J. Marshall & M. Protti (2001). Uplift patterns in the Forearc of the Middle America Trench, Costa Rica: implications for mass balance and fore-arc kinematics. *Eos, Transactions of the American Geophysical Union*, 82, F1151.

Kolarsky, R.A. & P. Mann (1995). Structure and neotectonics of an oblique-subduction margin, southwestern Panama. In: *Geologic and tectonic development of the Caribbean Plate boundary in Southern Central America*: (Mann, P. ed.). Geological Society of America Special Paper 295, p. 131-157.

Mann, P. & J.D, Corrigan (1990). Model for late Neogene deformation in Panama: Geology, 8, 558-562.

Montero, W. (1994). Neotectonics and related stress distribution in a subduction-collisional zone, Costa Rica. In: Geology of an evolving island arc (Seyfried, H. and Hellmann, W, eds.). *Profil* (University of Stuttgart, Germany, 7, 125-141.

Montero, W., P. Denyer., R. Barquero., G.E. Alvarado., H, Cowan., M.N, Machette., K.M, Haller & R.L.Dart (1998). Map and database of Quaternary faults and folds in Costa Rica and its offshore regions: *U.S. Geological Survey Open-File Report 98-481*, 63 p., 1 plate (1:750,000 scale).

Mora, S (1979). Estudio geológico de una parte de la región sureste del Valle del General, Provincia Puntarenas, Costa Rica: San José, University of Costa Rica, *unpubl. Senior Undergraduate thesis*, 185 p.

Morales-Simfors, N; et. al. A contribution to the study of the Osa-Golfo Dulce Seismicity, Costa Rica: March 11-14 earthquakes. *Int. J. Earth Sci.* (Submitted).

Rojas, W., Bungum, H & C, Lindholm (1993). Historical and recent earthquakes in Central America. *Revista Geológica de América Central*, 16, 5-21.

Rojas, W. (2008). Informe anual del proyecto de investigación de monitoreo sísmico de Zona Sur de Costa Rica VI-113-A7-170, *RSN*, San José, 13 pp.

EARTHQUAKE ARCHAEOLOGY

INQUA PALEOSEISMOLOGY AND ACTIVE TECTONICS

GEODETIC STUDIES IN THE ZAFARRAYA FAULT (BETIC CORDILLERAS)

Ruano, Patricia (1,2), Antonio J. Gil (3), Jesús Galindo-Zaldívar (1,2), Gracia Rodríguez-Caderot (4), María Clara de Lacy (3), Antonio M. Ruiz (3), María Jesús Borque (3), Juan A. Armenteros (3), Antonio Herrera (3), Antonio Jabaloy (1), Angel C. López-Garrido (2), Antonio Pedrera (5), Carlos Sanz de Galdeano (2)

(1) Dept. Geodinámica, Universidad de Granada. Campus Fuentenueva 18071-Granada, Spain. Email: pruano@ugr.es
(2). Instituto Andaluz de Ciencias de la Tierra, Facultad de Ciencias, 18071 Granada, Spain
(3). Dept. Ing. Cartográfica, Geodésica y Fotogrametría. E.P.S., Universidad de Jaén, Campus Las Lagunillas, 23071 Jaén, Spain.
(4). Dept. Astronomía y Geodesia, Universidad Complutense de Madrid, Ciudad Universitaria s/n, 28040 Madrid, Spain.
(5). Instituto Geológico y Minero de España. C/ Alcázar del Genil, 4. 18006 Granada, Spain.

Abstract (Geodetic studies in the Zafarraya fault (Betic cordilleras): *The Zafarraya Fault Zone constituted the seismic source of the 1884 Andalucian earthquake with an estimated magnitude of 6.5 – 7. It is a normal fault zone located in the northern limb of the Sierra Tejeda antiform and intersects the Internal and External Zone boundary of the Betic Cordillera. Two non- permanent GPS networks made up of 16 sites have been installed and surveyed in September 2004 and February and July 2010 in order to constrain the present-day motion of these structures. Result in 6 years elapsed time may help to discuss about coseismic and aseismic motions of the fault and elastic deformation before faulting.*

Key words*: GPS network, Zafarraya Fault, Sierra Tejeda antiform, present-day deformation*

THE ZAFARRAYA FAULT AND SIERRA TEJEDA ANTIFORM

The Betic Cordillera is located in the Western Mediterranean built up by the distributed deformations related to the Eurasian-African plate boundary and characterized by a present day moderate seismicity.

The Zafarraya Fault Zone is located in the Southwest of Granada Basin, which is one of the most important Neogene intramountain basins in the Cordillera that cover the Internal and External zones boundary. It is placed at the northern limb of the Sierra Tejeda antiform, and could be interpreted as a collapse structure developed along the external arch of the uplifted fold.

The main normal fault trends roughly E-W and includes other minor faults like Llanos de la Dona Fault. The whole fault system constitutes a set of fractures extending 23 km in length and 4 km in width that runs obliquely to the boundary between the External and Internal zones. The main fault segment has associated a rectilinear mountain front formed in Jurassic limestones of the External Zone and Triassic marbles of the Internal Zone. This mountain front is divided into several segments of E-W to NW-SE orientations. The kinematics of the fault is mainly normal with a minor dextral component as can be deduced by the observed slicken-lines. This fault controls the main features of the Zafarraya polje, an endorheic area developed in its hanging wall, and filled by Tortonian to Quaternary sediments (López-Chicano et al., 2002). The throw of this fault zone is 1500 m, considering the displacement of the External-Internal zone boundary. Taking into account the regional geological setting, most of the slip probably occurred since the Tortonian. The Zafarraya Fault was the causative fault of the largest historical earthquake registered in Spain (the Andalusian Earthquake, December 25, 1884) with a maximum intensity of X (MSK scale) from which a magnitude of 6.5 - 7 has been calculated (Muñoz and Udías, 1981) with an estimated total rupture of 16 km.

The slip-rate of the fault calculated from geological markers (10 Ma, Tortonian) is 0.125 mm/yr (Sanz de Galdeano et al., 2003) and 0.17 mm/yr (Reicherter et al., 2003). Whereas, from paleoseismological studies the slip-rate estimated is 0.35 mm/yr (Reicherter et al., 2003), 0.3 and 0.45 mm/yr with a recurrence period of 2-3 kyr for major, surface rupturing earthquakes (Reicherter et al., 2010).

THE GPS NETWORKS

Two non-permanent GPS networks were installed in Zafarraya Fault Zone and Sierra Tejeda antiform in 2004. The 16 GPS sites (Fig. 1) are located in a local and a regional network that extends up to the coast line in order to study the local motion along the Zafarraya fault and the regional development of the Sierra Tejeda antiform. These networks were made up of sixteen reinforced concrete pillars anchored to rock with an embedded forced centring system to assure that the antennas are placed exactly at the same position in different reoccupations. The local network comprises the sites 811, 812 and 816, located on the hanging wall of the fault. Most of them were built up on Jurassic limestones of the External Zones. The sites 810, 813, 814 and 815 are located in the footwall, and were build-up mainly on limestones and marbles. Although these sites are

located across the contact between External and Internal Zones, this contact is inactive at Present, and the southern part of the network may constitute a reference for the activity of the most recent Zafarraya Fault. The regional network that extends from the site 800, located on Jurassic limestones of the External Zones, crosses southwards the Zafarraya Fault and the contact between External and Internal Zones and reaches the uppermost part of Sierra Tejeda in the site 850, located on Triassic Alpujarride marbles. The southern part of the network is located along the southern limb of Sierra Tejeda, which is deformed by NW-SE oriented normal faults, and reaches the coast line (sites 890 and 880, builds up respectively on Alpujarride metapelites and marbles). The regional network also covers the WNW periclinal end of the Sierra Tejeda antiform (Fig. 1).

All sites meet the following requirements: no obstruction above 15 degrees; no high power lines nearby; easily accessible.

The first survey was done in September 2004 (Borque et al. 2005) and a. second survey in February 2010, for local network and in July 2010 for regional one.

The GPS constellation was tracked throughout a three-day campaign with 24-hour sessions per day in the local network and a six-day campaign in two settles with 2 shared sites in the regional one.

For data acquisition we used 6 dual frequency carrier phase GPS receivers Leica System 1200, consisting of GX1230 receivers and AX1202 antennas.

The GPS data processing was performed by using Bernese 5.0 software in the following way: single sessions were computed in multibaseline mode. The first step (preprocessing) related to receivers clocks calibration, performed by code pseudoranges, and detection and repair of cycle slips and removal of outliers, was carried out simultaneously for L1 and L2 data. The final solution for each session was obtained using the iono-free observable with precise ephemeris and absolute antenna phase centre variation files. The fixed solution of the coordinates was estimated using the QIF method to fix integer ambiguities. Troposphere parameters every two hours were estimated.

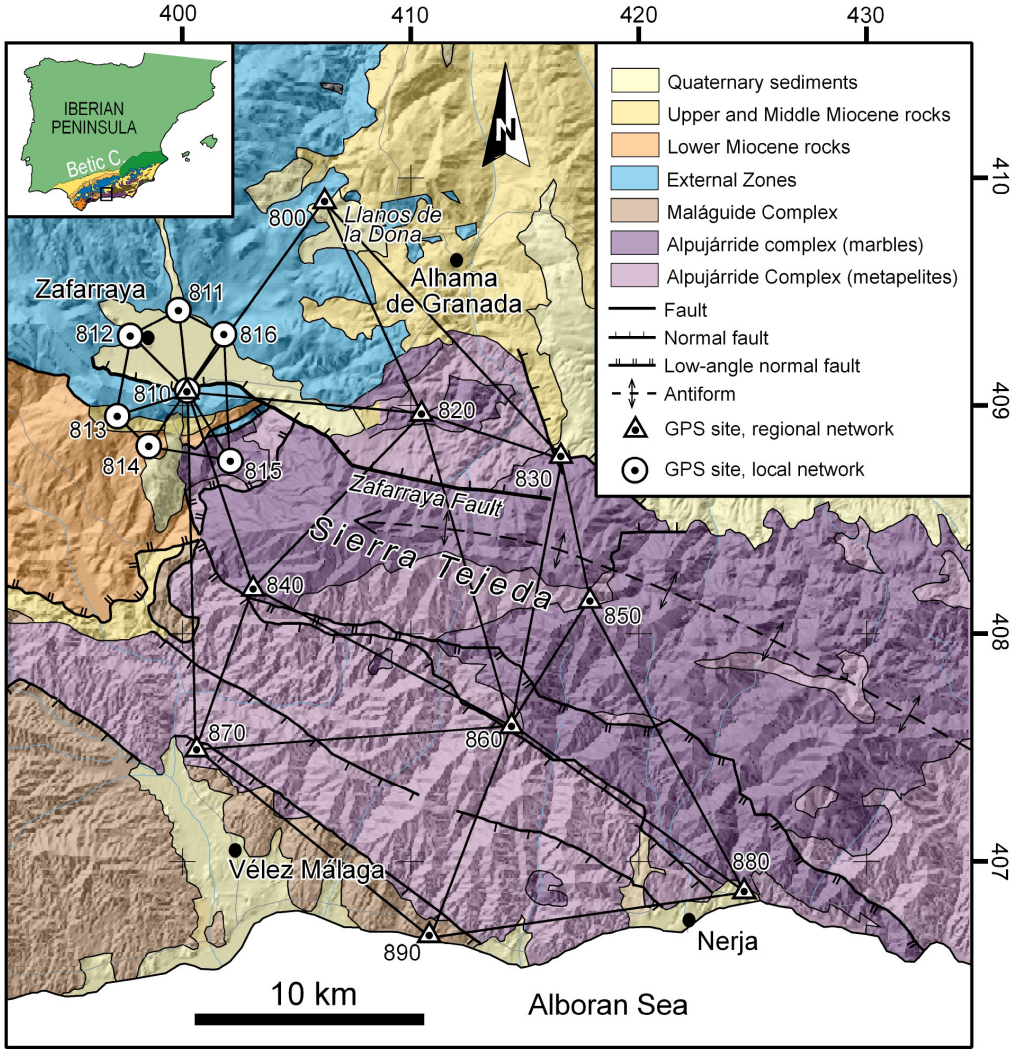

Fig. 1: Geological map and GPS network locations of Sierra Tejeda and Zafarraya fault.

RESULTS AND DISCUSSION

These geodetic surveys provide new insights on the Zafarraya fault (ZF) and Sierra Tejeda antiform (STA). Slow-motion faults need long periods of measurements to have suitable information.

The obtained results for both networks suggest a slow to moderated motion of the structures during the last 6 years. In Figure 2 are shown the present-day crustal deformation rates in terms of the annual velocity vectors with Eurasia fixed reference frame. These deformation rates are in order of several mm per year. Although velocity vectors must be quoted with its standard ellipses even largest of some annual velocity vector, all the vectors are consistent with a WNW trend. There are small differences due to the local activity of tectonic structures. To facilitate the interpretation of the presented results apart from a Eurasia fixed reference frame the results are presented (blue arrows, Fig. 2) in a frame were we fix the station 810, shared by both networks and located southward ZafarRaya fault. This way, it is easy to appreciate the motion of ZF and STA. South of the ZF most of the statiofs show very small northward motion that sugest a very slow activity of STA that constitutes the footwall of the fault. However, in the hanging wall the behavior od the sites is variable. While site 812 and the western end underline its dextral character, sites 811 and 816 may show a combination of motion with a cover NW-SE normal fault producing active NW-SE extension. The sites

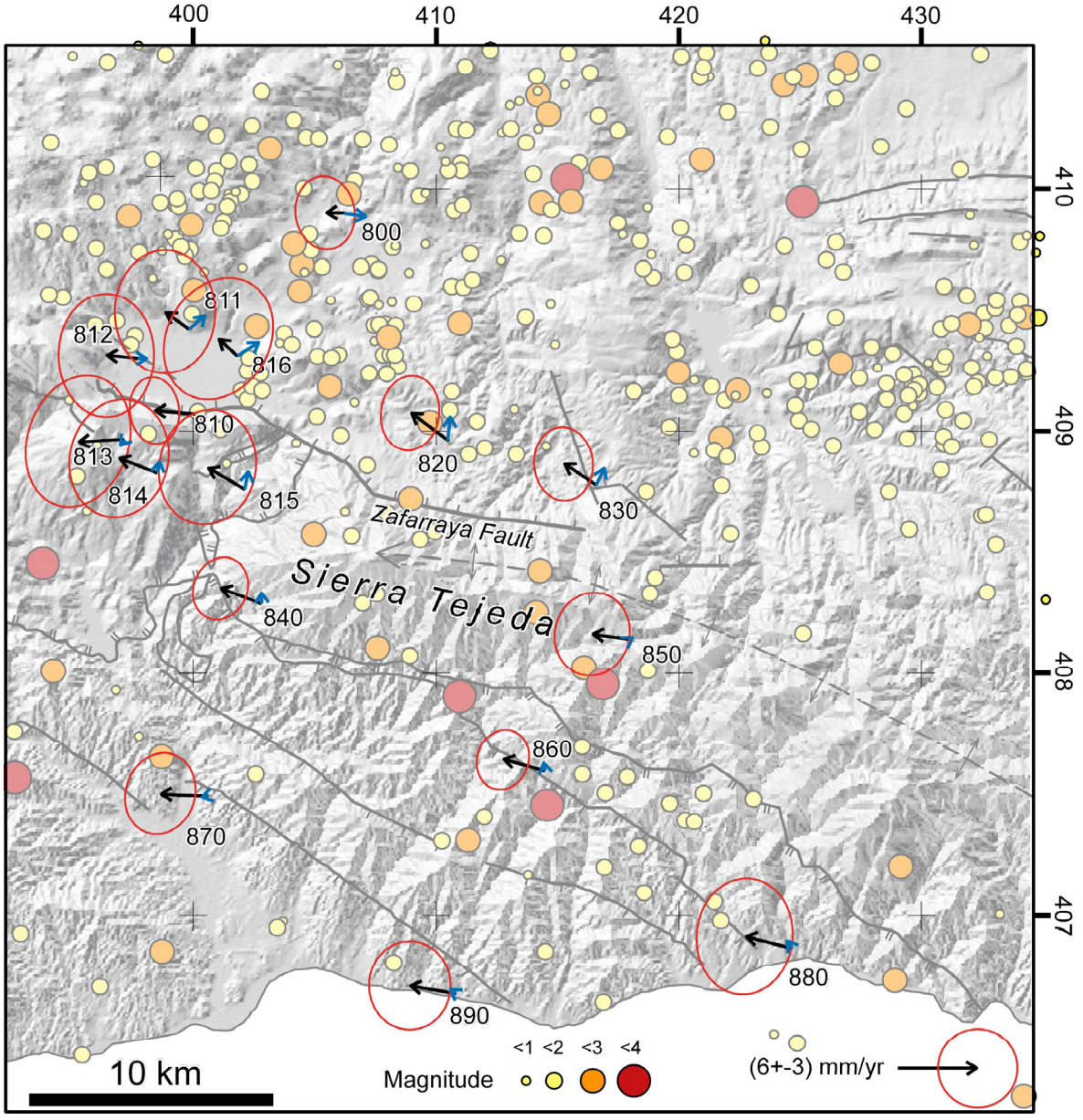

Fig. 2: GPS Velocity vectors in mm/yr with standard error ellipses. Black arrows: Eurasia fixed reference frame; Blue arrows: Site 810 fixed reference frame. The seismicity from September 2004 to July 2010 from IGN data base is shown.

820 and 830 located in its eastern area show its normal motion. Toward the North, the vector of site 800 could be related to the dextral motion of the Llanos de la Dona Faults.

From these results a NW-SE to N-S extension up to 2 mm/yr could be estimated for the Zafarraya fault zone. These rates are higher than those estimated by paleoseismological studies. Moreover, the paleoseismic data suggests that recent activity is higher that neotectonic activity. However, it is not well-constrained the importance of creep motions in the fault and the accommodation of elastic deformation in the area before seismic activity.

The historical and instrumental (Fig. 2) data support that Zafarraya fault has a seismic activity with discontinuous slip-rate. The occurrence of at least two seismic series in the area (Sep 2005 and Aug-Sep 2007), during elapsed time between surveys, could be the responsible of these highest rates that confirm the coseismic behavior of the ZF.

The present and future results will be very significant for a better understanding of the active tectonic structure interaction providing short-term mode of deformation and slip rates of one the most active sectors of the Betic Cordilleras.

Acknowledgements: Projects CSD2006-00041, CGL-2008-03474-E/BTE, CGL2010-21048, P09-RNM-5388 AYA2010-15501, and research groups of Junta de Andalucía RNM282, RNM370 and RNM148 are acknowledged.

References

Borque, M.J., Galindo-Zaldívar, J., Gil, A.J., Jabaloy, A., Lacy, M.C., López, A.C., Rodríguez-Caderot, G., Ruiz, A.M., Sanz de Galdeano, C. (2005): Establishment of a non-permanent GPS network to monitor the deformation in Zafarraya Fault and Sierra Tejeda Antiform (Spain). *Física de la Tierra*, 17, 23-31.

López Chicano, M.; Calvache, M. L.; Martín-Rosales, W. y Gisbert, J. (2002). Conditioning factors in flooding of karstic poljes—the case of the Zafarraya polje (South Spain). Catena, 49, 331-352.

Muñoz, D., Udias, A. (1981) - El Terremoto de Andalucía del 25 de Diciembre de 1884. *Instituto Geográfico Nacional*, Madrid.

Reicherter, K., Jabaloy, A., Galindo-Zaldívar, J., Ruano, P., Becker-Heidmann, P., Morales, P., Reiss, S. & González-Lodeiro, F. (2003) Repeated palaeoseismic activity of the Ventas de Zafarraya fault (S Spain) and its relation with the 1884 Andalusian earthquake. *Int. J. Earth Sci.*, 92, 912-922.

Reicherter, K., Jabaloy, A., Galindo-Zaldívar, J., Becker-Heidmann, P. & Sanz de Galdeano, C. (2010). Trenching results of the Ventas de Zafarraya Fault (Southern Spain). In: *Contribución de la Geología al Análisis de la Peligrosidad Sísmica* (J.M. Insua y F. Martín-González, eds.). Sigüenza (Guadalajara, España). 125.

Sanz de Galdeano, C., Pelaéz Montilla, J.A. & López Casado, C. (2003) Seismic Potential of the Main Active Faults in the Granada Basin (Southern Spain). *Pure and Applied Geophysics*, 160, 1537-1556.

NEOTECTONIC ACTIVITY OF THE GRANADA BASIN – NEW EVIDENCE FROM THE PADUL-NIGÜELAS FAULT ZONE

Rudersdorf, Andreas, Jochen Hürtgen, Christoph Grützner, Klaus Reicherter

Lehr- und Forschungsgebiet Neotektonik und Georisiken, RWTH Aachen, Lochnerstraße 4-20, 52056 Aachen (Germany).
E-Mail: andreas.rudersdorf@rwth-aachen.de , jochen.huertgen@rwth-aachen.de

Abstract (Neotectonic activity of the Granada Basin – New evidence from the Padul – Nigüelas fault zones): *The Padul-Nigüelas Fault Zone (PNFZ) is situated at the south-western mountain front of the Sierra Nevada (Spain) in an extensive regime and belongs to the internal zone of the Betic Cordilleras. The aim of this study is a collection of new evidence for neotectonic activity of the fault zone with classical geological field work and modern geophysical methods, such as ground penetrating radar (GPR). Among an apparently existing bed rock fault scarp with triangular facets, other evidences, such as deeply incised valleys and faults in the colluvial wedges, are present in the PNFZ. The preliminary results of our recent field work have shown that the synsedimentary faults within the colluvial sediments seem to propagate basinwards and the bed rock fault is only exhumed due to erosion for the studied segment (west of Marchena). We will use further GPR data and geomorphologic indices to gather further evidences of neotectonic activity of the PNFZ.*

Key words*: Active faulting, ground penetrating radar (GPR), neotectonics, Granada Basin*

INTRODUCTION

The Granada Basin is a seismically active intramontane basin in the Betic Cordillera of Andalucía, Southern Spain. Earthquakes have been documented both in the historic and the instrumental record (Reicherter (2001) among others). Situated in an extensive regime, normal faults delimit basins of Neogene and Quaternary ages. In this study, modern geophysical methods like ground penetrating radar (GPR) have been combined with classical geologic field work to gain new insight into neotectonic activity of the Padul-Nigüelas Fault Zone.

GEOLOGY

The convergence of the Eurasian and African plates resulted in coupled extension and compression during the Oligocene and Miocene whereas recent stress fields designate a NW-SE oblique convergence with a velocity of 4 mm/a (McClusky et al., 2003). As a result the Betic Cordillera orogeny formed a highly folded mountain belt simultaneously with associated normal faults. Uplift and exhumation resulted in erosion of stacked lithological units (Galindo-Zaldívar et al., 2003). The Betic Cordilleras are subdivided into an External Zone and an Internal Zone, which is subdivided into the Malaguide-Complex, the Alpujárride-Complex and the Nevado-Filábride-Complex because of different metamorphic facies.

The Padul-Nigüelas Fault Zone (PNFZ), situated in the internal zone of the Betic Cordilleras, is part of a NW-SE trending system of normal faults adjacent to sedimentary basins. They usually show a sedimentary succession from Tortonian ages (11.6 - 7.2 Ma BP) on and consist of calcarenites, evaporites, terrigenous clastics as well as carbonate intercalations. The youngest sequences are composed of Quaternary colluvial and alluvial deposits. The footwall, the Alpujárride complex, comprises several units, such as metapelites, metapsammites and quartzites at the base and carbonate rocks as uppermost formation. (Azañón et al., 2002)

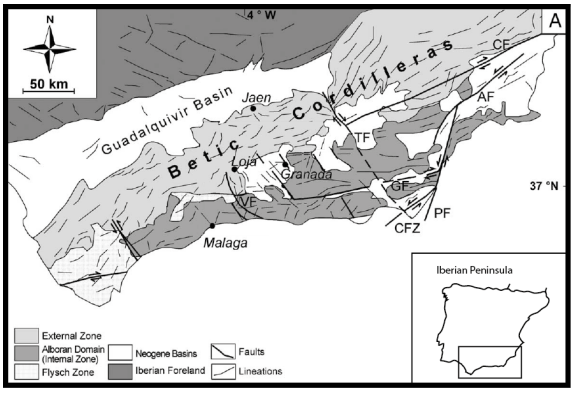

Fig. 1: Geological Map of the southern Iberian region (after Reicherter & Peters, 2005).

The PNFZ (Fig. 2) is well documented in the westernmost and easternmost parts whereas faults are circumspectly indicated in the central part north of Dúrcal. Due to the hard-rock carbonate lithology of the Alpujarrian basement, active faults in this segment are commonly preserved as bedrock fault-scarps.

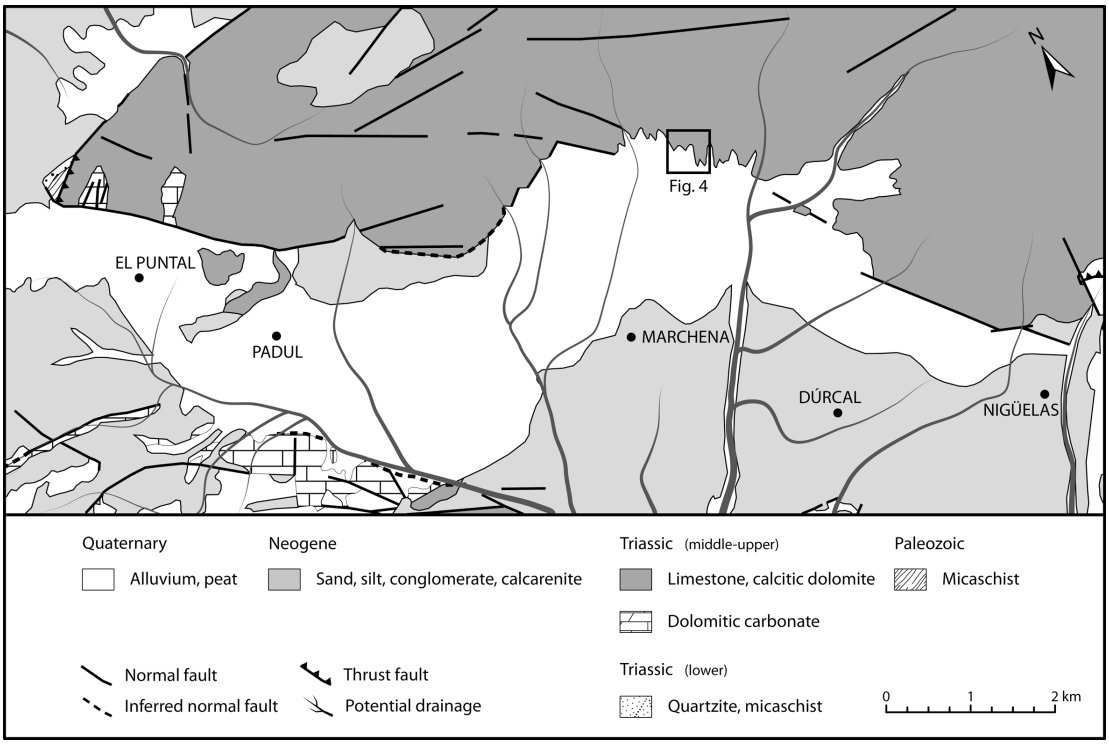

Fig. 2: Geological Map of the Padul-Nigüelas Fault Zone, simplified and composed from Sanz de Galdeano et al. (1975) and González Donoso et al. (1978).

METHODS

Apart from classical field methods, such as geological mapping, we used geophysical survey methods like ground penetrating radar and laser distance measurements to get a detailed image of both subsurface and outcropping structures in order to give evidence for historic and recent seismic activities in the Padul-Nigüelas Fault Zone.

Fig. 3: Illustration of a laser distance measurement. Exhumed scarp near the natural monument "Nigüelas Fault".

Laser distance measurements

Laser distance measurements (LDM) have been done with a compact rangefinder (LTI TruPulse 360) with an integrated tilt sensor and compass to measure slope, horizontal distance, vertical distance, inclination and azimuth of points in outcrops. LDM was used (1) to describe undulating scarp geometries and their dimensions and (2) to get exact relationships between several faults in outcrops of colluvial wedges and alluvial fans. The method of LDM is illustrated in Fig. 3. The rangefinder is mounted on a tripod and the position of the tripod is stationary during a measurement. With a narrow grid, it is possible to get detailed information about exhumed scarp planes or faults in colluvial wedges. We have recorded these measurements at several sites in the PNFZ.

Ground penetrating radar

Ground penetrating radar is a non-invasive geophysical method which uses electromagnetic waves for shallow subsurface surveys. Due to changing magnetic and electric properties in the underground, reflections of transmitted waves can be registered and the two way travel time (TWT, in ns) of the waves gives information about the depth of a reflector. We used a 270 MHz antenna to record the raw data, which have to be interpreted by various filtering and correction tools. According to subsurface conditions (permittivity, conductivity, presence of water-saturated or clay-rich sediments), the penetration depth varies between 5 and 10 m with high-resolution data. In our study area, we especially

investigated the colluvial wedges and alluvial fans of the Padul-Nigüelas Fault Zone with the aim to find basinwards trending faults in the subsurface.

PRELIMINARY RESULTS

The 3-week field work for this study has just been completed in the end of April 2011 and the evaluation and processing of recorded data is still in progress. Therefore, we present some preliminary results, especially from the central part of the Padul-Nigüelas Fault Zone on the Marchena fan.

During our field work, we have found several obvious evidences which suggest geologically recent fault activity in the PNFZ, such as triangular facets, deeply incised channels, faultward dipping layers and faults in both colluvial wedges and alluvial fans at numerous sites within the PNFZ. These features were also observed and documented by other authors (e.g. Alfaro et al. (2001), Galindo-Zaldívar (2003)).

The morphology of the PNFZ is characterized by the exhumed fault scarp, developed on the Alpujarrian bedrock. We could confirm the observations from Alfaro et al. (2001), who has already mentioned that the scarp is exhumed due to erosion and not due to fault activity. The exhumed fault scarps of the PNFZ are specified by lateral as well as downslope undulations of the main fault plane surface in a widespread range. The dip angle varies in a range from 20° to 65° and the dip direction from 190° to 260°. These undulations were documented and combined with laser distance measurements on several sites along the exhumed fault scarp of the entire fault zone.

Due to the apparently inactive main fault, our investigations in the field brought the colluvial wedges and alluvial fans in front of the PNFZ into focus. We gathered multiple profiles of faults in the colluvium and alluvium by classical field methods and by laser distance measurements. We have found active as well as buried faults in the sediments (see also Hamdouni et al. (2008)). Most of the outcrops are created naturally by strong river incision into the sediments and are situated adjacent to the bedrock fault scarp.

For this state of our study, we have concentrated the field-work on the widespread alluvial fan deposits located between the two segments of the Padul-Nigüelas Fault Zone developed on the Alpujarrian bedrock north of Marchena, which is axially dissected by the river Dúrcal. We collected several GPR profiles and documented several outcrop profiles in the proximal colluvial wedges developed at fault-fan contacts. One example is located in the northern part of the Marchena fan (Fig. 2). Fig. 4 shows a photograph of the outcrop (A) with interpreted faults in the sediments and a sketch (B) with the simplified geometry and certain marker horizons. On the basis of these horizons, we can preliminary determine the offset of the larger faults between a few cm and 1.8 m. Noticeable features in the faults are aligned clasts with their longitudinal axis along slip direction and carbonate-coated clasts, which indicate water circulation on the faults. Some of the faults are traceable up to the surface and build small scarps in the topology.

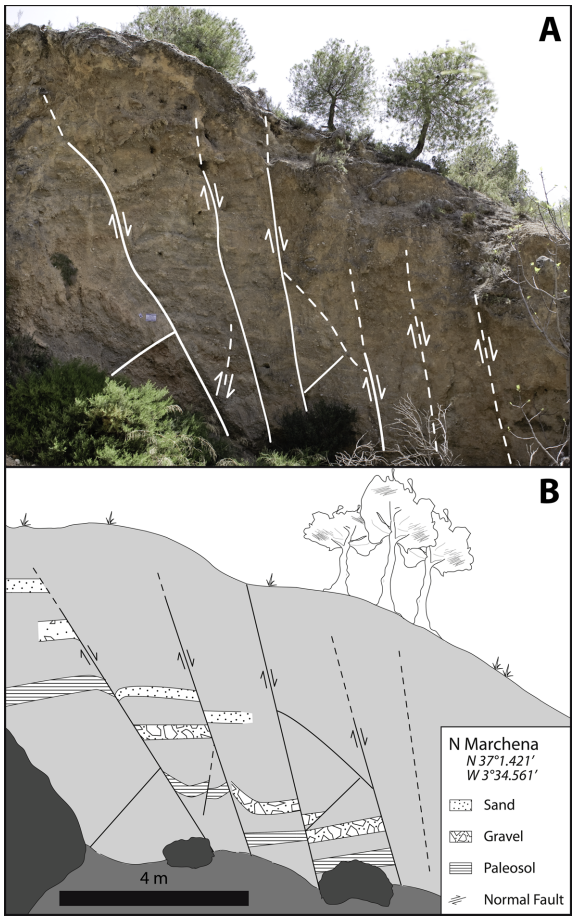

Fig. 4: Outcrop of an incised channel in the alluvial and colluvial fan in the north of Marchena. A: Photograph of the colluvial sediments and existing faults. B: Sketch of the same outcrop with a few traceable layers.

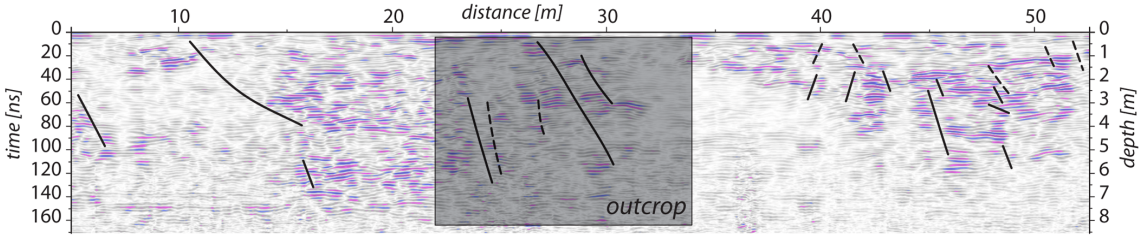

Fig. 5: GPR profile on the upper surface of the outcrop (Fig. 4). The profile is not topographically corrected and a velocity of 0.1 m/ns is assumed for the time-depth conversion. Grey box: excerpt of the outcrop. Black lines: interpreted faults.

In addition to the documentation of the faults in the colluvial wedge, we achieved a GPR profile on the upper surface of the outcrop (Fig. 5). The processed data is not topographically corrected, but first interpretations allow inferring a few faults in the profile. An exact correlation between the outcrop and the radar profile was not done so far. This profile as well as profiles in other studies (Reicherter et al. (2001)) demonstrates that GPR surveys are a useful method to locate faults and faultward dipping layers within colluvial wedges along presumably active range-front faults, such as the case of the Padul-Nigüelas Fault Zone.

The above mentioned features also occur at sites NW of El Puntal, Padul and Nigüelas which points to similar fault activity in this stage of our research.

DISCUSSION & OUTLOOK

The Padul-Nigüelas Fault Zone has been examined extensively for decades and is considered as active since instrumental and historical seismicity indicate several earthquakes in the Granada Basin. In our field study we found the fault scarps exposed because of erosion instead of fault activity. The colluvial wedges are not undisturbed, they show both buried and active faults, therefore we consider basinwards trending fault activities for this sector, as well as for the entire PNFZ.

Since our study is not finished, GPR data and geomorphologic indices will be used to give further evidence for either active or inactive faults in the Padul-Nigüelas Fault Zone.

References

Alfaro, P., J. Galindo-Zaldívar, A. Jabaloy, A.C. López-Garrido & C. Sanz de Galdeano, (2001). Evidence for the activity and paleoseismicity of the Padul fault (Betic Cordillera, southern Spain). *Acta Geologica Hispanica* 36 (3-4), 283-295.

Azañón, J.M., J. Galindo-Zaldívar, V. García-Dueñas and A. Jabaloy (2002). Alpine tectonics II. Betic Cordillera and Balearic Islands. In: W. Gibbons and T. Moreno (eds.), *The Geology of Spain* 16, 401-416.

Galindo-Zaldívar, J., A.J. Gil, M.J. Borque, F. González-Lodeiro, A. Jabaloy, C. Marín-Lechado, P. Ruano, C. Sanz de Galdeano (2003). Active faulting in the internal zones of the central Betic Cordilleras (SE, Spain). *Jorunal of Geodynamics* 36, 239-250.

González Donoso, J.M., V. Garcá-Dueñas, J.A. Gallegos, J. Avidad Castañeda (1978). Mapa Geologico de España - 1041 Dúrcal. Instituto Geológico y Minero de España.

Hamdouni, R., Irigaray, C., Fernández, T., Chacón, J., Keller, E.A. (2008). Assessment of relative active tectonics, southwest border of the Sierra Nevada (southern Spain). *Geomorphology* 96, 150-173.

McClusky, S., R. Reilinger, S. Mahmoud, D. Ben Sari, A. Tealeb (2003). GPS constraints on Africa (Nubia) and Arabia plate motions. *Geophysical Journal International* 155 (1), 126-138.

Reicherter, K.R. (2001). Paleoseismologic advances in the Granada basin (Betic Cordilleras, southern Spain). *Acta Geologica Hispanica* 36 (3-4), 267-281.

Reicherter, K., G. Peters (2005). Neotectonic evolution of the Central Betic Cordilleras (Southern Spain). *Tectonophysics* 405,191-212.

Sanz de Galdeano, C., J.M. González Donoso, J.A. Gallegos (1975). Mapa Geologico de España - 1026 Padul. Instituto Geológico y Minero de España.

HOLOCENE SEAFLOOR FAULTING IN THE GULF OF CORINTH: THE POTENTIAL FOR UNDERWATER PALEOSEISMOLOGY

Sakellariou, Dimitris (1), Lykousis Vasilis (1), Rousakis Grigoris (1)

(1). Institute of Oceanography, Hellenic Centre for Marine Research, 47km Athens-Sounio Ave., 19013 Anavyssos, Greece.
Email: sakell@ath.hcmr.gr, vlikou@ath.hcmr.gr, rousakis@ath.hcmr.gr

Abstract (Holocene seafloor faulting in the Gulf of Corinth: the potential for underwater paleoseismology): *The techniques used for the marine geological – geophysical investigation of the seafloor of the Gulf of Corinth were suitable for the mapping of the offshore faults and for the detection of recent, Holocene faulting activity. The available seismic data provide clear evidence that several faults have moved repeatedly in Holocene times and have produced cumulative offsets of up to several meters during the last 14-13 kyrs. The next step in the investigation of the offshore faulting in the Gulf of Corinth will be to use higher resolution methods to perform on-fault seismic profiling and to recognize individual earthquake ruptures along the faults on the seafloor of the Gulf of Corinth.*

Key words*: seafloor faults, Holocene earthquakes, recent movements*

INTRODUCTION

The Gulf of Corinth is an active continental rift developed within the stretching Aegean region, perpendicular to the alpine Pindos mountain chain. It is a 100 km-long rift characterized by high extension rates in N-S direction (currently up to 20 mm/yr, Clarke et al. 1998), localized mostly within the narrow, 15-20 km wide, marine basin. With a very high seismicity and more than ten earthquakes of magnitude M>6 in the last 50 years, the Gulf of Corinth is an ideal site to study active tectonics and recent fault movements.

The offshore fault pattern shown in Fig. 1 has been recognized on numerous seismic reflection profiles

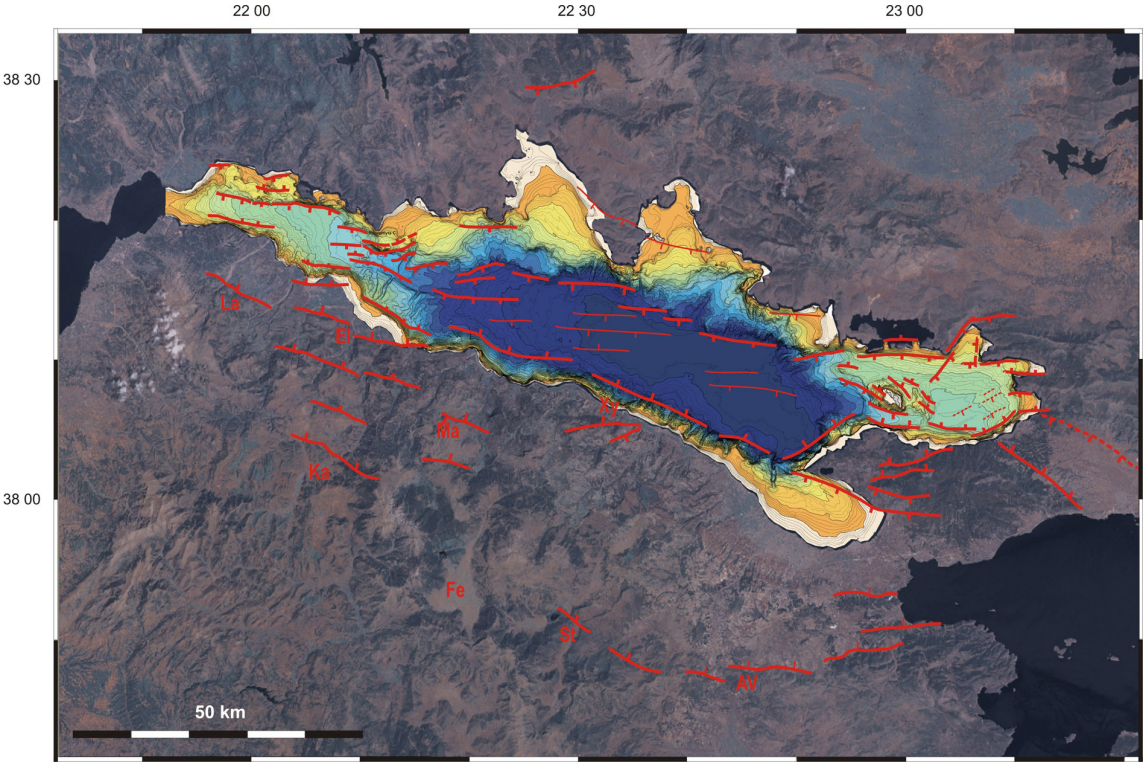

Fig. 1: Landsat image with main active offshore faults in the Gulf of Corinth rift. Swath bathymetry after Alexandri et al. (2003) and Nomikou et al. (this volume)

(airgun, boomer, 3.5 kHz) acquired during several cruises of R/V Aegaeo between 1995-2005 and R/V Alkyon recently (Sakellariou et al., 2001; 2004; 2007; Lykousis et al., 2007). More marine geophysical studies have been conducted by other Greek or international teams and have contributed to the understanding of the structure of the Gulf of Corinth (Stefatos et al., 2002; Moreti et al., 2004; Zelt et al., 2004; McNeill et al., 2005; Bell et al., 2008)

Although the scope of the above campaigns was mostly to study the neotectonic structure of the rift with relatively low to medium resolution techniques, many seafloor faults were identified to have moved in Holocene or even in historic times. The aim of this paper is to shed light these faults and explore the potential for high resolution underwater paleo-seismological studies in the Gulf of Corinth.

LECHAION GULF

Sakellariou et al. (2004b) showed that the Lechaion Gulf is currently a half graben developed on the hangingwall of the south-facing on/offshore Loutraki fault. Antithetic, north facing faults run E-W on the shallow southern shelf of the Gulf. Recent Boomer profiles and older Airgun 10 in^3 and 5 in^3 seismic profiles show that these faults cut through the 10-15m thick Holocene deposits.

The Boomer profile of Fig. 2 shows one of the north-facing athithetic faults of the Lechaion Gulf crosscutting the submerged Last Glacial Maximum (LGM) landscape and the Holocene drape. The offset of 6-7 m must have been accumulated after the inundation of the LGM Corinth lake about 14 ka ago.

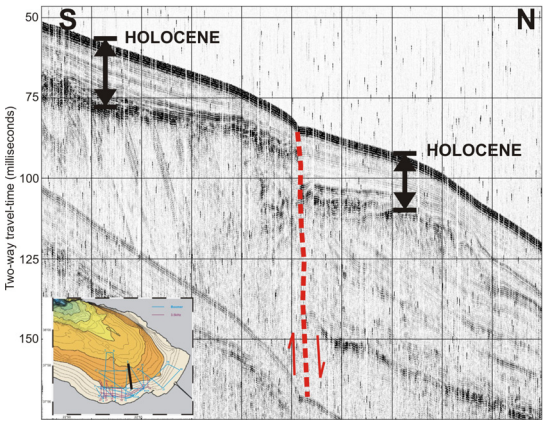

Fig. 2: Boomer profile, 175 Joules, 1-2,5 kHz, Lechaion Gulf.

CENTRAL GULF OF CORINTH

A dense grid of Airgun 10 in^3 single channel reflection profiles revealed the shallow structure and the seismic stratigraphy of the Central Gulf of Corinth deep basin (Lykousis et al., 2007). Gravity coring from R/V Aegaeo and long piston coring from R/V Marion Dufresne (Moreti et al. 2004) validated the interpretation of the seismic data and recovered a continuous sequence of Holocene mud and sand turbidites. Correlation of the seismic data with the sedimentary sequence recovered in the cores enabled absolute dating of basin-wide reflectors, which are frequently offset by faults. Careful and detailed analysis of the shallow seismic stratigraphy led Lykousis et al. (2007) to estimate Holocene slip rates of the basin bounding faults.

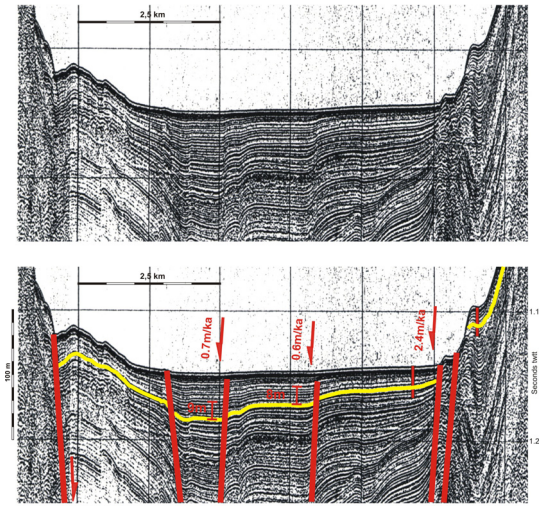

Fig. 3. Airgun 10in^3 single channel reflection profile through the deep basin of the Central Gulf of Corinth, south of Itea bay. Left=South, right=North. Top: Raw profile. Down: Interpreted profile and line drawing. The yellow line marks the 14 ka old interface between LGM lacustrine and Holocene marine sedimentation. Slip rates of the individual faults have been estimated from the vertical offset (Lykousis et al., 2007).

Vertical slip rates of 0.6-0.7 m/ka have been calculated for the intra-basin faults, while rates of 2.4-3.7 m/ka were estimated for the basin bounding faults. Still, the resolution of the technique is not sufficient high to allow recognition of individual earthquakes and rupturing events.

The deep basin of the Gulf of Corinth is an ideal site for on-fault and off-fault underwater paleo-seismological studies. The geophysical record of the shallow subseafloor sedimentary sequence with the continuous succession of mud and sand turbidites, potential well defined seismic reflectors, may resolve characteristic structures associated with individual fault ruptures. High resolution seismics with deep-towed vehicles in combination with carefully selected coring sites on the hangingwall and footwall of the faults will provide recognition and dating of dislocated layers and thus define individual earthquakes.

WESTERN GULF OF CORINTH

After the 1995 Aegion earthquake the western part of the Gulf of Corinth has been the site of intensive on- and offshore surveys by Greek and international teams. Numerous field surveys and marine geological-geophysical campaigns have been conducted and yielded very wealth data sets on

active tectonics and faulting. Onshore paleioseismological studies on the Heliki Fault and the broad region of Aegion provide new knowledge and understanding of the fault behaviour onshore. Systematic offshore seismic reflection profiling enabled detailed mapping of the seafloor faults of the western Gulf of Corinth. Nevertheless, as in the rest part of the Gulf, more precise data on the activity of specific offshore faults has been only occasionally gained. Two examples are given here below.

Medium resolution Airgun 5 in^3 single channel seismic reflection profiling has been conducted on the shelf and upper slope off Aegion – Diakofto region. A couple of the shot profiles crossed the eastward offshore prolongation of the well studied onshore Aegion fault (Fig. 4).

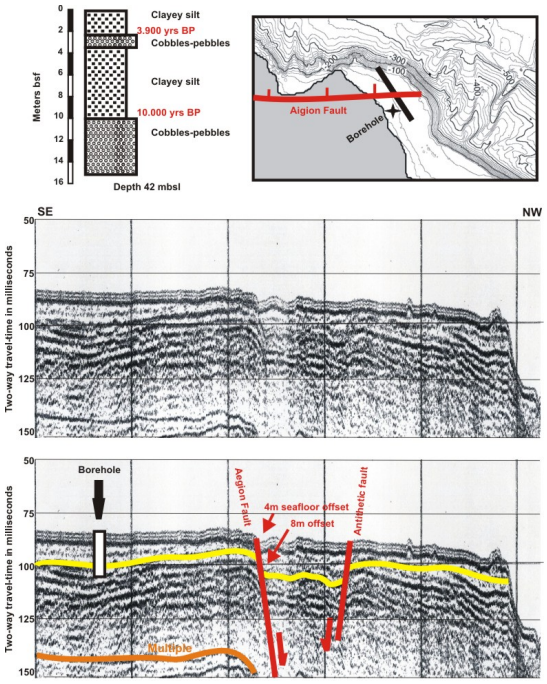

Fig. 4: Medium resolution Airgun 5 in^3 single channel seismic reflection profiling crosscutting the Aigion fault. Upper image: Map of Aigion area with the trace of the Aigion fault, the location of the profile and the sedimentological description and radiometric ages of an offshore drilling (Schwartz & Tziavos, 1979). Middle: raw profile. Down: Interpretation of the seismic profile. The north-facing Aigion fault and an antithetic, south-facing fault are marked in red. The yellow reflector marks the interface between clayey silt above and cobbles-pebbles below, dated to about 1o ka. Note that the Aegion fault offset vertically the yellow reflector by about 8 m and the seafloor by about 4 m.

Careful interpretation of the seismic profiles from the Aegion shelf along with the sedimentological data from the offshore drillings (Schwartz & Tziavos, 1979) indicate that the Aegion fault has produced a cumulative vertical offset of at least 4m during the last 10 kyrs.

Further on, Airgun 10 in^3 seismic profiles and 3.5 kHz profiles have been acquired from the deep basin of the western Gulf of Corinth and show significant fault movements in Holocene in the basin.

More precisely, significant fault movements have been detected on the south facing South Eratini fault, between Psaromyta Cape and Aegion (Fig. 5). The Airgun profile of Fig. 5 shows the multiplefaulting of the basin between Psaromyta Cape (North) and Aegion (South). The 3.5 kHz profiles through the South Eratini Fault indicate that the stratified Holocene drape of the basin has been vertically dislocated by about 5 m.

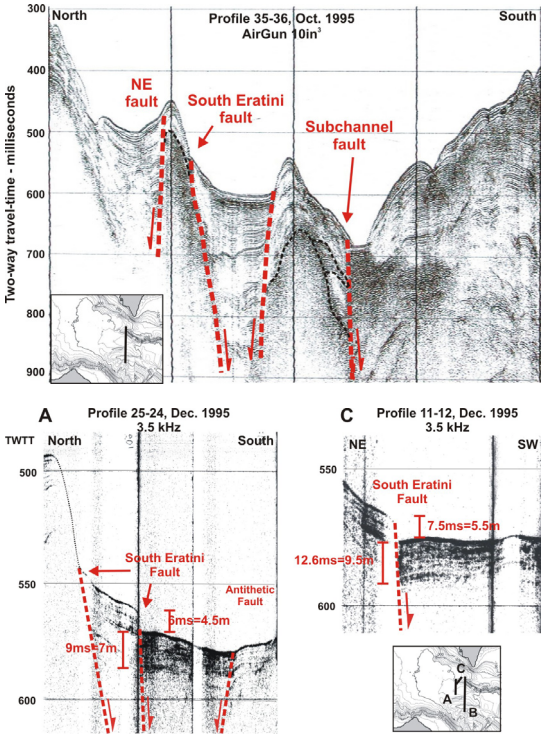

Fig. 5: Airgun 10 in^3 seismic profile (top) and 3.5 kHz profile (bottom) through the South Eratini Fault. Note that the 3.5 kHz profile shows vertical offset of the Holocene drape by about 5.5-4.5 m.

CONCLUSIONS

The techniques used for the marine geological – geophysical investigation of the seafloor of the Gulf of Corinth were suitable for the mapping of the offshore faults and for the detection of recent, Holocene faulting activity. The available seismic data provide clear evidence that several faults have moved repeatedly in Holocene times and have produced cumulative offsets of up to several meters during the last 14-13 ka. The next step in the investigation of the offshore faulting in the Gulf of Corinth will be to use higher resolution methods to perform on-fault seismic profiling and to recognize individual earthquake ruptures along the faults on the seafloor of the Gulf of Corinth.

References

Alexandri M., Nomikou P., Ballas D., Lykousis V. & Sakellariou D. (2003): Swath bathymetry map of Gulf of Corinth. Geoph. Res. Abstracts, Vol. 5, 14268, EGS 2003

Bell, R., McNeill, L.C., Bull, J.M., and Henstock, T.J., 2008. Evolution of the western Gulf of Corinth continental rift, Greece. Geological Society of America Bulletin, 120, 156-178.

Clarke, P.J., Davies, R.R., England, P.C., Parson, B., Billiris, H., Paradissis, D., Veis, G., Cross, P.A., Denys, P.H., Ashkenazi, V., Bingley, R., Kahle, H.-G., Muller, M.-V., and Briole, P., 1998, Crustal strain in central Greece from repeated GPS measurements in the interval 1989-1997: Geophysical Journal International, 135, 195-214.

Lykousis, V., Sakellariou, D., Moretti, I., and Kaberi, H., 2007, Late Quaternary basin evolution of the Gulf of Corinth: Sequence stratigraphy, sedimentation, fault slip and subsidence rates: Tectonophysics, 440, 29-51

Leeder, M.R., Portman, C., Andrews, J.E., Collier, R.E.L., Finch, E., Gawthorpe, R.L., McNeill, L.C., Perez-Arlucea, M., and Rowe, P., 2005, Normal faulting and crustal deformation: Alkyonides Gulf and Perachora peninsula, eastern Gulf of Corinth rift basin, Greece: Journal Geological Society of London, 162, 549-561.

McNeill, L., Cotterill, C., Stefatos, A., Henstock, T., Bull, J., Collier, R., Papatheoderou, G., Ferentinos G., and Hicks, S. 2005, Active faulting within the offshore western Gulf of Corinth, Greece: implications for models of continental rift deformation: Geology, 33, 241-244.

Moretti, I., Lykousis, V., Sakellariou, D., Reynaud, J.-Y., Benziane, B., and Prinzhoffer, A., 2004, Sedimentation and subsidence rate in the Gulf of Corinth: what we learn from Marion Dufresne's long-piston coring: Comptes Rendus Geoscience, 336, 291-299.

Nomikou, P., Alexandri, M., Lykousis, V., Sakellariou, D. & Ballas, D. (2011). Swath bathymetry and morphological slope analysis of the Corinth Gulf. 2nd INQUA-IGCP-567 International Workshop on Active Tectonics, Earthquake Geology, Archaeology and Engineering, Corinth, Greece (2011), this volume

Sakellariou, D., Lykousis, V. & Papanikolaou, D. (2001) Active faulting in the Gulf of Corinth, Greece. In: 36th CIESM Congress Proceedings, 36 pp. 43.

Sakellariou, D.,Kaberi, H. & Lykousis,V. (2004) Influence of active tectonics on the recent sedimentation of the Gulf of Corinth basin. In: 10th International Congress of Greek Geological Society, Abstracts 15-17 April, p. 232-233, Thessaloniki.

Sakellariou D., Fountoulis I. & Lykousis V. (2004b). Lechaion Gulf: the last descendant of the Proto-Gulf-of-Corinth basin. 5th Int. Symp. On East. Mediterranean Geology, Proceedings 2/881-884, Thessaloniki

Sakellariou, D., Lykousis, V., Alexandri, S., Kaberi, H., Rousakis, G., Nomikou, P., Georgiou, P., and Ballas, D., 2007, Faulting, seismic-stratigraphic architecture and late Quaternary evolution of the Gulf of Alkyonides basin – East Gulf of Corinth, Central Greece: Basin Research, 19, 273-295.

Schwarz M.L. & Tziavos C. (1979): Geology in the search for Ancient Helice. J. Field Archaeology, 6, p. 243-252

Stefatos, A., Papatheoderou, G., Ferentinos, G., Leeder, M., and Collier, R., 2002, Active offshore faults in the Gulf of Corinth, Greece: Their seismotectonic significance: Basin Research, 14, 487-502.

Zelt, B.C., Taylor, B., Weiss, J.R., Goodliffe, A.M., Sachpazi, M., and Hirn, A., 2004. Streamer tomography velocity models for the Gulf of Corinth and Gulf of Itea, Greece. Geophys. J. Int., 159, 333-346.

EARTHQUAKE ARCHAEOLOGY

INQUA PALEOSEISMOLOGY AND ACTIVE TECTONICS

DAMAGE ASSESSMENT IN ARCHAEOSEISMOLOGY: METHODS AND APPLICATION TO THE ARCHAEOLOGICAL ZONE COLOGNE, GERMANY

Schreiber,Stephan (1), Klaus-G. Hinzen (1)

(1) Earthquake Geology and Archaeoseismology Group, Cologne University, Vinzenz-Pallotti-Str. 26, 51429 Bergisch Gladbach. GERMANY. Email: stephan.schreiber@uni-koeln.de

Abstract (Damage Assessment in Archaeoseismology: Methods and Application to the Archaeological Zone Cologne, Germany): *A work flow to investigate archaeoseismological problems including the use of modern surveying equipment and quantitative methods was developed. We exemplify a comprehensive damage assessment in the historic city center of Cologne, Germany. During the construction of an underground museum (Archeological Zone Cologne), parts of the Roman and medieval city are being excavated. The remains exhibit structural damages spread over an area of 150 x 200 m. The structures were mapped using a phase-based 3D laser scanner. The acquired data were analyzed and the results lead to a quantitative damage database for the investigation area.*

Key words*: Damage Analysis, Laser Scanning, Quantitative Methods, Roman*

INTRODUCTION

One of the first steps in modern archaeoseismology is the precise mapping of damages with potential seismogenic origin. In addition to the archaeo-seismologic working scheme proposed by Galadini et al. (2006) and specified by Hinzen et al. (2009) and Hinzen (2011), Schreiber & Hinzen (2011) presented a site-specific modification for the situation in Cologne (Fig.1). The investigation of the archaeo-logical site is structured into four major categories: (1) investigation of the constructions, (2) surface topography, (3) subsurface conditions, and (4) geo-logical setting of the region.

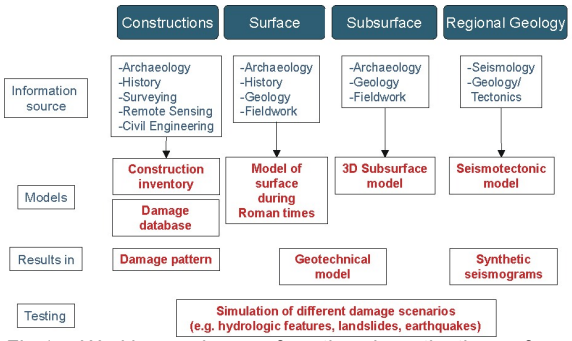

Fig.1: Working scheme for the investigation of an archaeological site with four major thematic groups (after Schreiber & Hinzen, 2011.

METHODS

This contribution focuses on the first category and shows how a comprehensive quantitative dataset is collected, analyzed, and prepared for further model-ling and estimation of the damage cause.

Data Acquisition & Processing

In this study the constructions were mapped using a phase-based 3D laser scanner (FARO Photon80). The scanner emits a permanent bundled infrared beam towards the measurement target via a rotating mirror. The target reflects the beam and the reflected signal is detected by the measuring device. The scanner records the phase shift between transmitted and received signal and calculates the distance to the target. Combined with instrumental parameters including the position of the rotating mirror during the measurement and the recording position of the scanner, the Cartesian coordinates are calculated for each discrete reflection point. The resolution of 0.00076° in horizontal and 0.009° in the vertical direction, which correlates to 0.13 mm and 1.57 mm at a distance of 10 m, allows a distance resolution in the range of 1-2 millimeters (Schreiber et al., 2011b). Due to the fast data acquisition rate of 120.000 pt/s measurement times are short and ongoing excavations are not significantly disturbed. The data were processed with the software JRC 3D Reconstructor 2 (Sequieira et al., 1999, Sgrenzaroli & Wolfart, 2002) which is a capable tool to handle large 3D point clouds.

After the application of different automatic filters to remove erroneous points (e.g. points at edges or points acquired in the open sky) and the manual cleaning of the point clouds to remove vegetation or modern structures, the scans were merged into models of substructures of the investigation area. Due to smaller file sizes (5-20% of the overall data volume) these “submodels” are easier to handle in the analysis phase.

Damage Analysis

The substructure models were used to perform a detailed analysis of the scanned structures and their

damages. The structural damages were (1) identified, (2) located within the global reference system, (3) classified (rotation, displacement, tilting, cracking), and (4) quantified with damage-dependent methods. All results were merged into a damage database. The damage database is linked to a construction inventory, where information about the buildings from (1) previous and recent archaeological excavations, (2) city annals and historical reports and (3) historical maps were collected. In addition to these archaeological and historical sources, information about the construction type, the building material and the function of the building was collected.

WORKING AREA

The working area is located in the historic city center of Cologne, on the top of the slope to a former side arm of the Rhine River (Fig. 2). The excavations are part of the Archaeological Zone Cologne (AZC), a large museum area, which will exhibit remains from 2000 years of history after its completion. During several building phases the constructions expanded over the edge of the slope, towards the Rhine River, so the excavated buildings are founded partially in artificial fillings. The topography, the complexity of the construction ground, the position next to a large river and the seismic potential of the region suggest several possible causes for the observed damages.
The following paragraphs present three examples of the data acquisition and damage analysis methods applied to different structures in a rather complex excavation environment. Since 2008 over 200 laser scans were collected in the AZC resulting in a point cloud of 2.4 billion individual points. This data were combined to ten models of substructures within the AZC. The analysis of the data leads to a damage database with currently 2000 detected damages.

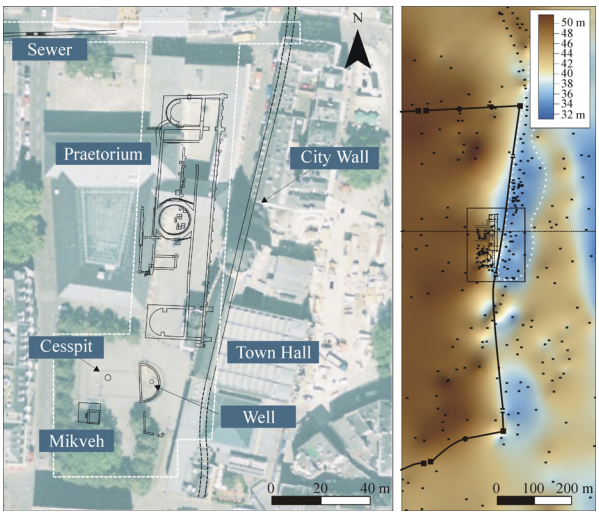

Fig.2:(Left) Aerial photo of the historic city center of Cologne with the main structures of the excavations. The white line indicates the planned museum area. (Right) 3D surface model of the natural ground. The position of the Roman city wall is indicated and the black rectangle marks the excavation area (Schreiber et al., 2011a). Circles give the location of borings used to construct the model. The former sidearm of the Rhine River is marked with the dotted white line.

Example: Praetorium
The praetorium, the palace of the Roman governor was the main administrative building of the province *germania inferior*. The first building phase of the praetorium started with the beginning of the first century AD followed by three more phases (end of the 1st century, end of the 2nd century and 4th century). The structure was completely demolished in the 9th century (Gechter & Schütte, 2000). The foundations of the northern half of this former 90 m long and 25 m high building were excavated in the 1950s and 1970s. We mapped the remains of the construction in 97 scans from different height levels and combined them to four models of the main parts of the building.

The models were used to identify, locate and classify different damages. The main damage type in the praetorium is the tilting of walls; 822 tilt measurements were made on virtual cross-sections of the point cloud, which were exported to CAD software. Figure 3 shows the distribution of directional tilting found in the praetorium.

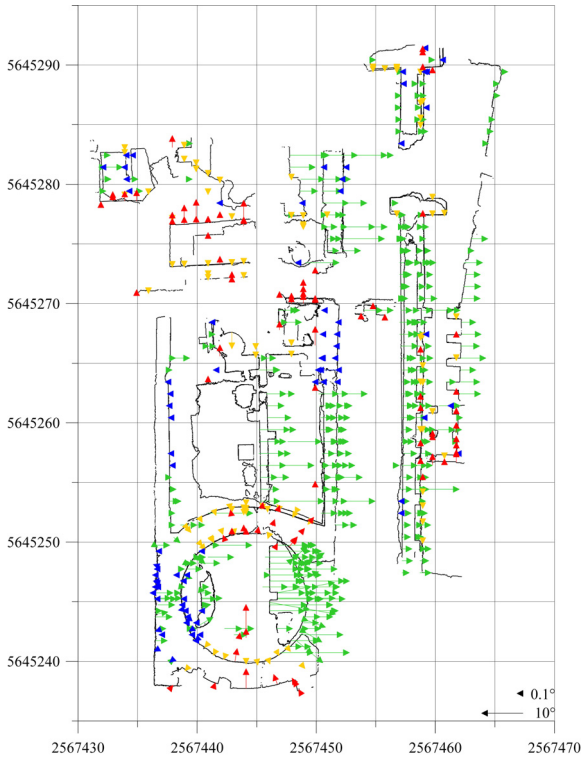

Fig.3: Floor plan of the praetorium with directional tilting vectors. Color indicates the orientation sector (blue: west, green: east, red: north, yellow: south). The vector length gives the amount of tilting.

The eastern part of the praetorium is tilted eastward. The distribution of tilting correlates well to a change in the subsurface where the constructions expand over the edge of the former slope towards the Rhine River and are partly founded in artificial fillings. The maximum observed tilt is 15.1° towards east. Average tilt of all eastward tilted walls is 3.1°± 2.4°. Maximum tilt towards west is 12.9° with an average of 1.5°± 1.8°, and the maximum tilts towards north and south are 5.6° and 11.4°, respectively. In

addition to tilting, 104 cracks with opening widths of up to 25 cm were quantified from the point cloud; 39 horizontal displacements in the walls with opening width up to 9 cm were detected. It is the first time the documentation focuses on the damage of the buildings. Before only some of the damages were documented as a side product in archaeological drawings; however, not quantified.

Example: Roman Well

A 12.5 m deep Roman well is located west of the Cologne city hall (Fig.2). The well was mapped in two campaigns with 20 scans. The scans were acquired using a special retaining device. The scanner was installed upside-down and lowered down the well with an electrical winch; the position was fixed using air-pressured stamps (Fleischer et al. 2010).

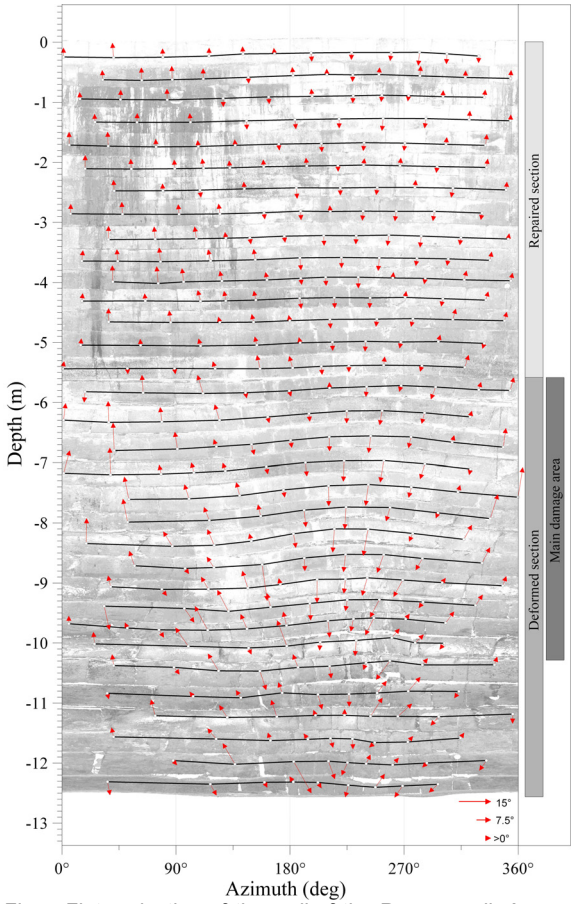

Fig.4: Flat projection of the wall of the Roman well. Arrows give the direction of tilting and rotation of the normal of virtual planes, fitted to the front side of each block. The length of the arrows gives the amount of tilting. The white points are the centre points of the fitted planes connected by the black lines indicating the trend of the layer centers (after Fleischer et al., 2010). The bars at the right give the locations of the repaired section, the deformed section and the main damage area.

The structure shows two sections (Fig. 4): The upper 5.5 m were reconstructed probably during medieval times, while the lower 7 m remained deformed. For the analysis of the orientation, virtual planes were fitted in a least square sense to the front sides of 338 blocks in 33 layers. This technique allowed the quantification of the tilting and the rotation of each block using the position of the plane normal. Figure 4 shows the tilting vectors for each block on top of a unrolled cylindrical scan of the inside of the well. The damage analysis showed that the block layers are tilted up to 11° within the damage zone (layers between –8 m and –9 m in Fig. 4). The average tilting of the discrete blocks is 4.2°± 3.3°. The maximum tilt is 15.8°.

Example: Roman Sewer

The 180 m long sewer located north of the excavation area is part of the complex Roman dewatering system of the city. The eastern and western sections of the sewer were built with different construction techniques. The latter is made of large tuff blocks. This 120 m long section was scanned with 25 scans. Damages include displaced blocks in the roof (Fig. 5) and shell-like spallings on the sidewalls.

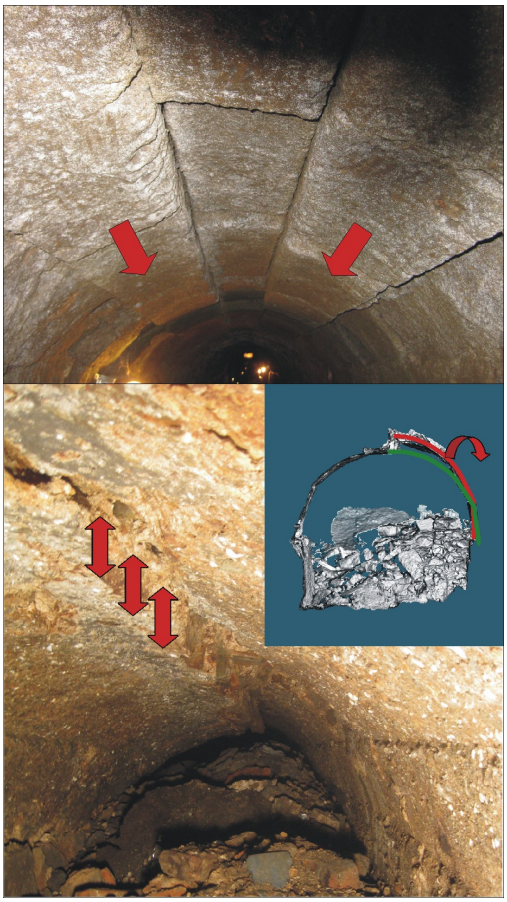

Fig.5: (Upper) Displacement of blocks in the vault of the western part of the Roman sewer. (Lower) Cracking of the vault in the eastern part of the sewer. In the bottom, the top of the filling of the sewer is still in place. The inset shows a cross-section of the point cloud when the sediment filling of the sewer was still in place. The green curve shows the original shape of the vault, the red line follows the rotated and displaced vault in the damaged area.

The eastern section, which ends in an outlet through the eastern Roman city wall of Cologne, was scanned in an emergency campaign before the excavations were stopped due to critical static conditions of the sewer. Therefore only four scans were

made so far. In this part the vault of the sewer is made of *opus caementicium*. Here massive shell-like spallings were found on the bottom parts of the sidewalls. The roof shows a large crack with displacements of up to 15 cm on a length of minimum 10 m (Fig. 5). Currently the damages in the western part are investigated in detail using virtual cross-sections in 1 m intervals. For the eastern part additional scans are necessary to perform a complete damage analysis.

CONCLUSIONS

The application of 3D laserscanning in the AZC shows that this technique is an appropriate tool especially when complex structures are analyzed. The main challenge during the mapping of the Cologne praetorium was the widespread and complex damage pattern, which required a large amount of scans. In the Roman well the vertical shaft, required a complete different approach. The scanner was mounted upside down in order to avoid shadowing effects and the time consuming construction of different plateaus in the shaft. The scanning of the sewer required a careful selection of scanning positions to avoid shadowing effects due to steep angles in the only 1.6 m wide structure. It could be shown that the analysis of the damages needs a site-specific approach in order to quantify the different types of damages. In comparison to traditional mapping techniques laser scanning provides a large amount of high-resolution data in a short period of time. In case of fragile conditions of the excavated objects, repeated scanning can virtually conservate the original conditions before these are alterated due to ongoing restoration and/or excavation. The accuracy of the measurements allows a detailed analysis even when the original finding is no longer accessible.

The results of the damage analysis are the base for further studies on the damage cause. The type and the amount of the damages can be used to narrow down possible damage scenarios. However, as shown in Figure 1, the mapping and the analysis of the damages are one of the first steps in the workflow. Further steps, e.g. the surface and subsurface analysis (Schreiber et. al 2011a) and the modelling of scenarios (e.g. Hinzen et al., 2010, 2011b) are necessary for an accurate investigation of an archaeoseismological problem.

Acknowledgements:
We are grateful to the staff of the Archaeological Zone Cologne. We thank the staff of the Seismological Station Bensberg, especially Claus Fleischer for his dedication to the fieldwork

This work is beeing financed by Deutsche Forschungsgemeinschaft DFG (HI 660 / 2-1).

References

Fleischer, C., K.-G. Hinzen and S. Schreiber, (2010). Laserscanning eines römischen Brunnens in der Archäologischen Zone Köln. *AVN Allgemeine Vermessungs Nachrichten* 5/2010, 176-181.

Galadini, F., K.-G. Hinzen and S. Stiros, (2006). Archaeoseismology: Methodological Issues and Procedure. *Journal of Seismology* 10, no. 4, 395-414.

Gechter, M. and S. Schütte, (1999). Ursprung und Voraussetzung des Mittelalterlichen Rathauses und seiner Umgebung. *Stadtspuren* 22, 69-195.

Hinzen, K.-G., C. Fleischer, S.K. Reamer, S. Schreiber and S. Schütte, (2009). Quantitative Methods in Archaeoseismology. In: *Archaeoseismology and Palaeoseismology in the Alpine-Himalayan Collisional Zone* (Pérez-López, R., Grützner, C., Lario, J., Reicherter, K., Silva, P.G. eds). Baelo Claudia, Spain, 50-51.

Hinzen, K.-G., S. Schreiber and B.Yerli, (2010). The Lycian Sarcophagus of Arttumpara, Pinara (Turkey) -Testing Seismogenic and Anthropogenic Damage Scenarios. *Bulletin of the Seismological Society of America* 100 (6), 3148-3164.

Hinzen, K.-G., (2011). Earthquake, Archaeoseismology. In: *Encyclopedia of Solid Earth Geophysics* (Gupta, H. K., ed.) Springer, Heidelberg, DOI 10.1007/978-90-481-8702-7.

Hinzen, K.-G., H. Kehmeier, S. Schreiber and S.K. Reamer, (2011). Test Of Earthquakes And Rockfall As Possible Cause Of Damage To A Roman Mausoleum In Pinara, Sw Turkey. In: *Proceedings of 2nd INQUA-IGCP-567 International Workshop on Active Tectonics, Earthquake Geology, Archaeology and Engineering* (Papanikolaou, I.D., Reicherter, K., Vött, A., Silva, P.G. eds.) Corinth, Greece, submitted.

Schreiber, S., I. Wiosna, M. Wegner and K.-G. Hinzen, (2011a). Archeoseismological Study in the Historic City Center of Cologne, Germany. *71. Jahrestagung der Deutschen Geophysikalischen Gesellschaft*, 21.-24.2.2011, Cologne, Germany.

Schreiber, S., K.-G. Hinzen and C. Fleischer (2011b). Excavation Parallel Laser Scanning of a Medieval Cesspit in the Archaeological Zone Cologne, Germany. *Journal of Computing and Cultural Heritage,* submitted.

Schreiber, S. and K.-G. Hinzen, (2011). Archeoseismological Investigations in the Historic Center of Cologne, Germany. *Seismological Research Letters* 82, No. 2, 334.

Sequieira, V., K. Ng, E. Wolfart, J.G.M. Goncalves and D. Hogg, (1999). Automated Reconstruction of 3D Models from Real Environments. I*SPRS J. Photogramm.* 54, 1-22.

Sgrenzaroli, M. and E. Wolfart, (2002). Accurate Texture-Mapped 3D models for Documentation, Surveying and Presentation Purposes. In: *CIPA WG 6 International Workshop on Scanning For Cultural Heritage Recording*, Greece, Corfu, 1-2 September 2002.

EARTHQUAKE
ARCHAEOLOGY

INQUA PALEOSEISMOLOGY
AND ACTIVE TECTONICS

EARTHQUAKE TRIGGERING, CLUSTERING, AND THE SYNCHRONIZATION OF FAULTS

Christopher H. Scholz

Lamont-Doherty Earth Observatory, Columbia University. Palisades, NY. USA

Abstract (Earthquake Triggering, Clustering, and the Synchronization of Faults): *Large earthquakes are sometimes observed to trigger other large earthquakes on nearby faults. The magnitudes of the calculated Coulomb stress transfers presumed to cause the triggering are 10^{-2} – 10^{-3} the earthquake stress drop and the triggering delay times are similarly small with respect to the natural recurrence time of the earthquakes. This requires that both faults be simultaneously very close to the ends of their seismic cycles. Paleoseismological data show that for the same regions prior earthquakes have occurred in clusters in space and time separated by long quiescent periods. Both observations suggest that synchronization is occurring between faults. Theory and observations indicate that synchronization can occur between nearby faults with positive stress coupling and intrinsic slip velocities within an entrainment threshold. In the south Iceland seismic zone, the central Nevada seismic belt and the eastern California shear zone several synchronous clusters that apparently act independently, can be recognized. This behaviour is the 3D equivalent of the phase locking those results in the seismic cycle being dominated by large characteristic earthquakes, and for synchronization of fault segments along a single fault. Rupture patterns of repeated individual earthquakes or earthquake clusters are not identical in either the 2D or 3D cases. The state of this system, which exhibits strong indications of synchrony without exact repetition, may be called fuzzy synchrony.*

EARTHQUAKE ARCHAEOLOGY

INQUA PALEOSEISMOLOGY AND ACTIVE TECTONICS

RELIEF PRODUCTION, UPLIFT AND ACTIVE TECTONICS IN THE GIBRALTAR ARC (SOUTH SPAIN) FROM THE LATE TORTONIAN TO THE PRESENT

Silva, Pablo G. (1), Alex Ribó (1), Moises Martín Betancor (2), Pedro Huerta (1), M. Ángeles Perucha (3), Cari Zazo (4), Jose L. Goy (1), Cristino J. Dabrio (5), Teresa Bardají (6)

(1) Dpto. Geología, Escuela Politécnica Superior de Ávila, Universidad de Salamanca. Avda. Hornos Caleros, 50. 05003-Ávila. SPAIN. pgsilva@usal.es, aribo@usal.es, phuerta@usal.es, joselgoy@usal.es
(2) Dpto. Cartografía y Expresión Gráfica en Ingeniería, Universidad de Las Palmas de Gran Canaria, Campus Tafira Baja 35017-Las Palmas de Gran Canaria, SPAIN. mmartin@dcegi.ulpgc.es
(3) Instituto Geológico y Minero de España. Ríos Rosas, 23. 28003-Madrid. SPAIN. ma.perucha @igme.es
(4) Dpto. Geología, Museo Nacional de Ciencias Naturales (CSIC), 28006-Madrid SPAIN
(5) Dpto. Estratigrafía. Facultad CC. Geológicas. Universidad Complutense de Madrid. 28040-Madrid. SPAIN.
(6) Dpto. Geología, Universidad de Alcalá de Henares, 28871- Alcalá de Henares, Madrid SPAIN

Abstract (Relief production, uplift and active tectonics in the Gibraltar Arc (South Spain) from the Late Tortonian to the present): *This work analyzes the topographic evolution of the Gibraltar Arc (Betic Cordillera) from the Tortonian to the present. This first preliminary approach is based on the morphometric analysis of drainage basins and the identification of stratigraphic markers for ancient positions of the sea-level. Computed data indicate that mean thickness of eroded materials by fluvial erosion is 593 m, generating an overall isostatic rebound of about 495 m. These data fit with computed mean elevations for individual basins, suggesting a quasi-isostatic equilibrium in the zone. However uplift is differentially distributed indicating that the main tectonic structures outcropping in the zone (ancient Betic thrusts and main tectonic contacts) are accommodating differential uplift, and therefore have been actives throughout Late Neogene to Quaternary times.*

Key words*: Differential Uplift, Geophysical relief, Erosional unloading, Gibraltar Arc, Betic Cordillera, Spain.*

INTRODUCTION

Isostatic uplift in response to erosional unloading of single faulted range fronts, mountain ranges and entire cordilleras has been proved to be a key process for the long-term landscape evolution in tectonically active areas (e.g. Molnar and England, 1990; Bishop, 2007; Fernández-Ibáñez et al., 2010). Denudational unloading promotes relevant lithospheric upward flow, and subsequent surface uplift, controlling the topographic evolution of active orogens and backfeeding the rhythms of mass rock-transfer between ranges, local sedimentary basins and oceans/seas (e.g. Watts, 2001). Some authors envisage this process to explain regional surface uplift in relation to active fluvial erosion in mountain chains (Gilchrist et al., 1994; Small and Anderson, 1998; Brocklerhurst & Whipple, 2002), oceanic islands (Menéndez et al., 2008) or even single faulted-fronts (Fernández-Ibáñez et al., 2010). On the other hand, aside of the backfeeded contribution of tectonic and isostatic uplift, cyclic or unique events of base-level drop can affect to the related rates of erosion and uplift. This study is a preliminary analysis focused on the topographic development of the Gibraltar Arc (Betic Cordillera, South Spain) since Late Neogene times, and it is part of a large project within the framework of the EUROCORES-TOPOMED Program on the topographic evolution of the Betic-Rif Cordillera in the Western Mediterranean Basin.

GEOLOGICAL BACKGROUND

The development of the Betic–Rif orogen on top of the Africa–Iberia plate boundary across the transition zone between the Atlantic Ocean and the Mediterranean Sea resulted in a complex structural framework mostly developed during the Alpine orogeny. The role of fluvial unloading within the northern segment of the Gibraltar Arc is analyzed by means of the morphometric analysis of the main "direct" river basins draining towards the Gulf of Cádiz (west) and the Alboran Basin (East) from the fluvial outlets of the Guadalete river (Cádiz)) up to Motril (Granada). The study comprises the analysis of the computed bulk volume of rock-mass removed by erosion since the Tortonian until the present, as well as the analysis of this same parameter for discrete time-windows: Tortonian, Messinian, Pliocene and Quaternary. This last sequenced analysis will allow establishing time-dependent differential uplift, but also discrete temporal pulses of uplift for the whole studied zone, especially before and after the "Messinian Salinity Crisis". This event occurred between 5.96 and 5.33 Myr ago triggering the disconnection of the Mediterranean Sea from the Atlantic Ocean in response to the final stages of build-up of the Gibraltar Arc, as well as a rapid episode of desiccation in the Mediterranean basin with a related sea-level drop of about 1000 metres in the western Mediterranean (e.g. Blanc, 2006). In fact, recent studies (i.e. Iribarren et al., 2009) indicate that the continentalization (i.e. emersion or uplift) of this sector of the Betic Cordillera took place around 5.3 Myr ago, probably linked to this event. In fact computed data of sedimentary budget (5,490 km^3/Myr) and sedimentation rates (0.18 mm/yr) within the Alboran Basin during the Late Neogene were higher than those recorded for previous and

subsequent time-periods. The Messinian sea-level drop generated an unusual topographic scenario along the growing emerged tectonic wedge of the Gibraltar Arc, with an oceanic (Atlantic) foreland basin to the West and a large desiccated basin to the East. This situation gave place to an abrupt asymmetry in the base-level at both sides of the growing tectonic wedge and therefore, triggered asymmetric fluvial erosion, probably backfeeding differential uplift in mountain building. The subsequent Zanclean Flooding (García Castellanos et al., 2010) inundated again the entire Mediterranean basin in an instantaneous time-span of about 2 years dissipating a gravitational potential energy of about 1.63×10^{22} J and balancing again base-levels at both sides of the Gibraltar Arc. Sea level reached a maximum of ca. + 70 m during the Pliocene previous to the eventual growing of the Antarctica ice sheet.

ANALYSIS OF RELIEF AND UPLIFT

A digital elevation model of 40x40m pixel resolution has been used in order to extract main ridgelines and drainage basins of the Gibraltar Arc from Cádiz (West) to Motril (East), differentiating 50 individual drainage basins larger than 18 km^2 over a bulk area of 14552 km^2, which excludes the western slope basins draining towards the Guadalquivir Basin. 11 drainage basins dissect the western Atlantic slope of the Gibraltar Arc with an area of 5849 km^2, and 39 ones are located in the Mediterranean slope over an area of 9063 km^2. For a preliminary estimation of the volume of removed materials by fluvial erosion a pre-incision surface was computed for each individual basin from the present elevation of their ridgelines perimeters and representative erosional surfaces. The results indicate eroded budgets of 8632.9 km^3 for the bulk of the studied section of the Gibraltar Arc, of which 836.7 km^3 corresponds to the Atlantic slope and 7765.2 km^3 for Mediterranean one. Dividing the obtained removed volumes by the present drained areas results in the theoretical equivalent thickness of removed materials or "geophysical relief" (Small and Andersson, 1998), which for the bulk studied area is of 593 m.

In a second step hypsometric curves were computed for each individual drainage basin in order to obtain the distribution and values of mean and maximum present elevations for the studied basins, resulting in a mean value for the whole studied area of 411.4 m above the sea-level, but with a clear asymmetry between the Atlantic (108 m) and Mediterranean (492.3 m) slope of the Gibraltar Arc, with computed percentual weights over the total analyzed area always above of 70% and therefore statistically representative. Comparing the values of mean elevations and computed geophysical reliefs offer well fit linear regressions, with correlation coefficients close to 0.9 for the whole studied zone and their zonations. This fact implies a good correlation between the present elevation and the theoretical thickness of removed materials by fluvial erosion, suggesting near-isostatic equilibrium conditions for the zone. From this approach, in a third step the zone was divided in individual crustal/lithospheric sectors corresponding to the analyzed basins in order to calculate the consequent uplift in response to erosional unloading following the Airy-Heiskannen isostatic model. Different approaches have been applied in this study in order to obtain the isostatic response (e.g. Gilchrist et al., 1994; Fernández-Ibáñez et al., 2010), but the best fitting ratios between computed uplift and present mean elevation

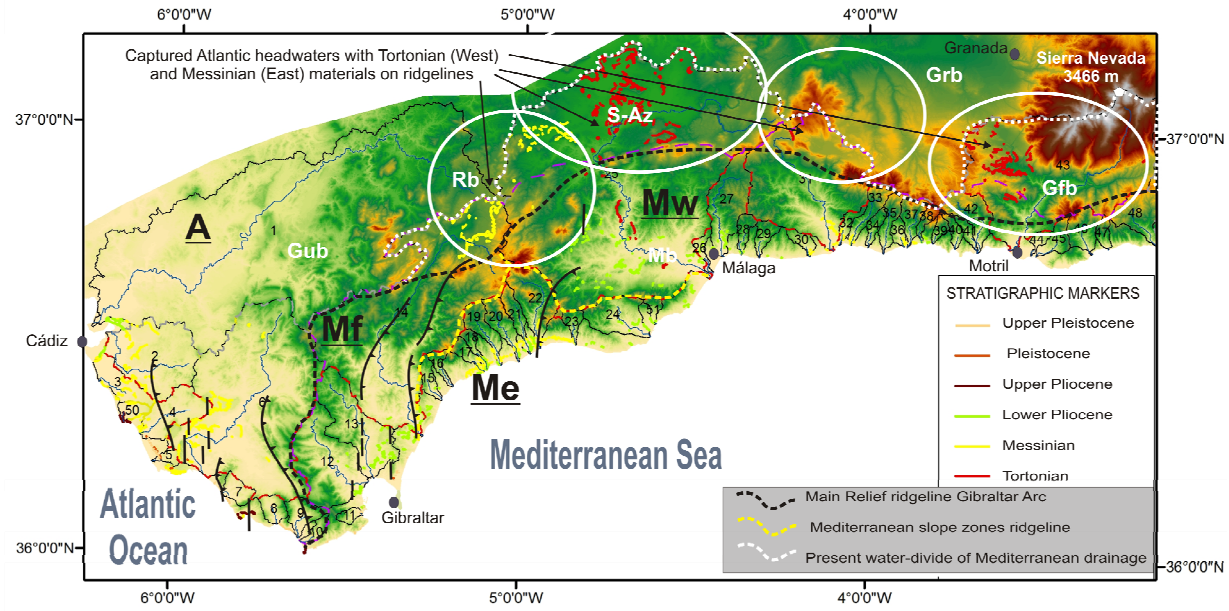

*Fig. 1: Digital Elevation Model of the Gibraltar Arc (Western Betic Cordillera) displaying the main elements of the present relief, drainage basins and stratigraphic markers (littoral sediments) analyzed in this study. Mapped Betic thrusts and normal faults (conventional symbols) are those controlling differential uplift from the Messinian. **A**: Atlantic Slope; **M**: Mediterranean Slope, subdivided in Frontal Flysch (**Mf**), Eastern (**Me**) and Western (**Mw**) analyzed sectors. Gub: Guadalete Neogene basin; Rb: Ronda Neogene basin; S-Az: Setenil-Antequera zone; Grb: Granada Neogene basin; Gfb: Guadalfeo Neogene basin. Numbers corresponds to the individual analyzed drainage basins.*

correspond to the application of the Gilchrist et al. (1994) isostatic constant, which offer linear regression lines with correlation indexes up to 88%. This fact suggests that isostatic compensation is more related to crust/mantle models rather to lithosphere/ asthenosphere models, but also that the studied zone should be in near-isostatic equilibrium at present. The application of crust/mantle isostatic constant yields a value of +495 m for the mean uplift of the whole investigated area of, but differentially distributed from the Atlantic flysch sector (+74.8 m), the Mediterranean flysch sector (+170.4 m), the Mediterranean mantle-core complex of the Ronda Range sector (+417.2 m) and the Mediterranean sector west to the Málaga basin along the Mijares Range (+592.8 m). However, taking into account the present mean maximum elevation of the analyzed area (1195.8 m), maximum denudational isostatic rebound represent the 41-49% of the recorded uplift since the Tortonian, the remaining 59-51 % should be achieved by the African-Eurasian plates convergence.

Implementation of digital geological data obtained from the IGME data base (GEODE) in the digital elevation model allows the extraction of representative linear and punctual stratigraphic markers for different Late Neogene sea-level positions. The geological data implemented in the DEM only correspond to littoral, shallow marine and proximal delta units and the intersection of their upper contacts with the present relief sketch or depict approximate paleo-shorelines with a confidence of ± 40m forced by the DEM resolution. These relative paleoshorelines has been obtained for different time-windows corresponding to the Late Tortonian, Messinian, Lower Pliocene, Upper Pliocene and Lower Pleistocene. These appear identified by means of different colours in the map of figure 1.

The analysis of these stratigraphic markers is still in progress, but the preliminary analysis of their spatial/elevation distribution clearly indicates that the main stage of relief production in the studied zone was attained after the relevant Messinian sea-level drop (5.96 Myr). Most of the littoral Messinian depostis identified in the GEODE data base in the Mediterranean slope of the studied zone may mainly correspond to younger Pliocene sediments. Therefore “true” Messinian deposits in the studied area are only present northwards and westwards of the main ridgeline of the Gibraltar Arc (Fig. 1) along the ancient Atlantic front of the growing tectonic wedge. In this zone Messinian, but also Tortonian deposits, occur at ridgeline locations on the headwaters of the present drainage basins, which obviously indicate that main fluvial dissection stages are post-Messinian.

The occurrence of sediments of these ages in the present headwaters of the Mediterranean slope is consequence of Messinnian and post-Messinian aggressive headward erosion of the largest fluvial basins trespassing the ancient main ridgeline of the Gibraltar Arc (Fig. 2) such as those corresponding to the Guadalfeo, Guadairo, Guadarranque and Guadalhorce rivers (Fig.1). This ridgeline was already emerged during the Tortonian limiting the Noegene basins of Ronda and Granada by the south. The main emerged ridgeline was only interrupted (inundated) during the pre-Messinian times in the Málaga Basin along the present Guadalhorce corridior, the unique location in which there are outcrops of littoral/shallow marine Tortonian sediments eastwards the ancient ridgeline of the Gibraltar Arc within the studied zone (Fig. 1). The Pliocene and Pleistocene littoral materials in the Mediterranean simply partially filled the main fluvial basins generated during the Messinian. These deposits never appear in ridgeline positions along the entire Mediterranean slope.

The elevation distribution of post-Messinian sea-levels markers strongly support that the aforementioned differential uplift is being conducted along the more relevant NNE-SSW or N-S thrust contacts developed during the final stages of the construction of the Gibraltar Arc broadly delineated in

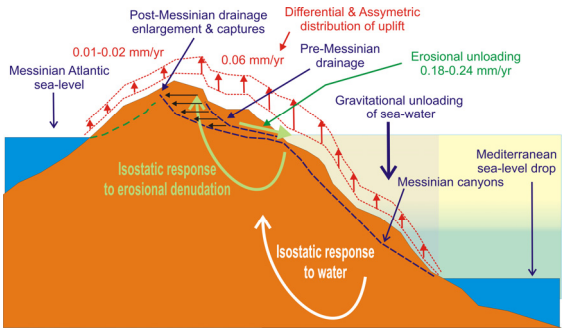

Fig. 2: Conceptual Model for the interaction of fluvial unloading and gravitational unloading triggering the subsequent differential uplift along the Gibraltar Arc during the Messinian sea-level drop (rates from Iribarren et al., 2009).

Figure 1. These tectonic structures can be considered as active ones in which a vertical partition of tectonic and isostatic movements seems to occur in order to distribute regional differential uplift. In the central sector of the Gibraltar Strait these tectonic structures controlled the generation of N-S subsiding troughs (controlled by normal faulting) during the Pliocene, clearly control the distribution of differential uplift of the Last Interglacial marine terraces and are presently related with instrumental seismicity (Zazo et al., 1999; Silva et al., 2006).

CONCLUSIONS

The analysis of relief of the Gibraltar Arc presented in this work is a preliminary approach to decode the evolution of the onshore topography of this sector of the Betic Cordillera from the Tortonian to the present. Initial computed data indicate that the equivalent thickness of erosional unloading (geophysical relief) is of 593 m for the whole studied area. Isostatic uplift response to fluvial unloading is of 495 m, but differentially distributed, with maximum values in the eastern studied sector south of Sierra Nevada (Motril) and minimum values in the western Atlantic sector (Cádiz). Subsequent analyses will be also

focused in the relationships of seismotectonic activity of the more outstanding North-South tectonic structures accommodating differential uplift in the central-axial sector of the Gibraltar Arc.

The sequential analysis of eroded volumes during discrete periods will allow to establish theoretical values of uplift for the different studied drainage basins and sectors. The preliminary results in this study indicate an accumulated mean uplift of +495 m since the end of the Tortonian (c.a. 7.2 Myr) which suggest broad mean uplift rates of 0.068 mm/yr for this time-period, clearly decreasing towards the Gibraltar Strait area where uplift rates are of ca. 0.01-0.02 mm/yr. The obtained values are within the range of the estimated uplift rates by other authors, and other methods, for the whole Betic Cordillera (i.e. Iribarren et al., 2009) which is of 0.05 mm/yr, but decreasing to 0.02 mm/yr to the Gibraltar Strait (Fig. 2).

A final preliminary remark is that isostasy triggered by mass-rock transfer between the growing tectonic wedge of the Gibraltar Arc and two the adjacent marine basins can explain about the 40-50% of the recorded uplift since the end of the Tortonian. On the other hand, the volume of post-Tortonian sediments accumulated in the Alboran basin indicates mean rates of sedimentation of about 0.18-0.24 mm/yr (Fig. 2). The conversion of these sedimentation rates to erosion rates will allow checking the uplift response by means of different isostatic crust/mantle and lithosphere/asthenosphere conceptual models. These models will also take into account the isostatic rebound related to sea-water unloading in the Mediterranean slope triggered by the relevant sea-level drop occurred during the Messinian (Fig.2).

Acknowledgements: This work has been supported by the EUROCORES-TOPOMED PROGRAM through the Spanish research project CGL2008-03474-E/BTE (CSIC) produced by the TopoMed-Spain Onshore Research Group of the University of Salamanca. Also financial support has been obtained from the research projects CGL08-03998BTE, CGL08-04000BTE

References

Blanc, P. L. (2006). Improved modelling of the Messinian Salinity Crisis and conceptual implications. *Palaeogeogr. Palaeoclimatol. Palaeoecol.* 238, 349–372.

Bishop, P. (2007). Long-term landscape evolution: Linking tectonics and surface processes. *Earth Surface Processes and Landforms,* 32, 329–365.

Brocklehurst, S.H., Whipple, K.W. (2002). Glacial erosion and relief production in the Eastern Sierra Nevada, California. *Geomorphology* 42 , 1-24.

Fernández-Ibáñez, F., Pérez-Peña, J.V., Azor, A., Soto,J. Azañón, J.M. (2010). Normal faulting driven by denudational isostatic rebound. *Geology,* 38, 643-646.

Garcia-Castellanos, D., Estrada, F., Jiménez-Munt, I., Gorini,C., Fernández, M., Vergés, J. & De Vicente, R. (2009). Catastrophic flood of the Mediterranean after the Messinian salinity crisis. *Nature,* 462, 778-782.

Gilchrist, A.R., Kooi, H. & Beaumont, C. (1994). Post-Gondwana geomorphic evolution of southwestern Africa: Implications for the controls on landscape development from observations and numerical experiments: *Journal of Geophysical Research,* 99, 12,211–12,228.

Iribarren, L., Vergés, J. & Fernandez, M. (2001). Sediment supply from the Betic–Rif orogen to basins through Neogene. *Tectonophysics,* 475, 68–84

Menéndez, I., Silva, P.G., Martín Betancor, M., Pérez Torrado, F.J., Guillou, H. & Scaillet; S. (2008). Fluvial dissection, isostatic uplift, and geomorphological evolution of volcanic islands (Gran Canaria, Canary Islands, Spain). Geomorphology, 102, 189 – 203.

Molnar, P. & England, P. (1990). Late Cenozoic uplift of Mountain ranges and global climate change: Chicken or egg?: *Nature,* 346,,29– 34.

Silva, P.G., Goy, J.L., Zazo, C., Bardají, T., Lario, J., Somoza, L., Luque, L. & González Fernández, F.M. (2006). Neotectonic fault mapping at the Gibraltar Strait Tunnel area, Bolonia Bay (South Spain). Eng. Geology, 84, 31–47

Small, E. & Anderson, R. (1998). Pleistocene relief production in Laramide mountain ranges, western United States: *Geology,* 26, 123–126.

Watts, A.B. (2001). Isostasy and flexure of the lithosphere. Cambridge University Press, Cambridge, UK, pp. 458.

Zazo, C., Silva, P.G., Goy, J.L., Hillaire-Marcel, C. Lario, J. Bardají, T. & González, A. (1999). Coastal uplift in continental collision plate boundaries: Data from the Last interglacial marine terraces of the Gibraltar Strait area (South Spain). *Tectonophysics*, 301, 95-119.

REASSESSING ANCIENT EARTHQUAKES ON MINOAN CRETE GETTING RID OF CATASTROPHISM

Sintubin, Manuel (1), Simon Jusseret (2,1), Jan Driessen (2)

(1) Geodynamics & Geofluids Research Group, Department of Earth & Environmental Sciences, Katholieke Universiteit Leuven, Celestijnenlaan 200E, B-3001 Leuven. BELGIUM. Email: manuel.sintubin@ees.kuleuven.be
(2) Aegean Interdisciplinary Studies Research Group (AegIS-CEMA-INCAL), Université Catholique de Louvain, Place B. Pascal 1, B-1348 Louvain-la-Neuve. BELGIUM. Email: jan.driessen@uclouvain.be; simon.jusseret@uclouvain.be

Abstract(Assessing ancient earthquake on Minoan Crete. Getting rid of catastrophism): *Early in the 20th century Arthur Evans invoked catastrophic earthquakes to explain the destruction encountered in the Palace of Knossos. Ever since, these earthquake catastrophes have been used as reference events to which structural damage or destruction layers on Minoan sites are indiscriminately attributed in archaeological and archaeoseismological publications. However, structural damage to archaeological remains cannot be unequivocally attributed to earthquakes. A detailed analysis of Late Minoan contexts moreover reveals that multiple moderate earthquakes occurred during this 200-year period (c. 1600 – 1400 BC). All evidence suggests that earthquakes did not play a crucial role in Minoan history and did certainly not cause the decline of Minoan civilization. This reassessment of the Minoan case clearly demonstrates that earthquakes in itself are incapable of causing the collapse of a civilization.*

Key words*: Minoan Crete, Late Bronze Age, catastrophism, earthquake archaeology*

Early in the 20th century Arthur Evans invoked catastrophic earthquakes to explain the destructions encountered during the excavations of the Minoan Palace at Knossos, Crete (Fig. 1). Such seismic catastrophes were considered to have ended the Protopalatial period (c. 1700 BC), to have been responsible for the *"great destruction"* during the Neopalatial period (c. 1600 BC), and to have ultimately caused the collapse of Minoan civilization around 1450 BC (Evans, 1928).

Fig. 1: The "house of the fallen blocks" at the palatial site of Knossos, a particular damage interpreted by Evans (1928) to have been caused by a catastrophic earthquake.

Ever since, these earthquake catastrophes have been taken for granted and used as reference events to which structural damage to buildings and other cultural remains or earthquake-related destruction layers are indiscriminately attributed in archaeological (e.g., Sakellarakis & Sapouna-Sakellaraki, 1991) and archaeoseismological publications (e.g., Monaco & Tortorici, 2004; Vallianou, 1996). But is there any reliable evidence to support the existence of such catastrophic earthquakes and can we parameterize them?

First, it is extremely difficult to attribute unequivocally structural damage to Minoan archaeological remains to earthquakes. In most cases it cannot be excluded that other physical and/or anthropogenic agents have generated the damage observed (cf., Driessen, 1995). A macroseismological parameterization of these ancient earthquakes based on the detailed archaeological record remains a very challenging prospect.

Secondly, a detailed analysis of Late Minoan (c. 1600 – 1400 BC) archaeological contexts (cf., Driessen & Macdonald, 1997) shows that earthquake-related damage, repairs, adjustments (e.g., Driessen, 1987) and/or abandonment are all rather isolated and local phenomena within and not necessarily contemporaneous between the different sites. This evidence reveals that most probably multiple moderate earthquakes occurred during this 200-year time period, rather comparable to today's seismicity of the island.

There is seemingly only consistent archaeological evidence for widespread, earthquake-related damage on Crete, as well as on Thera (Santorini), Kos, and

Rhodes at c. 1600 BC (transition of ceramic stage MM IIIB to LM IA), known as the *"great destruction"* (Evans, 1928). This potentially "catastrophic" event is, however, followed by a sudden increase of the number of secondary sites, in particular in eastern Crete (cf., Driessen & Macdonald, 1997), new palatial architecture with new architectural (anti-seismic?) elements, such as 'pier-and-door partitioning' (cf., Driessen, 1987), and the greatest construction program of any prehistoric era in the Aegean. The heyday of Minoan civilisation followed this major seismic event.

Between c. 1520 and c. 1480 BC (ceramic stage LM IA) this prolific building program came to an abrupt end. Monumental buildings were left unfinished. This heralded the demise of Minoan society. In a period of one to two generations – from c. 1480 to c. 1425 BC (ceramic stage LM IB) – a wave of fire destruction raged over the island. Settlements were abandoned, population density declined. Both a "crisis architecture" (cf., Driessen, 1995) and a "crisis cult" took hold of Minoan society. Evidence for earthquake-related damage in that period indicates multiple moderate earthquakes affecting local communities rather than island-wide destructive events. Most of the destruction was indeed caused by man. All evidence indicates that the socio-political and economic landscape of Minoan society completely disintegrated and collapsed in that period, leaving behind a "failed state". The power vacuum was later – during ceramic stage LM II (c. 1425 to c.1400 BC) – filled by the Mycenaens.

Although Late Minoan society can clearly be characterized as a society in crisis (cf. Driessen & Macdonald, 1997), no hard evidence exists to link this societal decline with (catastrophic) earthquakes. Even the existence of such seismic catastrophes during Minoan history – except for the c. 1600 BC event – should be questioned. Minoans lived with earthquakes, very much as modern Cretans do. Earthquakes did not play a crucial role in Minoan history and did definitively not cause the decline of Minoan civilization. At most, they added some extra stress to a society already in crisis.

This reassessment of the Minoan case illustrates that earthquakes, irrespective of their magnitude and recurrence, provoke different societal responses, largely depending on the political, social, economic and military context. Earthquakes in itself are incapable of causing the collapse of a community, let alone a civilization. It's therefore time to get rid of the catastrophism that has burdened earthquake archaeology for too long (e.g., Nur, 2008; Nur & Cline, 2000).

Acknowledgements: This contribution frames in the UNESCO-IUGS funded International Geoscience Programme IGCP 567 *Earthquake Archaeology*. S. Jusseret is currently a Intercommunity Scientific Postdoctoral Collaborator of the Francqui Foundation (Belgium) at the K.U.Leuven.

References

Driessen, J. (1987). Earthquake-Resistant Construction and the Wrath of the "Earth-Shaker". *Journal of the Society of Architectural Historians* 46, 171-178.

Driessen, J. (1995). "Crisis Architecture". Some observations on Architectural Adaptations as Immediate Responses to Changing Socio-Cultural Conditions. *Topoi* 5, 63-88.

Driessen, J., Macdonald, C. F. (1997). *The Troubled Island. Minoan Crete before and after the Santorini Eruption*, Liège & Austin.

Evans, A. (1928). *The Palace of Minos, part II.*, London.

Monaco, C., Tortorici, L. (2004). Faulting and effects of earthquakes on Minoan archaeological sites in Crete (Greece). *Tectonophysics* 382, 103-116.

Nur, A. (2008). *Apocalypse. Earthquakes, Archaeology, and the Wrath of God*. Princeton University Press, Princeton.

Nur, A, Cline, E. H. (2000). Poseidon's Horses: Plate Tectonics and Earthquake Storms in the Late Bronze Age Aegean and Eastern Mediterranean. *Journal of Archaeological Science* 27, 43-63.

Sakellarakis, J. A., Sapouna-Sakellaraki, E. (1991). *Archanes*. Ekdotike Athenon S.A., Athens.

Vallianou, D. (1996). New Evidence of Earthquake Destructions in Late Minoan Crete. In: *Archaeoseismology* (edited by Stiros, S. C. & Jones, R. E.). *Fitch Laboratory Occasional Paper* 7. Institute of Geology & Mineral Exploration & The British Scholl at Athens, Athens, 153-167.

PALEOTSUNAMIS EVIDENCE FROM A COMBINED INLAND AND OFFSHORE STUDY IN THE AUGUSTA BAY AREA (EASTERN SICILY, ITALY)

Smedile, Alessandra (1), Paolo Marco De Martini (1), Daniela Pantosti (1)

(1) Istituto Nazionale di Geofisica e Vulcanologia. Via di Vigna Murata, 605. 00143- Roma. ITALY.
Email: alessandra.smedile@ingv.it, paolomarco.demartini@ingv.it, daniela.pantosti@ingv.it

Abstract (Paleotsunamis evidence from a combined inland and offshore study in the Augusta bay area (eastern Sicily, Italy): *We present the geological evidence for a 4000 year-long record of repeated tsunami events along the coast of the Augusta Bay derived from the combination of inland and offshore cores data. The research was carried out through a multi-theme approach which benefited from an long historical record that we used to guide detailed geomorphologic, geologic, and geophysical surveys, that were performed both inland and offshore. These surveys served to locate and characterize the best sites were to perform the coring collection that where studied through and several laboratory analyses. The Augusta Bay represents a unique case study because besides showing a long record of paleotsunami events, it contains the first inland and offshore evidence for the Crete AD 365, and Santorini Late Minoan tsunamis in the central-western Mediterranean area.*

Key words*: Eastern Sicily, tsunami deposits, AD 365 Crete and Santorini events.*

Eastern Sicily (Italy) was repeatedly affected by tsunami waves related to large local historical earthquakes (e.g. 1908, 1693, 1169) (CPTI Working group, 2004) as well as to far-field sources (e.g. AD 365 Crete earthquake) (Jerome, 380). Along the eastern Sicily coasts, we selected the Augusta Bay, a natural gulf about 15 km wide and with a 25 km-long shoreline (Fig.1), as the key area of this study. In fact, it is one of the locations where both information available from historical written reports on tsunami effects (hit localities, inundated areas and run-up distribution) (Gerardi et al., 2008) and local geomorphology suggest it is very favorable for the research of the geological signature of past tsunamis. Well-targeted sediment samples have been collected both inland and offshore through coring at different depths. Small ponds, marshes and lagoons characterize the coastal area, while a relatively wide continental shelf with a thick late-Holocene record has been investigated offshore through the acquisition of a tight grid of CHIRP-sonar profiles. The integrated interpretation of the geophysical and geological data has been carried out in order to recognize, date and correlate key-layers in the sediment column that may be directly or indirectly related to tsunami events.

A total number of 22 cores were collected inland at two different sites with a maximum distance of 530 m from the present coastline (De Martini et al., 2010). The dominant fine to very fine stratigraphy is intercalated by at least 6 high-energy depositional layers, repeatedly found in several cores. These relatively thin (about 10 cm) single massive and structureless beds with abrupt erosional lower contact are made of coarse to fine sand and present a bioclastic component (sometimes predominant) made of microfauna (benthic and planktonic foraminifera, from both shallow and open marine environment) and shell fragments both suggestive of a marine origin. Chronological constraints on the age of these deposits are based on 8 AMS radiocarbon datings and on the attribution of a tephra layer to the 122 BC Etna eruption. For the marine shell samples (details in De Martini et al., 2010 and Smedile et al., 2011), measured C14 ages were dendro-chronologically corrected using a marine calibration curve that incorporate a time-dependent global ocean reservoir correction of about 400 yrs (Reimer et al., 2009). Moreover, the marine palaeo-reservoir effect was subjected to the local effect (ΔR offset) that, in the Mediterranean Sea, appears to be constant for the past 6 or 7 ka (Reimer and McCormac, 2002). The appropriate ΔR offset can be selected from the Chrono Marine reservoir Database (Reimer and Reimer, 2001).

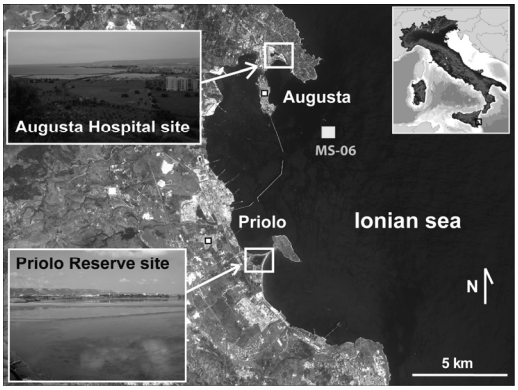

Figure 1: The Augusta Bay area in eastern Sicily, Italy. The Augusta Hospital and Priolo Reserve sites are marked with white empty rectangles, while a white box locates the offshore coring site (MS-06). Two panoramic pictures of the in-land investigated sites are also shown.

On the basis of the combination of all the data collected, the inland sequence spans the last 4100 yrs. In terms of tsunami timing, we could list them as follow (PR= Priolo Reserve site; AU= Augusta Hospital site): younger than 1420–1690 AD (PR-01), 650–770 AD (AU-00), 160–320 AD (PR-02), 600–400 BC (AU-01), 800–600 BC (PR-03), 975–800 BC (AU-02) and 2100–1635 BC (PR-04).
Three of the tsunami deposits found at the Priolo Reserve site may be associated with historical tsunamis: PR-01 with the 1693 local event, PR-02 with the 365 AD Crete event and PR-04 with the ca. 3600 BP Santorini event.

The offshore record was derived from a 6.7 m-long piston-core sampled 2 km offshore the Augusta harbor at 72 m depth (Fig.1). The core study includes X-ray imaging, isotopic dating, tephrachronology, grain-size and foraminiferal analyses (Smedile et al., 2011). The homogeneous sequence of dark grey mud is interrupted at -2.9 m b.s.f. (below sea floor) by the same Etna tephra deposit found inland. Through the analysis of tephrostratigraphy, radiocarbon dating and radioactive tracers, the entire core sequence has been dated back to the last 4500 yrs. Furthermore, we estimated an age range for the 12 high energy intervals as follows: E1 (AD 1820-1920), E2 (AD 1430-1810), E3 (AD 930-1170), E4 (AD 590-800), E5 (AD 430-660), Ex (AD 90-370), E6 (BC 350-130), E7 (BC 580-320), E8 (BC 660-400), E9 (BC 800-560), E10 (BC 1130-810), E11 (BC 1720-1200). Moreover, the quantitative micropaleontological (on the benthic foraminifera assemblage) and sedimentological analyses highlighted 12 anomalous layers marked by high concentration of displaced epiphytic foraminifera (species growing in vegetated substrates like the *Posidonia oceanica*) and subtle grain size changes.
These anomalous layers are likely to have been caused by high-energy events, with tsunamis (back-wash wave) as best candidates. This hypothesis is also supported by the fact that the ages of 5 of these peculiar layers coincide with that of historical tsunamis [1908 (E1), 1693 (E2), 1169 (E3), AD 365 Crete (Ex) and ca. 3600 BP Santorini (E11)].
Moreover, to better detail and replicate the MS06 results at least for the recentmost sequence, new cores were collected in the northern part the Augusta Bay. These cores were sampled in order to define a W-E oriented transect along the shelf from 58 to 110 m water depth.

The Augusta Bay represents a unique case study because it allows a comparison between geological (both inland and offshore) and historical records. For the 365 AD Crete tsunami and the Late Minoan Santorini event, our findings represent the first inland-offshore evidence in the central-western Mediterranean area. On the basis of these results we can propose, for the past 4 ka in the Augusta Bay, an inland and offshore geologic average tsunami recurrence interval of about 550-650 and 320 years, respectively. This difference is conceivably due to the better preservation of the stratigraphic record in the offshore with respect to coastal areas, commonly affected by intermittent erosional and sedimentation events as well as by antrophic activities .

Acknowledgements: This work was funded by the Italian Dipartimento della Protezione Civile in the frame of the 2004–2006 and 2007–2009 agreements with Istituto Nazionale di Geofisica e Geofisica e Vulcanologia — INGV with contribution of the EU Transfer project. We have to warmly thank M.S. Barbano, F. Gerardi, C. Pirrotta from Catania University, L. Gasperini, L. Bellucci, A. Polonia from ISMAR-CNR Bologna and P. Del Carlo and E. Boschi from INGV for their enthusiastic and productive collaboration.

References

CPTI Working group, 2004. Catalogo Parametrico dei Terremoti Italiani, version 2004 (CPTI04). INGV, Bologna. http://emidius.mi.ingv.it/CPTI/

De Martini, P.M., Barbano, M.S., Smedile, A., Gerardi, F., Pantosti, D., Del Carlo, P., Pirrotta, C, (2010). A 4000 yrs long record of tsunami deposits along the coast of the Augusta Bay (eastern Sicily, Italy): paleoseismological implications. *Marine Geology*, 276, 42-57, doi: 10.1016/j.margeo.2010.07.005

Gerardi, F., Barbano, M.S., De Martini, P.M., Pantosti, D., 2008. Discrimination of tsunami sources (earthquake vs. landslide) on the basis of historical data in eastern Sicily and southern Calabria. *Bulletin of the Seismological Society of America*, 98 (6), 2795–2805.

Smedile A., P.M. De Martini, D. Pantosti, L. Bellucci, P. Del Carlo, L. Gasperini, C. Pirrotta, A. Polonia, E. Boschi (2011). Possible tsunamis signatures from an integrated study in the Augusta Bay offshore (Eastern Sicily–Italy), *Marine Geology*, 281, 1-13, doi: 10.1016/j.margeo.2011.01.002.

Reimer, P.J., McCormac, F.G., 2002. Marine radiocarbon reservoir corrections for the Mediterranean and Aegean Seas. Radiocarbon 44, 159–166.

Reimer, P.J., Reimer, R.W., 2001. A marine reservoir correction database and on-line interface. *Radiocarbon* 43, 461–463 suppl. mat.URL: http://www.calib.org.

Reimer, P.J., Baillie, M.G.L., Bard, E., Bayliss, A., Beck, J.W., Blackwell, P.G., Bronk Ramsey, C., Buck, C.E., Burr, G.S., Edwards, R.L., Friedrich,M., Grootes, P.M.,Guilderson, T.P.,Hajdas, I., Heaton, T.J., Hogg, A.G., Hughen, K.A., Kaiser, K.F., Kromer, B., McCormac, F.G., Manning, S.W., Reimer, R.W., Richards, D.A., Southon, J.R., Talamo, S., Turney, C.S.M., van der Plicht, J., Weyhenmeyer, C.E., 2009. IntCal09 and Marine09 radiocarbon age calibration curves, 0–50, 000 years cal BP. *Radiocarbon* 51 (4), 1111–1150.

BULGARIAN NATIONAL DIGITAL SEISMOLOGICAL NETWORK

Solakov D. (1), L.Dimitrova (1), S.Nokolova (1), St. Stoyanov (1), S. Simeonova (1), L. Zimakov (2), L.Khaikin (3)

(1) Dpt. Seismology, National Institute of Geophysics, Geodesy and Geography. Acad. G. Bonchev str.,bl. 3, 1113 – Sofia, BULGARIA, Emails: dimos@geophys.bas.bg, lidim@geophys.bas.bg, sbnik@geophys.bas.bg, stoyan@geophys.bas.bg, stelas@geophys.bas
(2) Refraction Technology, Inc., USA. l.zimakov@reftek.com
(3) Russia, leonidh@ramblert.ru

Abstract (Bulgarian national digital seismological network): *The Bulgarian National Digital Seismological Network (BNDSN) consists of: National Data Centre (NDC); 13 stations equipped with RefTek Seismic Recorders DAS130 and 1 station equipped with Quanterra 680; broadband seismometers and accelerometers. The real-time data acquisition and processing are performed by a system for signal detection; evaluation of the signal parameters; phase identification and association; source estimation. Seismic interactive analysis system and Early warning system are running in the NDC also. Modern digital equipment installed at Bulgarian seismic stations, careful selection of the software packages running in the data centre proved to be suitable choice for the purposes of BNDSN – to ensure reliable automatic localization of the seismic events and rapid notification of the governmental authorities in case of felt earthquakes on the territory of Bulgaria, to provide a modern basis for seismological studies in Bulgaria.*

Key words*: Bulgarian National Digital Seismological Network, digital equipment, data processing*

INTRODUCTION

In 2005, the Geophysical Institute (with governmental support) performed overall modernization of the Bulgarian National Seismological Network (BNDSN) *(Fig.1)*. Modern digital equipment and broadband seismometers were installed in all stations.

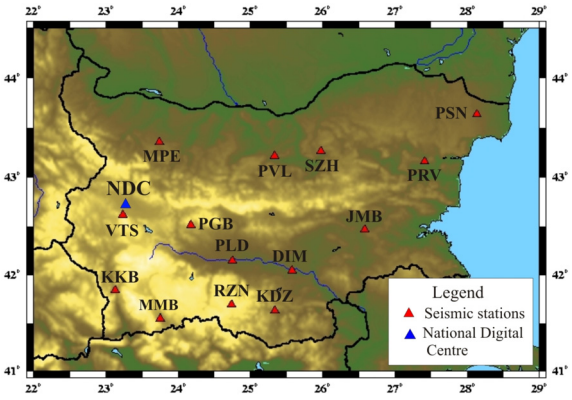

Fig. 1: Bulgarian National Seismological Network

At present the upgraded network consists of a National Data Centre (NDC), 13 stations equipped with RefTek High Resolution Broadband Seismic Recorders – model DAS 130-01/3, 1 station equipped with Quanterra 680 (installed in 1996 in station VTS by project PLATO1/MEDNET as a station from VBB Mediterranean Network) and sensors: very broadband - STS2, STS1, KS2000, RefTek151/120; broadband - CMG 3ESPC, CMG40T; short-period - S13 and accelerometers RefTek 131/03.

Data acquisition

Real-time data transfer from seismic stations to NDC is realized via Virtual Private Network (VPN) of the Bulgarian Telecommunication Company (BTC) *(Fig.2)* with the following characteristics: 64kbps baud rate from each individual site to the digital network of BTC; high security – closed Internet access; broadband 2Mbps optical line established between the NDC and the Centre of Communication Company in Sofia. This solution proved to be very stable and has ensured a reliable communication system through the six years of exploitation.

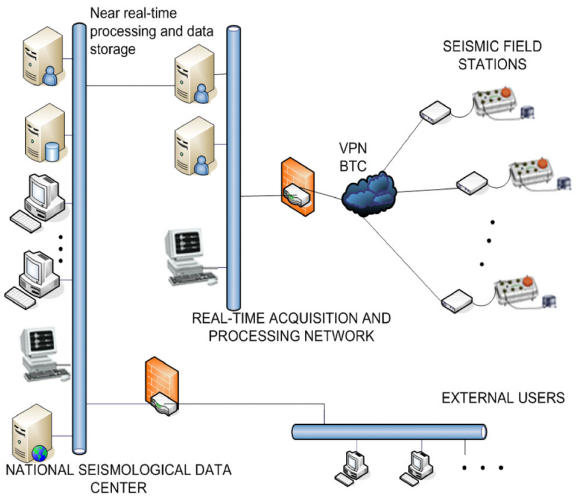

Fig.2. Real-time data transfer from seismic stations to NDC via Virtual Private Network (VPN) and three layer local network

The network availability exceeded 99.99%. The communication interruptions did not cause any data loss at the NDC. The data is backed up in the field station recorder 4Mb RAM memory and is retransmitted to the NDC immediately after the communication link is re-established. The recorders are equipped with 2 compact flash storages able to save more than 1 month long data. The data from the flash disks can be downloaded remotely using FTP.

The data acquisition and processing hardware redundancy at the National Data Center is achieved by two clustered SUN Fire V240 servers with swappable software module and two Blade 1500 Workstations. In the case of server failure the swappable module re-directs the real-time data flow. To secure the acquisition, processing and data storage processes a three layer local network is designed at the NDC. First layer incorporates acquisition and real-time processing equipment, the second layer consists of interactive processing and archiving modules and external users belong to the third layer *(Fig.2)*. Real-time data acquisition is performed using REFTEK's full duplex error-correction protocol RTPD. Data from the Quanterra recorder and foreign stations are fed into RTPD in real-time via SeisComP/SeedLink protocol. Using SeisComP/SeedLink software the NDC transfers real-time data to INGV, Roma and NEIC, USA. The BNDSN is a part of European Virtual Broadband Seismograph Network and the NDC transmits real-time data to the ORFEUS Data Centers. Regional real-time data exchange with Romania, Macedonia, Serbia and Greece is established at the National Data Center also. The data flow from neighbor countries is incorporated in the real-time data stream in the NDC and is used together with BNDSN data for localization of the local, regional and distance seismic events.

Data processing

Data processing is performed by the Seismic Network Data Processor (SNDP) (Haikin and Kushnir, 2005; Haikin et al., 2009) software package running on the both Servers. SNDP includes subsystems:

- *Real-time subsystem* (RTS_SNDP) – for signal detection; evaluation of the signal parameters; phase identification and association; source estimation;
- *Seismic analysis subsystem* (SAS_SNDP) – for interactive data processing;
- *Early warning subsystem* (EWS_SNDP) - based on the first arrived P-phases.

The signal detection process is performed by traditional STA/LTA detection algorithm. Input data streams are band-pass filtered with band limits described in a parametric file. The filter parameters of the detectors are defined on the base of previously evaluated ambient noise at the seismic stations.

The annual noise distribution at the BNDSN stations is presented on *Fig. 3* (the 14 figures around the map).

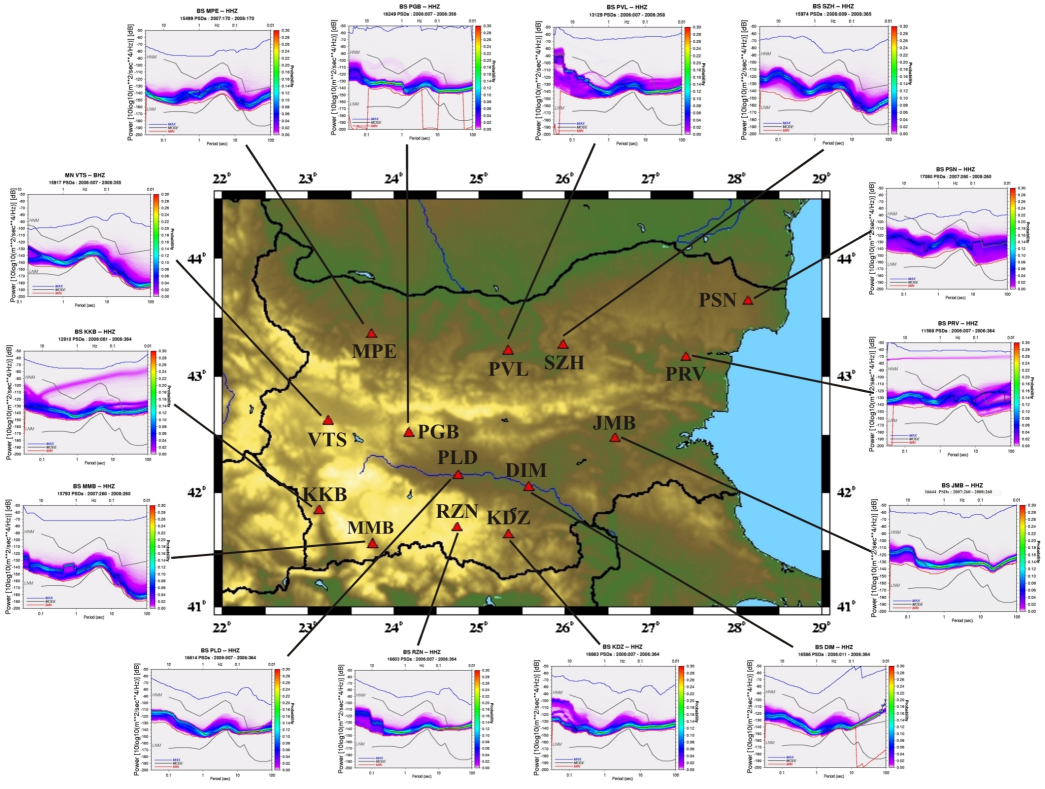

Fig. 3. Evaluation of ambient seismic noise at BNDSN stations

For the analysis purposes, the range of recorded periods from 0.1s to 100s is divided into two sub-periods:
1. The periods longer than 1s, where the microseisms are spread;
2. The periods shorter than 1s, where the most common noise source is the man-made one.

The results show that:

– For the periods greater then 1s the mode curve of Power Spectral Density (PSD) closely tracks the New Low Noise Model (NLNM) *(Fig.3)* and even low magnitude events should be reliably detected. There is no need to filter the signal in this frequency range and no need to add parameters in the parametric detector file.

– For the periods lower then 1s the distribution of PSD has unique model for every station depending on specific noise sources (Dimitrova, 2009). The most significant noise sources are often related to human activities at or near the Earth´s surface. In this frequency range the filter parameters of detectors are selected on the base of the corresponding station noise model *(Fig.3)*.

The output of the Real-time subsystem data processing is a daily bulletin with the hypocentral determinations. The event localizations are visualized on a map and an e-mail is sent to the list of subscribers. In case of felt (M>=2.5) or damaging earthquake on the territory of Bulgaria the NDC issues information to the government authority, mass media and broad public. The NDC in close cooperation with the Civil defense carries out macroseismic investigation in the epicentral region.

The interactive processing of the seismic event parameters and magnitude determinations are performed by manual graphic analysis of the seismogram *(Fig. 4)*. An advantage of SAS_SNDP is easy access to the automatic arrivals and waveforms collected in a disk loop with capacity more than 365 days. Additional advantage of the subsystem is the ability to operate with the waveforms for rapid manual relocation of the events in time interval close to real time.

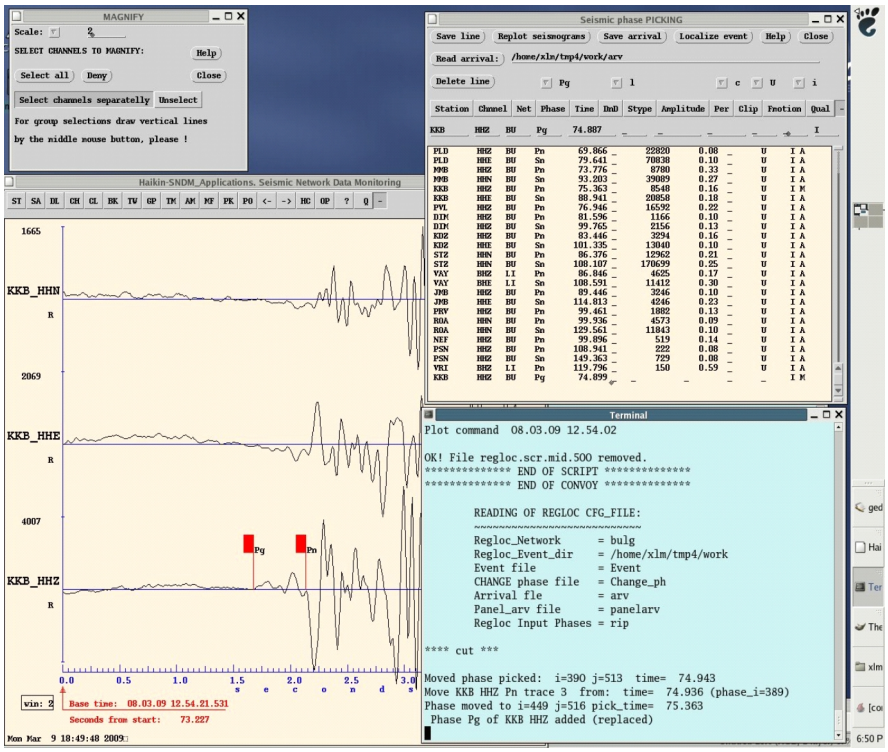

Fig. 4. Interactive data processing by means of Seismic analysis subsystem – SAS_SNDP - tuning of the seismic phase parameters

The Early warning subsystem provides messages on the based of first arrived P-phases within 5 to 8 seconds. An alarm module is switched on and the epicenter of the strong event is visualized on a map.

Some extra modules for network command/control, state-of-health network monitoring and data archiving are running as well in the National Data Centre. Three types of archives are produced in the NDC - two continuous - miniSEED format and RefTek PASSCALI format; and one event oriented in CSS3.0 scheme format.

CONCLUSIONS

Modern seismological equipment installed at Bulgarian seismic stations, carefully selected and developed software packages for data processing proved to be suitable choice for the purposes of BNDSN and NDC. Currently, the NDC and BNDSN allow reliable automatic localization of magnitude

events ML>=1.5 within the network, and ML>=2.5 at regional distances.

Presently BNDSN is a world-class broadband digital network providing reliable, high quality real-time seismic monitoring and rapid earthquake information to both scientific communities and authorities in Bulgaria and international community for seismic hazard mitigation and research.

Acknowledgements: The modernization of the BNDSN was carried out within the projects: Decision SB - 3/04.05.2005 of Permanent Commission for Prevention of the Population from Natural Disasters, Technological Accidents and Catastrophes (PCPNDTAC), Bulgaria,
Contract N IKI -11/01.09.2005 with Bulgarian National Science Fund, Ministry of Education and Science: "Environmental Monitoring Implement for Risk Assessment of natural and man-made hazard (EMIRA)".

References:

Dimitrova L., (2009). Noise level on selected digital stations of the National Operative Teleseismic System for Seismic Information (NOTSSI). *Comptes rendus de l'Academie bulgare des Sciences.* Vol 62, No4, pp 515-520.

Haikin, L. and A. Kushnir, (2005). Seismic Network Data Processor (SNDP) - Comprehensive Software for UNIX Networks. *SYNAPSE Science Center*, pp. 122.

Haikin L., L. Begun and M. Morskov, (2009). Haikin-SNDM-Applications. Seismic Network Data Monitoring.Comprehensive Software for UNIX Networks. *Introductory Software manual*. Version 2.0.

EARTHQUAKE ARCHAEOLOLOGY

INQUA PALEOSEISMOLOGY AND ACTIVE TECTONICS

VERIFICATION OF SEISMIC SCENARIO USING HISTORICAL DATA-CASE STUDY FOR THE CITY OF PLOVDIV

Solakov, Dimcho(1), Stela Simeonova(1), Irena Alexandrova(1), Petya Trifonova(1), Metodi Metodiev(1)

(1) National Institute of Geophysics, Geodesy and Geography-BAS, Acad. G. Bonchev Str., Bl.3, Sofia 1113, BULGARIA. Email: solakov@geophys.bas.bg

Abstract (Verification of seismic scenario using historical data-case study for the city of Plovdiv): *The territory of Bulgaria represents a typical example of high seismic risk area. Over the centuries, Bulgaria has experienced strong earthquakes.*
The main purpose of this work is to compare the calculated and observed intensity values and to judge if they are meaningful and can be used to "validate" forecasting scenario. To make this, a test scenario for the city of Plovdiv is generated and the obtained intensity values are compared to the observed data from real earthquakes.
Plovdiv is the second-largest city in Bulgaria with a population of about 400 000. It is situated in the southern part of the country along the Maritsa River valley. History of the city of Plovdiv spans some 6000 years, with traces of a Neolithic settlement dating to roughly 4000 BC. The earthquakes that mainly influence the hazard for Plovdiv originate near the city. The intensity assessments used for verification are from the 1928 earthquakes (on April 14th, M=6.8 and the earthquake on April 18th , 1928, M =7.0).

Key words*: earthquake, seismic scenario, Bulgaria*

INTRODUCTION

Earthquakes are the most deadly of the natural disasters affecting the human environment; indeed catastrophic earthquakes have marked the whole human history. Global seismic hazard and vulnerability to earthquakes are increasing steadily as urbanization and development occupy more areas that are prone to effects of strong earthquakes. Additionally, the uncontrolled growth of mega cities in highly seismic areas around the world is often associated with the construction of seismically unsafe buildings and infrastructures, and undertaken with an insufficient knowledge of the regional seismicity peculiarities and seismic hazard. The assessment of seismic hazard and generation of earthquake scenarios is the first link in the prevention chain and the first step in the evaluation of the seismic risk. The implementation of the earthquake scenarios into the policies for seismic risk reduction will allow focusing on the prevention of earthquake effects rather than on intervention following the disasters.

The territory of Bulgaria (situated in the eastern part of the Balkan Peninsula) represents a typical example of high seismic risk area (Fig. 1). Over the centuries, Bulgaria has experienced strong earthquakes (Shebalin et al., 1974). At the beginning of the 20-the century (from 1901 to 1928) five earthquakes with magnitude larger than or equal to M_S=7.0 occurred in Bulgaria (Boncev et al., 1982). However, no such large earthquakes occurred in Bulgaria since 1928 (Solakov, Simeonova, 1993), which may induce non-professionals to underestimate the earthquake risk. The 1986 earthquake of magnitude M_S=5.7 occurred in the central northern Bulgaria (near the town of Strazhitsa, studied in Oncescu et al., 1990) is the strongest quake after 1928. Moreover, the seismicity of the neighboring countries, like Greece, Turkey, former Yugoslavia and Romania (especially Vrancea-Romania intermediate earthquakes), influences the seismic hazard in Bulgaria (Simeonova et al., 2006).

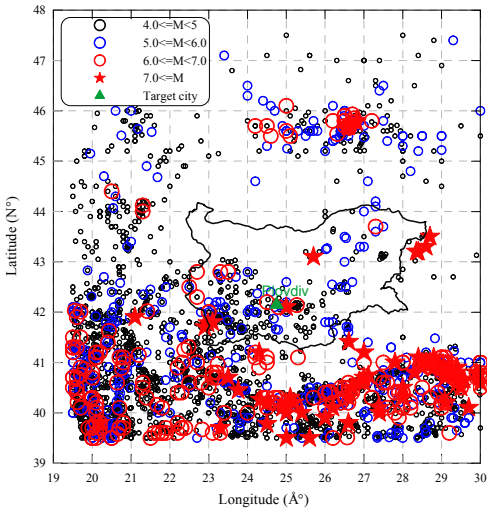

Fig. 1 Seismicity in and near Bulgaria (M_S≥4.0)

In the present study deterministic scenario (expressed in seismic intensity) for the city of Plovdiv is presented. The work on scenarios was guided by the perception that usable and realistic (also in the sense of being compatible with seismic histories of cities that are several centuries long) ground motion maps had to be produced for urban areas. By deterministic scenario it is mean a representation of the severity of ground shaking over an urban area,

using one or more hazard descriptors. Such representation can be obtained: - either from the assumption of a “reference earthquake” specified by a magnitude or an epicentral intensity, associated to a particular earthquake source - or, directly, showing values of local macroseimic intensity generated by a damaging, real earthquakes of the past (Report, GFI and CLSMEE, 2002).

The first consideration in this work is weather comparison between calculated and observed intensity values are meaningful and if they can be used to “validate” forecasting scenario. To make this test scenario for the city of Plovdiv is generated and the estimated intensity values are compared to the observed data from real destructive earthquake in the past.

EARTHQUAKE SCENARIO FOR THE CITY OF PLOVDIV

The Bulgarian city of Plovdiv is located in the Southern/Central part of Bulgaria. Being the second largest city in the country, it has a population of about 400 000. Plovdiv is situated along the two banks of the river Maritsa with its slow water, and also on a number of picturesque hills (called “tepe” by the local people) that are part of the town's charm and beauty. The city has historically developed on seven syenite hills, some of which are 250 m high. Because of these seven hills, Plovdiv is often referred to in Bulgaria as "The City of the Seven Hills.

a)

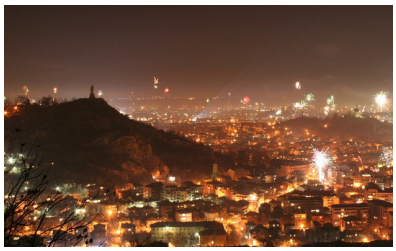

b)

c)

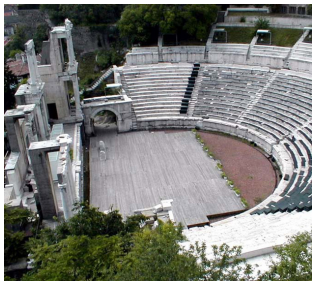

Fig. 2 The city of Plovdiv: a) now; b) in 19th century; c) in ancient time

History of the city of Plovdiv spans some 6,000 years (Fig. 2), with traces of a Neolithic settlement dating to roughly 4000 BC. In 4th century BC the city was a centre of a trade fair (called *panegyreis*). In 342 BC, it was conquered by Philip II of Macedon, the father of Alexander the Great, who renamed it "Φιλιππόπολις", *Philippopolis* or "the city of Philip" in his own honour. Later, it was reconquered by the Thracians who called it *Pulpudeva*, and was the largest and most important city in Northern Thrace. It gained a city status in late 1st century AD. Although it was not the capital of the Province of Thrace, the city was the largest and most important centre in the province. In the Middle Ages, it retained its strategic regional importance, changing hands between the Byzantine and Bulgarian Empires. It came under Ottoman rule in the 14th century. In 1878, Plovdiv was made the capital of the autonomous Ottoman region of Eastern Rumelia; in 1885, it became part of Bulgaria with the unification of that region and the Principality of Bulgaria.

At present Plovdiv is one of the most populated industrial and cultural regions of Bulgaria that faces considerable earthquake risk. The earthquakes that mainly influence the hazard in Plovdiv originate near the city. The contemporary tectonic activity of the area is associated with Maritsa fault system with WNW-ESE direction. The Maritsa fault with its satellites belongs to structures with a longlasting development, which continues in the neotectonic period. The oblique Maritsa Fault striking N 116º, and the dipping towards N is of length of about 36 km. Significant slip rate during the neotectonic stage. It is known with the surface rupturing during the M = 7.0 earthquake of 18 of April 1928 (Yankov, 1935). The strongest earthquakes occurred on the fault system are those in 1928 (the Chirpan earthquake of April 14, 1928 with M =6.8 and the Plovdiv earthquake of April 18, 1928 with M =7.0, I = 9-10 MSK). The 1928 earthquakes completely destroyed 74000 buildings in the towns of Plovdiv, Chirpan and Parvomay (Kirov, 1945). Some of the damages in the city of Plovdiv are presented in Fig.3.

Fig. 3 Damages in the city of Plovdiv caused by the 1928 Maritsa earthquakes.

APPROACH USED FOR DEVELOPING EARTHQUAKE SCENARIO:

The approach adopted for developing ground motion hazard maps (earthquake scenarios) includes the following stages (Report, GFI and CLSMEE, 2002):

1. Compilation of regional seismotectonic data base (region with in a radius of 150 km surrounding the considered urban area);
2. Analysis of regional seismotectonics (identification of the tectonic feature(s) capable of generating the scenario earthquake with the associated magnitude level, and representation of seismic sources for the different methods of analysis .
3. Seismo-tectonic zonation, the aim of which is to highlight the relationships between seismicity and active geological structures;
4. Geotechnical characterization of the studied urban area;
5. Seismic hazard assessment.

Base of seismic history of the city of Plovdiv the 1928 earthquake (I=9-10 MSK) was considered as responsible of the macroseismic intensity scenario.

The "reference earthquake" with magnitude value of M_S=7.0 and maximum macroseismic intensity 9-10 MSK was used for intensity hazard scenario. The simplified source representation is adopted that consists of WNW-ESE trending (striking N 116°), normal fault at a minimum distance of 20 km from the center of the city.

The intensity map was created using the generalized macroseismic model for earthquakes on the territory of Bulgaria presented in Glavcheva et al. (1982, 1983). The intensity isoseismal is approximated to an ellipse in the modelling. The ellipse is defined by the following equations:

$$\text{Lg } Q(I, M) = c(I)*M + d(I)$$

$$\text{Lg}(a*b^2) = c_1(I)*M + d_1(I)$$

$$\text{Lg}(b^2/a) = c_2(I)*M + d_2(I)$$

where M-earthquake magnitude; I- macroseismic intensity; Q-size of an ellipse at a fixed I; *a* and *b*-semi-axes of an ellipse at a fixed I; c, c_i, d, d_i– empirical coefficients (i=1,2) coefficients were determined on the based of historical data for earthquakes in and near Bulgaria by using the least square method.

The intensity scenario map is presented in Fig. 4. It is accepted that the scenario map is generated for middle soil conditions-stiff soils and an increment in intensity of +/-0.5 degrees is applied for rock and soft soils respectively. The soil properties of the urban area were incorporated in the scenario generation by using a simplified geotechnical map for the city of Plovdiv. The intensity values range between 7.5 and more than 9 (MSK) and although a general decreasing trend with increasing distance from the source is obvious, a certain complexity in the spatial distribution arises because of the influence of soil conditions (as for example the amplification in the northern part of the city).

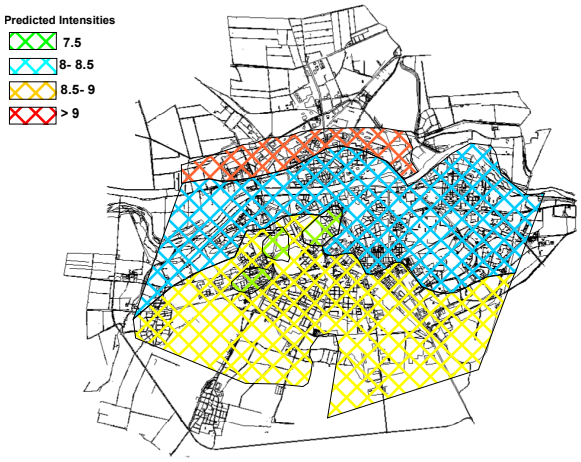

Fig. 4 Scenario map of the predicted intensity value (Ip - in MSK intensity scale) for the city of Plovdiv

The second deterministic scenario based on observed macroseismic effects caused by the 1928 earthquakes is illustrated in Fig.5

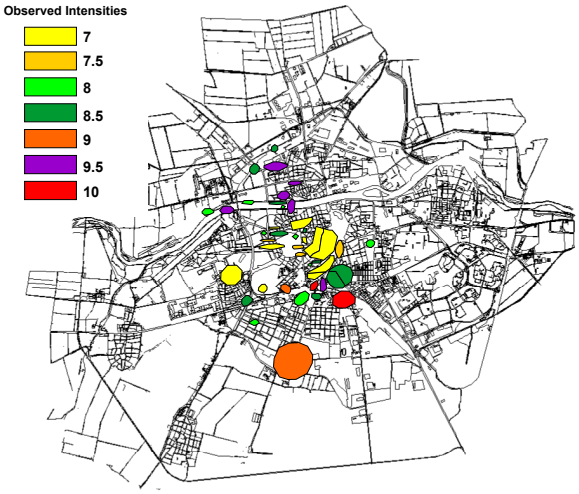

Fig. 5 Observed macroseismic effects (I_o- in MSK intensity scale) for the city of Plovdiv caused by the 1928 (M=7.0) earthquake

The generation of intensity scenario use directly the intensity assessment of the strongest past earthquake (the 1928 quake with M=7.0) damaged the city. Distribution of macroseismic effects along the city is estimated on the base of descriptions, documents and analyses presented in DIPOZE (1931).

The scenario map illustrates the distribution of the maximum values of macroseismic intensity (MSK) along the central part of the city of Plovdiv (at the beginning of the 20th the size or the urban area was much less the present one) generated by 1928 earthquakes.

For a comparison difference between observed (I_o) and predicted (I_p) intensities is illustrated in Fig. 6.

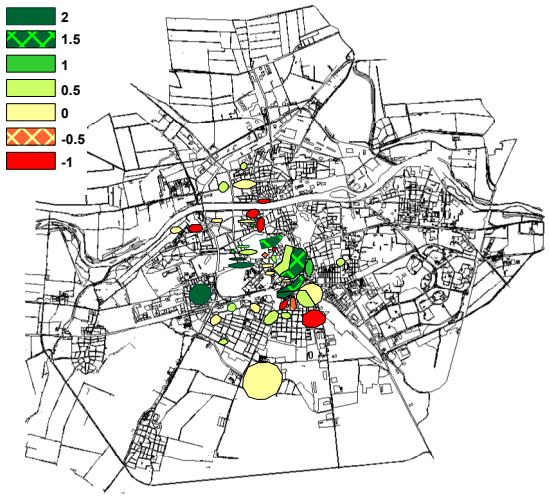

Fig. 6 Comparison between predicted and observed intensity values for the city of Plovdiv

The results indicate a relatively good coincidence of the predicted and observed intensity values. The difference values are varying between -1 and + 2. The maximum difference (I_o-I_p)=2 - underestimation) between I_o and I_p is identified in two small dark green areas in the central and western part of the city (Fig.6). Higher observed than predicted intensity values could be considered as design and building problems (according to the analysis presented in DIPOZE, 1931). The maximum negative values (I_o-I_p=-1 – overestimation) are spread over the city (red sports in Fig.6). These overestimated predicted values could be related to the specific soil conditions (detail soil properties could not inferred from the schematic geotechnical map for the urban we have used in the analysis).

CONCLUSIONS

From our analysis it can be concluded that:

1. The generated intensity scenario map is reliable and can be used for developing risk scenario, for risk and engineering decisions, in infrastructure planning and insurance.
2. The earthquake scenario for the city of Plovdiv will be improved if a more accurate geotechnical map is obtained.
3. A archaeo-seismological survey of the region will be an useful tool for further studies in seismology.

Acknowledgements: The financial support for presenting this work was provided by a project co-financed by the European Social Fund of EU under grant BG051PO001-3.3.04-33.

References

Boncev E., V.Bune, L.Christoskov, J.Karagjuleva, V.Kostadinov, G.Reisner, S.Rizhikova, N.Shebalin, V.Sholpo, D.Sokerova, 1982. A method for compilation of seismic zoning prognostic maps for

DIPOZE, 1931. Report for post earthquake activities that were undertaken in the time interval April 1928 - November 1931. State Press, Sofia, pp 421 (in Bulgarian).

Glavcheva R., S. Simeonova, D. Solakov, 1982. A generalized macroseismic model of the high intensities fields for Bulgaria. B.G.J.,8, 3,77-83.

Glacheva, R., S. Simeonova, Tz. Hristova, D. Solakov, 1983. Generalized Isoseismals of the High Intensities for Earthquakes in Bulgaria. *B. G. J.*, 9, 3, 69-77.

Kirov, K, 1945. Tremblements de terre en Bulgarie 29-32. Liste des tremblements de terre ressentis pendant les annees 1928-1930. Inst. Meteorol. Sentr. De Bulgarie, S. pp 140. (in Bulgarian and abstract in French)

Oncescu M., C.Trifu, C.Hristova, S.Simeonova, D.Solakov, 1990. A detailed analysis of the Strazhitza (Bulgaria) seismic sequences of 1986: location, focal mechanism and regional stress tensor, Tectonophys, 172, 121-134.

Report, GFI and CLSMEE, 2002.WP2 Seismic hazard assessment and ground motion scenarios for the city of SOFIA, Contract: EVK4-CT-2000-00014.

Shebalin, N., V. Karnik and D. Hadzievski (Editors), 1974. Catalogue of Earthquakes, Part I and Part II, UNDP/UNESCO Survey of the seismicity of the Balkan region, Skopje, pp 600.

Simeonova S. D., D. E. Solakov , G. Leydecker , H. Busche , T. Schmitt , D. Kaiser , 2006, Probabilistic seismic hazard map for Bulgaria as a basis for a new building code. Nat. Hazards Earth System Sciences, 6, 881–887.

Solakov, D., S. Simeonova (Editors), 1993. Bulgaria Catalogue of Earthquakes 1981-1990, BAS, Geoph.Inst., Seism.Dep., Sofia, pp 39.

Yankov, Y., 1935. Regional deformations caused by the 14 and 18 April 1928 earthquakes. Earthquakes in Bulgaria No.20-21, Centr. Meteorol. Stat., Imprimerie de l'Etat, Sofia, pp 93. (in Bulgarian and French).

PALEOSEISMIC STUDY OF THE SUDETIC MARGINAL FAULT AT THE LOCALITY BÍLÁ VODA (BOHEMIAN MASSIF)

Štěpančíková Petra (1), Nývlt Daniel (2), Hók Jozef (3), Dohnal Jiří (4)

(1). Dpt. Engineering, Institute of Rock Structure and Mechanics, Academy of Sciences of the Czech Republic, V Holešovičkách 41, 182 09 Prague 8.CZECH REPUBLIC. E-mail: stepancikova@irsm.cas.cz
(2). Czech Geological Survey, Brno Branch, Leitnerova 22, 658 69 Brno, CZECH REPUBLIC, E-mail: daniel.nyvlt@geology.cz
(3). Dpt. Geology and Paleontology, Faculty of Natural Sciences, Comenius University in Bratislava, Mlynská dolina, 842 15 Bratislava 4, SLOVAKIA, E-mail: hok@fns.uniba.sk
(4). Faculty of Sciences, Charles University in Prague, Inst. Hydrogeology, Engineering Geology and Applied Geophysics, Prague Albertov 6, Prague 2, 128 43, CZECH REPUBLIC, E-mail: dohnalj@natur.cuni.cz

Abstract (Paleoseismic study of the Sudetic Marginal Fault at the locality Bílá Voda (Bohemian massif): *The study area is situated in the north-eastern part of the Bohemian Massif and comprises SE part of the Sudetic Marginal Fault zone (SMF) with pronounced mountain front, which borders the Sudeten Mts. Paleoseismological trenches at the locality of Bílá Voda municipality performed across the SMF were carried out in order to study potential prehistoric morphogenic earthquakes responsible for the present-day morphology. Geomorphologic analysis and electrical resistivity tomography enabled to position the trenches at suitable site. The trenches revealed prevailing strike-slip character of the late Quaternary faulting. Faulted deposits were dated by OSL and radiocarbon dating methods and the results are discussed here. At least four or five events creating a surface rupture during late Quaternary (Holocene) were inferred. Due to strike-slip character, the horizontal displacement and the related slip-rate on the SMF is still under investigation. From the previous study, minimum magnitude **M** 6.3 is expected for the SMF.*

Key words*: active tectonics, trenching, paleoseismology, Sudetic Marginal Fault*

The study area is situated in the north-eastern limit of the Bohemian Massif in the Czech Republic (central Europe). The studied Sudetic Marginal Fault (SMF) is a part of the Elbe Fault System, which comprises WNW-striking zone from SE North Sea to the front of Outer Carpathian nappes and disrupts the Variscan central Europe at the length of several hundreds of kilometers. The SMF is about 200km long and divides the Variscan Sudetic Mountains block from upland-like Fore-Sudetic block hosting Cenozoic cover. For a length of 130, km it controls the pronounced mountain front of the Sudetic Mountains (Fig. 1).

Quaternary activity of the fault has been demonstrated e.g. by Middle and Upper Pleistocene fluvial terraces that are truncated by the SMF and expressed by 5 - 20 m high scarp in their longitudinal profiles in the Polish portion of the fault (e.g. Krzyszkowski et al., 1995). Local historic earthquakes recorded within the SMF had epicentral intensity estimated to reach only I_0=4 -7 (MSK), which would correspond to macroseismic magnitude M_M=3-4.9 (Guterch and Lewandowska-Marciniak, 2002). They include the events from years 1594 and 1778 (Zlotoryja/Legnica), and 1615 and 1786 near Bardo/Dzierżoniźów. Other historic earthquakes with

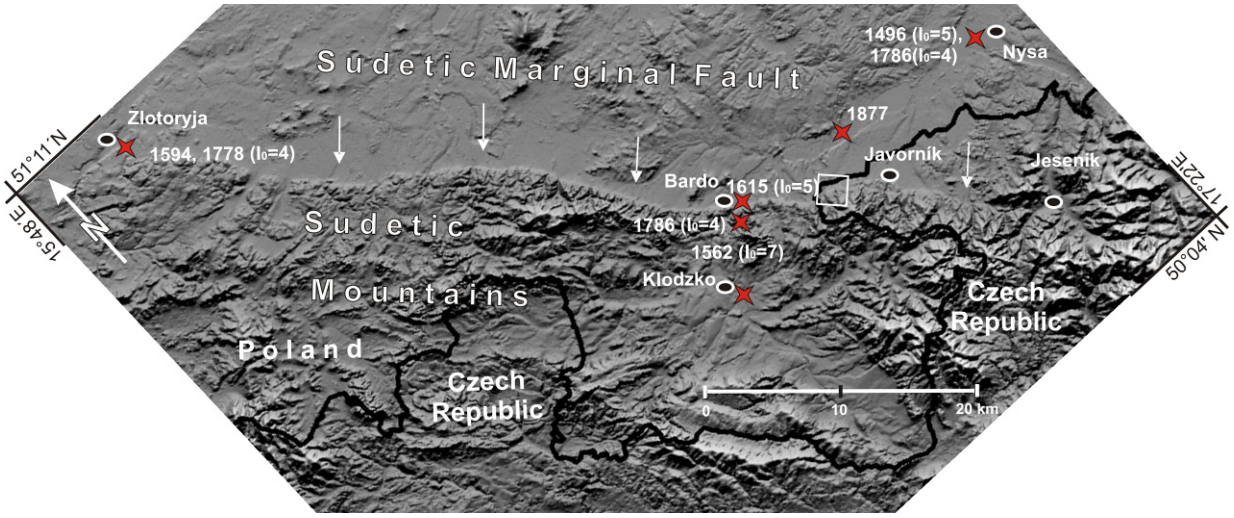

Fig. 1. Digital elevation model of the morphologically distinctive Sudetic Marginal Fault (SMF) that controls the Sudetic Mountains front. Red stars - historic earthquakes, I_0= epicentral intensity; white square – study area.

more distant epicentres or those being felt in the zone parallel to the SMF (*Fig. 1*) include events in 1496, 1562, 1786, 1823, 1877, and 1895 (Kárník et al., 1958; Olczak, 1962; Pagaczewski, 1972; Guterch and Lewandowska-Marciniak, 2002).

As the historic earthquakes were not large enough to create the morphology (I_0=4-7 MSK; cf. Guerrieri and Vittori, 2007), the study of potential presence of larger prehistoric earthquakes responsible for the growth of the mountain front was carried out. This paper presents results from investigation of the mountain front at the locality Bílá Voda municipality (Czech Republic). The results from three parallel trenches (C, D, F) performed across the SMF are discussed here.

In order to determine the position of the fault for the following trenching, electric resistivity tomography with electrode spacing 2 m was performed (*Fig. 2*). The fault appeared to be expressed by the presence of a remarkable resistivity gradient, which divided high-resistivity of anticipated metamorphic rocks on the footwall and low-resistivity of Miocene deposits on the hanging-wall (Štěpančíková et al., 2011). This was confirmed in the trenches C, D, F (Fig 2b). All the trenches revealed a subvertical fault zone striking 135°-150° dividing Paleozoic crystalline rocks (phyllites, schists, granitic aplite) and late Quaternary colluvial deposits overlaying warped Miocene sediments. The SMF has been generally considered as a normal fault having experienced inversion during Late Cretaceous/Paleogene and extensional reactivation since Miocene during Alpine cycle (c.f. Badura et al., 2007). Nevertheless, our trenches revealed that the movements on the fault, at least the youngest ones, had very probably prevailing strike-slip character. The strike-slip on the main marginal fault with strike and dip of 135°/75°NE is suggested by a flower structure within the 4-m wide zone of tectonic breccia and fault gouge displayed both on the trench walls and on the floor, and by completely different lithologies on the both sides without any matching points.

The down-thrown block is composed by Miocene (unit A; *Fig 3),* strongly kaolinised clayey silty sand with a small pebble admixture of local lithology. The clay originated by chemical weathering of feldspars and granite groundmass. These sediments may be correlated with Member C described few km to the SE by Štěpančíková et al. (2010) and interpreted as to be deposited in a fluvio-limnic environment during the Carpatian and lower Badenian (i.e. early to mid Miocene, ~18–15 Ma). These deposits are upwarped, which was indicated also by preceding ERT profiles (see *Fig 2*), and covered by colluvial deposits (unit B). The colluvial deposits represent matrix-supported intermediate to sandy diamicts with gravel clast content between 5 and 25% and sandy to silty matrix. Largest clasts are up to 20–25 cm and are made of angular to subangular gneiss clasts, granodiorite and quartz clasts. The colluvial sediments have a sharp erosional base and their lowermost part is enriched by Mn oxides as a result of manganese precipitation from percolating water just above the impermeable Miocene clayey sand.

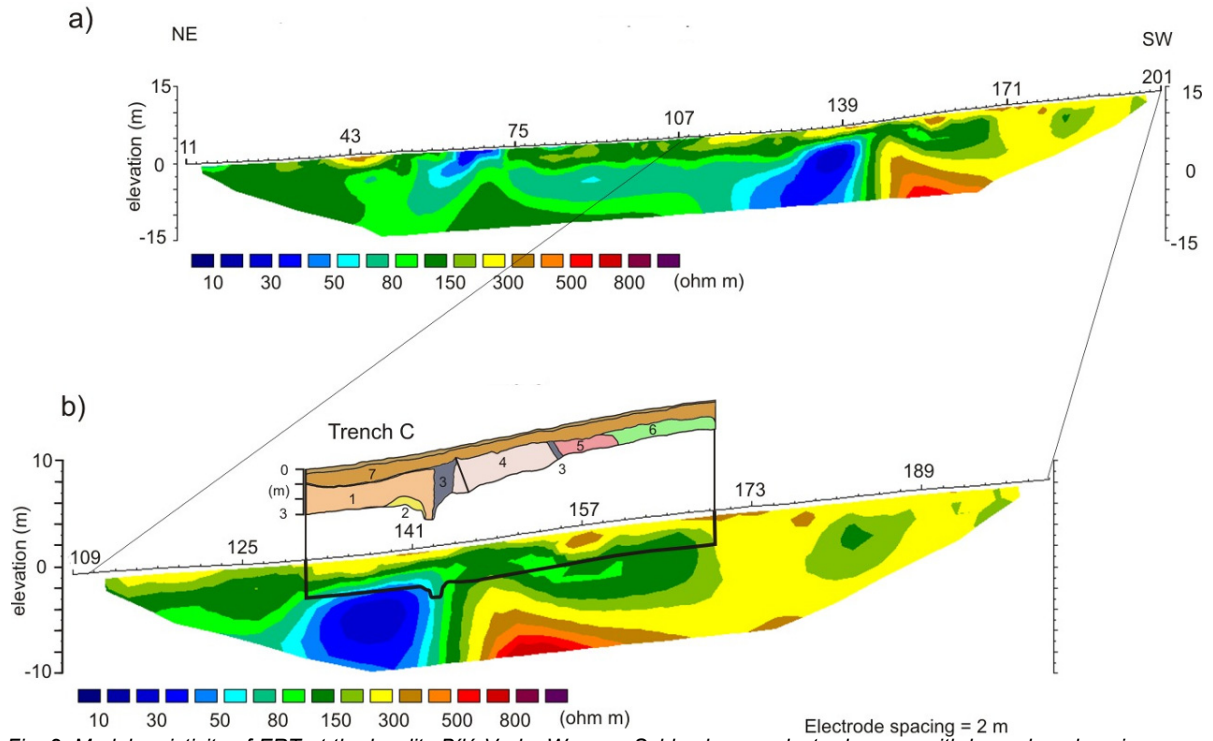

Fig. 2. Model resistivity of ERT at the locality Bílá Voda, Wenner–Schlumberger electrode array with logged geology in Trench C. a) Resistivity in ohm m; vertical exaggeration=1; iteration 3; RMS error=2.3%. The SMF lies within the expressive resistivity gradient between Stations 143 and 145. b) Geology in the trench 1 – Late Quaternary colluvium; 2 – Miocene lacustrine deposits, 3 – fault zone with tectonic breccia and fault gauge, 4 – micashists, 5 – granitic aplite, 6 – gneisses, 7 – Late Holocene colluvium.

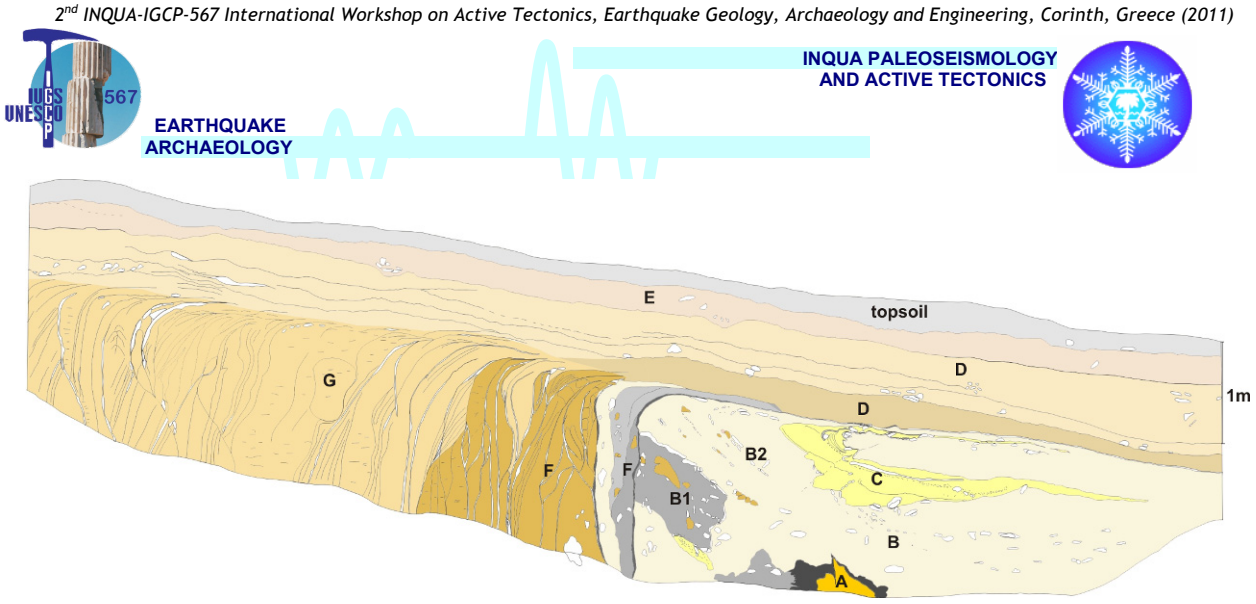

Fig. 3. Log of the trench F. See text for explanation of units A to E. Unit F – fault zone with tectonic breccia, G – metamorphic rocks.

The colluvium close to the fault is obviously fault-related and is interpreted to be derived from the fault scarp created after an earthquake (c.f. McCalpin, 2009); it includes material from the fault zone and particularly clasts of the fault breccia. Although the colluvium does not display completely clear discrete sedimentological units that could be ascribed to individual events, there are some indications; in trench F (*Fig 3*), the part of colluvium that includes blackish matrix with breccia clasts have wedge shape (B1) and seems to be covered by another wedge-shaped colluvial unit (B2), which includes the fault rocks at lesser amount. This would indicate at least two faulting events, which resulted in the origin of the colluvial wedges. This fault-related colluvium is then covered by 35–40 cm thick beige to grey lens composed of beds of slightly clayey silt, sand and granule (unit C). They bear a very fine lamination, especially in silty layers. The upper part of the lens is dominated by bands of Mn and Fe oxides, which percolate fine to medium sand with some granule clasts. The sedimentary body is fault-parallel oriented and it was very probably a small pool emerging in front of the fault scarp. After its deposition the lens were tilted and displaced by minor faults (*Fig 4*), which displayed various sense of movement on the both walls of trench F. In trench C the deposit is only tilted. This must have been a result of another younger faulting (3rd event). Unfortunately, no pollen or macro-remains were found within the silty sediment and only residual sediment carbon was dated by AMS ^{14}C dating.

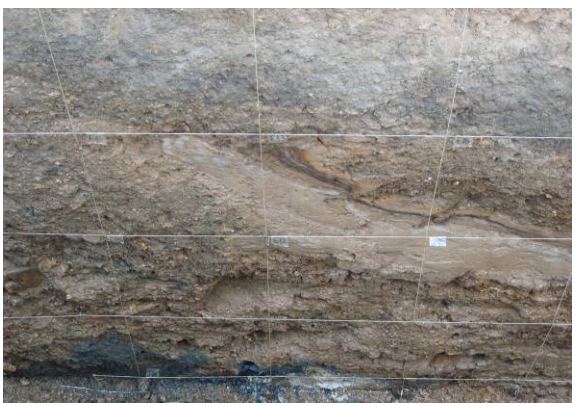

Fig. 4. Tilted and displaced unit C - lens composed of beds of clayey silt, sand and granule; trench F.

We have a set of 3 OSL dates from this colluvial unit ranging from 25.8 ± 1.6 ka to 9.5 ± 0.9 ka. We accept only the youngest one as reliable age, because the age corresponds to ~1 m long lens of sorted sand, which imply better zeroing before burial of this material. The older dates are probably influenced by residual signal. This is supported by 2 radiocarbon dates (all radiocarbon ages given here are calibrated ages using IntCal09 calibration dataset; Reimer et al., 2009) falling into the early Holocene – 7,997 ± 23 a and 6,433 ± 29 a. Both ages originate from residual sediment carbon, as no plant macro-remains were found in this unit. The exact age may therefore be slightly older than the ages given above.

The above-mentioned fault-derived colluvium is then cut by the youngest faults of the flower structure, which would indicate the following (4th) faulting event unless it was simultaneous with the deformation of the silty lens (3rd event), which is ambiguous. Both the colluvium (incl. the silty lens) and the fault zone is sealed by banded layers due to superficial flow processes (unit D). They create individual bands 3 to 10 cm thick, which continue >5 m downhill. The thickness of bands is much smaller, than it was described in other trenches studied along the Sudetic Marginal Fault at Vlčice (Štěpančíková et al., 2010), where up to 20 cm thick layers were interpreted to be deposited by a sheet gelifluction and ascribed to the Late Glacial, which was also supported by radiocarbon dating. So, the banded layers here in Bílá Voda were considered to be of similar origin and age, i.e. from Late Glacial, which would have important implication for inferring the age of the faulting (c.f. Štěpančíková et al., 2009, 2011). However, new data on both OSL and radiocarbon age of the banded layers here give similar ages of 2.6 ± 1.2 ka and 2,610 ± 108 a respectively. The thickness and dating of the layers here may show on the frost creeping of this material, which does not imply flow processes connected with seasonal thawing of the active permafrost layer, which was not present here during the Holocene. Frequent and

usually rapid diurnal frost creep processes may affect the superficial layer typically 5–10 cm thick even at the warm margin of the solifluction-affected environment (Matsuoka, 2001). Therefore, the presence of these processes at low altitude as here (~360 m) during the Holocene is feasible.

In trench C on the footwall, these banded layers display around 35cm high step just coinciding with minor faults with opposite dip. These faults also do not show any displaced matching points, so horizontal movements with minor reverse component might be inferred here. On the hanging wall, these banded layers are slightly up-warped, which might have been related to a transpression responsible for the above–described step in the banded layers. This would imply another, potentially 5th or 4th event.

The banded layers are covered by late Holocene colluvial deposits usually 0.5 to 1.5 m thick (unit E). These are matrix-supported, with the matrix composed predominantly of sandy fraction originating from the weathering of local Javorník granodiorite, which is mixed with silt and mostly pebble to fine cobble clasts. Gravel clast typically first cm large are mostly subangular to less subrounded and are made of Javorník granodiorite, quartz, (ortho)gneiss and schist, rather rare are clast of Nordics (originating from tills and glaciofluvial deposits left here by Pleistocene ice sheets; Nývlt et al., 2011) and pieces of bricks pointing to young age. Radiocarbon dates of charcoals from these young Holocene colluvial deposits range from 1,145 ± 89 a to 757 ± 30 a. On the top of these colluvia a cambisol type of recent soil is developed with 25–30 cm thick light grey-brown A-horizon with ploughed erosional base.

To summarize, the results from the trenches at the Bílá Voda locality show potentially four to five movements on the SMF during late Quaternary (Holocene). Due to lack of kinematic indicators in the trenches perpendicular to prevailing movements, the sense of the strike-slip is still under investigation. Since the perpendicular trenches across strike-slips do not show the amount of horizontal slip, also slip-rate could not be assessed with reasonable confidence. Nevertheless, based on the previous trenching (Štěpančíková et al., 2010), according to empirical relationship 'magnitude versus maximum vertical displacement' (Wells and Coppersmith, 1994), the minimum moment magnitude **M** 6.3 is expected on the SMF.

Acknowledgements: The research was supported by the Grant Agency of the Czech Republic No. Czech Science Foundation No. 205/08/P521. The work has been elaborated within the Institute Research Plan of the Institute of Rock Structure and Mechanics, Academy of Sciences of the Czech Republic, No. AVOZ30460519.

References

Badura, J., Zuchiewicz,W., Štěpančíková, P., Przybylski, B., Kontny, B., Cacoń, S., (2007). The Sudetic Marginal Fault: a young morphotectonic feature at the NE margin of the Bohemian Massif, Central Europe. *Acta Geodynamica et Geomaterialia* 4 (148), 7–29.

Guerrieri, L., Vittori, E. (Eds). (2007). Intensity scale ESI 2007. Mem. Descr. Carta Geologica d´Italia, 74, Servizio Geologico d´Italia – Dipartimento Difesa del Suolo, APAT, Rome, Italy, 41pp.

Guterch, B., Lewandowska-Marciniak, H., (2002). Seismicity and seismic hazard in Poland. *Folia Quaternaria* 73, 85–99.

Kárník, V., Michal, E., Molnár, A., (1958). Erdbebenkatalog der Tschechoslowakei bis zum Jahre 1956. Geofysikální Sborník 69, 411–598.

Krzyszkowski, D., Migoń, P., Sroka, W., (1995). Neotectonic Quaternary history of the Sudetic Marginal fault, SW Poland. *Folia Quaternaria* 66, 73–98.

Matsuoka, N., (2001). Solifluction rates, processes and landforms: a global review. *Earth-Science Reviews* 55, 107–134.

McCalpin, J. (Ed.) (2009). *Paleoseismology*. Second Edition. Academic Press. 613 pp.

Nývlt, D., Engel, Z., Tyráček, J., (2011). Pleistocene Glaciations of Czechia. In: Ehlers, J., Gibbard, P. L., Hughes, P. D., (Eds): Quaternary Glaciations – Extent and chronology, A closer look. *Developments in Quaternary Science* 15, 37–46, Elsevier.

Olczak, T., (1962). Seismiczność Polski w okresie 1901–1950. *Acta Geophysica Polonica* 10, 3–11.

Pagaczewski, J., (1972). Catalogue of Earthquakes in Poland in 1000–1970 years. *Mat. I Prace Inst. Geofiz.*, vol. 51. 36 pp.

Reimer, P.J., Baillie, M.G.L., Bard, E., Bayliss, A., Beck, J.W., Bertrand, C., Blackwell, P.G., Buck, C.E., Burr, G., Cutler, K.B. Damon, P.E., Edwards, R.L., Fairbanks, R.G., Friedrich, M., Guilderson, T.P., Hughen, K.A. Kromer, B. McCormac, F.G., Manning, S. Bronk Ramsey, C., Reimer, R.W., Remmele, S., Southon, J.R., Stuiver, M., Talamo, S., Taylor, F.W., van der Plicht, J., & Weyhenmeyer, C.E., (2009). Intcal09 and Marine09 Radiocarbon Age Calibration Curves 0-50,000 Years Cal BP. *Radiocarbon* 51, 1111–1150.

Štěpančíková P., Dohnal J., Pánek T., Łój M., Smolková V., Šilhán K., (2011). The application of electrical resistivity tomography and gravimetric survey as useful tools in an active tectonics study of the Sudetic Marginal Fault (Bohemian Massif, central Europe). *Journal of Applied Geophysics* 74, 69-80.

Štěpančíková, P., Hók, J., Nývlt, D., (2009). Trenching survey on the south-eastern section of the Sudetic Marginal Fault (NE Bohemian Massif, intraplate region of central Europe). In: *Archaeoseismology and Palaeoseismology in the Alpine-Himalayan Collisional Zone* (Pérez-López, R., Grützner, C., Lario, J., Reicherter, K., Silva, P.G. eds). Baelo Claudia, Spain, 149–151.

Štěpančíková, P., Hók, J., Nývlt, D., Dohnal, J., Sýkorová, I., Stemberk, J., (2010). Active tectonics research using trenching technique on the south-eastern section of the Sudetic Marginal Fault (NE Bohemian Massif, central Europe). *Tectonophysics* 485, 269–282.

Wells, D.L., Coppersmith, K.J., (1994). Empirical relationships among magnitude, rupture length, rupture area, and surface displacement. *Bulletin of the Seismological Society of America* 82, 974–1002.

TOWARD DEVELOPMENT OF A LONG RUPTURE HISTORY OF THE IMPERIAL FAULT IN MESQUITE BASIN, IMPERIAL VALLEY, SOUTHERN CALIFORNIA

Tsang, Rebecca Y. (1), Thomas K. Rockwell (2), Aron J. Meltzner (3), Paula M. Figueiredo (4)

(1) Dept. of Geol. Sci., San Diego State University, San Diego, California 92182, U.S.A. Email: tsang.y.rebecca@gmail.com
(2) Dept. of Geol. Sci., San Diego State University, San Diego, California 92182, U.S.A. Email: trockwell@geology.sdsu.edu
(3) Earth Observatory of Singapore, Nanyang Technological University, Singapore. Email: meltzner@ntu.edu.sg
(4) IDL / FCUL - Geology Department, Lisbon University, Lisbon, Portugal. Email: pmfigueiredo@fc.ul.pt

Abstract (Toward Development of a Long Rupture History of the Imperial Fault in Mesquite Basin, Imperial Valley, Southern California): *We conducted a paleoseismic study on the northern Imperial fault at the Dogwood site in Mesquite Basin, southern California, to extend the record of late Holocene surface ruptures. New trench exposures have revealed evidence for up to 17 events in the past 1300 years, yielding an average recurrence interval of 80 years, and the large CV suggests the fault ruptures in a non-episodic manner. Our data indicate that the connection between lake and earthquake cycles is either very weak or non-existent as many of the ruptures occurred during dry periods between lakes. However, there is a strong correlation between the earthquake chronologies in the southern San Andreas fault and those on the northern Imperial fault, suggesting surface rupture at the southern portion of San Andreas fault may have triggered surface slip on the northern Imperial fault, or vice versa.*

Key words*: clustering, Imperial, paleoseismology, recurrence*

INTRODUCTION

The Imperial fault is a northwest-striking, dextral fault located in the Mesquite Basin, an area in which the seismicity patterns have been interpreted in terms of spreading and transform faulting (Sharp, 1982). The North American-Pacific plate boundary rate is approximately 45±1 mm/yr for southern California (DeMets et al., 1994). The Imperial, along with the San Jacinto and Elsinore faults, are considered as part of the San Andreas fault system and accommodate a significant proportion of the plate-boundary motion (Hill et al, 1990). The 70-km fault crosses the U.S.-Mexico Border and terminates in the south at a right stepover to the Cerro Prieto fault, and in the north at the Brawley Seismic Zone which

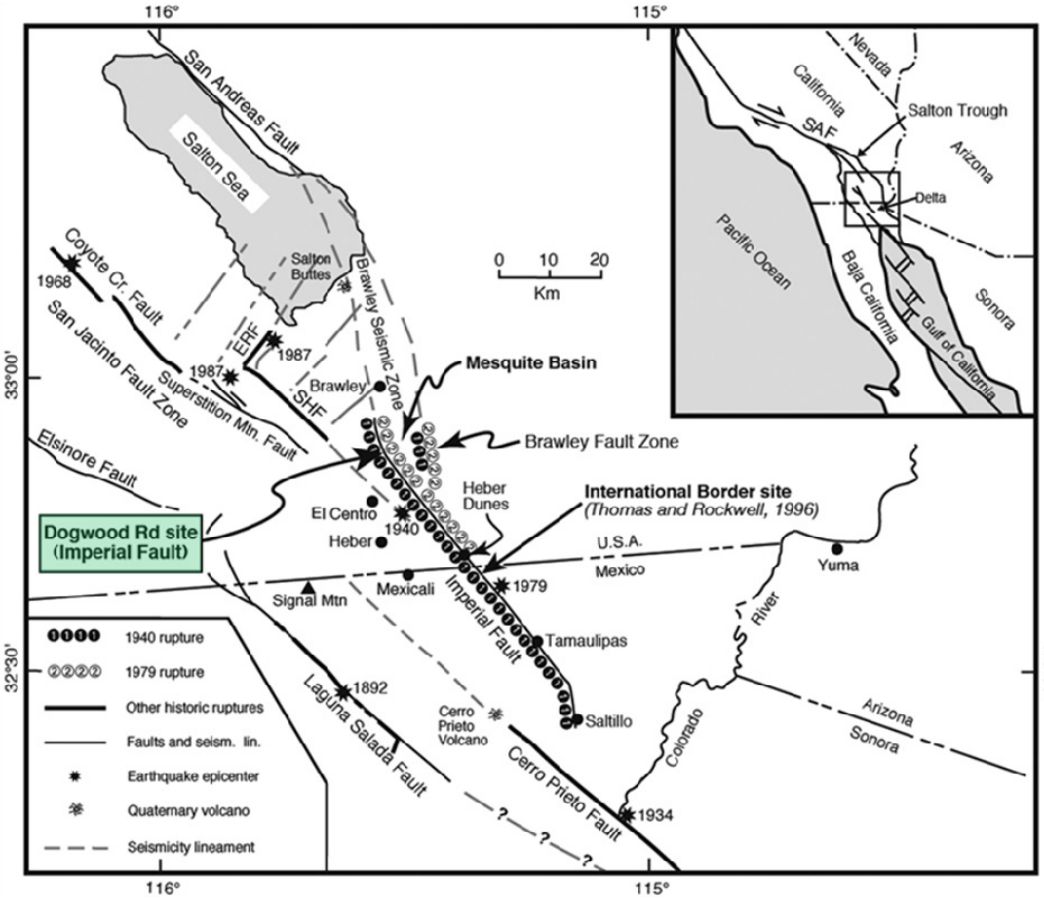

Fig. 1: Map showing the major structures and the Dogwood site in the Imperial Valley (modified from Thomas and Rockwell, 1996).

extends farther north to the Salton Sea (Figure 1). The fault was not recognized until the 1940 M_L 7.1 earthquake that was caused by an end-to-end rupture propagating mostly to the southeast (Buwalda and Richter, 1941; Richter, 1958). Thirty-nine years later, the fault ruptured again to produce a M_L 6.6 earthquake (Chavez et al, 1982). Besides surface ruptures, the area is also characterized by regular aseismic creep and high levels of microseismicity (Cohn et al., 1982; Lyons et al.,2002; Shearer, 2002).

In earlier work, we resolved the timing and displacement for the six most recent surface ruptures, all of which have occurred in the past 500 years. In this study, we conducted new paleoseismic studies on the northern Imperial fault to extend the record of late Holocene surface ruptures to better understand the behaviour of this plate boundary strike-slip fault. Twelve new trench exposures at the Dogwood site in Mesquite Basin, near El Centro, California have revealed evidence for up to 17 events in the past 1300 years.

The Dogwood Site

Our study area is located about 10 km north of Interstate Highway 8, next to Dogwood Road which makes it easily accessible (Figure 2). El Centro has an arid climate and is covered by farmland, but the lack of vegetation particularly at our site makes excavation easier. The Imperial fault at this site is expressed surficially as a single strand, which

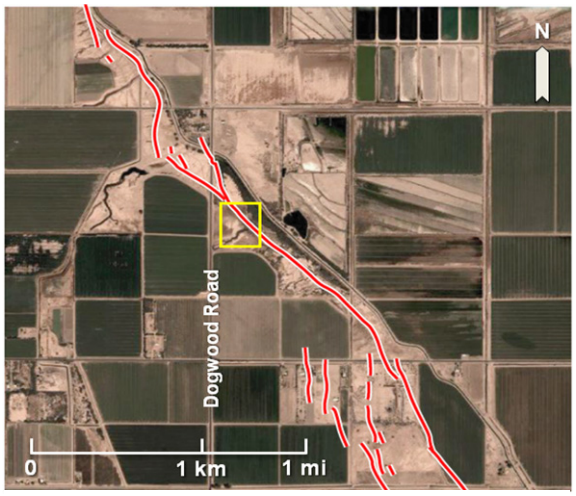

Fig. 2: Satellite image of the study area (yellow box) in the Imperial Valley, southern California.

reduces the structural complexity that might mask evidence for past surface ruptures (Figure 2). Most importantly, the Dogwood site has preserved a remarkable stratigraphy of Lake Cahuilla which is an ephemeral freshwater body formed when the floodwaters of the Colorado River intermittently filled the Salton depression during the Holocene (Sharp 1982a). This allows us to identify event horizons and to obtain ages for past surface ruptures by radiocarbon dating of detrital charcoal that was embedded within the stratigraphy.

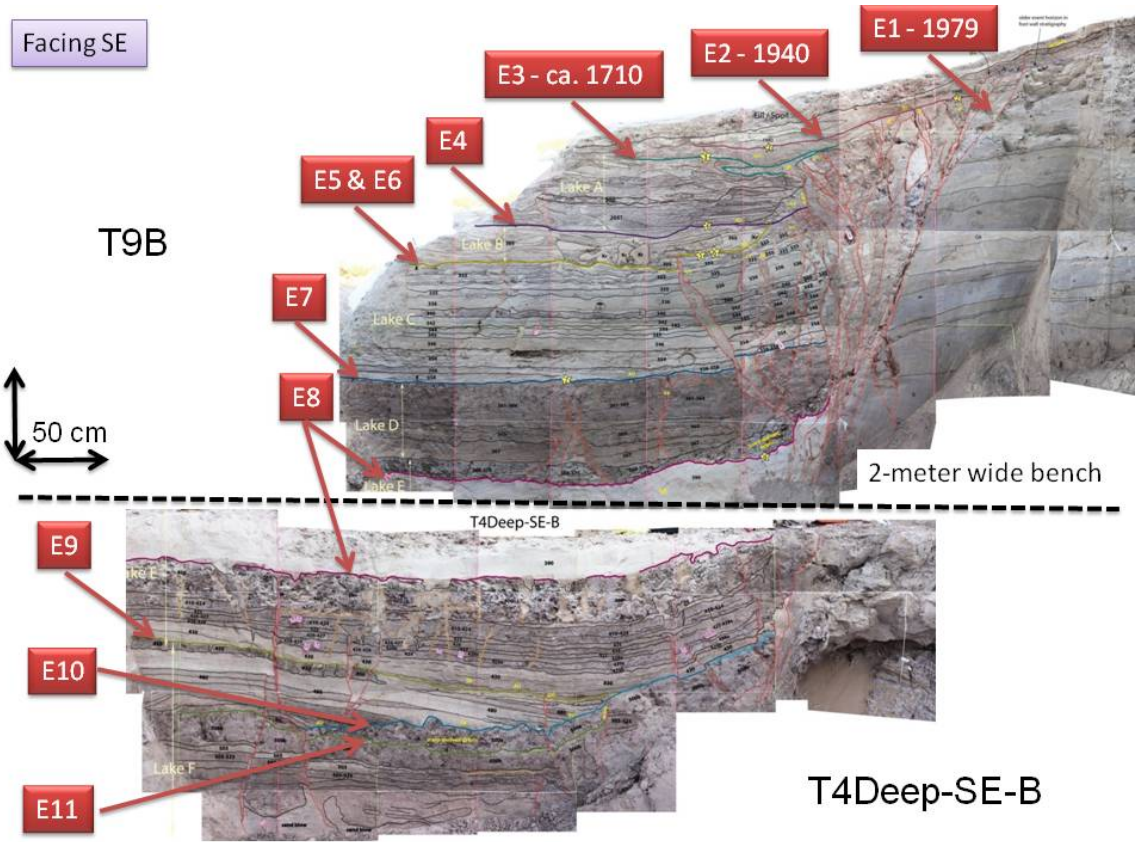

Fig. 3: Composite trench logs of T9B-SE (top) and T4Deep-SE (bottom) showing the remarkable Lake Cahuilla stratigraphy and the event horizons identified in these two exposures.

Stratigraphy and Lake Chronology

The stratigraphy consists of lacustrine, deltaic and fluvial sediments that were deposited during the filling and drying periods of Lake Cahuilla. Up to a total of 5 m of stratigraphy below ground surface was exposed in our trenches which contains a record of 6 to 7 lake episodes. The lacustrine deposits consist of massive and bedded clay; the deltaic deposits are characterized by interbedded fine silt, silty clay and clay; and the fluvial deposits contain planar and cross-bedded silt and fine sand. In some exposures, the strata above the most recent lake deposition (post 1720 AD) comprises of localized flood deposits and spoil. A well-sorted sandy unit (Unit 390) of 1 to 2 m in thickness was preserved in 10 trench exposures and was interpreted as a sand blow. Other sand blows also appear in five exposures of the lower section. The well-bedded stratigraphy at this site allows us to resolve the age of past earthquakes relative to the stratigraphy rather precisely (Figure 3).

Calendar years of past earthquakes were determined by using the lake chronology that Meltzner and Rockwell had developed (unpublished data). They submitted over 180 detrital charcoal and peat samples from the Lake Cahuilla strata at different localities for ^{14}C analysis. About 50 ^{14}C dates were used in the OxCal program to calculate calendar years of the different lake episodes. (For details of OxCal, please refer to Lienkaemper and Ramsey, 2009). Identifying and locating an event horizon within the lake stratigraphy would then allow us to obtain calendar years of past surface ruptures.

Evidence for Surface Ruptures

Common paleoseismic indicators were used to identify event horizons for past surface ruptures, including upward fault termination, fissure fill, sand blow, angular unconformity, colluvial wedges and scarp-derived debris, liquefaction pipes and downward growth of displacement. For example, in Figure 4, several indicators and their geometrical relationships define the event horizon for Event 8. A fissure fill is bounded by two fault splays terminating upward at the same horizon, where a sand blow unit was deposited at the paleosurface rather horizontally, forming an angular unconformity with the strata below.

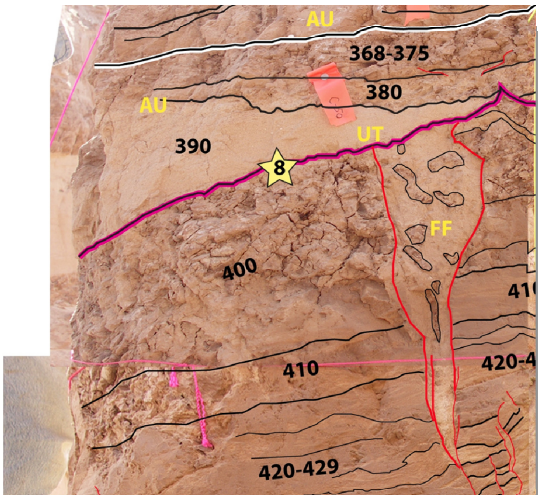

Fig. 4: Paleoseismic indicators used to identify the horizon of Event 8 include upward fault termination (UT), angular unconformity (AU) and fissure fill (FF).

A rating scheme of the paleoseismic indicators for each event horizon was devised to better qualify the likelihood of a past earthquake. Each indicator receives a rating of 1 to 4, with 1 being the weakest and 4 being the strongest. For example, an angular unconformity is a strong line of evidence hence it has a rating of 4. On the contrary, downward growth of displacement might be a result of fault dying out upward rather than cumulative displacement of multiple events on the same fault. Therefore, this indicator has the lowest rating of 1 due to the ambiguity in interpretation. The frequency (F) of these indicators is another factor to determine the likelihood of an event. In this method, the value of F is calculated by dividing the number of exposures where the indicator was observed by the number of exposures where the indicator *should be* observed. Finally, R is multiplied by F for the R*F value which indicates the likelihood of a paleoearthquake. The higher the R*F value, the more likely an event had occurred (Figure 5). Event 4 although receives a low R*F value, its occurrence was assured by a buried offset channel study by Meltzner and Rockwell (unpublished data). Among all 17 events, almost all events receive an R*F value higher than 1 except for Events 4, 8.5, 8.7 and 9. These events could be interpreted as unlikely or as events with small displacement.

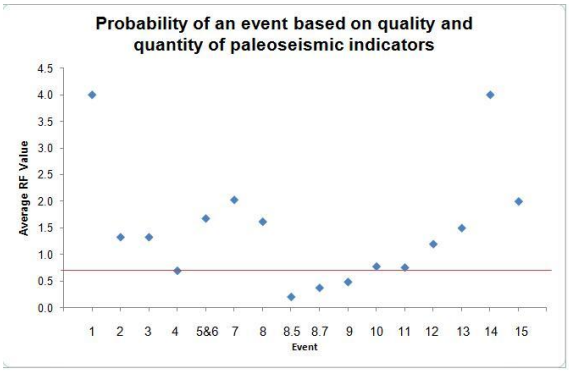

Fig. 5: Likelihood of an event based on quality and quantity of paleoseismic indicators as seen in the plot of average RF values of each event. Higher values indicate more likelihood.

CONCLUSION

We conducted this paleoseismic study on the northern Imperial fault at the Dogwood site in Mesquite Basin, southern California, to extend the record of late Holocene surface ruptures to better understand the behavior of this plate boundary strike-slip fault. Event horizons in 12 trench exposures were identified within the Lake Cahuilla stratigraphy using the standard paleoseismic indicators such as angular unconformity, fissure fill and upward truncation of faults. By using the lake chronology model that Meltzner and Rockwell (unpublished data) developed for Lake Cahuilla in the Imperial Valley, we

developed an earthquake chronology of the northern Imperial fault. Our study has revealed evidence for up to 17 events in the past 1300 years, yielding an average recurrence interval of about 80 years, albeit with a large standard deviation and coefficient of variation (Figure 6). We tested the hypothesis of a connection between lake and earthquake cycles, however, our data suggest that the connection is either very weak or non-existent as the majority of the ruptures occurred during dry periods between lakes. On the other hand, we do find a strong correlation between the earthquake chronologies determined for the southern San Andreas fault and the rupture history on the northern Imperial fault, suggesting surface rupture at the southernmost portion of San Andreas fault may have triggered earthquakes on the northern Imperial fault (Figure 7).

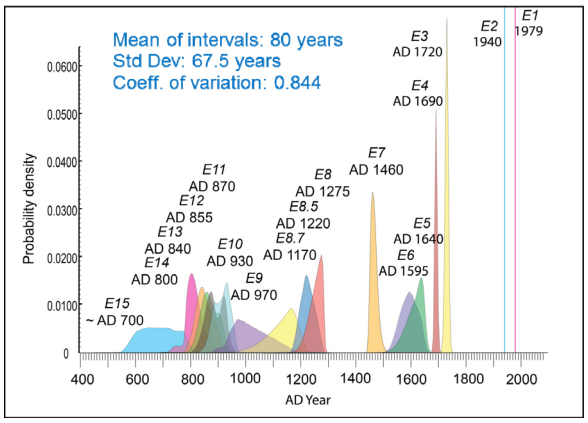

Fig. 6: Earthquake calendar ages obtained from OxCal. The higher the probability density, the more well-constrained the ages are. The height of a peak does not give any information about the likelihood of a paleoearthquake.

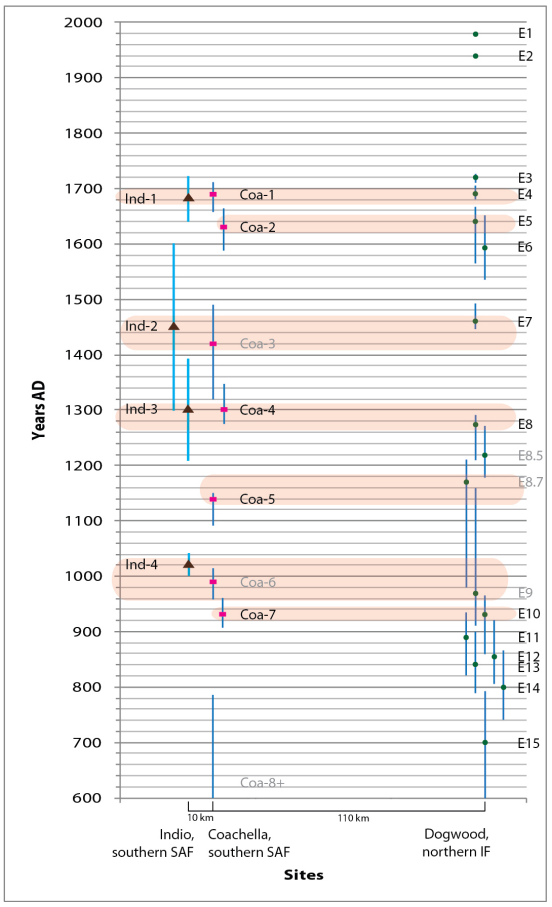

Fig. 7: Earthquake chronologies from paleoseismic sites on the southern San Andreas fault and the northern Imperial fault. The possible earthquakes Coa-3 and Coa-6, and the less likely events E8.5, E8.7 and E9 are shown in gray text. Correlations of events at the three paleoseismic sites are highlighted in pink.

Acknowledgements: We are grateful for the help we received to make this project possible. We thank the landowner for permission to excavate on his property and Jim Little for the backhoe operation. Field assistants including Gayatri Marliyani, Nissa Morton, Barrett Salisbury, Mike Buga, Petra Štěpančíková, Eulàlia Masana and Katie Anderson offered much help in the exposure preparation. This project was funded by the National Earthquake Hazards Reduction Program (NEHRP).

References

Buwalda, J. P., & C. F. Richter (1941). Imperial Valley earthquake of May 18, 1940. *Geological Society of America Bulletin*, 52, 1942-1943.

Chavez, D., J. Gonzales, A. Reyes, M. Medina, C. Duarte, J. N. Brune, F. L. Verson, III, R. Simons, L. K. Hutton, P. T. German, and C. E. Johnson. (1982). Mainshock location and magnitude determination using combined U.S. and Mexican location and magnitude determination using combined U.S. and Mexican data. The Imperial Valley, California, Earthquake, October 15, 1979. United States *Geological Survey Professional Paper*, 1254, 51-54.

Cohn, S. N., C. R. Allen, R. Gilman, & N. R. Goulty. (1982). Preearthquake and postearthquake creep on the Imperial fault and the Brawley fault zone. United States *Geological Survey Professional Paper*, 161-167.

DeMets, C., R. G. Gordon, D. F. Argus, and S. Stein. (1994). Effects of recent revisions to the geomagnetic reversal time scale on estimates of current plate motions. *Geophysical Research Letters*, 21, 2191-2194.

Hill, D. P., J. P. Eaton, and L. M. Jones (1990). Seismicity: 1980-1986, in Wallace, R.E., ed. The San Andreas Fault System, U.S. Geol. Surv. Profess. Pap. 1515, 114-151.

Lienkaemper, J. J., and C. B. Ramsey (2009). OxCal: Versatile Tool for Developing Paleoearthquake Chronologies. *Seismol. Res. Lett.*, 80, 431-434.

Lyons, S. N., Y. Bock, and & D. T. Sandwell (2002). Creep along the Imperial Fault, southern California, from GPS measurements. *J. of Geophysical Research*, 107 (B10).

Richter, C. F. (1958). Elementary seismology: San Francisco. W. H. Freeman, 768.

Sharp, R. V. (1982). Tectonic Setting of the Imperial Valley Region. United States *Geological Survey Professional Paper*, 5-14.

Shearer, P. M. (2002). Parallel fault strands at 9-km depth resolved on the Imperial Fault, Southern California. *Geophysical Research Letters*, 29 (14).

Thomas, A. P., and T. K. Rockwell (1996). A 300- to 550-year history of sip on the Imperial fault near the U.S.-Mexico border: Missing slip at the Imperial fault bottleneck. Journal of Geophysical Research, 101, 5987-5997.

EARTHQUAKE ARCHAEOLOGY

INQUA PALEOSEISMOLOGY AND ACTIVE TECTONICS

MAPPING PALEO SHORELINES IN LESVOS ISLAND: NEW CONTRIBUTION TO THE LATE QUATERNARY RELATIVE SEA LEVEL CHANGES AND TO THE NEOTECTONICS OF THE AREA

Vacchi, Matteo (1,2), Alessio Rovere (1,2), Nickolas Zouros (3), and Marco Firpo (1)

(1) Department for the Study of the Territory and its Resources, University of Genova, Genova. (Italy)
(2) SEAMap srl, Seascape Evaluation Assessment and Mapping, Genova (Italy)
(3) Department of Geography, University of Aegean, Mytylene, Lesvos Island (Greece)

Abstract (Mapping paleo-shorelines in Lesvos Island: new contribution to the late quaternary relative sea level changes and to the neotectonics of the area): *This study attempts to delineate the late Quaternary morphotectonic evolution of the coastal zone of southern Lesvos Island (NE Aegean Sea) on the basis of detailed field mapping of different sea level indicators. The geomorphological analysis of the markers, coupled with radiometric dating, allowed to identify a Late Quaternary regional uplift trend controlled by the footwall of a large normal fault (Lesvos Fault) located between Lesvos and Chios Islands. At local scale, superimposed to this trend, the area is characterized by many indicators of rapid vertical displacements (uplift and subsidence) related to the high seismicity. The most important co-seismic event has been found to have happened between 3365 and 3924 BP which uplifted of about 0.8 m a large sector of the southern Lesvos coastline.*

Key words*: raised shorelines; coastal uplift, Lesvos Island; Relative sea level changes.*

INTRODUCTION

Due to the geodynamic setting, several sectors of the Mediterranean basin exhibit evidence of differential vertical movements during the late quaternary (Stewart & Morhange, 2009). In particular, several papers investigated the coastal morphotectonics of the Aegean region, one of the most seismically active areas not only at Mediterranean scale (Stiros et al., 2000; 2009 Palyvos et al., 2008; Cundy et al., 2010). In many cases geomorphological approaches became very practical solutions to get quantitative information on late quaternary uplift and paleoseismicity of coastal areas (Palyvos et al. 2008). For this reason, detailed mapping of paleo-sea level markers has been often used as a tool to quantify coastal uplift and relative sea level changes in several areas of the Aegean Sea (Pirazzoli et al., 2004; Stiros et al., 2009). In this study we analyzed the coastal geomorphology of the southern sector of Lesvos Island, located in the NE Aegean Sea. Here, despite several papers already dealt with the neotectonics of this area, detailed information on the coastal morphotectonics of the Island is lacking. Morphological, biological and sedimentary records of past sea level were mapped, analyzed and, where possible, sampled and dated.

Lesvos islandis located in a geotectonically complex area, because directly affected by the North Anatolian Fault Zone (NAFZ), its westward continuation in the Aegean Sea, known as the North Aegean Trough (NAT) and the West Anatolia Graben System (WAGS) in Asia Minor with significant historical seismicity (Papazachos and Papazachou, 1997; Papazachos and Kiratzi, 1996). As a result of the interaction between those tectonic systems, Lesvos Island presents a strong diversity in fault setting and is presently characterized by the parallel activity of both normal and strike slip faults (Roumelioti et al., 2011).The study area is located in the south eastern part of the Island, in the coastal area comprised between Tarti and the entrance of the Kalloni gulf (Fig.1). From the geomorphological point of view, it is mainly characterized by steep cliffs alternated with gravel pocket beaches, often with beachrocks outcrops. The outcropping lithologies are composed by a basement of Alpidic and pre-Alpidic rocks, mainly Triassic limestones, marbles and schists. In the whole sector the tidal range does not exceed 0.2 m (Vousdoukas et al., 2009).

Marine and coastal processes produce many kinds of geomorphologic markers, especially on rocky shores, that are related to the contemporary sea-level position (Pirazzoli, 2007). Among them tidal notches, and the inner edge of benches and shore platform are considered precise indicator of paleo sea level stands in microtidal environment such as the Mediterranean Sea. Endolithic organisms often leave morphological signs that can be used as sea-level indicator and, at Mediterranean scale, *Lithophaga* boreholes horizontal upper limit represent a good biological indicator of former m.s.l. (Laborel and Laborel-Deguen, 1994).

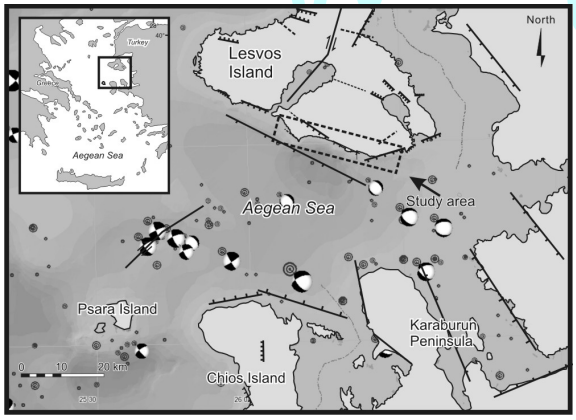

Fig.1. Geographical location and active faults of the study area. Focal mechanism represent the > 4M earthquakes after the 1928.

A detailed mapping of paleo-shorelines including erosional, biological and depositional sea level markers was carried out in the island during three field campaigns between September 2009 and October 2010. Although debates in literature (Kellettat, 2006; Desruelles et al., 2009), in this study we considered beachrocks as markers of past relative sea level mainly because of their strict altimetric correlation with other sea level markers such as benches, tidal notches or wave cut platforms. In fact, the combined analysis of erosive and depositional paleo-shoreline indicators is of timely importance because, although marine erosional forms are more precise indicators of sea level in coastal settings, they rarely preserve dateable materials, which are more frequent in depositional landforms (Pirazzoli, 2005; Pirazzoli, 2007).

Markers elevations were measured using a 3 m metal bar with centimeter sub-division and in-built spirit level in order to achieve better vertical and horizontal accuracy. Elevations were measured with reference to SL at the time of measurement with a maximum error of 10 cm and the markers location was measured using a handheld GPS (± 5m). Underwater transects were carried out up to – 10 m to map and sample the submerged markers (mainly notches and beachrocks).

RESULTS

The most evident morphological marker was represented by a uplifted wave cut platform developing for about 6 km eastwards and westward to Agios Fokas cape (Fig. 2).

The platform is continuous (despite the several changes of lithologies occurring in the area) and presented an inner margin often characterized by an abrasion notch with the roof positioned at about + 0.9 m a.s.l. This level was confirmed by the presence of isolated limestones blocks lying on the platform showing the presence of *lithophaga* boreholes up to 0.8 m above the present sea level.

Along the platform fragments of marine shells (vermetids, serpulids, gastropods) were found still preserved in growth position at about .0.5 m a.sl. AMS radiocarbon dating were performed on 3 samples of marine shells (gastropods and serpulids) sampled at about 4 km of distance one from the other. Calibrated ages dated the samples respectively 3365 – 3648 BP (K1 beta); 3460 – 3812 BP (AF1 beta); 3609 – 3924 BP (AF3 poznan).

A second level of uplifted wave cut platform was mapped along this sector at an elevation ranging from 5 to 6 m. This level is recurrent in 4 sites along the coastline and is always covered by beach deposits rich in marine fauna. Two samples of marine shells (*Patella ferruginea*) were sampled. AMS radiometric dating gave calibrated ages of 29160 ± 150 (V1 beta) and 27410 ± 120 (Ag2 beta).

Fig. 2. Uplifted wave cut platforms in the sector of Agios Fokas and Vrisa. They often showed an inner margin often characterized by an abrasion notch with the roof at about + 0,9 m a.s.l. as indicated by the dashed line in the photo above.

On the vertical limestone cliffs, a modern tidal notch was always present (width 50- 70 cm). Recurrent uplifted relict of tidal notches were also observed at different elevation varying from + 0.7 up to +12 m a.s.l. (Fig.3c) locally interrupted where lithological conditions are unfavorable for their formation and preservation (i.e., schists).

Their lateral continuity, until the village of Melinta was however confirmed by examination by boat. Morphology and elevation of the notches showed discrepancies and altimetric correlations has been very difficult. However, a recurrent morphology was observed on tidal notches positioned at + 9 to +11 m. They always presented a double concavity that appeared smoothed in exposed areas and well preserved in the sheltered ones (Fig. 3b). In front of the village of Melinta a large limestone rock presented an uplifted wave cut platform characterized by an inner margin at +11.2 m clearly indicated by the upper limit of a well preserved *lithophaga* boreholes band (Fig.3a).

The area of Tarti is characterized by almost vertical cliffs carved in Triassic limestones. Evidence of *Lithophaga* boreholes bands were observed on both sides of the Tarti cape. The upper limit is located at + 1.8 m. Any evidence of uplifted erosional markers or modern tidal notches was observed despite the favorable lithology of the area. On the contrary, a submerged tidal notch was mapped all along the cape. The maximum concavity was measured at -0,7 m below the modern sea level (Fig.4).

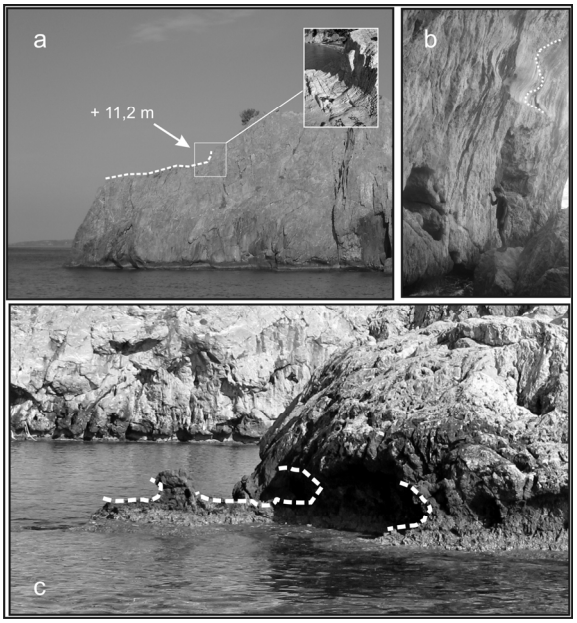

Fig.3. Raised shorelines mapped in the area of Kryfty and Melinta. a) wave cut platform with inner limit positioned at + 11.2 and characterized by lithofaga boreholes. b) double concavity notch occurring in Kryfty cove. c) raised tidal notches carved in the Triassic limestones of Kryfty area. The maximum concavity is at + 0.8 m.

Uplifted beachrocks outcrops were observed along the whole SE sector of the island. The beachrocks are often organized in multiple slabs reaching up to about + 3.1 m a.s.l. The only exception is represented by Tarti site where beachrocks developed from – 1.1 m up to intertidal zone.

DISCUSSION

Raised sea stands have been identified along the whole south eastern coast. Altimetric distribution of the different markers pointed out some recurrent levels especially in the areas comprised between Agios Fokas cape and the village of Melinta.
The first is positioned at + 0.8 ± 0.2 m. According to Pirazzoli, (2007) and Stiros et al., (2009), the good preservation of both morphological and biological markers suggests a very rapid uplift probably related to a co-seismic event.
The second paleo-shoreline is positioned at + 4.80 ± 0.2 m and, according with the dating, was referred to MIS 3. The highest recurrent sea level stand is positioned at 10.9 ± 0.2 m. No radiometric dating was possible because the lack of datable material.
The geographical limit of these recurrent levels has been positioned in the village of Plomari. In fact, eastward to Plomari, although indicators of raised shorelines were still present, however their altimetric distribution was significantly different with respect to the Agios Fokas and Melinta sectors. The site of Tarti is the only one that showed both evidence of uplift and subsidence.

The detailed analysis of morphologies and distribution of the markers, coupled with radiometric dating, allowed to identify a Late Quaternary regional uplift trend controlled by the footwall of a large normal fault (Lesvos Fault) located between Lesvos and Chios Islands (Mascle & Martin, 1990) (Fig.1).

Fig.4 . Underwater tidal notch occurring all along the Tarti cape.

At local scale, superimposed to this trend, the area is characterized by many indicators of rapid vertical displacements (uplift and subsidence) related to the high seismicity. According to the radiomentric dating and geomorphological evidence,an important co-seismic event has been found to have happened between 3365 and 3924 BP. This rapid event uplifted of about 0.8 m a large sector of the southern Lesvos coastline.

According to Lambeck (1996) and Siddal et al., (2008), the position of the MIS 3 shorelines at about + 5 m on the present position allowed to quantify the

rate of uplift during the late quaternary. However, as pointed out by several indicators, the average rate is a sum of gradual and co-seismic uplifts and more accurate consideration strongly needs further radiometric dating. If further studies will confirm our data, Lesvos Fault is among one of the less documented active fault in this sector of the Aegean Sea to have ruptured in recurring earthquake within a relatively recent timespan.

In conclusion, geomorphological markers of past sea levels are well known for being one of the main means to estimate neotectonic trends and historical recurrence and magnitude of co-seismic events. The scientific value of this kind of studies is flanked by the value assumed for society. The latter is twofold: on one side, very active sites like Lesvos Island are a potential source of data to tune global sea level models and therefore global estimates of future sea level rise; on the other side, they have a local value in terms of earthquake risk assessment.

References

Cundy, A.B., Gaki-Papanastassiou, K., Papanastassiou, D. Maroukian, H., Frogley, M.R., Cane, T.(2010) Geological and geomorphological evidence of recent coastal uplift along a major Hellenic normal fault system (the Kamena Vourla fault zone, NW Evoikos Gulf, Greece) *Marine Geology* 271, 156–164

Desruelles, S., Fouache, É., Ciner, A. Dalongeville, R., Pavlopoulos, K., Kosun, E., Coquinot, Y., Potdevin, J.L. (2009). Beachrocks and sea level changes since Middle Holocene: Comparison between the insular group of Mykonos–Delos–Rhenia (Cyclades, Greece) and the southern coast of Turkey. *Global and Planetary Change Volume* 66, 1-2, 19-33.

Kellettat, D. 2006. Beachrock as Sea-Level Indicator? Remarks from a Geomorphological Point of View. *Journal of Coastal Research* 22 (6), 1558-1564.

Mascle, J. ,Martin, L. (1990). Shallow structure and recent evolution of the Aegean Sea: a synthesis based on continuous reflection profiles. *Marine Geology* 94, 271–299.

Lambeck, K. (1996) – Sea-level changes and shore-line evolution in Aegean Greece since Upper Paleolithic time. *Antiquity*, 70, 588-610.

Palyvos, N., Lemeille, F., Sorel, D., Pantosti, D. Pavlopoulos, K. (2008). Geomorphic and biological indicators of paleoseismicity and Holocene uplift rate at a coastal normal fault footwall (western Corinth Gulf, Greece). *Geomorphology* 96, 16–38

Papazachos, C.B. and Kiratzi, A.A., (1996). A detailed study of the active crustal deformation in the Aegean and surrounding area, *Tectonophysics* 253(1-2), 129-153.

Papazachos, B., Papazachou, C., 1997. *The earthquakes of Greece*, Ziti editions. Thessaloniki

Pirazzoli, P.A. (2005). A review of possible eustatic,isostatic and tectonic contributions in eight late-Holocene relative sea-level histories from the Mediterranean area. *Quaternary Science Review* 24, 1989–2001

Pirazzoli, P.A., Stiros S.C., Fontugne M., Arnold M. (2004). Holocene and Quaternary uplift in the central part of the southern coast of the Corinth Gulf (Greece). *Marine Geology* 212, 35-44

Pirazzoli, (2007). Sea level studies. Geomorphological Indicators. *Encyclopedia of Quaternary Science*, 2974-2983.

Roumelioti, Z., Kiratzi, A., Benetatos, C., (2011). Time Domain Moment Tensors of earthquakes in the broader Aegean Sea for the years 2006-2007: the database of the Aristotle University of Thessaloniki, *Journal of Geodynamics* 51, 179-189.

Siddal, M., Rohling, E.J., Thompson, W.G., Waelbroeck, C. (2008). Marine isotope stage 3 sea level fluctuation: data synthesis and new outlook. *Reviews of Geophysics* 46, 1-29.

Stewart, I.S. Morhange, C. (2009), Coastal geomorphology and sea-level change, in J. C.Woodward (ed.), *The Physical Geography of the Mediterranean.* Oxford University Press, Oxford, 385–413

Stiros, S.C., Laborel, J., Laborel-Deguen, F., Papageorgiou S., Evind J., Pirazzoli P.A.. 2000. Seismic coastal uplift in a region of subsidence: Holocene raised shorelines of Samos Island, Aegean Sea, Greece. *Marine Geology* 170, 41-58

Stiros, S.C. Pirazzoli, P.A. Fontugne, M., (2009). New evidence of Holocene coastal uplift in the Strophades Islets (W Hellenic Arc, Greece). *Marine Geology* 267, 207–211.

Vousdoukas, M.I., Velegrakis, A.F., Karambas, T.V. (2009). Morphology and sedimentology of a microtidal beach with beachrocks: Vatera, Lesbos, NE Mediterranean. *Continental Shelf Research* 29, 1937–1947.

BOULDER DEPOSITS IN SOUTHERN LESVOS: AN EVIDENCE OF THE 1949'S CHIOS-KARABURUM TSUNAMI?

Vacchi, Matteo (1), Alessio Rovere(1), Marco Firpo (1) and Nickolas Zouros (2)

(1) Department for the Study of the Territory and its Resources, University of Genova, Genova. (Italy)
(2) SEAMap srl, Seascape Evaluation Assessment and Mapping, Genova (Italy)
(3) Department of Geography, University of Aegean, Mytylene, Lesvos Island (Greece)

Abstract (Boulder deposits in southern Lesvos: an evidence of the 1949's Chios-Karaburum tsunami?): *Aim of this study was to understand the mechanism of deposition of clusters of large boulders, consisting of beachrock slabs, which were found on the southern coasts of Lesvos Island (NE Aegean Sea). An integrated study was carried out in order to detect whether transport and accumulation can be related to an exceptional storm or a tsunami event. The results provided evidence of a tsunami wave impact during the last century. Specifically, the boulder accumulation is likely to have been deposited by the tsunami that was triggered by the 6.7M Chios-Karaburum earthquake of 1949. Lesvos island, on the basis of the seismic sources, was already listed as tsunami affected area but field evidence was previously lacking. The results represent a new contribution that could be of primary importance in assessing the degree of vulnerability of the local coastal communities of southern Lesvos to future tsunami events.*

Key words*: boulder deposits; catastrophic waves; Lesvos Island; coastal hazard.*

INTRODUCTION

Identification of boulders displaced and eventually transported by tsunami or exceptional storm waves plays a crucial role in the assessment of the occurrence of past catastrophic events (Goto et al., 2009). Understanding the nature and impact of these events is fundamental in terms of evaluation, mitigation and management of current coastal hazards. In the Mediterranean, historical tsunamis were often reported as consequences of destructive earthquakes (Soloviev et al., 2000). In the Ionian and Aegean Seas, geomorphological records of tsunamis were detected in several areas (Mastronuzzi and Sansò., 2000; Scheffers and Kellettat, 2003; Scheffers and Scheffers, 2007, Scicchitano et al., 2007; Scheffers et al., 2008). In particular, the area surrounding western Turkey and Greece is among the most seismically active and rapidly deforming regions in the world (Nyst and Tatcher, 2004), and thus has historically been strongly affected by tsunami events (Papadopoulos & Chalkis, 1894; Soloviev, 1990; Soloviev et al., 2000,Fig. 1).

The aim of this study is to understand the mechanism of deposition of clusters of large boulders (weighing up to 17 tons) which were found on the southern coasts of Lesvos Island (NE Aegean Sea). In particular, studies of boulder morphology, tectonic setting, wave climate and historical context were carried out in order to detect whether transport and accumulation can be related to an exceptional storm or a tsunami event.

The study area (Fig. 1) is located in the southern part of the island, near the villages of Plomari and Agios Isidoros. From a geomorphological point of view, this area is characterized by cliffs alternating with sandy to gravel beaches, often with beachrock outcrops. The main lithologies are represented by Triassic schists and limestones. Due to the southern facing, this costal sector is characterized by a relatively low wave regime because of the protection from the main swells of the Aegean sea generated by northern winds (Soukissian et al., 2007). The maximum fetch does not exceed 100 nautical miles, and main waves (coming from SE) reach maximum off-shore wave height of about 1,8 m (Vousdoukas et al., 2009).

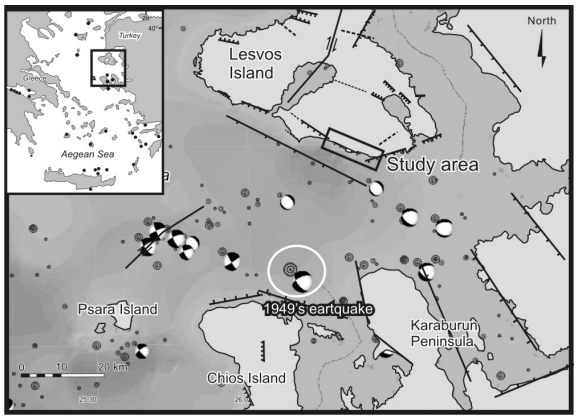

Fig. 1. Geographical location and seismo-tectonic setting of the study area. Focal mechanism of the > 4M earthquakes after the 1928. The white circle indicates the 1949's M. 6.7 event triggering a tsunami wave recorded in Chios and in the Karaburun peninsula. Black dots in the small square represent the historical tsunamigenic earthquakes according to Soloviev, 1990.

A total of 47 boulders was found in the study area. Some of them are organized in clusters, others are scattered along the shoreline (Fig. 2). After a first general mapping, more detailed measures

concentrated on the 26 boulders showing a major axis ≥ 1 m. The boulders consisted of beachrock slabs (Fig. 2) of which having unit weight of 2.6 tm^{-3}. The boulders had a maximum size of 4.5 × 2.5 × 0.6 m with a volume of about 7 m^3 and a maximum weight of about 17 t. Some peculiar features are constant on the majority of the beachrock boulders:
i) the boulders are scattered up to about 20 m from the shoreline and their elevation does not exceed 0.5 m asl;
ii) many boulders are upside down, as proved by erosive features normally cut upon the upper surface of a beachrock and presently facing the ground (Fig. 2);
iii) Several boulders, especially in the area of Agios Isidoros, are completely buried in the sand (Fig. 2).
The presence of biogenic encrustations (mainly vermetids and serpulids) suggests a mid-sublittoral pre-transport position of the boulders (as these organisms usually live within this environment, Laborel, 1987).

These settings were validated by the transects carried out along the whole seaward extension of the beachrock outcrop: the high degree of fracturing coupled with the presence of scattered broken pieces mainly at the seaward edge of the beachrock outcrop (about -3 m) confirmed the hypothesis of an original submerged position or a submerged joint bounded scenario. In fact, geometrical analysis of the boulders and of large holes in the submerged part of the beachrock itself revealed a close correspondence between the shapes of the boulders and the shapes of the holes. On the basis of the pre-transport settings individuated, values of storm wave height (Hs) and tsunami wave height (Ht) theoretically required for the boulder displacement were calculated using the equations proposed by Nott, (2003), Pignatelli et al., (2009), Benner et al., (2010).

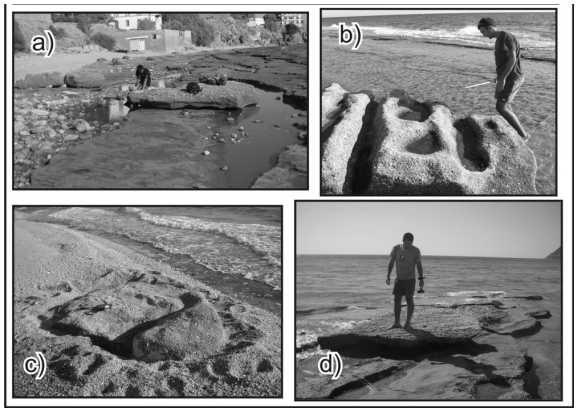

Fig. 2 a) and b) examples of large boulders mapped in the site of Plomari; c) and d) examples of large boulders mapped in the site of Agios Isidoros

DISCUSSION

Significant discrepancies were observed between the different hydrodynamic approaches. For the submerged boulders (SMBS), the Nott equation calculated storm wave values (Hs) up to 15 m to displace the largest boulder. The maximum storm wave values (Hs) computed using the Benner et al. approach are considerably smaller, slightly exceeding 8 m.

Nott's joint bounded equation (JBBS) computed storm waves values (Hs) exceeding 20 m whereas storm wave values derived from Pignatelli et al. equations reached maximum values of about 10 m.

The Aegean Sea is characterized by relatively short fetch and relatively small swells, mainly generated from northern winds (Soukissian et al., 2007). It is very unlikely that waves exceeding 10 m could be generated in this sector of the Aegean, especially in a south-facing area, characterized by a maximum fetch not exceeding 100 nautical miles and by maximum off-shore significant wave height (Hs) not exceeding 2 m.

These hydrodynamic results suggest that a tsunami could have been responsible for on-shore deposition of the boulders, but the discrepancies between the different approaches did not provide unambiguous evidence. Further analyses were then performed in order to test the reliability the tsunami hypothesis.

Some considerations based both on geomorphological indicators and on seismotectonic sources, support the hypothesis that the boulder accumulation in southern Lesvos was caused by tsunami.

The morphology and lithostructural settings of the coastal area play a crucial role in boulder detachment and transport by catastrophic waves. Mastronuzzi et al., (2006) indicated the presence of layered units and bedrock fracturing as important pre-conditions for boulder displacement. Coastal sectors characterized by beachrock outcrops and affected by tsunami wave impact often showed on-shore broken slab accumulation (Vött et al., 2007, 2009; Scheffers and Scheffers, 2007). In the study area, the slabs were probably torn out of the original beachrock unit which was already fractured by several seismic events affecting the whole coastal sector. Moreover, on the majority of boulders, a fragile layer of biogenic encrustation was observed. Its preservation is a clear indicator of short transport generated by a single wave (Mastronuzzi et al., 2006).

Other evidence can be gathered by subdividing the a-axis orientation of the boulders on the basis of the relative Hs values. Most of the boulders presenting Hs values exceeding 7,5 m (i.e. not compatible with calculated extreme storm events) had their elongated axis almost perpendicular to the shoreline and oriented between 170°N and 200°N. However, other boulders are oriented mainly between 130° and 150°N. This is the direction of the major swells in the area (Vousdoukas et al., 2009). This orientation pattern reflects a scheme already present in other Mediterranean boulder accumulations (Mastronuzzi and Sansò, 2004; Scicchitano et al., 2007) and was explained with re-orientation by storm waves after a tsunami event. According to the previous

considerations, we hypothesize that a single tsunami wave displaced all the boulders from the submerged position to the shore. Subsequent storm wave events, coming from S-SE, reworking the deposited boulders were able to re-orient only the smaller ones.Further confirmation was provided by the literature dealing with Mediterranean regions most frequently affected by tsunamis (Papadopoulos and Chalkis, 1984; Altinok and Ersoy, 2000; Soloviev et al., 2000; Papadopoulos and Foakefs, 2005; Yolsal et al., 2007; Papadopoulos, 2009). These papers provided spatial distribution of tsunami hazard in the Aegean area based on the historical occurrence of tsunami events as well as on the triggering seismic sources (Papadopoulos and Chalkis, 1984; Papazachos and Dimitriou, 1991; Papadopoulos and Foakefs, 2005). On the basis of the distribution of tsunamigenic earthquakes and of the historical data of past events, several authors listed Southern Lesvos as an area vulnerable to tsunami events (Fig.3) (Papadopoulos and Chalkis, 1984; Soloviev et al., 1990 Papadopoulos and Foakefs, 2005; Yolsal et al., 2007). This integrated study, ranging from geomorphological to seismotectonic data, corroborated the tsunami hypothesis and most probably ruled out extreme storms as the cause of transport and displacement of the boulders.

The high seismic activity affecting this sector of the Aegean Sea often triggered tsunami waves that caused damage to the surrounding coastal areas (Papazachos and Papazachou, 1997; Altinok et al., 2005). Historical data are available on six main events which took place 20th March 1389, 24th November 1772, 13th November 1856, 19th January 1866, 3rd April 1881 and 23rd July 1949 (Soloviev et al., 2000; Altinok et al., 2005).

Radiocarbon age determinations were performed on two samples of biological encrustation, the first, (serpulids) from the Plomari cluster and the second (vermetids) from Agios Isidoros cluster. AMS radiocarbon age determination indicated that both were of recent origin (fraction of modern carbon, ~1950). Because of this, it was possible to carry out an historical investigation with the help of the cultural association "*to polion*" of Plomari. Aged inhabitants of the village confirmed the sudden appearance of the boulders on the shoreline but the people who were interviewed could not recall precise dates. Important data were achieved by using an historical photograph of Plomari taken in 1896 (Fig. 4). In the same area where boulders are presently found the photograph shows no traces dislocated blocks.

This photograph allows us to place a further temporal limit on the date of the boulders deposition. In 1896 there is no evidence of broken beachrock slabs on the shoreline. This is consistent with the theory of a single pulse wave as the depositional mechanism as opposed to a continuous action of the waves on the beachrock outcrops. These historical data supported the results obtained by radiometric dating, indicating a tsunami event that cannot be earlier than the year 1896.

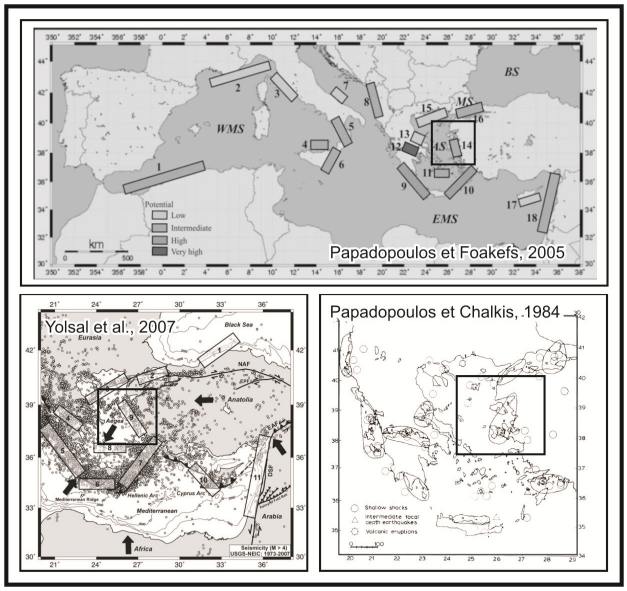

Fig. 3 Maps of the tsunami affected area compiled by Papadopoulos & Foakefs, 2005; Papadopoulos & Chalkis, 1984; Yolsal et al., 2007.

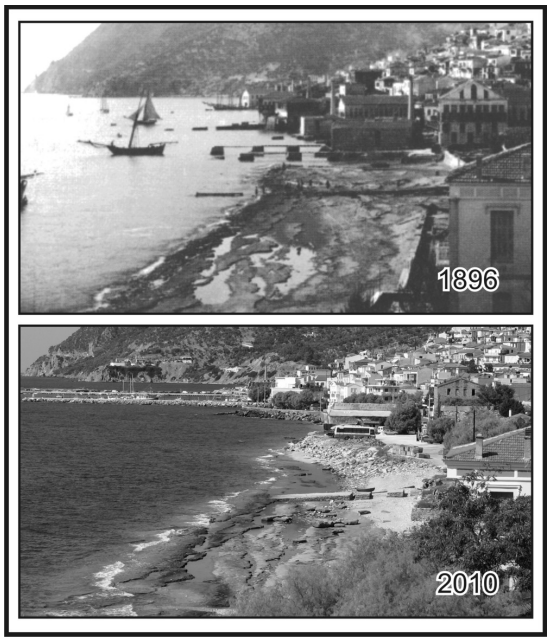

Fig. 4 Plomari today and in the 1896. Boulder deposits are missing in the 1896's photograph.

Analysis of the historical tsunami catalogs isolated the Chios-Karaburum earthquake of 1949 as the only known event capable of creating the boulder deposit. The epicenter of the earthquake (M=6.7 Papazachos and Papazachou, 1997) was located offshore of Chios Island (Fig.1) at about 40 km from Plomari. The tsunami triggered by the earthquake affected the coasts of Chios Island, and Karaburum historical reports are available in both sectors (Altinok et al., 2005).

This paper presents results of geomorphologic traces of catastrophic wave impact in a coastal sector

included in the lists of areas affected by tsunami, but where field evidence of paleo-tsunamis was previously lacking. The enigmatic large boulders observable on the southern coast of Lesvos Island were investigated without excluding, *a priori*, any possible cause of deposition. The integrated study of geomorphological, hydrodynamic, seismotectonic and historical data provided evidence of a tsunami wave impact during the last century. Specifically, the boulder accumulation is likely to have been deposited by the tsunami that was triggered by the 6.7M Chios-Karaburum earthquake of 1949.

Plomari (founded in 1849) home to about 6000 people, is the second largest town of Lesvos Island and is the only sizable settlement on the southern coast of Lesvos. Its geographical position justifies the creation of serious policies related to seismic hazard. In fact, Papazachos et al. (2004) indicated the possibility of a strong seismic event in the near future (up to M 6.5–6.7) in the area of Lesvos and Chios. The above results represent a new contribution that could be of primary importance in assessing the degree of vulnerability of the local coastal communities to future tsunami events.

Acknowledgements: The authors would like to thank Prof. G. Mastronuzzi (Bari, IT) for his suggestions and to C.N. Bianchi (Genoa, IT) for the identification of biological marine encrustation.

References

Altinok, Y., Ersoy., S. (2000). Tsunamis Observed on and Near the Turkish Coast. Natural Hazards 21, 185–205.

Altinok, Y., Alpar, B., Ozer, N., Gazioglu, C. 2005. 1881 and 1949 earthquakes at the Chios-Cesme Strait (Aegean Sea) and their relation to tsunamis. Natural Hazard and Earth System Science, 5, 717–725.

Benner, R.; Browne, T.;Brückner, H.; Kelletat, D.; Scheffers, A. (2010). Boulder Transport by Waves: Progress in Physical Modelling. Zeitschrift für Geomorphologie NF. Supp., 54, (3), 127-146.

Goto, K., Okada, K., Imamura, F., (2009). Characteristics and hydrodynamics of boulders transported by storm waves at Kudaka Island, Japan. Marine Geology 262, 14–24

Laborel J, 1987. Marine biogenic constructions in the Mediterranean—A review. Scientific report of Port-Cros Natural. Park (France) **13**: 97–126.

Mastronuzzi, G., Pignatelli, C., Sanso, P., (2006). Boulder fields: a valuablemorphological indicator of Paleotsunami in the Mediterranean Sea. Zeitschrift für Geomorphologie, NF 146, 173–194

Mastronuzzi, G., Sanso, P., (2000). Boulder transport by catastrophic waves along the Ionian coast of Apulia (Southern Italy). Marine Geology 170, 93–103.

Mastronuzzi, G., Sansò, P., (2004). Large boulder accumulations by extreme waves along the Adriatic Coast of southern Apulia (Italy). Quaternary International 120, 173–184.

Nyst, M., Thatcher, W. (2004). New constraints on the active tectonic deformation of the Aegean. Journal of Geophysical Resources 109, B11406, doi:10.1029/2003JB002830.

Nott, J., (2003). Tsunami or storm waves?—Determining the origin of a spectacular field of wave emplaced boulders using numerical storm surge and wave models and hydrodynamic transport equations. Journal of Coastal Research 19, 348–356.

Papadopoulos, G. A. (2009). Tsunamis, in J. C. Woodward (ed.), The Physical Geography of the Mediterranean. Oxford University Press, Oxford, 493–512.

Papadopoulos, G. A., Fokaefs, A. (2005). Strong tsunamis in the Mediterranean Sea: a re-evaluation. ISET Journal of Earthquake Technology, 42, 159–170.

Papadopoulos, G. A., Imamura, F.: (2001). A proposal for a new tsunami intensity scale. ITS 2001 Proc., Session 5, N. 5-1, 569–577

Papadopoulos, G.A., Chalkis, B.J., (1984). Tsunami observed in Greece and the surrounding area from antiquity up to present times. Marine Geology 56, 309–317

Papazachos B. C., Dimitriou P. P., (1991). Tsunamis In and Near Greece and Their Relation to the Earthquake Focal Mechanisms. Natural Hazards 4, 161-170.

Papazachos, B., Papazachou, C., (1997). The earthquakes of Greece, Ziti editions. Thessaloniki

Papazachos, C.B., Karakaisis, G.F., Scordilis, E.M., and Papazachos, B.C., (2004). Probabilities of activation of seismic faults in critical regions of the Aegean area, Geophysical Journal International 159, 679–687.

Pignatelli, C., Sansò, P., Mastronuzzi, G. (2009). Evaluation of tsunami flooding using geomorphologic evidence. Marine Geology 260, 6–18.

Scheffers, A., Kelletat, D., (2003). Sedimentologic and geomorphic tsunami imprints worldwide—a review. Earth-Science Reviews 63, 83–92.

Scheffers, A., Scheffers, S.R., (2007). Tsunami deposits on the coastline of West Crete (Greece). Earth and Planetary Science Letters 259, 613–624.

Scheffers A., Kelletat, D., Vött A., May, S.M., Scheffers, S.R., (2008). Late Holocene tsunami traces on the western and southern coastlines of the Peloponnesus (Greece). Earth and Planetary Science Letters 269, 271-279.

Scicchitano, G., Monaco, C., Tortorici, L., (2007). Large boulder deposits by tsunami waves along the ionian coast of south-eastern Sicily (Italy). Marine Geology 238, 75–91.

Soloviev, S.L., (1990). Tsunamigenic zones in the Mediterranean Sea. Natural Hazards 3, 183–202.

Soloviev, S.L., Solovieva, O.N., Go, C.N., Kim, C.S., Shchetnikov, N.A., (2000). Tsunamis in the Mediterranean Sea 2000 B.C.-2000 A.D. Kluwer, Dordrecht.

Soukissian, T.H., Hatzinaki, M., Korres, G.,, Papadopoulos, A., Kallos, G., Anadranistakis, E. (2007). Wind wave atlas of the Hellenic seas. Hcmr publication, 300 pp.

Vött, A., Brückner, H., May, M., Lang, F., Herd, R., Brockmüller, S., (2007). Strong tsunami impact on the Bay of Aghios Nikolaos and its environs (NW Greece) during classical-Hellenistic times. Quaternary International 181, (1), 105-122

Vött, A., Brückner, H., Brockmüller, S., Handl, M., May, S.M., Gaki-Papanastassiou, K., Herd, R., Lang, F., Maroukian, H., Nelle, O,. Papanastassiou, D. (2009). Traces of Holocene tsunamis across the Sound of Lefkada, NW Greece. Global and Planetary Change 66, 112-128.

Vousdoukas, M.I., Velegrakis, A.F., Dimou, K., Zervakis V., Conley, D.C. (2009). Wave run-up observations in microtidal, sediment-starved pocket beaches of the Eastern Mediterranean. Journal of Marine Systems 78, 537–547.

Yolsal, S., Taymaz, T., Yalciner, A., C. (2007). Understanding tsunamis, potential source regions and tsunami-prone mechanisms in the Eastern Mediterranean.In: Taymaz, T., Yilmaz, Y. Dilek, Y. (eds) The geodynamics of the Aegean and Anatolia. Geological Society, London, Special Publications, 291, 201–230.

ACTIVE FAULTING AND EARTHQUAKE-INDUCED SLOPE FAILURES IN ARCHEOLOGICAL SITES: CASE STUDY OF DELPHI, GREECE

Valkaniotis, Sotiris (1), George Papathanassiou, Spyros Pavlides

(1) Dept of Geology, Aristotle University of Thessaloniki, Greece, email gpapatha@auth.gr

Abstract (Active faulting and earthquake-induced slope failures in arcacheological sites: case study of Delphi, Greece): *The archeological area of Delphi is one of the most visited places in Greece. However, as it is described in historical reports, severe ground deformations triggered by earthquakes took place. In order to assess the rockfall potential and the relevant hazard within this area, the parameters of the 1870 earthquake were taken into account. Afterwards, the GIS-based Newmark's displacement method was applied in order to compute the permanent displacement values in the study area. The outcome provided by this study, indicates that the zone located at the archaeological area is characterized as very unstable. Moreover, the value of the critical acceleration within this zone is very low and even a small magnitude seismic event could generate rockfalls. Thus, the hazard and consequently the risk is extremely high and permanent mitigation measures should be developed.*

Key words*: Delphi, earthquake, rockfall, hazard*

INTRODUCTION-GEOLOGICAL SETTING

The WNW-ESE-trending Gulf of Corinth separates the northern coast of the Peloponnese from mainland Greece (Figure 1). To the east it is bounded by the Isthmus of Corinth through which the Corinth Canal passes into the Saronic Gulf. The Gulf of Corinth cuts across the NNW-SSE regional trend of the Hellenic mountain chain and overlies the Pindus, Parnassos and Othris zones of the internal Hellenides. This has resulted in a NNW-SSE and NW-SE structural grain to the area, which may have had some control on the later extensional deformation (McKenzie, 1972; 1978; Papazachos & Papadopoulos, 1977; Makris, 1976; 1978; Le-Pichon & Angelier, 1979; Angelier et al., 1982; Papadopoulos et al., 1986; Doutsos et al., 1988; Jackson & McKenzie, 1988). In the northern part of the Gulf of Corinth Rift, the mountain chains of Elikonas, Parnassos – Giona and part of Pindos are situated.

DELPHI-ARAHOVA-AMFISSA FAULT ZONE

One of the most important and impressive fault zones of the Central Greece area is the Amfissa – Delphi – Arahova Fault Zone (Pèchoux, 1977; Sebrier, 1977; de Boer & Hale, 2000). Detailed field mapping along with a wealth of historical documents and references for strong earthquakes back to 373 BC unveil an important and complex active fault structure (Piccardi, 2000; Valkaniotis, 2009). The fault zone extends along the southern rims of Mt Parnassos for a total length of more than 25 km and terminates to the west in Mt Giona over the plain of Amfissa (Figure 2). Normal- to oblique-slip displacement in the fault zone (Delphi – Arahova faults) is undergoing a intriguing transition to strike-slip displacement in the western part (Agia Efthimia fault) documented during field mapping (Valkaniotis, 2009). The mountainous area between Kifissos Basin and Amfissa – Delphi – Arahova Fault zone contains smaller fault structures following pre-existing alpine fault zones reactivated in the present extensional stress regime.

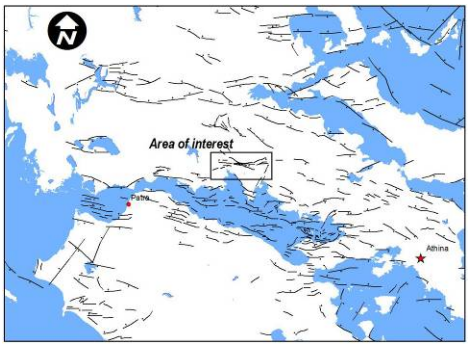

Fig. 1: Active and possible active faults in Central Greece. Fault data from Pavlides et al. (2007, 2008)

Delphi fault is a normal-oblique normal fault, with dipping to the south and strike direction NW-SE to WNW-ESE for the western part and W-E for the central part (Figure 2). Bedrock lithology is compiled by alpine (Jurassic-Creataceous) limestones of Parnassos-Giona geotectonic unit. In the hanging-wall, these limestones are overlain by flysch sediments, and a thick unit of Quaternary consistent and loose breccias and scree.

The Delphi fault cuts through the archaeological site of the Delphi Oracle. Clearence of recent (historical) depostis in the site due to archaeological excavations provide a detailed examination of the fault zone structure and earthquake fault displacement. The fault zone, reaching a thickness of 500-2000 m in Delphi-Arahova valley, consists of sub-parallel fault planes, with a mean dip of 70-80^0, converging in a depth of ~2 km with the main fault surface of 60^0 dip (Valkaniotis, 2009).

The entire set of monuments that constitute the archaeological area of Delphi (Stadium, Sanctuary of Apollo, Castalia spring, High School, Temple of Athena) are placed in front of the main surface of the fault at Delphi, which forms a striking morphological vertical scarp. The archaeological site of Delphi is situated in an active scree deposition area, with

continuous rock and debris due to the high relief and tectonic weakening of the bedrock. Severe damages and surface ruptures are reported in Delphi (Piccardi, 2000; Papadopoulos, 2000; Valkaniotis, 2009) for numerous historical earthquakes (373BC, 278BC, 326AD, 552AD, 1870AD). Rock falls in the vicinity of Delphi are reported during numerous other small-large earthquakes in the broader area. The last strong earthquake in the Delphi-Arahova-Amfissa fault zone was the 1870 event, with a magnitude of 6.8 and a possible rupture of the whole fault zone (Schmidt, 1879; Ambraseys & Pantelopoulos, 1989; Papadopoulos, 2000).

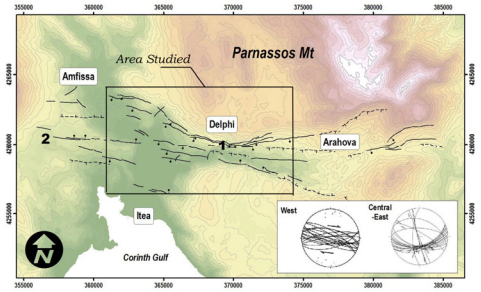

Fig. 2: The Delphi-Arahova-Amfissa Fault Zone. Fault plane projections for western and central-east part. After Valkaniotis (2009).

EVALUATING THE EARTHQUAKE-INDUCED LANDSLIDE HAZARD

The potential of a slope failure triggered by an earthquake, can be evaluated by three main methods; pseudostatic, permanent or statistical analysis (Miles & Keefer, 2000). The latter accesses the landslide hazard by assuming the past predicts the future and the pseudostatic employs a static slope stability analysis with the addition of a horizontal force modeling the earthquake ground motion (Miles & Keefer, 2009). The second analysis, proposed by Newmark (1965), provides information regarding actual slope stability based on accepted characterization of the severity of the earthquake shaking (Miles & Keefer, 2009).

The development of a Newmark analysis requires the evaluation of the parameters of the expected earthquake shaking and the capability of the geological unit to resist this dynamic effect. The latter parameter is quantified as the critical acceleration (a_c), a threshold ground acceleration necessary to overcome basal sliding resistance and initiate permanent downslope movement (Jibson, 2007). The computation of critical acceleration is based on the following equation proposed by Newmark, (1965)

$$a_c = (FS - 1) g \sin a \qquad (1)$$

where FS is the factor of safety, α is the angle of the sliding surface (slope angle), *g* is the acceleration of gravity.

According to Jibson et al. (1998), the factor of safety is evaluated using a relatively simple limit-equilibrium model of an infinite slope in material having both frictional and cohesive strength and is given by:

$$FS = \frac{c'}{\gamma t \sin a} + \frac{\tan \varphi'}{\tan a} - \frac{m \gamma_w \tan \varphi'}{\gamma \tan a} \qquad (2)$$

where φ' is the effective friction angle, c' is the effective cohesion, α is the slope angle, γ is the material unit weight, γ_w is the unit weight of water, t is the thickness of the mass at right angles to the slope and m is the proportion of the slab thickness that is saturated.

A Newmark analysis can be extended to regional analysis using GIS software (Miles & Keefer, 2000), *Arcinfo*, by applying equations 1 and 2 to raster data layers created for each input variable.

APPLYING THE NEWMARK APPROACH TO DELPHI AREA

The first step in the Newmark approach is the calculation of the factor of safety of the slope using equation 2. Therefore, the strength parameters of the geological units in the specific area should be evaluated. In our study, for the heavily jointed and weathered limestone in the study area, mean values of 30 ^{o} (angle of friction) and 15 kPa (cohesion) were employed and 30 ^{o} and 10 kPa for the formation of flysch, respectively, based on literature review.

Information from the literature was used to estimate the thickness of the failed material parallel to the slope. Khazai & Sitar (2000) proposed a correlation between slope angle and the thickness of the failed mass in which a slope angle between 40-60^{o} corresponds to a thickness of 1m; this was adopted in the present study.

Finally, the value of the topographic slope angle α (figure 3) was obtained from the DEM of a 30 m grid prepared from contour lines on the 1:5000-scale topographic maps using ArcInfo Software. In the study area the slope angle varies from 0^{o} to 60^{o} , however in this research we took into consideration only the areas where slope angle α>20 ^{o}.

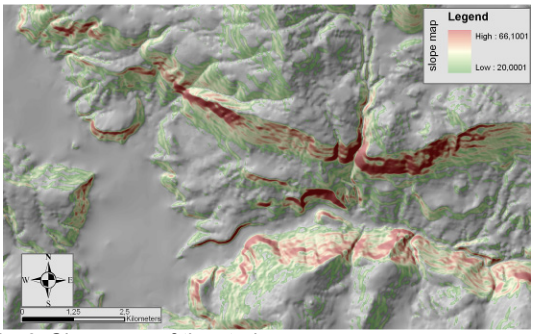

Fig. 3: Slope map of the study area.

Having computed the factor of safety, the next step was the estimation of the critical acceleration using equation 1. However, it was first necessary to modify estimated values of Fs <1, as the model should be stable before the earthquake shaking occurs (Jibson

et al., 1998). In order to achieve this, the cohesion of the geological units was increased, mainly in steep areas, until a factor of safety equal to one was accomplished. In order to avoid unrealistic cohesion values, the procedure suggested by Jibson et al. (1998) was used and an Fs of 1.001 was assigned to the unstable cells (figure 4).

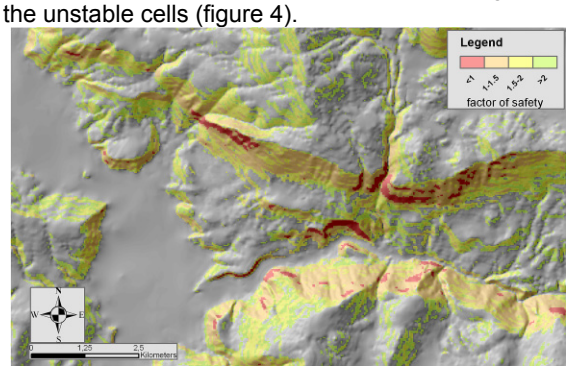

Fig. 4: Map showing the distribution of the fact of safety against slope instability.

The critical acceleration value for each 30 m-grid pixel was then computed and a relative map was compiled for the whole area of Delphi using the spatial analysis of ArcInfo Software. The critical-acceleration map (figure 5) can be characterized as a seismic landslide susceptibility map as it delineates areas prone to slope failure independent of any ground-shaking scenario (Jibson et al., 1998).

The value of the peak ground acceleration (PGA) that was employed in our study was estimated using the attenuation relationship proposed by Skarlatoudis et al. (2003) and by taking into consideration as earthquake magnitude the relevant seismic event of 1870.

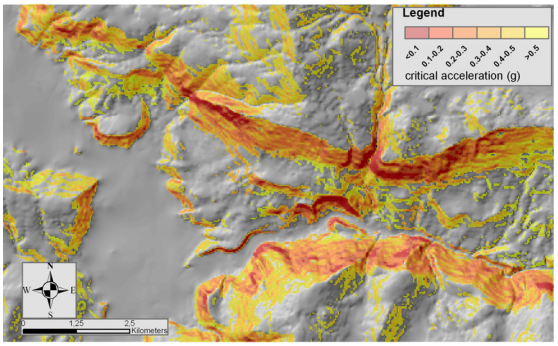

Fig. 5: Map showing the distribution of the value of critical acceleration

As an outcome, a PGA contour map of the study area was developed based on the computed values of ground motion using the Euclidean distance model provided by ArcInfo software. As can be seen in figure 6, the value of PGA in the study area varies from 0.32 to 0.71g.

The next step in the analysis developed by Newmark (1965) is the calculation of the cumulative permanent displacement of the slopes for the given level of ground shaking. According to Jibson et al. (1998), Newmark's method is based on a fairly simple model of rigid-body displacement and thus does not necessarily precisely predict measured landslide displacements in the field. Rather, Newmark's displacement is a useful index of how a slope is likely to perform during seismic shaking.

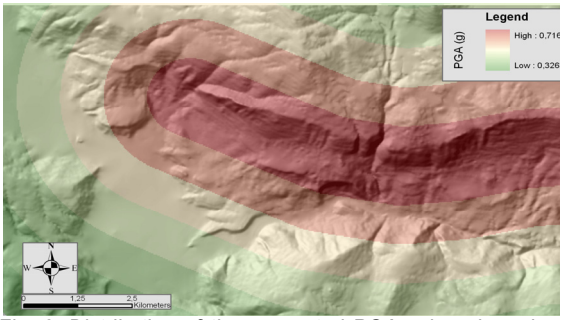

Fig. 6: Distribution of the generated PGA values based on the scenario of 1870 earthquake.

In the present study, the Newmark displacement was computed using equation [3] proposed by Jibson (2007), valid for a magnitude from 5.3 to 7.6. This equation estimates rigid-block Newmark displacement as a function of the critical acceleration and peak ground acceleration.

$$\log D_n = -2.710 + \log\left[\left(1-\frac{a_c}{a_{max}}\right)^{2.335}\left(\frac{a_c}{a_{max}}\right)^{-1.478}\right] + \quad (3)$$

$$+0.424 \times M \pm 0.454$$

where D_n is Newmark displacement in centimeters, a_c is critical (yield) acceleration in g's, and a_{max} is the peak horizontal ground acceleration in g's.

The distributions of the estimated values of Newmark displacement are shown in figure 7. The boundary values taken for the applied approach of Newmark's displacement were 2, 5, 10, 25, 50 and 100 cm. Sites where the estimated Dn is >5 cm can be considered as prone to slope failure while failure is unlikely where Dn < 5 cm. As it is shown in figure 7, most of the study area is considered as a low potential to earthquake-induced rockfalls zone since the computed newmark displacement ranges between 2 and 5 cm. However, a "hotspot", an area of high potential to slope failures, is delineated at the eastern part of the archeological area of Delphi where the estimated displacement is >100 cm.

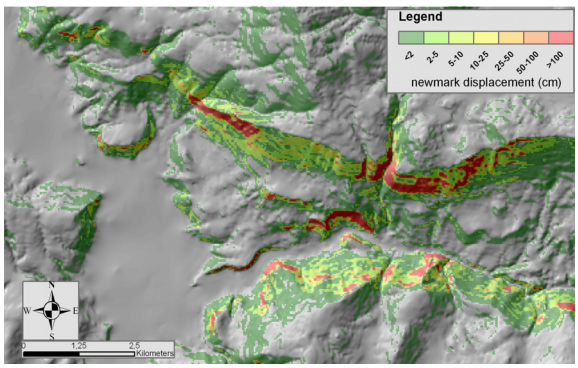

Fig. 7: map showing the estimated Newmark displacement values in the area of Delphi

CONCLUSIONS

The goal of this study was the evaluation of the potential of rockfall occurrence generated by seismic events in the vicinity of the archaeological site of Delphi, Greece. In order to achieve this, the scenario of 1870 earthquake was taken into account. The outcome provided by this research indicates that the value of Newmark displacement close to the archaeological site is low and the area is considered as low potential to earthquake-induced rockfalls. However, high values of displacement were estimated at the archaeological area where the factor of safety against slope failure and the critical acceleration are less than 1 and 0.1g, respectively. Thus, even a small magnitude seismic event could generate rockfalls.

Acknowledgements: The study of active faults and the evaluation of their potential have been financial supported by the General Secretariat for research and technology of Greece. The authors of this study would like to thank the anonymous reviewers for their constructive comments.

References

Ambraseys, N. Pantelopoulos, P. (1989). The Fokis earthquake of 1 August 1870. *Journal European Earthquake Engineering*, 3, 10-18.

Angelier, J., Lyberis, N., Le-Pichon, X., Barrier, E., & Huchon, P. (1982). The tectonic development of the Hellenic Arc and the Sea of Crete: a synthesis. *Tectonophysics*, 86, 159 -196.

De Boer J.Z., J. R. Hale (2000). The geological origins of the oracle at Delphi, Greece, in: McGuire, B. et al., (eds) The archaeology of geological catastrophes. *Geological Society of London*, Special Publication, 171, 399–412.

Doutsos, T., Kontopoulos, N. & Poulimenos, G. (1988): The Corinth-Patras rift as the initial stage of continental fragmentation behind an active island arc (Greece). *Basin Research*, 1, 177-190.

Jackson, J.A. McKenzie, D.P. (1988). The relationship between plate motions and seismic tensors and the rate of active deformation in the Mediterranean and Middle East. *Geophysical Journal*, 93, 45-73.

Jibson, R.W, (1993). Predicting earthquake-induced landslide displacements using Newmark's sliding block analysis. Transp Res Rec 1411:9–17

Jibson, R.E, (2007). Regression models for estimating coseismic landslide displacement. *Engineering Geology* 91:209–218

Jibson, R.W., Keefer, D.K, (1993) Analysis of the seismic origin of landslides: examples from the New Madrid Seismic Zone. *Geological Society America Bulletin* 105(4):521–536

Jibson, R.E., Harp, E.L., & Michael, J.A, (1998) A method for producing digital probabilistic seismic landslide hazard maps: an example from the Los Angeles, California area. USGS open-file report, pp 98–113

Keefer, D, (1984) Landslides caused by earthquakes. *Geological Society America Bulletin* 95:406–421

Keefer, D.K., Wilson, R.C, (1989) Predicting earthquake-induced landslides, with emphasis on arid and semi-arid environments. In: Landslides in a semi-arid environment. *Inland Geological Survey Society*, 2:118–149

Khazai, B., Sitar, N, (2000). Landsliding in native ground: a GIS-based approach to regional seismic slope stability assessment, report. http://www.ce.berkeley.edu/*khazai/research

Le-Pichon, X. Angelier, J. (1979). The Hellenic arc and trench system a key to the neotectonic evolution of the eastern Mediterranean area. Tectonophysics, 60, 1-42.

Makris, J. (1976). A dynamic model of the Hellenic arc deduced from geophysical data. *Tectonophysics*, 36, 339-346.

Makris, J. (1978). The crust and upper mantle of the Aegean region from deep seismic soundings. *Tectonophysics*, 46, 269-284.

McKenzie, D.P. (1972). Active tectonics of the Mediterranean region, *Geophysical Journal Research Society*, 30, 109-182.

McKenzie, D. (1978). Active tectonics of the Alpine-Himalayan belt: the Aegean Sea and surrounding regions. *Geophysical Journal Research Society*, 55, 217-254.

Miles, S.B., Keefer, D.K, (2000). Evaluation of seismic slope performance models using a regional case study. *Environmental Engineering Geoscience* 6(1):25–39

Miles, S.B., Keefer, D.K, (2009). Evaluation of CAMEL–Comprehensive Areal Model of Earthquake-induced Landslides. *Engineering Geology* 104: 1–15

Newmark, N.M, (1965). Effects of earthquake on dams and embankments. *Geotechnique* 15(2):139–160

Papadopoulos, G.A. (ed.) (2000). Historical earthquakes and tsunamis in the Corinth rift, central Greece. National Observatory of Athens, Institute of Geodynamics, Publication No 12. 128p.

Papadopoulos, G.A., Kondopoulou, D.P., Leventakis, G.A. & Pavlides, S.B. (1986). Seismotectonics of the Aegean region. *Tectonophysics*, 124, 67-84

Papazachos, B.C. and Papadopoulos, GA. (1977). Deep tectonic and associated ore deposits in the Aegean area. Proc. 6th Colloq. Geology Aegean Region, 3, 1071-1080.

Pavlides, S., Chatzipetros, A. & Valkaniotis, S. (2007). Seismically Capable Faults In: *Aegean Broader Area: Criteria For Classification. Geological Society Bicentenary Conference: Earth Sciences in the Service of Society*, 10-12 September 2007, London. Abstract Book, 124-125.

Pavlides, S., Chatzipetros, A. & Valkaniotis, S. (2008). Active faults of Greece and surroundings. In Proceedings of the 33rd International Geological Congress, Oslo, Norway. Abstract.

Pèchoux, P. Y. (1977). Nouvelles remarques sur les versants Quaternaires du secteur de Delphes. *Revue de Gèographie Physique et de Gèologie Dynamique*, 19:83–92

Piccardi, L. (2000). Active faulting at Delphi, Greece: Seismotectonic remarks and a hypothesis for the geologic environment of a myth. *Geology*, 28: 651–654.

Schmidt, J. (1879). Studien ueber Erdbeben, ed. Georgi, A. (Leipzig), 352p.

Sebrier, M. (1977). Tectonique recente d'une tranversale a l'Arc Egeen . These de Docteur, Academie de Versailles, Universite de Paris XI, 100p.

Skarlatoudis, A.A., Papazachos, C.B., Margaris, B.N., Theodulidis, N., Papaioannou, Ch., Kalogeras, I., Scordilis, E.M., & Karakostas, V, (2003). Empirical peak ground-motion predictive relations for shallow earthquakes in Greece. *Bulletin of Seismological Society of America* 93(6): 2591–2603

Valkaniotis, S. (2009). Correlation Between Neotectonic Structures and Seismicity in the broader area of Gulf of Corinth (Central Greece). Unpublished PhD Thesis, Aristotle University of Thessaloniki, 2009, 247pp.

EARTHQUAKE ARCHAEOLOGY

INQUA PALEOSEISMOLOGY AND ACTIVE TECTONICS

SEDIMENTARY BURIAL OF ANCIENT OLYMPIA (PELOPONNESE, GREECE) BY HIGH-ENERGY FLOOD DEPOSITS – *THE OLYMPIA TSUNAMI HYPOTHESIS*

Vött, Andreas (1), Fischer, Peter (2), Hadler, Hanna (1), Handl, Mathias (3), Lang, Franziska (4), Ntageretzis, Konstantin (1), Willershäuser, Timo (1)

(1) Institute for Geography, Johannes Gutenberg-Universität, 55099 Mainz, GERMANY. E-Mail: voett@uni-mainz.de
(2) Institute for Geography, Universität zu Köln, Albertus-Magnus-Platz, 50923 Köln, GERMANY. E-mail: peter.fischer@uni-koeln.de
(3) Philipps-Universität Marburg, Biegenstraße 10, 35037 Marburg, GERMANY
(4) Department of Classical Archaeology, Technische Universität Darmstadt, El-Lissitzky-Str. 1, 64287 Darmstadt, GERMANY. E-mail: flang@klarch.tu-darmstadt.de

Abstract(Sedimentary burial of ancient Olympia (Peloponnese, Greece) by high-energy flood deposits – The Olympia tsunami Hypothesis): *Detailed geo-scientific studies were carried out in the Kladeos and lower Alpheios River valleys in order to clarify the mystery of the rapid burial of Olympia under 4-6 m of sediments after the 6th cent. AD and subsequent erosion of the Kladeos River by 8-10 m down to the ancient flow level. Sedimentological, geophysical, geochemical and microfaunal analyses were conducted along the Olympia terrace by means of 22 vibracores and 70 resistivity tomography transects. Geomorphological studies revealed strong discrepancies between the present hydraulic potential of the Kladeos River and the dimension and structure of the Olympia terrace. Our results show that the Kladeos River valley and Olympia experienced at least four distinct phases of catastrophic high-energy flood events. Sedimentary, geochemical and faunal traces found in the adjacent Basin of Flokas-Pelopio clearly document multiple tsunami impact. Identical fingerprints and strong stratigraphical correlations were also detected along the Kladeos River beyond the Ridge of Flokas-Platanos. We thus set up and discuss the* Olympia Tsunami Hypothesis *saying that the shallow saddles of the ridge were repeatedly overflowed by tsunami waters and the cult site Olympia was rather destroyed by tsunami than by fluvial processes related to the Kladeos River.*

Key words*: Olympia, high-energy deposits, tsunami, geoarchaeology*

INTRODUCTION

Olympia, used as famous cult site for Panhellenic games between Archaic times and the 4th cent. AD, is located at the confluence of the Kladeos and Alpheios Rivers in the western Peloponnese (Greece). The sedimentary burial of ancient Olympia is one of the most interesting geoarchaeological mysteries in the Mediterranean world. The sedimentological evolution since early medieval times shows two different steps. After the 6th cent. AD, the site was covered by 4-6 m of sediments; subsequently, the nearby Kladeos River eroded its bed by 8-10 m approximately reaching the level existing during antiquity.

Previous studies presented different explanations for this setting. Büdel (1981), together with Dufaure & Fouache 1988, Fouache & Pavlopoulos 2011, are in favour of anthropogenically induced soil erosion as main factor for enhanced sediment accumulation at the mouth of the Kladeos River during phases of uncontrolled landuse, especially after the Slavic invasion in early medieval times. On the contrary, Fountoulis & Mavroulis (2008) hold distinct periods of wet climate responsible for accelerated sediment accumulation. However, both scenarios do not give explanations for the change from accumulation to subsequent erosion dynamics within the past 1500 or so years.

Before systematic excavation of the site by the German Archaeological Institute started in 1875, the archaeological remains of Olympia were integrated into a wide terrace, the so called Olympia terrace. From a geomorphological point of view, this terrace can be traced both downstream the Alpheios River towards the present coast of the Gulf of Kyparissia and upstream all along the lower and middle Kladeos River valley. In the Kladeos area (Fig. 1), the Olympia terrace is up to 300-500 m wide. It is present on both sides of the Kladeos River with a distance of up to 200 m between the opposite terrace faces. Considering that the Kladeos River is rather a creek than a river with a perennial runoff concentrated within a maximum 5-8 m-wide secondary river channel and maximum water flow depths of 2-3 m during winter and heavy rain events, there is a considerable discrepancy between the dimension and the hydraulic potential of the Kladeos River on the one hand, and the local geomorphology of the Olympia terrace on the other hand.

The objectives of our investigations thus were (i) to establish a well-based stratigraphy of the Olympia terrace along the Kladeos River by detailed geomorphological and sedimentological studies, (ii) to compare these results with stratigraphies found along the Alpheios River, especially in the adjacent Basin of Flokas-Pelopio, and (iii) to find a geomorphological model which best explains the hydro-dynamic finger-

print and distribution pattern of the encountered sediments.

METHODS

We carried out geomorphological mapping of the Olympia terrace using topographical and geological maps and remote sensing data. Stratigraphical studies are based on 22 vibracores, 16 of which were drilled in the Kladeos River valley and 6 in the Alpheios River valley by means of a handheld Cobra mk1 vibracorer (Atlas Copco) and a Nordmeyer drill rig (type RS 0/2.3). We used core diameters of 6 and 5 cm. Maximum coring depth was 17 m below ground surface (m b.s.). Earth resistivity tomography (ERT) was conducted to study subsurface structures and stratigraphies along 70 transects using a multi-electrode geo-electrical Iris instrument (type Syscal Junior Switch 48). Selected sediment samples were analysed by their microfossil content. Key cores were additionally cored with an inliner system and analysed using the X-ray fluorescence technique (XRF). We also conducted grain size analyses for selected samples. Vibracoring sites and ERT transects were measured by means of a differential GPS (type Topcon HiPer Pro) with an accuracy of 2 cm or better. A local geochronostratigraphical framework was established using age estimations of diagnostic ceramic fragments, radiocarbon dating and Optically Stimulated Luminescence (OSL) approaches.

RESULTS

Vibracores ALP 3, 4, 5 and 8, drilled in the environs of ancient Olympia, especially on top of the Olympia terrace towards the south of the southeastern Roman baths and on top of the Olympia terrace to the west of the Kladeos, revealed characteristic sequences of light brown, silt- and clay-dominated alluvial or colluvial deposits with remains of freshwater fauna which are repeatedly interrupted by up to four sections out of light brown sand and gravel. These coarse-grained deposits were found in comparable stratigraphic positions in every core and thus indicate synchronous flooding of wide areas related to high flow velocities. Associated to these deposits, we found sedimentary structures such as basal erosional unconformities in underlying silt deposits, fining upward sequences with mud caps and abundant marine shell debris and marine microfauna. XRF analyses revealed clear maximum peaks of the Ca/Ti ratio for the coarse-grained sections. The calcium content documents the input of calcium carbonate from biogenic and bedrock sources, the titan content reflects terrigenous input by subaerial weathering into the sedimentary system. Results were also tested for masking and matrix effects which can be excluded as major sources of bias. Apart from a distinct and ca. 1 m-thick palaeosol found on top of a coarse-grained section at ca. 4 m b.s. in core ALP 8 (Fig. 2), which includes Roman sherds, palaeosols are missing. A charcoal fragment from a fining upward sequence out of sand and gravel deposited under high-energy conditions at site ALP 5 was ^{14}C AMS radiocarbon dated to 585-647 cal AD (2σ interval, 3.74 m b.s.).

Vibracores ALP 12-15 and 19 were drilled in the middle Kladeos River valley around the villages of Mageiras and Kladeos on top of the Olympia terrace. Here, we also found predominating clayey to silty deposits accumulated under quiescent to moderate flow conditions. These deposits are grey in colour, partly include lots of plant material and freshwater shell and thus document a permanent water body of fluvio-limnic nature. Similar to the situation at Olympia, we found up to four intersecting layers of sand and gravel, partly grey (base and mid-section), partly light brown in colour (top), associated to high-energy sediment type structures such as basal unconformities, muddy intraclasts, fining upward sequences and including abundant faunal remains of marine origin. Based on XRF measurements, the Ca/Ti ratio again shows clear maximum peaks stratigraphically corresponding to the intersecting coarse-grained layers. Thus, all along the Kladeos River valley between Kladeos, Mageiras and Olympia, the Olympia terrace shows a similar inner structure with the individual coarse-grained high-energy layers lying in stratigraphically consistent positions. The same is true for both distal and proximal parts of each specific terrace section as documented by ERT transects.

We thus conclude, in a first step, that the Olympia terrace between Kladeos and Olympia documents at least four phases of high-energy flood events that obviously affected the whole valley bottom to an extent far beyond the dimensions of the present Kladeos river channel.

Vibracores 9-11 were drilled at the eastern fringe of the Basin of Flokas-Pelopio at a distance of 1 to 2 km to the west of the Kladeos River valley across the Flokas-Platanos Ridge. Vibracore ALP 10 lies around 2.2 km distant from the Alpheios River at a right angle opposite to its seaward flow direction. Despite the vicinity to the Alpheios River, vibracore ALP 9 does not include any pieces of gravel; it consists of homogeneously light brown (top) to grey (base), clayey to silty deposits accumulated in a low-energy freshwater lake environment. Associated to basal unconformities, we found several intersecting layers of sand with fining upward sequences and mud caps and marine faunal remains which clearly document episodic high-energy interruption of the allochthonous environment. Vibracore ALP 10, drilled at the western hill slope of the Flokas-Platanos Ridge, revealed a similar stratigraphic pattern with distinct interruptions of limnic (base and mid-section) and colluvial (top) deposits by predominantly sandy to gravelly high-energy deposits reaching up to 20 m above present sea level (m a.s.l.). In each case, at least the upper part of the intersecting layer consists of brown sediments of mostly terrestrial origin. The Ca/Ti ratios for both cores show distinct maximum peaks for the intersecting coarse-grained allochthonous material (Fig. 3).

Fig. 1: View of the middle Kladeos River valley (foreground) towards the west. The valley is separated from the adjacent Basin of Flokas-Pelopio (middleground) by the homonymous ridge. The Alpheios River valley connects the basin and the Gulf of Kyparissia (left background) in a direct line. Photo taken by A. Vött, 2011.

In the more seaward vibracore ALP 7, drilled some 8 km inland in the midst of the Alpheios River valley halfway between ALP 9 and the present coast, we found autochthonous marine sand at approx. 2.50 m below present sea level (m b.s.l.). Covered by a 10 m-thick layer of sandy gravel, this unit documents that the Gulf of Kyparissia extended far into today's Alpheios valley during the Holocene.

DISCUSSION

Sedimentary structures, geochemical fingerprints and faunal remains encountered at the western fringe of the Basin of Flokas-Platanos indicate episodic high-energy marine flooding from the sea side. Stratigraphies of cores ALP 9 and 10 clearly show tsunami-type marine incursions into a shallow lake and runup-backflow sequences at the adjacent hillside, respectively. Considering that at least parts of the lower Alpheios River valley were flooded by the sea during the Holocene and manifold traces of palaeotsunami are known from the present coast (Vött et al. 2011), these findings are plausible.

Considering, however, that both the geochemical and the overall stratigraphic patterns of the cores from the west of the ridge and from the Kladeos River valley itself are principally identical – documenting episodic high-energy input of coarse-grained marine sediments into prevailing quiescent environments – we hypothesize that marine flooding also affected the Kladeos River valley and Olympia. Our main arguments thus are of sedimentological and geochemical nature and based on consistent stratigraphies on either side of the Flokas-Platanos Ridge. We call this scenario the *"Olympia Tsunami Hypothesis"*.

As a major argument against our hypothesis one may bring forward the fact that Neogene bedrock units in the catchment area of the Kladeos River also include conglomerate and sand units, the latter being characterized by abundant remains of a Plio-Pleistocene marine fauna (IGME 1982). However, especially around Olympia and in most parts of the middle Kladeos River valley, Plio-Pleistocene marl and not sand is the predominant bedrock material provoking many landslides (IGME 1982, Christaras et al. 2002). Moreover, microfaunal analyses of selected core sections revealed freshwater ostracods in fine-grained silt-dominated deposits but exclusively marine species in high-energy flood sediments. In case, these were transported by a mega-Kladeos River with a width of several hundreds of meters – dimensions which are necessary to explain the consistent lateral distribution of this facies across the entire Olympia terrace – one would have to expect admixed freshwater or even river-borne species. This was not the case in the samples which we analysed. However, further attempts are needed to fully understand the fossil record of the high-energy flood deposits in the environs of Olympia.

Geomorphological studies carried out within our project revealed erosion as well as scouring features across the lower saddles of the Flokas-Platanos Ridge lying at about 60 m a.s.l. which indicate possible flow paths across the ridge.

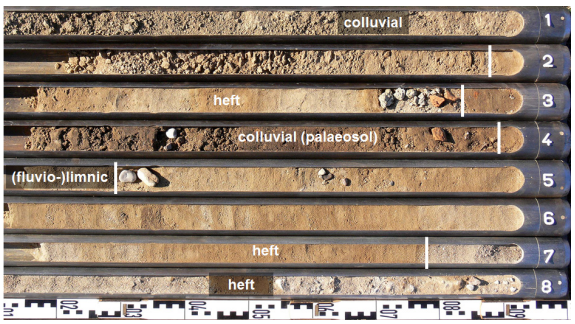

Fig. 2: Facies distribution pattern of vibracore ALP 8 (38.37 m a.s.l.) drilled on top of the Olympia terrace to the west of the Kladeos River some 250 m to the west of the Kronos hill. Several sandy to gravelly high-energy flood type (heft) deposits can be seen alternating with fine-grained colluvial or (fluvio-)limnic deposits. The mid-core palaeosol dates to Roman times. Please note the three fining upward sequences encountered in the uppermost heft unit. Photo taken by T. Willershäuser, 2010.

Concerning the elevation which, at a first glance, seems to be too high for tsunami flooding, one has to consider (i) channelling and accelerating effects of the tube-like and ca. 8 km-long lower Alpheios River valley during inflow, (ii) backwatering and boosting of inundating marine water masses because of blocked backflow in the Alpheios River valley itself and at the

breakthrough through Drouva Ridge, where the modern Alpheios dam is located, (iii) the arrival of subsequent waves of a longer wave train before backflow was completely accomplished, as well as (iv) potential interim changes in the topography due to landslides of the predominating Tertiary marls typical for the ridge. From the nearby coast, there is evidence of multiple tsunami landfall since the mid-Holocene and for tsunami run-up up to 18 m a.s.l. around the ancient site Pheia, one of the harbours of Olympia (Vött et al. 2011).

By the *Olympia Tsunami Hypothesis*, we suggest that tsunami waters repeatedly overflowed the lower saddles between Flokas and Platanos and then partly flowed upstream and partly downstream the Kladeos River valley, hereby creating a vast terrace structure way above the flow level of the Kladeos at that time. Subsequently, tsunami backflow concentrated along the Kladeos creek eroding an up to 200 m-wide gap into the terrace. Tsunami backflow through the breakthrough of the Alpheios across the Drouva Ridge was hindered and possibly blocked, at least during tsunami inundation of the Basin of Flokas-Pelopio. One of the high-energy flood deposits encountered near Olympia was dated to 585-647 cal AD which fits well with the earthquake in 551 AD during which Olympia is reported to have been destroyed. However, there are no historic accounts on catastrophic flooding of Olympia.

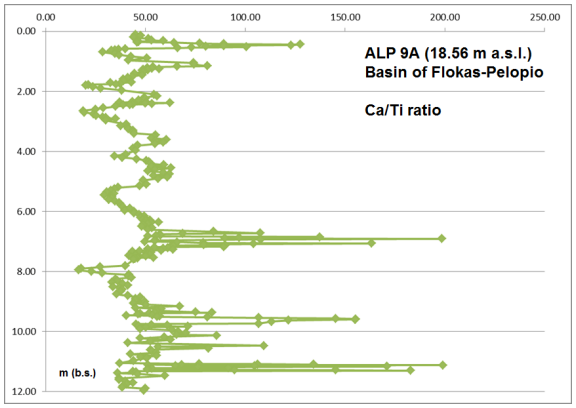

Fig. 3: Ca/Ti ratios for vibracore ALP 9A drilled at the western fringe of the Basin of Flokas-Pelopio at the foot of the homonymous ridge nearby Olympia. Allochthonous silt-dominated deposits of a quiescent limnic environment are characterized by a Ca/Ti base level around 50. Episodic interferences from the sea side by tsunami waves left behind marine sand deposits with Ca/Ti ratios up to 200. Similar Ca/Ti profiles and stratigraphies were found for vibracores in the Kladeos River valley and nearby Olympia.

CONCLUSIONS

Detailed geomorphological, sedimentological, geophysical, geochemical and microfaunal studies of the Olympia terrace in the Kladeos and the lower Alpheios River valleys allow to draw the following conclusions. (i) The Kladeos valley and the environs of Olympia were affected by at least four distinct phases of high-energy flood events by which the site was finally covered completely by sediments. (ii) Similar high-energy flood deposits were also encountered at the eastern fringe of the adjacent Basin of Flokas-Pelopio; due to their fossil content, their geochemical fingerprint, their geomorphological position and their stratigraphical pattern, they are interpreted as of tsunamigenic origin. (iii) In both areas, the high-energy facies is associated to sedimentary structures known from historic to recent tsunami events (basal unconformity, fining upward sequences, mud caps, ripped up intraclasts etc.) and is characterized by abundant fragments of a marine fauna. (iv) Geomorphological features such as marks of scouring and undercutting let us assume that tsunami overflow occurred across the comparatively shallow saddles between the villages of Flokas and Platanos wheras backflow was accomplished along the river valley as soon as blocking of the entrance of the Alpheios River into the Basin of Flokas-Pelopio by tsunami waters had ceased. We call this scenario "*The Olympia Tsunami Hypothesis*". (v) Our results, together with manifold geoarchaeological destruction patterns at Olympia, rather indicate catastrophic event-related flooding by tsunami than by the River Kladeos itself.

Acknowledgements: Sincere thanks are due to our cooperating partners G. Chatzi-Spiliopoulou (Olympia), I. Fountoulis (Athens), H.-J. Gehrke (Freiburg), A. Hoppe, R. Lehné (Darmstadt), K. Reicherter (Aachen), D. Sakellariou (Athens) and R. Senff (Athens/Olympia). Work permits were kindly issued by the Greek Institute for Geology and Mineral Exploration (IGME). We gratefully acknowledge funding by the German research Foundation (DFG, VO 938/3-1).

References

Büdel, J. (1981). *Klima-Geomorphologie*. 2nd edition. Bornträger. Berlin, Stuttgart. 304 p.

Christaras, B., Mariolakos, I., Dimitriou, A., Moraiti, E. & D. Mariolakos (2002). Slope instability at Olympia archaeological site in southern Greece. *Intern. Symp. "Landslides Risk Mitigation and Protection of Cultural and Natural Heritage", Abstract Volume.* Kyoto. 339-342.

Dufaure, J.-J. & E. Fouache (1988). Variabilité des crises d'âge historique le long des vallées d'Elide (Ouest du Peloponnèse). *Cahier Inter-universitaire d'Etudes Méditerranéennes,* 12: 259-278. Poitiers.

Fouache, E. & K. Pavlopoulos (2011). The interplay between environment and people from Neolithic to Classical times in Greece and Albania. In: *Landscapes and societies. Selected cases* (Martini, I.P., Chesworth, W. eds.). Springer. Dordrecht. 155-166.

Fountoulis, I., Mariolakos, I., Mavroulis, S. & I. Ladas (2008). Flood periods during prehistoric and Roman times in the Kladeos torrent basin – ancient Olympia (Greece). In: *8th Intern. Hydrogeol. Congr. Greece, 3rd MEM Workshop Fissured Rocks Hydrology, Abstract Volume* (Migiros, G., Stamatis, G., Stournaras, G. eds.). Athens. 809-818.

Institute for Geology and Mineral Exploration (IGME, 1982). Geological map of Greece, 1:50,000, Olympia Sheet. Athens.

Vött, A., Bareth, G., Brückner, H., Lang, F., Sakellariou, D., Hadler, H., Ntageretzis, K. & T. Willershäuser (2011). Olympia's harbour site Pheia (Elis, western Peloponnese, Greece) destroyed by tsunami impact. *Die Erde* (in press).

LANDSLIDE MAPPING TO ANALYSE EARTHQUAKE ENVIRONMENTAL EFFECTS (EEE) IN CARMONA, SPAIN – RELATION TO THE 1504 EVENT?

Vollmert, Andre (1), Klaus Reicherter (2), Pablo G. Silva (3), Tomas M. Fernandez-Steeger (4)

(1) Lehrstuhl für Ingenieur- und Hydrogeologie, RWTH Aachen University, Lochnerstr. 4-20, 52056 Aachen. GERMANY. Email: andre.vollmert@rwth-aachen.de
(2) Lehr- und Forschungsgebiet Neotektonik und Georisiken, RWTH Aachen University, Lochnerstr. 4-20, 52056 Aachen. GERMANY. Email: k.reicherter@nug.rwth-aachen.de
(3) Dpto. Geología, Escuela Politécnica Superior de Ávila, Universidad de Salamanca. Avda. Hornos Caleros, 50. 05003-Ávila. SPAIN. Email: pgsilva@usal.es
(4) Lehrstuhl für Ingenieur- und Hydrogeologie, RWTH Aachen University, Lochnerstr. 4-20, 52056 Aachen. GERMANY. Email: fernandez-steeger@lih.rwth-aachen.de

Abstract (Landslide mapping to analyse earthquake environmental effects in Carmona, Spain – relation to the 1504 event?): *The 1504 Carmona earthquake (intensity IX EMS) claimed the loss of human life and caused a number of Earthquake Environmental Effects. On the basis of historical data reported by George Bonsor (1918) this study is intended to estimate coseismic slope performance. The aim is to combine field investigations, geotechnical parameters and computerized models to generate digital probabilistic seismic landslide hazard maps on a local scale. GIS-based simulations of mass movements driven by hydrodynamical and gravitational processes are performed by means of the factor of safety, which is calculated for dry and fully water saturated conditions. Following Newmark´s sliding block model these approaches are extended to assess the potential of earthquake-triggered slope movements. Assuming a Peak Ground Acceleration of 0.3 g, representing the 1504 event, the most affected areas show a failure probability of 33.5 %.*

Key words*: 1504 Carmona Earthquake, Seismic Landslide Hazard Assessment, South Spain*

INTRODUCTION

In 1918 the archaeologist George Bonsor was the first scientist who published the effects of a strong earthquake near Carmona (South Spain) in 1504 (Bonsor, 1918). Based on the ESI-2007 Intensity Scale, Silva et al. (2009) attract notice again on this event in order to update Bonsor´s data. They focus on ground cracks, liquefaction, anomalous waves, flooding in rivers, temporary turbidity changes in wells and, especially, on mass movements, since landslides and rock falls belong to the most relevant phenomena of all EEE being observed in Carmona. This study provides different approaches to calculate the site scaled slope instability in terms of the 1504 earthquake (IX EMS) as a potential triggering factor for a number of observed landslides. Each of the methods combines geotechnical results and slope angles derived from a Digital Elevation Model (DEM). Figure 1 points out the sequential steps leading to the hazard-mapping procedure of the study. All simulations have been performed under dry and fully water saturated conditions.

LANDSLIDES IN CARMONA

Within the southern margin of the Guadalquivir river valley Carmona is founded on a small NE-SW trending ridge (Los Alcores). It consists of Miocene blue marls and grey clays coming from the southeast located Betic Cordillera front.

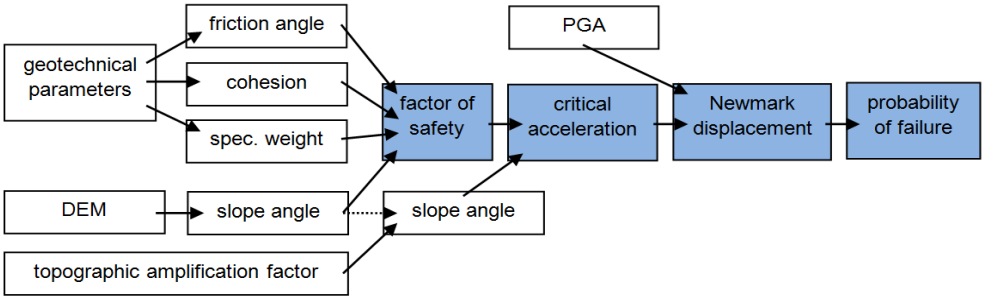

Fig. 1: Flow chart showing the steps involved in producing a seismic landslide hazard map; white: input parameters; blue: results (modified after Jibson et al., 2000).

This substratum is covered by a Late Neogene calcarenite unit, which outcrops in a steep cliff, surrounding large parts of the city. Both units can be subjected to massive landslides. In order to distinguish seismically triggered slope movements from others driven by hydrodynamical and gravitational processes, all landslide phenomena are classified according to type of movement, material and size of the displaced mass. Furthermore, all possible causes including geological, morphological, physical and human influences are determined as an important aim.

All important investigation sites are indicated in figure 2 showing the studied area around Carmona. The map also includes joint diagrams from

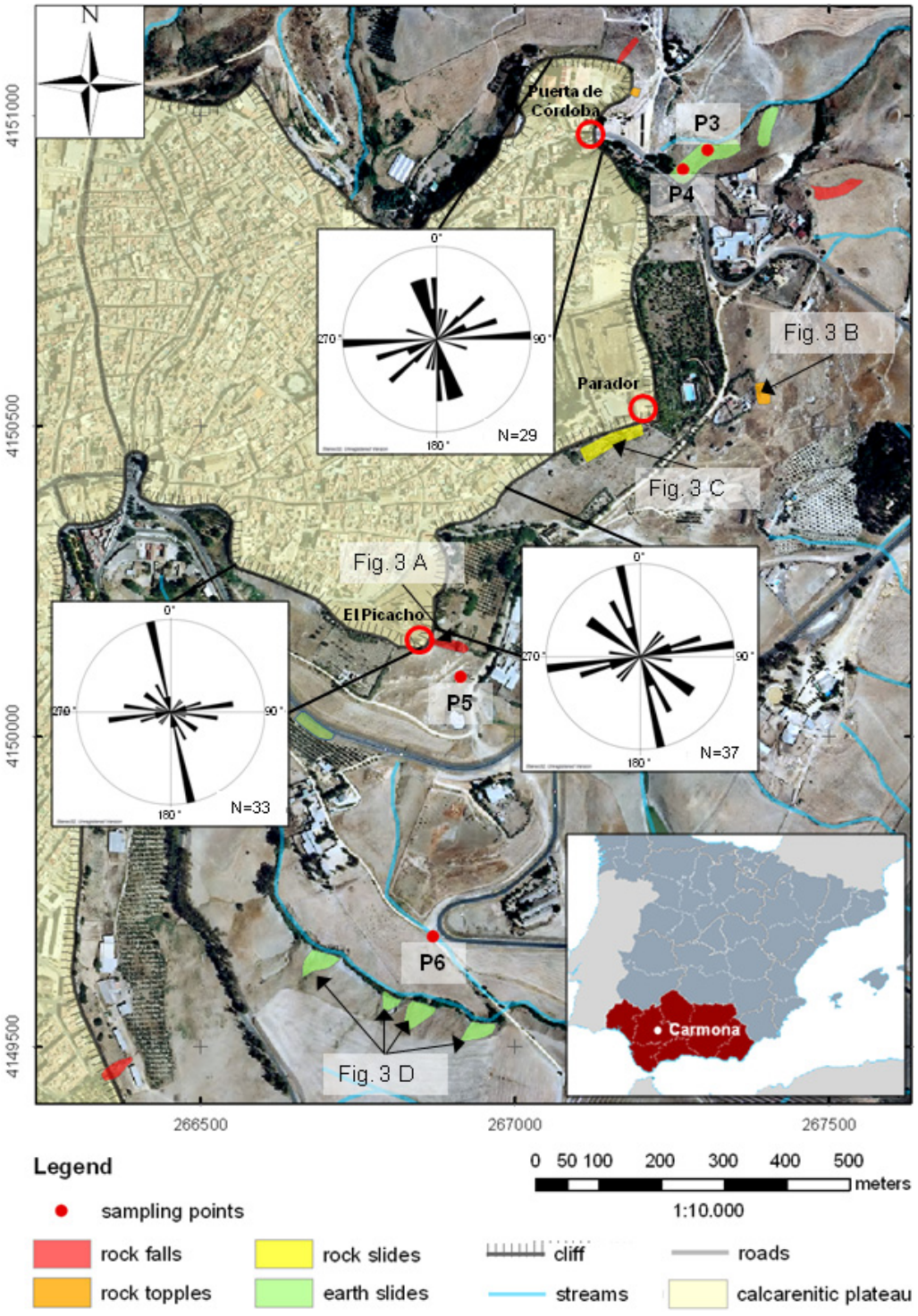

Fig. 2: Map of Carmona showing the sampling points for later geotechnical investigations, joint diagrams and the location of landslide phenomena illustrated in figure 3 (Gauss-Krüger coordinates).

calcarenite strata and the location of observed rock falls, topples and slides as well as earth slides in the unit of blue marls and grey clays. Typical examples of these types are illustrated in Figure 3.

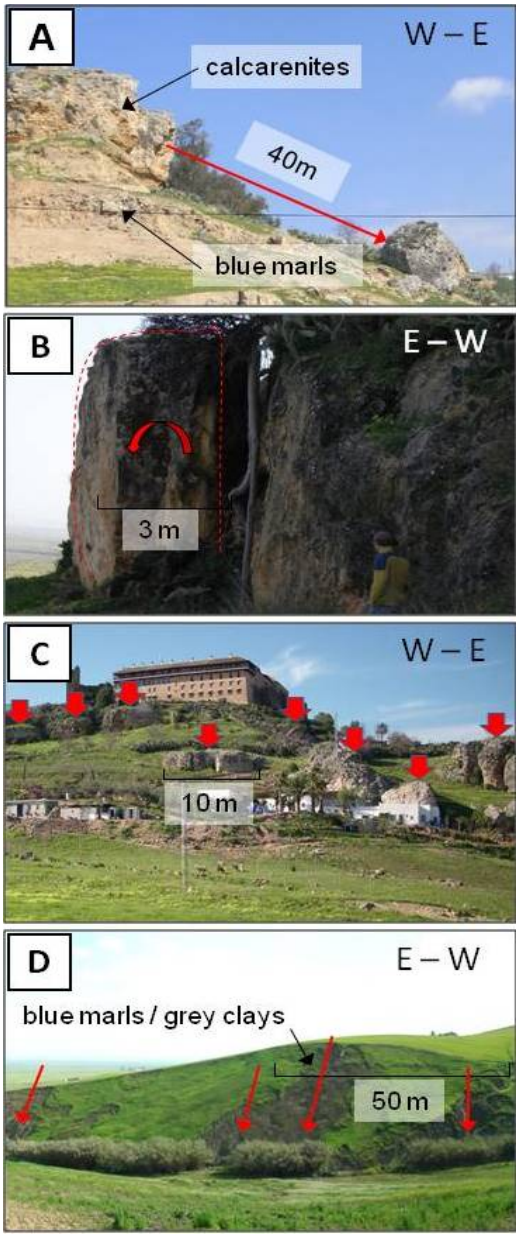

Fig. 3: Huge rock fall underneath the Picacho (A); Toppling process of a column of calcarenite rock (B); Calcarenitic boulders are transported downslope on softer clayey materials (C); Earth slides due to water saturated conditions and steep slope angles (D).

Landslides in Carmona are related to a number of preparative and triggering factors. Observed rock falls and topples in calcarenite strata can be mainly subjected to SSE- and ENE-striking tension cracks (fig. 2) and relatively low shearing parameters (c´ = 17 MPa; φ´ = 41°). Laboratory results of analysed loose material samples indicate effective cohesions between 13.04 and 20.16 kPa and angles of internal friction between 17.35 and 26.23°. This data and the high contents of clay minerals (35 – 66 %) are supposed to be essential for the occurrence of massive earth slides on steep slopes along the courses of streams.

Apart from these invariant parameters, both, water saturated soils caused by intensive rainfalls and earthquake shaking can be seen to be the most relevant causal factors for landslides in Carmona. Therefore, these triggering factors are considered in the following simulations.

SIMULATION OF SLOPE STABILITY

First slope stability has been simulated be means of the factor of safety, which is calculated by the ratio of the sum of the resisting forces that act to inhibit a slope failure to the sum of the driving forces that tend to cause a failure. The application of a Geographical Information System (ArcGIS 9.3) allowed a differentiated calculation for every grid cell (2 x 2 m), where input parameters vary due to different slope angles.

Based on the factor of safety the site-specific critical acceleration was calculated in a second step. According to Newmark´s sliding block analogy (Newmark, 1965) the critical acceleration is defined as the minimum horizontal seismic acceleration that is necessary to overcome the shear resistance of a friction block, resting on an inclined plane. That means, the higher the degree of slope stability, the higher the critical acceleration, which is needed to cause a failure.

To estimate the cumulative slope displacement during an earthquake, Wilson & Keefer (1983) developed a double integration approach based on numerically cumbersome calculations performed by Newmark (1965). Thereby, those sections of an earthquake accelerogram that exceed the critical acceleration of a slope are integrated two times to obtain the velocity and the cumulative displacement of the sliding block. Considering also the PGA of the Carmona earthquake (0.3 g) it was possible to determine the Newmark Displacement.

Newmark displacement rates are not directly correlated to the potential of earthquake-triggered landslides. For this reason, Jibson et al. (2000) developed a probabilistic empirical model, which allows the estimation of the probability of a failure for every grid cell (Eq. 1):

$$Pf = 0.335 + \left[1 - \exp\left(-0.048 D_N^{1.565}\right)\right] \quad [1]$$

They have calibrated these parameters with data from Southern California and anticipate that the mapping procedure is applicable in any areas susceptible to seismic slope failure. Therefore the model was used to compile digital probabilistic landslide hazard maps for dry and fully water saturated conditions in the study area (fig. 4).

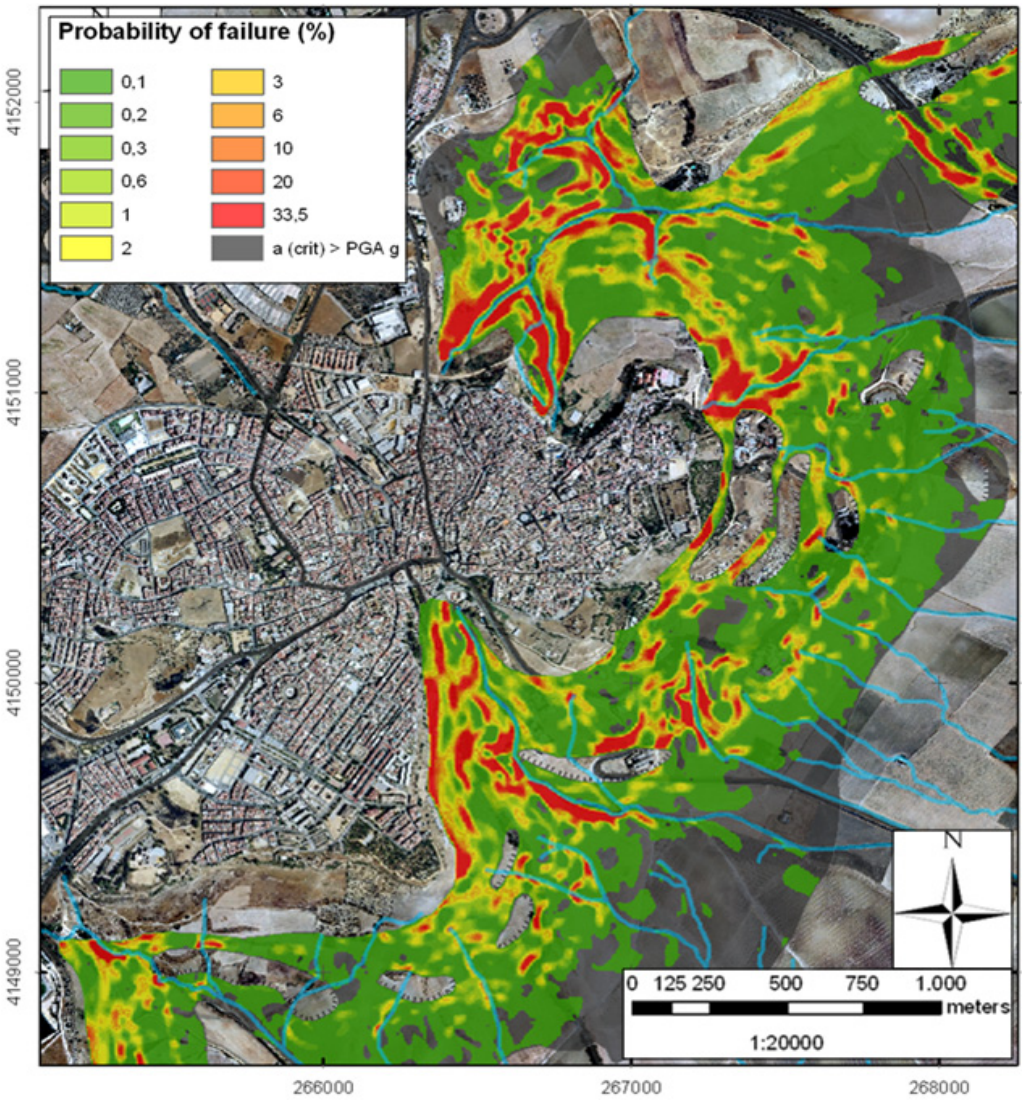

Fig. 4: Probabilistic landslide hazard map showing the probability of failure in case of an intensity-IX (EMS) earthquake under fully water saturated conditions (Gauss-Krüger coordinates).

The most affected areas show a failure probability of 33.5%. They are generally related to the same slopes indicating a higher potential of landslides under non-seismic conditions, however, they are extended.

CONCLUSION

The performed assessment of earthquake-triggered landslides provides useful information to estimate potential damages during future earthquakes. In this sense, the designation of vulnerable areas can be used to predict interruptions of access roads, gas and water pipes or electrical lines in case of another strong earthquake in Carmona when landslides of large volumes will be triggered with high probability.

Acknowledgements: This work would not have been possible without the support of many persons. It is a pleasure for me to thank those who always helped and inspired me during this project.

References

Bonsor, J. (1918): El terremoto de 1504 en Carmona y en Los Alcores. Boletín de la Real Sociedad Española de Historia Natural, 18, 115-123.

Jibson, R. W., Harp, E. L. & Michael, J. A. (2000): A method for producing digital probabilistic seismic landslide hazard maps. Engineering Geology, 58, 271-289.

Newmark, N. M. (1965): Effects of earthquakes on dams and embankments. Géotechnique, 15, 139-160.

Silva, P.G., M.A Rodríguez-Pascua, R. Pérez-López, J.L. Giner-Robles, J. Lario, T. Bardají, J.L. Goy & C. Zazo, (2009). Geological and archaeological record of the 1504 AD Carmona earthquake (Guadalquivir Basin, South Spain): a review after Bonsor, 1918. In: *Archaeoseismology and Palaeoseismology in the Alpine-Himalayan Collisional Zone* (Pérez-López, R., Grützner, C., Lario, J., Reicherter, K., Silva, P.G. eds). Baelo Claudia, Spain, 139-142.

Wilson, R. C. & Keefer, D. K. (1983): Dynamic analysis of a slope failure from the 6 August 1979 Coyote Lake, California, earthquake. Bulletin of the Seismological Society of America, 73, 863-877.

STORM SURGE LAYERS WITHIN A CHANGEFUL HOLOCENE ENVIRONMENT OR SEDIMENTARY TRACES OF PALAEO-TSUNAMIGENIC EVENTS. PROS AND CONS OF ON-SITE FINDINGS, JADE BAY, SOUTHERN NORTH SEA, GERMANY

Wartenberg, Wolfram (1), Andreas Vött (2), Hanna Hadler (2), Timo Willershäuser (2), Holger Freund (1), Stefanie Schnaidt (1)

(1) Institute for Chemistry and Biology of the Marine environment (ICBM), Carl von Ossietzky Universität Oldenburg, 26382 Wilhelmshaven. Germany. Email: wolfram.wartenberg@uni-oldenburg.de

(2) Institute for Geography, Johannes Gutenberg-Universität, 55099 Mainz. Germany. Email: voett@uni-mainz.de

Abstract (Storm surge layers within a changeful Holocene environment or sedimentary traces of palaeo-tsunamigenic events. Pros and cons of on-site findings, Jade Bay, Southern North Sea, Germany): *Tsunamigenic events are well known to occur within the Mediterranean and along many seismo-tectonically active coasts all over the world. Their incidence is almost excluded for the southern North Sea, a shore line well known to be prone to storm surges that in parts occur at a regional scale. Accordant chronicles describe floods of sheer enormity, for instance affecting the Dutch and the German coastal sections at the same time (e.g. Cosmas and Damian flood, 1509).*

Key words*: tsunami, storm, North Sea, Germany*

INTRODUCTION

The Jade Bay in Lower Saxony, northwest Germany, is the largest tidal inlet of the German North Sea coast. The modern embayed tidal flat system shows a changeful Holocene sedimentary record from terrestrial-driven to seaward-influenced environments (Streif, 2004). The Jade area has been investigated interpreting sedimentary markers, pollen and macro remains taken from 45 cores. Probing was carried out between 2009 and 2011. The sedentary chronology is based on 36 radiocarbon and pollen datings. Direct age determination of clastic sediments will be complemented in late 2011 using optical dating.

The palaeo-geomorphology of the Jade area is influenced by a major north-south trending channel (Sindowski, 1972), representing the structural rudiment for an early stage of the advancing sea. From approximately *4500* cal BC onwards, the palaeo-coastline must have been close, starting to increase the groundwater level. *Alder* carr to *Cyperaceae* fen peat started to develop extensively before marine conditions became dominant from ~3000 to ~2800 cal BC (Wartenberg & Freund, in press). Two different palaeo-environments are related to the present-day Jade Bay, each identifying a distinctive local depositional development (Wartenberg & Freund, in press). From the west to the centre, the equivalent early Holocene landscape morphology is drainage-driven, feeding the associated pronounced basal peat with minerogenic water but being autonomous from isochronic relative sea-level. To the east, basal peat is absent within the sedimentary succession. Here, the facies zone is dominated by tidal flat to brackish-lagoonal sediments, in places intercalated by fen peat layers dating back to minimum 4490 cal BC.

Comparing the western and the eastern palaeo-environments reveals different sedimentary signals identifying coincident event-stratigraphic markers of early to late Holocene age (Fig 1). Their event-stratigraphic signal may be linked to distinct sedimentary horizons at a regional scale. The clastic material deposited in parts shows rhythmic layers of coarser material within one event horizon (Fig. 2).

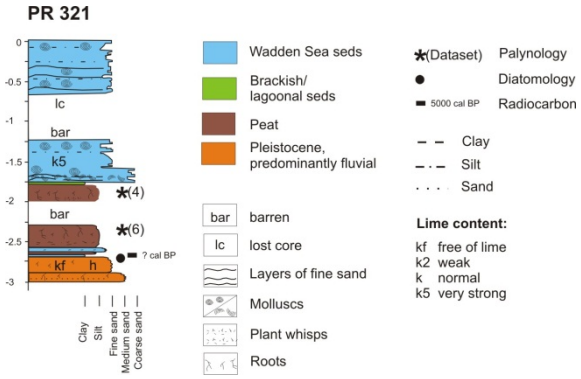

Fig. 1(above): Description of core PR 321, tidal flat Arngast Sand, central Jade Bay. Drawing: Stefanie Schnaidt.
Fig. 2 (below): Event layer of core PR 321 at 1.77 to 1.64 m.

The poster presents detailed discussion on the origin of these high-energy event layers with respect to major storm or tsunami influence. Feasible Tsunami triggers may have been landslides in the northern North Sea area (alike the Storegga event at ~8000 BP) or earthquakes along active faults at the coastal sections of

southern Spain and Portugal.

Acknowledgements: The geological field work was accomplished as part of an interdisciplinary study of the Jade Bay. We gratefully acknowledge project funding by the Ministry for Science and Culture of Lower Saxony (Sponsorship program: "Niedersächsisches Vorab der Volkswagen Stiftung").

References

Sindowski, K.-H. (1972): Zur Geologie des Jadebusen-Gebietes. *Oldenburger Jahrbuch 72, 175-181.*

Streif, H. (2004): Sedimentary record of Pleistocene and Holocene marine inundations along the North Sea coast of Lower Saxony, Germany. *Quaternary International 112, 3-28*.

Wartenberg, W., Freund, H. (2011): Late Pleistocene and Holocene sedimentary record within the Jade Bay, Lower Saxony, Northwest Germany – new aspects for the palaeo-ecological record. *Quaternary International (in press).*

TESTING EARTHQUAKE RECURRENCE MODELS WITH 3D TRENCHING ALONG THE DEAD-SEA TRANSFORM

Wechsler, Neta (1, 2), Thomas K. Rockwell (2), Yann Klinger (1), Amotz Agnon (3), Shmulik Marco (4)

(1) Equipe de Tectonique, Institut de Physique du Globe de Paris, CNRS, Paris, France. Email: wechsler@ipgp.fr
(2) Department of Geological Sciences, San Diego State University, San Diego, CA, United States.
(3) Institute of Earth Sciences, Hebrew University of Jerusalem, Jerusalem, Israel.
(4) The Department of Geophysics and Planetary Sciences, Tel Aviv University, Tel Aviv, Israel

Abstract (Testing earthquake recurrence models with 3D trenching along the Dead-Sea Transform): *We propose to test earthquake recurrence and slip models via high-resolution three-dimensional trenching of the Betieha site on the Dead Sea Transform (DST) in northern Israel. We extend the earthquake history of this simple plate boundary fault to establish how often earthquakes have occurred in the Holocene (past 50-100 centuries), to determine the amount of slip per event, and to test competing rupture models (characteristic, slip-patch, slip-loading, and Gutenberg Richter type distribution). We do this by 3D trenching and documentation of offset buried streams of various ages across the DST. This information is critical for improving seismic hazard analysis and earthquake forecast models in general, and for establishing the current earthquake risk in Israel and the surrounding Middle East.*

Key words*: Dead Sea Transform, 3D Paleoseismology, slip per event, historical earthquakes*

INTRODUCTION

Understanding earthquake production along major plate-boundary faults is critical for improving seismic hazard assessment and earthquake forecast models. Models used to forecast future seismicity make fundamental assumptions about fault behavior, whether it ruptures in a random, quasi-periodic, or clustered pattern. Those models are based on limited observations of recurrent slip at a point along a fault, or variations in recurrence times at multiple paleoseismic sites along individual faults. Models such as the "characteristic earthquake" model (Schwartz and Coppersmith, 1984) or the "slip-patch" model (Sieh, 1996) rely on assessments of fault segmentation and assume that large ruptures terminating at invariant segment boundaries (Wesnousky, 2008). However the self-similarity of large ruptures, both in terms of magnitude and of slip distribution, is not clearly established thus far, as there is yet to be a recorded repeated large event since the advent of modern instrumental measurements. In order to better understand long-term earthquake recurrence there is need for comprehensive event records that includes magnitude, location and displacement data. The Beteiha (Bet-Zayda) site, located on the Dead-Sea Transform fault (DST), provides us with an opportunity for constructing long term record for an active plate-boundary via high-resolution three-dimensional trenching. The data can be used to test earthquake recurrence and slip models, as well as to address other key issues such as slip-rate variation with time, or GPS-geological slip-rate disparity.

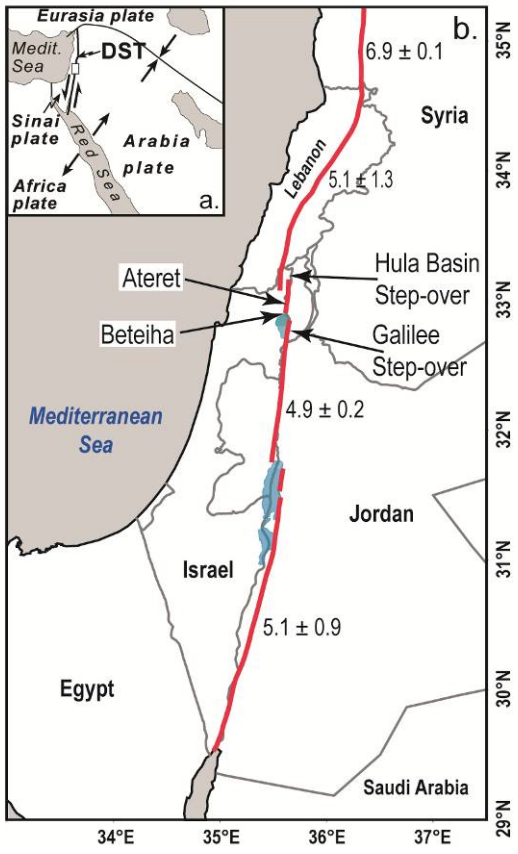

Fig. 1: a) Generalized tectonic framework of the Middle East. b) The DST (on land) from the Red Sea northward to the East Anatolian fault (EAF) in Turkey. Slip rate data are shown in black (Daeron et al., 2004, Ferry et al., 2007, Le Beon et al., 2010, Meghraoui et al., 2003).

Geological Background

The DST is a major plate boundary and a source of significant hazard in the Middle East, accommodating the relative motion between the African and Arabian

plates. It transfers slip northward from the oblique opening at the Red Sea to the Taurus-Zagros collision zone, and a consequence of this northward motion of Arabia and collision with Asia is the westward extrusion of Anatolia along the North Anatolian Fault system (Fig. 1a). The cumulative offset of the DST is ~105 km, representing the total motion between the Arabian plate and Sinai sub-plate since the mid Miocene (e.g., Freund et al. 1968; Garfunkel 1981). The rate of sinistral motion measured across the fault is estimated to be between 3 and 7 mm/year in northern Israel (Le Beon et al. 2008 and references therein, Figure 1b). Despite the rich record of historical seismicity in the Middle-East, not enough data exists to constrain surface rupture extent for historical earthquakes. Previous work (Ellenblum et al., 1998; Marco et al., 2005) on this segment of the DST obtained slip per event for the last 2 historical earthquakes (1759 and 1202 CE) and established that they indeed ruptured this far south.

Results

We present results from a 2 year trenching campaign in the Beteiha valley, on the northern shore of Lake Tiberias. Previous trenches in the same locale by Marco et al. (2005) exposed 5 buried paleo-channels which provided slip-per-event data for the last two earthquakes, as well as slip-rate estimate for the last 5k years. In the first year, we established the feasibility for an extended 3D trenching project in that locale by excavating a 300m long fault parallel trench (Figure 2) and exposing at least 7 additional buried channels that can be used as offset markers, in addition to the 5 channels that were originally mapped by Marco et al. (2005). In order to constrain each paleo-channel's age, 30 ^{14}C samples were dated. The obtained dates span the range 915 years BP to more than 4000 years BP. A re-dating of charcoal from the channel (CH1) previously dated to 5kyr using bulk soil ^{14}C, found it to be younger by at least 1kyr (4k and not 5k). Based on the new dates, the slip-rate estimate of 3 mm/yr based on 15m offset measured for CH1 is revised to 3.7 mm/yr. The ages of the buried channels cover the period between the last large event on this segment (1202 CE) and over 4000 years ago.

The second year's trenching season will commence in May 2011, with the main goal to follow the paleo-channels across the fault and measure the amount of offset for each, thus refining the slip-rate and slip-per-event history. We plan to have several of the channels excavated and mapped by July, and we will present our results in Corinth, 2011.

Acknowledgements: Thanks are due to all the trenching assistants, especially to K. Farrington, J. B. Salisbury and E. Bowles-Martinez. We thank the village of Almagor for letting us trench in their fields, with special thanks to Avshi Herzog for his assistance. This project is funded by NSF grant EAR-1019871 to T. K. Rockwell and by a grant from the city of Paris to N. Wechsler and Y. Klinger.

References

Ellenblum, R., Marco, S., Agnon, A., Rockwell, T.K., and Boas, A., 1998, Crusader castle torn apart by earthquake at dawn, 20 May 1202, *Geology* 26, 303–306.

Daeron, M., Benedetti, L., Tapponnier, P., Sursock, A., and Finkel, R.C., 2004, Constraints on the post 25-ka slip rate of the Yammouneh fault (Lebanon) using in situ cosmogenic ^{36}Cl dating of offset limestone-clast fans, *Earth Planet. Sci. Lett.*, 227, 105–119.

Ferry, M., M. Meghraoui, N. Abou Karaki, M. Al-Taj, H. Amoush, S. Al-Dhaisat, and M. O. Barjous, 2007, A 48-kyr-long slip rate history for the Jordan Valley segment of the Dead Sea Fault, *Earth Planet. Sci. Lett.*, 260, 394–406.

Freund, R., Zak, I., and Garfunkel, Z., 1968, Age and rate of the sinistral movement along the Dead Sea Rift, *Nature*, 220, 253– 255.

Garfunkel, Z., Zak, I., and Freund, R., 1981, Active faulting in the Dead Sea rift, *Tectonophysics*, 80, 1-26.

Le Béon, M., Klinger, Y., Amrat, A. Q., Agnon, A., Dorbath, L., Baer, G., Ruegg, J. C., Charade, O., and Mayyas, O., 2008, Slip rate and locking depth from GPS profiles across the southern Dead Sea Transform, *J. Geophys. Res.*, 113, B11403, doi:10.1029/2007JB005280.

Le Beon, M., Klinger, Y., Al□Qaryouti, M., Mériaux, A-S, Finkel, R. C., Elias, A., Mayyas, O., Ryerson, F. J., and Tapponnier, P., 2010, Early Holocene and Late Pleistocene slip rates of the southern Dead Sea Fault determined from ^{10}Be cosmogenic dating of offset alluvial deposits, *J. Geophys. Res.*, 115, B11414, doi:10.1029/2009JB007198.

Marco, S., Rockwell, T.K., Heimann, A., Frieslander, U., Agnon, A., 2005, Late Holocene activity of the Dead Sea Transform revealed in 3D paleoseismic trenches on the Jordan Gorge segment. *Earth Planet. Sci. Lett.*, 234, 189–205.

Meghraoui, M., et al., 2003, Evidence for 830 years of seismic quiescence from palaeoseismology, archaeoseismology and historical seismicity along the Dead Sea Fault in Syria, *Earth Planet. Sci. Lett.*, 210, 35–52.

Schwartz, D. P., and K. J. Coppersmith, 1984, Fault behavior and characteristic earthquakes: Examples from the Wasatch and San Andreas fault zones, *J. Geophys. Res.*, 89, 5681–5698.

Sieh, K., 1996, The repetition of large-earthquake ruptures, *Proc. Natl. Acad. Sci. U.S.A.* 93, 3764-3771.

Wesnousky, S.G., 2008, Displacement and geometrical characteristics of earthquake surface ruptures: Issues and implications for seismic-hazard analysis and the process of earthquake rupture, *Bull. Seismol. Soc. Am.* 98(4), 1609-1632.

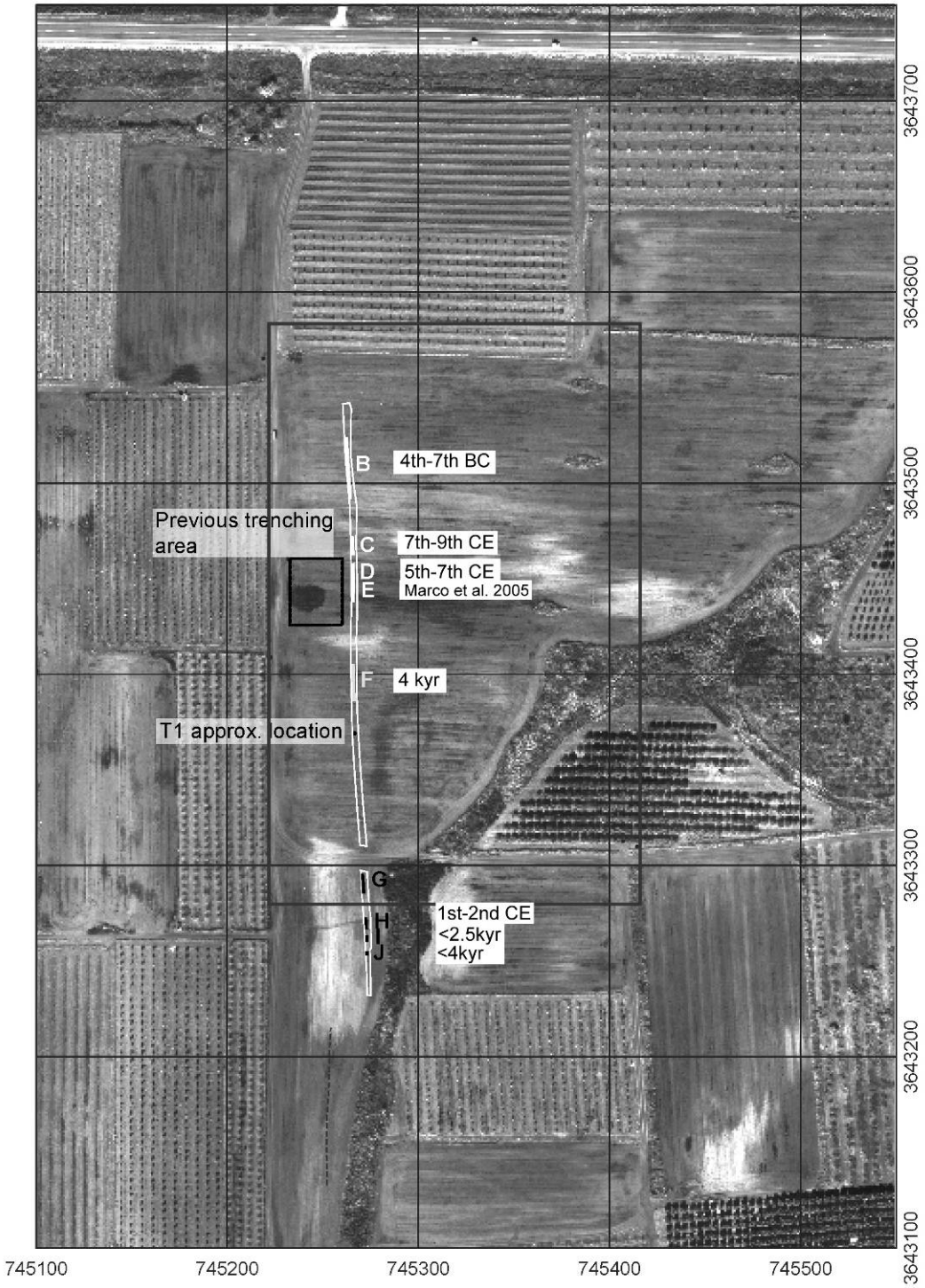

Fig. 2: Location of first year trenches, on an aerial photograph of the field from summer 2009. Approximate location of previous trenches is marked with a blue rectangle. The buried paleo-channel locations are marked in the trench by letters, and the youngest 14C calibrated date is given for each. Marco et al. (2005) followed sub-units of channel E to constrain slip for the 1202 and 1759 events. Their CH1, used to estimate the last 5kyr slip-rate, was exposed in T1, and its approximate location is marked on the photo, just south of our paleo-channel F.

EARTHQUAKE ARCHAEOLOGY

INQUA PALEOSEISMOLOGY AND ACTIVE TECTONICS

A TERRESTRIAL CLOSE RANGE VIEW OF THE NORMAL FAULT ZONE NEAR ARCHANES (EAST YIOUCHTAS MT., HERAKLION BASIN, CRETE)

Wiatr, Thomas (1), Ioannis D. Papanikolaou (2, 4), Klaus Reicherter (1), Tomás Fernández-Steeger (3)

(1) RWTH Aachen University, Neotectonics and Natural Hazards Group, Lochnerstr. 4-20, 52056 Aachen, Germany
(2) Laboratory of Mineralogy & Geology, Department of Sciences, Agricultural University of Athens, 75 Iera Odos Str., 11855 Athens, Greece
(3) RWTH Aachen University, Department of Engineering Geology and Hydrogeology, Lochnerstr. 4-20, 52064 Aachen, Germany
(4) AON Benfield UCL Hazard Research Centre, Department of Earth Sciences, University College London, WC 1E 6BT, London UK

Abstract (A terrestrial close range remote sensing view of the normal fault zone near Archanes (East Yiouchtas Mt., Heraklion basin, Crete): *The focus of investigation in this paper is the reconstruction of different fault plane conditions and the primary interpretation of them, based on terrestrial close range LiDAR (Light Detection and Ranging) data. For reconstruction the slip per event along the bedrock scarp and where possible (e.g. postglacial scarp) an estimate regarding the slip rate of the individual faults we used the backscattered signal of the laser beam, the geomorphological geometry and the fault plane conditions. In this paper we discuss the N-S striking normal fault near Archanes in the Heraklion basin. To the north of this fault zone the ancient Minoan temple Anemospillia (caves of the wind) is located, which was destroyed by an earthquake around 1700 BC and forms the nearest seismic source to the site.*

Key words*: close range LiDAR, normal fault, fault scarp morphology, Crete*

INTRODUCTION

Crete is the largest Greek island with an area of ~ 8300 km² and approx. 900 km coastline. The development of a multidirectional tectonic regime on Crete is interpreted as a result of the Hellenic subduction zone in the south and the westward extrusion of the Anatolian plate in the north. The island is forms a horst structure in the Hellenic fore arc zone, which is also influenced by the roll back of the African plate. Rapid uplift of ~ 1.2 mm/yr can be observed on the entire island (Meulenkamp et al., 1994). Crete has been uplifted since the Middle Miocene from 1 up to 2 km depending on the influence of different tectonic blocks. The island of Crete lies on top of the active subduction zone for about 30 ma years, implying that it experiences high strain rates and constant deformation processes (Papanikolaou, 1993). Crete is characterised by a complex geological and tectonic structure that results from: i) the successive thrusting of the alpine geotectonic units on top of each other (Bonneau, 1984), ii) the activity of major detachment faults (Fasoulas et al., 1994, Papanikolaou and Vassilakis, 2010, Zachariasse et al., 2011), iii) by the intense neotectonic and active faulting (Monaco and Tortorici, 2004, Peterek and Schwarze, 2004, Caputo et al., 2010). Crete is located in a high seismicity area. Over the last 40 years the active Hellenic subduction zone produced earthquakes in a depth range from 18 to 162 km with magnitudes of M = 4.9 up to 6.1 (Benetatos et al., 2004). Hypocentral depths of earthquakes showed that the north dipping Wadati-Benioff seismic zone close to the low angle subduction along the convex side of the Hellenic arc trench is located in a depth of around 60 to 90 km near Crete (Papazachos et al., 2000). But this region has also experienced strong thrusting paleoearthquakes with magnitudes up to M > 7.5 - 8.0 and hence one of the most intense seismic activity area of the Aegean region (Papazachos & Papazachou, 1997).

Decoding paleoearthquakes in fault bedrock scarps is important for seismic hazard assessment. Shallow earthquakes greater than M_S6 can produce an imprint in the landscape named fault scarps (Stewart & Hancock, 1990). Bedrock fault scarps are indicators of large surface faulting events and may provide not only slip rates, but also information on slip per events when they are analysed with cosmogenic isotope dating (Benedetti et al., 2003). Fault scarps are preserved in the landscape when the slip rate is greater than the erosion rate. Therefore, these are regarded as postglacial scarps that were formed since the last glaciation (Benedetti et al., 2002). The Neogene fault plane solutions and the seismic activities indicate large earthquakes and a rapid uplift with complex tectonic settings of Crete (Dewey & Sengör, 1979; Papazachos et al., 1987).
This paper is focused on the N-S striking fault zone in the Heraklion basin to the south of Knossos (Fig.1). This basin is characterized by block tectonics and the Yiouchtas Mt. represent a neotectonic horst structure which is subdivides the Heraklion Basin in a western and an eastern subbasin (Papanikolaou and Nomikou 1998). Major aims of the investigation were to find quantitative and qualitative data for the reconstruction of surfaces and to analyze the tectonic geomorphology and paleoseismicity of active faults with terrestrial laser scanning (TLS) to reconstruct fault history and activity along surface rupturing scarps.

The varying scale of structural heterogeneity and discontinuous geometry of the exhumed foot wall slip plane along a fault zone and the complexity of the surface features like the subslip-plane breccia sheet, brecciated colluvium or frictional water-wear striations on the rupture plane, makes it difficult to recognize the paleoevents on the fresh fault scarp

above the level of exhumation (Stewart & Hancock, 1991; Roberts, 1996). Even, more the detail geometrical characterisation of the slip surface depends on the view direction to the strike-slip direction (parallel or perpendicular), the calculation approaches and the scaling size of the analysis, because the anisotropy properties and fractal dimensions of fault morphology are decisive (Mandelbrot, 1985; Fardin et al., 2001, 2004; Rahman et al., 2006; Renard et al., 2006; Sagy et al., 2007, 2009; Candela et al., 2009). Additionally, several time-dependent and overlapping processes influence the condition of the free face fault plane that become degraded. These processes involve weathering, pedogenesis of the unbrecciated colluvium, vegetation, karstification and erosion of the colluviums and the fault outcrop.

PRIMARY RESULTS OF THE LiDAR INVESTIGATION ON THE NORMAL FAULT ZONE NEAR ANEMOSPILIA *"CAVES OF THE WIND"* (1900-1700 BC MM II/III) IN THE HERAKLION BASIN

In the northern part of the Mount Juktas about 7 km south of Knossos, the legendary area and tomb of Cretan Zeus is situated, which is considered to be one of the earliest Minoan temples: Anemospilia (Fig.1).

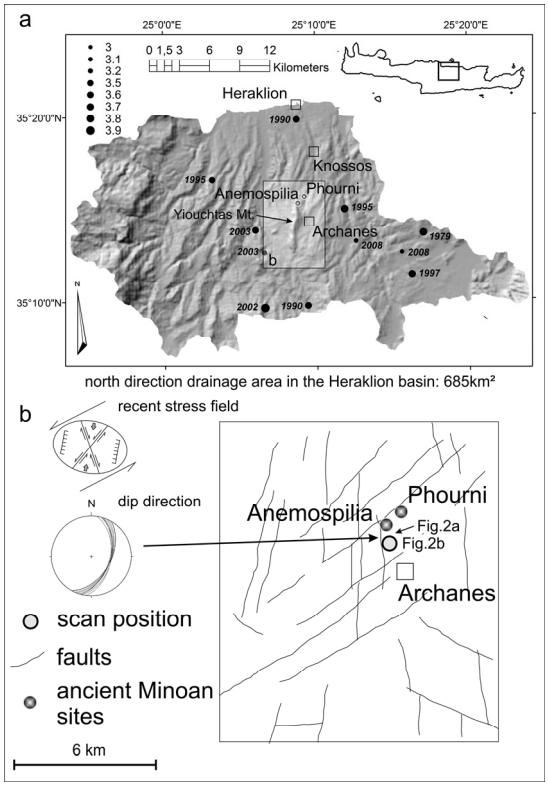

Fig. 1: Investigation area near Archanes in the Heraklion basin of Crete including earthquakes recorded since 1979 (a) (SRTM, USGS, www.usgs.gov) and the main faults, the LiDAR position, location and looking direction of photos (see Fig.2), dip direction of the scanned fault plane, recent stress field and ancient sites (b) (modified from Fassoulas, 2001; ten Veen & Meijer, 1998).

The three small rooms, each of them opened into a corridor, were described and discovered by Sakellarakis during the 1979 expedition. They assumed that the temple was destroyed by a sequence of large earthquakes around 1700 BC and based this conclusion on pottery and artefacts (Nur, 2008). Furthermore, they found a skeleton with broken legs under an ash layer implying that the earthquake was strong enough to damage the massive temple and was followed by a fire. Five different close range LiDAR scans were made in the middle of the N-S striking normal fault 2 km south of the Anemospilia temple (Fig.2). The free natural fault plane in the interesting area is around 6 m high and the scanned area is around 30 m wide. The whole outcrop is by this location around 70 m continuous wide. Our primary goal in this study was to use the TLS for fault tectonomorphology reconstruction. The TLS data have a point to point range between 3 and 7 mm. The examples in this paper (Fig.3/4) had around 2.8 and 3.8 million numbers of shots (points) and the average range between LiDAR and defined scan window was 10 m. This allowed a spatial reconstruction of the scan sequence without gaps and ensured a good data quality and spatial resolution for the interpolation between the points and for the analysis of the plane morphology. The detailed structural analysis of rock surfaces has shown that the surface conditions are changing from base to top (Fig.4). The hillshades in figure 3b and 4b illustrates the plane morphology with different karstic features and degradation in the upper part of the scarp plane (variance of rougher surface conditions in section III, IV, V, VI in Fig.3).

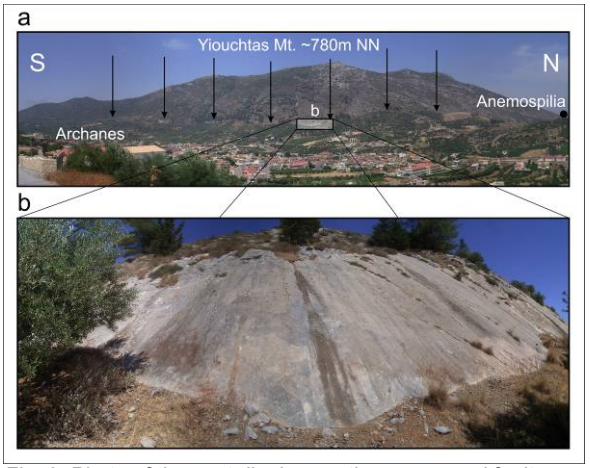

Fig. 2: Photo of the east dipping continuous normal fault zone western Archanes and eastern Mount Yiouchtas within the ancient Minoan site Anemospilia in the northern part of Mount Juktas (a). b) Zoom in photo of the fault plane.

Parts I and II of this section have no significant karstification. The sections are dominated by striation, slickensides and small fractures (compare Fig.4). The combination of the plane morphology with the detected backscattered signal of the LiDAR is shown in figure 3d/3e and 4d. By using this technique, a different point of view allowed that the detected near infrared laser signal can be used for the classification of different functions of weathering, morphological and erosion features on the fault plane

and also reveals the exhumation history. The signal intensity can be used to identify vegetation (including lichen) and its influence on the fault plane. The results shown the influence of the colluvium on the base of the scarp (I in Fig.3e), which can be detected by a change of the backscattered intensity. Furthermore it is possible to distinguish between the different parts of the fault plane, which are characterised and dominated by 1) degradation; 2) karstification; 3) slickensides; and 4) the influence of the colluvium. Following Giaccio (2002) and the model of natural free normal bedrock scarp, we identified different weathering mircomorphologies depending on the scarp height (Fig.4e). The different sections with determinates features on the fault plane represent the time-dependent fault scarp evolution (Stewart, 1996).

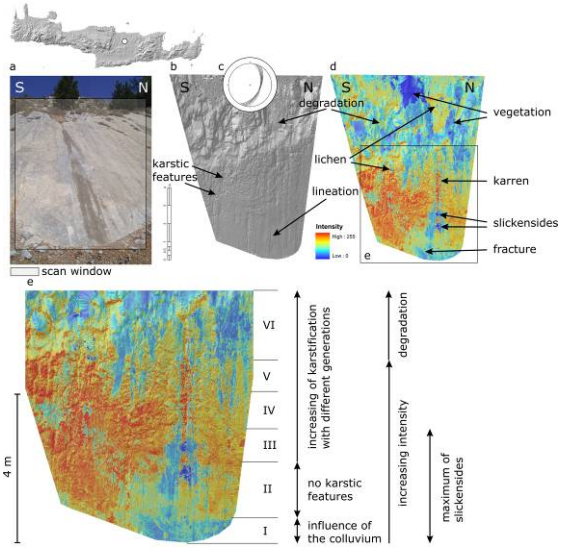

Fig. 3: Primary results of the LiDAR investigation based on the model in Fig.1. a) photo of the fault plane includes the LiDAR scan window, b) hillshade of the fault plane for geometrical and morphological analysis, c) dip direction of the plane, d) distribution of the backscattered signal with primary surface interpretation, e) primary interpretation of all fault plane conditions.

The time- and height-dependent features of bedrock fault scarps are shown figure 4e. The boxes illustrate examples of the fault plane morphology from bottom to top (young to old; brown, red, green, yellow). Conspicuous is the increasing roughness from young to old (brown to yellow) and the specific surface features in different heights. The reason could be the different bio-karstic, bio-erosional, physical and biochemical processes which depend on time (Giaccio et al., 2002). The brown box shows the striation in the lower part of the fault. The red box illustrates small fractures and a rougher surface than in the brown box. The green box the gradation of the karstification and the yellow box show the rillen karst in an advanced stage. Close range LiDAR investigation on postglacial natural normal fault scarps has shown that reconstruction of the spatial distribution of different plane evolution indicators is possible.

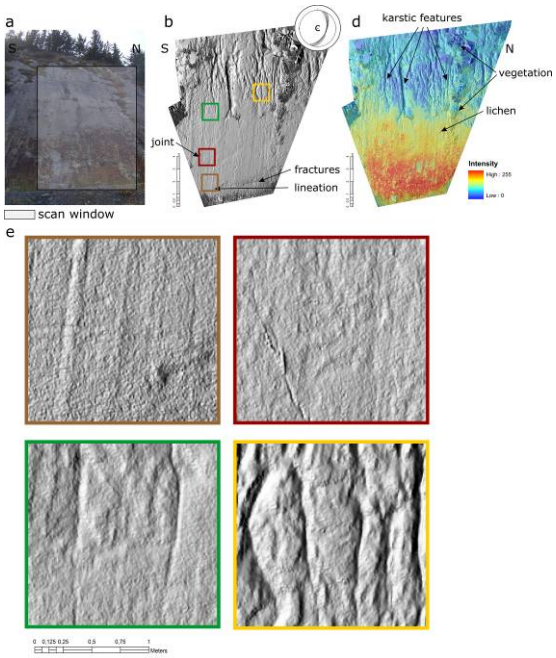

Fig.4: a) photo of the fault plane includes the LiDAR scan window, b) hillshade of the fault plane for geometrical and morphological analysis, c) dip direction of the plane, d) distribution of backscattered signal with primary surface interpretation, e) brown, red, green and yellow boxes are demonstrate the different surface conditions on the fault plane in depending on the scarp height.

These fundamental phenomena can be realized by and imaged with a high resolution digital elevation model (HRDEM) in combination with the backscattered laser impulse. The primary interpretations of the fault surface conditions and their interaction are described in figure 3. Based on the LiDAR results and the field survey we created a principal model of fault scarp alteration for the East Yiouchtas fault, following the general model of Giaccio et al. 2002 (Fig. 5).

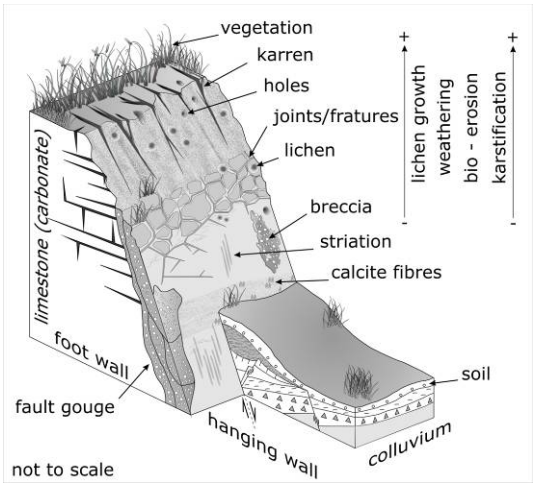

Fig. 5: The model of a normal fault with fault plane evolution indicators (modified from Giaccio et al. 2002).

The investigation with LiDAR and the field survey has shown that the eastern Yiouchtas fault is active with several events in the post-glacial time period.

References

Benedetti, L., Finkel, R., King, G., Armijo, R., Papanastassiou, D., Ryerson, F., Flerit, F., Farber, D. & Stavrakakis, G., 2003: Motion on the Kaparelli fault (Greece) prior to the 1981 earthquake sequence determined from 36Cl cosmogenic dating. Terra Nova, 15:118-124.

Benedetti, L., Finkel, R., Papanastassiou, D., King, G., Armijo, R., Ryerson, F., Farber, D. & Flerit, F., 2002: Post-glacial slip history of the Sparta Fault (Greece) determined by ^{36}Cl cosmogenic dating: evidence for non-periodic earthquakes. Geophys. Res. Lett., 29: 87-1–87-4.

Bonneau, M., 1984: Correlation of the Hellinides nappes in the south-eastern Aegean and their tectonic reconstruction. Special Publication of the Geological Society of London 17, 517-527

Benetatos, C., Kiratzi, A., Papazachos, C., & Karakaisis G., 2004: Focal mechanisms of shallow and intermediate depth earthquakes along the Hellenic Arc. J. Geodyn., 37, 253-296, doi:10.1016/j.jog.2004.02.002.

Candela, T., Renard, F., Bouchon, M., Brouste, A., Marsan, D., Schmittbuhl, J. & Voisin, C., 2009: Characterization of fault roughness at various scales: implications of three-dimensional high resolution topography measurements, Pure appl. geophys. doi: 10.1007/s00024-009-0521-2.

Caputo, R., Catalano, S., Monaco, C., Romagnoli, G., Tortorici G. & Tortorici, L., 2010: Active faulting on the island of Crete (Greece). Geophys. J. Int., 183, 111–126, doi: 10.1111/j.1365-246X.2010.04749.x.

Dewey, J.F. & Sengör, A.M.C., 1979: Aegean and surrounding regions: Complex multiplate and continuum tectonics in a convergent zone. Bull. geol. Soc. Am., 90, 84-92.

Fardin, N., Stephansson, O. & Jing, L., 2001: The scale dependence of rock joint surface roughness. Int. J. Rock Mech. & Min. Sci., 38, p. 659-669.

Fardin, N., Feng, Q. & Stephansson, O., 2004: Application of a new in situ 3D laser scanner to study the scale effect on the rock joint surface roughness. Int. J. Rock Mech. & Min. Sci., 41, p. 329-335.

Fassoulas, C., 2001: The tectonic development of a Neogene graben at the leading edge of the active European margin, The Heraklion basin, Crete, Greece, J. Geodyn., 31, 49–70, doi:10.1016/S0264-3707(00)00017-X.

Giaccio, B., Galadini, F., Spasato, A., Messina, P., Moro, M., Zreda, M., Cittadini, A., Salvi, S. & Todero, A., 2002: Image processing and roughness analysis of exposed bedrock fault planes as a tool for paleoseismological analysis: results from the Campo Felice fault (central Apennines, Italy). Geomorphology, 49, 281-301.

Mandelbrot, B.B., 1985: Self-affine fractals and fractal dimension, Phys. Scripta, v. 32, p. 257-260.

Meulenkamp, J.E., van der Zwaan, G.J., van Wamel, W.A., 1994. On late Miocene to recent vertical motions in the Cretan segment of the Hellenic arc. Tectonophysics, 234, 53-72.

Monaco, C. & Tortorici, L., 2004: Faulting and effects of earthquakes on Minoan archaeological sites in Crete (Greece). Tectonophysics, 382, 103-116.

Nur, A., Burgess, D., 2008: *Apocalypse: Earthquakes, Archaeology and the Wrath of God*. Princeton University Press. Princeton and Oxford. 309 p.

Papanikolaou, D. (1993). Geotectonic evolution of the Aegean. Bull. Geol. Soc. Greece, 28/1, 33-48.

Papnikolaou, D.J. & Nomikou, P.V., 1998: Neotectonic blocks and planation surfaces in Iraklion basin, Crete, Greece. Bull. Geol. Soc. Greece, XXXII/1, 231-239.

Papanikolaou, D. and Vassilakis, E. (2010). Thrust faults and extensional detachment faults in Cretan tectono-stratigraphy: Implications for Middle Miocene extension. Tectonophysics 488, 233-247

Papazachos, B.C., Papadimitriou, E.E., Kiratzi, A.A., Papaioannou, C.A. & Karakaisis, G.F., 1987: Probabilities of Occurrence of Large Earthquakes in the Aegean and Surrounding Area During the Period 1986-2006. Pageoph., 125, 4, 597-612.

Papazachos, B. & Papazachou, C., 1997: The Earthquakes of Greece. Zitis, Thessaloniki.

Papazachos, B.C., Karakostas, V.G., Papazachos, C.B. & Scordilis, E.M., 2000: The geometry of the Wadati–Benioff zone and lithospheric kinematics in the Hellenic arc. Tectonophysics, 319, 275-300.

Peterek, A. & Schwarze, J., 2004: Architecture and Late Pliocene to recent evolution of outer-arc basins of Hellenic subduction zone (south-central Crete, Greece). J. Geodyn., 38, 19-55.

Rahman, Z., Slob, S. & Hack, R., 2006: Deriving roughness characteristics of rock mass discontinuities from terrestrial laser scan data. Proceedings of the 10th IAEG Congress, Engineering geology for tomorrow's cities, Nottingham, United Kingdom, 6-10 September 2006. Engineering geology for tomorrow's cities.

Renard, F., Voisin, C., Marsan, D. & Schmittbuhl, J., 2006: High resolution 3D laser scanner measurements of a strike-slip fault quantify its morphological anisotropy at all scales, Geophys. Res. Lett. 33, L04305, doi: 10.1029/2005GL025038.

Roberts, G.P., 1996: Variation in fault-slip directions along active and segmented normal fault systems. J. Struct. Geol., Vol. 18, No. 6, 835-845.

Sagy, A., Brodsky, E.E. & Axen, G.J., 2007: Evolution of fault-surface roughness with slip. Geology, 35: 283-286.

Sagy, A. & Brodsky, E.E., 2009: Geometric and rheological asperities in an exposed fault zone. J. Geophys. Res., 114, B02301, doi: 10.1029/2008JB005701.

Sakellarakis, Y. & Sapouna-Sakellaraki, E., 1981: Drama of death in a Minoan temple. National Geographic, February 1981.

Stewart, I.S. & Hancock, P.L., 1990: Brecciation and fracturing within neotectonic normal fault zones in the Aegean region. In: Knipe, R.J. and Rutter, E.H., (eds.) Deformation Mechanisms, Rheology and Tectonics. Geol. Soc. Spec. Publ., 54: 105-112.

Stewart, I.S. & Hancock, P.L., 1991: Scales of structural heterogeneity within neotectonic normal fault zones in the Aegean region. J. Struct. Geol., Vol. 13, No. 2, 191-204.

Stewart, I., 1996: A rough guide to limestone fault scarps. J. Struct. Geol., 18,1259-1264.

ten Veen, J.H. & Meijer, P.T., 1998: Late Miocene to Recent tectonic evolution of Crete (Greece): geological observations and model analysis. Tectonophysics, 298, 191-208.

Zachariasse, W.J., van Hinsbergen, D.J.J., & Fortuin, A.R., 2011: Formation and fragmentation of a late Miocene supradetachment basin in central Crete: implications for exhumation mechanisms of high-pressure rocks in the Aegean forearc. Basin Research, doi: 10.1111/j.1365-2117.2011.00507.x.

THE DISCONTINUITY OF A CONTINUOUS FAULT: DELPHI (GREECE)

Wiatr, Thomas (1), Klaus Reicherter (1), Ioannis D. Papanikolaou (2, 3) & Tomás Fernández-Steeger (4)

(1) RWTH Aachen University, Neotectonics and Natural Hazards Group, Lochnerstr. 4-20, 52056 Aachen, Germany
(2) Laboratory of Mineralogy & Geology, Department of Sciences, Agricultural University of Athens, 75 Iera Odos Str., 11855 Athens, Greece. papanikolaou@ucl.ac.uk
(3) AON Benfield UCL Hazard Research Centre, Department of Earth Sciences, University College London, WC 1E 6BT, London UK. papanikolaou@ucl.ac.uk
(4) RWTH Aachen University, Department of Engineering Geology and Hydrogeology, Lochnerstr. 4-20, 52064 Aachen, Germany. fernandez-steeger@lih.rwth-aachen.de

Abstract (The discontinuity of a continuous fault: Delphi (Greece): *We used a terrestrial laser scanning system for the reconstruction and analysis of the morphotectonic features on a fault segment near the ancient Delphi, Greece. Delphi is located on the northern part of the Gulf of Corinth and embedded in a seismic landscape and is the major onshore fault north of the Corinth Gulf. This paper concentrates on the LiDAR long range investigation of the fault for generating a digital elevation model. The model was used for estimating the natural fault plane height by using several vertical profiles. The results show a high horizontal and vertical variability on a 120 m long fault scarp.*

Key words*: long range LiDAR, discontinuous fault, Corinth Gulf, Delphi*

INTRODUCTION

The ancient Delphi with its oracle dedicated to the god Apollo, was the most popular place of worship around 700 B.C. to 400 A.D. in ancient Greece. Delphi is located at the southern flank of Mount Parnassus that is compiled by thick-bedded neritic Mesozoic limestones with significant bauxite deposits. The mountain range is situated on the northern coast of the Gulf of Corinth and bounded by an active fault zone that dips southwards (Fig.1).

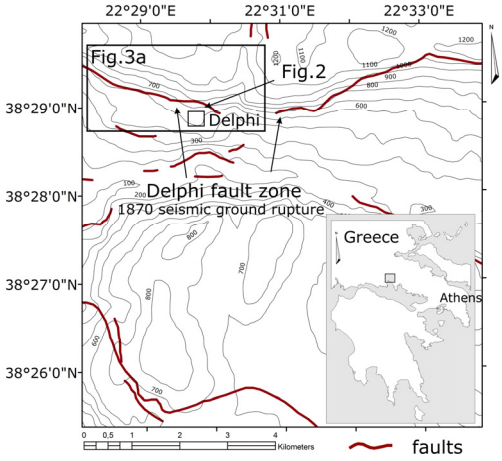

Fig. 1: Tectonic and topographic overview map of the Delphi area.

The Gulf of Corinth is a graben like tectonic structure with E-W trending normal faults and characterized one of the fastest extending regions worldwide with up to 20 mm/yr rate (Billiris et al., 1991; Briole et al., 2000). Destructive historical earthquakes in the area are reported for 373 B.C. (Piccardi, 2000), 515 A.D. (Ambraseys & Jackson, 1998; Papazachos & Papazachou, 2003) and 1870 (1st of August, Ms=6.7, Ambraseys & Jackson, 1998; Papazachos & Papazachou, 2003 and Pavlides & Caputo, 2004). Piccardi (2000) described the 373 B.C. earthquake, which partly destroyed the ancient Delphi showing that there is a post-earthquake reconstruction phase at the shrine of Athena (located around 500 m east of the Temple of Apollo) (Fig.2).

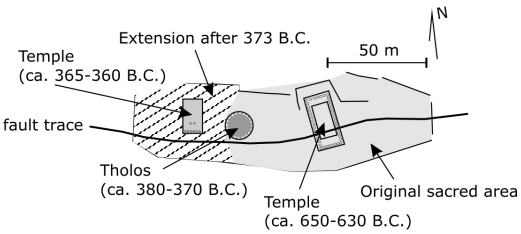

Fig. 2: Setting of the archaeological site of the shrine of Athena Pronaia (modified from Piccardi, 2000).

Furthermore, he postulates that the Temple of Athena was relocated from its original position.
Aim of our study was the reconstruction of the morphotectonic features of the Delphi fault scarp, located 2 km west of the Temple of Apollo by using a terrestrial remote sensing technique. We scanned a 120 m long fault scarp with long range LiDAR. We used a terrestrial LiDAR (Light Detection and Ranging) system from Optech Inc.

METHODS

The ground-based LiDAR (Light Detection And Ranging) or TLS (terrestrial laser scanning) remote sensing method has been established as a versatile data acquisition tool in photogrammetry, engineering technologies, atmospheric studies and as a good data acquisition tool in geosciences and geological engineering in difficult accessible areas.

As the TLS has a high spatial and temporal resolution it is an effective remote sensing technology for reconstruction, monitoring and observation of geosciences phenomena.

The fundamental principle of ground-based LiDAR is to generate coherent a laser beam with little divergence by stimulated emission. LiDAR is a contact- and destructionless, non-penetrative active recording system which is stationary during the recording. The electromagnetic waves are reflected by surfaces and the receiver detects portions of the backscattered signal. All scan sequences were mapped with first pulse detection mode. The laser ranging system is based on measuring the time-of-flight (two-way travel time) of the short wave laser signal. Advantages of the terrestrial method are the flexible handling, a relatively quick availability of an actual dataset, and a very high spatial resolution of the object with information about intensity, x-y-z-coordinates and range. The combination with a digital camera allows combining the point cloud with panchromatic information in order to achieve additionally the RGB colour-coding.

Laser scanning allows 3D surface data acquisition, which is specifically characterized by a digital data record and a computerized data analysis. Furthermore, an implementation of the dataset in a geographical information system (GIS) is uncomplicated with accurate digital elevation models (DEM) or digital terrain models (DTM) sourced directly from the raw dataset.

The infrared laser scanner detected the monochromatic information of the backscattered intensity in 256 grey values. The information of the monochromatic wavelength, the detected backscattered intensity, reflexes the surface properties in the near infrared range. This wavelength is invisible for human eyes. Hence, the results show a different kind of view of the surface conditions. The quality of the reflection depends on the inclination angle of the laser beam, the range between the object and scanner, the material, the colour, the surface condition (weathering/roughness), and the spatial resolution.

DISCONTINUOUS FAULT SEGMENT ON A CONTINUOUS FAULT NEAR DELPHI

The scan position for the long range investigation was 250 m south of the fault plane (Fig.3). The raw data point cloud includes around 6.2 million points for an 130 m long and 60 m wide scan window. For this study a point resolution of 2 cm was chosen. Moreover, we recorded 9 close range scans with 4 mm point resolution (Fig.4).

After data validation and cleaning, the point cloud has been geo-referenced and imported into a GIS. In the GIS, the scans have been converted in a triangulated irregular network (TIN) and in a raster format. With the grid format it is possible to calculate the basic applications for morphologic specifications.

For the morphological analysis twelve vertical profiles with 10 m distance to each other were generated from the LiDAR data. All profiles start on the same height level on top of the fault zone on the foot wall and are perpendicular to the fault plane towards the hanging wall.

Results show a variation of the free face fault height with a difference of 5.4 m. The height data range of the natural bedrock fault plane is between 4 and 9.4 m. Furthermore, horizontal variations of 3 m were detected (Fig.5).

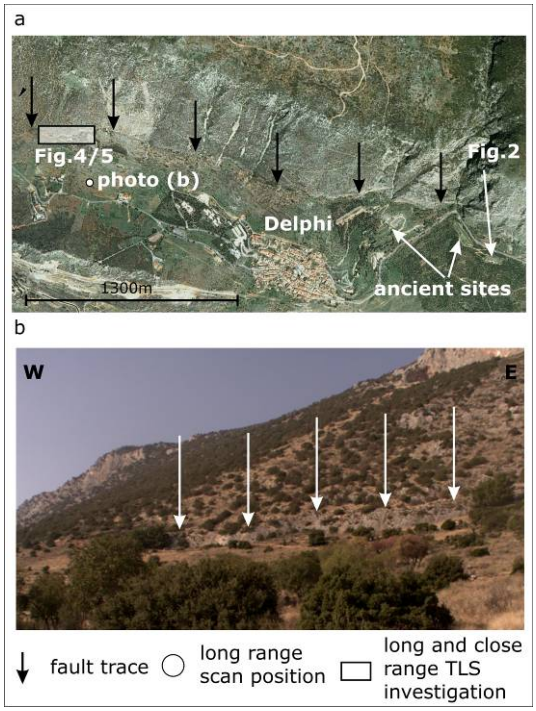

Fig. 3: Panchromatic images of the investigation area. a) The geoeye satellite image shows the continuous fault by Delphi and includes the long range LiDAR study area (modified from Google earth). b) Photo of the south dipping continuous fault zone 2 km westward from the ancient shrine of Apollo by Delphi.

We found that the Delphi fault has an oscillation in three dimensions (horizontal and vertical displacement), across the 120 m long scan sequence. The absolute elevation range of all profiles on the natural free face fault surface (vertical range of the fault plane) is between 574.5 m and 588.7 m above sea level (see Fig.5 right site number 1) and the horizontal variation is between 11.2 m and 21 m (see Fig.5 number 1 under the profiles). The horizontal and vertical value range (number 1) includes the variation of the knick point on top of the free face to the foot wall (number 2) and the knick point of the bottom of the free face to the hanging wall (number 3). Furthermore, the results had shown a variability of the alluvial deposits (vertical and horizontal displacement) of the hanging wall (number 3).

It turns out that the long term slip rate for postglacial scarps (last 19 ka ± 3 ka) in this case ranges between 0.21 ± 0.04 mm/yr and 0.49 ± 0.09 mm/yr

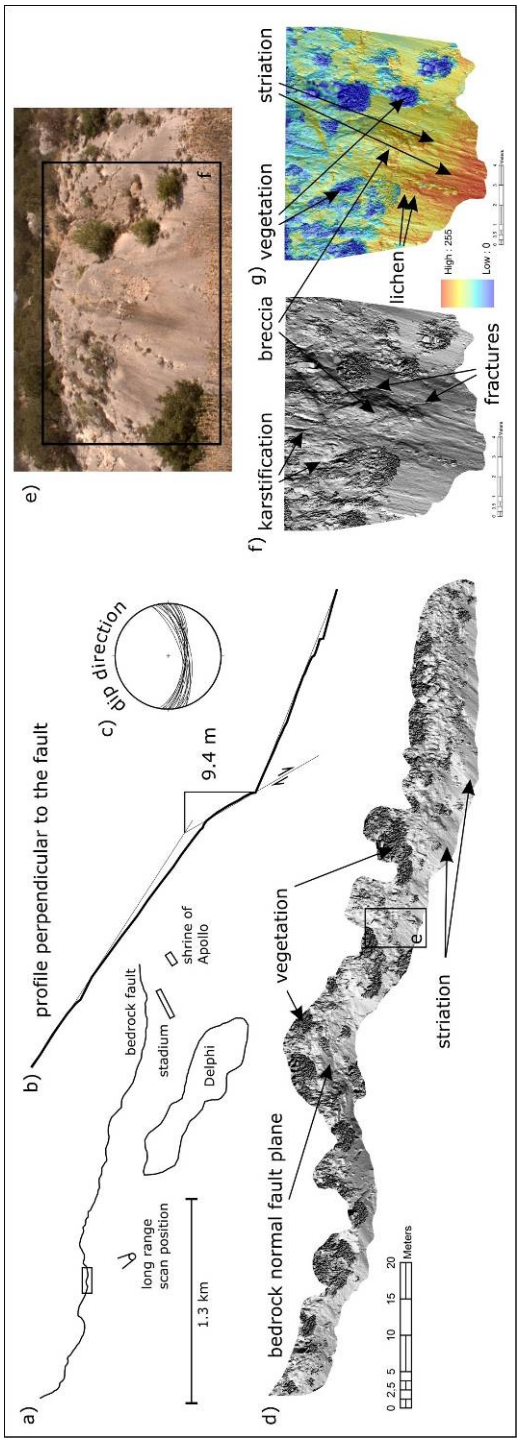

Fig. 4: Close and long range terrestrial LiDAR investigation for morphological analysis on the southwards dipping continuous bedrock fault scarp 2 km west of the archaeological site of Delphi (a). b) Illustrates the calculation of the largest postglacial vertical displacement in the scan window on one profile. c) Fault plane dip direction derived from structural mapping in the scan area. d) Fault plane reconstruction based on LiDAR data was realised by a hillshade in a GIS environment. e) Photo of the fault plane including the LiDAR scan window. f) Hillshade of the close range fault plane and g) distribution of backscattered signal with primary surface interpretations.

depending on the fault segment analysed, and between 0.3 and 0.72 mm/yr for the last 13 ka (The 13 ka pertains to Benedetti et al., 2002; 2003). Hence, the long term slip rate had a range between 0.25 ± 0.05 mm/yr and 0.58 ± 0.09 mm/yr for the last 16 ka ± 3ka. This implies for the long term slip rate estimation a variation of 0.28 mm/yr (19 ka ± 3 ka (0.4 mm/yr worst case scenario)) and 0.42 mm/yr (13 ka), which is enormous.

CONCLUSION

Post-glacial throw variation along strike is evident, even over short distances, including locations that are apparently undisturbed by incision or deposition processes (Papanikolaou et al., 2005). This is the natural variation associated with coseismic surface slip and constitutes a major source of uncertainty that in central Apennines was measured at ± 20% (Papanikolaou et al., 2005). A fairly irregular surface slip distribution has been documented from several normal faulting events such as the 1981 Alkyonides earthquake sequence (Jackson et al., 1982). Herein, in Delphi we measured a higher variability of around ± 28 %. Processes like erosion, deposits and debris as well as catchments analysis are not including in this research until now.

But the LiDAR investigation on a fault scarp segment in Delphi has shown a massive variation in the vertical and horizontal displacement. The data collection for calculation of the long term slip rate with the profile method, it is necessary to produce a lot of profiles in the field, to get an impression of the fault variation. Due to the digital elevation model of the long range LiDAR data with 2cm spatial resolution and without gaps it is possible to get a high data quality for morphological analysis and ensured a documentation in a tectonic environment.

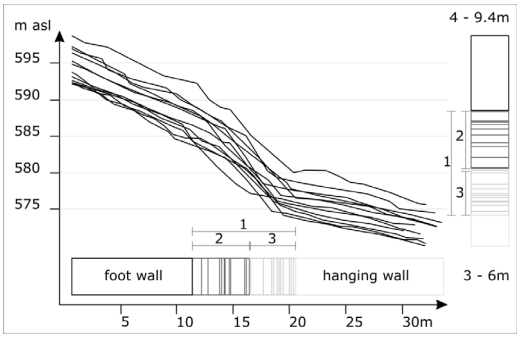

Fig. 5: Twelve perpendicular profiles from the 120 m long Delphi scarp segment show the horizontal and vertical discontinuity of the fault plane. 1) Variations of the free face fault plane. 2) Top knick point of the free face to the foot wall. 3) Bottom knick point of the free face to the hanging wall.

References

Ambraseys, N.N. & Jackson, J.A., 1998: Faulting associated with historical and recent earthquakes in the Eastern Mediterranean region. Geophysical Journal International, 133, 390–406.

Benedetti, L., Finkel, R., Papanastassiou, D., King, G., Armijo, R., Ryerson, F., Farber, D. & Flerit, F., 2002: Post-glacial slip history of the Sparta Fault (Greece) determined by ^{36}Cl cosmogenic dating: evidence for non-periodic earthquakes. Geophys. Res. Lett., 29: 87-1–87-4.

Benedetti, L., Finkel, R., King, G., Armijo, R., Papanastassiou, D., Ryerson, F., Flerit, F., Farber, D. & Stavrakakis, G., 2003: Motion on the Kaparelli fault (Greece) prior to the 1981 earthquake sequence determined from 36Cl cosmogenic dating. Terra Nova, 15:118-124.

Billiris, H., Paradissis, D., Veis, G., England, P., Featherstone, W., Parsons, B., Cross, P., Rands, P., Rayson, M., Sellers, P., Ashkenazi, V., Davison, M., Jackson, J. & Ambraseys, N., 1991: Geodetic determination of tectonic deformation in central Greece from 1900 to 1988. Nature, 350, 124– 129, doi:10.1038/350124a0.

Briole, P., A. Rigo, H. Lyon-Caen, J. C. Ruegg, K. Papazissi, C. Mitsakaki, A. Balodimou, G. Veis, D. Hatzfeld, & Deschamps, A., 2000: Active deformation of the Corinth rift, Greece: Results from repeated Global Positioning System surveys between 1990 and 1995, J. Geophys. Res., Solid Earth, 21, 25, 605–625.

Jackson, J., Gagnepain, A., Houseman, J., King, G., Papadimitriou, G.C.P., Soufleris, P. & Virieux, C., 1982: Seismicity, normal faulting, and the geomorphological development of the Gulf of Corinth (Greece): the Corinth earthquakes of February and March 1981. Earth and Planetary Science Letters 57, 377– 397.

Papanikolaou, I.D., Roberts, G.P. & Michetti, A.M., 2005: Fault scarps and deformation rates in Lazio-Abruzzo, Central Italy: comparison between geological fault slip-rate and GPS data. Tectonophysics 408, 147–176.

Papazachos, C. & Papazachou, C., 2003: The Earthquakes of Greece. Ziti, Thesaloniki [in Greek].

Pavlides, S. & Caputo, R. 2004. Magnitude versus faults' surface parameters: quantitative relationships from the Aegean Region. Tectonophysics, 380, 159–188.

Piccardi, L., 2000: Active faulting at Delphi: seismotectonic remarks and a hypothesis for the geological environment of a myth. Geology, 28, 651–654.

POSTSEISMIC DEFORMATION OF THE 2009 L'AQUILA EARTHQUAKE (M6.3) SURFACE RUPTURE MEASURED USING REPEAT TERRESTRIAL LASER SCANNING

Wilkinson, Maxwell (1), Ken McCaffrey (1), Gerald Roberts (2), Patience Cowie (3), Richard Phillips (4)

(1) Department of Earth Sciences, Durham Univerity, United Kingdom. Email: maxwell.wilkinson@durham.ac.uk
(2) School of Earth Sciences, Birkbeck College, University of London, United Kingdom.
(3) School of Geosciences, University of Edinburgh, United Kingdom.
(4) Institute of Geophysics and Tectonics, University of Leeds, United Kingdom

Abstract (Postseismic deformation of the 2009 L' Aquila Earthquake (M6.3) surface rupture measured using repeat terrestrial laser scanning): *We conducted an innovative survey using repeat terrestrial laser scan (TLS) technology at four sites on the surface rupture of the 2009 L'Aquila earthquake (M6.3), Central Italy. Between 8 – 126 days after the earthquake we repeatedly laser scanned four road sections cross-cut and vertically offset by the surface rupture. A method was developed to quantify the postseismic deformation. We modelled rupture afterslip and associated near-field postseismic deformation in the hangingwall at each site with millimetre to sub-centimetre precision. The observed postseismic deformation coincides with the coseismic slip deficit within the fault zone, which we suggest is the driving mechanism for afterslip and near-field postseismic deformation. Repeat TLS survey of actively deforming surface ruptures provide a new method to monitor and quantify postseismic deformation.*

Key words*: Postseismic deformation, Laser scanning.*

INTRODUCTION

We report the use of Terrestrial Laser Scan (TLS) technology to monitor near field postseismic deformation at four sites along the surface rupture of the 6th April 2009 L'Aquila earthquake, in the Abruzzo region, Apennines, central Italy. The main shock (Mw 6.3) occurred at 03:32 local time. The city of L'Aquila and its surrounding suburbs were subjected to the largest intensity shaking, resulting in 308 deaths, 1,500 injuries and over 50,000 people made homeless.

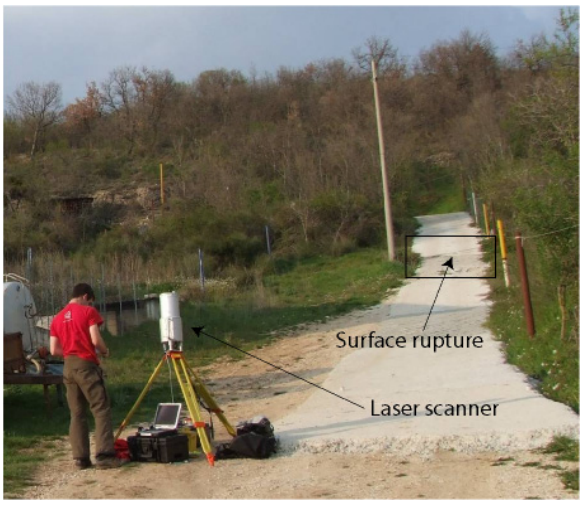

Fig. 1: Riegl LMS-z420i laser scanner set up at site PAG, one of the four surface rupture study sites.

The source of the L'Aquila seismicity was identified as the Paganica fault, to the NE of the city of L'Aquila, defined by focal mechanisms, aftershock distribution (Chiarabba et al. 2009) and differential interferometry. The earthquake created a discontinuous surface rupture, ~ 12 km in length (Falcucci et al. 2009) along the Paganica fault with normal sense displacement, down thrown to the SE, with a maximum throw of 0.1 m as defined by the EMERGEO working group (2009) and Vittori et al. (in press).

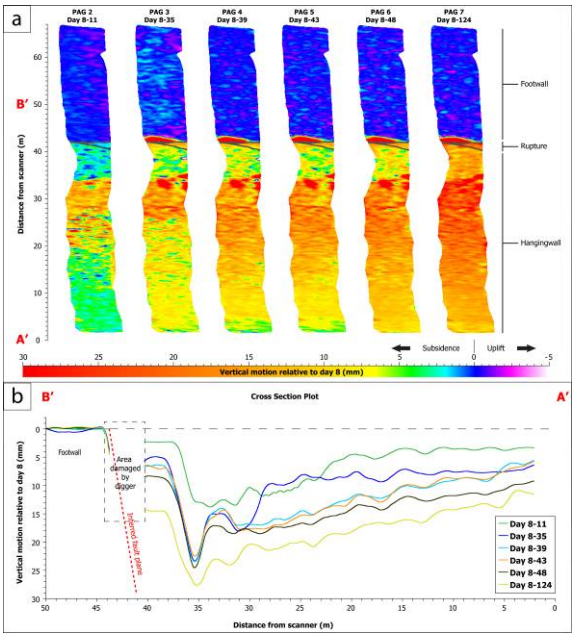

Fig. 2: Modelled postseismic deformation and rupture afterslip at PAG for the various time intervals. (From Wilkinson et al. 2010)

Between 8 – 124 days after the earthquake we repeatedly laser scanned four road sections cross-cut and vertically offset by the surface rupture (Fig. 1). By comparing each subsequently acquired dataset to the first at each site, we were able to

model the resultant near-field postseismic deformation and rupture afterslip over various time intervals with millimetre to decimetre precision. We used reflective targets to measure the horizontal component of deformation.

DISCUSSION

We observe progressive surface deformation in our modelled datasets whose rate decreases over time. We present the modelled data from site PAG in figure 2 as this is site with the greatest magnitude of deformation. The three equations shown in figure 3 are used to describe afterslip and postseismic deformation for three different studies of the Guatemala (1) and Superstition Hills (2 & 3) earthquake surface ruptures. The three equations differ slightly as they were derived using a mix of theoretical and empirical approaches, as well as datasets from different earthquakes or study sites. In figure 4 we compare these three equations with their earthquake specific parameters to our measurements for the L'Aquila earthquake derived from figure 2. We find that our data, with a decaying rate over time is consistent with previously published theoretical and empirical laws derived to explain afterslip phenomenon.

$D = a + b\log T$ (1)[1]	$U^P = U_C^S + \alpha' \ln\left[\left(\frac{\beta'}{\alpha'}\right)t + 1\right]$ (2)[2]	$D = at^b$ (3)[3]
[1]Model 1: Equation defined by least-squares regression of observed displacement data on logarithm of time from the 1976 Guatemala earthquake [*Buckham et al.*, 1978]. D = modeled displacement (mm) a = coseismic rupture offset (mm) b = gradient of best fit line through the data plotted as logarithm of time T = time since earthquake (days)	[2]Model 2: Two variable version of a closed-form solution for afterslip [*Marone et al.*, 1991, after *Scholtz*, 1990] modified to accommodate coseismic measurements, and used to model 1987 Superstition Hills afterslip data [*Sharp et al.*, 1989]. U_D^S = modeled displacement (mm) U_C^S = coseismic rupture offset (mm) α' = a parameter (mm) defining the friction rate parameter divided by spring stiffness, analogous to the thickness of the velocity strengthening region, the former obtained from best fit to data plotted as logarithm of time β' = coseismic slip velocity in the velocity strengthening region (mm/day)	[3]Model 3: Slip decay model [*Williams and Magistrale*, 1989] describing displacement data from the 1987 Superstition Hills earthquake sites 2M, 2T and 2U. D = modeled displacement (mm) a = coseismic rupture offset (mm) b = decay rate parameter t = time since earthquake (days)

a (mm)	b	U^P_C (mm)	α'	β'	a (mm)	b
0 (replacement of 50.9 as there is no coseismic component to be compared in our dataset)	13.9	0 (replacement of 237.1 as there is no coseismic component to be compared in our dataset)	65.69	518.1	14.6	0.131
Parameters calculated from data of the 1976 Guatemala earthquake, Zacapa site.		Parameters calculated from data of the 1987 Superstition Hills Earthquake site 2T [*Sharp et al.*, 1989].			Parameters calculated from data of the 1987 Superstition Hills Earthquake, Site 2T.	

Fig. 3: Theoretical and empirical afterslip models with parameters obtained from afterslip datasets of previous earthquakes.

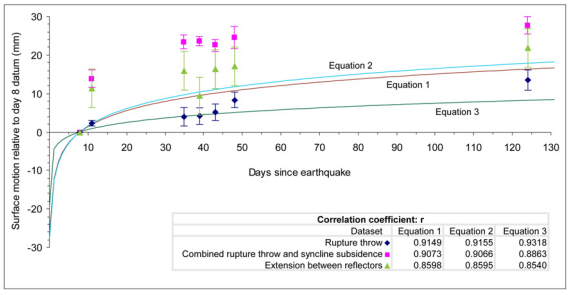

Fig. 4: Surface motion measurements of rupture throw (purple diamonds), hangingwall syncline subsidence (pink squares) and extension between reflective targets (green triangles), derived from the modelled data in Fig 2. Our measurements are compared to data for the three theoretical and empirical models for afterslip shown in figure 3. (Figure from Wilkinson et al. 2010)

At the study site PAG, we observe surface deformation of significant magnitude in the form of a developing syncline in the hangingwall, up to 30 m from the surface rupture. We interpret this deformation as the signal of shallow afterslip in the fault zone. Unpublished data from the three remaining study sites, plus a supplementary dataset of total station line of sight measurements from a fifth site show similar results, confirming postseismic deformation along the surface rupture is attributable to afterslip within the fault zone.

We note our study sites experienced significant postseismic deformation, and are located above a zone of coseismic slip deficit within the fault zone (Fig. 5, after Cheloni et al. 2010). The correlation between a coseismic slip deficit in the fault zone and significant postseismic deformation at the surface suggests the coseismic slip deficit as the driving mechanism for afterslip and near-field deformation.

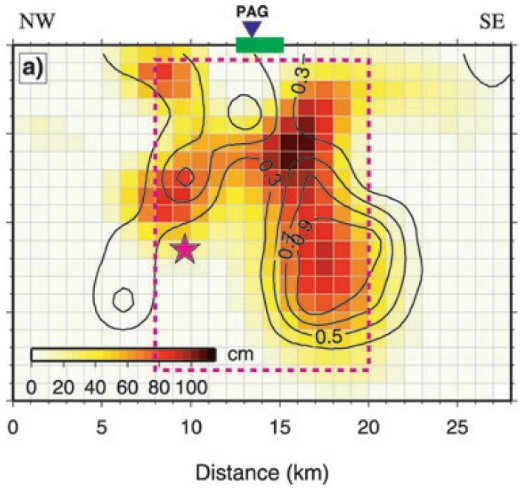

Fig. 5: Coseismic fault slip map derived from coseismic GPS data. The contours represent coseismic slip (m). Note the location of study site PAG at the surface and the coseismic slip deficit (white patch) within the fault zone beneath it. (Figure adapted from Cheloni et al, 2010)

CONCLUSIONS

Repeat TLS survey of actively deforming surface ruptures provide a new method to monitor and quantify postseismic deformation. We have measured near-field postseismic deformation at four sites along the surface rupture of the L'Aquila earthquake. We observe rupture afterslip and hangingwall deformation whose decay in rate over time is consistent with field observations from other earthquakes, as well as theoretical and empirical laws derived to explain such phenomenon. We interpret the near-field postseismic deformation as the signal of afterslip within the fault zone. We note the correlation between the location of our sites experiencing significant postseismic deformation and a coseismic slip deficit within the fault zone beneath them. We suggest that the coseismic slip deficit is the driving mechanism for near-field postseismic deformation and afterslip within the fault zone.

EARTHQUAKE ARCHAEOLOGY

INQUA PALEOSEISMOLOGY AND ACTIVE TECTONICS

Acknowledgements: Funded by NERC grants NE/H003266/1 and NE/E016545/1 and Durham University Doctoral Fellowship (M. Wilkinson). Thanks to A. Michetti, E. Vittori, L. Guerrieri, A. M. Blumetti, N. De Paola, A. Yates, A. Bubeck and G. Sileo for assistance in the field.

References

Buckham, R.C., G. Plafker, and R.V. Sharp (1978), Fault movement (afterslip) following the Guatemala earthquake of February 4, 1976. Geology, 6, 170-173.

Cheloni, D., et al. (2010), Coseismic and initial post-seismic slip of the 2009 M-w 6.3 L'Aquila earthquake, Italy, from GPS measurements. Geophys J Int, 181 (3), 1539-1546, doi: 10.1111/j.1365-246X.2010.04584.x

Chiarabba, C. et al. (2009), The 2009 L'Aquila (central Italy) Mw6.3 earthquake: Main shock and aftershocks. Geophys Res Lett, 36, L18308, doi:10.1029/2009GL039627

Emergeo Working Group (2010), Evidence for surface rupture associated with the Mw 6.3 L'Aquila earthquake sequence of April 2009 (central Italy). Terra Nova, 22, 43-51.

Falcucci, E., et al. (2009), The Paganica Fault and Surface Coseismic Ruptures Caused by the 6 April 2009 Earthquake (L'Aquila, Central Italy), Seismol. Res. Lett., 80, 940–950, doi:10.1785/gssrl.80.6.940.

Marone, C. J., S. H. Scholtz, and R. Bilham (1991), On the mechanics of Earthquake Afterslip, J. Geophys. Res., 96, 8441–8452, doi:10.1029/91JB00275

Scholz, C. H. (1990), The Mechanics of Earthquakes and Faulting, Cambridge Univ. Press, New York.

Sharp, R.V. et al. (1989), Surface faulting along the Superstition Hills fault zone and nearby faults associated with the earthquakes of 24 November 1987, Bull. Seismol. Soc. Am., 79, 252-281.

Vittori, E. et al. (2010), Surface faulting of the April 6th 2009 Mw 6.3 L'Aquila earthquake in central Italy. Bulletin of the Seismological Society of America, in press.

Wilkinson, M., et al. (2010), Partitioned postseismic deformation associated with the 2009 Mw 6.3 L'Aquila earthquake surface rupture measured using a terrestrial laser scanner, Geophys Res Lett, 37, L10309, doi: 10.1029/2010GL043099

Williams, P.L. and H.W. Magistrale (1989), Slip along the Superstition Hills fault associated with the 24 November 1987 Superstition Hills, California, Earthquake. Bull. Seismol. Soc. Am., 79, 390-410.

SEDIMENTARY EVIDENCE OF HOLOCENE TSUNAMI IMPACTS AT THE GIALOVA LAGOON (SOUTHWESTERN PELOPONNESE, GREECE)

Willershäuser, Timo (1), Andreas Vött (1), Georg Bareth (2), Helmut Brückner (2), Hanna Hadler (1), Konstantin Ntageretzis (1)

(1) Institute for Geography, Johannes Gutenberg-Universität Mainz, Johann-Joachim-Becher-Weg 21, 55099 Mainz. GERMANY.
Email: Timo.Willershaeuser@uni-mainz.de
(2) Institute for Geography, Universität zu Köln, Albertus-Magnus-Platz, 50923 Köln. GERMANY

Abstract (Sedimentary evidence of Holocene tsunami impacts at the Gialova Lagoon (Southwestern Peloponnese, Greece): *The coastal area around the Gialova Lagoon (southwestern Peloponnese, Greece), directly exposed to the tectonically highly active Hellenic Trench, was repeatedly affected by tsunamigenic impacts as known from historical sources. Detailed geo-scientific studies were carried out in coastal environments in search of corresponding tsunami deposits using terrestrial vibracorings. Geomorphological, sedimentological and geochemical methods were applied to reconstruct the sedimentary fingerprints of Holocene tsunami events and the palaeogeographical evolution. Our results show that the palaeogeographical setting was strongly affected by high-energy tsunami impacts. Coarse-grained allochthonous sediments of marine origin were found intersecting muddy deposits of low-energy lagoonal and limnic environments. The Voidokilia washover fan and beachrock structures along the coastline also seem to be of tsunamigenic origin. Both sedimentological and geochronological criteria suggest multiple tsunami landfall since the mid-Holocene.*

Key words*: Palaeotsunami, beachrock-type tsunami deposits, Holocene stratigraphy, washover fan.*

INTRODUCTION AND AIMS

The eastern Mediterranean is a tectonically active region with a high tsunami risk (Papazachos & Dimitriou, 1991). The plate boundary of the Hellenic Arc, where the African Plate is being subducted beneath the Aegean microplate, is a hot spot for earthquakes and therefore highly capable for triggering tsunamis. Numerous historical accounts show that the surrounding coastal areas and their geomorphology were affected by multiple tsunamigenic impacts (Soloviev, 1990). Thus, palaeotsunami research in the eastern Mediterranean has been distinctly intensified in the last 20 years. Sedimentary characteristics of recent and subrecent tsunami deposits comprise e.g. (a) shell debris layers, (b) mixture of littoral and sublittoral material, (c) multi-modal grain size distribution, (d) rip up-clasts, (e) basal erosional unconformities, (f) fining upward and thinning landward tendencies, (g) lithified beachrock-type tsunamites and (h) washover deposits (Dominey-Howes et al., 2006; May, 2010; Vött et al., 2009a, 2009b, 2010a, 2010b).

The main objectives of this study are (i) to detect allochthonous high-energy deposits in the local stratigraphical record and (ii) to reconstruct palaeotsunami events against the background of the palaeogeographical evolution of the Gialova coastal area during the Holocene.

REGIONAL SETTING AND METHODS

The coastal area of Pylos and the Gialova Lagoon are located in the southwestern Peloponnese. The study area is directly exposed to the subduction zone of the Hellenic Trench holding a high tsunami risk (Hollenstein et al., 2008, Sachpazi et al., 2000, Papazachos & Dimitriou, 1991). The Gialova Lagoon is located in the northern fringe of the Navarino Bay, a tectonic depression. The shallow lagoon is separated from the Bay of Navarino by a beach barrier system to the south and the semi-circular Bay of Voidokilia to the west (Fig. 1).

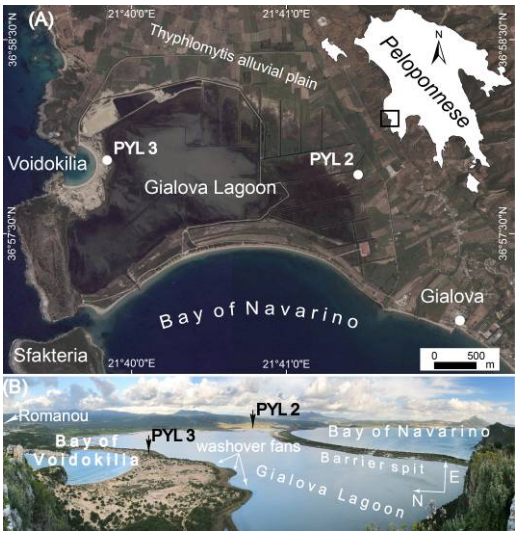

Fig. 1: (a) Topographic and geomorphological overview of the study area and selected coring sites. General map based on Google Earth images (2003). (b) Bird's eye view of Gialova Lagoon, view to the east. Photo taken by. T. Willershäuser, 2009.

Vibracores in the environs of the Gialova Lagoon were retrieved by an Atlas Copco mk1 corer. In the

field, vibracores were analyzed by sedimentological and pedological methods. Laboratory studies comprised analyses of organic content (loss on ignition), concentration of calcium carbonate, pH-value and electrical conductivity. All sediment samples were analysed for contents of Ca, Mn, Fe and more than 20 other elements using the XRF technique.

SEDIMENTARY RECORD IN QUIESCENT NEAR-SHORE ENVIRONMENTS

The Gialova geo-archive is dominated by quiescent low-energy conditions. For the Gialova Lagoon vibracoreprofiles PYL 2 and PYL 3 are considered to be most representative for the local coastal evolution and to detect potential high-energy signatures in the stratigraphical record.

Vibracoring site PYL 2 (N 36°57'46.9'', E 21°41'29.3'', ground surface at 0.47 m above sea level) and PYL 3 (N 36°57'51.6'', E 21°39'51.3'', ground surface at 0.22 m above sea level) are located at the eastern and western shores of the Gialova Lagoon, respectively (Fig. 1).

At its base, the stratigraphy of PYL 2 (based on sedimentological and geochemical parameters), consists of homogenous silty sediments showing quiescent, most probably limnic conditions. This basal stratum is intersected by high-energy deposits of unsorted coarse-grained material of marine origin. This event layer is overlain by homogeneous and well sorted silty clay indicating an immediate re-establishment of pre-existing quiescent conditions. The limnic environment was again influenced by a second input of unsorted allochthonous grus, gravel and limestone fragments embedded in a loamy matrix. The associated sharp basal erosional contact again documents that sediment input occurred abruptly. Towards the top, the high-energy sediments are covered by a sequence of peat, organic mud, limnic mud and finally by recent marshy sediments.

The base of PYL 3 is made out of well sorted fine sandy silt of a quiescent (fluvio-)limnic environment. This facies is separated by a sharp erosional unconformity from following allochthonous coarse-grained and unsorted sediments with distinct fining upward sequences and sublayers including well-rounded gravel. Subsequently, autochthonous limnic conditions were re-established. A second sharp erosional unconformity indicates another abrupt environmental change and the input of allochthonous marine material (Fig. 2). The fairly unsorted sediments consist of a mixture out of gravel, grus, sand and loam. This part of the profile is again characterized by distinct fining upward sequences and rip up-clasts of eroded underlying limnic sediments. After the event, quiescent limnic conditions were quickly re-established, subsequently turning into lagoonal conditions. Towards the top of vibracore PYL 3, the lagoon was influenced by another third distinct input of allochthonous marine sand. The intersecting event layer is characterised by rip up-clasts and several fining upward sequences. A stratum of lagoonal mud documents that the pre-existing quiescent conditions were again re-established. Finally, the lagoonal mud is covered by sandy sediments of the recent dunes and marshy deposits.

In summary, both Vibracores show distinct signatures of abruptly environmental changes in the sedimentary record. We detected a minimum of two distinct allochthonous layers of high-energetic conditions compared to the autochthonous, predominantly limnic pre-existing environments.

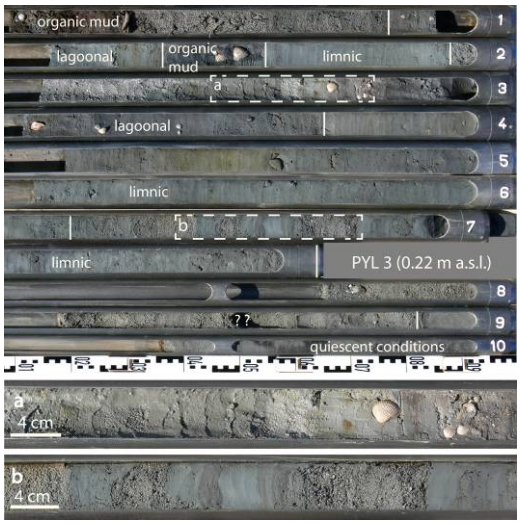

Fig. 2: Vibracore PYL 3 and facies interpretation. Details (a + b) show intersecting allochthonous marine sediments in between predominantly limnic deposits.

BEACHROCK AS LITHIFIED TSUNAMI DEPOSIT

First studies on the occurrence of beachrock along the coastline of Pylos were made by Kraft et al. (1980). These authors described that the beachrock includes sherds of probably Roman age, but no further information on the internal structure, geomorphological and sedimentary context was given. However, recent studies on beachrock-type calcarenitic deposits at adjacent coastal areas revealed that post-depositional pedogenetic decalcification and cementation of tsunami deposits must be assumed for their evolution (Vött et al., 2010a & Scheffers et al., 2008).

In the investigation area, several locations along the coastline show onshore and offshore occurrences of eroded and fragmented beachrock. The internal structure is characterized by typical sedimentological features of tsunami deposits. At Vromoneri (10 km to the north of Gialova Lagoon), we found beachrock sequences injected in between bedrock units and characterized by basal erosional discontinuities, partly well-laminated structure, embedded intra clasts and features of a distinct landward flow direction are detectable.

At Romanou (Fig. 3), the basal section of the beachrock is dominated by gravel, followed by coarse, medium and fine sand with distinct fining upward sequences. The sedimentary features are untypical of littoral environments and rather document high-energy flow dynamics. Thus, beachrock-type lithified sediments along the Pylos coastline are interpreted as deposits of high-energy impact.

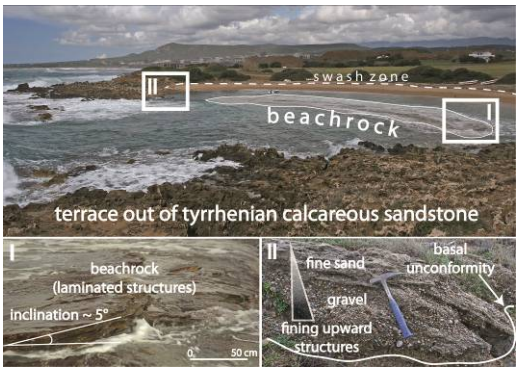

Fig. 3: Beachrock at Romanou (about 5 km to the north of the Gialova Lagoon - see Fig. 1). The present position of the fragmented beachrock is offshore (I) and onshore (II).

DISCUSSION AND CONCLUSION

Our case-study, based on sediment cores and geomorphological findings, show that tsunami signatures in coastal sedimentary environments are highly variable on large scales.

The sediment profiles recovered from near-shore environments are characterised by allochthonous gravelly to sandy high-energy deposits intersecting fine-grained autochthonous sediments of a lower energetic potential. As the energetic potential as well as the landward extent of storm influence in the Mediterranean are known to be restricted to the immediate littoral zone (Vött et al., 2010b), allochthonous coarse-grained deposits found in the environs of Gialova Lagoon are interpreted as of tsunamigenic origin. Moreover, numerous findings of beachrock along the coastline must not be considered as consolidated littoral sediments. We assume that the origin of the beachrock in this case is attributed to sediment deposition by high-energy events followed by post sedimentary cementation and calcification (Vött et al., 2010a). Associated sedimentary characteristics, such as laminated structures, erosional contact at the base, fining upward sequences and embedded stones and ceramic fragments are characteristic for tsunami influence but cannot be described by recent littoral processes. The paleogeographical evolution of the Pylos area is characterised by predominant limnic and lagoonal conditions. The shifting and destruction of the palaeo-environment is mainly controlled by high-energy tsunami impacts induced by earthquake focal mechanisms. Gradual changes seem to be merely responsible for the re-arrangement of sediments after high-energy impacts.

Acknowledgements: We acknowledge funding of the project by the German Research Foundation, DFG (Bonn, Gz. VO 938/3-1). Work permits were kindly issued by the Greek Institute of Geology and Mineral Exploration (IGME, Athens).

References

Dominey-Howes, D.T.M., G.S. Humphreys & P.P. Hesse (2006). Tsunami and palaeotsunami depositional signatures and their potential value in understanding the late-Holocene tsunami record. *The Holocene* 16 (8), 1095-1107.

Hollenstein, C., M.D. Müller, A. Geiger & H.G. Kahle (2008). Crustal motion and deformation in Greece from a decade of GPS measurements, 1993–2003. *Tectonophysics* 449, 17-40.

Kraft, J.C., G.R. Rapp, Jr. & S.E. Aschenbrenner (1980). Late Holocene Palaeogeographic Reconstructions in the Aerea of the Bay of Navarino: Sandy Pylos. *Journal of Archaeological Science* 7, 187-210.

May, S.M. (2010). Sedimentological, geomorphological and geochronological studies on Holocene tsunamis in the Lefkada – Preveza area (NW Greece) and their implications for coastal evolution. PhD Thesis 159 pp., Cologne, Germany.

Papazachos, B.C. & P.P. Dimitriu (1991). Tsunamis In and Near Greece and Their Relation to the Earthquake Focal Mechanisms. *Natural Hazards* 4, 161-170.

Sachpazi, M., A. Hirn, C. Clément, F. Haslinger, M. Laigle, E. Kissling, P. Charvis, Y. Hello, J. C Lépine, M. Sapin& J. Ansorge (2000). Western Hellenic subduction and Cephalonia Transform: local earthquakes and plate transport and strain. *Tectonophysics* 319(4), 301–319.

Scheffers, A., D. Kelletat, A. Vött, S.M. May & S. Scheffers (2008). Late Holocene tsunami traces on the western and southern coastlines of the Peloponnesus (Greece). *Earth and Planetary Science Letters* 269, 271-279.

Soloviev, S.L. (1990). Tsunamigenic Zones in the Mediterranean Sea. *Natural Hazards* 3, 183-202.

Vött, A., H. Brückner, S. Brockmüller, M. Handl, S.M. May, K. Gaki-Papanastassiou, R. Herd, F. Lang, H. Maroukian, O. Nelle & D. Papanastassiou (2009a). Traces of Holocene tsunamis across the Sound of Lefkada, NW Greece. *Global and Planetary Change* 66 (1-2), 112-128.

Vött, A., H. Brückner, S.M. May, D. Sakellariou, O. Nelle, F. Lang, V. Kapsimalis, S. Jahns, R. Herd, M. Handl & I. Fountoulis (2009b). The Lake Voulkaria (Akarnania, NW Greece) palaeoenvironmental archive - a sediment trap for multiple tsunami impact since the mid-Holocene. *Zeitschrift für Geomorphologie N.F., Suppl. Issue* 53 (1), 1-37.

Vött, A., G. Bareth, H. Brückner, C. Curdt, I. Fountoulis, R. Grapmayer, H. Hadler, D. Hoffmeister, N. Klasen, F. Lang, P. Masberg, S.M. May, K. Ntageretzis, D. Sakellariou & T. Willershäuser (2010a). Beachrock-type calcarenitic tsunamites along the shores of the eastern Ionian Sea (western Greece) – case studies from Akarnania, the Ionian Islands and the western Peloponnese. *Zeitschrift für Geomorphologie N.F., Suppl- Issue* 54 (3), 1-50.

Vött, A., et al. (2010b), Sedimentological and geoarchaeological evidence of multiple tsunamigenic imprint on the Bay of Palairos-Pogonia (Akarnania, NW Greece), Quaternary International (2010),doi:10.1016/ j.quaint.2010.11.002

IS THE RURRAND FAULT (LOWER RHINE GRABEN, GERMANY) RESPONSIBLE FOR THE 1756 DÜREN EARTHQUAKE SERIES?

Winandy, Jonas (1), Christoph Grützner (1), Klaus Reicherter (1), Thomas Wiatr (1), Peter Fischer (2), Thomas Ibeling (3)

(1) RWTH Aachen, Neotectonics and Natural Hazards Group, Aachen, Germany (jonas.winandy@rwth-aachen.de, +49 241 8096358),
(2) Köln University, Geographisches Institut, Köln, Germany
(3) Archäologische Grabungen und Sondagen GBR, Köln, Germany

Abstract (Is the Rurrand Fault (Lower Rhine Graben, Germany) responsible for the 1756 Düren earthquake series?): *In 1756, several strong earthquakes (M5-6.1) occurred close to Düren (Lower Rhine Graben, LRG) in Germany. The Rurrand Fault in the LRG located in the middle between Aachen and Cologne possibly indicates the Düren earthquake sequence. This fault is one of the most prominent NW-SE trending normal faults with a morphological expression in the area within the Lower Rhine Graben. Holocene sediments with significant offsets covered by thin colluvial sediments were found and a complex fault geometry was observed during archaeological excavations. DC geoelectrics and georadar were applied in order to image the deeper parts of the fault zone. Radiocarbon and luminescence dating of sediment samples are in progress, but the morphological expression of the fault, the shallow depths of the offset sediments, and geophysical data allow concluding on recent seismicity along this active fault with at least four surface-rupturing events.*

Key words*: earthquake, geophysics, Rhine Graben, Rurrand Fault*

INTRODUCTION: THE DÜREN EARTHQUAKES 1755/1756

The area between Aachen and Cologne in western Germany was hit by a series of earthquakes in 1755/1756. On 18th February, 1756, the strongest event took place most likely west of the city of Düren, leaving two people dead (some reports claim three fatalities) and causing significant damages also in Aachen, Cologne, and nearby villages. Chimneys were destroyed in up to 70 km distance (Liège, Belgium), light damages were recorded in Brussels, Gießen and Osnabrück (200 km distance). A landslide was triggered 15 km SW from Düren. The shaking was felt as far as 400 km from the epicentre in London, Magdeburg, Halle, Paris, and Strasbourg (Meidow, 1995). Epicentral intensities of VIII are reported by Skupin et al. (2008) for the Eschweiler area (15 km W of Düren). A magnitude of 6.3 is assumed for the main event by Skupin et al. (2008), Meidow (1995) assumes M_L=6.1. Our study shows that the Rurrand Fault was possibly activated during the Düren earthquake sequence.

GEOLOGY AND TECTONIC SETTING

The Lower Rhine Embayment (LRE) underwent subsidence from Miocene to recent, accompanied by uplift of the Rhenish Massif to the southwest and east of the study area. Tertiary and Quaternary sediments of more than 1 km thickness were deposited and also include lignites which are extracted in open pit mines. Fluvial and aeolian Pleistocene-Holocene sediments as well as loess cover wide areas.

The Lower Rhine Embayment and especially its western part is one of the tectonically most active areas in Germany and dominated by the Lower Rhine Graben. NW-SE trending normal faults form a horst and graben structure with a number of single blocks (Krefeld-, Köln-, Venlo-, Erft-, and Rur blocks, from NE to SW). The faults show offsets of more than 50 m in the Quaternary. Düren is situated in a NW-SE striking graben, which is flanked by the Rurrand Fault in the NE and the Stockheimer Sprung in the

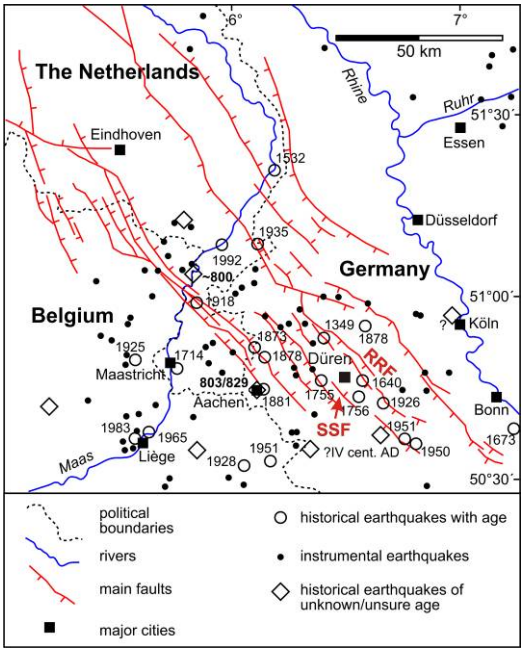

Fig. 1: Neotectonics and historical earthquakes in the study area, the Lower Rhine Embayment. RRF: Rurrand Fault; SSF: Stockheimer Sprung

SW (Fig. 1). The Rurrand Fault is a NW-SE striking normal fault dipping to the SW and expressed by an escarpment.

A large number of damaging earthquakes since Karolingian times has been reported for this area. The most recent one was the 1992 Roermond earthquake which reached M_L=5.9. Recent studies reported that active faults in the study area are characterized by recurrence periods in the order of tens of ka (Skupin et al., 2008; Camelbeeck et al., 2007), and that present day aseismic slip is assumed for the Rurrand Fault, resulting form the lowering of the groundwater level due to the nearby mining activities (Vanneste & Verbeeck, 2001). Active faults in Germany are often not visible in the field due to relatively high erosion rates. Therefore, the seismic hazard might be under-estimated. The Rurrand Fault was trenched already only approx. 2-3 km away, and only Pleistocene faulting evidence was found (Skupin et al., 2008).

METHODS

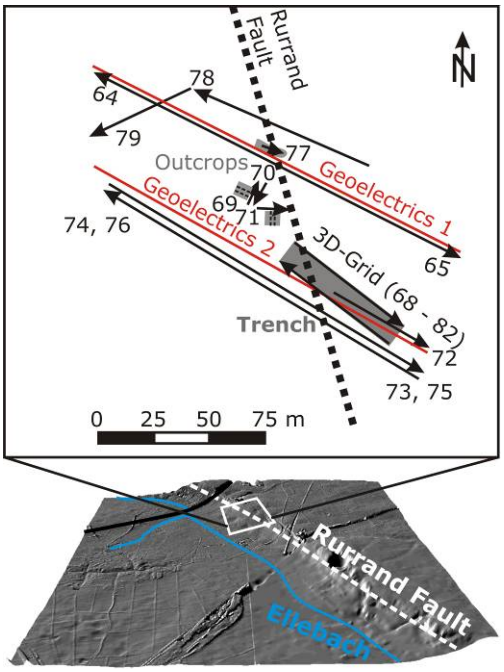

Fig. 2: Location of trenches, outcrops and geophysical profiles at the study area.

Due to construction works for a new highway, extensive archeological excavations have proven findings from Roman times until recent. At this occasion, the Rurrand Fault was trenched in several places, where we mapped layer offsets, sediment deformation, and structural data (Fig. 2). The trench walls were sketched and photographed. Ground penetrating radar (GPR) and electric resistivity measurements have been applied in order to image deeper sediment structures and to map the fault trace. We used the GSSI 100, 270, and 400 MHz antennas with the SIR 3000 controller, a survey wheel and a GPS data logger for georadar measurements. Data processing was done with ReflexW by Sandmeier Scientific Software. The geoelectrics data were gathered with the 4-point-light system (Lippmann), and 80 electrodes with 1.5 m spacing. Schlumberger, Dipole-dipole and Wenner configurations were applied. Soil samples were taken for radiocarbon and luminescence dating, which is currently in progress.

RESULTS

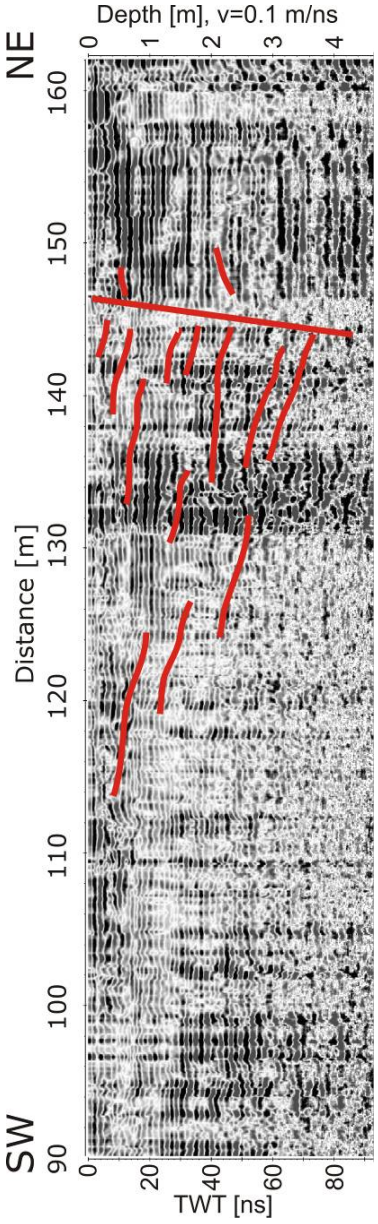

Fig. 3: 270 MHz GPR profile (64) crossing the fault with an angle of 45°.

The GPR data revealed sediment layers inclined towards the fault (Fig. 3). The fault cropped out 2 m away from the GPR profile, allowing a direct comparison. Down to a depth of 4 m several reflectors dip towards the NW.

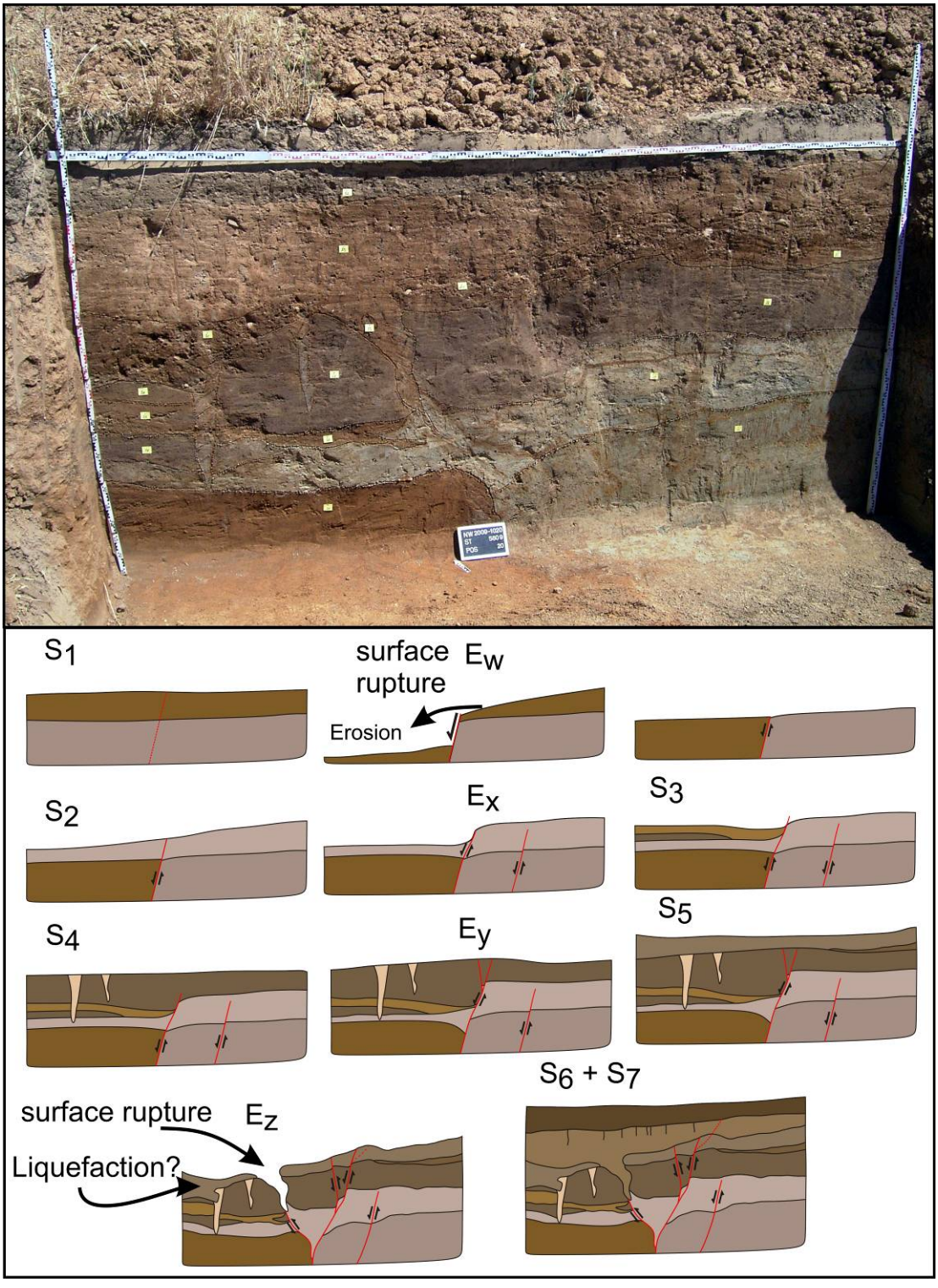

Fig. 4: Photograph of the fault, outcropped in an archeological trench (upper image), and reconstruction of the faulting history (lower image). S = sedimentation and erosional stages; E_W - E_Z = last earthquake events.

A sharp contrast in reflection amplitudes marks the fault itself. On the footwall, only few layers appear to dip towards the Rurrand Fault. Similar observations were made at other GPR profiles that crossed the fault. The high-frequency antennas allowed identifying tilted sediments and the fault itself at various locations. The resolution of the 100 MHz antenna was found too low for imaging fault features in this case. Geoelectrics data revealed low-resistivity anomalies (higher conductivities) at the fault zone, which are most likely related to an increase in water content at the fault zone.

Holocene surface-near sediments with significant offsets covered by thin colluvial sediments were found and a complex fault geometry was observed during the archaeological excavations (Figs. 4 - 6). Some deformation structures seem to be related to liquefaction. The offset of surface-near sediments is in the order of 5 cm (Fig. 5), deeper layers show greater offsets (Fig. 6). Growing displacement of the major fault downsection suggest more than one major, surface-rupturing earthquakes along the Rurrand Fault in the Holocene/Late Pleistocene. We developed a deformation model for the fault, assuming at least four surface-faulting events (E_W - E_Z) that led to the present day geometry (Fig. 4) and seven stages of seismic quiescence (S_1-S_7). Roots penetrated the soil at stage four, and liquefaction of fine grained material is likely to have occurred during the last earthquake event. Despite the results from dating are yet to come, we can assume four events since Late Pleistocene, which would result in slightly shorter recurrence periods than estimated by previous studies. The fault may also be responsible for the Düren 1756 events, as the evidence for surface-faulting earthquakes proves that it is capable for destructive events with magnitudes > 5.5. However, only the dating will allow associating the Düren earthquakes with the Rurrand Fault.

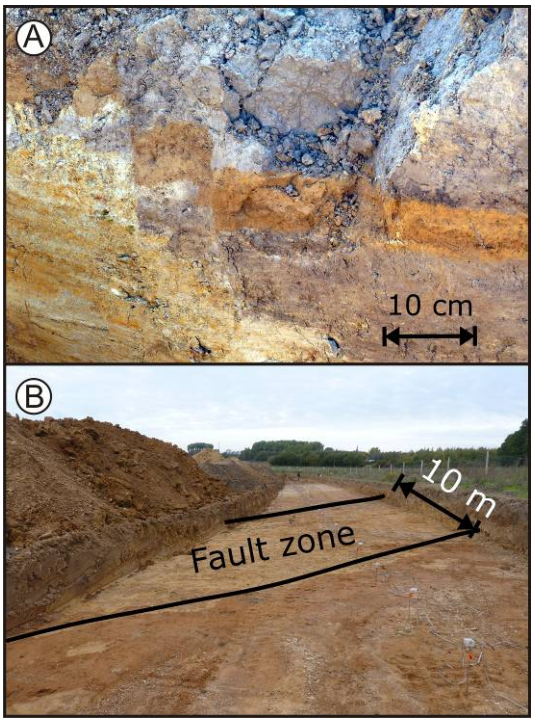

Fig. 5: A) Step-like offset clearly points to seismic deformation instead of soil creep. Displacement is about 5 cm. The offset reddish layer is made up of clayey-silty, loess material, 50 cm below the surface. B) The fault zone is clearly visible in the trenches, not only at the walls, but also on the floor. This enabled a very good correlation with the geophysical data and a precise analysis of subsurface features.

CONCLUSION

We found evidence for four surface-faulting events at the active Rurrand Fault close to Düren, which might be responsible for the 1755/1756 earthquake series. Offset sediments clearly point to seismic activity since Late Pleistocene and at least four earthquake events. Geophysical data allowed mapping the fault trace where there were no outcrops (Geoelectrics and GPR) and revealed the fault geometry in depths of up to 6 m (GPR).

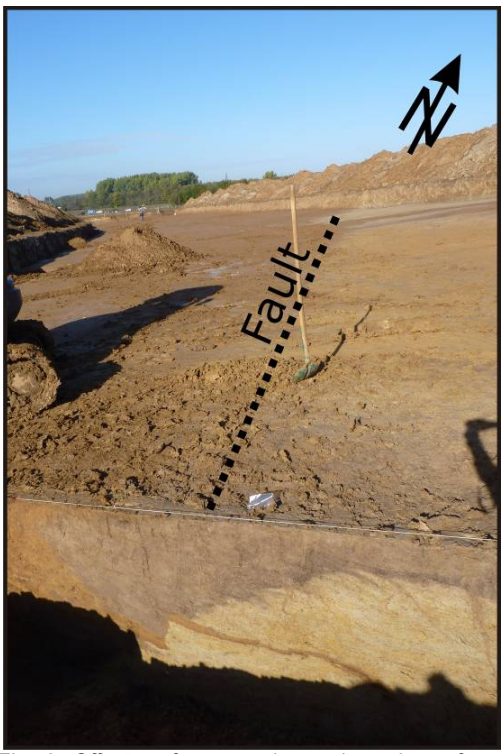

Fig. 6: Offset surface-near layers have been found during the archeological excavations

References

Camelbeeck, T., Vanneste, K., Alexandre, P., Verbeeck, K., Petermans, T., Rosset, P., Everaerts, M., Warnant, R. & Van Camp, M. (2007). Relevance of Active Faulting And Seismicity Studies To Assessments Of Long-Term Earthquake Activity and Maximum Magnitude In Intraplate Northwest Europe, between the Lower Rhine Embayment and the North Sea. In: *Geological Society of America, Special Paper*, vol. 425, pp. 193-224.

Meidow, H. (1995). *Rekonstruktion und Reinterpretation von historischen Erdbeben in den nördlichen Rheinlanden unter Berücksichtigung der Erfahrungen bei dem Erdbeben von Roermond am 13. April 1992.* Dissertation, Universität Köln, Leverkusen, 305 p.

Skupin, K., Buschhüter, K., Hopp, H., Lehmann, K., Pelzing, R., Prüfert, J., Salamon, M., Schollmayer, G., Techmer, A. & Wrede, V. (2008). Paläoseismische Untersuchungen im Bereich der Niederrheinischen Bucht. *Scriptum 17, Krefeld (Geol. Dienst Nordrh.-Westf.), 72 p.*

Vanneste, K. & Verbeeck, K. (2001). Paleoseismological analysis of the Rurrand fault near Jülich, Roer Valley graben, Germany: Coseismic or aseismic faulting history? *Netherlands Journal of Geosciences / Geologie en Mijnbouw,* 80 (3-4): 155-169.

EARTHQUAKE ARCHAEOLOGY

INQUA PALEOSEISMOLOGY AND ACTIVE TECTONICS

FIND AND PRIMARY SEARCH OF AN ACTIVE FAULT AT THE GAIXIA SITE, GUZHEN COUNTY, ANHUI PROVINCE, P.R. CHINA

YAO Da-quan (1), SHUO Zhi (2),TANG Ji-ping (3), WANG Zhi (2),SHEN Xiao-qi (1),CHEN An-guo (1) , LI Lin-li (1)

(1)Seismological Administration of Anhui Province,Hefei,Anhui P.R.China,230031. email: daquany@aheq.gov.cn
(2)Cultural Relic Archaeology Research Institute of Anhui Provine, Hefei,Anhui P.R. China,230001
(3)Institute of Cultural Relic Archaeology of Tongling City,Anhui Province,Tongling, Anhui P.R. China,244001

Abstract (Find and primary search of an active fault at the Gaixia Site, Guzhen County, Anhui Province, P.R. China): *Recently a large number of ancient sites were excavated due to construction works in eastern China, which makes it possible to identify and trace thousands of years of natural deformation history. With this opportunity, one can benefit from the precise archaeological layer technology. In a collaboration of earthquake research institutions and archaeological departments, we analysed Quaternary tectonic deformation, in particular the deformation phenomena hosted in the prehistoric cultural layer. This paper reports the working progress of a special excavation at the Gaixia archaeological site in Haocheng town (Guzhen county, Anhui province, P.R. China).*

Key words*: Quaternary deformation, prehistoric culture, Gaixia site, Anhui Province*

THE BASIC FEATURES OF THE VESTIGE

The Gaixia site is located east of the Tancheng-Lujiang fault (TanLu Fault on Fig. 1). In the west there is the Guzhen-Fengtai fault, where the Ms~ 6.2 earthquake event of 1831 took place in FengTai. The southern border is the NW-trending GuoHe fault, where a magnitude Ms~ 6 earthquake occurred in 1481 in Guoyang (Fig.1).

The Gaixia site lies in Bawangcheng village, Haocheng town, 24 kilometers eastward of Guzhen county, which is the centre battlefield of the competition between Chu and Han and the final Gaixia battle, where the 'Gaixia Battle' took place in 202 B.C. The entire archaeological area is about 150,000 km^2, with an earth wall around the main site, which is 2-3 m higher than the outer surface level. The inner terrain is higher at the sides and lower than the surroundings in the middle. West and north of the archaeological site there is the Tuohe River.

In order to clarify the specific age, the floor width and construction methods of the ancient city wall, archaeologists excavated a trench since March 2008 (serial number: 2008 GGTG3, TG3 for short) with a length of 40 m and a width of 3 m, about 70 m from a former excavation in 2007. The trench extends from the city wall to the inner moat, which completely reveals the whole section of the city wall and excavates some of the cultural layers in the inner wall. Just in the Dawenkou Cultural layer in both sides and at the bottom of TG3, seismologists and archaeologists discovered an active fault (Fig.2).

DISCOVERY AND ANALYSIS OF THE TENSION-SHEAR FAULT IN THE CULTURAL LAYER

On May 12th, 2008, when excavations reached grey-black ash layers, seismologists and archaeologists

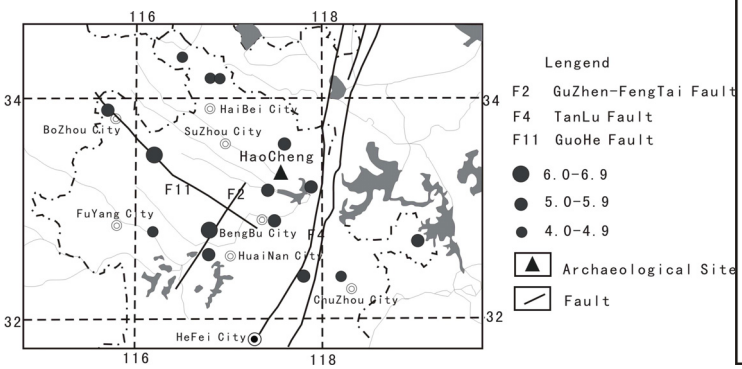

Fig. 1: A sketch of regional geology seismology of Gaixia ruins

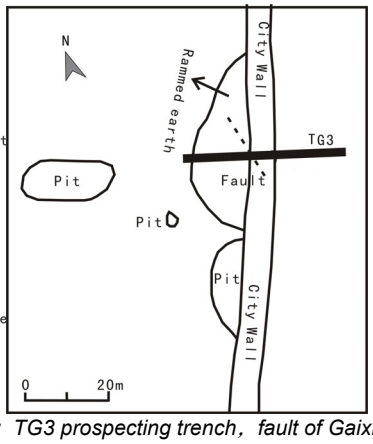

Fig. 2: TG3 prospecting trench, fault of Gaixia ruins

found fault dislocation evidence. According to this clue, they carefully scraped the pace of the layer again for further identification, and confirmed the range of fault dislocation.

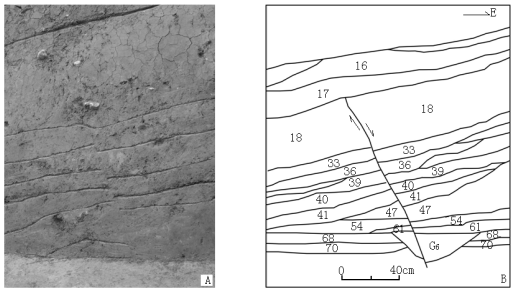

Fig.3: Tensile-shear fault on the northern wall. Left: Photo of the northern wall; Right: sketch of the northern wall.

The dislocation was located in TG3, and the west segment is about 15.4 m to the west wall. According to the change of quality and color of the soil and the analysis of samples taken at the dislocation position, it could be confirmed that the dislocation is beneath the 17th layer of the city wall (serial number: "the 17th layer wall", following are the same), and the dislocation extends from the 18th layer, including raw soil layer (undisturbed soil). A crack with a width of

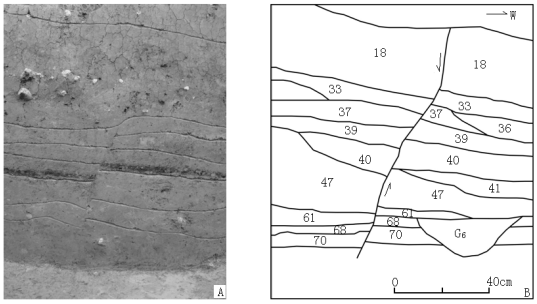

Fig.4: Tensile-shear fault on the southern wall. Left: photo of the southern wall; Right: sketch of the southern wall.

2 mm - 4 mm can be seen at both the plane and the profile of the dislocation, which was very clear to see on the bottom of the soil layer, gradually becoming thinner upwards in the 17th layer. The crack was filled with grey clay and had a different colour than the surrounding soil. The soil's thickness was symmetric and completely anastomosing on the two sides of the fault.

The western part of the fractured plane was 3.8 cm higher than the eastern (= 3.8 cm vertical offset). The trend of the fracture plane is 353°, and the section dipped towards the E with an angle of ~60°. The fault plane is curved, with its highest point 1.79 meters below the ground surface at the western wall of the trench, extending to the raw soil layer. The highest point on the south wall is 1.68 meters below ground surface, and also extends to the raw soil layer. From the 18th layer downwards, 12 layers of the north wall had dislocation, not including the raw soil layer: the fault penetrated the wall with the layers 18, 33, 36, 37, 39, 40, 41, 47, 54, 61, 68, 70, and also penetrated the narrow channel G6, which is S-N trending. The southern part of the prospecting trench also showed normal faulting (Fig.3). From the 18th layer downwards to the raw soil layer there are 10 layers that were dislocated, not including the raw soil layer, and also showing normal faults (Figs.4,5).

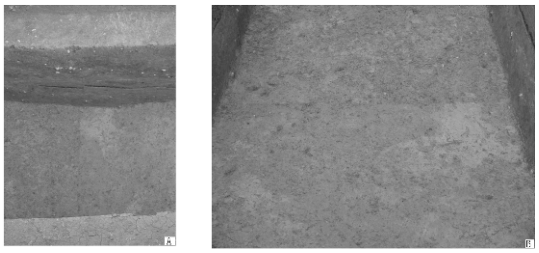

Fig.5: Tensile-shear fault on the trough bottom. Left: photo towards the southern overlook; Right: photo towards the eastern overlook.

DISCUSSION AND CONCLUSIONS

In conclusion, active faulting was found in the culture layers of the vestige belong to the Late Dawenkou Dynasty (about 4300a BP), and the observation of the fault plane shows the characteristic of high speed deformation (He Yong-nian et al.,1985; Yao Da-quan,2004).

The archaeological site is located right on the NNW trending Tancheng-Lujiang fault. According to the history records, several earthquakes of Ms~6 occurred near this area. Our discovery of this earthquake in the ruins enriches the seismotectonic knowledge in this area and completes the earthquake catalogue for future hazard studies.

Acknowledgements: This paper is a contribution to the Scientific Research Special Project of the Earthquake Calling（200808064）and Science and Technology Tackle Key Problem Plan Project of Anhui Province（08010302204）.

References

He Yong-nian, Yang Zhu-en. 1985. Research and the significance of microscopic marks of ancient earthquakes [J]. Earthquake Research in China,1(3):76-81(in Chinese).

Yao Da-quan 2004. Macroscopic and Microscopic Evidence of Periodical Stick-Slip Deformation in an Active Fault [J]. Recent Developments in World Seismology, (4):6-10 (in Chinese).

THE MOVRI MOUNTAIN EARTHQUAKE: UNDERSTANDING ACTIVE DEFORMATION OF THE NW PELOPONNESE

Zygouri, Vasiliki (1), Sotiris Kokkalas (1), Paris Xypolias (1), Ioannis Koukouvelas (1), Gerassimos Papadopoulos (2)

(1). Department of Geology, Division of General, Marine Geology and Geodynamics, University of Patras, Patras 26500, Greece. Email: iannis@upatras.gr
(2). Institute of Geodynamics, National Observatory of Athens, Lofos Nymfon, Thissio, 11810, Athens, Greece. Email: papadop@noa.gr

Abstract (The Movri Mt earthquake: understanding active deformation of the NW Peloponnese): *The Mw 6.4 June 8th 2008 Movri Mountain earthquake struck NW – Peloponnesus, Greece, caused widespread deformation and damage in buildings, as well as extensive ground hazards. Three surface ruptures were triggered by the earthquake, with the most promising for paleoseismology analysis lying near the epicenter of the event, attaining a maximum offset of 25 cm. In this surface rupture a paleoseismological trench was excavated. Based on seven ^{14}C samples, we identify two surface – rupturing earthquakes in the last 1Kyr prior the recent event. Thus, observations from paleoseismology suggest that the Nisi fault appear to be related to surface ruptures and events. In addition, our ^{14}C data support the view that the Nisi fault displays a slip rate in the order of 1.5 mm/yr during the last 1Kyr.*

Key words*: paleoseismology, surface ruptures, colluvial wedge.*

INTRODUCTION

On June 8th 2008, a Mw 6.4 strike – slip earthquake (hypocentral depth of almost 20 km) occurred in the northwestern Peloponnese (Greece) without obvious relation to any mapped fault. Although strong earthquakes are common in western Greece, this event took place in a region previously considered as seismically quiet. This earthquake ruptured along an unknown dextral strike slip fault segment striking NE-SW, resulted in new geological conclusions for the area. During the Movri Mt earthquake, three main fault ruptures emerged on the epicentral area, the 4.5 km long Vithoulkas surface rupture, the 5.0 km long Michoi surface rupture and the 6.0 km long Nisi surface rupture (Fig. 1).

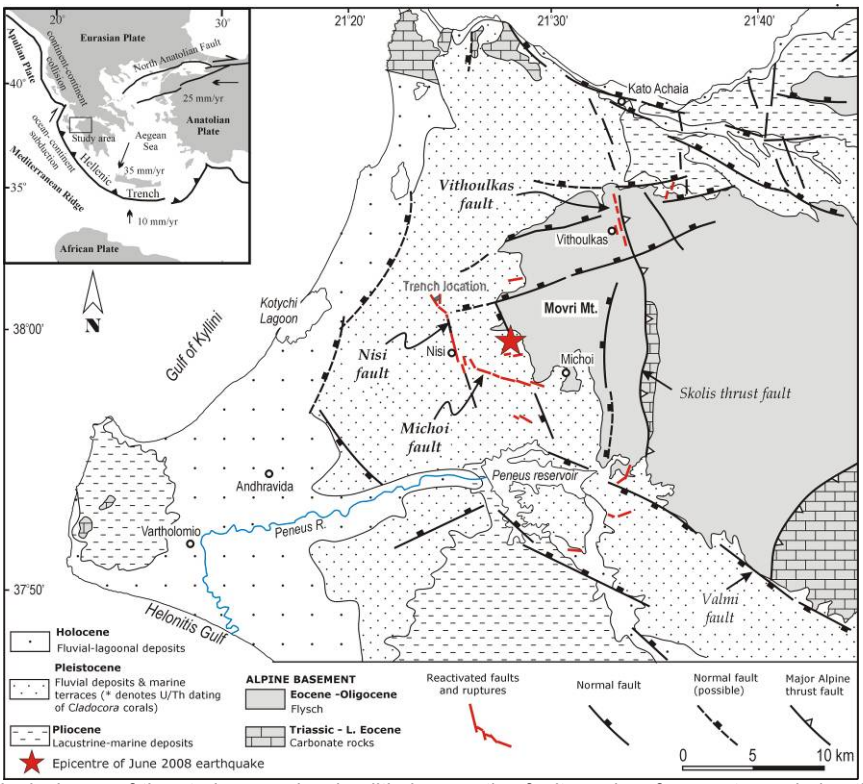

Fig. 1: Geological map of the study area showing lithology, active faults and surface ruptures during the Movri Mt earthquake.

In order to investigate whether these ruptures and associated fractures record an individual or unique tectonic offset or a response to strong ground motion we performed a paleoseismological study across the Nisi surface rupture. The Nisi rupture trends NNW-SSE and has an almost straight, segmented trace and attained a maximum offset of 25 cm during the event. The trench has a length of 10 m, a width of 1.5 m and a depth of 2.5 m.

DESCRIPTION OF THE NISI TRENCH

The sedimentary environment observed inside the trench suggests fine – grained coastal and fluvial to lagoonal sediments (fig. 2). It comprises sandy to clay horizons with generally yellow, brownish yellow and grey to dark brown sediments. Shallow coastal sediments are mostly found on the uplifted part of the trench. Shallow coastal sediments are overlain in the upthrown block of the fault either directly by the modern plowed soil, or by a succession of almost 0.5 m thick yellow sandy and grey clay fluvial sediments in the downthrown block. The fault zone is almost 1 m wide with open voids formed also during the latest event. The deeper excavated part of the fault zone includes rotated coastal sediments. Open voids allow the precipitation of meteoric water, and disturb the deposition of new material after every possible new event. The material inside the fault zone is characterized as an unconsolidated, unsorted and mixed assemblage of coastal sediments derived mainly from the fine grained footwall's coastal sediments. Two small colluvial wedges (fig. 3) with a maximum thickness of 30-40 cm, though obscure, can be detected. These colluvials are characterized by wedge geometry, thickest at the fault surface and thinning away from it, and colour differences.

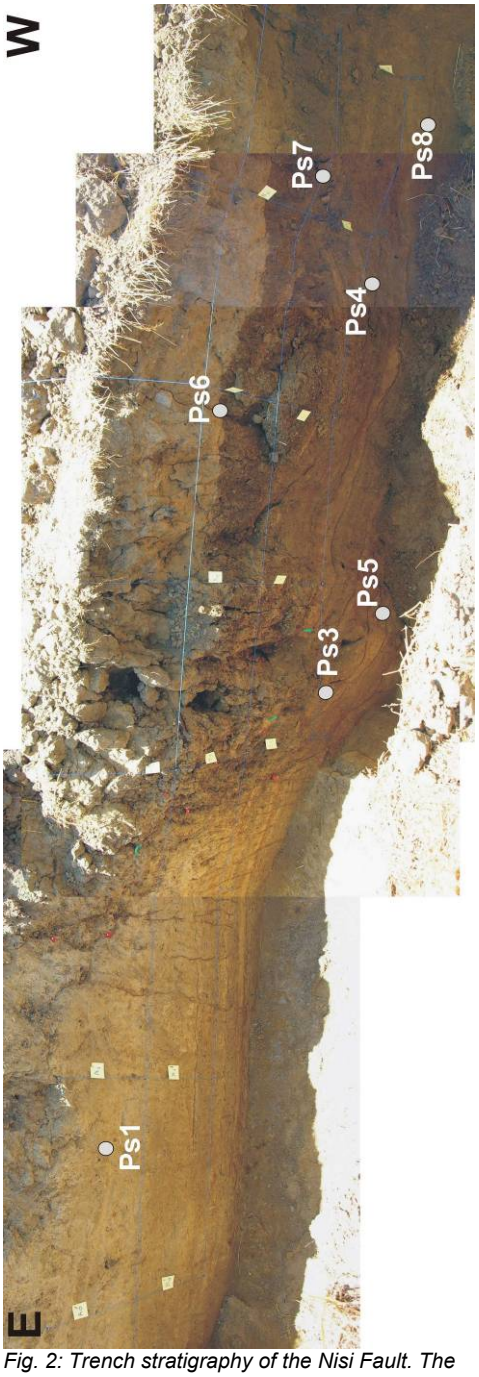

Fig. 2: Trench stratigraphy of the Nisi Fault. The sampling sites within the trench are mentioned with Ps abbreviation .

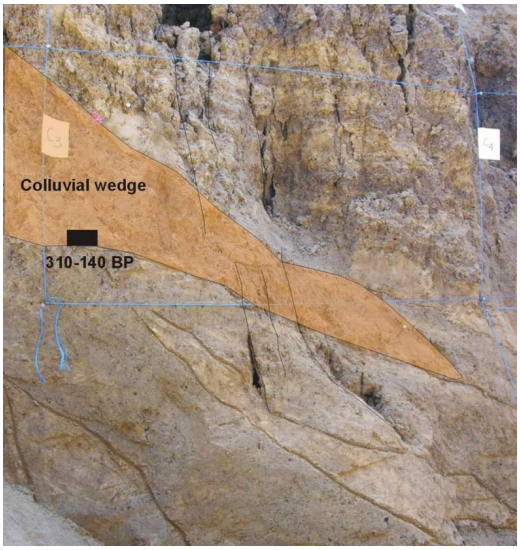

Fig. 3: Detailed view of the upper colluvial wedge formed in the Nisi fault zone (The black box shows the Ps3 sample).

DISCUSSION AND CONCLUSIONS

Despite the flat and rather featureless landscape, certain evidences support the view that Nisi rupture is a newly emerged fault with recent seismic history. The colluvial wedges in the trench fulfil most of the parameters defining deposits in fault zones such as their shape and chaotic sedimentation (sensu Pavlides et al., 2004). The colluvial deposits are supplied by fine grained material of the upthrown block, controlled by the sedimentation environment and the ruptured sediments and therefore is bound to be formed by the finer deposits accumulating on the downthrown block's free face. Open voids, filled cracks, the formation of at least one datable colluvial wedge and the increased deformation in upthrown horizons attests to possible episodic activity during the past 1000 years.

The seven samples (fig. 2) were collected from both the uplifted and subsided block of the fault as well as from the disturbed fault zone. The disturbed zone samples yielded two kind of ages, a younger one at the lowest part of the zone (sample Ps5) and an older one (sample Ps3) above the previous sample and at the base of the colluvial wedge (figs. 2, 3). This attests the effect of precipitation of meteoric water through the fault zone. After considering the full distribution of ^{14}C ages and taking into account the stratigraphy of the trench we interpret three events (with the more recent included) that can be evidenced.

Our trenching study showed a recurrence interval between 300 to 600 years, we suggest that the Nisi fault shapes fine grained colluvial wedges without following a constant time pattern. Thus, we assume a Quaternary slip rate in the order of 1.5mm/yr and strong slip-rate similarities to the Egion and Schinos faults in Gulf of Corinth (Koukouvelas, 1998; Koukouvelas et al., 2005).

.

Acknowledgements: We would like to express our appreciation to S. Pavlides, R. Caputo and A., Chatzipetros for fruitful discussion of the trench and S. Verroios and V. Chatzaras for their help during fieldwork.

References

Koukouvelas, I.K., (1998). The Egion fault, earthquake-related and long term deformation, Gulf of Corinth, Greece. *Journal of Geodynamics* 26, 501-513.

Koukouvelas, I.K., D. Katsonopoulou, S. Soter, & P. Xypolias, (2005). Slip rates on the Helike Fault, Gulf of Corinth, Greece: new evidence from geoarchaeology. *Terra Nova* 17, 158-164.

Pavlides, S., I. Koukouvelas, S. Kokkalas, L. Stamatopoulos, D. Keramydas & I. Tsodoulos, (2004). Late Holocene evolution of the East Eliki fault, Gulf of Corinth (Central Greece), Quaternary International 115-116, 139-154.

Index

Proceedings
INQUA - IGCP 567 CORINTH (GREECE), 2011

RWTH AACHEN UNIVERSITY
Neotektonik
Georisiken

ΕΘΝΙΚΟ & ΚΑΠΟΔΙΣΤΡΙΑΚΟ ΠΑΝΕΠΙΣΤΗΜΙΟ ΑΘΗΝΩΝ
ΕΡΓΑΣΤΗΡΙΟ ΠΡΟΛΗΨΗΣ & ΔΙΑΧΕΙΡΙΣΗΣ ΦΥΣΙΚΩΝ ΚΑΤΑΣΤΡΟΦΩΝ
LABORATORY OF NATURAL HAZARDS PREVENTION & MANAGEMENT
NATIONAL & KAPODISTRIAN UNIVERSITY OF ATHENS

Ο.Α.Σ.Π.

UCL
Aon Benfield UCL
Hazard Centre

JG|U
JOHANNES GUTENBERG UNIVERSITÄT MAINZ

VNiVERSiDAD D SALAMANCA

AEQUA

GSSI

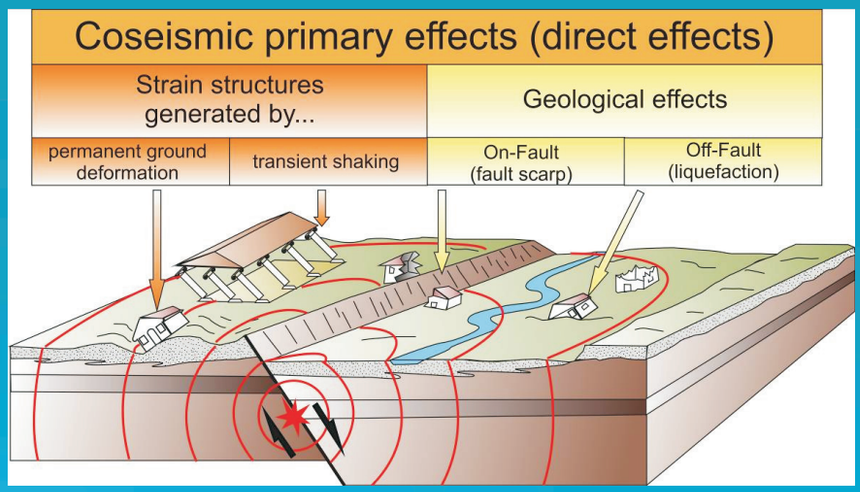

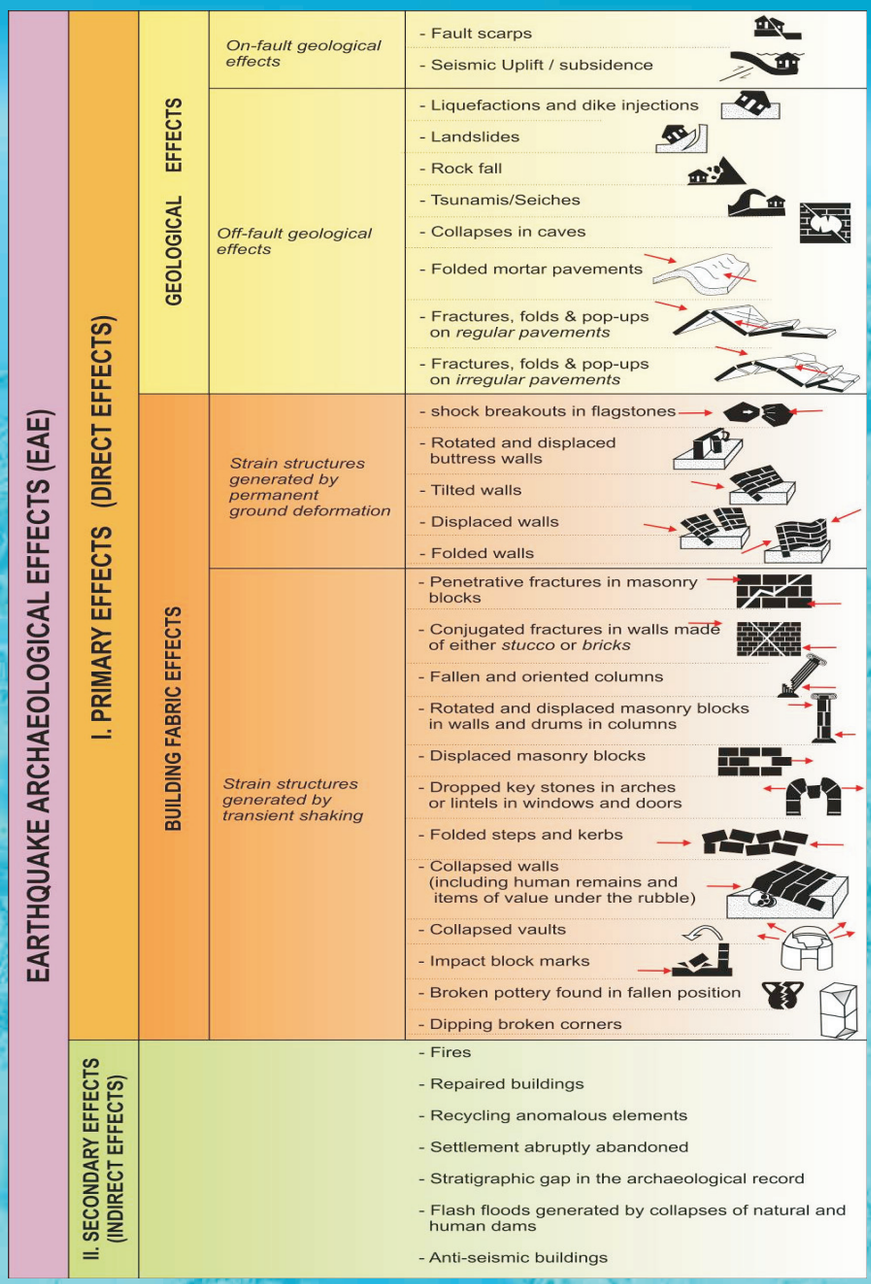

M.A Rodríguez Pascua et al. (2011). Quaternary International, 242 (1), 20-30. Sp. Vol. on Earthquake Archaeology and Paleoseismology (P.G. Silva, M. Sintubin & K. Reicherter Eds.)

MINISTERIO DE CIENCIA E INNOVACIÓN
Instituto Geológico y Minero de España

INQUA TERPRO Paleoseismology and ActiveTectonics

ESI-2007

IUGS UNESCO 567

paleoseismicity.org